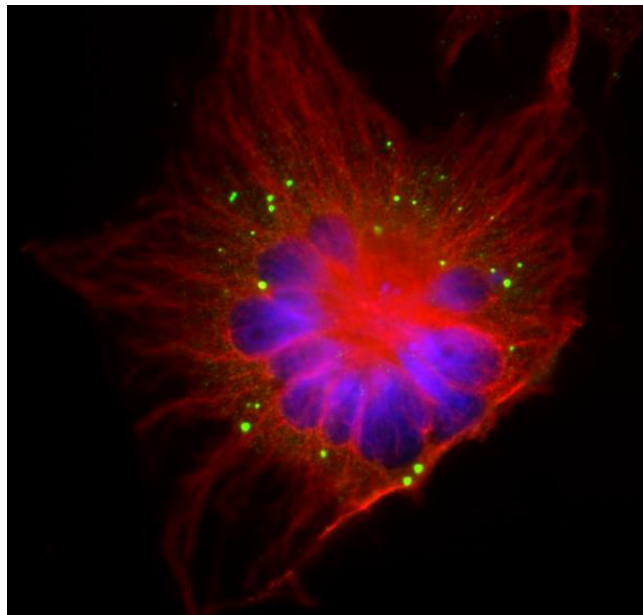




UNIVERSITÀ
DI PAVIA

Dipartimento di Biologia e Biotecnologie "L.Spallanzani"

**A new platinum-based prodrug: its anticancer effects
and *in vitro* approaches to understand novel targets to
treat Nervous System tumours**



Beatrice Ferrari

Dottorato di Ricerca in
Genetica, Biologia Molecolare e Cellulare
Ciclo XXXII – A.A. 2016-2019



UNIVERSITÀ
DI PAVIA

Dipartimento di Biologia e Biotecnologie "L.Spallanzani"

**A new platinum-based prodrug: its
anticancer effects and *in vitro* approaches
to understand novel targets to treat
Nervous System tumours**

Beatrice Ferrari

Supervised by Prof. Maria Grazia Bottone

Dottorato di Ricerca in
Genetica, Biologia Molecolare e Cellulare
Ciclo XXXII– A.A. 2016-2019

Abstract

To the Nervous System (NS) belong a heterogeneous group of cancers, whose classification, in the years, has undergone numerous implementations following the integrated use of genotypic and phenotypic parameters. This new approach has added a greater level of objectivity in diagnosis and the possibility of carrying out targeted therapies. Nevertheless, to date, some types of tumours, such as gliomas and neuroblastomas remain refractory to treatments. Despite the initial benefits, current therapies, *i.e.* clinical treatment with cisplatin (CDDP), are associated with severe systemic side effects and are unable to contrast the typical relapsing forms of these tumours. Furthermore, the standard therapy with Temozolomide (TMZ), although it has prolonged patient's life expectancy from 5 to 15 months, is still ineffective in some case studies due to the genetic characteristics of patients. To overcome the limits of classical oncotherapy, platinum(IV) prodrugs have been synthesised. Among these, the new (OC-6-44)-acetatodiamminedichlorido(2-(2-propynyl)octanoate)platinum(IV) prodrug, named Pt(IV)Ac-POA, synthesised by Prof. Osella and his team (Amedeo Avogadro University of Eastern Piedmont, Italy), represents a promising tool, able to generate a synergistic action in the hypoxic tumour cell microenvironment. This prodrug bearing as axial ligand (2-propynyl)octanoic acid (POA), a histone deacetylase inhibitor, has a higher activity due to the high cellular accumulation by virtue of high lipophilicity and to the inhibition of histone deacetylase which leads to increased exposure of nuclear DNA, thereby permitting higher platination levels and promoting cancer cells death. The first part of the present study investigated the effects induced by Pt(IV)Ac-POA on two types of rat cell lines, *i.e.* B50 neuroblastoma and C6 glioma cells and human U251 glioblastoma cells, evaluating toxic concentrations, morphological and functional alterations, after 48 hours of treatment of continuous exposure to the new compound.

The second part of the work focused mainly on the U251 line, a human glioblastoma multiforme (GBM) cell line, in order to identify whether Pt(IV)Ac-POA treatment could induce chemoresistance, as was often detected *in vitro* after treatment with CDDP. In this view, in collaboration with Dr. Facchetti of the National Center for Cancer Treatment (CNAO, Italy), the effects induced on the U251 line by carbon ion radiotherapy, in association or not with Pt(IV)Ac-POA, have been evaluated, with the aim to identify the most efficacy therapeutic combination to obtain the best long-term antitumor effect and consequently to reducing the possible phenomena of chemo- and radioresistance.

Parallely, this study investigated the response of U251 to different concentrations of the extract of Dandelion root (*Taraxacum officinale*) and a myco-phytotherapeutic supplement called “Ganostile” (Miconet s.r.l.), based on *Ganoderma lucidum* and containing several extracts of medicinal mushrooms, to evaluate antitumor activity on U251 cell line. Indeed, both the *Taraxacum officinale* and the *Ganoderma lucidum* are known in the literature not only for their beneficial effects but also for their use in the treatment of different types of tumours.

Lastly, in collaboration with Prof. Rossi (Neurobiology and Integrated Physiology Laboratory, University of Pavia, Italy), the localization and the possible functional role of the inwardly rectifying potassium channels, Kir4.1, and large-conductance Ca^{2+} -activated potassium channels (BK) were analysed in U251 cells. The study was conducted focusing on the changes observed performing “wound healing” as an assay to migration. In this context, several studies highlighted the role of ion channels and intracellular calcium levels in cell proliferation and migration processes, which are at the basis of GBM malignancy.

The results obtained showed the efficacy of the new prodrug Pt(IV)Ac-POA to induce cell death in all three cell lines at lower concentrations than the standard reference treatment with CDDP. Especially, this cytotoxic effect was observed in the U251 cell line even after 7 days from treatment (*recovery* condition), demonstrating a prolonged antitumor effect of the new compound. The combination of Pt(IV)Ac-POA pre-treatment with carbon ion irradiation showed very promising data in the treatment of the U251 line of glioblastoma multiforme. This efficacy was already detected at 48 hours of exposure, but the results obtained also showed a long-term effect of the combined treatment, compared to the one with the CDDP, demonstrating once again the greater efficacy of the Pt(IV)Ac-POA.

The use of phyto- and/or mycotherapeutic substances, thanks also to the basic benefits of which they are characterized, has shown promising effects in the treatment of GBM, suggesting a possible adjuvant effect to treatment, combining both an antitumor effect and an improvement in the quality of life of the patient in a context of clinical treatment.

Moreover, the better characterization of the BK and Kir4.1 channel involved in proliferation and migration could allow the implementation of new strategies in glioblastoma treatment, thus representing a possible new target for anticancer drugs.

This study is part of a broader project, aimed at connecting different methodological approaches to improve the overall view on the characterization and the problems related to the treatment of tumours of the

NS. Therefore, this work allowed to identify a new valid antitumor agent, such as Pt(IV)Ac-POA, for the treatment of different brain tumours cell line. Furthermore, the different investigations have led both to the identification of possible new antitumor targets and the feasible use of unconventional therapies *i.e.* hadrontherapy and myco- phytotherapy. Then, these new results could also improve GBM treatment and overcome the limitations of standard oncotherapy such as chemoresistance and toxicity related to the high dose of treatment, aimed at improving not only the patient's prognosis but also to improve his quality of life during therapy.

Acknowledgements

I would like to thank my supervisor Prof. Bottone for having welcomed me into her laboratory for all these years and for supporting my research work.

Thanks to Prof. Osella for providing us with Pt(IV)Ac-POA on which my thesis has been based.

Thanks to Prof. Rossi and Dr. Facoetti for the experimental implementations that allowed me to add essential data to this work.

Many thanks to Prof. Roda for support and kind suggestions for experiments and drafting of articles.

Thanks to Dr. Mazzini for the technical support of flow cytometric analyses.

Last but not least, I am very grateful to Mrs. Veneroni for her essential help in setting up cell cultures.

Abbreviations

$\Delta\psi_m$: mitochondrial transmembrane potential
 α -KG: α -ketoglutarate
AA: Anaplastic Astrocytoma
ABC: ATP-binding cassette protein
Acac: acetylacetonate
ACD: Accidental Cell Death
ADP: Adenosine Diphosphate
AIC: 5-aminoimidazole-4-carboxamide
AIF: Apoptosis-Inducing Factor
AGT: O⁶-alkylguanine-DNA-alkyltransferase
AMBRA: Activating Molecule in Beclin-1-Regulated Autophagy Protein
APAF-1: Apoptotic Protease Activating Factor-1
APE1: Abasic-AP Endonuclease-1
APNG: Alkylpurine-DNA-N-glycosylase
ATG: Autophagy-related Genes
ATM: Ataxia Telangiectasia Mutated
ATP: Adenosine Triphosphate
ATP7B: ATPase Copper Transporting Beta
ATP11B: ATPase Phospholipid Transport 11B
ATR: ATM and Rad3-related
Bak/Bak1: Bcl-2 Antagonist Killer
Barkor: Beclin -1-Associated Autophagy-Related Key Regulator
Bax: Bcl-2 associated X
BBB: Blood Brain Barrier
BCSF: Blood-Cerebrospinal Fluid Barrier
Bcl-2: B-cell lymphoma 2
bFGF: basic Fibroblast Growth Factor
BK: Big Potassium channel
BMB: Blood-Meningeal Barrier
BSA: Bovine Serum Albumin
BRAP: BRCA1-Associated Protein
b.w.: body weight
Ca²⁺: Calcium
CAD: Caspase-Activated DNAase
CaM: Calmodulin
CaMK: Ca²⁺/CaM-dependent Protein Kinase
CAR: Chimeric Antigen Receptor
CARD: Caspase-Recruitment Domain
CAT: Catalase

CB: Calbindin
CBDCA: CycloButane DiCarboxylic Acid
CBPs: Calcium Binding Proteins
CCDC178: Coiled-Coil Domain Containing 178
Chk1: Checkpoint kinase 1
CDDP: Cisplatin
CMA: Chaperone-Mediated Autophagy
COG: Children's Oncology Group
COX2: Cyclooxygenase 2
CNS: Central Nervous System
CR: Calretinin
CSCs: Cancer Stem Cells
CT: Continuous treatment
CTLA-4: Cytotoxic T-cell Lymphocyte Antigen-4
Ctr1: Copper Transporter 1
CYCS: Cytochrome c, somatic
CypA: Cyclophilin A
d-2-HG: d-2-hydroxyglutarate
Da: Dalton
DACH: Diaminocyclohexane
DAMPs: Danger-Associated Molecular Patterns
DBD: DNA Binding Domain
DCs: Dendritic Cells
DD: Death Domain
DDR: DNA Damage Response
DED: Death-Effector Domain
DFFA: DNA Fragmentation Factor subunit alpha
DFFB: DNA fragmentation factor subunit beta
DISC: Death Inducing Signaling Complex
DMEM: Dulbecco's Modified Eagle Medium
DMS: Dimethylsulphide
DNA: Deoxyribonucleic acid
dpi: dots per inch
DR: Death Receptor
DRE: Dandelion Root Extract
DYRK1B: Dual-specificity Y-phosphorilation regulated kinase 1B
ECM: Extracellular Matrix
EDTA: Ethylenediaminetetraacetic Acid
EGFR: Epidermal Growth Factor Receptor
EMEM: Eagle's Minimal Essential Medium
EP: ergosterol peroxide

ER: Endoplasmic Reticulum
ERBB2: Erb-b2 receptor tyrosine kinase 2
ERK: Extracellular Signal-Regulated Kinases
ESCRT: Endosomal Sorting Complexes Required For Transport
FAD: Flavin Adenine Dinucleotide
FBS: Fetal Bovine Serum
FDA: Food and Drug Administration
FIP200: Focal Adhesion Kinase
FLIP: FADD-like IL-1 β -converting enzyme-inhibiting protein
GABARAP: Gamma-aminobutyric acid receptor-associated protein
GAP: GTPase Activating Protein
GBM: Glioblastoma Multiforme
G-CIMP: Glioma CpG-Island Methylator Phenotype
GEF: Guanine Nucleotide Exchange Factor
GFAP: Glial Fibrillary Acidic Protein
GPx: Glutathione Peroxidase
GSC: Glioma Stem Cells
GSH: Glutathione
GSN: Gelsolin
GTP: Guanosine Triphosphate
GDP: Guanosine Diphosphate
GLPS: Ganoderma lucidum Polysaccharides
Gy: Gray
H₂O₂: Hydrogen peroxide
HAT: Histone Acetyltransferase
HDAC: Histone Deacetylase
HDACi: Histone Deacetylase inhibitors
HDR: Homology Directed Repair
HIF-1: Hypoxia-Inducible Factor 1
HMGB: High-Mobility Group Box
HSC70: Heat shock cognate 70 kilodaltons
HSP70: Heat Shock Protein 70 kilodaltons
HVA: High-Voltage-Activated
IAP: Inhibitors of Apoptosis Proteins
ICAD: Inhibitor CAD
IDH: Isocitrate Dehydrogenase
IKK: I κ B Kinase Complex
IL-1 β : Interleukin 1 beta
IL-4: Interleukin 4
IL-10: Interleukin 10
IL-13: Interleukin 13

INF- γ : Interferon gamma
 INRGSS: International Neuroblastoma Risk Group Staging System
 InsP3R: Inositol Triphosphate Receptor
 INSS: International Neuroblastoma Staging System
 IP3: Inositol Triphosphate
 JNK: c-Jun N-Terminal Kinase
 Kir: Inwardly rectifying potassium channel
 LAMP-2A: Lysosomal-Associated Membrane Protein type 2A
 LC3: Microtubule Associated Protein 1 Light Chain 3
 LDCD: Lysosome-Dependent Cell Death
 LET: Linear Energy Transfer
 LINAC: medical linear accelerator
 LMP: Lysosomal Membrane Permeabilization
 LPO: Lipid Peroxidation
 LSDs: Lysosomal Storage Diseases
 LVA: Low-Voltage-Activated
 MAPK: Mitogen-Activated Protein Kinase
 MCFA: Medium-Chain Fatty Acid
 MGMT: O⁶-methylguanine-DNA-methyltransferase
 MHC: Major Histocompatibility Complex
 mHCX: mitochondrial H⁺/Ca²⁺ exchanger
 MMP: Mitochondrial Membrane Permeabilization
 MMR: Mismatch Repair
 mNCX: Na⁺/Ca²⁺ exchanger
 MAMs: Mitochondrial-Associated Endoplasmic Reticulum Membranes
 MCU: Mitochondrial Calcium-Uniport
 MeV: Megaelectron Volt
 MOMP: Mitochondrial Outer Membrane Permeabilization
 MPTP: Mitochondrial Permeability Transitional Pore
 MRP2: Multidrug Resistance-associated Protein 2
 mtDNA; mitochondrial DNA
 MTIC: 5-(3-methyltriazol-1-yl)imidazole-4-carboxamide
 mTOR: Mammalian Target of Rapamycin
 MTS:[3-(4,5-dimethylthiazol-2-yl)-5-(3-carboxymethoxyphenyl)-2-(4-sulfophenyl)-2H-tetrazolium]
 NADPH: Nicotinamide Adenine Dinucleotide Phosphate
 NCCD: Nomenclature Committee on Cell Death
 NEAA: Non-Essential Amino Acids
 NEMO: NF- κ B Essential Modulator
 NER: Nucleotide Excision Repair
 NF- κ B: Nuclear Factor kappa-light-chain-enhancer of activated B cells

NGF: Nerve Growth Factor
 NGS: Normal Goat Serum
 NMDA: N-methyl-D-aspartate
 NO: Nitric Oxide
 NOS: Nitric Oxide Synthases
 NS: Nervous System
 NSCs: Neural Stem Cells
 •OH: Hydroxyl radical
 O_2^- : Superoxide anion
 O_3 : Ozone
 1O_2 : Singlet oxygen
 OER: Oxygen Enhancement Ratio
 OMM: Outer Mitochondrial Membrane
 OPA1: Optic Atrophy type 1
 OPCs: Oligodendrocyte Precursor Cells
 P2XR: Purinergic ionotropic Receptor
 P62/SQSTM1: Sequestosome 1 protein
 PBS Phosphate-Buffered Saline
 PARP: Poly-ADP-Ribose Polymerase
 PAS: Phagophore Assembly Site
 PCD: Programmed Cell Death
 PD-1: Programmed Cell Death-1
 PDGFR: Platelet-Derived Growth Factor Receptor
 PE: Phosphatidylethanolamine
 PhB: Phenylbutyrate
 PI: Propidium Iodide
 PI3K: Phosphatidylinositol 3-class kinase III
 PIP: Phosphatidylinositol Phosphate
 PIP2: Phosphatidylinositol 4,5-bisphosphate
 PKA: Protein Kinase A
 PKC: Protein Kinase C
 PKC- α : Protein Kinase C-alpha
 PLC: Phospholipase C
 PMCA: Plasma Membrane Calcium ATPase
 PNS: Peripheral Nervous System
 PRR: Pathogen Recognition Receptor
 Pt(IV): Platinum(IV)
 Pt(IV)Ac-POA: (OC-6-44)-acetatodiamminedichlorido(2-(2-propynyl)octanoato)platinum(IV)
 PTEN: Phosphatase and Tensin homolog
 PTP: Permeability Transition Pore

PTPC: Permeability Transition Pore Complex
PV: Parvalbumin
PYD: Pyrin Domain
QoL: Quality of Life
RAB8A: Ras-related protein Rab-8A
RBE: Relative Biological Effectiveness
RCD: Regulated Cell Death
RCS: Reactive Chloride Species
REC: Recovery Condition
RIP: Receptor-Interacting Protein
RIPA: Radioimmunoprecipitation Assay
RIPK: Receptor-Interacting Protein Kinase
RNS: Reactive Nitrogen Species
RNPs: Ribonucleoproteins
ROS: Reactive Species of the Oxygen
RSS: Reactive Sulphur Species
RT: Room Temperature
RTK: Tyrosine Kinase Receptor
RyR: Rianodine Receptor
SAHA: Suberoylanilide Hydroxamic Acid
SEM: Standard error of the mean
SERCA: Sarco-Endoplasmatic Reticulum Calcium ATPase
SD: Standard Deviation
SDS: sodium dodecyl sulphate
SMAC/ DIABLO: Second Mitochondrial Activator of Caspases
SOBP: Spread-Out Bragg Peak
SOCE: Store Operated Calcium Entry
SOD: Superoxide Dismutase
STIM1: Stromal Interaction Molecular 1
SVZ: Subventricular Zone
TAK1: Transforming Growth Factor-Beta-Activated Kinase 1
TCR: Transcription-Coupled Repair
TERT: Telomerase Reverse Transcriptase
TET: Ten-Eleven Translocation
TF: Transcription Factors
TGF β : Transforming Growth Factor beta
TM: Tumour Microtubes
TME: Tumour Microenvironment
TMEM205: Transmembrane Protein 205
TMZ: Temozolomide
TNF: Tumor Necrosis Factor

TRAF: TNF Receptor-Associated Factor
TRAIL: TNF-related apoptosis-inducing ligand
Tregs: regulatory T-cells
TRP: Transient Receptor Potential
Ulk: Unc-51 Like Kinase
UVRAG: UV Irradiation Resistance-Associated Gene
VDAC: Voltage-Dependent Anion Channel
VDCC: Voltage-Dependent Calcium Channels
VEGF: Vascular Endothelial Growth Factor
VGCC: Voltage-Gated Calcium Channel
VPA: Valproate
WHO: World Health Organization
XIAP: X-Linked Inhibitor of Apoptosis Protein
ZBP1: Z-DNA Binding Protein 1

Contents

<i>Abstract</i>	3
<i>Acknowledgements</i>	6
<i>Abbreviations</i>	7
<i>Contents</i>	14
1. Review of the literature.....	15
2. Aims of the research.....	108
3. Materials and methods	110
4. Results	121
5. Discussion	205
6. Conclusions and perspectives	216
<i>References</i>	218
<i>List of original manuscripts</i>	282

1. Review of the literature

1.1 Nervous System tumours

Nervous System (NS) tumours belong to a heterogeneous group of cancers, and in the years, the classification has undergone numerous implementations following the integrated use of genotypic and phenotypic parameters (Louis DN et al. 2014). This new approach has added a greater level of objectivity in diagnosis, although some types of tumours, such as gliomas and neuroblastomas, remain refractory to treatments.

The tumours of the NS can be classified in different ways: a possible distinction is based on the localization, distinguishing cancers that affect the Central Nervous System (CNS) and those that originate in the Peripheral Nervous System (SNP). Another subdivision differentiates tumours of glial origin (the so-called gliomas) from those of neuronal derivation.

In this study the attention was focused on two types of tumours with different cell origins: neuroblastoma and glioma, subsequently deepening the analysis of one of the most malignant gliomas, the Glioblastoma multiforme.

1.1.1 Neuroblastoma

Neuroblastoma is the most frequent extra-cranial solid tumour that affects infants and children. This type of cancer represents 8-10% of all childhood tumours and 15% of causes deaths from paediatric cancers with only a 38% survival rate (Brodeur GM et al. 2011; Salazar BM et al. 2016; Spix C et al. 2006). Neuroblastoma is principally a tumour of young children. Indeed, neuroblastoma is usually diagnosed before 5 years of age, and in most cases, the diagnosis is established around 17 months of life (London WB et al. 2005). Moreover, neuroblastoma is slightly more frequent in boys than girls (Whittle SB et al. 2017). Neuroblastoma is often diagnosed concomitantly with other congenital anomalies such as Hirschsprung's disease, Congenital Central Hypoventilation Syndrome and Neurofibromatosis Type 1 (Park JR et al. 2010). Due to its neuroendocrine properties, neuroblastoma can secrete catecholamine, resulting in early-onset hypertension and tachycardia (Colon NC and Chung DH 2011). 65% of these tumours develop in the abdomen, while about half of them localized preferentially at the adrenal medullary. However, neuroblastoma can affect

the neck (5%), the chest (20%) or the pelvis (5%) (Kushner BH 2004; Park JR et al. 2010). If the primary tumour originates in the neck or upper chest, it can lead to the onset of Horner syndrome which is characterized by ptosis, miosis, and anhidrosis. Neuroblastomas can also affect the spinal column and spread through the intraforaminal spaces leading to a compression of the backbone with a consequent paralysis. Often these tumours penetrate the structures of the organs themselves going to surround importance nerves and vessels, such as the celiac tripod (**Figure 1**). Generally, neuroblastomas metastasize to the liver, regional lymph nodes, and bone marrow level through the hematopoietic system. Furthermore, metastatic tumour cells can also invade compact bone (Maris JM 2010).

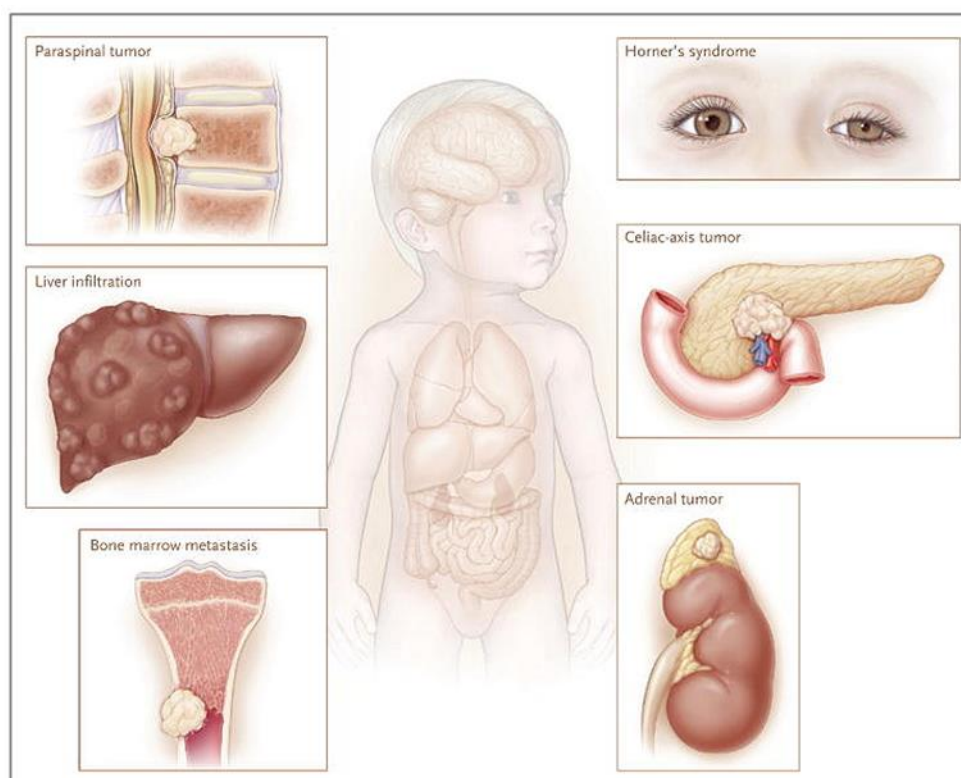


Figure 1. Most common sites of neuroblastoma localization (Maris JM 2010).

Neuroblastoma can be described as the result of a neural cell differentiation failure. Neuroblastoma derives from developing cells and grows within the neuronal ganglia of the Sympathetic Peripheral Nervous

System. These neuronal structures originate from the ventrolateral neural crest cells, which early migrate from the neural tube, during embryogenesis (Better E et al. 2010). The neural crest is a transient embryological tissue that derives from neuroectoderm (Hall BK 2000). In vertebrates, during the formation of the neural tube, a maturation process, strongly regulated by transcription and epigenetic factors, takes place within the neural crest (Mayanil CS 2013; Prasad MS et al. 2012). In the normal physiological process, the population of neural crests, on the border between neuroblast and epiblast, subsequently loses adhesion and migrates, forming the different tissues *i.e.* pigmented cells of the epidermis, portions of the PNS (neurons and sensory ganglia, ganglion and postganglionic motor neurons of the Autonomous Nervous System, Schwann cells, neuroglia cells), neuroendocrine cells (including those of the adrenal medulla), endocrine cells (including those of the adenohypophysis) and part of the neurocranium (**Figure 2**).

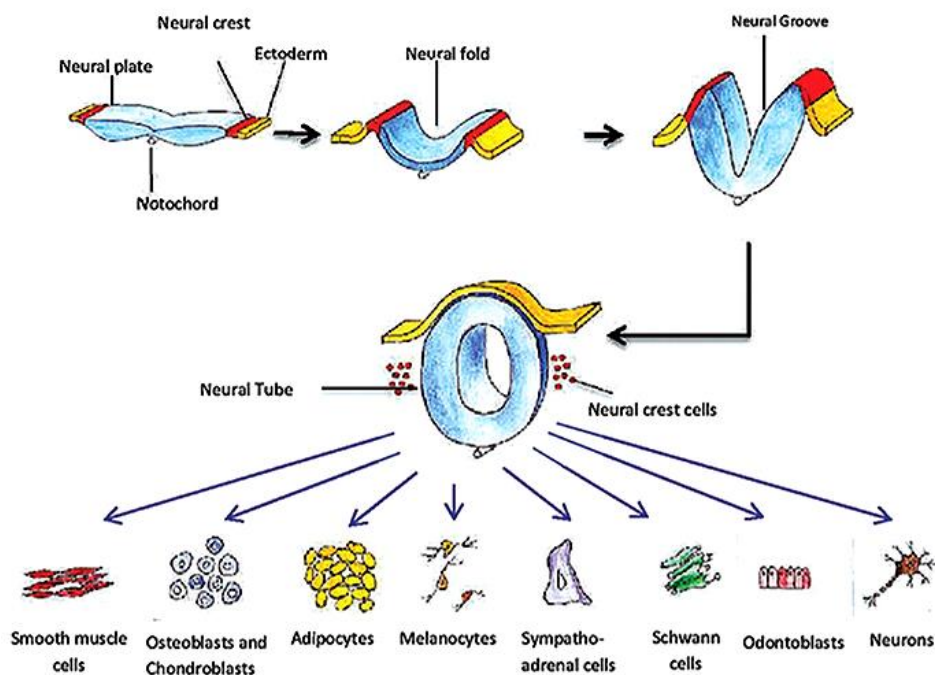


Figure 2. Neurulation and formation of neural crests: details of differentiation of neural crest cells (Shyamala K 2015).

The process of neural crests development is finely regulated in the various stages (including the acquisition of the typical characteristics of stem cells) thanks to a group of genes called “Neural Crest Gene Regulatory Network” (Adams M et al. 2008). However, some alterations in this strongly regulated cascade may increase the chances of neoplastic transformation of neural crest multipotent precursors (Louis CU and Shohet JM 2015). The clinical manifestation and the consequent outcome are highly variable: long-term survival appears to be mainly dependent on the degree of tumour cells differentiation, since that the most differentiated tumours determine a more favourable outcome compared to less differentiated ones (Fredlund E et al. 2008).

Neuroblastoma is distinct from other solid tumours due to its remarkable heterogeneity of biological, pathological, genetic and clinical features (Stallings RL 2009). These prognostic factors include clinical aspects such as the stage of the tumour and the patient’s age at the time of diagnosis, cancer biological features *i.e.* histology and ploidy of DNA, cytogenetic factors, including amplification of MYCN oncogene and the main chromosomal deletions or gains and other serum and molecular tumour markers. Based on these clinical and biological prognostic elements, patients with neuroblastoma can be divided into one of three risk groups: low-risk, intermediate-risk, and high-risk (Whittle SB et al. 2017). The two methods most used to classify neuroblastoma are the International Neuroblastoma Staging System (INSS) and the International Neuroblastoma Risk Group Staging System (INRGSS). The INSS developed in 1988 and modified in 1993, characterized by six stage/prognostic groups (1, 2A, 2B, 3, 4 and 4S), is based on the possibility to remove totally or partially the tumour, then on biopsies, on the infiltrating characteristics of tumour cells eventually present in the lymph nodes and on the spread of any metastases. This method is still used by several research groups, however, the INSS is a postsurgical staging system, based on the extent of tumour removal and is not suitable for the pre-treatment risk classification of patients (Brisse HJ et al. 2011; Monclair T et al. 2009). Therefore, the INRGSS was developed in 2008 to establish a classification of risk in pre-treatment conditions (Monclair T et al. 2009). This system is characterized by the presence of the so-called “Image-Defined Risk Factors” (IDRFs), which are radiographic and preoperative images, used to assess the possibility of tumour removal (Owens C and Irwin M 2012, Pohl A et al. 2016). This method is used to define two stages of localized (L1 and

L2) and two stages of metastatic disease (M and MS). Based on this classification, patients are assigned to distinct risk groups in very low, low, intermediate and high. In some cases, the tumour, low grade, can undergo spontaneous regression, with a favourable clinical prognosis or a total survival rate, otherwise, differentiate in benign ganglioneuromas. On the contrary patients with high-risk neuroblastoma have very aggressive tumours and it can be detected the onset of metastases at the level of the liver, bones, brain, and skin, which are not responsive to standard anticancer treatments (Moreno L et al. 2013; Park JR et al. 2013).

Two main genetic causes have been identified at the origin of the disease: one familial and one sporadic. The sporadic cases are the most frequent ones while the familial forms represent about 1% (Maris JM et al. 2007; Øra I and Eggert A 2011). Familial tumours are mainly caused by a germline mutation due to a loss of function of the PHOX2B gene (Paired-like Homebox2B), which together with the PHOX2A gene, drives the differentiation of neural crest precursors into sympathetic neurons (Pei D et al. 2013). This mutation has also been found in 4% of sporadic cases (Mosse YP et al. 2004; Trochet D et al. 2004). Furthermore, activating mutations in the ALK gene (Anaplastic Lymphoma Kinase) have been identified among the main causes of neuroblastoma of familial origin (Webb TR et al. 2009), as well as being implicated in 6-10% of sporadic cases (Mosse YP et al. 2008). The ALK gene, coding for a tyrosine kinase, was initially discovered in anaplastic large cell lymphoma (Morris SW et al. 1994), it is an important oncogene for neuronal proliferation and differentiation and normally present in embryonic neuronal cells, promoting cell proliferation, survival, and differentiation (Yao S et al. 2013). This gene is highly expressed in neuroblastoma cells and many studies have shown that ALK also promotes tumour cell growth (Speleman F et al. 2016). High expression of ALK seems to be closely correlated with an unfavourable clinical response in patients with neuroblastoma (De Brouwer S et al. 2010; Duijkers FA et al. 2012). However, the pathogenic role of ALK in these tumours is still not clear (Alshareef A et al. 2017). The sporadic origin of neuroblastoma is the result of chromosomal anomalies, such as the amplification of the MYCN gene (also present in more than ten copies), which was found in 20% of cases and is associated with a poor prognosis (Maris JM and Matthay KK 1999). Transgenic murine models confirm that the alteration of MYCN gene expression, at the level of the neural crest, is sufficient to induce

tumorigenesis (Hansford LM et al. 2004). MYCN is a transcription factor that acts either by activating or inhibiting different genetic targets, through a direct link with DNA or indirectly through protein-protein interaction mechanisms (Schramm A et al. 2013; Shohet JM et al. 2011). Moreover, its physiological effect is extremely significant, since it is able to intrinsically activate angiogenic factors, which lead to the formation of new blood vessels, to ensure an adequate supply of nutrients to tumour cells, and to repress angiogenic inhibitors (Shohet JM 2012). During normal embryogenesis and neural crest development, MYCN is transiently expressed in cells of the ventrolateral portion, destined to become sympathetic ganglia (Wakamatsu Y et al. 1997); therefore, it is not surprising to find high levels of MYCN in a subgroup of poorly differentiated and particularly aggressive neuroblastoma cells (Fredlund E et al. 2008). It was observed that downregulation of the MYC gene induces inhibition of cell proliferation and activates the apoptotic pathway, therefore, through downregulation of the MYC gene it may be possible to reduce the growth of neuroblastoma (Westermarck UK et al. 2011). However, several cases of high-risk neuroblastoma present minimal levels of MYCN expression, suggesting the implication of other mechanisms independent of the alteration of this gene in the genesis of the tumour (Maris JM 2010).

Specific epigenetic patterns may be implicated in tumour development; for example, an important epigenetic regulator is the methyltransferase DNMT3B, normally active in cells of the ectoderm, inducing differentiation in neural crest cells (Martins-Taylor K et al. 2012) but of which overexpression determines cisplatin resistance in murine tumour cells (Qiu YY et al. 2015).

Even non-coding RNAs (microRNAs, lncRNAs, piRNAs) are essential transcriptional regulators, involved in the development and maturation of the neural crest, and many of these, such as miR-9 and miR-17-92a, are directly implicated in some aggressive forms of neuroblastoma, promoting the development of metastases (Ma L et al. 2010; Stallings RL 2009).

Neuroblastoma treatments

To define the correct treatment strategy, the Children's Oncology Group (COG) has been developed as a risk group stratification for clinical trials. Combining the INSS/INRGSS classifications with the age at diagnosis, the histologic data, and the biology and genetics of the type of neuroblastoma,

allows to place the patient into a low-, intermediate-, or high-risk group (Swift CC et al. 2018). The biological heterogeneity of neuroblastoma strongly influences the choice of therapeutic approach. For the treatment of low-risk neuroblastoma cases, surgical removal can be carried out, according to the invasiveness, extension, and location of the tumour, while for high-risk patients a multimodal therapy is required. Induction chemotherapy is aimed at reducing tumour volume, allowing, when possible, a complete surgical removal. The drug treatment consists of different combinations of cyclophosphamide, doxorubicin, cisplatin, melphalan, carboplatin, etoposide, topotecan, ifosfamide, and vincristine. Subsequently, one or more cycles of high-dose chemotherapy are performed to induce bone marrow ablation with subsequent autologous hematopoietic stem cell transplantation (Yalçın B et al. 2015). Intermediate-risk patients are subjected to milder chemotherapy, followed by surgical resection of the remaining tumour mass, while low-risk patients receive minimal therapy. In some cases, patients can recover thanks to surgery alone or not need any treatment due to spontaneous tumour regression (Berlanga P et al. 2017; Shohet J and Foster J 2017). However, more aggressive neuroblastomas can show chemoresistance; about 50% -60% of high-risk patients show recurrence (Maris JM 2010). In addition, for the treatment of high-risk patients, radiotherapy is often necessary, in order to manage tumour localization and any metastases (Colon NC and Chung DH 2011; Modak S and Cheung NK 2010). However, radiotherapy is not recommended when the tumour is in the spinal cord, because serious side effects may occur; such as growth arrest, scoliosis and damage to the vertebral column (Ishola TA and Chung DH 2007). Currently, new biological therapies have been included in the treatment of high-risk patients, such as immunotherapy, which consists in activating the patient's immune system to recognise and fight the tumour (Louis CU and Shohet JM 2015). Anti-GD2 immunotherapy associated with dinutuximab is the standard therapy treatment (Swift CC et al. 2018), which improved 2-year survival to 66% (Yu AL et al. 2010). Other possible therapies try to identify a new therapeutic target, for the treatment of neuroblastoma. Among these new targets, the ALK gene was suggested, however, a resistance to the inhibitors of this gene has been discovered, including crizotinib (Alshareef A et al. 2017).

Neuroblastoma cell lines

Different neuroblastoma cell lines are extensively used for testing drug neurotoxicity such as anticancer agents, in order to better understand relationships between proliferation and differentiation mechanisms as well as the induction of apoptosis and chemoresistance.

In this work, the attention was focused on the B50 neuronal cell line that offers considerable advantages over primary CNS neurons for use in cell biology and biochemistry experiments, including simplicity of culture, and the possibility to establish stable cell lines. This cell line was derived from neuroblastoma in the neonatal CNS, induced by transplacental administration of ethylnitrosourea in *Rattus norvegicus* (Schubert D et al. 1974). B50 cells are excitable and can produce a regenerative action potential, thus highlighting the neural origin of the line (Kuffler SW and Nicholls JG 1966). The neuronal origin of B50 cells derives from the fact that the S100 and 14-3-2 proteins are widely expressed, moreover this cell line express higher levels of neurotransmitters and acetylcholine receptors and exhibit a more flattened morphology, suggesting that they may represent a more differentiated state (Schubert D et al. 1974). B50 cells came into wide use in the study of factors that control the morphological differentiation of CNS neurons. These cells can be also used to understand morphological differentiation and active neurite outgrowth (Audesirk T et al. 1991; Reboulleau CP 1990). B50 cells were also used in many toxicology experiments, such as the evaluation of different compounds and substances neurotoxicity, with attention on the activation of the cell death pathway (Capano M et al. 2002; Hayton S et al. 2017; Otey CA et al. 2003). Concerning to our research, the B50 rat neuroblastoma cells represent, to date, a good model for the study of *in vitro* neurotoxicity, resulting very useful to identify the mechanisms of cytotoxicity induced by treatment with cisplatin and other compound of interest (Bottone MG et al. 2008, Grimaldi M et al 2019; Rangone B et al. 2018). This feature has been useful in understanding the neuroblastoma and for development of newer therapies.

1.1.2 Gliomas and Glioblastoma multiforme

Most brain tumours in adults and children are derived from glial cells or their precursors and are referred to as “gliomas”. Gliomas are highly heterogeneous tumours, refractory to treatment and are the most commonly

diagnosed primary brain tumours (Poff A et al. 2019). They represent about 80% of all brain malignancies (Maugeri R et al. 2016) and are characterized by a high degree of malignancy and a low degree of patient survival (Sciumè G et al. 2010), presenting a rate of higher mortality than any other brain tumour (Wen PY et al. 2010). Several studies in transgenic mice demonstrate that gliomas can evolve from a variety of cell types, including neural stem cells, astrocytes, oligodendroglial progenitor or ependymal cells (Zong H et al. 2015).

For several years, gliomas have been classified by the World Health Organization (WHO) on histological criteria defined in 2007, by which histological variants were added thanks to evidence of different age distribution, location, genetic profile or clinical behaviour (Louis DN et al. 2007). After the publication of the revised WHO Classification of Tumours of the CNS in 2016, for the first time, molecular parameters in addition to histology was applied to define different tumour entities, thus making a significant improvement in the diagnosis of CNS tumours *i.e.* diffuse gliomas, medulloblastomas, and other embryonal tumours (Louis DN et al. 2016). Furthermore, each tumour is ascribed to a histological grade of anaplasia, from WHO grade I to IV. This WHO classification system indicates the degree of tumour malignancy and the possible natural disease course, with WHO grade I indicating slow-growing cancer usually related to a favourable prognosis, while WHO grade IV is assigned to highly malignant tumours (Reifenberger G et al. 2017). Generally, the most common types of glioma include glioblastoma (grade IV), astrocytic tumours (I-III), oligodendroglial tumours (grade II-III) and ependymomas (grade I-III) (Rasmussen BK et al. 2017). Gliomas are complex and may consist of both neoplastic and non-neoplastic cells, the latter population being mainly represented by tumour-associated macrophages (TAMs) which make up about 50% of the cellular fraction of gliomas (Yin J et al. 2017). A distinctive aspect of gliomas is to localize themselves in brain areas that exhibit greater functional activity such as the motor area, the language area and the visual one (Kiekow CJ et al. 2016), making difficult the possible removal interventions. Glioma cells are highly invasive (Markovic DS et al. 2009) and their main characteristic is the ability to infiltrate healthy brain tissue adjacent to the tumour mass. The propensity of malignant cells to spread widely in the brain, make these tumours more malignant, aggressive and refractory to therapy (Chakravarti A et al. 2002). Gliomas, in fact, can also be distinguished as a circumscribed or

diffused species. Depending on the location and low malignancy, the circumscribed gliomas can be surgically removed, on the contrary, diffuse gliomas are highly invasive. Due to the absence of a well-defined boundary between the tumour and the surrounding tissues surgical resection can never be performed completely and residual neoplastic cells can often lead to recurrences (Masui K et al. 2017; Soomro SH et al. 2017). Compared with the previous, the main improvement in the 2016 WHO gliomas classification, is the change in the identification of diffuse gliomas now defined based on the presence/absence of isocitrate dehydrogenase (IDH) mutation and 1p/19q codeletion (Wesseling P and Capper D 2018).

The discovery of IDH mutations in most WHO grade II and III gliomas have represented a revolution in the understanding of these cancers. Indeed, mutant IDH proteins acquire a different enzymatic activity, resulting in the conversion of α -ketoglutarate (α -KG) to d-2-hydroxyglutarate (d-2-HG), which in turn inhibits α -KG-dependent dioxygenases, such as ten-eleven translocation (TET) family 5-methylcytosine hydroxylases and the Jumonji C domain-containing histone-lysine demethylases (Pajtler KW et al. 2017). Consequently, IDH mutation produces aberrant DNA and histone methylation, eventually leading to the “glioma CpG-island methylator phenotype” (G-CIMP), a hypermethylation phenomenon of CpG islands (Collins VP et al. 2015). Based on these observations IDH mutation represents an important marker for glioma classification, leading to the introduction of the following, genetically defined subtypes: diffuse astrocytoma, IDH-mutant; anaplastic astrocytoma, IDH-mutant; oligodendroglioma, IDH-mutant; anaplastic oligodendroglioma, IDH-mutant; and glioblastoma, IDH-mutant, in addition, the definition a “not otherwise specified” category is used when molecular testing could not be performed or the results of such tests were inconclusive (Wesseling P and Capper D 2018). However, studies conducted in mice indicate that IDH mutation alone is not enough for tumorigenesis, but as occur in IDH-mutant astrocytoma, an additional mutation in TP53 and ATRX10 is required for cancer development (Suzuki H et al. 2015). Moreover, the accumulation of somatic mutations in genes that encode inhibitors of the G₁/S cell-cycle checkpoint is also implicated in the dysregulation of cell division, driving tumour progression (Ceccarelli M et al. 2016; Mazor T et al. 2015). Another biomarker for tumour, that emphasize the important role of epigenetic alterations, are mutations in the histone genes H3F3A or HIST1H3B K27M

(Ceccarelli M et al. 2016). The histone mutation H3K27 M is distinguishing for paediatric midline high-grade glioma and the H3G34R/V mutation for hemispheric high-grade glioma in young adults and children (Louis DN 2007). Interestingly, this epigenetic aberration is correlated with characteristic DNA methylation profiles, showing distinctive age distributions and tumour locations, suggesting a possible association with a phase of brain development and diseases (Gusyatiner O and Hegi ME 2018). Unlike other solid malignant tumours, gliomas very rarely metastasize outside the brain. Furthermore, glioma cells do not employ a lymphatic or intravascular pathway to migrate (Beauchesne P 2011) but move through the extracellular space of brain tissue (Cuddapah VA et al. 2014; Montana V and Sontheimer H 2011). In particular, these cancer cells migrate through pre-existing brain structures such as: the interstitial spaces of the cerebral parenchyma; the white substance; the subarachnoid space (Cuddapah VA et al. 2014) and the blood vessels, where a constant supply of oxygen and essential nutrients for growth is guaranteed (Manini I et al. 2018; Montana V and Sontheimer H 2011) (**Figure 3**). Furthermore, glioma stem cells (GSC), which are profoundly influenced by the local microenvironment, have been reported as the population responsible for glioma invasion and resistance (Roos A et al. 2017). Indeed, thank self-renewal properties and the bidirectional cross-talk between GSCs and the tumour microenvironment (TME), these cells can initiate and support tumour growth, being responsible for tumour recurrence (Chen J et al. 2012; Hanahan D and Weinberg RA 2011).

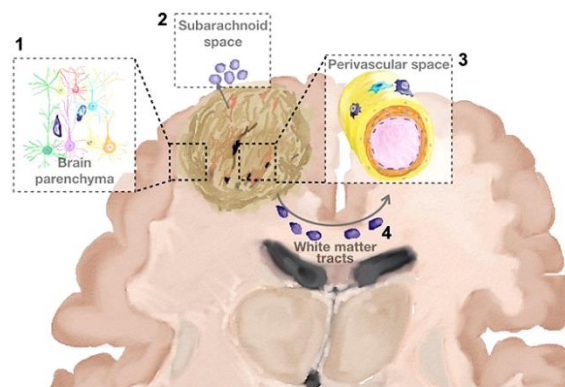


Figure 3. Preferential migration way of glioma cells. Interstitial spaces of the brain parenchyma (1); subarachnoid space (2); perivascular space (3) and white matter traits (4) (adapted from Manini I et al. 2018).

In addition when glioma cells move through the brain parenchyma, they interact with the extracellular matrix (ECM) molecules (Gritsenko PG et al. 2012) and migrate along the blood vessels, also modifying the organization of cerebral vasculature (Watkins S et al. 2014). Also important is a stromal component and soluble factors (Li G et al. 2017; Wu M and Swartz MA 2014) as the kinin signal molecules. Normally kinins are present in the brain but appear to be more expressed in physiopathological conditions (hypoxia, inflammation, tissue damage) that correlate with metastasis and tumour progression (Ratajczak MZ et al. 2006). The vascular endothelial cells of the brain synthesize bradykinin, which is a chemotactic signal and as such is able to attract glioma cells (Montana V and Sontheimer H 2011). Bradykinin performs numerous functions, including activating the secretion of matrix metalloproteinases, through its binding to one of the two B1R receptors. The latter is expressed in pathological conditions, while the B2R is constitutively active and is responsible for physiological responses. The bradykinin receptors are coupled to G proteins which, after interacting with the ligand, activate a signal transduction cascade leading to the activation of phospholipase C (PLC) and the mobilization of calcium (Higashida H et al. 2001). In fact, the inositol triphosphate (IP3) produced by the PLC binds to its receptor with the consequent release of calcium from the intracellular stores. Tests carried out on tissues derived from cancer patients showed an increase in B2R expression in gliomas. In rat glioma cells, low doses of Bradykinin (1 μ M) cause an increase in calcium intracellular concentration (Wang YB et al. 2007), while high doses of Bradykinin determine oscillations in the intracellular concentration of the ion (Giannone G et al. 2002). Just as the granular cells of the cerebellum under development, require intracellular calcium variations to migrate into the layers of the cerebellar cortex, glioma cells also show an oscillation of intracellular calcium during their migration (Bordey A et al. 2000; Ishiuchi S et al. 2002).

Glioblastoma multiforme (GBM) or grade IV astrocytoma, according to the WHO classification, is the most aggressive and frequent of all primary brain tumours (Li R et al. 2015). It represents 12% -15% of all intracranial tumours and 50% -60% of astrocytic tumours (Soomro SH et al. 2017). The average age of onset of GBM is 64 years and the onset is more common in males than females. This tumour has a higher incidence in the Caucasian race, followed by the African and Asian ones (Thakkar JP et al. 2014). Some risk factors are associated with GBM, on the other hand, although most GBMs

start sporadically, 5% are associated with hereditary syndromes, such as neurofibromatosis or Li-Fraumeni syndrome (Farrell CJ and Plotkin SR 2007). Furthermore, GBM, like other tumours, can grow thanks to the immunodepression of the microenvironment surrounding the tumour and often patients present non-specific signs and symptoms (Sasmita AO et al. 2018). It is estimated that the average survival of the patient is less than 15 months, but it does not seem to vary between the different races (Brandes AA et al. 2008; Johnson DR and O'Neill BP 2012; Shahar T et al. 2012).

The most common sites of GBMs development are the frontotemporal region and the parietal lobes, while it is rare to find them in the cerebellum and even more in the spinal cord (Taghipour Zahir S et al. 2018) (**Figure 4a**). These tumours begin mainly in the frontal lobe, growing in the two hemispheres simultaneously (overlapping tumours) rather than in the temporal or parietal lobe (Thakkar JP et al. 2014). Infiltration through the corpus callosum in the contralateral hemisphere leads to a bilateral and symmetrical lesion for which the tumour is called “butterfly glioma”. Unlike the other tumours, the GBM does not metastasize through the vascular system, and not from metastases in other organs, but it can spread so rapidly in the cerebral parenchyma and along the spinal cord that the infiltrated cells in tissues are already present at diagnosis, surrounding brain and making tumour eradication impossible, thus leading to a patient’s survival between 12-18 months (Catacuzzeno L et al. 2015).

The term “glioblastoma” means “blast of the glia”, this because in contrast to the other astrocytomas where the cells maintain the astrocytic morphology, in the glioblastoma the cells are blasts, that divide into other blasts and have lost their ability to differentiate. While, the term “multiforme”, on the other hand, illustrates the heterogeneity presented by this tumour in all its characteristics (Jacob G and Dinca EB 2009). Indeed, GBM is extremely heterogeneous at the microscopic level, with “pseudo-palisated” cells areas surrounding necrotic regions, pleomorphic nuclei and a very strong vascularization (Holland EC 2000). At the macroscopic level, the tumour area is characterized by a high proliferative rate (identifiable by the Ki-67, a proliferation marker), which results in extensive necrotic regions due to the high proliferation of the tumour mass and to the crushing inside the cranial theca (**Figure 4b**). Infiltrative growth is therefore associated with high recurrence rates, resistance to therapy, neurological deterioration and low survival rates (Kim SS et al. 2015). Low survival is partly due to the inability to deliver

chemotherapeutic agents through the blood-brain barrier (BBB) and to the low tumour response to radiotherapy (Natsume A and Yoshida J 2008).

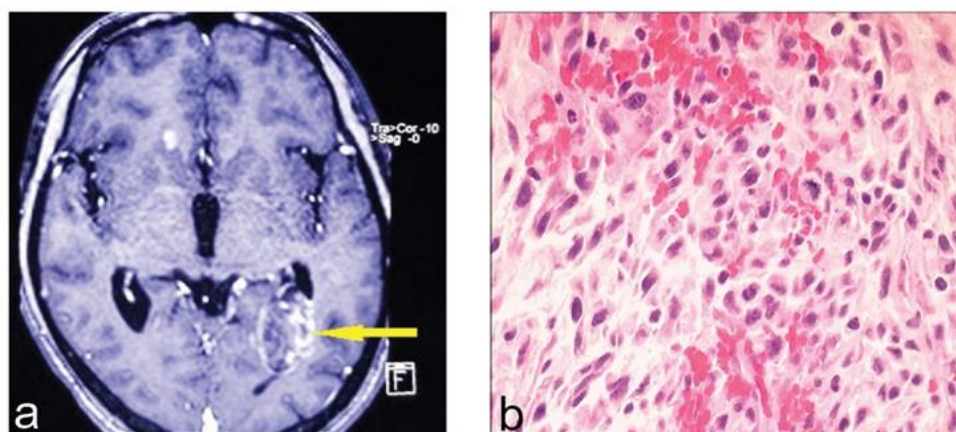


Figure 4. a) Magnetic resonance imaging. Multiple, well-defined round-to-ovoid lesions attached to frontal, occipital horn and septum pellucidum of lateral ventricles (yellow arrow). **b) Post craniotomy histopathology report.** Large areas of necrosis with peripheral pseudopalisade cells (hematoxylin and eosin stain) (Purkayastha A et al. 2018).

The vascular density in GBM is considerably higher than that of low-grade glioma and an increase in vascularization considerably worsens the prognosis of the disease. Vasculogenesis and angiogenesis have shown a distinct role in the pathogenesis of primary malignant glioblastoma and recurrences (Kioi M et al. 2010). Angiogenesis is one of the key events in the development of GBM, in fact among all solid tumours, GBM has been reported as the most angiogenic, as it shows a high degree of endothelial cell proliferation, hyperplasia and vascular proliferation (Folkerth RD 2000). Microvascular proliferation, necessary for tumour growth (McNamara MG and Mason WP 2012), is induced by vascular endothelial growth factor (VEGF) (Norden AD et al. 2009; Onishi M et al. 2011). Indeed, high levels of VEGF seem to be associated with adverse outcomes in patients with GBM (Flynn JR et al. 2008). Furthermore, GBM presents hypoxic regions (Yang L et al. 2012), which are fundamental for the aggressiveness of the tumour itself (Evans SM et al. 2004). Hypoxia has been associated with resistance to treatment, local invasion and worse prognosis (Keith B and Simon MC 2007). It is responsible for the resistance to chemotherapy through multiple mechanisms: *i*) hypoxic

cells are distant from blood vessels and therefore remain far from exposure to systemically administered antitumoral agents *ii*) hypoxia also reduces the proliferative potential of cells which is a critical factor for targeting of many chemotherapeutic compounds and increases the regulation of genes involved in chemotherapy resistance, such as P-glycoprotein (Sermeus A et al. 2008; Aghi MK et al. 2009). Furthermore, it has been shown that a hypoxic glial tumour microenvironment can create post-translational epigenetic modifications in tumour suppressors, such as at p53 (Cobbs CS et al. 2003).

To date, the origin of GBM is still controversial and several studies attempt to identify the “cell of origin”, which represents an important aspect in understanding tumour heterogeneity and in designing novel therapeutic strategies for glioblastoma. It should be noted that “cancer stem cell” (CSC) is a functional definition that can only be assessed by the ability of a cancer cell to initiate new tumours. Based on these elements, progress in the biology of neural stem cells (NSCs) and oligodendrocyte precursor cells (OPCs) offers novel insights into their candidacy as the cell of origin for human glioblastoma. Adult NSCs (also termed B1 cells) have been widely considered as the most feasible cell of origin for high-grade glioma, due to their property to self-renew, and the remarkable plasticity to differentiate into several neural cell types (Stiles CD and Rowitch DH 2008). In addition, CSCs isolated from human GBMs show several markers normally expressed by NSCs, *i.e.* Nestin, GFAP, CD133, and Sox2, also generating renewable NSC-like spheres in culture (Shao F and Liu C 2018). Interestingly, human glioblastomas were commonly diagnosed next to the subventricular zone (SVZ), further proving the possibility that they originated from NSCs. Moreover, it has also been observed that the increased possibility of developing recurrences in specific brain areas is associated with the presence of niches in which the NSCs reside (Barami K et al. 2009).

Nevertheless, NSCs do not constantly renew themselves in the adult brain, but exclusively in postnatal life, thus decreasing the ability to accumulate mutations (**Figure 5**). Furthermore, CSC markers detected in NSCs could result from a process of de-differentiation and niches could essentially be places of preference where GBM cells migrate (Batlle E and Clevers H 2017). On the contrary, the OPCs constantly divide during adult life, produce various cell types and therefore they are susceptible to an accumulation of mutations, showing markers in common with CSCs. Furthermore, as a result of the induction of mutations in the p53 protein gene, OPCs are transformed into

GBM cells. Thus, the hypothesis of their implication in the origin of GBM is being validated (Shao F and Liu C 2018). An important detail to take into consideration is that this evidence comes from studies on transgenic mice and the validity of a translation to humans is controversial. Therefore, the dynamics at the base of the cell origin of the GBM remain not entirely clear.

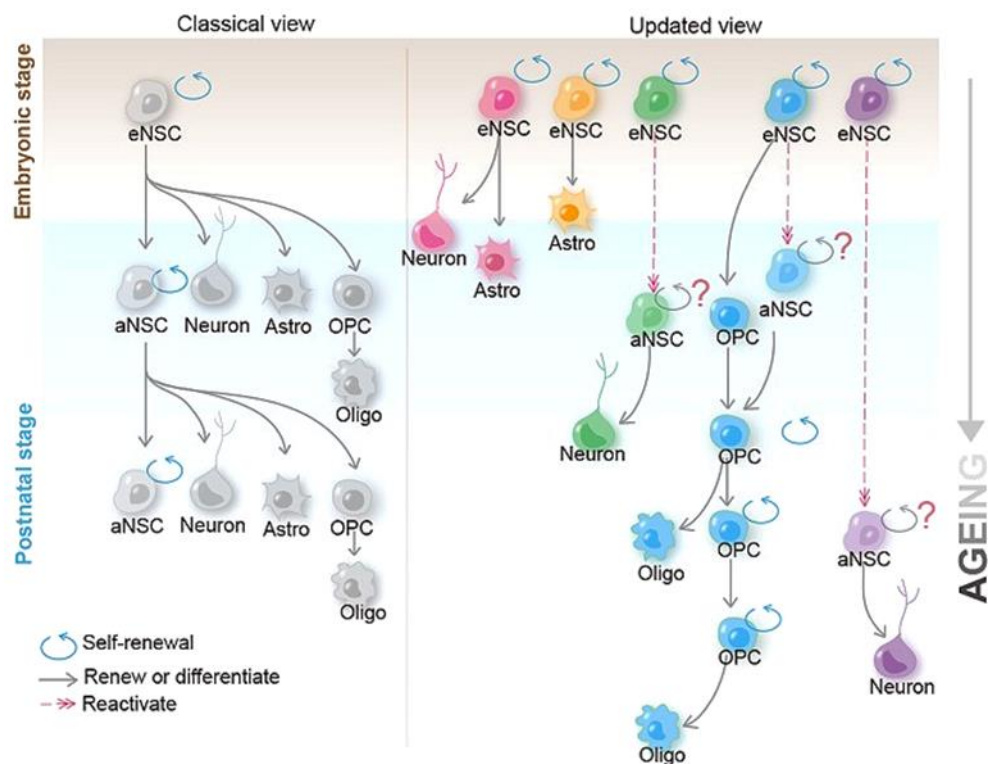


Figure 5. In the conventional (left) view, it was assumed that a single NSC can recurrently self-renew for many generations and generate new NSCs, as well as differentiate into neurons, astrocyte and OPCs, that can, in turn, differentiate into mature oligodendrocyte. The updated (right) analysis of the NSC, using a mouse model, suggest that adult form of NSCs (aNSC) are derived from embryonic NSCs (eNSCs) that actively proliferate at ~E14.5. These embryonic NSCs stay quiescent until they are reactivated at the adult stage. Moreover, the clonal analysis revealed that a single adult NSC can either give rise to neurons or glial cells (such as astrocytes and oligodendrocytes), but rarely to both cell types. On the contrary clonal analysis further revealed that adult OPCs can self-renew continuously (adapted from Shao F and Liu C 2018).

From a clinical and biological point of view, it is important to distinguish primary GBM (IHD wild-type) and secondary GBM (IHD-mutant), which are histologically indistinguishable, but differ in the expression of molecular markers, chromosomal aberrations, age of onset and prognosis (Louis DN et al. 2016; Mutlu H et al. 2014; Thakkar JP et al. 2014). Primary GBM is detected in about 90% of patients with GMB, and particularly in males, without evidence of previous less malignant lesions, thus originating *de novo* from glial cells (Furnari FB et al. 2007; Reardon DA and Wen PY 2006). It is the most common among patients of advanced age for whom the prognosis is poorer. Primary GBM is characterized by mutations and amplifications for the EGFR gene (Epidermal Growth Factor Receptor), mutations in PTEN (Phosphatase and Tensin homolog) and in the TERT promoter (Telomerase Reverse Transcriptase) (Larysz D et al. 2011).

In contrast, secondary glioblastoma develops more slowly, deriving from low-grade gliomas (grade II) or anaplastic astrocytoma (grade III). This tumour represents 15% of GBM, tends to develop in subjects under 45 years, is more frequent in women, and the prognosis is better than in primary GBM (Parsons DW et al. 2008). Secondary GBM is also characterized by TP53 mutations, alterations in ATRX, chromatin remodeling, and IDH1 (Larysz D et al. 2011). Some studies have shown how radiation, tobacco, alcohol, head trauma, exposure to N-nitroso compounds, may represent risk factors for the development of this tumour (Braganza MZ et al. 2012).

Among the alterations mainly involved in the tumour transformation of glial cells, we also find changes in membrane receptors. These receptors, in physiological conditions, activated by growth factors, allow the beginning of intracellular transduction signals, such as the MAPK and PI3K pathways, stimulating the cell cycle and survival. In tumorigenic conditions, these receptors are constitutively activated, independently of extracellular signals, and their expression can be increased, thus stimulating cell proliferation uncontrollably (Agnihotri S et al. 2013; Alifieris C and Trafalis DT 2015). The most involved receptors belong to the tyrosine kinase (RTKs) receptor family, the epidermal growth factor receptor (EGFR) and the platelet-derived growth factor receptor (PDGFR). The gene for EGFR is amplified in about 40% of all GBMs and the most frequent mutation, consisting in the deletion of exons 2-7 (known as variant three, EGFRvIII) found in 20-30% of cases, where an increased EGFR activity is detectable (Agnihotri S et al. 2013; Alifieris C and Trafalis DT 2015).

Recently, membranous extensions that start from the cells that compose astrocytoma have been discovered and identified as tumour microtubes (TMs). TMs approximately connect half of the tumour cells, forming syncytium with elongated extensions that invade areas of the adjacent healthy brain parenchyma. The formation of TMs may depend on the integrity of 1p/19q (possibly due to the presence of neurotrophic factors in these areas) and that it is mediated by tight junctions of the Cx43 type. This association could be also implicated in resistance to chemotherapy and recurrences formation (Lou E 2017; Osswald M et al. 2016).

Gliomas and Glioblastoma treatments

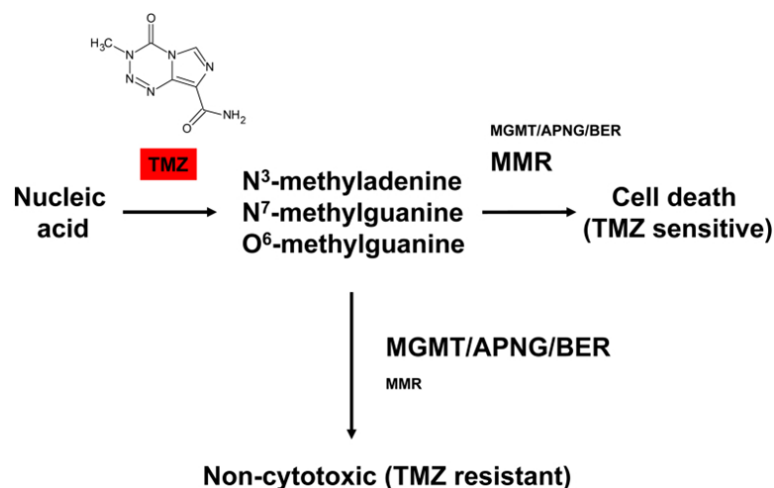
The first therapeutic approach in the treatment of gliomas is surgical resection. There is considerable evidence that the total eradication of the tumour mass is associated with an increase in the subject's survival (Chaichana KL et al. 2014). However, in most cases, complete surgical removal is impossible. In the case of very infiltrating tumours, such as the glioblastoma which presents an irregular perimeter, the tumour cells can migrate into the cerebral parenchyma far from the tumour mass. Tumour recurrence is commonly observed along the periphery of the tumour removal cavity (Hide T et al. 2013), also favoured by the presence of aberrant vasculature located around the tumour tissue (Wait SD et al. 2015). In addition, some regions of the brain, such as the basal ganglia and the brain root, are highly sensitive to surgery, which makes the disease prognosis even worse (Goffart N et al. 2013). Although the chemo- and/or radiotherapy protocols, which follow surgical resection (Brodbelt A et al. 2015), are very strong, patients with glioblastoma have a mean survival expectancy of 15 months. That because, in addition to the characteristics of the tumour, it is necessary to consider the presence of the BBB, which limits the availability of chemotherapeutic agents at the level of the cerebral parenchyma and consequently of the tumour site. The size of the molecules, the lipophilicity of the drug, the presence of active pumps and the integrity of the BBB, strongly influence the access of the drug to the tumour site and therefore the treatment outcome (Lebelt A et al. 2008; Neuwelt EA et al. 2011).

For decades, neurosurgical resection and postoperative radiotherapy have been the basis of treatment for patients with GBM (Weller M et al. 2010), but recent advances have improved patient survival, especially since the introduction of Temozolomide (TMZ) (Okada M et al. 2017), which has been

extensively used for the treatment of high-grade gliomas, including anaplastic astrocytoma (AA) and GBM. TMZ is an imidazotetrazine derivative of the alkylating agent dacarbazine with antineoplastic activity, it is a second-generation lipophilic prodrug with a molecular weight of 194 Da therefore capable of crossing BBB and is well tolerated by GBM patients so much to be administered orally (Liu YL et al. 2017). The access of TMZ into the CNS has been studied in rats and rhesus monkeys, showing that the levels of the drug in the brain and cerebrospinal fluid are around 30% to 40% of the plasma concentration, however its metabolite does not effectively diffuse in to the CNS (Agarwala SS and Kirkwood JM 2000). TMZ is stable at a pH less than 5 but at a pH higher than 7 it is spontaneously hydrolysed to 5-(3-methyltriazene-1-yl)imidazole-4-carboxamide (MTIC), thus allowing the drug to perform its function in the tumour tissue (Lee SY 2016). Subsequent intracellular reactions lead to the formation of methylhydrazine, CO₂ and 5-aminoimidazole-4-carboxamide (AIC) (Zhang J et al. 2012). The methyl diazonium ion formed by the breakdown of MTIC then yields the methyl groups to N⁷ guanine, to N³ adenine, and to a small extent to the O⁶ position of guanine. During replication, the alkylation of O⁶ guanine leads to the insertion of thymine instead of a cytosine opposite to methylguanine. The formation of O⁶-methylguanine adducts, if not repaired, lead to single and double-stranded DNA breaks, causing tumour cell block in the G₂ phase of the cell cycle and triggering apoptotic processes and senescence mechanisms in glial cells (Kheirleisid EA et al. 2013; Lee SY 2016). N⁷-methylguanine is moderately less cytotoxic because the nucleotide excision repair pathway can successfully remove these adducts without damaging the DNA. TMZ does not induce chemical cross-linking of the DNA strands, thus, it is less toxic to the hematopoietic progenitor cells in the bone marrow than other agents, such as platinum compounds, and procarbazine, which create cross-link the DNA (Agarwala SS and Kirkwood JM 2000). However, the difficulty in tumour treatment is also due to genetic instability, which causes the alteration of the genetic pool of the cells, thus making cancer cells different from one another. Indeed, the limited success of TMZ in the treatment, in particular, GBM treatment, appears to be related to the occurrence of chemoresistance and to the inability of TMZ to induce tumour cell death in some patients.

The key enzyme involved in the removal of methyl groups from O⁶-methylguanine is O⁶-alkylguanine-DNA-alkyltransferase (AGT), also known as O⁶-methylguanine-DNA-methyltransferase (MGMT). Overexpression of

the AGT enzyme may induce resistance to the cytotoxic effect induced by the active metabolite MTIC. The MGMT enzyme and the “mismatch repair” (MMR) system seem to be closely related to the failure of therapy with TMZ (**Figure 6**). The MMR system is fundamental to guarantee correct DNA replication and to induce adequate cellular responses in case of DNA damage (Hsieh P and Yamane K 2008). The MGMT enzyme eliminates the alkyl groups from the O⁶ position of guanine, the site of several chemotherapy-induced DNA alkylations, protecting the cellular genome from the mutagenic effects of some alkylating agents, including TMZ. The methylation status of the MGMT promoter is responsible for the regulation of MGMT expression and has been correlated to an increase in the survival of patients with glioblastoma (Melguizo C et al. 2012; Perazzoli G et al. 2015). Indeed, the MGMT enzyme removes the O⁶-alkylguanine-DNA adducts thus reducing the effect of TMZ (Donson AM et al. 2007; Marchesi F et al. 2007). Only 5-10% of methylated DNA adducts resulting from TMZ treatment are O⁶-methylguanine, but if MGMT is not active to repair the damage, these chemotherapy-induced alkylation lead to DNA damage in cancer cells, including DNA double-strand breaks and mismatches, which trigger apoptosis and cytotoxicity (Gerson SL 2002). In detail, the methylation of the CpG islands of the MGMT promoter leads to a reduced expression of the protein itself in the tumour tissue, resulting in a failure of MGMT action which consequently increases the possible alkylating effect of TMZ and increasing the survival of patients with GBM (Melguizo C et al. 2012). It has been shown that the loss of chromosome 10q26 on which the MGMT gene is located or the methylation of the MGMT promoter leads to inactivation of the enzyme and a positive response of patients to chemotherapy with TMZ (Hegi ME et al. 2005; Okada M et al. 2017; Riemenschneider MJ et al. 2010). The methylation of the MGMT promoter is, therefore, an important biomarker in patients with glioblastoma treated with TMZ (Wick W et al. 2014).



Alkylpurine-DNA-N-glycosylase (APNG), Base excision repair (BER),
DNA mismatch repair (MMR), O⁶-methylguanine-DNA methyltransferase (MGMT)

Figure 6. Mechanism of Temozolomide and chemoresistance. Temozolomide (TMZ) modifies DNA or RNA at N⁷ and O⁶ sites on guanine and the N³ on adenine by the adding of methyl groups. The methylated sites can *i*) stay mutated, *ii*) be fixed by DNA mismatch repair (MMR), *iii*) be eliminated by base excision repair (BER) by the action of a DNA glycosylase such as, alkylpurine-DNA-N-glycosylase (APNG), or dealkylated by the action of a demethylating enzyme such as O⁶-methylguanine methyltransferase (MGMT). When MMR is expressed and active cells are TMZ sensitive, on the contrary when MGMT, APNG, and BER proteins are functional, GBM cells are resistant to TMZ (Lee SY 2016).

TMZ therapy is often associated with radiotherapy, TMZ seems to increase DNA breakage in a proapoptotic environment induced by radiological treatment according to the standard daily dose of 60 Gray (Gy) in 30 fractions (Zhang M and Chakravarti A 2006). However, it has been shown that radiotherapy induces a self-protective attitude in the tumour cells, indeed, it seems that the treatment is able to induce the migration of tumour cells going to activate the Ca²⁺-dependent potassium channels. These channels together with the Cl⁻ channels are fundamental in the regulation of cell volume due to the change in cell morphology during the migration process (Steinle M et al. 2011), an extremely negative process in the formation of metastases and recurrences.

Survival with the use of TMZ is also improved in patients with low expression of Alkylpurine-DNA-N-glycosylase (APNG). APNG is also implicated in TMZ resistance, as it directly mediates the repair of alkylated bases in the N⁷ position guanine and N³ adenine (Agnihotri S et al. 2012). In addition to these resistance mechanisms, PARP-1 (Poly-ADP-Ribose Polymerase-1) and APE1 (Abasic-AP Endonuclease-1) are also implicated in base excision repair, and their inhibition shows increased sensitivity to TMZ (Wen PY and Kesari S 2008; Zhang J et al. 2012). At the same time, TMZ induces EGFRvIII and EGFR expansion, therefore the combined use of EGFR inhibitors such as Erlotinib (Tarceva) is recommended (Munoz JL et al. 2014).

The high progression and the relapse rate after therapy could be associated with the presence of cell populations with CSCs characteristics, as described above, which present a high tumorigenic activity (Warrier S et al. 2012; Würth R et al. 2013), thus supporting the mechanism of tumour recurrence and therapeutic resistance (Ahmed EM et al. 2018; Iwanami A et al. 2013). Since the CSCs are involved in tumour recurrence and drug resistance it is important, from a therapeutic point of view, to be able to identify them (Brescia P et al. 2013; Roy S et al. 2017). In this regard, a cell surface glycoprotein CD133, also known as prominin-1, could be a marker to identify this type of cells (Ahmed EM et al. 2018). CSCs can self-renew, differentiate, with metastatic properties and capable of repairing DNA (Liu YL et al. 2017), a skill that explains the resistance of GBM to therapies. Furthermore, CSCs also show drug resistance against TMZ (Lesueur P et al. 2018). GBM tumours that have relapsed after radiotherapy or chemotherapy show an increased percentage of CD133⁺ cells compared with the primary tumour, suggesting a key role for CD133 in tumour recurrence and invasion. However, not all stem cells express CD133, which so can be considered as a marker for progenitor cells (Bradshaw A et al. 2016).

Traditional therapies are therefore able to improve the patient's condition only slightly, so to date, biomedical research aim is to find new treatment approaches (Patel M et al. 2014; Zhang X et al. 2018). Strategies such as immunotherapy (Del Vecchio CA et al. 2012), the use of agents with epigenetic effects (Alvarez AA et al. 2015) and the application of miRNA inhibitors (Rolle K 2015), have shown to have synergistic effects with traditional approaches, as well as the employment of a targeted diet could not

only improve the patient's prognosis, but also the quality of life conditions (Santos JG et al. 2018).

Glioma cell line

Rat C6 glioma cell line represents an experimental model for the study of gliomas, in order to understand the mechanism of growth, angiogenesis and tumour invasion (Grobben B et al. 2002). The origin of these cells derives from the induction of carcinogenesis in Wistar-Furth rats, following exposure to N,N'-nitroso-methylurea (Benda P 1968; Chekhonin VP et al. 2007). C6 cells developed in Wistar rats show similar characteristics to human malignant glioma including nuclear pleomorphism, high mitotic index, foci of necrosis, haemorrhage and parenchymal invasion of healthy tissue. The invasion of tumour cells is due to the presence of metalloproteases, an endopeptidase with highly conserved metal ions that degrade most of the components of basement membranes and the extracellular matrix, playing an essential role both in tumour invasion and in angiogenesis (Takahashi M et al. 2002). Furthermore, C6 cells express different growth factors and their receptors including: PDGF-A and PDGF-B; bFGF (basic fibroblast growth factor); VEGF (Vascular endothelial growth factor); EGFR (Epidermal growth factor receptor) and IGF-1 (Insulin-Like Growth Factor), which are over-expressed in human malignant gliomas (Barth RF and Kaur B 2009; Chekhonin VP et al. 2007) In particular, VEGF is over-expressed in hypoxic conditions and VEGF upregulation, in response to a reduction in oxygen levels, is mediated by the HIF-1 protein (Hypoxia-Inducible Factor 1) (Damert A et al. 1997). *In vitro* C6 cell migration is induced by tenascin and fibronectin which are both secreted by C6 cells following stimulation with the neuronal growth factor (Yavin E et al. 1991), on the contrary, *in vivo* fibronectin has no effect (Ohnishi T et al. 1998). Laminin, type IV collagen, and fibronectin are released into the tumour microenvironment following contact with healthy brain tissue (Knott JC et al. 1998).

C6 cell line is, therefore, a good experimental model for the study of growth, metastasis formation, and invasiveness of glioblastoma. Furthermore, this cell line allows screening for future drug targets and the development of new therapies (Ferrari B et al. 2019; Grobben B et al. 2002; Krajc D 2006; Mares V et al. 2003).

Glioblastoma multiforme cell line

Glioblastoma is a solid tumour able to develop a stable cell line *in vitro* (Ponten J et al. 1978). GBM is characterized by a complex cellular heterogeneity and many cell lines derived from it have been used as a model to study the molecular mechanisms underlying the tumour. Several human glioblastoma cell lines are used in scientific research such as GL-15, U87MG, D54-MG, U251, and A175. To date, the human U251-MG cell line is widely used in several studies as a GBM model. This line was created in the Wallenberg laboratory in Uppsala, Sweden, by removing tumour tissue from a male patient with a malignant astrocytoma (Torsvik A et al. 2014). Human U251 cells have a fusiform, round and pleomorphic morphology, the size of the cells ranges from small cells to multinucleated giant cells. U251 cells are characterized by intense mitotic activity and positivity to the GFAP, which identifies the astrocytic nature of the tumour (Karsy M et al. 2012). In addition, U251 cell line may exhibit stem cell characteristics such as the formation of floating neurospheres, a lot of cells in the G₀/G₁ phase, resistance to hypoxia, to radiation and to some chemotherapy agents (Qiang L et al. 2009). Glioblastoma is characterized by a large number and variety of genetic mutations that negatively affect many pathways that control cell survival, proliferation, differentiation and invasion (Purow B and Schiff D 2009). In U251 cells, the glycolysis pathway was also found to be up-regulated (Li H et al. 2017). This phenomenon is referred to as the “Warburg effect” and it has been observed as a typical feature of cancer cells. This effect has been associated with adaptation to conditions of hypoxia and nutrient starvation, as well as immortalization, resistance to oxidative stress and apoptotic stimuli (Mikawa T et al. 2015). Based on the elements U251 cells may be more resistant to hypoxia and low glucose compared to other glioblastoma cell lines.

Among these altered pathways are those that control the expression of ion channels, which are transmembrane proteins with an ions permeable pore. Usually, ion channels are selective to a specific ion and can open and close their pore in response to physical or chemical stimuli such as neurotransmitters or due to changes in membrane potential. Also, ion channels are involved in the regulation of various processes such as proliferation, apoptosis and cell migration, but in most cases, their contribution consists in regulating mainly two important cellular parameters: cell volume and internal calcium concentration (Arcangeli A et al. 2009;

Kunzelmann K 2005). Many ion channels commonly involved in tumour cell transformation could, therefore, be considered as “oncochannels” (Huber SM, 2013). Midst the many channels examined, those of potassium have emerged to be involved in different pathways in gliomas (Turner K and Sontheimer H 2014). One of the main functions of glial cells in the brain is the potassium spatial buffering process that maintains ionic homeostasis during neuronal activity (Higashimori H and Sontheimer H 2007). Several studies show that in glioma cells Inwardly rectifying potassium channel (Kir), and specifically the barium sensitive Kir4.1 encoded by KCNJ10, are differentially expressed and mislocated compared to physiological condition (Olsen MI et al. 2004; Wart A et al. 2005). In tumour cells these channels are associated to the maintenance of a more depolarized resting membrane potential (-20 mV to -50 mV) than other non-cancer cells (Blackiston DJ et al. 2009; Molenaar RJ et al. 2011) and their involvement has been found in U251 cell line invasion process too (Thuringer D et al. 2017). Furthermore, the change in cell volume necessary to allow the cell to invade the surrounding tissue, called “cell shrinkage”, is also regulated by the potassium flow, associated with that of chlorine and the concomitant movement of water through the plasma membrane (Catacuzzeno L et al. 2015; Turner K and Sontheimer H 2014). Therefore, specific molecular motors that allow a cyclic modulation of membrane volume and rearrangements of the plasma membrane are essential to the cellular movement (Turner K and Sontheimer H 2014); a mechanism that appears to be at the basis of the tumour behaviour of glioblastoma cells (Molenaar RJ et al. 2011).

Another channel of interest in the study of glioma behaviour is large-conductance calcium-activated potassium channel (BK), or Big Potassium, sensitive to changes in intracellular calcium levels. It belongs to a heterogeneous family of calcium-dependent potassium channels also called maxi-potassium channels, encoded by the KCNMA1 gene. These channels differ in their amino acid sequence and show different single-channel conductance and characteristic pharmacological profiles (Vergara C et al. 1998). They are activated at positive potentials, greater than +60 mV, however, an increase in the concentration of intracellular calcium at micromolar levels shifts the voltage dependence of these channels to more negative values (Salkoff L et al. 2006). The BK channels of glioma cells are also much more sensitive to intracellular calcium concentration than BK channels expressed by healthy glial cells (Liu X et al. 2002; Ransom CB et

al. 2001). This typical variant of glioma cells of BK channels is called “gBK” and contains an insert of 34 amino acids near the channel calcium sensor (Liu X et al. 2002). This makes these channels much more sensitive to small but physiologically relevant changes in intracellular calcium concentration (Ransom CB et al. 2001). To date there are conflicting data on the characterization of these channels and their expression within the tumour cell (Catacuzzeno L et al. 2015), in fact as regards the U251 cell line there are different interpretations of the role of BK channels and subtypes of channels that these tumour cells express (Abdullaev IF et al. 2010; Fioretti B et al. 2006; Weaver AK et al. 2006).

However, the U251 cell line represents a valid physio-pathologic model to understand the trigger mechanisms of glioma. The analysis of changes in ion channels expression and functionality, and the study of the effects induced by chemotherapeutic agents on U251 cells may give us an overall vision not only on genetic and molecular characteristics of tumour, but also on functional aspects that sustain cancer, with the aim of finding potential pharmacological targets and new antitumoral strategies.

1.2 Cisplatin

Cisplatin (CDDP, cisPt), also called *cis*-diaminodichloroplatin(II), is a platinum-based compound with a square planar geometry (Dasari S and Tchounwou PB 2014). At room temperature the CDDP appears as a white crystalline powder that can take on colour variations from deep yellow to orange, it is slightly soluble in water and soluble in dimethylprimanide and N,N-dimethylformamide. CDDP is stable at normal temperatures and pressures but can slowly turn into its *trans* isomer (IARC 1981).

CDDP was first synthesized by Michele Peyrone in 1844, while in 1893 Alfred Werner characterized its chemical structure (Desoize B and Madoulet C 2002). However, the compound was not biologically investigated until 1960, when Barnett Rosenberg at Michigan State University pointed out that some platinum electrode electrolysis products, including CDDP, were able to inhibit cell division in *Escherichia coli* thus creating a growing interest in the possible use of platinum in chemotherapy (Rosenberg B et al. 1965). The discovery of CDDP in 1960, as an anticancer drug, opened a new era in cancer treatment (Chen D et al. 2009). CDDP was first administered to a cancer patient in 1971, becoming available for clinical practice in 1978, under the

name “Platinol”; it was the first Food and Drug Administration (FDA) approved platinum compound for the treatment of tumours (Kelland L 2007). The widespread clinical use of CDDP is due to its cytotoxic properties on a variety of cancer, such as ovarian and testicular cancer, and solid tumours of the head and neck; furthermore, its ability to fight tumours such as sarcoma, bone, muscle and blood vessel cancer has been clinically proved (Florea AM and Büsselberg D 2011).

The CDDP is composed of a doubly charged platinum ion surrounded by four ligands: two amino ligands, which form stronger interactions with the platinum ion, and two chloride ligands, forming outgoing groups that allow the platinum ion to form bonds with the bases of DNA (Goodsell DS 2006).

1.2.1 Mechanism of action

The antineoplastic activity of CDDP is attributed to its stereochemical characteristics (Connors TA et al. 1979), indeed, the effectiveness of the compound depends on the *cis* position assumed by the two amino groups (Sherman SE and Lippard SJ 1987). This agent is administered intravenously, with short-term infusions in saline, and spreads rapidly in the tissues due to its binding in the blood with albumin and other plasma proteins. That effect can be attributed to the ability of CDDP to interact with sulphur-containing amino acids cysteine and methionine (Judson I and Kelland L 2000). Then CDDP can permeate across the cell membrane by passive diffusion or enter in cells actively using transporters, such as those of some metals, such as the copper Ctr1 transporter (Copper Transporter 1) (Arnesano F et al. 2013; Ishida S et al. 2002).

CDDP is chemically inert until one or two of its chloride ions are replaced by water molecules. The hydrolysis of the molecule, following the loss of chloride ions, occurs spontaneously in the cytoplasm, because the concentration of chloride ions in the cell is relatively low (2-10 mM), compared to that of the extracellular space (100 mM) (Kelland L 2007; Michalke B 2010). The substitution of *cis*-chlorine groups with water molecules, leading to the formation of CDDP species mono- and bi-aquate which are highly reactive (Galluzzi L et al. 2012). Although the aqua-complex can interact with different cellular components, and DNA represents the main biological target of CDDP. Indeed, the central platinum atom forms covalent bonds with the nitrogen atoms of purine bases, especially guanine, preferably in position N⁷, reactive centre on purine residues, and forming

inter- or intrastrand crosslink inducing CDDP-DNA adducts (Perez RP 1998). The 1,2-intrastrand cross-links of purine bases with CDDP are the most significant among the changes in DNA. These include the 1,2-intrastrand d(GpG) adducts 1,2-intrastrand d(ApG) adducts representing about 90% and 10% of adducts, respectively (Dasari S and Tchounwou PB 2014). 1,3-intrastrand d(GpXpG) adducts and other adducts such as inter-strand crosslinks and no functional adducts have been reported to contribute to CDDP toxicity (Basu A and Krishnamurthy S 2010; Gonzales VM et al. 2001) (**Figure 7**).

The formation of these adducts causes a local distortion of the double helix (Kostova I 2006), inevitably causing the arrest of both replication and transcription and inducing the arrest of the cell cycle (Kelland L 2007). CDDP exposure increases the duration of S-phase and blocks cells in G₂, this arrest is related to the accumulation of the inactive phosphorylated p34cdc2 protein. After a protracted delay, the p34cdc2 protein is dephosphorylated, and aberrant mitosis occurs. Several agents that abrogate the G₂ cell cycle checkpoint and induce premature mitosis, have demonstrated enhancement of CDDP-induced cytotoxicity (Shah MA and Schwartz GK 2001). The damage is then recognized by about 20 proteins, which bind to the physical distortions in DNA caused by the CDDP-DNA adducts. These recognition proteins can, therefore, activate different repair mechanisms which, depending on the extent of the damage, may have different results in their turn. If the DNA lesions produced by the CDDP-DNA adducts are in limited quantities they can be recognized and effectively removed by different repair systems that normally operate in the context of a temporary cell cycle arrest (Vitale I et al. 2011); on the contrary, when CDDP-induced DNA damage becomes irreparable, a damage response is triggered.

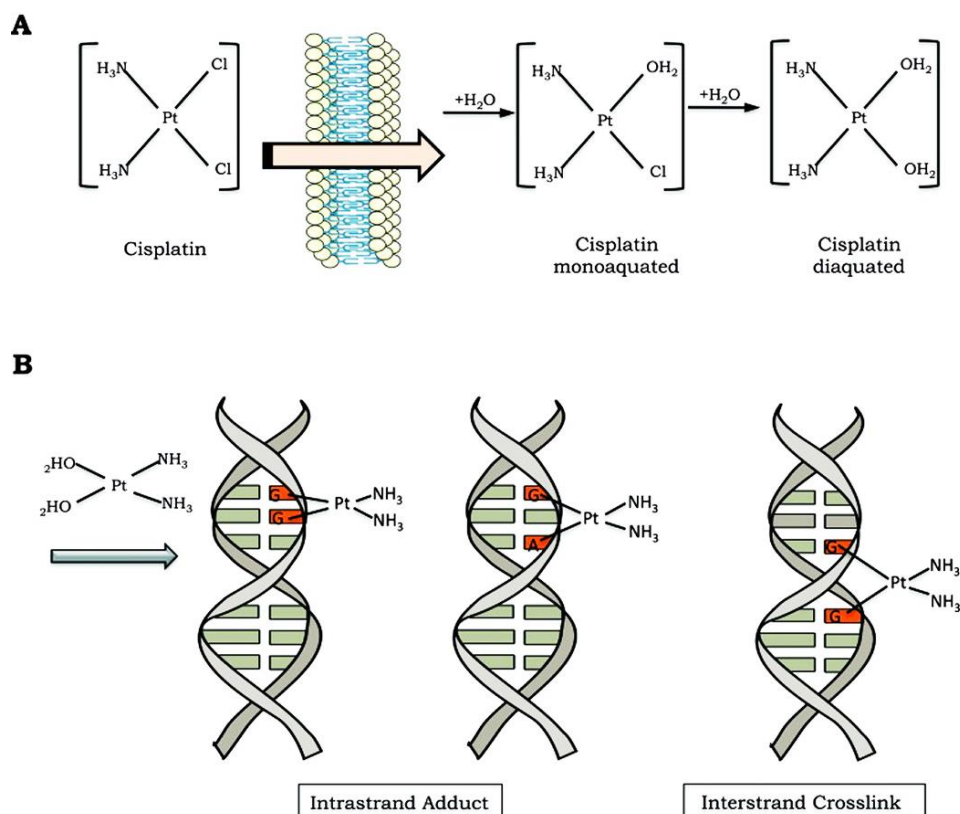


Figure 7. Mechanism of CDDP activation and DNA damage induction. A) The CDDP activation process occurs by replacing one or two of its chlorides with water molecules (monoquated and diaquated, respectively). **B)** CDDP can produce covalent bonds with DNA, inducing intrastrand DNA adducts and interstrand crosslinks (adapted from Rocha CRR et al. 2018).

The repair of DNA damage can be done by nucleotide excision repair (NER) (Galluzzi L et al. 2012). NER is an ATP-dependent multiprotein complex that recognizes DNA damage that can be caused by chemotherapy, radiation and oxidative stress, including intra-strand crosslinks, and it acts removing 27-29 nucleotides. Subsequently after the action of the DNA polymerase; if the damage is not too extensive, the cell survives, while if the damage is significant, the repair mechanisms are not enough, and cell death is triggered. As we shall see, strong activation of this reparative process is associated with chemoresistance mechanisms to CDDP (Basu A and Krishnamurthy S 2010). In addition to NER, CDDP can also activate

transcription-coupled repair (TCR). The intrastrand crosslink blocks RNA polymerase II to trigger TCR (Damsma GE et al. 2007). It has been described that p53 protects against apoptosis in a TCR-dependent manner (McKay BC et al. 2001). In addition, the homology-directed DNA repair (HDR) has been implicated in the repair of CDDP-induced DNA damage, allowing error-free repair of the double-strand breaks caused by the excision of CDDP-DNA adducts (Borst P et al. 2008). Mismatch repair (MMR) system identifies CDDP-induced DNA damage, but instead of increasing cell viability, the MMR system was shown to be crucial for CDDP-mediated cytotoxicity (Sedletska Y et al. 2007). The DNA damage caused by CDDP triggers DNA damage response (DDR) cascades which sustains a complex interaction of downstream pathways to define cell fate, including coordination of DNA repair, cell cycle arrest, and apoptosis. At the site of DNA damage, the DDR is initiated by the early (sensor) protein kinases: ataxia telangiectasia mutated (ATM), ATM and Rad3-related (ATR), which in turn activates the kinases CHK2 e CHK1, respectively, with the final activation of the onco-suppressor protein p53 (Galluzzi L et al. 2012; Huntoon CJ et al. 2013). The p53 protein can be activated as a result of DNA damage, but CDDP also acts directly on the ATR, CHK2 and MAPK proteins, activating them. ATR is also associated with the activation of Mitogen-Activated Protein Kinase (MAPK) (Tang D et al. 2002; Zhang Y et al. 2002), which phosphorylates the p53 protein in several sites, but in particular at Serine 15 (Persons DL et al. 2000) and Threonine 81 (Appella E and Anderson CW 2001). The MAPK family includes Extracellular Signal-Regulated Kinases (ERK); c-Jun N-Terminal Kinase (JNKs) and the p38 kinase. Therefore, when DNA damage is irreparable, p53 in turn allows the transcription of genes, of which protein products regulate the mitochondrial membrane permeabilization (MMP), triggering cell death by apoptosis through different pathways (Kroemer G et al. 2007) The high mobility group protein B1 and B2 (HMGB1 e HMGB2) is a family of chromatin-associated non-histone protein, that is also involved in the DNA damage response. They present a domain, formed by about 80 amino acid residues, which interacts with the minor groove of DNA and acts as a regulator in processes such as transcription, replication and repair; these proteins are able to bind to the adducts, preferably 1,2 intrastrand crosslinks, and to interfere with the activity of reparative enzymes (NER), leading to cell death (Zamble DB et al. 2002). It should be noted, however, that the cytostatic/cytotoxic effect of CDDP does not represent the single

consequence of its genotoxic activity but derives from both nuclear and cytoplasmic signalling pathways (Galluzzi L et al. 2012; Galluzzi L et al. 2014; Sancho-Martínez SM et al. 2012) (**Figure 8**).

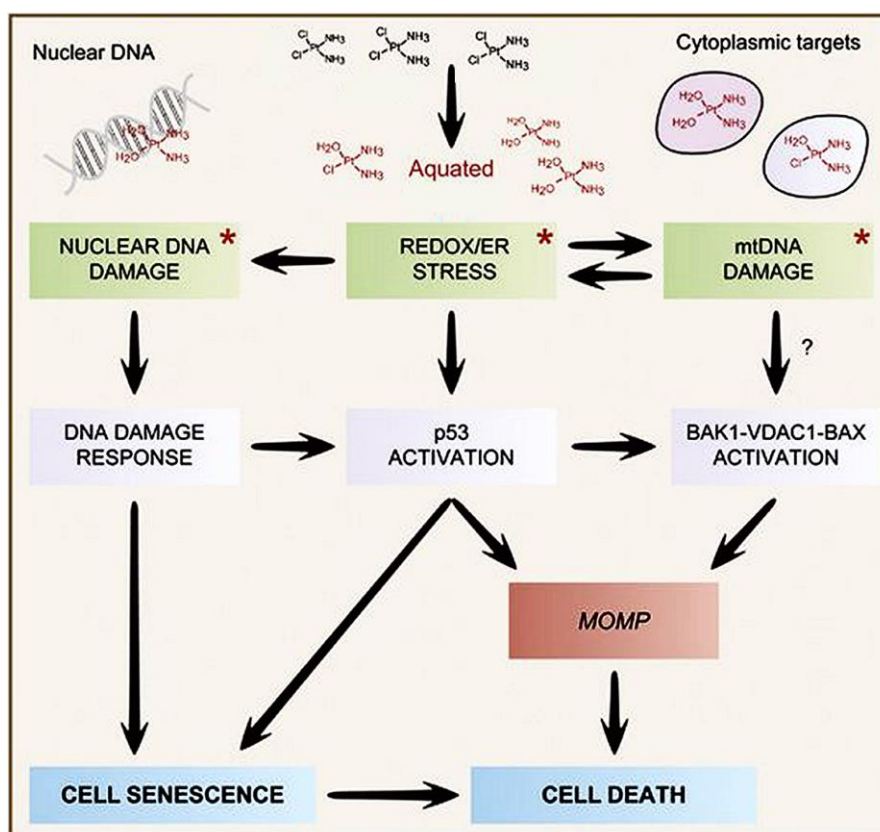


Figure 8. Mode of action of CDDP and different targets. In addition to DNA damage, CDDP can physically interact with different cytoplasmic nucleophiles, including mitochondrial DNA (mtDNA), several mitochondrial and extramitochondrial proteins. Other effects are the establishment of oxidative and reticular stress; induction of signal transduction cascade that involves BAK1 and BAX, as well as voltage-dependent anion channel 1 (VDAC1) and activation of the cytoplasmic pool of p53. Asterisks tag the primary consequences of CDDP reactivity (adapted from Galluzzi L et al. 2014).

Only about 1% of the intracellular CDDP forms covalent bonds with nuclear DNA (Gonzales VM et al. 2001), while among the remaining molecular mechanisms that support the cytotoxic potential of cytoplasmic CDDP there

is for example the accumulation of reactive species of the oxygen (ROS) and nitric oxide (NO), which not only aggravate the genotoxicity of CDDP, but also exert direct cytotoxic effects favouring the opening of the so-called PTPC complex (Permeability Transition Pore Complex) (Brenner C and Grimm S 2006; Godoy LC et al. 2012; Kroemer G et al. 2007). In addition, the mono- and bi-aquate forms of CDDP are highly electrophilic, therefore prone to form covalent bonds with methionine and with a large group of peptides and polypeptides containing cysteines, including reduced glutathione (GSH), which is present within the cell in high concentrations (0.5-10 mM) and metallothioneins (Timerbaev AR et al. 2006). The high affinity with GSH leads to the formation of ROS that can damage proteins, lipids and even the DNA itself. However, the CDDP-GSH conjugates are readily eliminated from the cell by Multidrug resistance-associated protein 2 (MRP2), a member of the ATPases of the ABC protein family, promoting the outflow of the drug itself and thus contributing to induction into the cell of the CDDP resistance (Dilruba S and Kalayda GV 2016). Several studies have shown that CDDP also induces damage directly to cytoplasmic organelles, causing apoptotic cell death (Ferri KF and Kroemer G 2001). The activation of a p53 cytoplasmic pool can promote MOMP (Mitochondrial Outer Membrane Permeabilization) through various mechanisms and by VDAC1 (Voltage-Dependent Anion Channel 1), a component of PTPC (Vaseva AV et al. 2012). Experiments carried out on mitochondria have shown that exposure to CDDP leads to calcium-dependent swelling, calcium release, depolarization of mitochondrial potential, and decay of NADPH (Custódio JB et al. 2009). Furthermore, following the increase in Bax protein expression, cytochrome c is released from the mitochondrial intermembrane space (Santin G et al. 2012). Cytochrome c binds both APAF-1 (apoptotic protease activating factor-1) and other proteins to form the complex known as apoptosome, which hydrolyzes ATP to recruit the procaspase initiator 9 and allow its cleavage to active caspase-9 (Yuan S et al. 2010). The latter then activates caspase-3 which mediates most of the events in the apoptosis execution phase, including cytoskeletal reorganization, phosphatidylserine membrane externalization, chromatin condensation and DNA fragmentation in the nucleus with the formation of apoptotic bodies (Núñez R et al. 2010). It has been shown that both the Golgi apparatus and the endoplasmic reticulum (ER) appear modified in rat neuroblastoma cells exposed to CDDP, and these alterations are connected to a reorganization of the cytoskeletal

tubulin, suggesting that the whole process is the basis of the generation of apoptotic bodies (Santin G et al. 2012). It has been shown that the CDDP-induced ER stress leads to the activation of caspase-12 and consequently of caspase-3, with consequent induction of apoptosis (Hodeify R et al. 2010; Santin G et al. 2011). After the lysosomal membrane permeabilization (LMP) by CDDP, with the consequent release of the organelle content in the cytosol, also lysosomes become inducers of cell death patterns. Lysosomes contain different proteases of the cathepsin family, which can activate the intrinsic apoptotic pathway, or cause massive proteolysis, which leads to necrosis (Sancho-Martínez SM et al. 2012). The CDDP also interacts with the cytoskeleton: at low concentrations, it prevents the polymerization of actin, while at higher concentrations, it causes the depolymerization of g-actin and f-actin (Sancho-Martínez SM et al. 2012). The α -tubulin also undergoes a rearrangement after treatment with CDDP that can cause the induction of the apoptotic pathway. Consequently, the reorganization of the cytoskeleton and fragmentation of the microfilaments confer plasticity to the whole cell and favour the decrease of cell volume (Bottone MG et al. 2013; Santin G et al. 2012).

1.2.2 Side effects of cisplatin treatment

The benefits produced using CDDP in anticancer treatments are compromised by severe systemic side effects, which determine a restriction in the dose of drug administration and limit the duration of treatment (Dasari S and Tchounwou P 2014). The main side effects include: nephrotoxicity, neurotoxicity and ototoxicity, but there are also phenomena of cardiotoxicity, hepatotoxicity, as well as myelosuppression (specifically neutropenia and thrombocytopenia), gastrointestinal toxicity (nausea and vomiting), and possible allergic reactions (Bloechl-Daum B et al 2006; Dugbartey GJ et al. 2016; Florea AM and Büsselberg D 2011). These elements not only aggravate the patient's already compromised state of health, but also worsen their quality of life (QoL).

Nephrotoxicity

Nephrotoxicity is one of the main side effects that occur during chemotherapy. It has been estimated that 20% of patients receiving high doses of CDDP show severe renal dysfunction, in some cases even just a few days

after starting treatment (Crona DJ et al. 2017). Nephrotoxicity is characterized by various types of symptoms; acute kidney damage, the most serious and frequent side effect, which occurs in 20-30% of patients. Other symptoms include hypomagnesemia, Fanconi-like syndrome, distal renal tubule acidosis, hypocalcemia, loss of salts in the kidney, hyperuricemia (Miller RP et al. 2010). The pathophysiological phenomena underlying the CDDP-induced renal damage include the sequential renal vasoconstriction, decrease in renal blood flow, reduction of glomerular filtration, increase in serum creatinine levels and a reduction in serum magnesium and potassium levels. Indeed, CDDP, being a non-charged molecule with a low molecular weight, can be freely filtered by glomeruli, internalized in renal tubular cells and finally reach the highest gradient at the proximal tubule, between the inner medullary and external cortical part causing damage, which can then extend to other tubular areas, including the distal tubule and the collecting duct (Pabla N and Dong B 2008). The long-term effects of CDDP at the renal level have not yet been completely clarified, but it is believed that they may be associated with a permanent reduction in renal function (Oh GS et al. 2014). The mechanism by which CDDP induces nephrotoxicity is complex and involves numerous cellular processes, such as cell death by necrosis and by apoptosis, oxidative stress, with production of free radicals of both oxygen and nitrogen, and inflammation, which leads to damage and cell death at the level of renal tubular cells (Miller RP et al. 2010). On the contrary, some literature data have shown that the inhibition of autophagy leads to an enhance in apoptosis, indicating a protective function of the autophagic process in the cellular response to CDDP (Kaushal GP et al. 2008). Although nephrotoxicity can be controlled using diuretics and adequate hydration of patients, its incidence, during CDDP therapy, is still high (Crona DJ et al. 2017; Oh GS et al. 2014).

Ototoxicity

Ototoxicity occurs in approximately 23-54% of patients treated with CDDP and in more than half of the children receiving this type of care, showing greater risk for developing hearing loss than adults (Sheth S et al. 2017; Waissbluth S and Daniel SJ 2013). Hearing loss is often verified in children who are undergoing treatment for brain tumours, such as neuroblastoma. Cisplatin-induced hearing loss is predominantly in the high-frequency range. The damage is bilateral and permanent and drastically

affects the quality of life for cancer patients, and, in childhood, it could affect early speech development and hamper social integration (Sheth S et al. 2017). Generally, platinum levels in the brain remain very low, the cochlea, however, exhibited distinctive pharmacokinetics among the other organs analysed. Indeed, it gradually accumulates platinum with each subsequent treatment cycle, indicating that the cochlea has a little capacity to eliminating CDDP and its derivatives (Breglio AM et al. 2017). The mechanism probably responsible for this side effect involves the accumulation in the cochlea of ROS and NO species which exert direct cytotoxic effects promoting cell death pathway activation, such as mitochondrial-mediated apoptosis (Callejo A et al. 2015). Unfortunately, no clinical treatment is currently available for CDDP-induced ototoxicity. However, it was shown that the calcium-channel blocker, flunarizine, can attenuate CDDP-induced cell death also by anti-inflammatory role (So H et al. 2008) and it is believed that exogenously administered antioxidants or other drugs can improve the local microenvironment and intracellular redox status to ensure otoprotection (Sheth S et al. 2017).

Hepatotoxicity

High doses of CDDP can lead to hepatotoxicity (dos Santos NA et al. 2007); several studies have reported a significant increase in the hepatic concentration of malonaldehyde and a reduction in antioxidant levels following treatment with CDDP (Mansour HH et al. 2006; Yilmaz HR et al. 2005). After cycles of CDDP therapy, there is an increase in levels of liver enzymes in serum, which are indicators of an impairment of liver functions (Iseri S et al. 2007); furthermore, histopathological changes were observed with necrosis and degeneration of hepatocytes, infiltration of hepatocytes at the level of the portal vein and dilation of the sinusoidal capillaries (Kart A et al. 2010). Hepatotoxicity studies suggest that augmented ROS generation, with consequent impairment of mitochondrial function and structure, could be a triggering negative effect. Indeed, the increased lipid peroxidation (LPO) may reduce mitochondrial membrane fluidity, enhance the negative surface charge distribution and alter membrane ionic permeability including protons permeability, which uncouples oxidative phosphorylation (Waseem M et al. 2015).

Cardiotoxicity

Among the cardiotoxic manifestations of the CDDP chemotherapy that have been described, there are heart failure, angina, acute myocardial infarction, thromboembolic events, autonomous cardiovascular dysfunction, both hypertension and hypotension, myocarditis, pericarditis and severe congestive cardiomyopathy (Patanè S 2014). Findings show that oxidative stress is strongly involved in the pathological process of platinum-induced cardiotoxicity. CDDP induces lipid peroxidation on cardiac cell membranes, leading to the loss of enzymes such as lactate dehydrogenase and creatine kinase at the level of cardiomyocytes. The histological changes induced by CDDP treatment, which lead to this type of toxicity, are degeneration and necrosis of cardiac muscle cells, with consequent formation of fibrous tissue, presence of vacuolations at the level of the cardiomyocytes cytoplasm and swelling of blood vessels (Al-Majed AA et al. 2006). Due to the limited regeneration capability of the cardiomyocyte, CDDP-induced cardiomyopathy is irreversible. In addition to temporary cardiotoxicity, CDDP can cause several persistent cardiac complications, and even lead to congestive heart failure (Demkow U and Stelmaszczyk-Emmel A 2013). Therefore, employ highly effective antioxidants to prevent ROS accumulation and oxidative damage is one of the most useful approaches to avoid cardiotoxicity of CDDP (Zhang P et al. 2017).

Neurotoxicity

The neurotoxicity caused by anticancer agents severely complicates the treatment of cancer patients, because the nervous tissue, besides being particularly sensitive to the cytotoxic action of chemotherapeutic agents, may be more exposed to high doses of treatment in a context of damaged BBB (Abbott NJ et al. 2010; Dubois LG et al. 2014). The greatest difficulty is limiting the damage caused by neurotoxicity during the treatment of paediatric tumours. During postnatal development, when the BBB is not yet fully formed, some areas of the CNS, *i.e.* hippocampus and cerebellum, are more sensitive to external agents, such as antitumour agents, that may cause severe neuronal damage, affecting the normal structural and functional development of the brain (Bernocchi G et al. 2015; Cerri S et al. 2011; Ikonomidou C 2017; John T et al. 2017). The toxicity of CDDP in the CNS mainly affects the ganglia of the dorsal root of the spinal cord and the

peripheral nerves, often affecting peripheral sensory neurotoxicity (Abdelsameea AA and Kabil SL 2018). The first manifestations of peripheral neurotoxicity consist of numbness, tingling or paraesthesia in the fingers and/or toes, dysesthesia and decreasing distal vibratory sensitivity (Hausheer FH et al. 2006). In addition, prolonged treatment can also influence proprioception with possible subsequent development of an ataxic gait (Avan A et al. 2015). Peripheral toxicity induced by platinum is manifested through two clinically distinct syndromes: an acute and transient paraesthesia at the distal extremities, more common following treatment with oxaliplatin and which normally occurs in the early phase of drug administration; or a chronic cumulative sensory neuropathy, which shows more persistent clinical alterations (Argyriou AA et al. 2012). Neuropathic symptoms can also interfere with treatment, leading to dose reduction or early cessation of chemotherapy, with a potential impact on patient survival (Park SB et al. 2013). The pathophysiology of neurotoxicity has not yet been completely clarified, based on the literature data, platinum compounds could actively enter the tumour and into normal cells through organic cationic transporters (Sprowl JA et al. 2013), organic cation/carnitine transporters (Jong NN et al. 2011), and some metal transporters, such as copper transporters. Another mechanism could involve oxidative stress, associated with mitochondrial dysfunction as a trigger for neuronal apoptosis. Therefore, peripheral neurotoxicity could be modulated by a reduction in the activity of enzymes involved in DNA base excision, in the repair of oxidative damage and redox regulation (Jiang Y et al. 2008).

1.2.3 Cisplatin and drug resistance

The benefits that treatment with CDDP entails in tumour therapies are often limited, in addition to toxicity, also by the acquired drug resistance that it induces. Cell resistance can originate from *i*) alterations in processes that precede the binding of CDDP with its targets, including DNA and cytoplasmic structures (pre-target resistance); *ii*) molecular damages directly caused by CDDP action (on-target resistance); *iii*) modifications involved in the pathways related to signals of cell death triggered by some molecular lesions (post-target resistance); *iv*) signals activated by CDDP (off-target resistance) (Galluzzi L et al. 2012) (**Figure 9**).

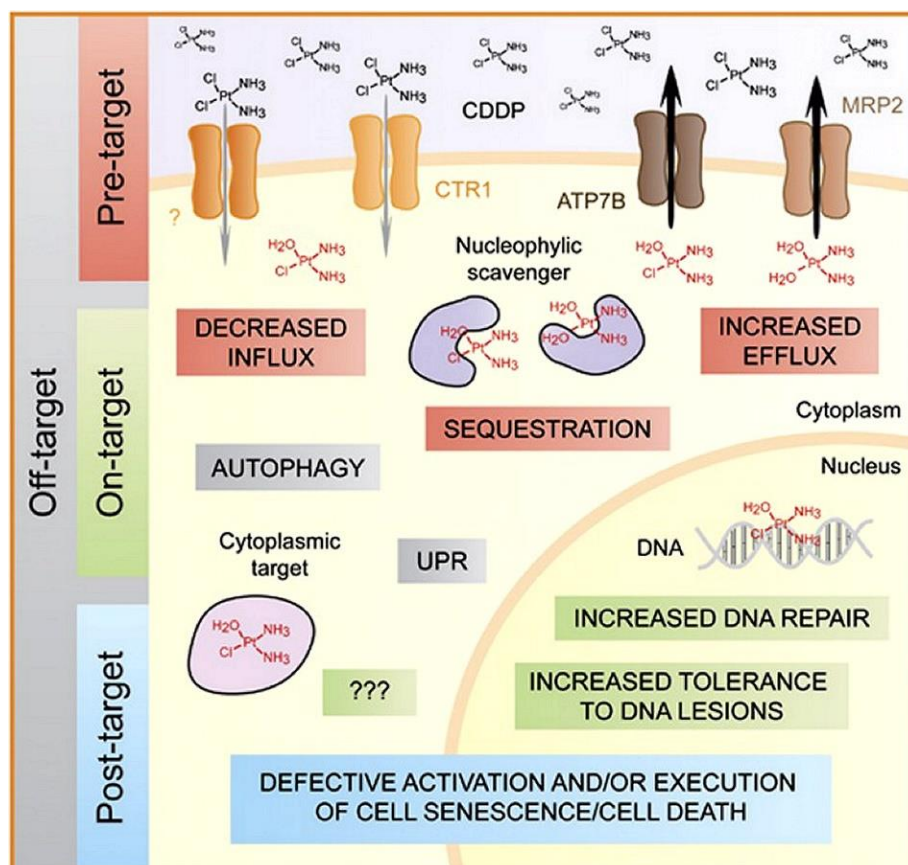


Figure 9. Molecular mechanisms of CDDP resistance. Different resistance pathways induced in malignant cells by CDDP treatment (Galluzzi L et al. 2014).

Pre-target resistance

CDDP resistance can develop through alterations that lead to a reduction in the amount of CDDP and its aqua-complexes in the cytoplasm. It has been observed that CDDP can enter cells by passive diffusion, but above all by transporters, such as the copper Ctr1 transporter, which is responsible for the internalization of a significant fraction of CDDP (Galluzzi L et al. 2012; Ishida S et al. 2002). In human cells, CDDP initiates a rapid degradation of transporter Ctr1, with a consequent decrease in the intracellular influx of CDDP, resulting in drug-induced resistance (Holzer AK et al. 2006). A recent study has shown that genetic Ctr1 knockout promotes

cellular CDDP resistance *in vivo*, whereas overexpression of Ctr1 has been associated with increased CDDP accumulation and sensitivity (Shen DW et al. 2012). On the contrary, an increase in Ctr1 expression could lead to an increase in CDDP accumulation and, in many cases, increase cell sensitivity to the compound itself (Kilari D et al. 2016). Conversely, the ATP7B transporter protein (ATPase Copper Transporting Beta), uses the metabolic energy produced by ATP hydrolysis to transport excess copper through cell membranes and plays a significant role in the extrusion of CDDP from cells (Ciarimboli G 2014). Thus, changes in expression levels, in the subcellular localization and/or functionality of the Ctr1 and ATP7B transporters, may represent possible targets associated with CDDP resistance, both in preclinical and clinical models (Kuo MT et al. 2012; Li T et al. 2017). Furthermore, it has been shown that other transporters present in the plasma membrane such as MRP2 (Multidrug Resistance-Associated Protein 2), the ABC transporter (ATP Binding Cassette) (Yamasaki M et al. 2011), and the ATPase ATP11B (ATPase Phospholipid Transport 11B) (Moreno-Smith M et al. 2018) can contribute to the CDDP extrusion from cells and therefore to the mechanism of resistance. Another protein with a possible role in cellular resistance to CDDP is Transmembrane Protein 205 (TMEM205). Analysis of TMEM205 expression profiles in normal human tissue indicates a differential expression pattern with high levels of expression in the liver, pancreas and adrenergic glands. The overexpression of TMEM205 in CDDP resistant cells could thus play a role in platinum cellular resistance in different types of tumour and could also be a valuable biomarker for cancer therapy (Schmit K and Michiels C 2018; Shen DW et al. 2012).

On-target resistance

The sensitivity of tumour cells to the cytostatic/cytotoxic effects of CDDP is limited by the presence of an efficient, and probably overexpressed, DNA repair apparatus. In particular, the NER system is believed to repair most of the DNA lesions caused by CDDP exposure (Furuta T et al. 2002, Galluzzi L et al. 2012; Rocha CRR et al 2018). Some components of the MMR system, normally implicated in the repair of incorrect insertions, deletions, and mis-incorporations of bases that may occur during DNA replication and recombination, are also implicated in this process of chemoresistance (Kunkel TA and Erie DA 2005; Rocha CRR et al 2018). Furthermore, the cytoplasmic components also considered the target of

CDDP extranuclear toxicity, such as cytoskeletal, mitochondrial and ribosomal proteins, could undergo frequent turnover phenomena, thus reducing the effect of CDDP damage and preventing the activation of the mechanisms associated with cell death (Sancho-Martínez SM et al. 2012).

Post-target resistance

Post-target resistance to CDDP can be the consequence of several alterations that affect signal transduction pathways that normally promote apoptosis but also problems with the cell death execution mechanisms (Galluzzi L et al. 2011). The neoplastic cells, due to the numerous alterations, are inherently more resistant to an adverse microenvironment, such as the accumulation of ROS, and are therefore more inclined to acquire genetic and epigenetic alterations that influence the susceptibility to drugs (Negrini S et al. 2010), promoting the activation of integrated adaptive responses, with the aim of re-establishing initial cellular homeostasis (Kroemer G et al. 2010). Tumour cells with a CDDP-resistant phenotype exhibit defects in the pro-apoptotic function of p53, resulting in inactivation of cell death and tolerance to CDDP-produced DNA adducts (Vousden KH and Lane DP 2007). This is due to the decreased ability of p53 to transactivate its genes, including, Bax. Furthermore, p53 loses its ability to regulate cell cycle checkpoints and thus block cells in G₁ phase, increasing resistance (Shah MA and Schwartz GK 2001). Further alterations that decrease the extrinsic pathway of apoptosis is the MAPK signalling pathway triggered by Fas/FasL. Furthermore, MAPK signalling also contributes to the post-transcriptional modification of p53, so a malfunctioning of p53 is not only due to defects in the transcription pathway or mutations in its gene, but also to the upstream mechanisms that support its activation (Mansouri A et al. 2003).

Off-target resistance

The susceptibility of tumour cells to CDDP can also be limited by the off-target mechanisms, which are molecular circuits that deliver compensatory survival signals, although these are not directly activated by chemotherapy (Galluzzi L et al. 2014). Among these processes, the upregulation of the DYRK1B kinase (Dual-specificity Y-phosphorylation regulated kinase 1B) appears to be involved, which increases the expression of antioxidant enzymes such as ferroxidase or superoxide dismutase,

contributing to tumour survival (Deng X et al. 2009). Recently, it has been observed that the TMEM205 protein appears to promote CDDP resistance through a molecular cascade involving the small Ras-like GTPase, RAB8A (Ras-related protein Rab-8A) (Shen DW et al. 2012). Finally, several non-specific adaptive responses to stress are implicated in CDDP resistance. These general stress responses include macroautophagy and the response of heat-shock proteins, which allow cells to adapt to treatment (Kroemer G et al. 2010). Concerning to mitochondria, more morphological aspect of the off-target CDDP resistance could be given by the increase in mitochondrial fusion. In fact, this process has been correlated with a reduction in apoptosis, would suggest that it could be a phenomenon of resistance to CDDP (Santin G et al. 2012).

1.3 Platinum-based compounds

In recent years, based on the antitumour properties of CDDP, the focus has been put on the use of platinum-based drugs in cancer therapy (Frezza M et al. 2010). Among these compounds, there are second-generation drugs, such as carboplatin, and third-generation drugs, such as oxaliplatin, which have already been approved by the FDA as chemotherapeutics (Boulikas T et al. 2007; Wheate NJ et al. 2010), but also promising compounds of new synthesis currently under study.

1.3.1 Platinum(II)

Carboplatin

In terms of its structure, carboplatin, sold under the trade name Paraplatin, differs from CDDP in that it has a bidentate dicarboxylate (the ligand is CycloButane DiCarboxylic Acid, CBDCA) in place of the two chloride ligands, which are the leaving groups in CDDP (**Figure 10**). Carboplatin and CDDP exert antineoplastic effects in a very similar way, so the non-distinguishable mechanism of action reflects the fact that the active form of these two drugs is identical. Carboplatin, while forming the same reaction products *in vitro* at doses equivalent to CDDP, has a longer-lasting action, attributable to a lower excretion and greater retention of the compound from the organism. Another difference with CDDP is the activation mode: it does not occur by “aquation”, but by nucleophiles such as glutathione, aspartic acid and other molecules containing sulfhydryl groups (Frezza M et

al. 2010). In contrast to CDDP, carboplatin has shown less nephro- and neurotoxic effects, it does not cause hearing loss and patients treated with this drug show a lower incidence of nausea and/or vomiting (Ardizzoni A et al. 2007). Carboplatin, having an activity spectrum identical to CDDP, is therefore ineffective against CDDP-resistant tumours (Moncharmont C et al. 2011). The main problem of carboplatin is its myelosuppressive effect that induces a cytotoxic action at bone marrow hematopoietic precursors and progenitors, promoting damage to the cells through the block of replication (Cheng YJ et al. 2017).

Oxaliplatin

Oxaliplatin, sold under the name Eloxatin, is a derivative of platinum consisting of the diaminocyclohexane ligand (DACH), in place of the two monodentate amine ligands, and of the oxalate representing a leaving group, making oxaliplatin a chemical entity distinct from the CDDP (**Figure 10**). The presence of bidentate oxalate significantly reduces the reactivity of the drug, which therefore presents immunological and pharmacological properties different from CDDP, correlated with a reduction in the effect on peripheral sensory neuropathy (Wheate NJ et al. 2010; Zou Y et al. 2016). Oxaliplatin has shown a wide antitumor effect both *in vitro* and *in vivo*, being effective in tumour cell lines resistant to CDDP and carboplatin (Dilruba S and Kalayda GV 2016; Stordal B et al. 2007). Oxaliplatin induces apoptosis following DNA-induced lesions, however, it shows several side effects including myeloablation, hemolytic anaemia, secondary immune thrombocytopenia and cases of acute leukaemia (Alcindor T and Beauger N 2011) have also been reported.

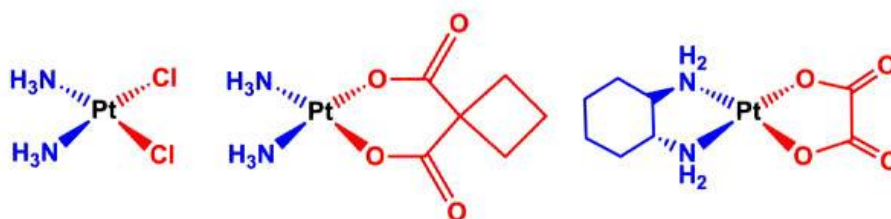


Figure 10. Platinum(II) compounds. The chemical structures of CDDP, carboplatin, and oxaliplatin. The leaving-group ligands are in red and the non-leaving-group ligands are in blue (Johnstone TC 2016).

[Pt(O,O'-acac)(γ -acac)(DMS)]

The synthesis of novel platinum(II) compounds is aimed to find platinum-based drugs, not only with higher antitumour activity and with a lower capability to induce side effects but also able to overcome CDDP resistance that occurs in many types of tumours (Muscella A et al. 2007). In this regard, Professor Fanizzi's team (University of Salento, Lecce, Italy) synthesized a new platinum(II) compound; the [Pt(O,O'-acac)(γ -acac)(DMS)], containing two acetylacetonate (acac) ligands: respectively one O,O'-chelate and the other σ -linked by methine in the γ position, and dimethylsulphide (DMS) in the metal coordination sphere (De Pascali SA et al. 2005). The [Pt(O,O'-acac)(γ -acac)(DMS)] has exhibited the capability to induce apoptosis not only in the endometrial tumour cells Hela, with activity about 100 times higher than that of CDDP, but also to induce a higher cytotoxic effect on resistant MCF-7 breast cancer cells (Muscella A et al. 2008).

The major effect of [Pt(O,O'-acac)(γ -acac)(DMS)] may be ascribable to its higher accumulation in the intracellular compartment (Muscella A et al. 2011) and the different mechanism of action. Indeed, previous studies showed that [Pt(O,O'-acac)(γ -acac)(DMS)] has a non-genomic target, suggesting that the mechanisms underlying its cytotoxicity not necessarily require reaction with DNA (Muscella A et al. 2007). The presence of DMS in the chemical structure of the molecule indicates its prevalence action on sulphur ligands such as thiols or thioethers attached to proteins (Muscella A et al. 2007). In this case, the principal targets may be represented by proteins, suggesting that the cellular targets could be amino acid residues of protein that could promote different apoptotic pathways and consequently an increase in cell death level (Muscella A et al. 2008). Furthermore, at sublethal concentration, [Pt(O,O'-acac)(γ -acac)(DMS)] is able to induce cell death in MCF-7 cells through anoikis and prevented events leading to cell migration (Muscella A et al. 2010). Indeed, anoikis, which acts as a physiological obstacle to metastasis, is a form of programmed cell death that occurs in anchorage-dependent cells, when they detach from the surrounding extracellular matrix (ECM) (Valentijn AJ et al. 2004). Moreover, in MCF-7 cells, [Pt(O,O'-acac)(γ -acac)(DMS)] can cause a decrease in the activity of PMCA1 (Plasma Membrane Calcium ATPase 1) (not SERCA or SPCA) and of membrane permeability to Ca^{2+} , resulting in the overall $[\text{Ca}^{2+}]_i$ increase (Muscella A et al. 2011). In addition, [Pt(O,O'-acac)(γ -acac)(DMS)] causes the activation of PKC- α (Protein

Kinase C-alpha) and the production of ROS that were responsible for the Ca^{2+} permeability (Muscella A et al. 2011), indicating a wide involvement of calcium in the mechanisms induced by the activity of the new compound (**Figure 11**). Other *in vitro* studies conducted on the B50 rat neuroblastoma line, revealed that the cytotoxic action of [Pt(O,O'-acac)(γ -acac)(DMS)] is already obtained at concentrations four times lower than the treatment standard with CDDP (Grimaldi M et al. 2016). The morphological and functional effects of exposure for 48 h to the new compound include damage of Golgi apparatus, loss of the actin and tubulin cytoskeletal organization, mitochondria fission and reduction of the mitochondrial membrane potential (Grimaldi M et al. 2016). Furthermore, preliminary data showed that the effects induced by treatment with [Pt(O,O'-acac)(γ -acac)(DMS)] may have a long-term cytotoxic effect on tumour cells, in contrast to cells treated with CDDP that show features of chemoresistance (Grimaldi M et al. 2019). *In vivo*, compared to CDDP, [Pt(O,O'-acac)(γ -acac)(DMS)] has shown less hepatotoxicity and nephrotoxicity, associated with a major concentration of platinum in the blood vessels (Muscella A et al. 2014). *In vivo* evaluations, conducted on Wistar male rats that had been subjected to [Pt(O,O'-acac)(γ -acac)(DMS)] injection at postnatal day 10, have shown that, one week after administration of the drug, no significant apoptotic events have been induced, but rather a less injury in the neuroarchitecture of both cerebellum and hippocampus have been observed (Bernocchi G et al. 2011; Cerri S et al. 2011; Piccolini VM et al. 2015). However, the mechanisms involving the buffering of calcium must be better understood, especially will be investigated the possible mechanisms of oxidative stress that the compound could induce at the level of healthy brain tissue.

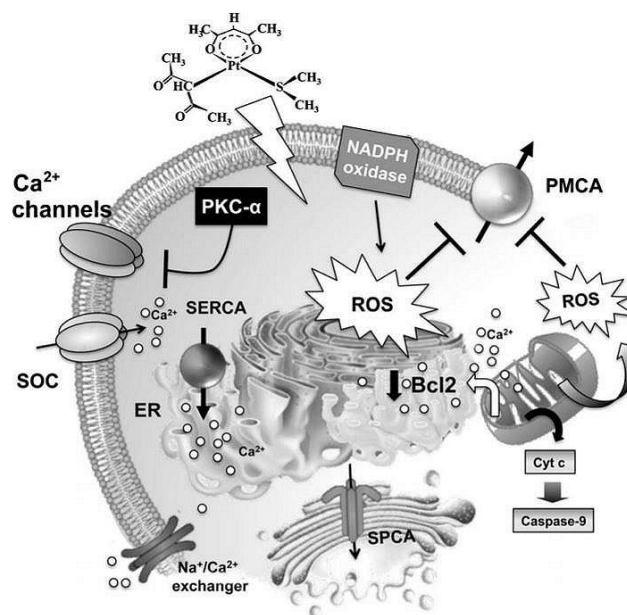


Figure 11. [Pt(O,O'-acac)(γ -acac)(DMS)] mechanism of action and targets.

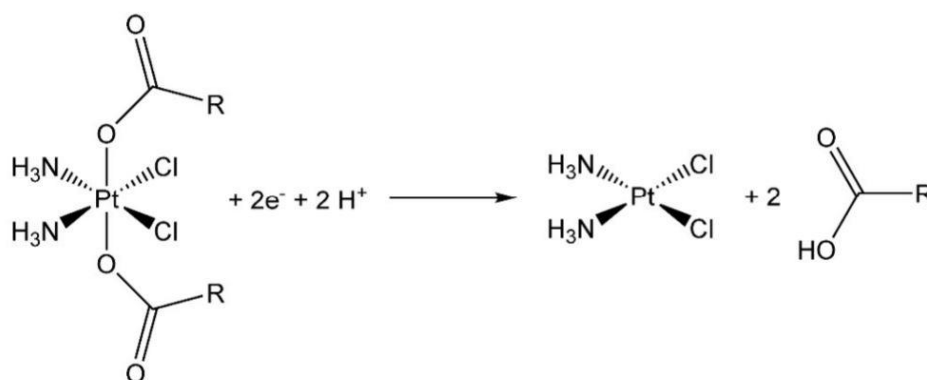
[Pt(O,O'-acac)(γ -acac)(DMS)] alters the $[Ca^{2+}]_i$, acting on the PKC- α -mediated closure of some channels and on PMCA activity. The compound also targets the mitochondria, causing a dissipation of the membrane potential, which may affect the role of mitochondria to Ca^{2+} homeostasis. Mitochondrial release cytochrome c leading to activation apoptosis cascade. In addition, [Pt(O,O'-acac)(γ -acac)(DMS)] decreases Bcl-2 expression, reducing its contribution to the ER Ca^{2+} uptake, an effect likely related to its antiapoptotic function (Muscella A et al. 2011).

1.3.2 Platinum(IV)

The efficacy of CDDP, and in general of other platinum(II), is therefore limited by a combination of different factors, such as toxicity, resistance and also a poor pharmacokinetic profile both at the cellular and systemic level (Wang D and Lippard SJ 2005). Furthermore, most platinum(II)-based drugs are lost before reaching their final target, because they interact with bloodstream proteins, giving rise to secondary reactions, which lead to the onset of undesirable side effects (Timerbaev AR et al. 2006).

Although some side effects can be alleviated, for years scientific research has concentrated on trying to obtain molecules with lower systemic toxicity and better pharmacological profiles (Wheate NJ et al. 2010).

A strategy to overcome the limitations of platinum(II)-based drugs may be the use of platinum(IV), Pt(IV). They are synthesized through an oxidative addition to the platinum(II) square planar geometry, usually of two hydrogen peroxides, which produces an octahedral complex, which maintains the original coordination structure of platinum(II) in equatorial position, with the addition of two hydroxides in axial position, finally the latter can be modified to give the desired properties to the complex (Chin CF et al. 2011; Galanski M et al. 2003) (**Scheme 1**).



Scheme 1. Mechanism of Pt(IV) compound. Activation by a reduction reaction of a generic CDDP-based Pt(IV) compound. R=alkyl or aryl substituent (Gabano E et al. 2017).

These octahedral compounds, thanks to their external electronic configuration, are stable outside the tumour cells, while they are activated through a reduction process only inside them, thus allowing their oral administration (Graf N and Lippard SJ 2012; Wilson JJ and Lippard SJ 2014). Intracellular activation is caused by reducing agents present inside the cell, for example, ascorbic acid or reduced GSH, and occurs through a reduction reaction with elimination of two electrons, which leads to the release of a molecule with planar geometry square of the platinum(II) family, often CDDP, and of the two axial ligands, which may be the same or different (Gibson D 2016; Ilangovan G et al. 2002).

The reduction of Pt(IV) complexes, from which the different products are obtained, represents an essential and critical step in the mechanism of action of these compounds (Ravera M et al. 2012). In fact, if the reduction occurs too quickly, before the drug reaches the tumour and is internalized by it, or if

the compound is resistant to reduction and cannot be activated within the tumour cells, then these compounds are almost inactive (Chen CKJ et al. 2013; Wexselblatt E and Gibson D 2012). Just due their specific mechanism of activation, *i.e.* they are reduced to cytotoxic platinum(II) analogues within the hypoxic tumour cells, it is generally accepted that Pt(IV) complexes act as prodrugs (Graf N and Lippard SJ 2012; Johnstone TC et al. 2016; Wexselblatt E and Gibson D 2012).

The two axial ligands, which detach themselves during the reduction of the Pt(IV) complexes, can be used in different ways to verify and improve the pharmacological properties of these prodrugs. A recent approach is to attack the prodrugs, through the axial ligands, to polymers, nanoparticles, or to other targets and transport systems, to increase the bioavailability and improve its specificity (Johnstone C et al. 2016). The axial ligands can increase the affinity to certain target receptors present on the surface of tumour cells, influencing the influence in the cell, mainly by passive diffusion, and consequently by acting on the cellular accumulation of Pt(IV) compounds (Ravera M et al. 2015). The Pt(IV) derivatives with one/two synergistic drug/s can be conjugated as axial ligand/s in the octahedral assembly, generating an ideally synergistic antineoplastic action when released along with CDDP upon reduction (Gabano E et al. 2017). For example, some Pt(IV) complex, derived from CDDP, carboplatin, and oxaliplatin, present as axial ligands ibuprofen, indomethacin, valproate or phenylbutyrate (Gibson D 2016).

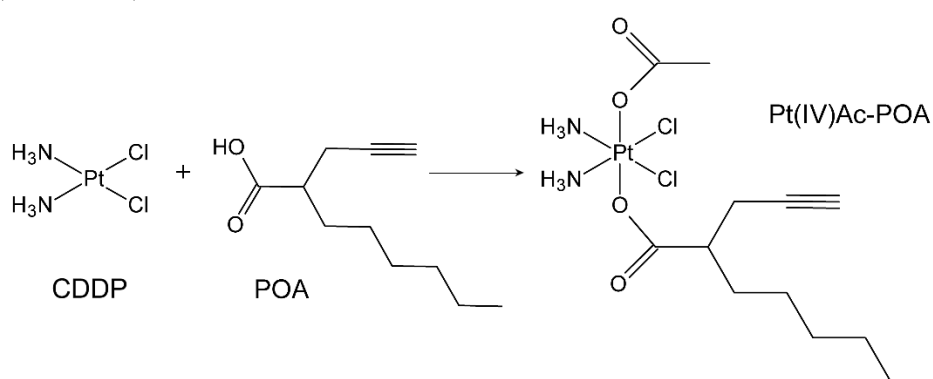
In particular, the conjugation of CDDP or oxaliplatin with histone deacetylase inhibitors (HDACi) is interesting. Histone deacetylase inhibitors are anticancer drugs that are attributed epigenetic properties, which can alter gene transcription and exert antitumor effects, such as the arrest of growth processes, differentiation, apoptosis, and inhibition of tumour angiogenesis; furthermore the inhibition of histone deacetylase leads consequently to hyperacetylation of histones, decreasing histone-DNA interactions DNA, thus leaving it in an open form and which allowing for chemo-sensitization versus DNA-damaging agents (Atadja PW 2011; Bolden JE et al. 2006; Lee MJ et al. 2008, Li Y and Seto E 2016). HDACi, modulating the expression and functions of DNA-repair proteins, further increase the persistence and efficacy of the Pt-DNA adducts (Falkenberg KJ and Johnstone RW 2014; Nikolova T et al. 2017).

HDACi consists of two main chemical families: hydroxamic acids such as suberoylanilide hydroxamic acid (SAHA or Vorinostat) and medium-chain fatty acids (MCFAs) or, more correctly (at physiological pH), their conjugated anions (Gabano E et al. 2017). Despite the highly effective of SAHA, it required heavy chemical modifications to coordinate the platinum(II) molecule core (Brabec V et al. 2012; Griffith D et al. 2009). On the contrary, MCFAs *i.e.* 2-propylpentanoate or valproate (VPA), clinically used as anticonvulsant agent, and phenylbutyrate (PhB) orphan drug applied in urea cycle disorders treatment (Manal M et al. 2016; Minucci S and Pelicci PG 2006) have been easily conjugated to the metal core via esterification reaction of hydroxido-Pt(IV) synthons (Raveendran R et al. 2016; Yang J et al. 2012), proving themselves as efficient HDACi. These derivatives, based on the square-plane arrangement of platinum(II) and carrying one or two MCFA molecule/s in the axial position, have been examined to better understand the possible antitumor dual- or multi-action (Gibson D 2006). In addition to using the elements present in the axial position in platinum(IV) complexes to obtain these prodrugs with different actions, the ligands can also be involved in the attack of platinum to specific target agents. There are several examples of the conjugation of platinum(IV) compounds to peptides to promote interaction with tumour targets or to facilitate internalization in cells. The target receptors that are mostly expressed in cancer cells, compared to healthy ones, represent a way to increase the selectivity of prodrugs and its cell uptake, which usually occurs by endocytosis (Massaguer A et al. 2015). Finally, one of the major challenges in the development of new drugs is to avoid unwanted interactions with serum proteins, and especially with albumin. As often happens with platinum(II) complexes; the formation of covalent bonds with these proteins occurs with consequent inactivation of the drug and a decrease in bioavailability. In contrast, platinum(IV)-based prodrugs are less inclined to form non-covalent bonds with serum proteins such as albumin. Anyway, this interaction could represent an *in vivo* strategy to improve the anticancer properties of these prodrugs; since human serum albumin has recently attracted attention for its transport system properties (Zheng YR et al. 2014; Pichler V et al. 2013).

The new Pt(IV)Ac-POA prodrug

To overcome limits of classical oncotherapy, the complex (OC-6-44)-acetatodiamminedichlorido(2-(2-propynyl)octanoato)platinum(IV), named

Pt(IV)Ac-POA, has been synthesised by Professor Osella and his team (University of Eastern Piedmont, Alessandria, Italy). Pt(IV)Ac-POA is synthesized starting from the CDDP which is oxidized with hydrogen peroxide to obtain an intermediate octahedral compound, which is then esterified with the addition of two long-chain carboxylic acids. Pt(IV)Ac-POA contains a different MCFA-HDACi, namely 2-(2-propynyl)octanoate (POA), along with an inert acetate (Ac) as axial ligands (Gabano E et al. 2017) (**Scheme 2**).



Scheme 2. Synthetic pathways for Pt(IV)Ac-POA synthesis. Cisplatin (CDDP), 2-(2-propynyl)octanoic acid, POA, and its Pt(IV) mixed derivative (OC6-44)-acetatodiamminedichlorido(2-(2-propynyl)octanoato)platinum(IV), Pt(IV)Ac-POA (Rangone B et al. 2018).

The Pt(IV)Ac-POA, acting as a prodrug, represents a promising tool, able to produce a synergistic action in the hypoxic tumour cell microenvironment. This prodrug, bearing as axial ligand POA, has a higher activity due to the high cellular accumulation due to high lipophilicity and to the inhibition of histone deacetylase which leads to increased exposure of nuclear DNA, thereby permitting higher platination levels at DNA, and promoting cancer cells death (Leng Y et al. 2010; Gabano E et al. 2017; Novohradsky V et al. 2017). Indeed, the HDACi activity of free POA has been established as an inducer of a strong histone H3 acetylation (at lysine 9 level), presumably acting at the HDAC8 level (Oehme I et al. 2009). Moreover, it has been reported that POA is more active than VPA to induce histone hyperacetylation in cerebellar granule cells, also exhibiting antiproliferative and neurotrophic activity (Gabano E et al. 2017; Leng Y et al. 2010).

Several studies have shown that the new prodrug Pt(IV)Ac-POA exhibited promising antitumor activity both *in vitro* and *in vivo* on different human tumour cell lines (Gabano E et al. 2017). As it may show fewer side effects than CDDP, as Pt(IV) derivatives generally do (Oehme I et al. 2009; Witt O et al. 2009), Pt(IV)Ac-POA is currently under investigation to understand its effect on other types of cancers such as nervous system tumours.

Role of HDAC inhibitors in therapy

As described above, the possibility of modifying histones acetylation levels could represent an effective strategy in reducing DNA packaging, leading DNA exposure to the chemotherapeutic agents and so increasing antitumoral effect. The genomes of eukaryotic organisms are tightly packaged in chromatin, which forms the structural basis of the nuclear processes associated with the genetic activity. The concept of epigenetics is defined to describe changes in the expression of genes or their function, but which does not involve alterations in the underlying DNA sequence (Altucci L and Stunnenberg HG 2009; Baylin SB and Schuebel KE 2007; Goldberg AD 2007). Many alterations in the epigenetic scenario, correlated with genetic changes, form the fundamental bases for the beginning and progression of many human diseases, especially cancer (Hirst M and Marra MA 2009; Szyf M 2009). In physiologic cell conditions, histone proteins contribute to gene expression control by modulating chromatin structure and function. Post-translational modifications of histone tails, such as acetylation, methylation, ubiquitination, and phosphorylation, determine how these histone proteins control chromatin remodelling (Bezecny P et al. 2014; Sturm D et al. 2014). There are two sets of antagonist enzymes: histone acetyltransferase (HATs), which adds acetyl groups to histone tails, neutralizing them and weakening their interactions with the nucleosome, and histone deacetylase (HDACs) which removes the acetyl groups from histones and drives compaction of chromatin and gene silencing on local DNA (Smith BC and Denu JM 2009). HDAC and HAT do not bind directly to DNA but interact with DNA through multi-protein complexes that include corepressors and coactivators (Marmorstein R 2001; Sengupta N and Seto E 2004). Cancer has been considered a disease promoted by genetic defects, *i.e.* gene mutations, chromosomal deletion, and abnormalities, resulting in a loss of function of tumour suppressor genes and/or gain of functionality or hyperactivation of oncogenes (Kops GJ et al. 2005; Torti D and Trusolino L 2011). Nevertheless,

the epigenetic regulation of genes and therefore, the plasticity of the epigenome, plays a key role in the development and progression of cancer (Herceg Z et al. 2013). Current studies found that class I HDAC expression was high in strongly proliferating and advanced tumours, sometimes founded in patients with poor prognosis (Weichert W 2009). In contrast, a reduction in class II HDAC expression was described in different types of tumours, including GBM (Lucio-Eterovic AK et al. 2008).

The treatment of cancer cells with HDACi can lead to histone acetylation and gene expression, resulting in increased susceptibility of cancer cells to apoptosis. The induction of apoptosis appears to be a predominant pathway in HDACi-induced cell death (Frew AJ et al. 2009) and this aspect is of considerable therapeutic value for the treatment of cancer (Marks PA and Xu WS 2009). HDACi can induce cell growth arrest, terminal differentiation, cell death and/or angiogenesis inhibition. Normal cells are relatively resistant to HDACi-induced cell death (Burgess A et al. 2004; Insinga A et al. 2005; Ungerstedt JS et al. 2005). The cell death pathways identified in the mediation of programmed cell death induced by HDACi include apoptosis (Bolden JE et al. 2006; Rosato RR and Grant S 2005; Minucci S and Pelicci PG 2006) by intrinsic and extrinsic pathways, autophagic cell death (Shao Y et al. 2004), senescence (Xu WS et al. 2005) and cell death induced by ROS (Cornago M et al. 2014; Rosato RR and Grant S 2005; Ungerstedt JS et al. 2005). HDACi can alter cell cycle progression by decreasing the expression of G₂ checkpoint kinases Wee1 and checkpoint kinase 1 (Chk1). In addition, HDACi reduces the expression of proteins involved in DNA repair (Cornago M et al. 2014).

Furthermore, HDACs can promote the deacetylation of structural proteins, chaperones, and transcription factors (TFs) with a significant impact on the physiopathological pathway (Benedetti R et al. 2015). The response to HDACi seems to depend, at least in part, on the nature of HDACi, on concentration and on exposure time, and, above all, on the cellular context. In tumours that poorly respond to chemotherapy, treatment with HDACi may increase the sensitivity of cancer cells to other drugs and treatments (Munshi A et al. 2005). To date, many HDACi are in pre-clinical and clinical stages of investigation, also due to HDACi's potential ability to penetrate the BBB (Sturm D et al. 2014). A good strategy in glioblastoma therapy in a pre-clinical setting may be to restore balance of histone HAT to HDAC activity, thereby enhancing the abilities of the body itself to recognise and fight cancer

and, in the same time, sensitizing tumour cells to HDACi, not only as monotherapeutic agents, but also in combination with chemo and/or radiotherapy (Lee P et al. 2015).

1.4 Cell death pathway activated by the platinum compounds

In order to obtain key elements that would allow identifying and characterizing the various types of cell death, over the last decade the Nomenclature Committee on Cell Death (NCCD) has drawn up guidelines for the definition and interpretation of various types of cell death on the bases of morphological, biochemical and functional aspects (Galluzzi L et al. 2018).

Two types of cell death are defined on the basis of the context in which they are activated and on the causes that induce them: *i*) Regulated cell death (RCD) that depends on a specific molecular pathway, which can be modulated in reaction times through genetic regulation but also pharmacologically; *ii*) Accidental cell death (ACD), very rapid and characterized by drastic effects, caused by events such as exposure to severe physical, mechanical and chemical insults (Galluzzi L et al. 2018).

RCD is activated in two different situations of cell death: RCD can occur as a physiological program for development or tissue turnover, without any exogenous environmental perturbation (Conradt B 2009; Fuchs Y and Steller H 2011) and can be referred to as programmed cell death (PCD). In contrast, RCD can be induced by alterations of the intracellular or extracellular microenvironment, when such perturbations are too severe or protracted for adaptive responses (Galluzzi L et al. 2016).

Each cell death manifests peculiar macroscopic morphological alterations, which in the past year have been applied to distinguish three different forms of cell death: *i*) type I cell death or apoptosis, characterized by cytoplasmic shrinkage, chromatin condensation (pyknosis), nuclear fragmentation (karyorrhexis), and the generation of plasma membrane blebbing. This process culminates with the formation of apoptotic bodies, an intact membrane small vesicles containing cytoplasm material, which subsequently are efficiently removed by cells with phagocytic activity and then degraded within lysosomes; *ii*) type II cell death or autophagy, is manifested with the creation of numerous cytoplasmic vacuolization and similarly ending to apoptosis with phagocytic uptake and following lysosomal degradation; *iii*) type III cell death or necrosis, displaying no typical features of type I or II

cell death and it concludes without phagocytic and lysosomal involvement, but it is often associated with the activation of inflammatory processes (Galluzzi L et al. 2007; Galluzzi L et al. 2018).

1.4.1 Apoptosis

Apoptosis is the most widespread form of programmed cell death that occurs during the development of the organism and regulates tissue homeostasis. It is a type of controlled and energy-dependent cell death, presenting some distinctive morphological and molecular features such as reduction of the cell volume, chromatin condensation, phosphatidylserine externalization and activation of caspases. Caspases are a class of cysteine-aspartic proteases that recognize aspartate residues on intracellular proteins such as other caspases, which then are cleaved along the proteolytic cascade; this recognition is possible by the presence of a cysteine residue, together with one of glycine, in the conserved sequence QACXG (Gln-Ala-Cys-X-Gly) where X corresponds to a residue of arginine, glutamine or glycine of such proteases, which contributes to the formation of the catalytic site (Cohen 1997; Cummings BS et al. 2000).

Caspase activation is a key step in the initiation of apoptosis; different stimuli can initialize these molecules, including those that activate death receptors at the plasma membrane (caspase-8), and those that cause mitochondrial dysfunction (caspase-9). These proteins are produced in inactive form, called zymogens or pro-caspases, the initiating caspases (2, 8, 9 and 10) are activated, through a process of self-proteolytic that is facilitated by the interaction with specific adapter molecules, through a domain of recruitment, defined as CARD (Caspase-Recruitment Domain); a protein-interaction module belonging to the death-domain superfamily, which includes the death domain (DD), death-effector domain (DED) and pyrin domain (PYD) (Park HH 2019). Executing caspases are responsible for apoptosis induction due to different biochemical features, including the cleavage and activation of poly ADP-ribose polymerase (PARP) and other inhibitors of the caspase protein activator domain, which leads to DNA fragmentation (Elmore S 2007).

Apoptosis is, therefore, a phenomenon that controls the programmed cell death at a certain point in its life cycle. On the other hand, other organelles do not undergo changes, such as mitochondria, which remain intact. In the apoptosis pathway three different stages of apoptosis can be distinguished: *i*) “Initiation” phase, in which a stimulus determines the recruitment of different

patterns, which respond to a specific stimulus; *ii*) “Effective” phase, in which every signal of initiation is integrated by the cell to decide its destiny of life or death; *iii*) “Execution” final phase, in which different proteins are degraded and the DNA fragmented (Apraiz A et al. 2011). Apoptosis is involved in physiological processes such as remodelling tissues, organs and maintaining the number of cells. However, this process is also implicated in different pathologies; excessive apoptosis has been linked to neurodegenerative diseases and organ function dysregulation. On the contrary, a lack of apoptotic pathway activation has been found in hyperproliferative diseases, such as cancer (Favaloro B et al. 2012). Cells that undergo apoptosis in response to stress and damage can release morphogenetic and mitogenic signal proteins to stimulate tissue growth and repair (Bergmann A and Steller H 2010). Several studies have shown that the overexpression of some molecules inhibiting the apoptotic process, such as Survivin and XIAP (X-Linked Inhibitor of Apoptosis Protein), is associated to the increase of CDDP resistance (Asselin E et al. 2001; Ikeguchi M et al. 2002). Indeed, these proteins directly or indirectly influence the activity of caspases, which we know to be the effectors of the apoptotic process. In CDDP-resistant cells, the activation of caspases-3,-8 and -9 is often reduced, resulting in a downregulation of apoptotic signals (Asselin E et al. 2001; Ono Y et al. 2001). Apoptosis can be triggered by two main mechanisms: the binding of specific ligands to death receptors in the extrinsic pathway, and the cytotoxicity that initiates the intrinsic (or mitochondrial) pathway (**Figure 12**). These mechanisms are not clearly separated and both pathways converge in the activation of a series of specific caspases that lead to the disassembling of the cell (Galluzzi L et al. 2018; Parrish AB et al. 2013).

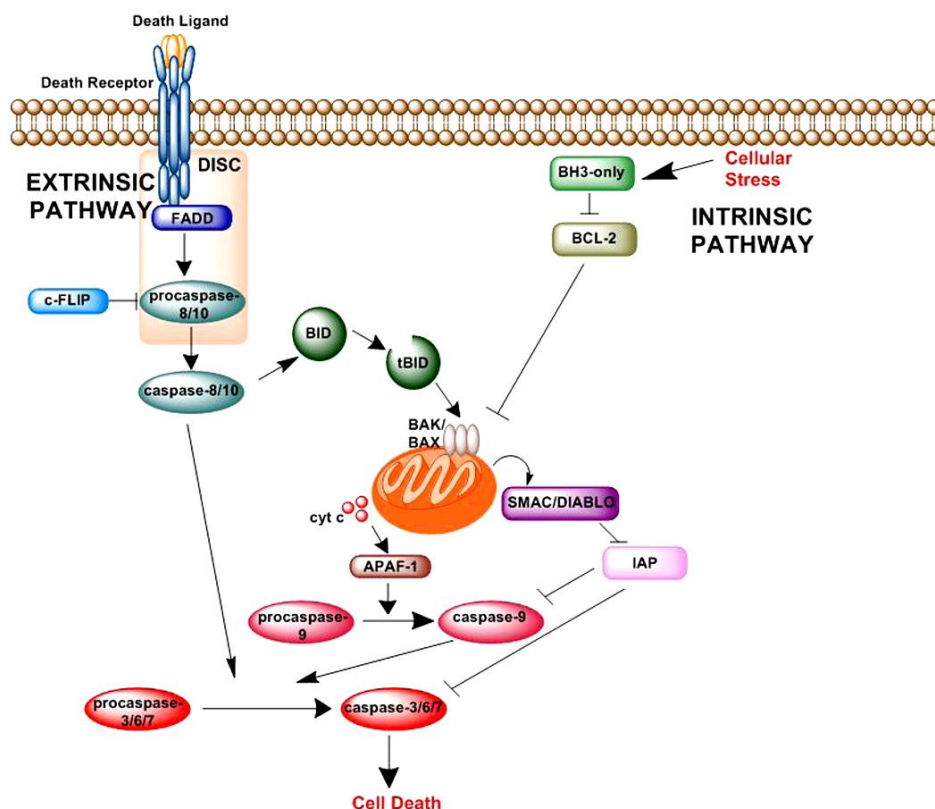


Figure 12. The intrinsic and extrinsic apoptotic pathway. The intrinsic pathway is triggered by cellular stress, while the extrinsic pathway is activated by death signals mediated by death ligands. Both pathways converge in the activation of a series of specific caspases that lead to cell death (Zaman S et al. 2014).

Intrinsic apoptotic pathway

Intrinsic apoptosis is a type of RCD caused by several microenvironmental stimuli including growth factor deletion, DNA damage, ER stress, ROS accumulation, microtubular alterations or mitotic faults (Brumatti G et al. 2010; Czabotar PE et al. 2014; Vitale I et al. 2017). The decisive step for intrinsic apoptosis is the irreversible mitochondrial outer MOMP and the consequent loss of the electrical potential of the inner membrane (Galluzzi L et al. 2016; Tait SE and Green DR, 2010). This pathway is finely regulated by pro-apoptotic and anti-apoptotic proteins of the Bcl-2 superfamily (Danial NN and Korsmeyer SJ 2004), a group of

proteins sharing one to four Bcl-2 homology (BH) domains (*i.e.* BH1, BH2, BH3, and BH4) (Czabotar PE et al. 2014; Shamas-Din A et al. 2013) and which control the permeability of the outer mitochondrial membrane (OMM). In response to apoptotic stimuli, MOMP is provoked by Bcl-2 associated X apoptosis regulator (Bax), and/or Bcl-2 antagonist/killer 1 (Bak1; best known as Bak), both of which contain four BH domains and a preserved transmembrane domain (Delbridge AR et al. 2016; Luna-Vargas MP and Chipuk JE 2016). The two proapoptotic factors, Bax and Bak, undergo structural changes, which lead to their activation: both proteins migrate to the mitochondria, where they form homodimers to expose dimer-dimer binding sites and introduce pores on the surface of mitochondria (Cory S and Adams JM 2002; Dewson G et al. 2009). Bax and Bak, containing a single BH3 domain, require the presence of some BH3-only proteins such as BIM (Bcl-2-interacting mediator of cell death), PUMA (p53-upregulated modulator of apoptosis) and BIDBH3 interacting domain death agonist to promote their activation by homo-oligomerization (Ren D et al. 2010). Other effects induced by Bax and Bak activation are the permeabilization of ER membranes and the consequent activation of the type 1 inositol triphosphate receptors (InsP3Rs) that induce the leakage of Ca^{2+} from ER to cytosol (Oakes SA et al. 2005).

MOMP can be antagonized by anti-apoptotic members of the Bcl-2 family, such as Bcl-2 itself, Bcl-2 like 1 (known also as Bcl-XL) that exert their effect inhibiting Bax and Bak and preventing their oligomerization and pore-forming activity (Barclay LA et al. 2015; Hardwick JM and Soane L 2013; O'Neill KL et al. 2016). This mechanism can occur either directly, upon physical sequestration at the OMM, or indirectly, following the sequestration of BH3-only activators.

MOMP induces, the opening of mitochondrial permeability transitional pores (MPTPs) located in the contact sites between the outer and inner membranes of the mitochondria, with the activation of the protein OPA1 (Optic atrophy 1) protein, a mitochondrial dynamic like GTPase (Tait SW and Green DR 2010). OPA1 is essential for preserving normal cristae structure and function, for maintaining the inner membrane organization and for protecting cells from apoptosis (Knowlton AA and Liu TT 2015). The dynamin-related protein OPA1, positioned on the inner mitochondrial membrane, protects against apoptosis by preventing the release of cytochrome c from the mitochondria (Frezza C et al. 2006). On the contrary,

the mitochondrial pathway is induced when the release of some molecules happens, *i.e.* cytochrome c, somatic (CYCS), which usually operates as an electron shuttle in the mitochondrial respiratory chain (Galluzzi L et al. 2012), and diablo IAP-binding mitochondrial protein (DIABLO; also known as second mitochondrial activator of caspases, SMAC) (Verhagen AM et al. 2000; Du C et al. 2000) which antagonize caspase inhibitory proteins (IAP) (Wu G et al. 2000; Srinivasula SM et al. 2001).

To note, MOMP, in the end, leads to the dissipation of the mitochondrial transmembrane potential ($\Delta\psi_m$), because of the respiratory impairment due by the loss of CYCS, and hence to the cessation of $\Delta\psi_m$ -dependent mitochondrial functions such as ATP synthesis and some forms of protein import (Schmidt O et al. 2010). In addition, when MOMP affects a restricted number of mitochondria, the consequent sublethal activation of caspases does not induce RCD but promotes genomic instability (Ichim G 2016).

The cytosolic pool of CYCS binds to apoptotic peptidase activating factor 1 (APAF-1) and pro-caspase-9 in a deoxy-ATP-dependent manner to form the complex known as apoptosome, which is responsible for caspase-9 activation (Jiang X and Wang X 2004) through the CARD domain (Hu Q et al. 2014; Riedl SJ and Salvesen GS 2007).

The active caspase-9 splits and cleaves caspase-3, -6 and caspase-7, which in turn activate the different intracellular substrates leading to morphological changes characteristic of apoptosis (Julien O and Wells JA 2017). Caspase-3 is responsible for the fragmentation of DNA in oligonucleosomal fragments of 50-300 kb, catalysing the inactivation of DFFA (DNA fragmentation factor subunit alpha) also known as ICAD (inhibitor of CAD), and initiates the catalytic activity of DFFB (DNA fragmentation factor subunit beta, or CAD, Caspase-activated DNase) (Nagata S 2000). Indeed CAD, in proliferating cells, is associated with its ICAD inhibitor; in apoptotic cells, however, caspase-3 cuts the inhibitor factor permitting the release of DNases (Sakahira H et al. 2015). Among caspase-3 substrates there is PARP-1, this protein possesses an N-terminal domain able to bind DNA thanks to the presence of a double zinc structure, called DBD (DNA Binding Domain), a nuclear localization signal, a C-terminal catalytic domain, and a “self-modifying domain” (Kim MY et al. 2005). The DBD binds with high affinity to single or double-stranded breaking sites and in the presence of low levels of DNA damage, PARP-1 acts as a survival factor, while in the presence of extensive damage it acts to promote cell death (Virag L and Szabo C 2002). Caspase-3

can inactivate the enzyme PARP-1, by a proteolytic cleavage between the residues of Asp214 and Gly215 of the damage repair enzyme, producing two fragments and so splitting the catalytic domain of 89 kDa from the DNA binding domain of 24 kDa (Los M et al. 2002). The p24 fragment can still bind DNA, but in the absence of the catalytic domain the protein is unable to act (Kim MY et al. 2005). Another target of caspase-3 is Gelsolin (GSN) which is a cytoskeleton-associated protein that regulates actin polymerization in the cell nucleus and can bind phosphatidylinositol 4,5-bisphosphate (PIP2). Gelsolin correlates cytoskeletal organization to signal transduction. An aberrantly regulation of Gelsolin has been observed in many tumour types, due to its implication in the promotion or inhibition of apoptosis depending on the pathological conditions and cell types (Wang PW et al. 2014).

Regulatory proteins of the intrinsic pathway, such as proapoptotic proteins of the Bcl-2 family, can promote also autophagy. The components of the autophagic system can also influence the way intrinsic apoptotic; for example, the Atg5 factor increases the susceptibility to permeabilization of mitochondria during treatment with DNA-damaging agents (Yousefi S et al. 2006). Furthermore, HDACs induce apoptosis in a series of cancer cells through the activation of the intrinsic mitochondria pathway by decreasing the expression of antiapoptotic proteins Bcl-2, Bcl-xl and improving the expression of proapoptotic proteins Bax and Bak (Bai LY 2010). Moreover, cytoskeletal actin also appears to be involved in the apoptotic pathway, as it would allow cytoplasmic proapoptotic proteins to translocate into the mitochondria via the cytoskeleton (Thomas SG et al. 2007).

Anoikis is indicated as a particular variant of intrinsic apoptosis, which is promoted by the loss of integrin-dependent attachment to the extracellular matrix (Paoli P et al. 2013). Generally, anoikis, preventing the anchorage-independent proliferation and the attachment to an improper matrix, is considered as an oncosuppressive process (Buchheit CL et al. 2012; Buchheit CL et al. 2014), indeed this mechanism prevent that cancer cells initiate and progress through the “metastatic cascade” (Galluzzi L et al. 2018).

Tumour cells can escape anoikis upon activation of the MAPK1, ERK2, caused by cellular aggregation and subsequent EGFR stabilization facilitated by Erb-B2 receptor tyrosine kinase 2 (ERBB2) (Rayavarapu RR et al. 2015), or by degradation of the negative ERK2 regulator BRCA1-associated protein (BRAP), which is favoured by coiled-coil domain containing 178 (CCDC178) (Hu X et al. 2017).

Extrinsic apoptotic pathway

Extrinsic apoptosis is an RCD modality induced by perturbations of the extracellular microenvironment (Strasser A et al. 2009) and it is triggered by the so-called death receptors (DRs). Death receptors include TNF (Tumor Necrosis Factor) receptor superfamily members and Fas cell surface death receptors *i.e.* FAS, CD95, and APO1 (Aggarwal BB et al. 2012; Dasari S and Tchounwou PB 2014; von Karstedt S et al. 2017). After the binding between receptors with their ligands such as TRAIL (TNF-related apoptosis-inducing ligand) ligand and FAS ligand (FASLG, CD95L, and APO-1), respectively, the subsequent formation of the Death Inducing Signaling Complex (DISC) occurs. Following this interaction, the receptors undergo a conformational change, necessary to attract cytoplasmic adaptive molecules, which expose in turn a DD: *i.e.* Fas-associated death domain (FADD) and TNFRSF1A associated via death domain (TRADD), which are required for the transmission of death signals (Dasari S and Tchounwou PB 2014).

Subsequently, this multiprotein complex triggers the activation of caspase-8 and 10 (Brenner D et al. 2015; Fu Q et al. 2016). The activation of caspase-8 in the DISC complex, in turn, determines the activation of caspase-3, which initiates the action of caspase-dependent deoxynuclease (Santin G et al. 2011). Most of the signals that inhibit caspase-8 act on its recruitment at the level of the DISC complex; for example the factor c-FLIP (FADD-like IL-1 β -converting enzyme-inhibitory protein) shows structural similarities with caspase-8 and this allows it to compete with it for the binding to specific sites and to replace itself in the complex DISC (Hughes MA et al. 2016; Kavuri SM et al. 2011).

Another mechanism of negative regulation of caspase-8 involves the recruitment of factors, such as IAP 1/2, which trigger survival signals and inhibit its activation (Gyrd-Hansen M and Meier P 2010).

Finally, the execution of apoptotic cascade can be initiated by caspase-3 and/or caspase-7 which are activated by caspase-8 (Barnhart BC et al. 2003). Caspase-8 can activate the cytoplasmic BH3-only protein Bid, which is a mediator of the apoptosis pathway following death receptor activation (Huang K et al. 2016). Death receptor activation by Fas or TRAIL, induced the cleavage of Bid (tBid formation) within this complex. tBid then shifted to separate mitochondria-associated complexes that contained other Bcl-2 family members (Schug ZT et al. 2011). Then the formation of the pore on the outer mitochondrial membrane allows the cytoplasmic release of factors

responsible for the intrinsic pathway (such as cytochrome c), suggesting a “cross-talk” between the intrinsic and extrinsic pathways (Huang K et al. 2016).

It was observed that HDACi increases signalling through the extrinsic apoptotic pathway according to several mechanisms that include cell surface receptors upregulation of death, and/or ligand expression, reduction in c-FLIP cytoplasmic levels and increased recruitment of DISC components. The effects of HDACi on the extrinsic pathway may increase the sensitivity of many types of tumour cells to activators of this pathway, such as TRAIL. For example, it has been observed that HDACi increases the expression of TRAIL-R2 and causes a decrease in the expression of c-FLIP in human malignant tumour cells, which results in the rapid production of DISC in the presence of TRAIL and the activation of caspases-8 (Carlisi D et al. 2009; Lagneaux L et al. 2007; VanOosten RL et al. 2005).

1.4.2 Autophagy

Autophagy is a dynamic and highly conserved process from eukaryotic microorganisms to humans. It is an energy-dependent cellular pathway that responds to different types of stress and cellular condition with the goal of self-preservation (Claudiu A et al. 2015). This process predominantly occurs during strong changes in environmental conditions, such as nutrient deprivation, oxidative stress and ultraviolet radiation (Levine B and Kroemer G 2008). In addition, autophagy can play an essential role in the multitude of physiological processes including cell differentiation and development, cellular quality control, tumour suppression, innate and adaptive immunity, energy homeostasis, the extension of life span and cell death (Deretic V et al. 2013; Puri P and Chandra A 2014). Autophagy promotes cell survival through the clearance of damaged organelles and aggregated proteins, provides for the elimination of intracellular pathogens and the recycling of essential macromolecules during nutrient limiting periods (Deretic V et al. 2015; Claudiu A et al. 2015). The involvement of autophagy in these different processes attributes a dual role to this mechanism. Indeed, if on the one hand, it represents a cell survival strategy, on the other, if induced in an excessive way, it can result in the death of the cell, called programmed type II cell death, which differs from the other forms of cell death (Galluzzi L et al. 2018). This double function of autophagy is also related to a wide range of human disorders including autoimmune diseases, neurodegeneration, infections, inflammatory processes, and even neoplasms, in which autophagy is often associated with chemoresistance (Deretic V et al. 2015; Grimaldi M et al. 2019; Jiang P and Mizushima N 2014).

For years, autophagy has been considered a non-selective degradation pathway within the cell, but recent evidence has shown that specific stimuli active selective types of autophagy to identify structures for lysosomal turnover (Farre JC and Subramani S 2016).

Autophagy can be classified into three groups: macroautophagy, microautophagy and chaperone-mediated autophagy (CMA), these mechanisms differ from each other for transport tools, for the specificity of the material to be degraded and for regulation, playing a different role in the ability to adapt to environmental changes (Yang Z and Klionsky DJ 2010; Yoshii SR and Mizushima N 2017).

Macroautophagy

Macroautophagy, usually referred to as simple autophagy, compared to the other two forms, is the predominant type and the most investigated process. The first information on macroautophagy derives from initial genetic studies on the vacuole system of the yeast *Saccharomyces cerevisiae*, akin to the lysosomal system of mammals (Huang WP and Klionsky DJ 2002). This process involves the turnover of aggregates of cytosolic proteins and damaged organelles, inside lysosomes, through the formation of a double membrane structure, known as autophagosome (Nixon RA 2013).

Macroautophagy begins with the formation of a pre-autophagosomal structure, called phagophore, which extends from both sides, and closes around the target, which must be eliminated, leading to the formation of autophagosome (Mizushima N et al. 2008), which is able to incorporate all the cytoplasmic components, including the organelles. The latter then uses a microtubular trace that allows it to melt and fuse with lysosomes, to form vesicles, called autolysosomes, within which hydrolytic enzymes degrade internalized substrates (Xie R et al. 2010). Autophagosomes can also merge with endosomes and with major histocompatibility complex (MHC) class II (Schmid D et al. 2007). This process takes place in all eukaryotic cells and is highly regulated by the action of various kinases, phosphatases and guanosine triphosphatases (Klionsky DJ and Emr SD 2000). Autophagy can be divided into several distinct stages: induction; vesicle nucleation; vesicle expansion and completion; retrieval; docking and fusion; breakdown and efflux (Amelio I et al. 2011; Harris and Rubinsztein 2012) (**Figure 13**).

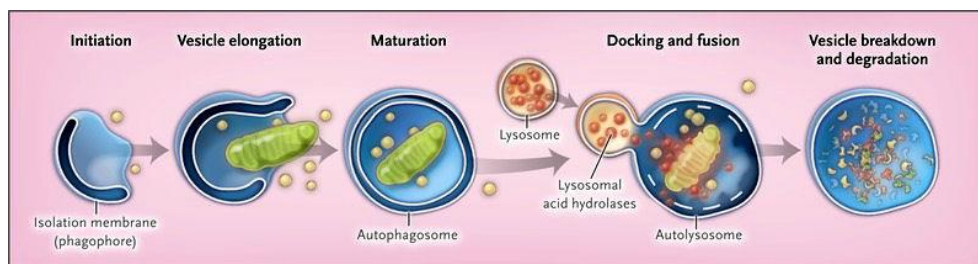


Figure 13. Steps of macroautophagy. Macroautophagy is characterized by well-defined phases, which lead to winding in a double-membrane vesicle of the material to be degraded, which will finally be demolished to obtain useful substances for the cell (Choi AM et al. 2013).

These steps are performed by proteins encoded by a group of autophagy-related genes (ATG). Atg proteins are grouped according to their respective functions and are divided into five subgroups: the Atg1/Ulk1 protein kinase complex, the Atg9-Atg2-Atg18 complex, the Vps34-Atg6/beclin1 class III complex phosphoinositide 3-kinase, Atg12 conjugation system and the Atg8/LC3 conjugation system (lipidation) (Ariosa AR and Klionsky DJ 2016). The formation of autophagosomes occurs at the phagophore assembly site (PAS) where the key proteins involved in the formation of the autophagosome are localized (Tooze SA and Yoshimori T 2010; Rubinsztein DC et al. 2012). However, in mammalian cells, the existence of PAS remains unclear, since more assembly sites for autophagosomes have been detected, including ER, Golgi, endosomes, and mitochondria (Tooze SA and Yoshimori T 2010; Weidberg H et al. 2011). Several studies suggest that the ER is crucial for autophagosome formation. The cisterns of the ER are often associated with the development of autophagosomes and from the analysis of electronic tomography direct connections between ER and autophagosomal membranes have been observed (Hayashi-Nishino M et al. 2009; Yla-Antilla P et al. 2009).

The activity of the Atg1 kinase in a complex with Atg13 and Atg17 is required for the formation of the phagophore in yeast (Klionsky DJ 2007).

Ulk-1 and Ulk-2 (Unc-51 Like Kinase), are a mammalian homologue of Atg1, the ULK complex, formed by Ulk1/2, Atg13, Atg101, and a scaffold protein FIP200 (Focal Adhesion Kinase), plays an important role in the initiation pathway of macroautophagy.

In nutrient-rich conditions, the serine-threonine kinase mTOR (Mammalian Target of Rapamycin), a mechanistic target of rapamycin, acts together with other proteins of the mTORC1 complex (mTOR Complex 1) to inhibit autophagy, through direct interaction with the Ulk1 complex (He C and Klionsky DJ 2009). On the contrary, in response to stressful conditions, such as fasting, mTOR is inhibited and dissociates from the ULK1 complex (Wong PM et al. 2013), which activates and catalyses the phosphorylation of Atg13, FIP200, and ULK1 itself, which is essential to initiate the macroautophagic process (Kim J et al. 2011). Furthermore, this complex can also be activated by AMPK (a protein kinase activated by AMP) through a mechanism of direct phosphorylation, at the level of serine residues at positions 317 and 777, which leads to the induction of autophagy in response to deprivation of glucose (Kim J et al. 2011; Egan DF et al. 2011).

Downstream of ULK1, the PI3K kinase complex (Phosphatidylinositol 3-class kinase III) intervenes, which assembles thanks to the action of the Beclin-1 factor, which acts as a platform through the bonding of different cofactors, such as Barkor (Beclin -1-Associated Autophagy-Related Key Regulator), p150 and UVRAG (UV Irradiation Resistance-Associated Gene) (Sun et al. 2008; Itakura E and Mizushima N 2009). This resulting complex plays an essential role in the nucleation and assembly of the initial phagophore membrane (Jaber N et al. 2012; Puri P and Chandra A 2014). The phosphorylation of the ULK1 complex can therefore promote the phagophore nucleation, mediated by the PI3K complex (Suzuki K et al. 2007), probably through the phosphorylation of key molecules, such as AMBRA (Activating Molecule in Beclin-1-Regulated Autophagy Protein 1) (Di Bartolomeo S et al. 2010) and Beclin-1 (Russell RC et al. 2013). This phase is followed by the expansion and completion of the vesicles. The membranes assemble and then seal themselves forming the autophagosome, two conjugation systems similar to ubiquitin are involved: the Atg12-Atg5 conjugation system and the LC3-PE system, between the LC3 (Microtubule Associated Protein 1 Light Chain 3) factor and the phosphatidylethanolamine (PE) (Puri P and Chandra A 2014). The first ubiquitin-like conjugation system is Atg12-Atg5: Atg7 (E1-like activating enzyme) activates the ubiquitin-protein Atg12 and transfers it to Atg10; finally, Atg10 (E2-like activating enzyme) covalently links the C-terminal glycine residue of Atg12 to a lysine residue of Atg5 (Kuma A et al. 2002). The Atg12-Atg5 conjugate possesses similar activity to the ligase facilitating the conjugation of Atg8 to the autophagic membranes. Atg12-Atg5 forms a constitutive complex of approximately 350 kDa, with the coiled-coil dimeric protein Atg16, which is essential for the biogenesis of autophagosome, but not necessary for the enzymatic activity of Atg12-Atg5 (Hanada T et al. 2007; Kuma A et al. 2002). This complex serves as the basis for stimulating the second conjugation reaction, which involves the LC3 factor. LC3 is processed and converted into a soluble LC3-I, immediately after its synthesis, by the enzyme Atg4, a cysteine protease that leaves a glycine residue uncovered in the C-terminal position; this is a target site for a thioester bond to a cysteine residue of Atg7, followed by transfer to Atg3 and finally by the establishment of an amide bond with PE (Kaufmann A et al. 2014; Romanov J et al. 2012). Thus LC3-II is localized at the level of the inner and outer membrane of the phagophore and is essential for the

biogenesis and closure of the autophagosome membrane (Nagatogawa H et al. 2007).

The autophagosome then fuses with the lysosomes to form autolysosomes, with consequent degradation of the vacuolar content by lysosomal hydrolases. Recent evidence indicates that autophagy is a more selective process than initially thought. Selective autophagy depends on the binding of the substrates with the inner surface of the growing phagophore, indicated as cargo, a process mediated by adapter proteins associated with both the substrate and the lipidated LC3, anchored to the phagophore.

The autophagic adapter protein p62, also known as Sequestosome 1 (SQSTM1), is a ubiquitously expressed protein and within cells it is distributed not only in the cytoplasm, but it is also localized in the nucleus, as well as in autophagosomes and lysosomes; in fact, in the presence of different stress factors, it is able to move substrates to be degraded within such vesicles, such as ubiquitinated proteins, protein aggregates, damaged mitochondria, and bacteria-infected cells (Katsuragi Y et al. 2015). Furthermore, p62/SQSTM1 acts as a scaffold protein for the transduction of different signals, through the interaction with other proteins, such as RIP (Receptor-Interacting Protein), TRAF6 (TNF Receptor-Associated Factor 6), ERK (Extracellular Signal-Regulated Kinase) and PKC (Protein Kinase C) (Jin Z et al. 2009; Moscat J et al. 2006). P62/SQSTM1 can polymerize through an N-terminal PB1 domain and can interact with ubiquitinated proteins through the C-terminal UBA domain. Furthermore, p62/SQSTM1 binds directly to the LC3 and GABARAP (Gamma-aminobutyric acid receptor-associated protein) family proteins via a specific sequence pattern. Furthermore, this protein is selectively degraded and acts to recognize ubiquitinated protein aggregates, linking them to autophagosomes, a process necessary for lysosomal degradation (Chen S et al. 2014; Liu WJ et al. 2016) (**Figure 14**).

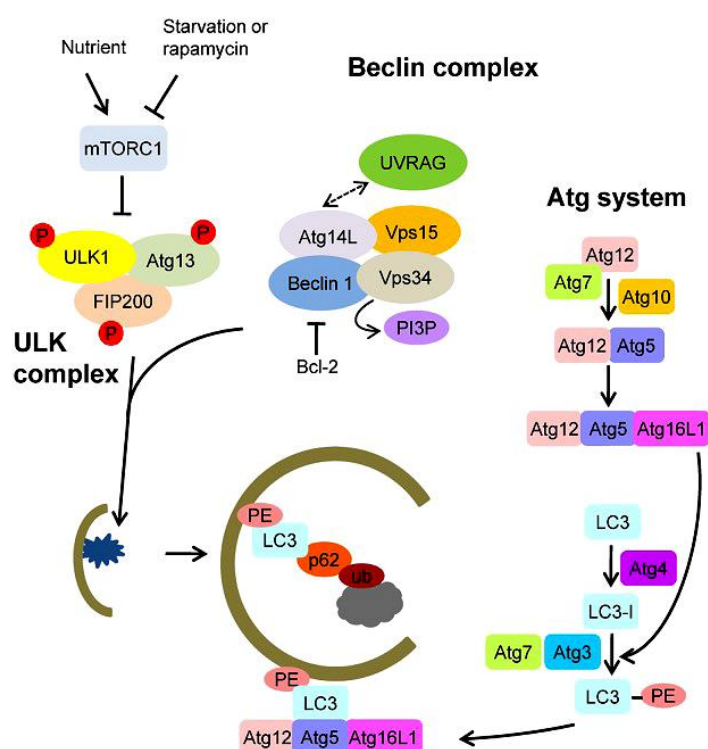


Figure 14. Molecular pathway of macroautophagy. Steps of autophagy induction and autophagosome formation (Quan W and Lee MS 2013).

Finally, in the process of fusion of autophagosomes with lysosomes, Rab proteins, monomeric GTPases that are activated following the action of a GEF (Guanine Nucleotide Exchange Factor) factor, which facilitates the replacement of GDP, are involved to form the polysomal linked to them with a GTP, which will then be again and rapidly hydrolyzed in GDP with the help of a GAP protein (GTPase Activating Protein) (Ao X et al. 2014). In addition, the autophagosome can form an amphisome, associating itself with the multivesicular body produced by an endocytic vesicle containing exogenous substances to be eliminated, called endosome, before melting with the lysosome, or performing this last step directly for degradation of the substrates; these processes are regulated in a similar way, also thanks to the intervention of common factors, such as the ESCRT (Endosomal Sorting Complexes Required For Transport) (Metcalf D and Isaacs AM 2010). Once

the macromolecules have been degraded within lysosomes, the monomeric units obtained, such as amino acids, can be exported to the cytoplasm for reuse (Sagnè C et al. 2001). Pro-inflammatory cytokines, *i.e.* IL-1 β (interleukin 1 beta), INF- γ (interferon-gamma) (Harris J et al. 2007; Singh SB et al. 2010) and TNF α (Mostowy S et al. 2011), can also stimulate autophagy, while it is inhibited by cytokines T helper 2, such as IL-4 (interleukin 4) and IL-13 (interleukin 13) (Harris J et al. 2007). The metabolites generated in these proteolytic processes, which include the amino acids, are actively removed by the autolysosomes, reported in the cytosol and reused by the cell (Ariosa AR and Klionsky DJ 2016).

Microautophagy

Microautophagy has been described in yeast but has not yet been well characterized in eukaryotic cells. Microautophagy works through direct invagination of lysosomes, leading to the formation of single membrane-limited vesicles (Li WW et al. 2012). The lysosome membrane is itself an active part of the process and there is no formation of intermediate vesicles, such as autophagosomes. Therefore, microautophagy does not depend on the canonical autophagic machinery (Li WW et al. 2012; Sahu R et al. 2011).

Microautophagy works in maintaining the organelle size, the composition of the membranes and promotes cell survival under nitrogen restriction conditions. This process can be induced by nitrogen starvation and rapamycin (Li WW et al. 2012); it has also been shown that this catabolic process is mainly performed by the cell to digest peroxisomes, the so-called “pexophagy” (Veenhuis M et al. 2000).

Like macroautophagy, microautophagy is induced through the TOR signalling complex and is also controlled by a second regulator, the EGO complex. This complex is composed of three proteins: Ego1, Ego3 and GTPase Gtr2 (Dubouloz F et al. 2005). Another important protein crucial for microautophagy is the VTC complex, composed of four proteins Vtc1, Vtc2, Vtc3, and Vtc4. This complex is in the vacuolar membrane, but also in other cell membranes (Uttenweiler A et al. 2007).

The mechanisms that drive the profound changes in lysosomal structure during invagination and cleavage of the nascent microautophagic vesicle are still unknown (Sattler T and Mayer A 2000).

Chaperone-mediated autophagy (CMA)

The third type of selective autophagy for the degradation of a subgroup of cytosolic proteins has been called chaperone-mediated autophagy (CMA) (Tekirdag K and Cuervo AM 2018; Wong E and Cuervo AM 2010). For this degradation process, vesicular trafficking is not required, therefore it differs from macroautophagy and microautophagy. The pathway is stress-activated such as prolonged starvation, exposure to toxic compounds or oxidative stress. The mechanisms of chaperone-mediated autophagy are like the mechanisms of protein import into mitochondria, chloroplasts, and ER (Cuervo AM and Wong E 2014; Majeski AE and Dice JF 2004). All the proteins internalized in lysosomes through CMA contain in their amino acid sequence a pentapeptide motif, KFERQ, which is necessary and enough for their targeting to lysosomes (Kaushik S and Cuervo AM 2012; Tekirdag K and Cuervo AM 2018).

This pentapeptide has been identified as a binding site for a cytosolic chaperone and this binding is necessary for lysosomal degradation of the substrate protein (Cuervo AM and Wong E 2014).

In the CMA pathway, cytoplasmic proteins are segregated and degraded within lysosomes in a highly selective manner. This selectivity is obtained from the heat shock protein of 70 kDa (HSC70), which identifies and transports the individual protein substrates one at a time to the surface of lysosomes (Puri P and Chandra A 2014). The substrate-chaperone protein complex is then bound to the LAMP-2A receptor (Lysosomal-Associated Membrane Protein type 2A), located on the lysosome membrane, and at this stage, LAMP-2A acts as a monomer. Subsequently, the binding of the substrate to this receptor leads to LAMP-2A multimerization, with the help of the lysosomal protein HSP90, since it is thought that the association of multiple LAMP-2A molecules can create a discontinuity in the membrane to facilitate the transport of the substrate. At this point, the substrate protein is unrolled and translocated in the lysosome lumen, thanks to the LAMP-2A complex, and with the help of a specific chaperone present in the lumen, lysosomal HSC70, the substrate is degraded by lysosomal proteases. Finally, the LAMP-2A multimer is disassembled and degraded for the subsequent chaperone-mediated autophagy cycle (Kaushik S and Cuervo AM 2012).

This finely regulated process (Cuervo AM and Wong E 2014) is maintained at basal levels and is activated following prolonged fasting and other types of stress. In fact, this mechanism represents an alternative energy source and a

control system to remove damaged proteins following various types of stress (Ravikumar B et al. 2010). Moreover, the capability of CMA to selectively degrade intracellular proteins involves in important functions such as regulation of transcription by the elimination of several transcription factors or control of proteins involved in the cell cycle (Tekirdag K and Cuervo AM 2018).

1.4.3 Necrosis

The type III cell death or necrosis consists of cellular swelling, loss of organelle homeostasis and integrity, rupture of the membrane and release of cellular contents into the extracellular space (Davidovich P et al. 2014). It is therefore not surprising that in this situation, the cells surrounding the necrotic cells are strongly influenced by their dying neighbours, triggering various responses such as inflammation and additional cell death (Fuchs Y and Steller H 2015). The excess of DNA damage produced by genotoxic stresses, such as oxidizing and alkylating agents, overactive PARP polymerase which operates by cutting coenzyme NAD⁺ and transferring ADP-ribose motifs to carboxyl groups of nuclear proteins. This depletes the reserves of NAD⁺/ATP and causing a metabolic catastrophe and the activation of the necrotic pathway (Van Wijk SJ and Hageman GJ 2005).

For several years necrosis has been considered a univocal form of ATP-independent cell death, referred to as a random and uncontrolled process that leads to “accidental” cell death. In the last decade, recent data have discovered a caspase-independent process that resembles necrosis mechanisms, suggesting that necrosis can occur in a highly regulated and genetically controlled manner (Vanden Berghe T et al. 2014).

1.4.4 Other type of cell death

In the last decade, numerous studies have proved the existence of different pathways of regulated necrosis, exhibiting the same features of non-regulated necrosis described above (Galluzzi et al. 2018; Vanden Berghe T 2014). Several molecular mechanisms characterise these processes, identifying different forms of regulated necrosis *i.e.* necroptosis, ferroptosis, oxytosis, parthanatos, ETosis, NETosis, pyronecrosis, and pyroptosis (Vanden Berghe T et al. 2014).

Necroptosis

Necroptosis is a type of RCD activated by alterations of extracellular or intracellular homeostasis detected by specific death receptors, including FAS and TNFR1 (Degterev A et al. 2008; Galluzzi L et al. 2014) or pathogen recognition receptors (PRRs), including TLR3, TLR4, and Z-DNA binding protein 1 (ZBP1) (Upton JW et al. 2010; 2012). This process takes its name from its morphological similarity with necrosis. Indeed necroptosis, just like necrosis, is characterised by cell swelling and rupture of the plasma membrane, with concomitant release of the cell contents in the extracellular environment, aspects that make it clearly distinct from apoptosis (Degterev A et al. 2005). The lytic nature of necroptotic cell death led to the formulation of a hypothesis according to which this process triggers inflammatory responses *in vivo*. This process is probably mediated by the release of DAMPs (Danger-Associated Molecular Patterns), a class of molecules of which release by damaged cells is read as a danger signal, and which may evoke a response from immune cells (Krysko DV et al. 2012). However, different data in the literature are in contrast (Kearney CJ et al. 2015).

Necroptosis is mediated by death receptors, such as Fas, TNFR1/2, TRAIL-R1/2, DR3 and DR6, and by their ligands, such as FASL, TNF, TRAIL, as well as by interferons, Toll-like receptors, intracellular DNA and RNA sensors, and may also from other mediators (Pasparakis M and Vandenabeele P 2015; Vandenabeele P et al. 2010). It has been added to the list of receptors capable of inducing necroptosis TAK1 (Transforming Growth Factor-Beta-Activated Kinase 1), which is activated through a set of different intra- and extracellular stimuli (Mihaly SR et al. 2014).

The most known pathway begins following the binding of TNF- α with its TNFR1 receptor, which triggers allosteric changes in the intracellular portion (Andera L 2009), and thus recruits a series of proteins containing death domains, including TRADD and FADD, and several E3-ligases, such as TRAF2/5 (TNF Receptor Associated Factor 2/5) and cIAP1 and cIAP2; all these proteins form the complex I (Wertz IE and Dixit VM 2008). TNFR1 also recruits the protein kinase RIP1 (Receptor-Interacting Protein 1), which is polyubiquitinated at the level of a lysine residue at position 63 by TRAF2/5, cIAP1 and cIAP2 (Mahoney DJ et al. 2008). This allows it to activate the IKK (I κ B Kinase Complex) and NEMO (NF- κ B Essential Modulator) complex, triggering the pro-survival pathway of NF- κ B. Conversely, when RIP1 is deubiquitinated by the action of the CYLD (Cylindromatosis) enzyme, it is

released into the cytoplasm and forms the complex II, with TRADD, FADD, the RIP3 kinase (Receptor-Interacting Protein 3) and caspase-8 (Hitomi J et al. 2008). Caspase-8, in its active form, cleaves RIPK3 and induces apoptosis through the caspase cascade; on the contrary inhibition of caspase-8 activity by FLIP, a catalytically inactive homolog of caspase-8 that can combine into complex II, can block RIPK1 cleavage and induce necroptosis (Feng S et al. 2007). The necrosome recruits, phosphorylates and consequently activates the MLKL, an effector protein that acts downstream of RIPK1 and RIPK3 (Sun L et al. 2012), which undergoes a conformational change and leads to the formation of a trimer and the exposure of a domain in N-terminal position, formed by four packed helices (Murphy M et al. 2013). This motif interacts with phosphatidylinositol phosphate (PIP), inside the plasma membrane, triggering the final stage of necroptosis, which leads to destruction of the membrane and consequent loss of ionic homeostasis, swelling and rupture of the cell, with dispersion of cellular content in interstitial space, and therefore cell death (Pasparakis M and Vandenabeele P 2015; Wang H et al. 2014) (Figure 15).

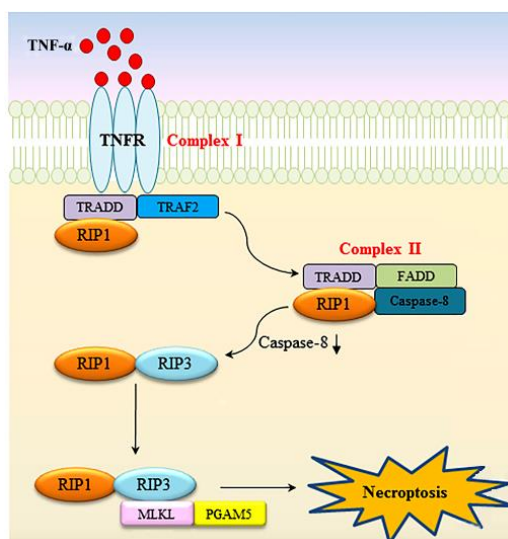


Figure 15. Necroptosis pathway. Upon TNF α binding to its receptor, TRADD, TRAF2, and RIP1 are recruited to form complex I. In turn, TRADD and RIP1 are bound to FADD and caspase-8, eventually forming the cytoplasmic complex II. In situations where caspase is inactivated, RIP1 interacts with RIP3 to trigger consecutive downstream signalling events, including the recruitment of MLKL, which transmit cytosolic death signals (Cho YS and Park HL 2017).

Regarding the regulation of necroptosis, IAP proteins also play an important function in its activation. They are ubiquitin-ligases E3, which play a key role in numerous cellular processes, able to mediate the proteasome-dependent degradation of the active RIPK1/3 complex, thus blocking the execution of necroptosis (Feoktistova M et al. 2011; Moulin M et al. 2012).

Recently, further regulators of necroptosis have been described, such as Ppm1 phosphatase, which directly dephosphorylates RIPK3, thus reducing necroptosis (Chen W et al. 2015); or on the contrary, it has been shown that a complex formed by chaperon proteins, such as HSP90 and CDC37, is able to associate with RIPK3 and enhance its activation (Li D et al. 2015).

Current research suggests that necroptosis acts a major role in cancer as well as numerous neurodegenerative diseases. Necroptosis is involved in metastasis formation; therefore, inhibition of the necroptotic pathway could limit tumour growth (Najafov A et al. 2017). Since apoptotic death of damaged or transformed cells is the key mechanism of tumour suppression, but the evasion of apoptosis is a classic feature of cancer, it could be interesting to find if some chemotherapeutic agents that cause DNA damage can trigger death by necroptosis (Tenev T et al. 2011).

Caspase independent cell death

This pathway is mediated by AIF (Apoptosis-Inducing Factor), a flavoprotein with NADH-oxidase activity containing a flavin adenine-binding domain of nucleotide (FAD-binding domain), located at the level of the mitochondrial intermembrane space and that is released into the cytosol during the execution of PCD (Candè C et al. 2002). AIF has a local redox function that is essential for optimal oxidative phosphorylation and efficient antioxidant defence (Modjtahedi N et al. 2006). The increase in mitochondrial permeability following specific apoptotic signals is mediated by the MPTP, allowing the release of apoptogenic effectors, such as AIF, which is released into the cytosol and subsequently transported into the nucleus (Bano D et al. 2010). In the cytosol, truncated AIF physically interacts with several proteins, such as HSP70 and cyclophilin A (CypA) (Bano D and Prehn JHM 2018). Once in the nucleus, AIF interacts directly with nuclear DNA and determines chromatin condensation, large-scale DNA fragmentation and cell death (Modjtahedi N et al. 2006). Furthermore, it was also shown that, in late apoptosis, AIF returns from the nucleus to the cytoplasm (Bottone MG et al.

2009; Scovassi AI et al. 2009), hypothesising that AIF could be degraded during this phase or re-synthesized in mitochondria (Bottone MG et al. 2009).

Recent studies have shown that AIF is involved in a caspase-independent cell death, which is known as parthanatos (Bano D and Prehn JHM 2018).

Parthanatos does not require the contribution of caspases for its execution but is mechanistically dependent on the nuclear translocation of the AIF. The time course of this type of cell death is related to the rapid activation of PARP-1 and other biochemical events such as synthesis and accumulation of PAR polymer, mitochondrial depolarization, and nuclear AIF translocation as describe above (Fatokun AA et al. 2014). In contrast to apoptosis, parthanatos does not promote the apoptotic bodies formation and it produces large-scale DNA fragmentation compared to small-scale DNA fragmentation observed in apoptosis (Wang Y et al. 2009).

As occurs in necrosis, parthanatic cell death produces a loss of cell membrane integrity, but without cell swelling (Wang H et al. 2004). Parthanatos and necroptosis may be considered two examples of regulated or programmed necrosis, while the co-involvement of PARP-1, PAR, and AIF, which is absent in other forms of programmed or regulated necrosis, still discriminates parthanatos from other types of cell death (Fatokun AA et al. 2014; Galluzzi L et al. 2018). To date, some data implicate PARP damage repair, and so parthanatos, in the pathogenesis of several human diseases such as cancer. To avoid the expression of this phenomenon, PARP blockers have been used as a strategy to avoid PARP hyperactivation and therefore parthanatos induction. The rationale for this use is that sustained inhibition of PARP in cancer cells promotes their death by blocking their DNA repair machinery needed for survival (Fatokun AA et al. 2014).

Lysosome-dependent cell death

The permeabilization of the lysosomal membrane, called LMP (Lysosomal Membrane Permeabilization), represents another process capable to positively regulate apoptosis (Foghsgaard L et al. 2001; Galluzzi L et al. 2018). LMP results from different signals, such as activation of death receptors, presence of ROS, ultraviolet radiation, proteasome inhibition, deprivation of growth factors and p53 activation (Appelqvist H et al. 2013; Serrano-Puebla A and Boya P 2016). Following an initial stimulus, the death

signals are transmitted to the lysosome in various ways, including through factors, such as Bax and caspase-8, following the activation of death receptors; or in the case of p53 activation, through the lysosome-associated apoptosis-inducing protein (Boya P and Kroemer G 2008; Chen W et al. 2005). Following a partial or total permeabilization of the membrane, lysosomes release hydrolases, such as cathepsins, in the cytoplasm, which can activate apoptosis through the caspase-dependent or independent pathways, optional involvement of MOMP, depending on the type of cells, in the context of lethal signal, the quantity of cathepsins released by the lysosome and the relative abundance of cathepsin inhibitors (Foghsgaard L et al. 2001).

Lysosomal activity is essential to maintain cellular homeostasis, in contrast, lysosomal dysfunction has been implicated in various disease conditions, including lysosomal storage diseases (LSDs), neurodegeneration, autoimmune diseases, and cancer. To better understand the pathological consequences of lysosome-dependent cell death (LDCD), lysosomes may constitute important novel therapeutic targets to blockade of metabolic dysfunctions and to treat human disease (Serrano-Puebla A and Boya P 2016; Wang F et al. 2018).

1.5 The role of calcium homeostasis and cytotoxicity

Calcium (Ca^{2+}) is an ion, called “the universal messenger” due to its property to be the most widespread transduction signal present in cells and its cytosolic concentration is about 20 000 times lower (100 nM) than extracellular concentration (2 mM) (Machaca K 2011; Parkash J and Asotra K 2010). Ca^{2+} takes part in many physiological processes *i.e.* increased bone mass, muscle contraction, blood coagulation, differentiation and cell death, immune response and enzymatic activation (Mori M et al. 2014). Especially at the neuronal level, Ca^{2+} is important for neurotransmitter release, synaptic plasticity, gene expression as well as for neuronal death (Calvo M et al. 2015; Segal M and Korkotian E 2016).

Ca^{2+} permeates through the membrane by the presence of several ion channels, which are subtyping in two superfamilies of Ca^{2+} channels: the channels of the plasma membrane, through which the extracellular Ca^{2+} enters the cell, and the intracellular channels that allow the release of Ca^{2+} from the intracellular stores. The main intracellular Ca^{2+} store is the smooth ER which has a Ca^{2+} -ATPase called SERCA (Sarco-Endoplasmatic Reticulum Calcium ATPase) whose function is to sequester the Ca^{2+} inside the cisterns (Manjarrés IM et al. 2010; Marchi S and Pinton P 2016). In addition to the smooth ER, mitochondria also play an important role in the Ca^{2+} uptake, which is performed thanks to the presence of the MCU system (Mitochondrial Calcium-Uniport) (Giorgi C et al. 2012; Mallilankaraman K et al. 2012). The action of this mechanism is counteracted by mitochondrial $\text{H}^+/\text{Ca}^{2+}$ exchanger (mHCX) and $\text{Na}^+/\text{Ca}^{2+}$ exchanger (mNCX) both situated in the inner membrane, while the permeability of the outer membrane is ensured by overexpression of the VDACs (Voltage-Dependent Anion Channel) (Rizzuto R et al. 2012).

To prevent cell damage induced by intracellular Ca^{2+} accumulation, there are several mechanisms of regulation such as PMCA, which pumps Ca^{2+} out of the cell (Nedergaard M et al. 2010), anti- $\text{Na}^+/\text{Ca}^{2+}$ proteins that are located on the plasma membrane and on the mitochondrial membrane, which allow Ca^{2+} transport by the electrochemical gradient of Na^+ (Gleichmann M and Mattson MP 2011) (**Figure 16**).

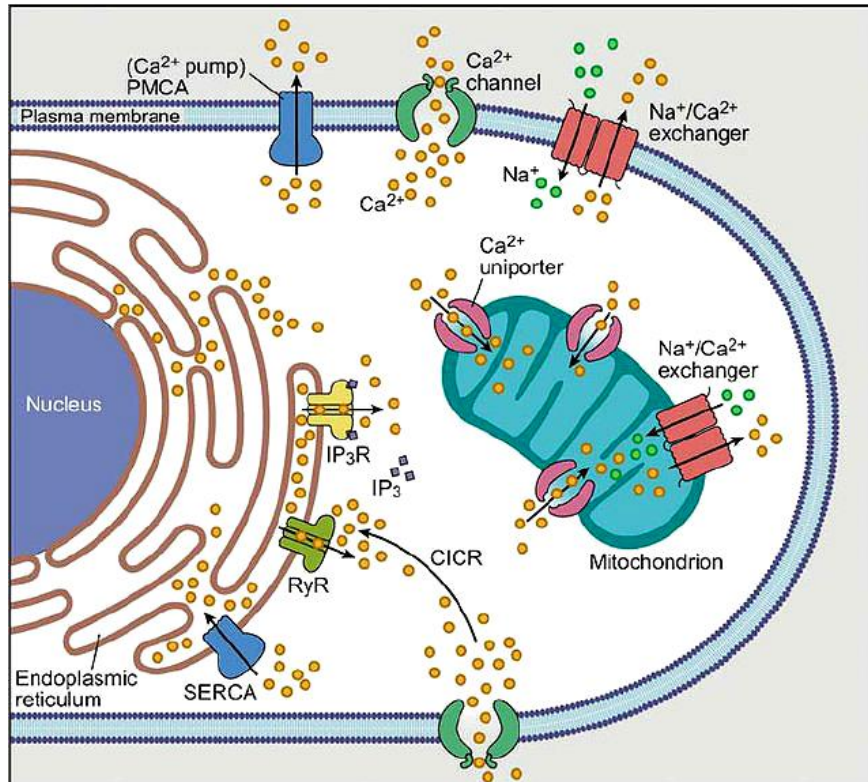


Figure 16. Calcium homeostasis in normal cells. Ca²⁺ concentration in the cytosol is normally maintained at 10-100 nM, to preserve this value, several mechanisms of regulation are involved such as endoplasmic reticulum (ER), and protein binding. Physiological increases of cytosolic Ca²⁺ take place by plasma membrane Ca²⁺ channels, the release of Ca²⁺ from the ER, upon binding of inositol trisphosphate (IP₃) to the inositol trisphosphate receptor (IP₃R) (Dong Z et al. 2006).

Another homeostatic mechanism is represented by the chelation of cytosolic free Ca²⁺ operated by the Calcium Binding Proteins (CBPs) (Yáñez M et al. 2012). The concentration of intracellular Ca²⁺ can increase following its massive access from the extracellular space, following the opening of voltage-gated calcium channels (VGCCs), also known as voltage-dependent calcium channels (VDCCs), or through the NMDA receptor, located on the postsynaptic membrane. Other channels are involved in Ca²⁺ homeostasis such as the non-voltage-gated channel P2XRs (purinergic ionotropic receptor families) and the transient receptor potential (TRP) channels, which mediate the influx of Ca²⁺ in response to several stimuli (Burnstock G and Di Virgilio

F 2013; Marchi S and Pinton P 2016; Montell C 2005). TRP channels modulate ion driving forces, the Ca^{2+} and Mg^{2+} transport machinery in the plasma membrane, where most of them are located. TRP channels play an important role in the mechanism known as SOCE (Store-operated calcium entry): the Ca^{2+} influx from the ER induces the opening of channels present in the plasma membrane taking an increase of this ion in the cytoplasm to restore the Ca^{2+} concentration in the cellular stores (Hogan PG and Rao A 2015). In this process, two TRP channels operate; ORAI1 (calcium release-activated calcium channel protein 1) and STIM1 (Stromal Interaction Molecular 1) (Hogan PG and Rao A 2015; Stathopoulos PB et al. 2013). The increase in intracellular Ca^{2+} levels can also be induced by the release of the ion from the ER through the InsP3Rs and the receptors for Rianodine (RyR) (Marchi S and Pinton P 2016).

A non-physiological increase in Ca^{2+} , as well as those induced by CDDP treatment, can lead to the activation of calpain, an activated Ca^{2+} protein that is involved in apoptosis (Chang L and Wang A 2013; Debatin KM et al. 2002; Smith MA and Schnellmann RG 2012). Calpain cleavages AIF protein, ensuring its translocation to the nucleus and consequently the DNA fragmentation (Norberg E et al. 2010). Increases in the cytosolic concentration of Ca^{2+} , and ROS accumulation can promote the opening of the PTP leading to a loss of the potential of mitochondrial membrane, to the release of cytochrome c from the mitochondria in the cytosol and consequently to the activation of caspases-9 and -3 triggering the apoptotic pathway (Marchi S and Pinton P 2016).

In neuronal cells, excessive activation of the NMDA receptor by glutamate produces a higher activation of the associated channels, increasing cytosol Ca^{2+} concentration that consequently causes excitotoxicity and eventually cells death (Carozzi VA et al. 2010).

When intracellular Ca^{2+} concentration is high, it can induce protein and nucleic acid aggregation, which can result in a collapse of the membrane lipid structure (Case RM et al. 2007). An alteration of Ca^{2+} homeostasis causes bone anomalies and an increased risk of developing epithelial tumours (Crosara Teixeira et al. 2014). Indeed, since the intracellular Ca^{2+} is fundamental for neuronal neurotransmitter release (Burnashev N and Rozov A 2005) anomalies in the Ca^{2+} signal homeostasis process, can lead to

disorders of various nature: migraine, ataxia (Lory P and Mezghrani A 2010), Alzheimer's disease (Sanz-Blasco S et al. 2008), stroke (Toescu EC 2004), epilepsy (Ben-Ari Y 2001; Lory P and Mezghrani A 2010) and cancers (Mignen O et al. 2017). In this context, several studies have been focused on the role Ca^{2+} channels, which have shown to be involved in progression and proliferation of cancer, migration, invasion, and metastasis (Abdullaev IF et al. 2010; Catacuzzeno L et al. 2015; Thuringer D et al. 2017). Another element that seems to have an important role in cancer is the mitochondrial-associated endoplasmic reticulum membranes (MAMs). MAMs are locating between ER and mitochondria making a contact between two organelles but maintaining ER and mitochondria biochemical distinct, therefore MAMs may have a role in cancer therapy response, especially during cell death processes by the modulation of Ca^{2+} signalling pathway (Morciano G et al. 2018).

1.5.1 Calcium Binding Proteins (CBPs)

The CBPs contain EF-hand motifs (helix-loop-helix) that allow binding Ca^{2+} (Lewit-Bentley A and Réty S 2000; Yáñez M et al. 2012). The structure of these EF-hand motifs refers to the anatomy of the right hand, where the two helices can be traced back to the thumb and index, while the bent middle finger reproduces the Ca^{2+} -binding loop (Schwaller B 2009). CBPs are divided into two large groups: *i*) Ca^{2+} sensing proteins, which following the bond with Ca^{2+} , undergo a conformational change and interact with a series of targets, activating the signal transduction cascade; *ii*) cytosolic Ca^{2+} buffers that do not undergo a conformational change and have the function of dissipating local Ca^{2+} (Alpàr A et al. 2012). However, in addition to this first distinction between these two classes of CBP, the classification of CBP also depends on their expression and the effective function they perform within the cell and the targets with which they interact. Some CBPs such as calreticulin and calsequestrin are involved within intracellular Ca^{2+} stores, while synaptotagmin, calmodulin and S100 families are recruited during neuronal processes (Alpàr A et al. 2012). Therefore, the function of individual proteins can depend on their focal concentration, the availability of interacting partners in signalling networks, and the cellular context. In conclusion, there are also extracellular CBPs that can be classified according to their Ca^{2+} binding structures which exert several functions also with ECM (Yáñez M et al. 2012).

Parvalbumin

Parvalbumin (PV) is a CBP of the albumin family, with a PM of 10-12 kDa, encoded by the PVALB gene located on chromosome 22 in humans and on chromosome 15 in the mouse (Hara E et al. 2012). It is an important protein for signal transduction, for gene expression and it is involved in muscle relaxation following the contraction phase (Wilwert JL et al. 2006).

PV consists of two EF-hand motifs with a high affinity for Mg^{2+} and low affinity for Ca^{2+} . The PV tends to slowly dissociate from Ca^{2+} and therefore takes longer to restore Ca^{2+} intracellular homeostatic concentrations. This suggests that PV is involved in the modulation of slow and transient Ca^{2+} signals, not appearing to be involved in the phasic release of neurotransmitters and in the control of rapid Ca^{2+} signals (Collin T et al. 2005). PV is also present at the neuronal level and its expression can be found in about 50% of the interneurons of the basolateral amygdala (McDonald AJ and Betette RL 2001). It is also expressed in the cerebral cortex, in the hippocampus, in the spinal cord and in Purkinje cells (Celio MR 1990), where it is located at the level of the soma, dendrites, and axon. PV appears to be expressed above all in those myelinated neuronal cells with thin projections, such as Golgi interneurons of type II (Plogmann D and Celio MR 1993).

Calbindin

Calbindin (CB) is a CBP of 28 kDa which acts as both a Ca^{2+} sensor protein and a buffering protein, interacts with several proteins localized in the cytoplasm, intracellular membranes and in the nucleus (Schwaller B, 2010). This protein is typical of neurons, but is also present in renal cells, in the pancreas and in the intestine (Yew DT et al. 1997). It has six EF-Hand domains of which four can bind the Ca^{2+} ion. CB has also a binding site for vitamin D, being its vitamin D dependent activity, and for some metals including zinc.

In the CNS, CB is localized in Golgi neurons of type I, in nigrostriatal neurons, in the neurons of the Meynert Basal Nucleus, in Purkinje cerebellar cells and in ganglion cells of the vestibular, cochlear, retinal and spinal nuclei (Celio MR 1990). Physiologically, in the cerebellum, CB, like PV, is expressed in dendrites, axons and the soma of Purkinje cells. (Schwaller B et al. 2002).

Calretinin

Calretinin (CR), also known as calbindin 2, is a CBP protein having a PM 29 kDa and encoded by the CALB2 gene located on chromosome 8. Its name is since this protein has been discovered at the level of retinal cells (Camp AJ and Wijesinghe R 2009). CR, as well as other CBPs, has EF-Hand domains, in this case, six Ca²⁺-binding EF-Hand domains. The domains that can bind the Ca²⁺ are the first five, while the sixth would seem to be inactive (Schwaller B 2014).

CR is particularly expressed in neuronal cell and high expression of this protein have been found at the level of the granular cells of the cerebellum (Marini AM et al. 1997; Résibois A and Rogers JH 1992; Schiffmann SN et al. 1999), where it modulates neuronal excitability (Schurmans S et al. 1997). CR is not expressed only at the neuronal level, but its presence has also been demonstrated in other cell types such as mesothelial cells, neuroendocrine cells and sweat glands (Camp A and Wijesinghe JR 2009).

Calmodulin

Calmodulin (CaM) is a ubiquitous CBP having a PM of 16.7 kDa and is expressed in all eukaryotic cells (Mori M et al. 2003). CaM, binding four calcium ions, undergoes conformational changes that can increase its affinity for the target proteins. This protein can interact with different targets which include: cellular proteins, enzymes, ion channels, transcription factors, and cytoskeleton proteins. Furthermore, CaM also interacts with a series of receptors, including G protein-coupled receptors (Wang D et al. 1999). Recently it has been shown that CaM interacts with the EGFR (Li H and Villalobo A 2002). Although total CaM levels in the brain are elevated (10 μM), the concentration of free protein appears to be reduced (Persechini A and Stemmer PM 2002).

CaM participates in the regulation of various biological processes including energy metabolism, cell motility, and exocytosis (Berchtold MW and Villalobo A, 2014). Indeed, CaM plays an important role in the recruitment of synaptic vesicles following activation of the Ca²⁺/CaM-dependent Protein Kinase (CaMK) I and II, and through the phosphorylation of synapsin, a protein located on the synaptic vesicle membrane. This phosphorylation allows the synaptic vesicles to free themselves from the cytoskeletal filaments

of actin and to reach the presynaptic active zones (Valtorta F et al. 1992; Benfenati F et al. 1993; Hilfiker S et al. 1998).

1.5.2 PMCA (Plasma-Ca²⁺-ATPase Membrane)

The PMCA protein belongs to the family of P-type ATPase pumps, whose name derives from the fact that a high energy phosphorylated compound is formed (Di Leva F et al. 2008) and it was discovered in erythrocytes at the level of the cell membrane (Schatzmann HJ 1966). Together with the other transport systems, it is involved in the control of Ca²⁺ homeostasis and uses ATP to eject a Ca²⁺ ion to the outside (Brini M et al. 2013). The PMCA has the same membrane topology as the SERCA pump; it has ten transmembrane domains, two broad intracellular loops, an N-terminal chain and a C-terminal, both cytoplasmic. The C-terminal chain is very long and has specific binding sites for CaM and for other proteins such as kinase A (PKA) and kinase C (PKC). The N-terminal chain possesses the regulation sites as well as the sites of PMCA inhibitory proteins binding (Linde CI et al. 2007; Rimessi A et al. 2005). The pump can exist in two different conformational states defined E1 and E2. E1 differs for the diverse binding affinity that PMCA presents to Ca²⁺. In E1 configuration, the pump binds Ca²⁺ with high affinity on the cytoplasmic side, while in the E2 configuration, PMCA binds Ca²⁺ with low affinity, releasing Ca²⁺ in the extracellular space (Brini M et al. 2013). The passage of the protein from the E1 to the E2 conformation occurs following the phosphorylation of a residue of aspartic acid, a constituent of the PMCA protein itself, by the ATP. At this point, the E2 configuration is cleaved and the protein returns to the E1 state. The protein can transport a Ca²⁺ ion for each ATP molecule consumed (Di Leva et al. 2008). In mammals, 4 distinct genes (ATP2B1-4) encode for 4 isoforms of the PMCA protein; PMCA2 is poorly expressed at the tissue level and significant expression of this protein has been found in CNS, in Purkinje cell dendrites (Brini M et al. 2013). This protein has two isoforms: the PMCA2a and the PMCA2b, with different locations; the first is detectable in the presynaptic terminal, while the second is in the postsynaptic level (Burette A and Weinberg RJ 2007). As well as the PMCA2 pump, the PMCA3 protein is also poorly ubiquitous and its localization is confined to the CNS (Brini M et al. 2013), in the axonal terminals of granular cells. The PMCA1 and PMCA4 pumps are ubiquitous and perform the function of housekeeping proteins (Brini M et al. 2017). The PMCA4 isoform is particularly expressed

in the sperm tails; mice having a deletion of the gene encoding the PMCA4 protein survive but are not fertile due to the inability of sperm to move (Schuh K et al. 2004). The PMCA1 protein is widely expressed in tissues and embryonic tissues (Brini M et al. 2013). Deletion of the gene that codes for this protein leads to the premature death of the embryo, underlining the important role of PMCA1 in development and organogenesis. This protein also regulates and maintains levels of Ca^{2+} around life-compatible values (Okunade GW et al. 2004). The PMCA1 isoform is a very important protein, able to compensate for the absence of other isoforms (Okunade GW et al. 2004). There are two isoforms of the PMCA1 pump: PMCA1a and PMCA1b. PMCA1b is mainly expressed during development and is then replaced by the 1a variant in the brain of adult mice (Kenyon KA et al. 2010). Several studies have shown that loss, mutation or inappropriate expression of different PMCAs is associated with pathologies ranging (Strehler EE 2013). It has been demonstrated that alterations in the expression of PMCA isoforms have been described in a variety of cancer types, including those of breast and colon (Curry MC et al. 2012; Lee WJ et al. 2005; Roberts-Thomson SJ et al. 2010). In turn, the characterization of the different PMCA isoforms could improve the understanding of the role played by these proteins in the various types of neoplasias, representing a strategy for the conception of more specific and targeted treatments.

1.6 The role of oxidative stress in cells

Reactive species involved in cell stress can be classified into four groups: ROS, RNS (Reactive Nitrogen Species), RSS (Reactive Sulphur Species) and RCS (Reactive Chloride Species). The family of ROS includes the superoxide anion (O_2^-), the hydroxyl radical ($\bullet\text{OH}$), the hydrogen peroxide (H_2O_2), singlet oxygen ($^1\text{O}_2$) and ozone (O_3) (Sosa V et al. 2013). In physiological conditions, the presence of antioxidant molecules guarantees the equilibrium between reactive species and antioxidant species, by balancing their generation and elimination. The scavenger systems consist in SOD (superoxide dismutase) that is the principal enzyme involved in the neutralization of ROS and catalyses the dismutation of O_2^- into H_2O_2 which, in turn, is transformed in water by CAT (catalase) enzyme and GPx (glutathione peroxidase) (Desoize B 2002; Halliwell B 2007, Pacher P et al. 2007). At lower levels, ROS act as intracellular signal transduction molecules

which can regulate kinase-driven pathways, in turn mediating cellular responses to external stimuli, such as growth factors, nutrient deprivation, or hypoxia (Gough DR and Cotter TG 2011).

However, in some conditions such as prolonged starvation, the excessive levels of ROS produced can damage cellular proteins, lipids, DNA and RNA leading to functional alterations, which can contribute to cell death and, in some cases, to carcinogenesis and metastasis formation (Sabharwal SS and Schumacker PT 2014; Veskoukis AS et al. 2012). Indeed, oxidative stress can produce mutation at DNA and can also compromise the function of DNA damage repair mechanisms, inducing the onset of cancers (Gupta RK et al. 2014). Cancer cells exhibit high levels of ROS compared to normal cells, this is partly due to oncogenic stimulation, which increases metabolic activity and mitochondrial breakdown. Mitochondria are the main source of ROS and their dysfunction may represent a link to tumorigenesis (Kongara S and Karantza V 2012; Starkov AA 2008).

Notably, in the tumoral context, several pathways are implicated in the downstream of the increase of ROS production, such as MAPK and PI3K pathways that are associated with the induction of tumours proliferation (Seo JH et al. 2005; Tobiume K et al. 2001). High ROS level can also produce negative effect by the interaction with a lot of proteins involved in: *i*) inflammation such as NF- κ B and cyclooxygenase 2 (COX2) that has a central role in the inflammation/cancer signalling axis and has been correlated poorer prognosis among patients with estrogen-independent breast cancer (Chikman B et al. 2014; Schexnayder C et al. 2018) *ii*) invasion as well as HIF1 and matrix metalloproteinases; *iii*) angiogenesis process *i.e.* VEGF and its receptor (Hu Z et al. 2017; Sosa V et al. 2013).

The family of nitric oxide synthases (NOSs) synthesises nitric oxide (NO) that plays an important role in genotoxic mechanisms, antiapoptotic effects, promotion of angiogenesis and metastasis, and limits the effect of the anticancer immune system. It has been associated with several types of cancers *i.e.* cervical, breast, CNS tumours and others (Choudhari SK et al. 2013).

Oxidative stress is one of the most important mechanisms involved in CDDP toxicity. Mitochondria are the first target of CDDP in inducing oxidative stress, which is expressed in a decrease in the sulfhydryl group of mitochondrial proteins, inhibition of Ca^{2+} uptake and reduction of mitochondria membrane potential. The formation of ROS depends on the

intracellular concentration of CDDP and the duration of exposure to it (Brozovic A et al. 2010). By inducing an increase in the ROS level, CDDP can thus promote DNA damage and consequently induce cell death.

1.7 Unconventional alternative therapies

In order to improve the effects induced by standard anticancer therapies and overcome the negative effects that can seriously compromise the quality of life (QoL) of the cancer patient, scientific research has adopted different methods to overcome the limits of conventional therapies.

Immunotherapy

In recent years, immunotherapy has gained more interest from the scientific community, resulting in a good tool for the treatment of different types of cancers and to date, several immunotherapy approaches are currently in clinical development or have reached FDA approval.

Antagonistic antibodies to the CTLA-4 (Cytotoxic T-cell Lymphocyte Antigen-4) pathways have been accepted for the treatment of different forms of cancer and the first anticancer drug targeting an immune checkpoint was Ipilimumab, a CTLA-4 blocker approved in metastatic melanoma therapy (Hodi FS et al. 2010). In addition PD-1 (Programmed Cell Death-1) blocking drugs such as nivolumab or pembrolizumab have shown unprecedented activity in patients with advanced melanoma and other cancers (Robert C et al. 2014; 2015). To date, the oncolytic herpes virus has been approved for the treatment of metastatic melanoma and Chimeric Antigen Receptor (CAR) T cells that target CD19 are employed for acute lymphoblastic leukaemia and diffuse large-cell lymphoma.

For decades, the brain has been considered an immune-privileged system due to unique anatomical, physiological, and immunological barriers (Roth P et al. 2016). Indeed, it was thought that the brain to be devoid of lymphatics, but current studies show that lymphatics are present in the arachnoid meninges and dura and that lymphocytes exit the brain via this system to deep cervical lymph nodes (Schläger C et al. 2016).

It has been demonstrated that malignant brain tumour can induce a pathological neuroimmune response that promotes a heterogeneous cellular milieu composed of a network of immune-activating and immune-tempering cells (Kipnis J 2016). Indeed, higher grade brain tumours promote the

intensification of irregular vascularization, BBB disruption, the formation of necrosis foci, and antigen expulsion (Charles NA et al. 2012; Domingues P et al. 2016; Dubois LG et al. 2014; Yang I et al. 2011). The leaking of antigens from brain parenchyma, leading by the fenestration of the BBB, and in this case, its rupture, is significant to promote the attraction and invasion of immunomodulatory cells from the periphery system (**Figure 17**). Although this mechanism contributes to increasing the immune infiltrate at the tumour level, it is not necessarily associated with better survival results. This is due to the presence of the BBB which, although it can be considered “permeable”, can be intact inside the tumour core, representing an obstacle for immunotherapy (van Tellingen O et al. 2015).

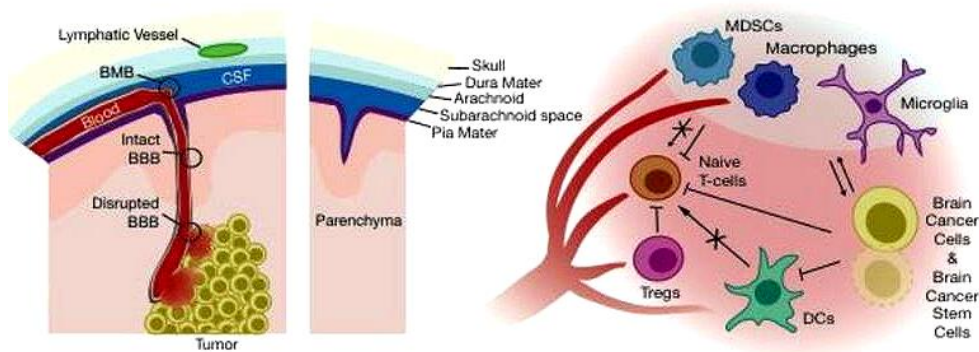


Figure 17. The neuro-immune environment in brain tumour. The BBB, Blood-Meningeal Barrier (BMB), and the Blood-Cerebrospinal Fluid Barrier (BCSF) all actively prevent blood-borne cells from entering the brain parenchyma. In the presence of a brain tumour, the BBB is damaged and blood-borne signals and immune cells can more readily infiltrate the brain parenchyma (on the left). Simplified overview of immune-suppressed cellular regulation in brain tumours (on the right) (Lyon JG et al. 2017).

It is known that naive cytotoxic T-cells ($CD8^+$) and T-helper cells ($CD4^+$) are attracted by the brain tumour microenvironment which actively modulates their phenotypes (Han S et al. 2014). $CD8^+$ T-cells confer an antitumour response, while $CD4^+$ T-cells seem to control the tumour-associated microglia/macrophage phenotype toward a more tumour-supportive one. Despite the ratio of infiltrated $CD8^+$ to $CD4^+$ T-cells is a prognostic indicator in brain tumours (Dunn GP et al. 2007), T-cell function is blocked by cytokines, such as VEGF, $TGF\beta$, IL-10, expressed in the tumour

microenvironment (Domingues P et al. 2016; Razavi SM et al. 2016). Impaired T-cells have minor proliferation and an attenuated response to pro-inflammatory signals that therefore induce an overall down-regulation of MHCs and Dendritic Cells (DCs) maturation (Albesiano E et al. 2010; Razavi SM et al. 2016). Massive infiltration of regulatory T-cells (Tregs) has been described in many high-grade brain cancers, via tumour-secreted chemokines *i.e.* CCL22, TGF β (Crane CA et al. 2012; Jacobs JFM et al. 2010).

More aggressive brain tumours have been correlated with activated Tregs that can repress proliferation and the cytokine-production of tumour-infiltrating lymphocytes; depletion of Tregs in mice has demonstrated to prolong survival and lead to non-immunosuppressive myeloid cell infiltration (Maes W et al. 2013).

To date, many clinical trials are being conducted in brain cancer treatment and checkpoint blockade alone or in combination with engineered T-cell therapies also may effectively overcome tumour heterogeneity (Grada Z et al. 2013; Hegde M et al. 2012). Ipilimumab and pembrolizumab have been shown to have acceptable safety and some efficacy in patients with brain metastasis from melanoma or non-small-cell lung cancer (Goldberg SB et al. 2016; Margolin K et al. 2012). However, patients treated with VEGF antibody bevacizumab showed a decline in global neurocognitive function, most obvious after prolonged treatment, compared to untreated patients, but further studies are still in progress (Fathpour P et al. 2014).

The EGFRvIII is a tumour-specific mutation mostly expressed on the lethal primary malignant neoplasm of the brain, such as primary GBM, with a prevalence of 20-30% (Babu R and Adamson DC 2012). The potential immunogenicity of the EGFRvIII mutation, first recognised in 2002, resulted in the development of Rindopepimut (CDX-110), a peptide vaccine containing the specific novel amino acid sequence created by the EGFRvIII deletion mutation conjugated to keyhole limpet hemocyanin (Elsamadicy AA et al. 2017; Weller M et al. 2017). Rindopepimut has shown clinical efficacy in phase I and II clinical trials, with a phase III clinical trial recently discontinued. Indeed, it seems that Rindopepimut does not improve survival in patients with newly diagnosed GBM, but combination approaches potentially including Rindopepimut are currently under study to show the efficacy of immunotherapy in GBM (Weller M et al. 2017).

Hadrontherapy with carbon ions

Radiotherapy stands out in “conventional” that uses mostly photons (X-rays) produced by a medical linear accelerator (LINAC), which accelerates electrons to a dozen MeV (MegaelectronVolt) and “unconventional”, known as hadrontherapy, based on charged particles.

Hadrontherapy is a form radiotherapy in which hadrons are used *i.e.* atoms with electrons torn off, one in the case of proton therapy and six in the case of carbon ion therapy. Hadrontherapy has been in constant progress in the past decades, bringing technical innovations both in clinical and scientific research (Marvaso G et al. 2017; Rossi S 2015).

Hadrontherapy has shown to be less invasive than conventional radiotherapy and more effectiveness than radiotherapy with X-rays (Combs SE et al. 2013). The advantage in the use of charged hadron beams is that a proton nanoampere, accelerated to 200 MeV, and a tenth of carbon ion nanoamperes, accelerated to 4 800 MeV, make it possible to irradiate deep tumours (*i.e.* those that they are also found at 25 cm below the skin) following the contour with millimetre precision. In addition, carbon ion therapy represents an advancement in the field of radiotherapy. Indeed, it has the same characteristics as proton therapy, but carbon ion beams allow improved dose distribution, leading to the concentration of enough dose within a target volume while minimizing the dose in the adjacent healthy tissues (Kamada T et al. 2015). Therefore, these properties allow the use of carbon ion beams in deep localized tumours and nearby organs particularly susceptible (**Figure 18**). Furthermore, in contrast to X-rays, protons and ions are heavy particles, so they can penetrate the tissue without deviating much from the initial direction and with their electric charge they tear electrons from the tissue molecules depositing most of their energy in the last centimetres of the path, providing a higher action (Kamada T et al. 2015) and so using a greater relative biological effectiveness (RBE).

Carbon ion beams provide a greater amount of energy per unit length (Linear Energy Transfer, LET) in the matter than low-LET radiation such as photons. Consequently, carbon ion beams generally cause the breakup of both DNA strands, resulting in the most significant event for tumour cell death (Hamada N et al. 2010). Compared to conventional photonic irradiation, carbon ions are less dependent on Oxygen Enhancement Ratio (OER), which in radiobiology refers to the increased effect of ionizing radiation due to the presence of oxygen. This would allow carbon ion therapy to eradicate hypoxic

glioblastoma cells, for example following an antiangiogenic therapy. The induction of apoptosis, autophagy, and cellular senescence are a set of mechanisms underlying the killing of glioblastoma cells mediated by irradiation of carbon ions (Jinno-Oue A et al. 2010; Tomiyama A et al. 2010). Furthermore, it has been demonstrated that such radiations would be able to inhibit the migratory capacity of glioma cells through a reduction in the expression of integrins (Rieken S et al. 2012). It has also recently been hypothesized that carbon ion radiation is able to overcome the intrinsic radioresistance of cancer stem cells (Pignalosa D and Durante M 2012), in addition, may be a promising therapy for paediatric brain tumours decreasing side effect related of CNS sensibility (Laprie A et al. 2015). Although clinical studies need to be more thoroughly investigated, to date this therapy, in the case of low-grade tumours, is associated with a potential reduction in long-term morbidity, while in cases of high-grade neoplasms, better tumour control and improve patient survival (Combs SE 2018).

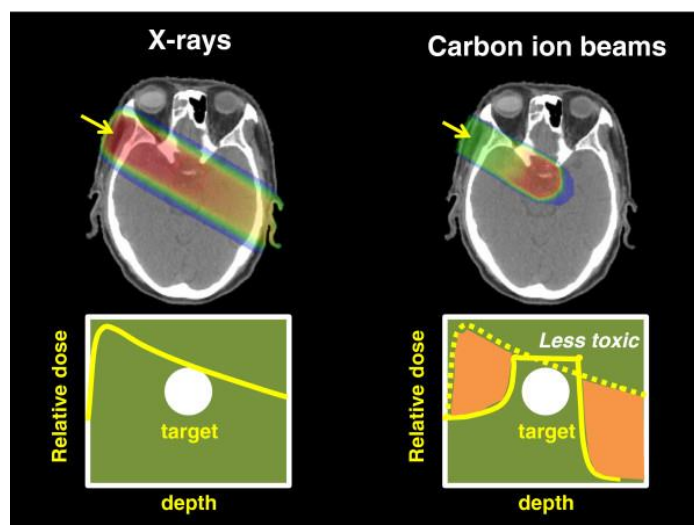


Figure 18. The difference of dose distribution by one port between X-rays and carbon ion beams. The figure represents the difference of dose distribution by one port between X-rays and carbon ion beams. The lateral fall-off around the target area obtained with the carbon ions beam is steeper than proton beams. Primary carbon ions undergo nuclear interactions and fragment into particles with a lower atomic number, producing a fragmentation tail beyond the peak. The consequent effect is that in the region beyond the distal end of the peak, almost no dose is deposited with protons, while a small dose is deposited with carbon ions (Ohno T 2013).

The accelerators used to produce the collimating beams are the cyclotrons and synchrotrons. The National Center of Oncologic Hadrontherapy (CNAO) of Pavia (Italy) uses for therapeutic purposes beams of carbon ions and protons. The accelerator assembly is based on a synchrotron with a diameter of 25 m able to accelerate carbon ions up to 400 MeV/u and protons up to 250 MeV/u. Inside the ring are the two sources, the two injection lines, and the linear accelerator. Outside the ring, there are four extraction lines, of about 50m each, which carry the extracted beam into the three treatment rooms. In one of the three rooms, a vertical beam and a horizontal beam are located, while in the remaining two rooms the treatment is administered only with horizontal beams. The time required for the beam to make a turn in the circle depends on the speed of the particles and therefore on its energy; however, for the range of bundles used for therapeutic purposes and in the synchrotrons used, the time is usually less than 1 μ s. So, if the radius was extracted after one revolution, the pulse duration would be less than 1 μ s. For clinical use, it is advantageous to have a modulable intensity in a range of time ranging from hundreds of milliseconds up to a few seconds. In summary, the main components of the synchrotron are described in **Figure 19**.

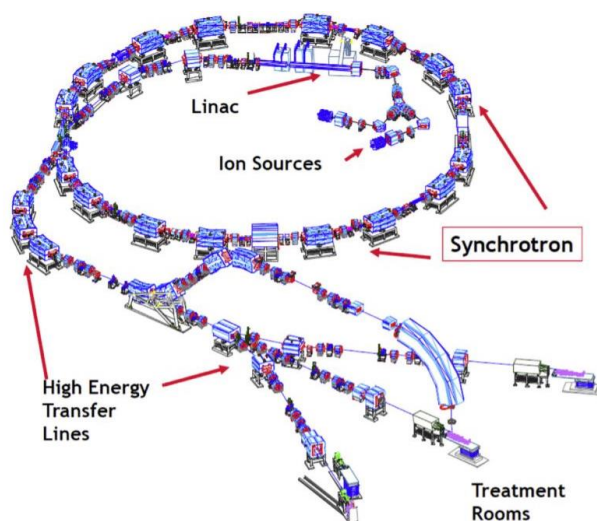


Figure 19. The layout of the high technology of CNAO. Sources; low energy transport line (LEBT line); radio frequency quadrupole (RFQ); linear accelerator (LINAC); medium energy transport line (MEBT line); synchrotron; high energy transport line (HEBT line) (Rossi S 2015).

Phyto- and mycotherapy

In recent years the therapeutic power of ancient medicinal herbs has become very popular in alternative medicine, so much so that many of the medicines used in the treatments have been created starting from them (Kolasinski SL 2014). To date, the use of phyto- and mycotherapy, already used in alternative therapies for the treatment of many diseases, could represent a new strategy to assist the treatment of different tumours, thanks to the numerous benefits that these substances bring to the whole organism and therefore to the patient's QoL.

Taraxacum officinale (Dandelion) originates from Europe, it is a plant of genus *Taraxacum* and a member of the Asteraceae family, and its extracts have long been used in traditional oriental medicine (Wirngo FE et al. 2016). Thanks to its benefit properties such as diuretic, antiangiogenic, antirheumatic and anti-inflammatory effects (Jeon HJ et al. 2008; Schütz K et al. 2006), *Taraxacum officinale* is widely used in the treatment of several inflammatory or infectious diseases including hepatitis, upper respiratory tract infections, bronchitis, pneumonia obesity and cardiovascular disease (Sweeney B et al. 2005; Wirngo FE et al. 2016).

In recent years, different forms of *Taraxacum officinale* extracts have been studied extensively also for its antidepressant and anti-inflammatory effects. Phytochemical analyses of the extract showed complex multi-component composition of the root extract (DRE), that includes some known bioactive phytochemicals such as α -amyrin, β -amyrin, lupeol, β -carotene, which protects cells from oxidation and cellular damage, and taraxasterol (Khoo HE et al 2011; Wirngo FE et al 2016). Taraxasterol is a pentacyclic triterpene, which greatly reduces the expression of NOS and COX2, decreasing the production of nitric oxide and prostaglandin induced by the lipopolysaccharide, and inhibiting NF- κ B thereby decreasing the level of inflammatory mediators such as TNF- α , IL-1 β , and IL-6 (Zhang X et al. 2012; Xiong H et al. 2014). This suggested that this natural extract could engage and effectively target multiple vulnerabilities of cancer cells. Current *in vitro* works have shown the anticancer potential of an aqueous DRE in several cancer cell models, without inducing cytotoxicity on non-cancer cells (Ovadge P et al. 2016) and acting to reduce pro-inflammatory response (Xiong H et al. 2014). It has been demonstrated that *Taraxacum officinale* caused apoptosis and loss of mitochondrial integrity as well as inhibition of invasion and

migration. In addition, the simultaneous therapy with *Taraxacum officinale* and the mistletoe extract has shown synergistic effects on neuroblastoma cell line SH-SY5Y compared to human fibroblast. These preclinical data support the use of *Taraxacum officinale* as a potential adjuvant application in paediatric oncology (Menke K et al. 2018).

Regarding mycotherapy, among the most known and studied fungi for their use or adjuvant action to conventional therapies are *Cordyceps sinensis*, *Hericium erinaceus*, and *Ganoderma lucidum*.

Cordyceps is a genus of mushrooms to which different species belong, including *Cordyceps sinensis*, the only one to have been recognized as a medicinal mushroom and used for more than 300 years in the traditional Chinese pharmacopoeia as a tonic, which gives the body greater energy and vitality (Ma L et al. 2015). The countless beneficial properties are conferred by its biological components, the most important of which is cordycepin (cordycepic acid), a secondary metabolite (Kuo HC et al. 2015) to which many research groups have attributed anticancer properties, antidepressants, anti-inflammatory, hypoglycemic, antimicrobial and antiviral.

Hericium erinaceus is a fungal species belonging to the *phylum* of the Basidiomycetes (Shen T et al. 2015) and it has always been an integral part of the Japanese and Chinese diet. Scientists have recently begun to study it for its powerful properties against neurodegenerative disorders (Brandalise F et al. 2017), moreover behavioral studies have demonstrated the effectiveness of this fungus in improving the performance of recognition memory in mouse models of Frailty during aging (Rossi P et al. 2018; Ratto D et al. 2019). Among its biological components, erinacines and hericenones are the two active elements responsible for increasing the synthesis of NGF (Nerve Growth Factor) in nerve cells (Li IC et al. 2014). These discoveries have given way to further studies on the possible use of this fungus in the treatment of senile dementia, degenerative diseases such as Alzheimer's disease, Parkinson's disease, multiple sclerosis, amyotrophic lateral sclerosis and many others (Samberkar S et al. 2015).

Ganoderma lucidum, also known as Ling Zhi in China or Reishi in Japan, is an oriental fungal species belonging to the Polyporaceae family of Basidiomycetes (Qu L et al. 2017), perennial fungi, saprophytes that grow and develop on broadleaf stumps, oak and chestnut (Prasad M and Naik ST

2002). The *Ganoderma lucidum* is characterized by a large fruiting body: the cap of the mushroom has a circular shape, reddish-brown, concentric streaks and a peculiar shiny appearance from which derives its scientific name *Ganoderma lucidum* (Sheena N et al. 2003). The stem may be in a vertical position or oblique, but it is almost always eccentric and of the same colour as the hat or darker (**Figure 20**). For over 2 000 years it has been used in traditional oriental medicine, purely Chinese, thanks to its multiple beneficial effects as a therapeutic agent for health and longevity, showing great efficacy in the treatment of many diseases including cancer (Jiang D et al. 2017). Due to the beneficial properties of this fungus, the researchers focused attention on the study of its bioactive compounds present mainly in the basidiocarp (basidiomycetes fruit-body) in the mycelium and in the spores (Cilerdžić J et al. 2014; Sanodiya BS et al. 2009).

Different classes of bioactive substances have been isolated and identified from *Ganoderma lucidum*, such as triterpenoids, polysaccharides, nucleosides, sterols, and alkaloids. Among all the various bioactive compounds mentioned, triterpenoids and polysaccharides represent the main constituents responsible for the anticancer activity of the fungus. The potential role of the polysaccharides of *Ganoderma lucidum* (GLPS) consists of the targeting immune cells and immune correlated cells including B lymphocytes, T lymphocytes, dendritic cells, macrophages, and natural killer cells. Recent data suggest that GLPS suppresses tumorigenesis or inhibits tumour growth through the direct cytotoxic effect and antiangiogenic actions (Xu Z et al. 2011). Triterpenoids have antiproliferative, antimetastatic and antiangiogenic activity (Wu GS et al. 2013). More in-depth studies have already been started to better understand the molecular mechanisms of action of the various compounds of the fungus and highlight the behaviour of the cells involved. The use of *Ganoderma lucidum* extracts could be a new therapeutic opportunity also in the treatment of breast cancer, melanoma and as a support during chemotherapy, considering its anti-inflammatory and antimetastatic actions (Barbieri A et al. 2017). Literature data show that ergosterol peroxide (EP) promotes anti-proliferative effects through G₁ phase cell cycle arrest, apoptosis induction via caspase-3/7 activation, and PARP cleavage on triple-negative breast cancer cells (Martínez-Montemayor MM et al. 2019). Furthermore, *Ganoderma lucidum* can be associated with other types of myco-phytotherapeutics in order to improve the conditions of oxidative stress present in the organism, fundamental as a method of

prevention of other diseases (Rossi P et al. 2014). This represents a prime example of how an ancient remedy can take on great importance in the modern era (Paterson RR 2006), whose next step will be to produce medicines.



Figure 20. The lingzhi mushroom (*Ganoderma lucidum*). *Ganoderma lucidum* is large, with a glossy exterior and a woody texture. The Latin word *lucidus* means “brilliant” and refers to the varnished appearance of the surface of the mushroom (Wachtel-Galor S et al. 2011).

2. Aims of the research

The aim of this research was mainly to characterize the effects of the newly synthesized platinum-based compound Pt(IV)Ac-POA (Prof. Osella, Amedeo Avogadro University of Eastern Piedmont, Alessandria, Italy) evaluating whether the new platinum compound may be more efficient than CDDP in treating different tumours of NS. The analysis was carried out on three different types of cells in order to increase the spectrum of analysis and understand the possible applications of the new compound.

1. In detail, two tumoral rat cell lines with different characteristics were examined: the B50 neuroblastoma cell line, with staminal properties, and the C6 glioma cell line, with differentiated features. Following the identification of the efficacious dose by flow cytometric techniques, the main cell death pathways were analysed by electron microscopy, immunocytochemical techniques, and western blot. Furthermore, in these two cell lines, the involvement of calcium was evaluated in order to understand a possible induction of cytotoxicity and the mechanisms of intracellular homeostasis sustained by CBPs and the PMCA pump. Finally, the effect of histone deacetylase inhibition of the new prodrug was evaluated, analysing the effects at both the molecular and ultrastructural cellular levels. This study was conducted in expectation of feasible employ of Pt(IV)Ac-POA *in vivo*, to characterize the possible cytotoxic effects, especially during the development stages of the CNS, when the BBB is not fully formed.

2. In the second part of the study, U251 human glioblastoma cells were used. The analyses carried out were based on the same approach described above, to understand the different induced cell death pathways. However, in this case, the analysis focused on possible new *in vitro* treatment targets and strategies, with a view to developing methods that can then guarantee a better quality of life for the cancer patient. The different experimentation approaches were based on different collaborations:

Hadrontherapy with carbon ions (Dr. Facoetti, CNAO, Pavia, Italy); study the effect of irradiation, discriminating the efficacy dose. Evaluating the implementation of chemotherapy and hadrontherapy, analysis of the long-term action of treatment.

Treatment with two different natural compounds to understand a possible adjuvant action to conventional therapies, focusing on the possible beneficial effects that could be useful in improving the QoL of cancer patients:

The watery root extract of *Taraxacum officinale* (Dr. Veltri, ICS Maugeri Spa IRCCS, Pavia, Italy);

Ganoderma lucidum-based myco-phytotherapeutic supplement called “Ganostile” (Miconet s.r.l.) (Prof. Rossi, Neurobiology and Integrated Physiology Laboratory, University of Pavia, Pavia, Italy).

Finally, characterization of Ca²⁺-activated potassium channels, in order to identify the mechanisms, underlying proliferation and migration of GBM cells (Prof. Rossi, Neurobiology and Integrated Physiology Laboratory, University of Pavia, Pavia, Italy).

3. Materials and methods

3.1 Cell Culture

B50 neuroblastoma rat cells (Lombardy and Emilia Romagna Experimental Zootechnic Institute - IZSLER, catalogue no. BS TCL 115) and C6 glioma rat cells (ATTC CCL 107, Rockville, Md, USA) were cultured in Dulbecco's Modified Eagle Medium (DMEM) supplemented with 1% L-glutamine, 1% penicillin/streptomycin and 10% fetal bovine serum (FBS). Human U251 MG cell line (Sigma-Aldrich, Rome, Italy) was cultured in Eagle's minimal essential medium (EMEM) supplemented with 1% glutamine, 1% non-essential amino acids (NEAA), 1% sodium pyruvate, 10% foetal bovine serum, 1% penicillin/streptomycin. All cell culture reagents were purchased from Celbio s.p.a. and Euroclone s.p.a. (Pero, Milan, Italy). All type of cell culture was maintained at 37°C in a humidified atmosphere (95% air/5% CO₂).

3.2 Treatments

3.2.1 Pharmacological treatment

Twenty-four h before experiments, cells were seeded on glass coverslips (200 000 cells) for fluorescence microscopy or grown in 75 cm² plastic flasks for flow cytometric, western blotting and ultrastructural analysis at transmission electron microscope. Cell exposure to different treatment was performed at 37°C. To compare the efficiency of the new prodrug to CDDP standard treatment, the administered concentration of 40 µM CDDP (Teva Pharma, Milan, Italy) was selected considering previous *in vitro* investigations (Bottone MG et al. 2008) as well as *in vivo* experimental designs (Bottone MG et al. 2008; Cerri S et al. 2011), employing a single subcutaneous injection (*i.e.* a single injection of 5 µg/g b.w.) in 10-days old rats, corresponding to the therapeutic dose proposed by Bodenner et al. (1986) and Dietrich et al. (2006), already used in clinical practice. Cell lines were exposure to platinum compounds according to the following protocols:

- i) standard acute test (48h continuous treatment, CT) to Pt(IV)Ac-POA or CDDP, for all cell lines (B50, C6, and U251);

- ii) standard acute test (48h-CT) to Pt(IV)Ac-POA or CDDP, followed by a 7 day-recovery phase in drug-free normal DMEM, namely recovered condition (only U251).

3.3.2 Carbon ion irradiation

Twenty-four h before experiments, U251 cells (400 000 cells) were seeded on culture flask sterile on slide 18 x 50 mm (Thermo Scientific™ Nunc™ Lab-Tek™) for fluorescence microscopy (**Figure 1A**). Cell lines were exposure for pre-treatment to platinum compounds for 48h-CT. At the end of the pre-treatment U251 cells were irradiated with a horizontal beam according to the protocol envisaged for clinical use of carbon ion therapy in CNAO (Facoetti A et al. 2015; Mirandola A et al. 2015). The flasks were positioned vertically immersed in a container full of water, 15 cm deep from the water surface (**Figure 1B, 1C**). The spread-out Bragg peak (SOBP), homogeneous in terms of dose absorbed in water, of 6 cm of thickness, was obtained with a modulation of the beam and of the pencil beam, using 31 different energies in the range from 246-312 MeV/u. The LET at a depth of 15 cm is equivalent to about 46 keV/u. For this study, the cellular samples were irradiated with 2 Gy or 4 Gy. At the end of the experiment, the medium was discarded; samples were divided into “standard acute test” and “recovered condition” (following the procedure described above). Finally, samples were with 4% formalin for 20 min and post-fixed with 70% ethanol at -20°C for at least 24 h for immunocytochemical procedures.

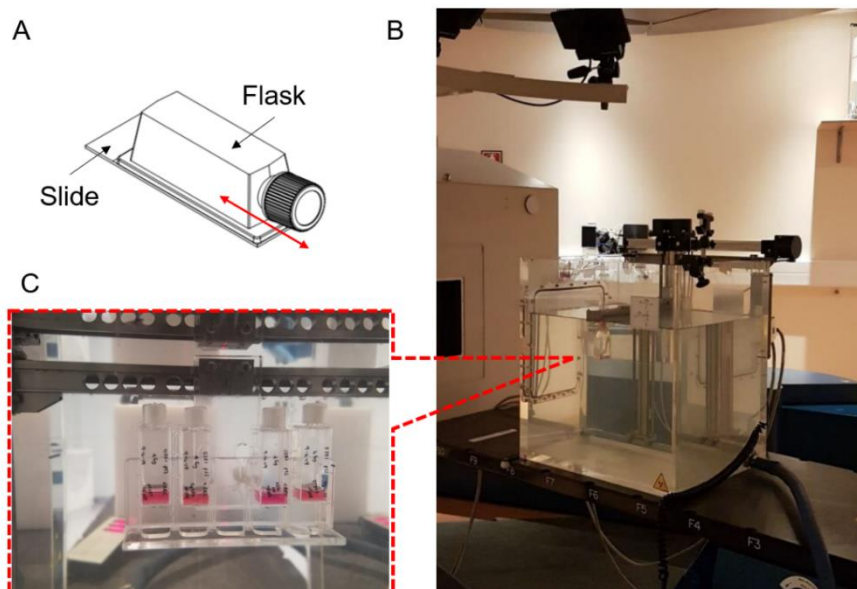


Figure 1. Irradiation with carbon ions. **A)** Flask sterile on slide used for U251 cell culture. **B)** Set-up for the irradiation of cultured cells in the treatment room of the CNAO Foundation. **C)** The flasks were placed vertically, immersed in the water chamber of the set-up.

3.3.3 Treatment with natural compounds

Before each experiment, the concentration to be used was evaluated through MTS [3-(4,5-dimethylthiazol-2-yl)-5-(3-carboxymethoxyphenyl)-2-(4-sulfophenyl)-2H-tetrazolium] assay on U251 cell lines.

Briefly, the cell viability test was performed using the CellTiter 96® Aqueous One Solution Cell Proliferation Assay (Promega) kit. A volume of 200 μL of cells was suspended at a density of 10 000 cells/well and transferred to a 96-well plate (0.1 ml per well) and incubated at 37 °C for 24 h, in a humidified atmosphere containing 5% of CO_2 . Subsequently, the culture medium was replaced with a fresh medium to then carry out the requested treatment. As a control, cells incubated with the culture medium alone were used, while for the treatment a range of concentrations was obtained dissolving the compound in the specific culture medium for the cells under examination. Each condition was repeated at least 4 times, to which 4 specific “whites” were then associated with normalization of absorbances. After the

incubation time for 48 h at the treatment, the culture medium was replaced with fresh medium and to each well 20 μ l of MTS solution, previously brought to RT, was added. This operation was performed in the dark and subsequently, the plates were incubated for about 3 h at 37 °C. At the end of the 3 h, the plates were read at 490 nm, using the ELx808™ Absorbance Microplate Reader (Bio-Tek Instruments, Inc.) plate reader. Percent cell viability was calculated using the following formula:

$$\text{Cell viability (\%)} = (\text{Abs}_{490} \text{ treated cells} / \text{Abs}_{490} \text{ control cells}) \times 100$$

This protocol was executed in triplicate to obtain statistical data.

Taraxacum officinale treatment: U251 cells were first exposed to aqueous extract of *Taraxacum officinale* root (from 694 mg of dandelion root in 15 ml) alone for 48 h-CT. Then was also evaluated the combine effect of this extract with Pt(IV)Ac-POA for 48 h-CT. The concentrations tested were chosen based on data already present in the literature and in order to be within the tolerability range of healthy cells (Sigstedt SC et al. 2008; Zhu H et al. 2018).

Ganoderma lucidum treatment: A myco-phytotherapeutic supplement based on *Ganoderma lucidum*, called “Ganostile” (Miconet s.r.l, Italy) was used to treat U251 for 48-CT. The supplement composition is: echinacea (*Echinacea purpurea* (L.) Moench., root) dry extract, eleutherococcus (*Eleutherococcus senticosus* (Rupr et Maxim) Maxim., root) dry extract, ganoderma (*Ganoderma lucidum* (Curtis) P.Karst., fungus) dry extract, astragalus (*Astragalus membranaceus* Moench., Root) dry extract, bulking agent: calcium phosphate; anti-caking agent: silicon dioxide, magnesium salts of fatty acids. The tested concentration was chosen considering the maximum daily dose recommended and based on the effect on the primary culture of human fibroblasts were cultured in RPMI 15% FBS, supplemented with 1% L-glutamine, 1% penicillin/streptomycin.

3.4 Flow cytometry

After 48h-CT of treatment, cells were detached by mild trypsinization (0.25% in phosphate-buffered saline, PBS, with 0.05% EDTA) to obtain single-cell suspensions to be processed for flow cytometry with a Partec PAS III flow cytometer (Münster, Germany), equipped with argon laser excitation

(power 200 mW) at 488 nm. Data were analysed with the built-in software (Flowmax, Partec).

3.4.1 Cell cycle analysis

Cells were washed in PBS, permeabilized in 70% ethanol for 10 min, treated with RNase A 100 U mL⁻¹ and then stained for 10 min at room temperature (RT) with Propidium Iodide (PI) 50 µg mL⁻¹ (Sigma-Aldrich, Milan, Italy) 1 h before flow cytometric analysis. PI red fluorescence was detected with a 610 nm long-pass emission filter. At least 20 000 cells per sample were measured to obtain the distribution among the different phases of the cell cycle and the percentage of apoptotic cells.

3.4.2 Identification of apoptotic cells with Annexin V assay

Single-cell suspensions, obtained as described above, were incubated with Annexin V-FITC (Annexin V-FITC Apoptosis Detection Kit, Abcam, Italy) for 10 min in the dark at RT. PI was used as a counterstain to discriminate necrotic/dead cells from apoptotic cells. Fluorescence was revealed by means flow cytometry at 488 nm excitation and with 530/30 (FITC) and 585/42 nm (PI) band-pass emission filters.

3.5 Ultrastructural analysis at TEM

Control cells and treated were harvested by mild trypsinization (0.25% trypsin in PBS containing 0.05% EDTA) and collected by centrifugation at 800 rpm for 5 min in fresh tubes. The samples were immediately fixed with 2.5% glutaraldehyde in culture medium (2 h at RT), centrifuged at 2000 rpm for 10 min and washed several times with PBS. Later, samples were post-fixed in 1% OsO₄ for 2 h at RT and washed in water. The cell pellets were pre-embedded in 2% agar, dehydrated with increasing concentrations of acetone (30, 50, 70, 90 and 100%, respectively). Finally, the pellets were embedded in Epon resin and polymerized at 60 °C for 48 h. Ultrathin sections were obtained with ultramicrotome Rechter, then located on nickel grids and stained with uranyl acetate and lead citrate. Sections were observed under a Zeiss EM 900 transmission electron microscope operating at 80kV. The plates, after being developed, have been computerized through Epson Perfection 4990 Photo scanner at a resolution of 800 dpi and then processed using the Epson Scan software.

3.6 Western blotting

Treated and control cells were washed twice with PBS and lysed in RIPA (Radioimmunoprecipitation assay) buffer (Tris HCl 1M pH 7.6, EDTA 0.5M pH 8, NaCl 5M, NP40 Nonidet 100%, with the addition of proteases and phosphatases inhibitors at 4°C for 30 min. Proteins were quantified using the Bradford reagent (Sigma Aldrich, Italy). Samples were electrophoresed in a 15% SDS-PAGE minigel and transferred onto a nitrocellulose membrane (BioRad, Hercules, CA) by semidry blotting for 1.30 h under a constant current of 60 mA. The membranes were saturated for 30 min with PBS containing 0.2% Tween-20 and 5% skim milk and incubated overnight with antibody reported in **Table 1**. After several washes with PBS-Tween, the membranes were incubated for 30 min with the proper secondary antibody conjugated with horseradish peroxidase (1:2000, Dako, Italy). Immunoreactive bands were detected with the reagent Luminata™ Crescendo (Merk Millipore, Billerica, MA), according to the appropriate instructions, and revealed on Amersham Hyperfilm™ ECL (GE Healthcare, Little Chalfont, UK) slabs. The density of the protein bands was normalized with the respective actin and subsequently with the loading control using ImageJ software.

Table 1 Antibodies used in western blot.

	Primary antibody	Dilution
PCNA	Mouse monoclonal [PC10] anti-PCNA ~ 29 kDa (Abcam, Cambridge, USA)	1:5000
Acetyl-H3	Rabbit polyclonal anti-Histone H3 ~ 17 kDa (acetyl K9) (Abcam, Cambridge, USA)	1:500
PARP-1	Rabbit monoclonal anti-PARP-1 ~ 116 kDa full length, ~ 89 kDa cleaved (Cell Signaling Technology, Danvers, USA)	1:1000
Calbindin	Mouse polyclonal anti-calbindin D-28k ~ 28 kDa (Swant, Switzerland)	1:1000
Calmodulin	Rabbit polyclonal anti-Calmodulin [EP799Y] ~ 17 kDa (Abcam, Cambridge, USA)	1:500
Calretinin	Rabbit polyclonal anti-Calretinin ~ 29-30 kDa (Swant, Switzerland)	1:1000
PMCA1	Rabbit polyclonal anti-PMCA1 ~130-134 kDa (Abcam, Cambridge, USA)	1:1000
Actin	Mouse monoclonal anti-actin ~ 43 KDa (Developmental Studies Hybridoma Bank, Iowa City, USA)	3:500

3.7 Evaluation of Ca^{2+} -activated potassium channels BK and Kir4.1

3.7.1 Wound healing assay

For the cell migration assay, U251 cells were seeded on glass coverslips (22×22 mm) located in cell culture dishes (35×10 mm). Once the cells have reached 90% confluence, a disposable pipette tip (1-mL volume) was used to scratch wounds on the midline of the coverslip (**Figure 2**).

Therefore, with t_0 was indicated the time at which the scratch was made, while with t_1 was specified the condition after 24 h from scratch. These samples were performed in duplicate both non-invasive perforating patch experiments in whole-cell conditions (D'Angelo E et al. 1998) and fluorescence immunocytochemical experiments following the standard protocol. The study was focused principally on the cells defined as “polarized”, a morphology often associated with migration, which was detected at the scratch level.

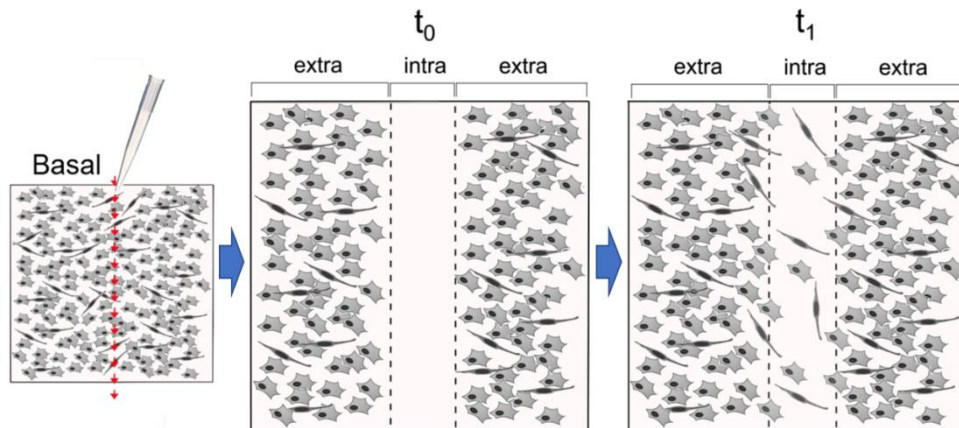


Figure 2. Experimental condition of wound healing assay. t_0 represents the condition immediately after the scratch. t_1 identifies coverslip after 24 h from scratch. To note, the schematic drawing describes the presence of migrated cells in scratch.

3.7.2 Analysis of Ca^{2+} -activated potassium channels localization

U251 cells were grown in 75 cm^2 flasks, harvested using mild trypsinisation and collected by centrifugation as described above. The samples were immediately fixed with 2% formaldehyde in PBS (2 h, at RT), centrifuged (2 000 rpm for 10 min) and washed with PBS. The cell pellets

were pre-embedded in 2% agar and dehydrated with increasing concentrations of ethanol (30, 50, 70, 90 and 100%). Finally, the pellets were embedded in LR-white resin (Sigma-Aldrich, Italy) and polymerised at 60°C for 24 h.

Ultrathin sections were obtained using ultramicrotome Rechter and then placed on nickel grids. The grids were floated on normal goat serum (NGS) diluted 1:100 in PBS for 3 min at RT and incubated with rabbit polyclonal anti-KCa1.1 or anti-Kir4.1 antibody (**Table 2**) overnight at 4 °C. The primary antibody was diluted 1:200 and 1:100, respectively, in PBS containing 0.1% Bovine Serum Albumin (BSA) and 0.05% Tween 20. The samples were rinsed with PBS-Tween two times for 5 min and equally with PBS. After incubation in NGS (1:50 in PBS) for 5 min at RT, the grids were treated with the specific secondary antibody (Jackson ImmunoResearch) coupled with colloidal gold of 6 nm diluted 1:20 in PBS for 30 min at RT. The sections were rinsed with PBS for 5 min twice and then with H₂O.

Sections were then stained for ribonucleoproteins (RNPs) following the regressive EDTA technique procedure. The grids were incubated in uranyl acetate for 2 min, in EDTA for 10 sec to remove uranyl from DNA and finally in lead citrate for the other 2 min.

Lastly, sections were observed under a Zeiss EM 900 transmission electron microscope operating at 80kV, computerised through Epson Perfection 4990 Photo scanner at a resolution of 800 dpi, and then processed using the Epson Scan software.

3.8 Immunocytochemical reactions at the fluorescence microscope

Control and treated cells were grown on coverslips were fixed with 4% formalin for 20 min and post-fixed with 70% ethanol at -20°C for at least 24 h. Samples were rehydrated for 10 min in PBS and then immunolabeled with primary antibodies diluted in PBS for 1 h, at RT in a dark moist chamber. After 3 washes in PBS of 5 minutes each, coverslips were incubated with secondary antibodies in PBS (1:200, Alexa Fluor, Molecular Probes, Invitrogen) for 45 min. At the end of the incubation and after other washing in PBS, sections were counterstained for DNA with 0.1 µg mL⁻¹ Hoechst 33258 (Sigma-Aldrich, Milano, Italy), washed with PBS, and mounted in a drop of Mowiol (Calbiochem, Inalco, Italy), for fluorescence microscopy analysis. An Olympus BX51 microscope equipped with a 100-W mercury lamp was used under the following conditions: 330-385 nm excitation filter

(excf), 400 nm dichroic mirror (dm) and 420 nm barrier filter (bf) for Hoechst 33258; 450-480 nm excf, 500 nm dm and 515 nm bf for the fluorescence of Alexa 488; 540 nm excf, 580 nm dm and 620 nm bf for Alexa 594. Images were recorded with an Olympus MagniFire camera system and processed with the Olympus Cell F software.

Primary and secondary antibodies used for immunocytochemical reactions at the fluorescence microscope are reported in **Table 2**.

Table 2 Antibodies used for immunofluorescence reactions

	Primary antibody	Dilution	Secondary antibody
Caspase-9	Rabbit polyclonal anti-caspase-9 (Cell Signaling Technology, Danvers, USA)	1:200	Alexa 594-conjugated anti-rabbit antibody
Caspase-3	Rabbit monoclonal anti-caspase-3 (Cell Signaling Technology, Danvers, USA)	1:200	Alexa 594-conjugated anti-rabbit antibody
PARP-1	Rabbit monoclonal anti-PARP-1 (Cell Signaling Technology, Danvers, USA)	1:200	Alexa 594-conjugated anti-rabbit antibody
Caspase-8	Rabbit monoclonal anti-caspase-8 (Cell Signaling Technology, Danvers, USA)	1:100	Alexa 594-conjugated anti-rabbit antibody
RIP1	Rabbit polyclonal anti-RIP1 (Santa Cruz Biotechnology)	1:200	Alexa 594-conjugated anti-rabbit antibody
MLKL	Mouse monoclonal Anti-MLKL Antibody, clone 3H1 (Sigma-Aldrich)	1:200	Alexa 594-conjugated anti-mouse antibody
Golgi	Human autoimmune serum recognizing proteins of Golgi Apparatus ^a	1:200	Alexa 594-conjugated anti-human antibody
Mitochondria	Human autoimmune serum recognizing the 70 kDa E2 subunit of the pyruvate dehydrogenase complex ^b	1:200	Alexa 594-conjugated anti-human antibody or Alexa 594-conjugated anti-human antibody
LC3B	Rabbit polyclonal anti-LC3B (Cell Signaling Technology, Danvers, USA)	1:400	Alexa 594-conjugated anti-rabbit antibody
p62/SQSTM1	Mouse monoclonal anti- p62/SQSTM1 (Abcam, Cambridge, USA)	1:100	Alexa 488-conjugated anti-mouse antibody
Lysosomes	Human autoimmune serum recognizing lysosomal proteinase	1:400	Alexa 488-conjugated anti-human antibody
PCNA	Mouse monoclonal [PC10] anti-PCNA (Abcam, Cambridge, USA)	1:200	Alexa 594-conjugated anti-mouse antibody
Active-Cdc42	Mouse monoclonal anti-Active Cdc42 (BIOMOL GmbH, Hamburg, Germany)	1:100	Alexa 488-conjugated anti-mouse antibody
Acetyl-H3	Rabbit polyclonal anti-Histone H3 (acetyl K9) (Abcam, Cambridge, USA)	1:200	Alexa 488-conjugated anti-rabbit antibody
BK channel	Rabbit polyclonal anti-KCa1.1 (KCNMA1) (Alomone Labs, Jerusalem, Israel)	1:200	Alexa 594-conjugated anti-rabbit antibody
KIR4.1 channel	Rabbit polyclonal anti-Kir4.1 (KCNJ10) (Alomone Labs, Jerusalem, Israel)	1:100	Alexa 594-conjugated anti- rabbit antibody
Bcl-2	Rabbit polyclonal anti-Bcl-2 (N-19) (Santa Cruz Biotechnology)	1:200	Alexa 594-conjugated anti-rabbit antibody

3. Materials and methods

Bax	Rabbit polyclonal anti-Bax (Cell Signaling Technology, Danvers, USA)	1:200	Alexa 594-conjugated anti-rabbit antibody
AIF	Rabbit polyclonal anti-AIF (Cell Signaling Technology, Danvers, USA)	1:200	Alexa 594-conjugated anti-rabbit antibody
NOS2	Mouse monoclonal anti-NOS2 (C-11) (Santa Cruz Biotechnology)	1:200	Alexa 594-conjugated anti-mouse antibody
COX2	Mouse polyclonal anti-COX2 (M-19) (Santa Cruz Biotechnology)	1:200	Alexa 594-conjugated anti-mouse antibody
Calbindin	Mouse polyclonal anti-calbindin D-28k (Swant, Switzerland)	1:200	Alexa 488-conjugated anti-mouse antibody
Calmodulin	Rabbit polyclonal anti-Calmodulin [EP799Y] (Abcam, Cambridge, USA)	1:200	Alexa 488-conjugated anti-rabbit antibody
Calretinin	Rabbit polyclonal anti-Calretinin (Swant, Switzerland)	1:2000	Alexa 488-conjugated anti-rabbit antibody
Parvalbumin	Rabbit polyclonal anti-Parvalbumin (Abcam, Cambridge, USA)	1:200	Alexa 488-conjugated anti-rabbit antibody
PMCA1	Rabbit polyclonal anti-PMCA1 (Abcam, Cambridge, USA)	1:300	Alexa 488-conjugated anti-rabbit antibody
α -tubulin	Mouse monoclonal anti- α -tubulin (Cell Signaling Technology, Danvers, USA)	1:1000	Alexa 488-conjugated anti-mouse antibody
Actin	Alexa 488-Phalloidin /Alexa 594-Phalloidin (Molecular Probes, Invitrogen)	1:500	

(^a Santin G et al. 2011; ^b Bottone MG et al. 2008)

3.8.1 Immunofluorescence quantification

After immunocytochemical reactions, images acquisition was performed by Cell F software. To make the fluorescence intensity comparable, during image acquisition the exposure time to detect every single fluorescence was selected based on the control sample and then maintained constant for the respective experimental conditions, thus avoiding the insertion of any variables in the analysis. The fluorescence intensity of the proteins of interest was analysed with the ImageJ software. The channels of each fluorescence have been split to obtain the single images in a greyscale where the minimum value is 0 (black) and the maximum value is 255 (white), as shown in the lower right panel reported in **Figure 3**. Then the mean values were normalized to control and expressed in percentage.

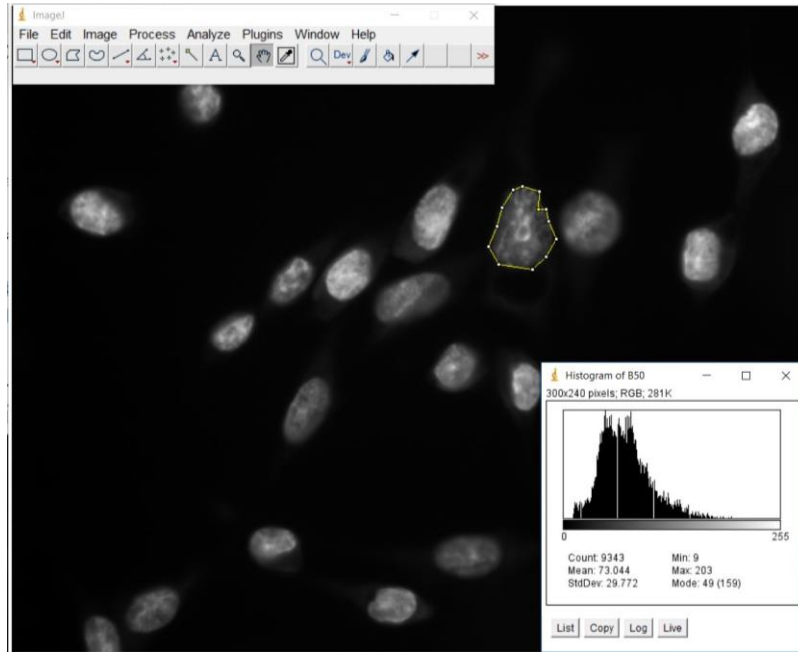


Figure 3. Screenshot of the software ImageJ working area. Greyscale used to measure the fluorescence intensity signal. The greyscale is included in a range that goes from 0 which represents the minimum value (black) and 255 which represents the maximum value of signal intensity (white). The yellow line indicates the measurement area.

3.9 Statistical analysis

Each experiment described above, on which a statistical evaluation was performed, was carried out as three independent replicates. In particular, for the immunofluorescence quantifications, three independent experiments were performed for each condition related to the marking of interest. Subsequently, for each condition, 11 quadrants were evaluated for a random analysis of cell fluorescence. In the end, the values obtained were expressed as mean \pm SEM (standard error of the mean). Data differences were analyzed for statistical significance utilizing Student's *t*-test or with one-way ANOVA and post hoc Bonferroni's test (software package GraphPad Prism Inc.). ρ values ranging from < 0.001 to < 0.05 were considered statistically significant.

4. Results

4.1 The effect of Pt(IV)Ac-POA on B50 neuroblastoma rat cells

Based on the viability test data obtained on the B50 rat neuroblastoma cell line (Randone B et al. 2018), some concentrations of interest of Pt(IV)Ac-POA have been tested *i.e.* 10, 4 and 1 μM . Control and treated samples were analysed by cytofluorimetric techniques to evaluate the efficacy of the new platinum-based compound. Effects of CDDP exposure on rat B50 neuroblastoma cells have already been extensively investigated in literature (Bottone MG et al. 2008; Grimaldi M et al. 2016, 2019; Santin G et al. 2011, 2012, 2013).

4.1.1 Cell cycle distribution

In **Figure 1** the data of 48h-CT to Pt(IV)Ac-POA at different concentrations (10, 4 and 1 μM) are reported. The cytograms represent the distribution of DNA in treated cells after PI-staining, compared to the control condition (CTR). Untreated cells were distributed among the different cell phases (G_1 , S, G_2), the presence of a large S phase denoted that the cells were proliferating. Conversely, the treatment with 10 μM 48h-CT intensely modified the histogram distribution. To note, the presence of a massive number of cells in the sub- G_1 peak (dead cells), while G_1 , S, and G_2 phases were almost lacking. After 4 μM 48h-CT the sub- G_1 peak was still evident, while the presence of G_1 and S peaks and the absence of G_2 peak, indicating an arrest of proliferation. After 1 μM 48h-CT, the cells redistributed in the different phases of the cell cycle, with a small sub- G_1 peak still visible.

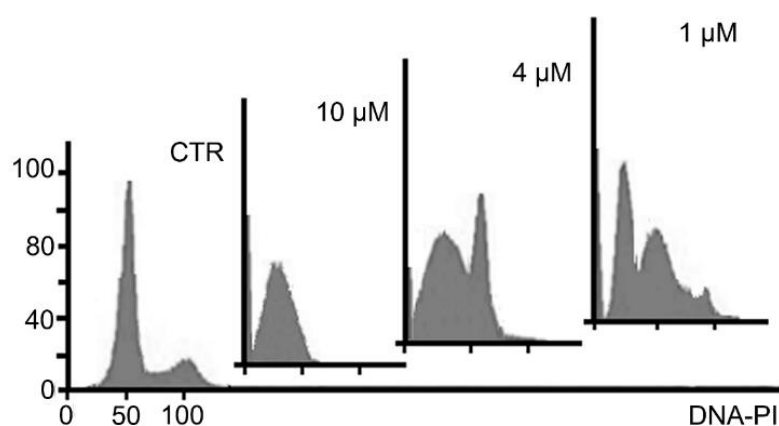


Figure 1. Flow cytometry after PI staining. Cytograms of DNA content in B50 control cells (CTR) and treated for 48h-CT with Pt(IV)Ac-POA at different concentrations (10, 4 and 1 μ M).

4.1.2 Ultrastructural analysis

The control cell (**Figure 2a**), exhibited a healthy nucleus with decondensed chromatin and an evident nucleolus. After 48-CT to Pt(IV)Ac-POA at 10 μ M strong subcellular disorganization and disaggregation of organelles and cytoskeletal components were observed, suggesting the activation of necrosis (**Figure 2b**). Moreover, the fragmentation of the nucleus and highly condensed chromatin (karyorrhexis) were also detectable. Treatments at 1 μ M (**Figure 2c**) and, even more, at 4 μ M (**Figure 2d**) seem to promote the autophagy pathway. A reduction in nucleus volume (pyknosis) and an increase of lysosomes and autophagic vacuole were observed. In addition, some vac

uoles included membranous cytoplasmic residues in the degradation phase, which can be ascribable to autophagosomes. In **Figure 2e** and **2f** a cell in apoptosis and necroptosis, respectively, were evidenced after treatment with Pt(IV)Ac-POA at 4 μ M.

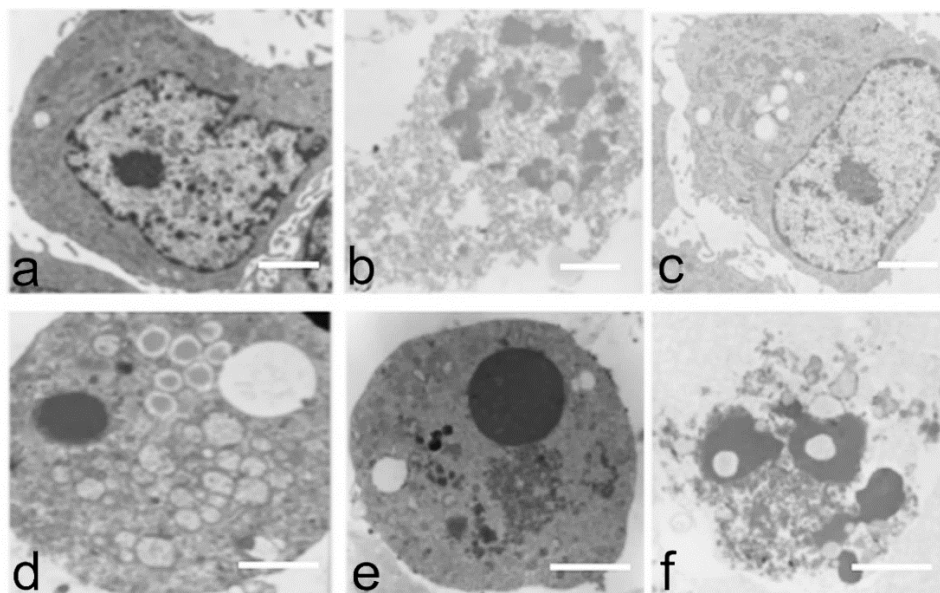


Figure 2. Ultrastructural analysis at electron microscopy. **a)** B50 cell in the control condition. **b)** B50 cell after 48h-CT with Pt(IV)Ac-POA at 10 μM . **c)** B50 cell after treatment 48h-CT with Pt(IV)Ac-POA at 1 μM . **d), e), f)** B50 traded-cells for 48h-CT at 4 μM Pt(IV)Ac-POA. Images **d-f** show examples of **d)** autophagy, **e)** apoptosis, and **f)** necroptosis. Bars: 1.5 μm .

4.1.3 Flow cytometric analysis by Annexin V assay

A test with Annexin V/PI staining was performed to investigate the possible induction of apoptosis after 4 and 10 μM 48-CT with Pt(IV)Ac-POA, the concentrations at which the compound was most effective. **Figure 3** shows a high number of vital cells in the control, while after treatments this value decreased drastically. At 4 μM an increase of late apoptotic cells compared to control (62.6 ± 0.8 vs 2.1 ± 0.2) was observed. Instead at 10 μM 48-CT, necrotic cells strongly increased compared to 4 μM 48h-CT sample (45.79 ± 0.32 vs 10.88 ± 0.44). For this reason, the concentration of 4 μM of Pt(IV)Ac-POA was chosen hereafter for the standard treatment with the new compound.

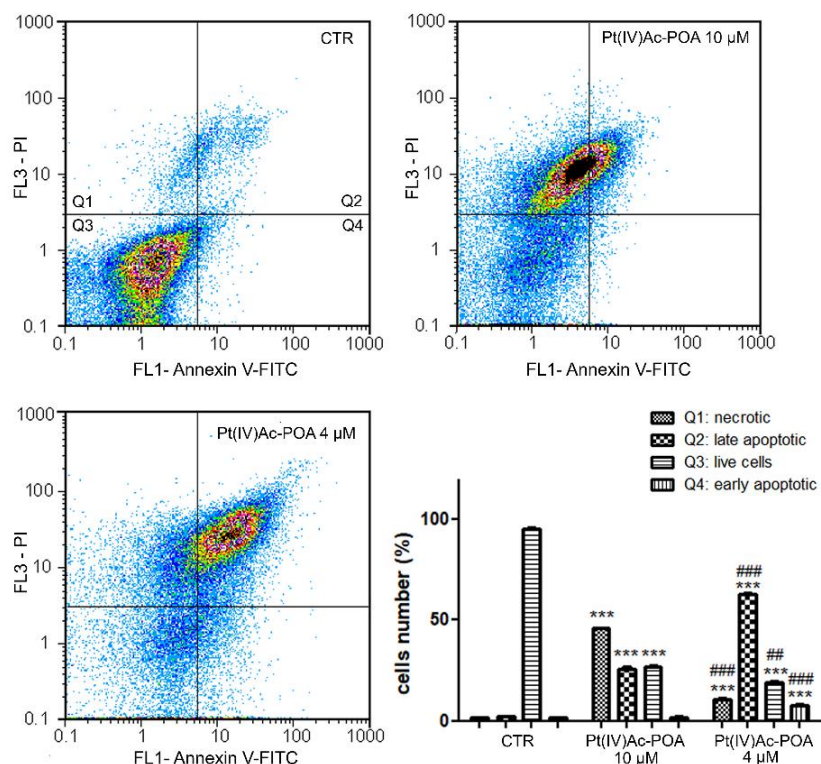


Figure 3. Dual parameter cytograms of FITC-labelled Annexin V (FL1) versus PI staining (FL3) of the control. Cytograms represent control cells (CTR) and treated cells 48h-CT with Pt(IV)Ac-POA at 10 or 4 μM . The bar chart represents the average of three independent experiments and shows the percentage of Annexin V/PI positive cells. *Statistical significance between control and Pt(IV)AC-POA-treated cells, 10 μM , and 4 μM , respectively; #statistical significance between the two treatments Pt(IV)Ac-POA at 10 μM vs Pt(IV)Ac-POA at 4 μM . ρ values: (***) < 0.001 ; (###) < 0.001 ; (##) < 0.01 .

4.1.4 Activation of different apoptotic pathways

The activation of cell death pathways, following treatment with the new compound, was analysed by immunocytochemical reactions, studying the main proteins involved in these processes. After immunolabeling (**Figure 4**), in control cells, Bax was present in the cytoplasm and not colocalize with the mitochondria. On the contrary, after 48h-CT with Pt(IV)Ac-POA at 4 μM , the distribution of Bax labeling was detectable at the mitochondria level with

a clear colocalization of both related fluorescence. Furthermore, the expression of Bax increased in treated cells, compared to control, especially in cells with an apoptotic nucleus in which Bax fluorescence increased. Also, a reducing in cell size was evident after exposure to Pt(IV)Ac-POA, moreover, the mitochondria lost their elongated morphology and clustered as suggested by an increase in fluorescence in the perinuclear area.

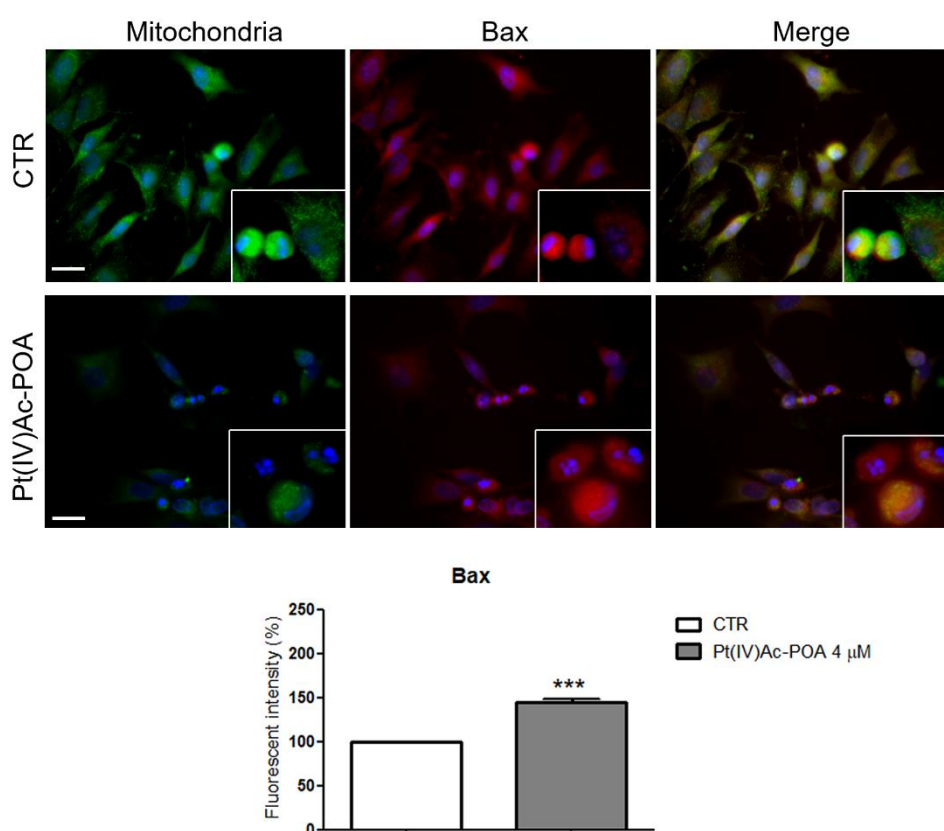


Figure 4. B50 control cells (CTR) and after treatment with Pt(IV)Ac-POA 4 μM. Mitochondria: green fluorescence, Bax: red fluorescence, Hoechst 33258 counterstaining for the nuclei (blue). Inserts show a detail of immunolabelling in control and in apoptotic nucleus cells. Bars: 40 μm. The bar chart shows the percentage of mean fluorescence intensity per cells normalised to control. Student's *t*-test: *statistical significance between control and Pt(IV)Ac-POA; p values: (***) < 0.001.

The images in **Figure 5** show double immunolabeling for Bcl-2 and the mitochondria. Following treatment with Pt(IV)Ac-POA at 4 μ M for 48h-CT, reduced labeling of Bcl-2 and an increase of apoptosis was observed. Furthermore, it was no longer possible to observe colocalization of Bcl-2 fluorescence at mitochondria compared to control condition. In addition, in treated cells, the mitochondria appeared smaller and more rounded, with a clear aggregation at the perinuclear level.

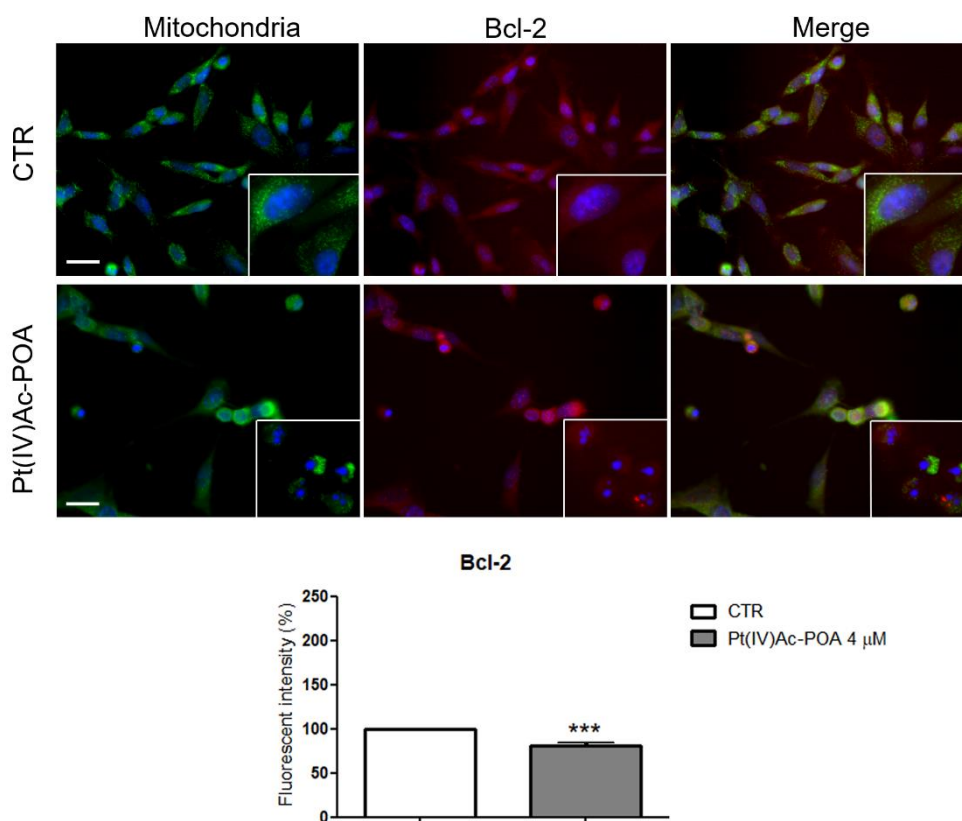


Figure 5. B50 cells in control condition and after 48-CT with Pt(IV)Ac-POA 4 μ M. Mitochondria: green fluorescence, Bcl-2: red fluorescence and Hoechst 33258 counterstaining for the nuclei (blue). Inserts show a detail of immunolabelling in control and in apoptotic cells. Bars: 40 μ m. The bar chart shows the percentage of mean fluorescence intensity per cells normalised to control (CTR). Student's *t*-test: *statistical significance between control and Pt(IV)Ac-POA-treated cells; p values: (***) < 0.001.

In B50 control cells, the AIF immunolabeling colocalized with the mitochondria (**Figure 6**). After treatment with Pt(IV)Ac-POA at 4 μM for 48h-CT, the fluorescence related to AIF was no associated with labeling for mitochondria but was found at the level of the nucleus, which following treatment, appeared fragmented and with apoptotic features.

The difference in morphology of the mitochondria, between the B50 control cells and those exposed to treatment, was significant. In control conditions, the mitochondria colocalized with the AIF protein, with a fusiform aspect, and with cytoplasmic localization. In contrast, following Pt(IV)Ac-POA treatment, the mitochondria lost their structure and arranged themselves on the periphery of the nucleus. To note, as fluorescent signal suggested, mitochondria collapsed in dense masses around the nucleus.

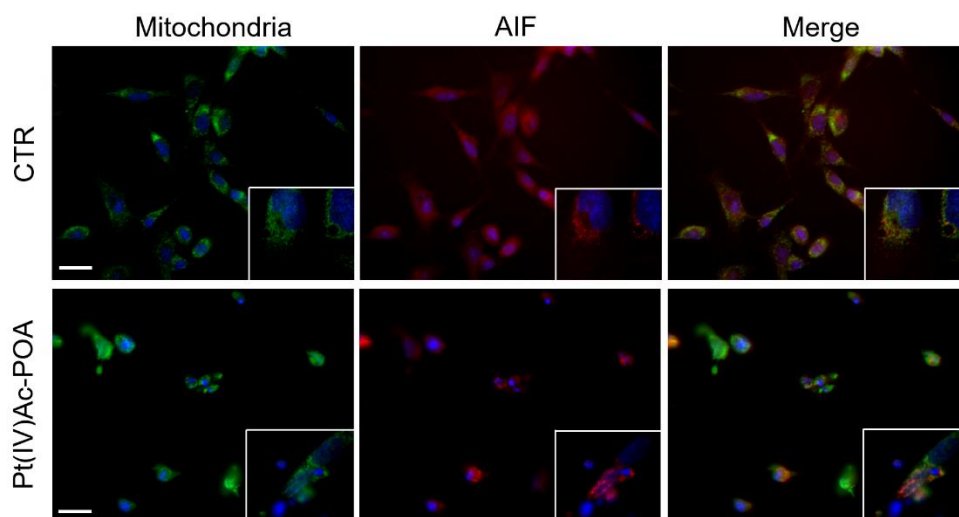


Figure 6. B50 cells in control condition and after treatment with Pt(IV)Ac-POA 4 μM . Mitochondria: green fluorescence, AIF: red fluorescence and Hoechst 33258 counterstaining for the nuclei (in blue). Inserts show a detail of immunolabelling in control and in apoptotic cells. Bars: 40 μm .

To corroborate the data obtained, the activation of the intrinsic apoptotic pathway was assessed by an immunocytochemical detection for active caspase-9,-3 and for PARP-1 was performed.

In the control condition, cells were not immunopositivity to active caspase-9 or -3, as testified by the presence of only viable cells (**Figure 7**). In this condition, the actin cytoskeletal was well structured in filaments within all

cytoplasm. After treatment, the cells underwent apoptosis: the immunopositivity of both active caspase-9 and caspase-3 was increased, as demonstrated also by the quantification cleaved caspase-3 positive cells. In this condition, cell morphology was altered: the cells had a round shape and their nucleus appeared fragmented. The actin cytoskeleton collapsed, with in homogeneous distribution localized around the nucleus.

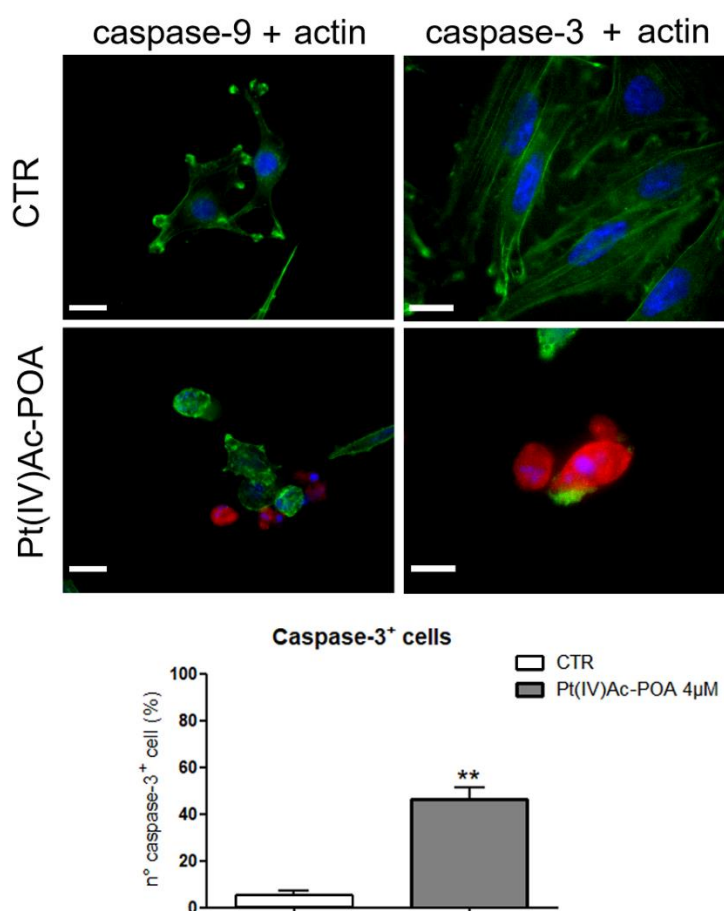


Figure 7. B50 cells in control condition and after treatment with Pt(IV)Ac-POA 4 μ M. Active caspase-9 and -3: red fluorescence, actin: green fluorescence, Hoechst 33258 counterstaining for the nuclei (in blue). Bars: 20 μ m. The bar chart represents the number of cleaved caspase-3 positive cells. Student's *t*-test: *statistical significance between control and Pt(IV)Ac-POA-treated cells; p values: (**) < 0.01 .

PARP-1, involved in DNA damage repair processes, acts as a survival factor in the presence of low levels of DNA damage, whereas extensive DNA damage promotes cell death (Virag L and Szabo C 2002). During apoptosis, the longer fragment moves from the nucleus to the cytosol, due to its lower DNA-binding affinity (Chaitanya GV et al. 2010). Indeed, when severe DNA damage is present, active caspase-3 cleaves PARP-1 in two fragments: p89 and p24 (Aredia F and Scovassi AI 2014; Soldani C et al. 2001). Therefore, p89 is considered an apoptotic marker, that was evaluated by immunocytochemistry.

In control cells PARP-1 was found colocalized in nuclei, on the contrary, in treated cells, it moved to the cytoplasm in late apoptotic cells, where nuclei resulted clearly fragmented. The cytoskeletal tubulin showed alterations after exposure to Pt(IV)Ac-POA and formed aggregates, no longer able to give structure to the cell (**Figure 8**). The presence of PARP-1 cleaved form (89 kDa), and consequently the activation of the intrinsic apoptotic pathway, was confirmed by western blot.

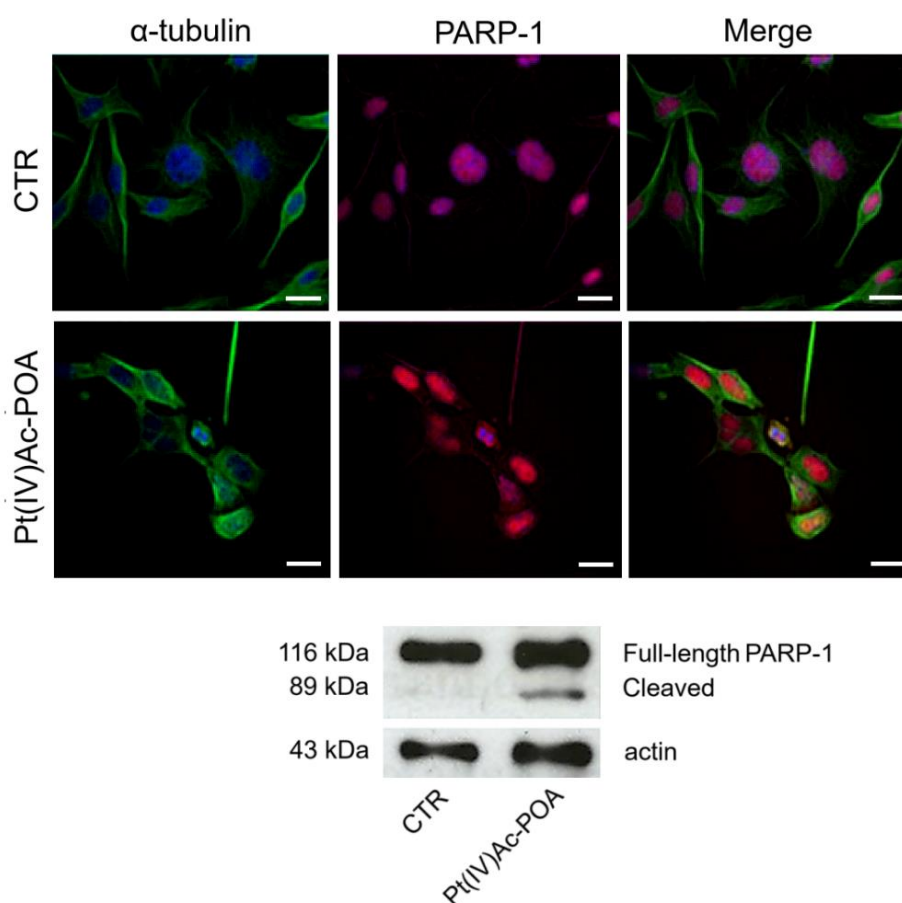


Figure 8. Double immunocytochemical detection in control (CTR) and 48h-CT to Pt(IV)Ac-POA at 4 μ M treated B50 cells. PARP-1: red fluorescence, α -tubulin: green fluorescence, Hoechst 33258 counterstaining for the nuclei (in blue). Bars: 20 μ m. Western blot analysis shows the bands of full-length PARP-1 (116 kDa) and cleaved PARP-1 (89 kDa) compared to the loading control (CTR) and actin (43 kDa).

Caspase-8 is implicated in the extrinsic apoptotic pathway, and its activation was evaluated by the immunofluorescence technique. In **Figure 9**, a high increase in the number of active caspase-8 positive cells was detected in treated cells compared to control conditions. In those cells that have shown immunolabeling for cleaved caspase-8, it was possible to observe the loss of

the structure of the tubulin cytoskeleton, which collapses around the apoptotic nuclei.

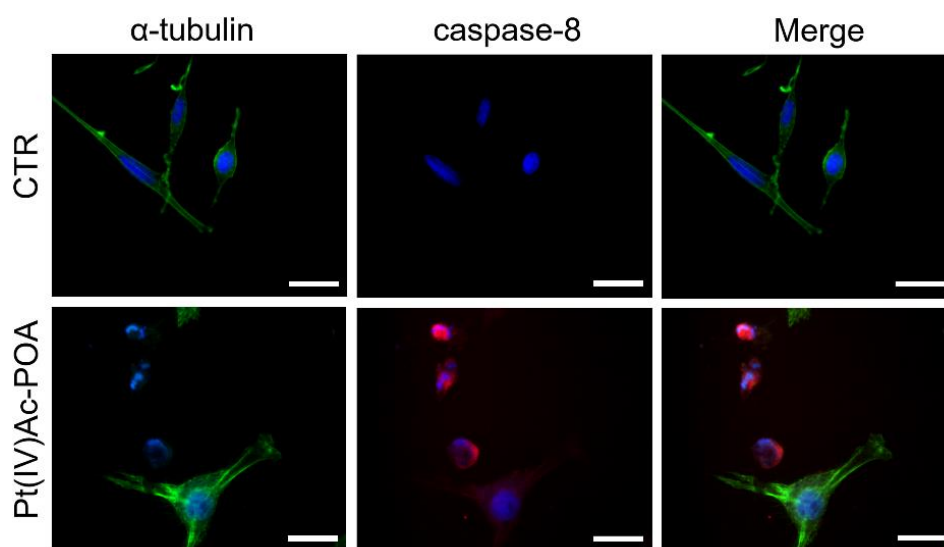


Figure 9. B50 control cells (CTR) and 48h-CT to Pt(IV)Ac-POA at 4 μ M treated cells. Active caspase-8: red fluorescence, α -tubulin: green fluorescence, Hoechst 33258 counterstaining for the nuclei (in blue). Bars: 20 μ m.

To confirm the activation of the extrinsic apoptotic pathway, an immunocytochemical detection of RIP1 was performed. RIP1 is involved in a preliminary step of the necroptosis process, which is promoted *inter alia* by oxidative stress (Hitomi J et al. 2008). Necroptosis is a form of cell death that is activated by the autophosphorylation of RIP1, which is a caspase-8 substrate, and RIP3, thus forming a necrosis complex (Feng S et al. 2007). In control cells (**Figure 10**), RIP1 was expressed in the cytoplasm with a homogeneous distribution, but the treatment caused a redistribution of RIP1 from the cytoplasm to a perinuclear zone, indicating that active RIP1 translocated from the cytoplasm, which appeared destroyed in tardive apoptosis.

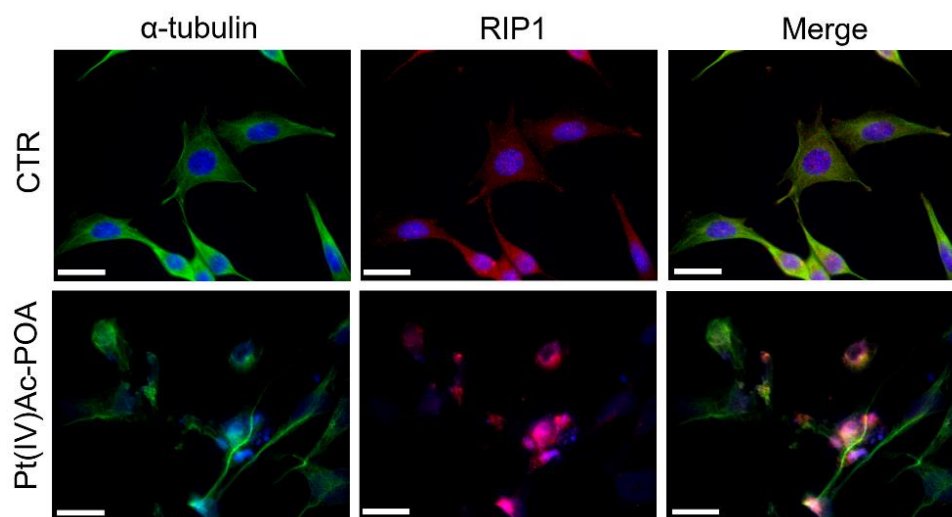


Figure 10. B50 control cells (CTR) and 48h-CT to Pt(IV)Ac-POA at 4 μ M treated cells. RIP1: red fluorescence, α -tubulin: green fluorescence, Hoechst 33258 counterstaining for the nuclei (in blue). Bars: 20 μ m.

4.1.5 Evaluation of autophagy

Autophagy is a form of cell death, but which can also represent a cell survival strategy in some stress condition. The ubiquitin-like protein LC3 is cleaved at its C-terminus to form LC3B-I, which is then conjugated with phosphatidylethanolamine in the autophagosome membrane to form LC3B-II (Kabeya Y et al. 2000), suggesting the activation of autophagy, which can contribute to type II cell death. LC3B-I is involved in autophagosome formation and interacts with another essential protein p62/SQSTM1. After immunoreaction, in control cells, LC3B was located in the cytoplasm and did not colocalize with lysosomes present in the cytoplasm. On the contrary after 48-CT to Pt(IV)Ac-POA at 4 μ M, LC3B moved mostly into the cytoplasm of cells with altered morphology, compared to control cells (**Figure 11**). In early apoptosis LC3B colocalized with lysosomes in the cytoplasm, whereas in late apoptosis there was no colocalization, and lysosomes number decreased.

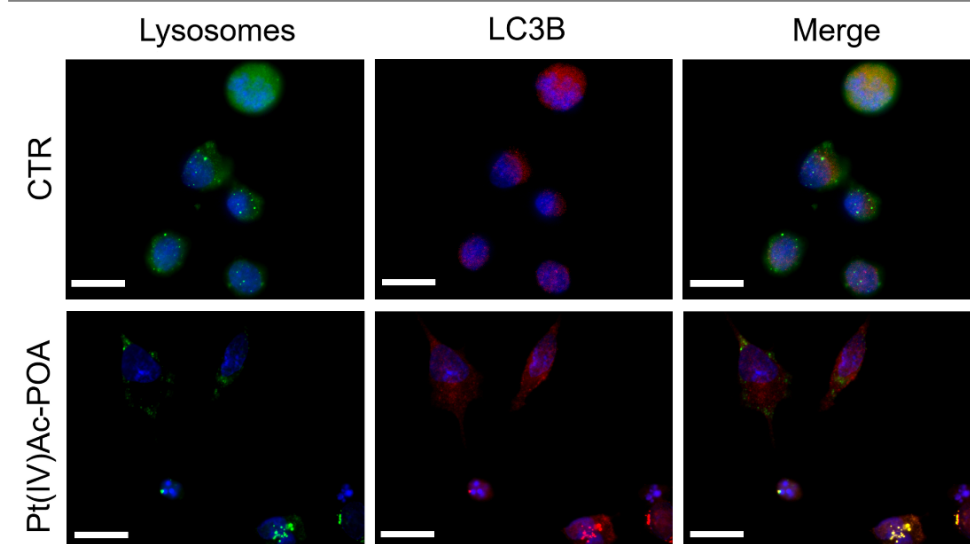


Figure 11. B50 control cells (CTR) and 48h-CT to Pt(IV)Ac-POA at 4 μ M treated cells. LC3B: red fluorescence, lysosomes: green fluorescence, Hoechst 33258 counterstaining for the nuclei (in blue). Bars: 20 μ m.

4.1.6 Effects of Pt(IV)Ac-POA on intracellular organelles

The action of Pt(IV)Ac-POA was also evaluated on cytoplasmic organelles, such as Golgi Apparatus and mitochondria. In control cells (**Figure 12A**), immunofluorescence for Golgi Apparatus appeared homogeneous with a perinuclear localization while the tubulin cytoskeleton maintained its organization. After 48-CT, cells underwent death showing evident alterations. In treated cells, the nucleus was fragmented, and the tubulin cytoskeleton collapsed around it; Golgi Apparatus lost its tubular connections, spreading in the cytoplasm. In control cells, mitochondria appeared with a spotted-like shape and localized in the cytoplasm near the nucleus (**Figure 12B**). Compared to control, treated cells exhibited mitochondria with evident morphological alterations, resulting in homogeneous fluorescence and clusterization in dense masses around the nucleus. Also, in this case, actin cytoskeleton underwent strong alterations collapsing around fragmented nuclei.

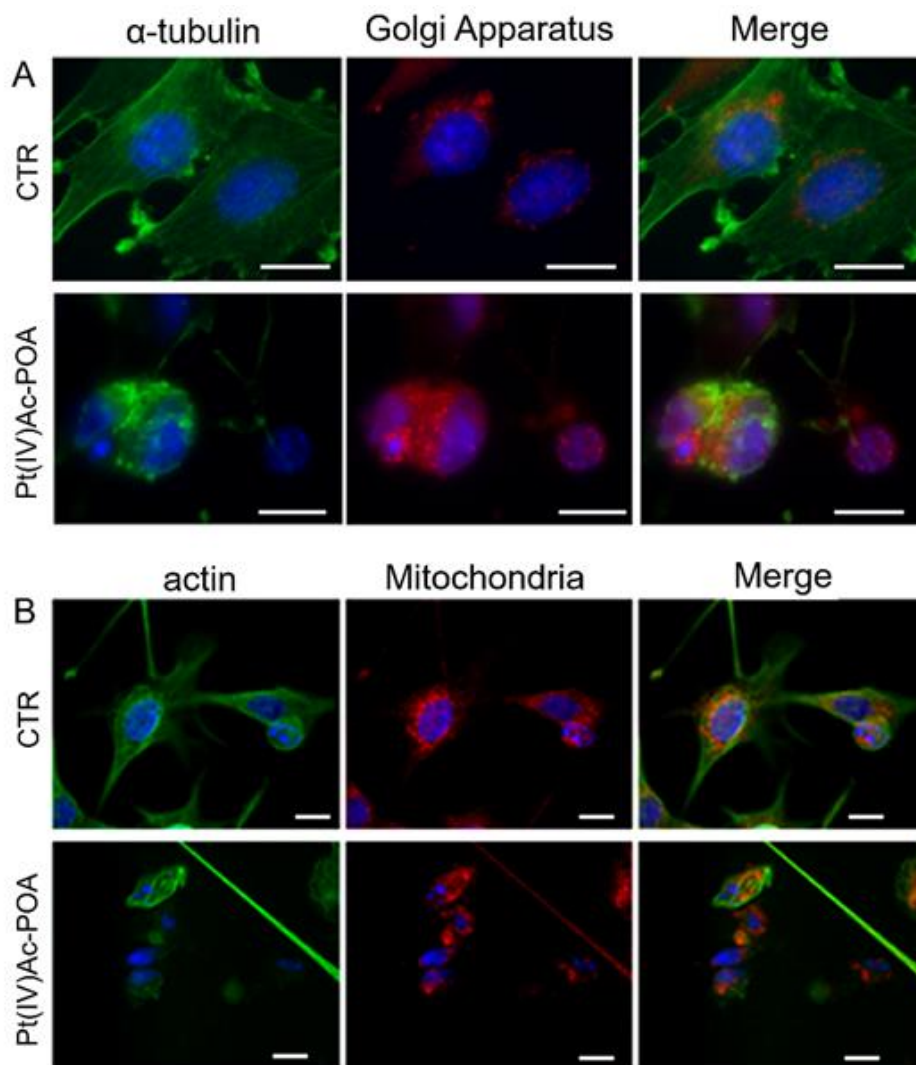


Figure 12. **A)** Double immunocytochemical detection of Golgi Apparatus (red fluorescence) and actin (green fluorescence) in control and 48h-CT Pt(IV)Ac-POA at 4 μ M treated cells. **B)** Double immunocytochemical detection of mitochondria (red fluorescence) and α -tubulin (green fluorescence) in control and 48h-CT Pt(IV)Ac-POA at 4 μ M treated cells. DNA was counterstained with Hoechst 33258 (in blue). Bars: 20 μ m.

4.1.7 Evaluation of CBPs after treatment with Pt(IV)Ac-POA

To evaluate the effects, following 48h-CT Pt(IV)Ac-POA 4 μM , on the expression of CBPs in B50 cells, immunocytochemical reactions were conducted to highlight the proteins involved in Ca^{2+} homeostasis. This preliminary study also investigated the effects induced by the treatment with CDDP, at the condition of 48h-CT at 40 μM , as there is no data in the literature concerning the action of CDDP on CBPs in rat B50 neuroblastoma cell line. The double immunoreactions were carried on marking the respectively CBPs (green fluorescence) and actin cytoskeleton (red fluorescence) (**Figure 13**). In addition, to better understand the qualitative data, quantification of each CBPs fluorescent signal intensity was performed (lower part of **Figure 13**).

Typically expressed in interneurons, in control cells the PV fluorescence was cytoplasmic, while following 48h-CT with CDDP 40 μM or with Pt(IV)Ac-POA 4 μM , protein-associated labeling was still cytoplasmic, but a higher related fluorescence intensity was observed in cells treated with CDDP compared to treatment with Pt(IV)Ac-POA. Moreover, after treatment with CDDP and Pt(IV)Ac-POA, cells that underwent cell death have a fragmented nucleus and the actin cytoskeleton loses its morphology, collapsing around the nucleus. Quantitative analysis showed a statistically significant reduction in the fluorescence intensity of the PV signal after Pt(IV)Ac-POA compared to CDDP-treated and control cells.

CR is a cytosolic buffering protein implicated in the modulation of Ca^{2+} homeostasis and neuronal excitability. In **Figure 13**, in control cells, CR is homogeneously distributed in the cytoplasm. Following 48h-CT with CDDP 40 μM or with Pt(IV)Ac-POA 4 μM , protein-associated labeling was still visible at the cytoplasmic level, showing an increase in its fluorescence intensity. In control condition the cytoskeleton appears well structured, conversely, after both treatments, cells show evident structural alterations and fragmented nuclei, typical of cell death. Bar chart displayed a statistically significant increase in the fluorescence intensity of the CR signal, which was observed after both treatments compared to the control samples. No differences between CDDP- and Pt(IV)Ac-POA-treated cells were observed. CaM is a ubiquitous CBP involved in the regulation of several biological processes, including energy metabolism, cell motility, and exocytosis. The image presented in **Figure 13** displays a double immunolabeling for CaM and actin cytoskeleton. In B50 control cells and after 48h-CT with CDDP at 40

μM or with Pt(IV)Ac-POA at $4 \mu\text{M}$, the labeling for CaM was diffused in the cytoplasm. In detail, the CaM fluorescence signal was increased in cells treated with Pt(IV)Ac-POA compared to control cells and treated with CDDP, as confirmed by the quantitative analysis of fluorescence intensity. Immunolabeling for the actin cytoskeleton displayed morphological and structural alterations of the cytoskeleton component after both treatments. Indeed, compared to control cells in which the actin cytoskeleton had a well-defined and regular organization in thin filaments, following treatment with CDDP and Pt(IV)Ac-POA, changes in cell morphology and cytoskeleton were visible, associated to the fragmented nucleus in apoptotic cells.

CB is involved in the development of neurons, neurite elongation and the growth and formation of dendritic spines. The image presented in **Figure 13** shows a double immunolabeling for CB and actin cytoskeleton, in B50 control cells the labeling for CB protein was recorded at the level of the cytoplasm, while after 48h-CT to CDDP at $40 \mu\text{M}$ or to Pt(IV)Ac-POA at $4 \mu\text{M}$, the fluorescence relative to the CB was still in cytoplasm, but a significant increase in fluorescence intensity was observed, especially after exposure to CDDP. In addition, between control B50 cells and those exposed to both treatments, some differences were evaluated in cell morphology. To note, control cells actin cytoskeleton had the typical well-defined organization, instead, following treatments, the nucleus appeared fragmented in apoptotic cells and cytoskeleton changes were also visible. Indeed, the actin cytoskeleton appears to be collapsed and perinuclearly localized.

All these preliminary data obtained by immunofluorescence reactions were then corroborated by western blot analysis. The data obtained, shown in **Figure 14**, were found to be in line with what was previously seen in immunofluorescence. Western blot conducted to quantify CR in B50 cells revealed a significant increase in protein expression in the treated samples compared to the control. The trend of the values seems to confirm the data obtained by fluorescence intensity quantification, although there were no substantial differences between the two treatments. Quantification of CaM showed differences between treated samples and control conditions, confirming a statistically significant increase in CaM expression especially after exposure to Pt(IV)Ac-POA. Analysing the western blot data about CB, it was evident how the treatments with CDDP and with Pt(IV)Ac-POA have induced changes in the expression of the protein, compared to the control, but not between the two treatments.

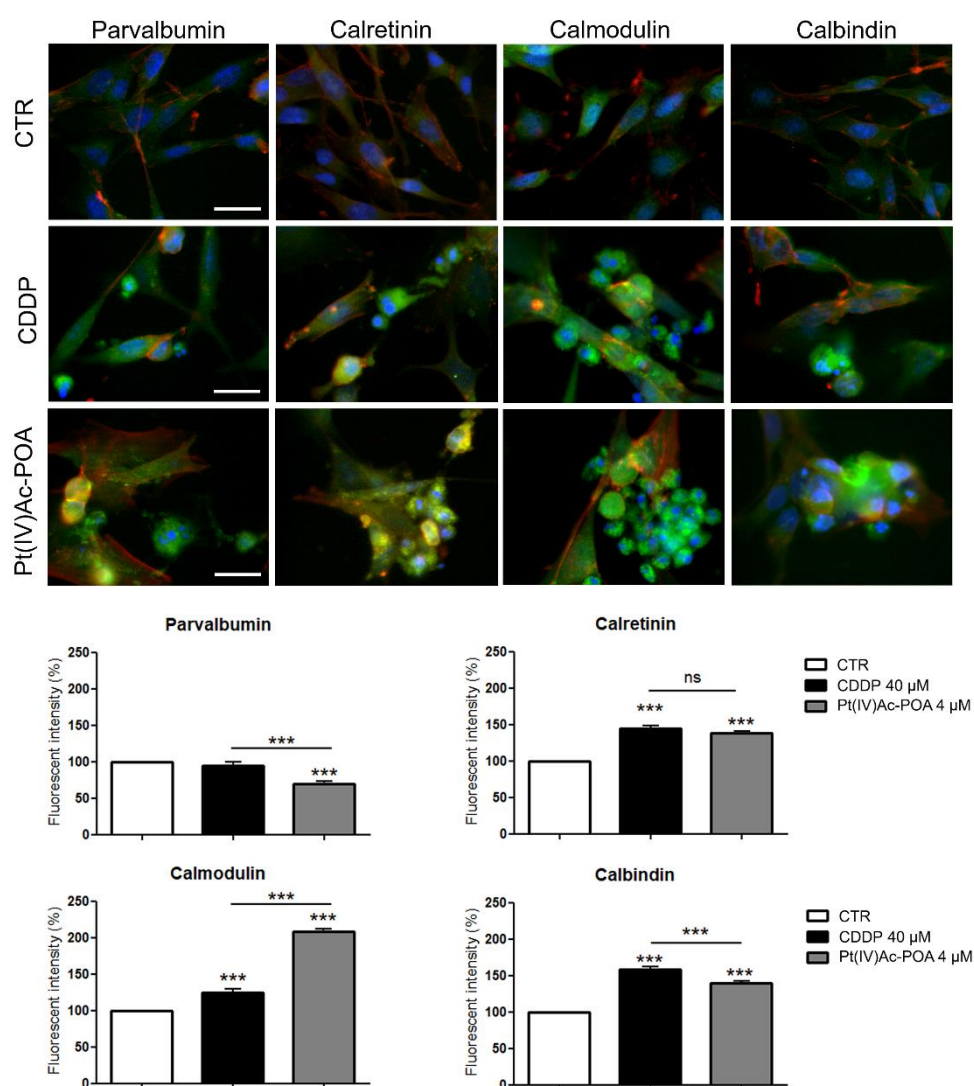


Figure 13. Immunocytochemical detection of CBPs: parvalbumin, calretinin calmodulin and calbindin (red fluorescence) and actin cytoskeleton (green fluorescence) in control B50 cells and after 48h-CT with CDDP 40 μ M or Pt(IV)Ac-POA 4 μ M. DNA was counterstained with Hoechst 33258 (in blue). Bar: 40 μ m. Bar charts with the percentage of fluorescence intensity for each CBPs in control and treated cells with CDDP and Pt(IV)Ac-POA. *Statistical analysis: control vs each treatment and CDDP vs Pt(IV)Ac-POA; p values: (***) $p < 0.001$, ns: not significant.

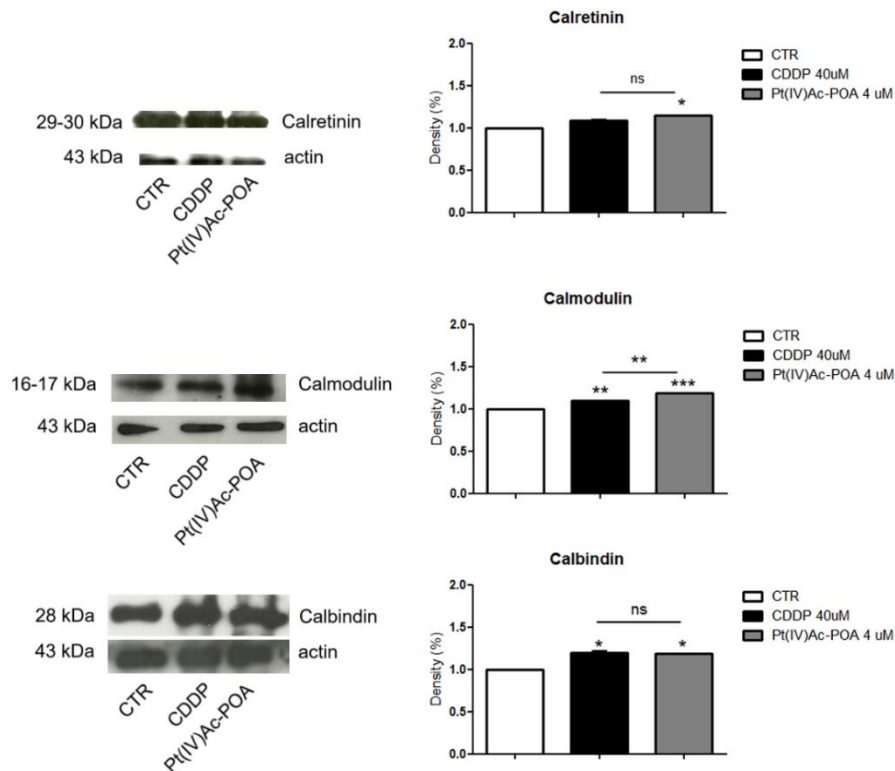


Figure 14. Western blot bands of CBPs calretinin, calmodulin, and calbindin after 48h-CT to CDDP 40 μ M or Pt(IV)Ac-POA 4 μ M, compared to the loading control (CTR) and actin 43 kDa. On the right of each western blot the respective bar chart of density bands quantification. *Statistical analysis: control vs each treatment and CDDP vs Pt(IV)Ac-POA; ρ values: (*) $\rho < 0.05$, (**) $\rho < 0.01$, (***) $\rho < 0.001$, ns: not significant.

4.1.8 Evaluation of PMCA1 after treatment with Pt(IV)Ac-POA

PMCA1 is an ATPase pump involved in the control of Ca^{2+} homeostasis, using ATP to expel a Ca^{2+} outside, in development and organogenesis. As reported in the images in **Figure 15**, the immunolabeling for PMCA1, in green, and the actin, in red, revealed a profound difference between the control cells and the 48h-CT CDDP- and Pt(IV)Ac-POA-treated cells. In control conditions, PMCA1 was cytoplasmatic but weakly expressed. In contrast, the cells exposed to CDDP showed an increase in the PMCA1

fluorescence intensity, while after Pt(IV)Ac-POA this increase was less evident (**Figure 15A**). Immunolabeling for actin revealed that the cytoskeleton was well structured in the control cells, instead, it lost its organization and collapsed near the nucleus following both treatments. The quantitative analysis concerning PMCA1 fluorescence displayed a statistically significant increase of the marking in the two treatments compared to the control condition. However, western blot analysis corroborated the data observed for CDDP treatment but evinced no significant differences between control and Pt(IV)Ac-POA-treated cells (**Figure 15B**).

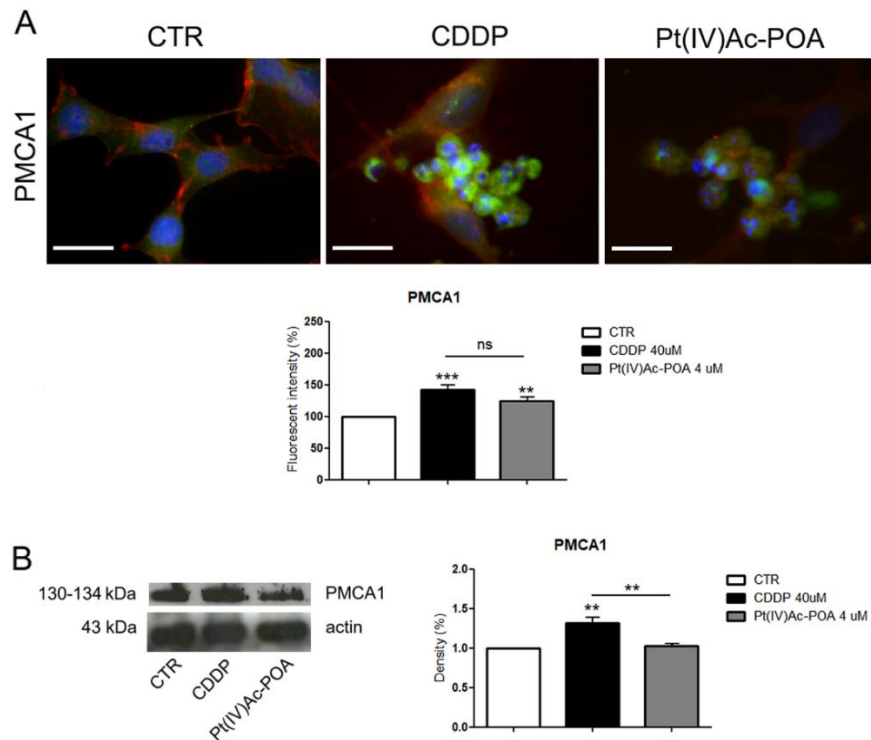


Figure 15. A) Double immunofluorescence for PMCA1(green fluorescence) and actin (red fluorescence) in B50 cells in control condition and after 48h-CT with CDDP 40 μ M or Pt(IV)Ac-POA 4 μ M. DNA was counterstained with Hoechst 33258 (in blue). Bar: 40 μ m. Bar chart with the percentage of fluorescence intensity for PMCA1 in the three conditions. **B)** Western blot density bands and the respective graph of density bands quantification. *Statistical analysis: control vs each treatments and CDDP vs Pt(IV)Ac-POA; p values: (**) $p < 0.01$, (***) $p < 0.001$, ns: not significant.

4.1.9 Analysis of the deacetylation effects induced by POA in B50 cells

To identify the action as HDACi and consequently the induction of deacetylation, the free acid POA was analysed individually to separate it from the action of the CDDP contained in Pt(IV)Ac-POA. For this analysis the same concentration used for the standard treatment with Pt(IV)Ac-POA was employed, therefore using the POA alone at the concentration of 4 μ M. The preliminary data obtained showed that after 48h-CT with POA at 4 μ M no significant difference in cell cycle distribution was observed (**Figure 16A**). The only significant difference was a sub-G₁ peak evaluated after treatment, but not ascribable to an increase of the amount of apoptotic cell after evaluation with Annexin-V assay (**Figure 16B**).

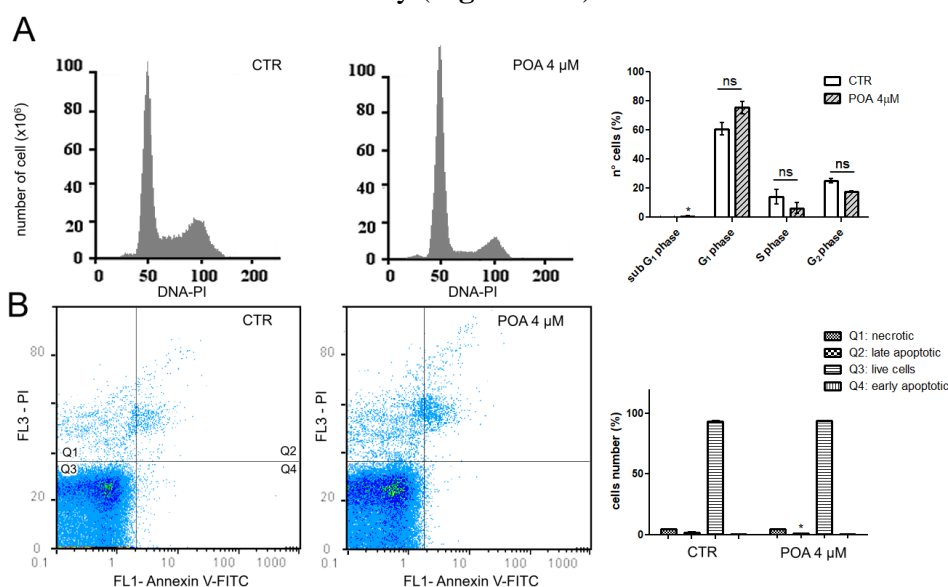


Figure 16. **A)** Cytograms of DNA content in B50 control cells (CTR) and treated for 48h-CT with POA at 4 μ M after PI staining. On the right, the quantification bar chart represents the percentage of cell number in the respective cell cycle phases. **B)** Dual parameter cytograms of FITC-labelled Annexin V (FL1) vs PI staining (FL3) representing control cells (CTR) and treated cells 48-CT with POA at 4 μ M. The bar chart shows the percentage of Annexin V/PI positive cells. Student's *t*-test: *statistical significance between the respective conditions of control and POA-treated cells; p values: (*) $p < 0.05$, ns: not significant.

Double immunolabeling for the acetylated histone H3 and PCNA was carried out in order to evaluate the expression of these proteins after treatment for 48h-CT with POA 4 μ M. PCNA, in this case, a specific antibody for proliferation and not for DNA damage, was used as a reference nuclear protein for immunolabeling. In **Figure 17A** the images related to the immunofluorescence show how after treatment there was an increase in fluorescence intensity for acetyl-H3, on the contrary, a significant decrease in the PCNA fluorescent signal was observed, supporting the presence of dead cells in the image and the previous data observed in cytofluorimetry. Following western blot analysis, although not significant, in the samples treated with POA there was an increase in histone H3 acetylation. Furthermore, the reduction of PCNA expression in treated cells was confirmed by western blot evaluation.

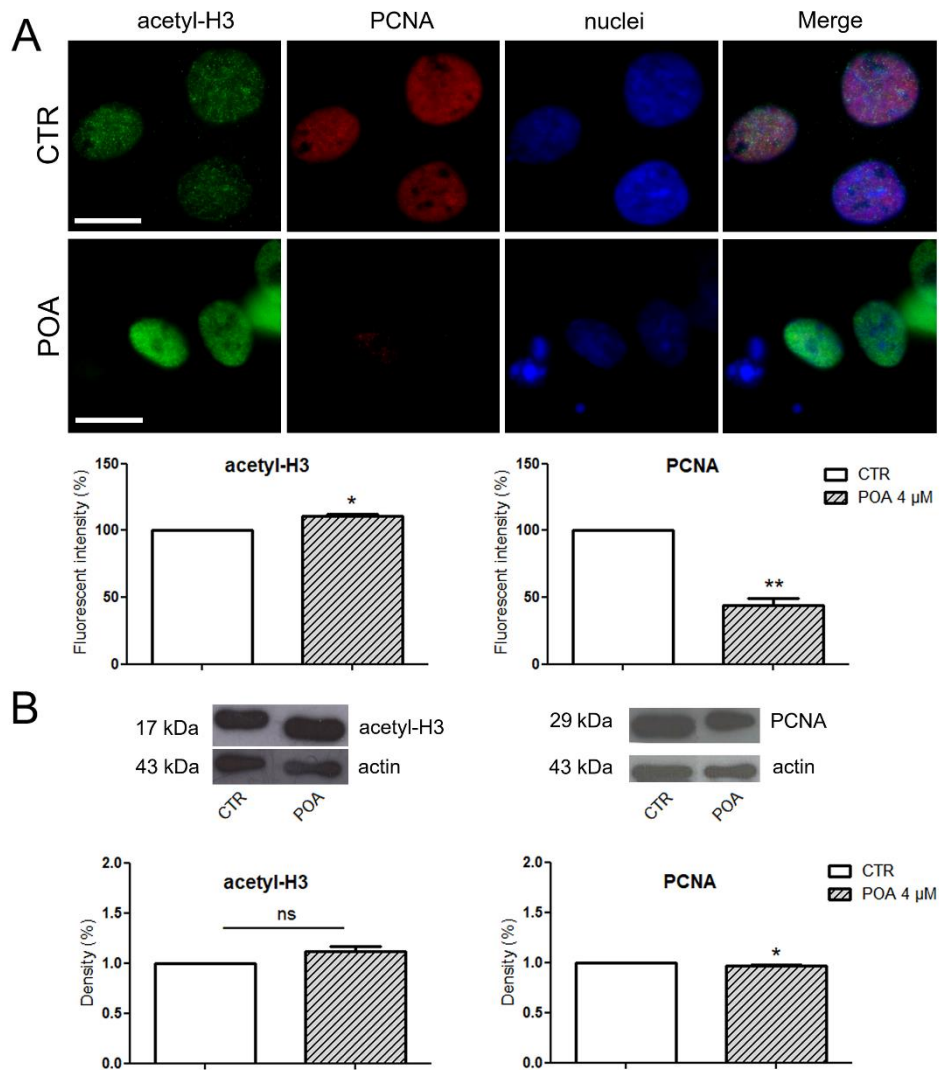


Figure 17. **A**) Double immunofluorescence reaction, with the relative quantification, for acetyl-H3 (in green) and PCNA (in red), nuclei were counterstained with Hoechst 33258 (in blue). Bar: 20 μ m. **B**) Western blot bands and density bar charts of acetyl-H3 and PCNA quantifications. Student's *t*-test: *statistical significance between control and POA-treated cells; p values: (*) $p < 0.05$, (**) $p < 0.01$, ns: not significant.

Despite the data obtained from the previous analysis, through the ultrastructural observations at electron microscopy, a visible decondensation in the chromatin was not found in 48h-CT POA-cells compared to controls (**Figure 18**). This led to the assumption that acetylation could only be a local effect and not induce a structural chromatin modification.

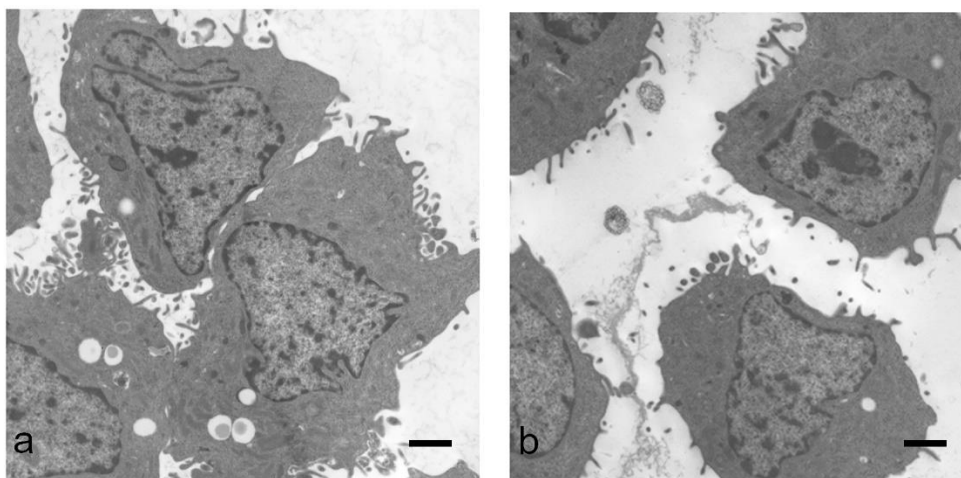


Figure 18. Ultrastructural analysis at the electron microscope reveals no difference in chromatin decondensation between control (**a**) and treated cells at 48h-CT with POA μM (**b**). Bars: 1.1 μm .

To elucidate this mechanism of action induced by the free acid POA, short times treatment (*i.e.* 2h, 4h, 8h, and 24h) have been evaluated which, as shown in **Figure 19**, revealed how the decondensation effect of 4 μM POA treatment was detectable at 4h of continues exposure. At 2h of exposure to POA and in time after 4h the level of chromatin decondensation was like to control conditions described above.

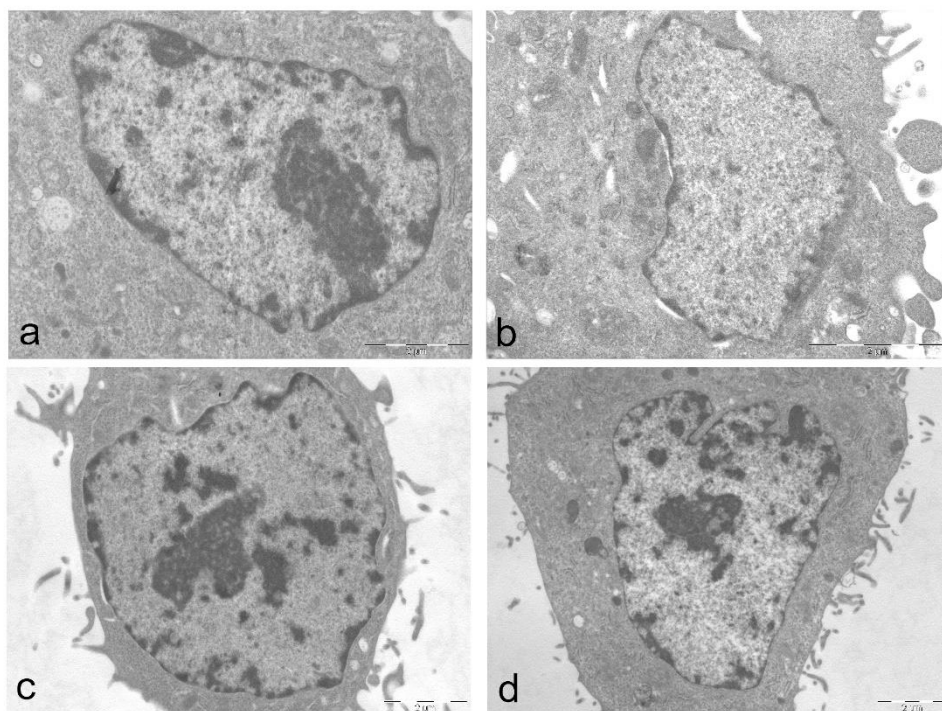


Figure 19. B50 cells after 4 μM POA treatment at 2h (a), 4h (b), 8h (c) and 24h (d), respectively. To note the strong chromatin decondensation after 4h of continuous exposure to POA: Bars: 2 μM .

Once the effect of 4h-CT POA at 4 μM was evaluated, the expression of acetyl-H3 and PCNA was quantified. Double immunolabeling revealed a significant increase for acetyl-H3 after treatment with POA compared to the respective control at 4h (**Figure 20A**). The data was also confirmed by the western blot analysis, where a significant increase of this marker was observed compared to the control cells (**Figure 20B**). Instead, the evaluation of PCNA after 4h-CT with POA at 4 μM , showed no difference compared to the control samples, both after fluorescence intensity analysis and after western blot evaluation.

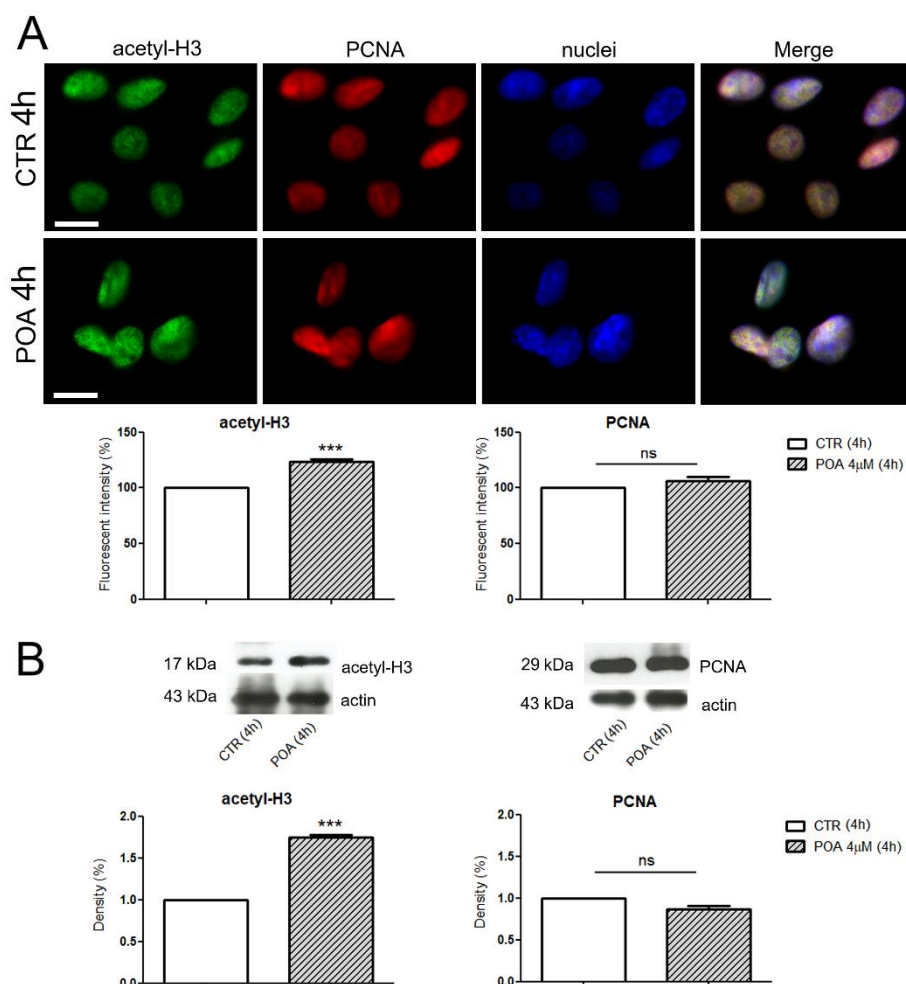


Figure 20. **A)** B50 control cells and treated with 4 μ M POA at 4h-CT. Double immunofluorescence reaction, with the relative quantification, for acetyl-H3 (in green) and PCNA (in red), nuclei were counterstained with Hoechst 33258 (in blue). Bar: 20 μ m. **B)** Western blot bands and density bar charts of acetyl-H3 and PCNA quantification. Student's t-test: *statistical significance between control and POA-treated cells; p values: (***) $p < 0.001$, ns: not significant.

No changes induced by the treatment 48h-CT with POA at 4 μ M were found on B50 cells compared to control, in the analyses on the pathway and CBPs previously described and carried out for 48h-CT Pt(IV)Ac-POA at 4 μ M.

4.2 The effect of Pt(IV)Ac-POA on C6 glioma rat cells

Pt(IV)Ac-POA treatment has shown encouraging results, exhibiting a strong anticancer effect on B50 neuroblastoma rat cells already at the concentration of 4 μM (Rangone B et al. 2018). Therefore, further analysis was conducted on the rat glioma C6 cell line, focusing on the activation of cell death pathways and evaluating morphological and functional changes induced by the novel prodrug Pt(IV)Ac-POA (Ferrari B et al. 2019). The C6 line was widely used in the study of the gliomas and mechanisms underlying the action of CDDP (Krajčí D et al. 2006; Mares V et al. 2003; Mohamadi N et al. 2017; Noda S et al. 2001) thus the 48h-CT with CDDP at 40 μM was introduced to have a comparison with the data already obtained on other lines and to perform a treatment comparable to that with Pt(IV)Ac-POA.

4.2.1 Cell cycle distribution and cell death

First of all, the concentrations of Pt(IV)Ac-POA were evaluated on C6 cells in order to obtain the most effective dose to be used for subsequent procedures. Based on the analysed in Rangone B et al. 2018, the respective concentrations of Pt(IV)Ac-POA *i.e.* 10, 4 and 1 μM were tested. Cytograms in **Figure 21** represent the distribution of DNA content in C6 control cells and after treatment for 48h-CT with CDDP (40 μM) or Pt(IV)Ac-POA (10, 4 and 1 μM). In the control condition (CTR), cells were distributed among the different cell phases (G_1 , S, G_2), where an intense S phase indicated active proliferation. After CDDP exposure, the cell cycle lost its physiological distribution and a sub- G_1 peak (dead cells) was observed. After 48h-CT Pt(IV)Ac-POA at 10 μM , DNA content distribution was deeply modified, and debris was detectable. In addition, at this concentration peaks G_1 , S, and G_2 were almost absent. After 48h-CT at 4 μM cytogram exhibited an enlarged sub- G_1 peak, representing high cell mortality, moreover, the distribution of the cell DNA content was comparable to those obtained with CDDP treatment, but which was already achieved at a concentration ten times lower than reference treatment. Conversely, cells treated with the new prodrug at a concentration of 1 μM returned to be distributed in the different phases of the cycle, but a small sub- G_1 peak can be still distinguishable. Based on these results, like for the B50 cell line, the concentration of 4 μM of Pt(IV)Ac-POA was chosen for the standard 48-h CT to compare with CDDP 40 μM treatment.

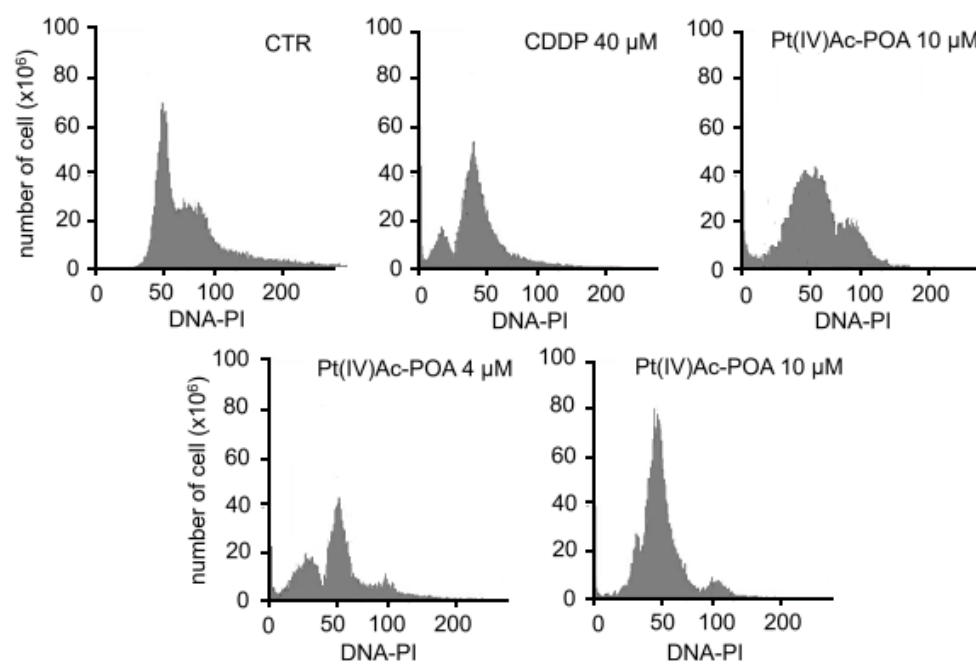


Figure 21. Cytograms of DNA content after staining with PI in C6 control cells and after treatment with CDDP (40 μM) or Pt(IV)Ac-POA (10, 4 and 1 μM) for 48h-CT.

A test with Annexin V/PI staining was performed to assess the induction of apoptosis after 48h-CT with 4 μM Pt(IV)Ac-POA. To note, in **Figure 22**, that in control condition almost cells were living, while treatments induced a strong reduction in the number of viable cells. Bar chart displays that compared to control condition, after CDDP exposure there was an increase in the necrotic cell concentration (35.96 ± 1.14 vs 0.42 ± 0.03) and late apoptotic cells (37.36 ± 1.86 vs 7.06 ± 0.34), while a concentration of live cells (23.97 ± 0.75 vs 86.58 ± 4.36) was still preserved. At 4 μM of Pt(IV)Ac-POA, the number of late apoptotic cells increased (62.81 ± 1.32), on the contrary, the amount of necrosis decreased (23.68 ± 0.83) compared to CDDP treated sample.

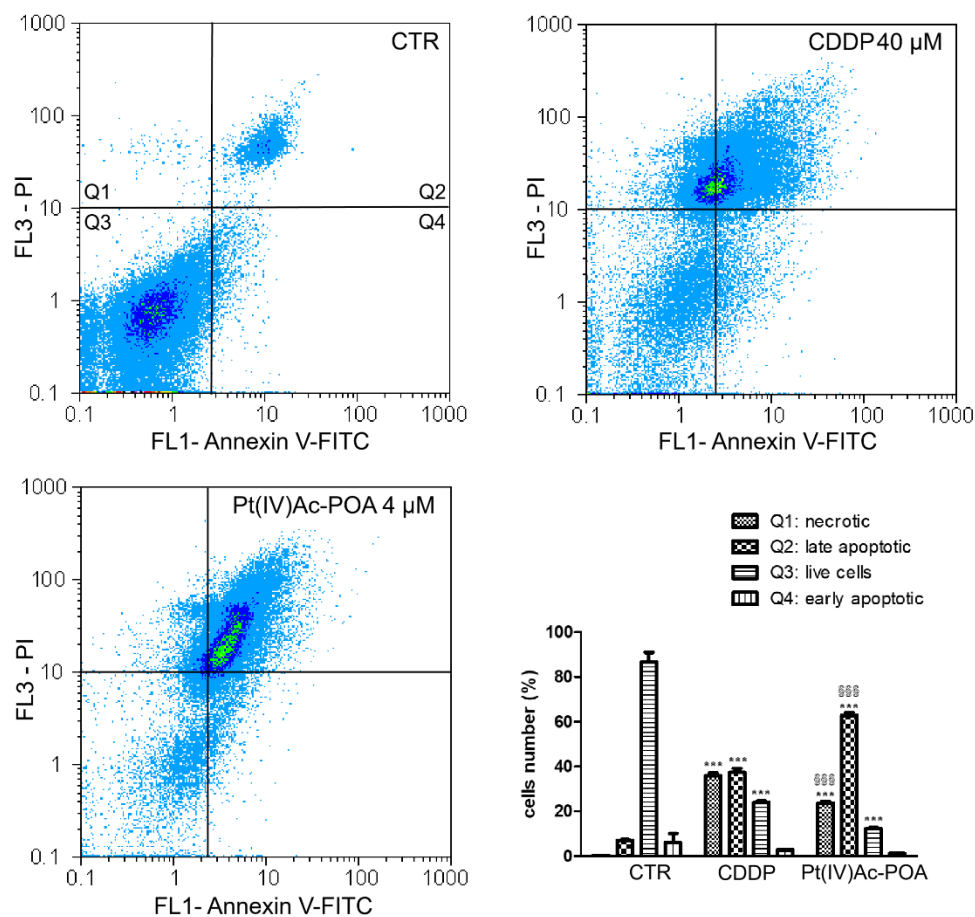


Figure 22. Dual parameter cytograms of FITC-labelled Annexin V (FL1) versus PI staining (FL3) of the control (CTR) and of cells treated with CDDP at 40 μM or Pt(IV)Ac-POA at 4 μM concentrations, respectively. The bar chart represents the average of three independent experiments, shows the percentage of the value of Annexin V/PI positive cells: in quadrant Q1 (necrotic), Q2 (late apoptotic), Q3 (viable cells) and Q4 (early apoptotic). *Statistical analysis: control vs treated samples: (***) $p < 0.001$; §statistical analysis CDDP vs Pt(IV)Ac-POA treated samples: (§§§) $p < 0.001$.

4.2.2 Ultrastructural analysis

Through investigations at electron microscopy, CDDP treatment has been shown to induce apoptosis in C6 cells (Krajcǐ D et al. 2000). Based on these data, the effect of Pt(IV)Ac-POA on the rat glioma line was analysed, to identify the possible structural alterations and classify the potential cell deaths induced by the treatment. Control cell, (**Figure 23a**) showed the presence of a nucleus in a central position with decondensed chromatin, Golgi Apparatus was structured in the perinuclear zone. In addition, in cytoplasm medium size mitochondria were detectable and cytoplasmic extensions at the cellular periphery level and sporadic lysosomes suggested a possible basal autophagic activity. In **Figure 23b** after 48h-CT Pt(IV)Ac-POA at 4 μ M, cell exhibited the typical apoptosis features: chromatin condensation, absence of nuclear envelope and cytosol in part degraded. As showed in **Figure 23c**, some characteristics of autophagy were detectable after prodrug treatment. Indeed, many cytoplasmatic autophagic vacuoles were observed, probably autophagolysosomes, characterized by a double membrane and containing degraded cytoplasmic components (insert, black arrowhead). Furthermore, a necroptosis reported in **Figure 23d** showed some characteristics similar to the apoptosis, such as the karyorrhexis, and aspects analogous to necrosis as well as cytoplasmic vacuolations and rupture of the plasma membrane.

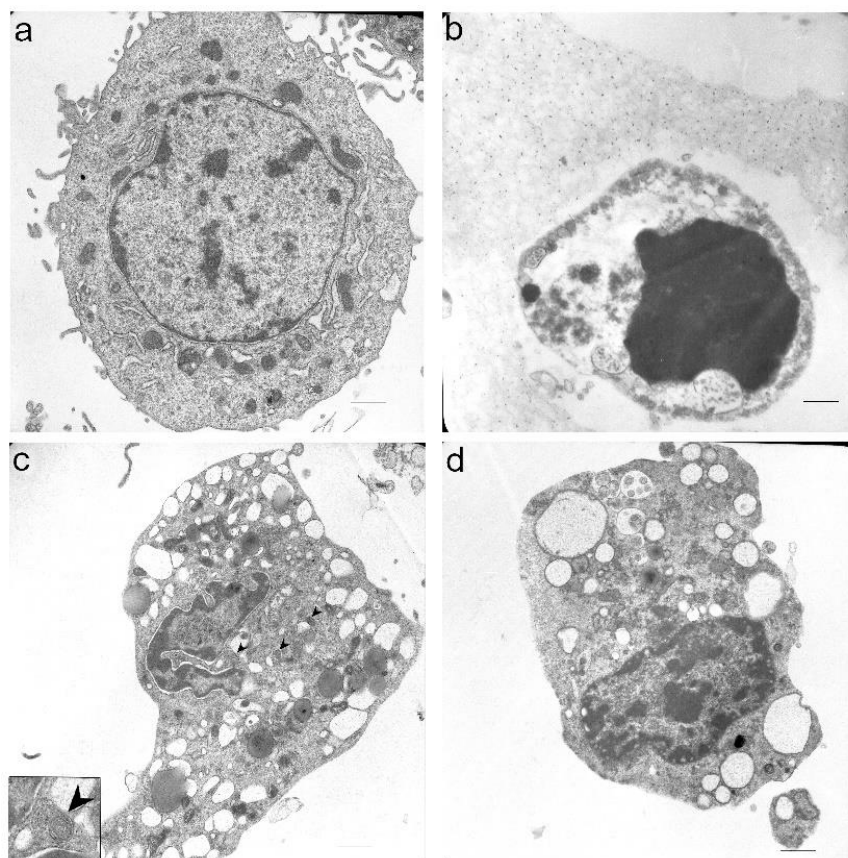
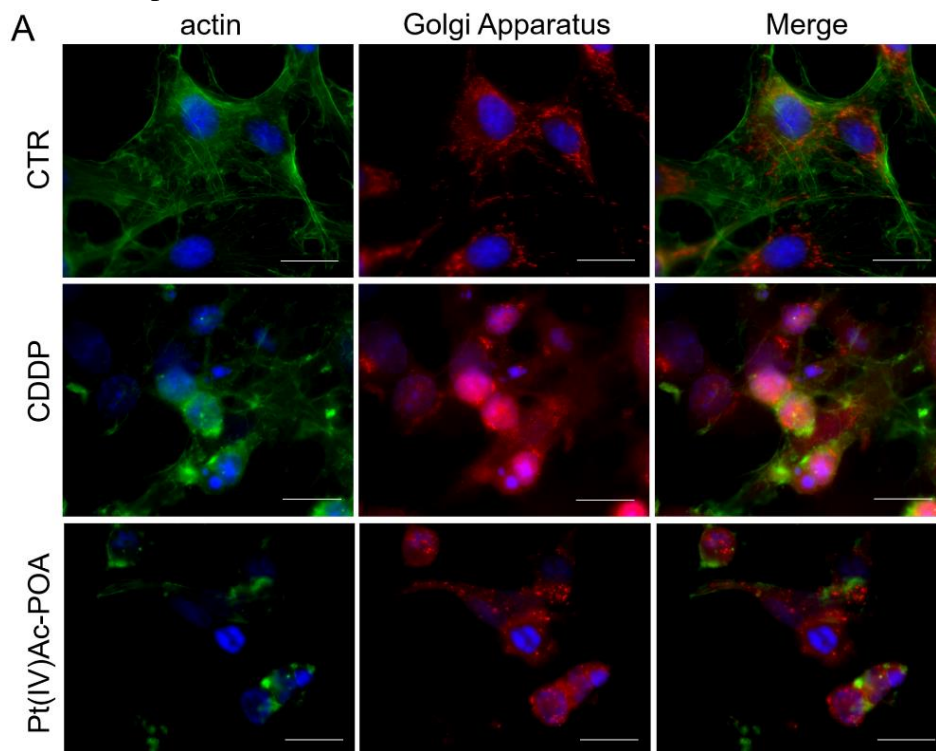


Figure 23. C6 cells ultrastructural analysis in the control condition (a) and after 4 μM Pt(IV)Ac-POA 48h-CT (b-d). Apoptosis (b), autophagy (c) with some autophagolysosomes (insert, black arrowhead), necroptosis (d) are shown. Bars: 1.1 μm .

4.2.3 Effects of Pt(IV)Ac-POA on intracellular organelles

Previous studies conducted on the B50 neuroblastoma cell line, after 48h-CT with CDDP at 40 μM , have shown that cytoplasmic organelles, such as Golgi Apparatus and mitochondria, are possible targets of drug exposure (Santin G et al. 2012; Santin G et al. 2013). Thus, the effects of 48-CT with Pt(IV)Ac-POA at 4 μM on Golgi Apparatus and mitochondria were evaluated. In control cells (Figure 24A), Golgi Apparatus immunofluorescence showed a usual appearance, with a homogeneous

distribution in the perinuclear zone, moreover, the actin cytoskeleton was well-structured. After 48h-CT with Pt(IV)Ac-POA, cells showed evident alterations related to cell death: actin cytoskeleton collapsed around the cell fragmented nuclei, and Golgi Apparatus lost its physiological tubular connections, exhibiting a globular appearance distributed in the cytoplasm. Regarding mitochondria, in control cells, immunolabelling had a spotted-like shape with cytoplasm and perinuclear distribution (**Figure 24B**). Compared to control cells, after CT exposure, treated cells showed morphological alterations; mitochondria immunofluorescence resulted homogeneously and these organelles clustered around apoptotic nuclei, forming dense masses. Also, in this case, the tubulin cytoskeleton collapsed, and cells lost their fusiform shape.



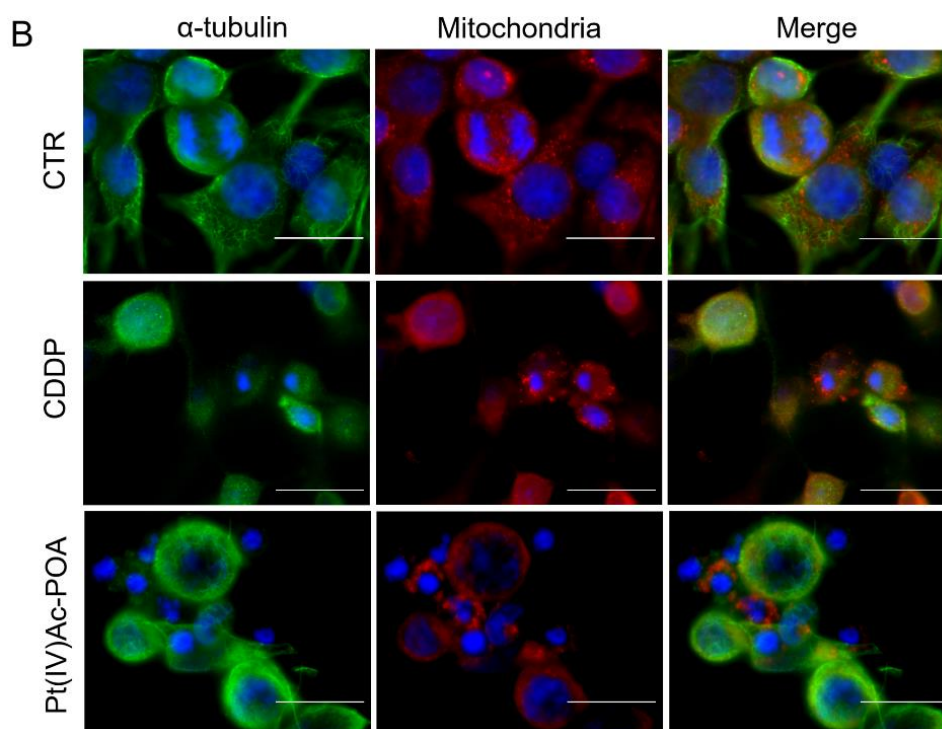


Figure 24. Intracellular organelles investigation by fluorescence microscopy, C6 control cells and after 48h-CT with CDDP 40 μ M or Pt(IV)Ac-POA 4 μ M. **A)** Double immunocytochemical detection of Golgi Apparatus (red fluorescence) and actin (green fluorescence). **B)** Double immunocytochemical detection of mitochondria (red fluorescence) and α -tubulin (green fluorescence) in control and treated cells. DNA counterstaining with Hoechst 33258 (in blue). Bars: 20 μ m.

4.2.4 Activation of different apoptotic pathways

Similarly, to the B50 cell line, for C6 cells a double immunolabel was carried out for proteins involved in cell death pathways. In particular, the images shown in **Figure 25** reported double immunolabeling for the Bax protein and mitochondria. As has been observed in B50 cells, even in the C6 control cells, Bax-related fluorescence has a purely cytoplasmic localization, without any colocalization with the mitochondria. Instead, at 48h-CT with CDDP 40 μ M or with Pt(IV)Ac-POA 4 μ M, an increase in mitochondrial localization of the Bax immunolabeling was observed. After treatment with Pt(IV)Ac-POA, in early apoptosis, the fluorescence intensity for Bax appears

to be strongly increased, compared to cells exposed to CDDP. While immunolabeling for mitochondria shows a visible morphological difference between C6 control cells and treated to the compounds. In control conditions the mitochondria were distributed evenly in the cytoplasm, in contrast, following treatment with CDDP the mitochondria tend to be clustered, losing their classic tapered shape. This aspect was more evident after treatment with Pt(IV)Ac-POA, where the mitochondria, changing their morphology, moved mainly around the nucleus. The quantification of Bax fluorescence intensity showed that in C6 cells there was a statistically significant increase after Pt(IV)Ac-POA and CDDP, compared to control. This value was increased after treatment with Pt(IV)Ac-POA, compared with that obtained after exposure to CDDP.

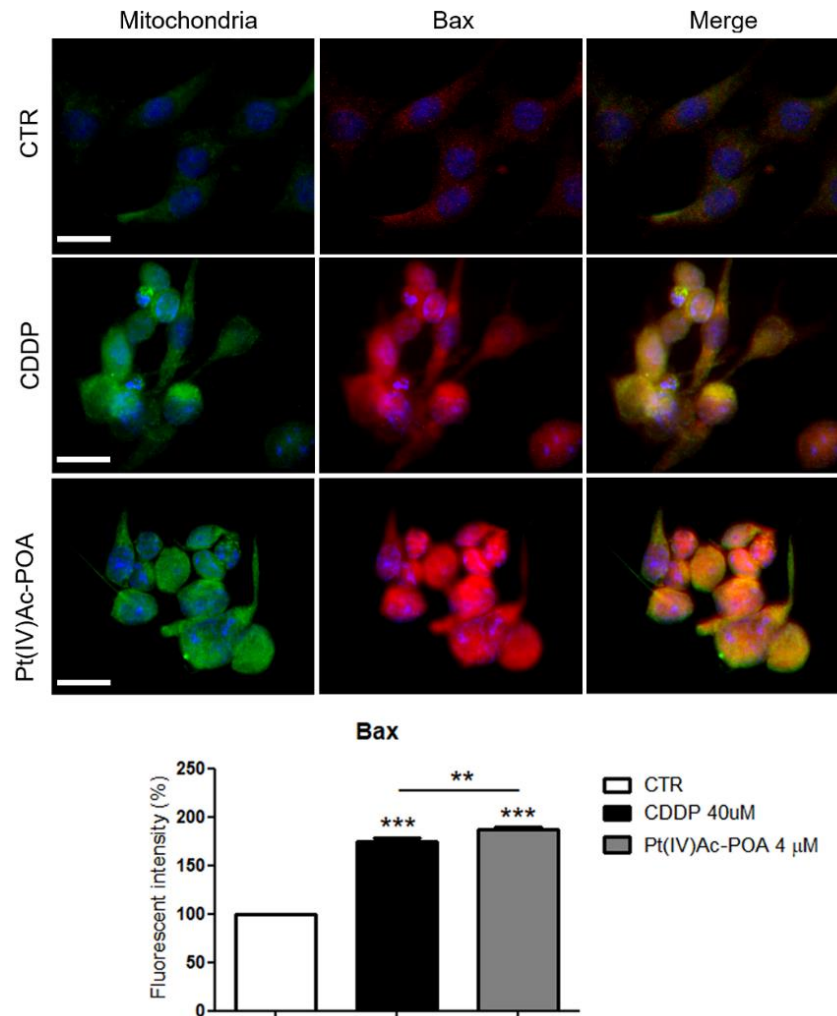


Figure 25. Double immunoreaction for mitochondria (green fluorescence) and Bax (red fluorescence) in control and treated cells with CDDP or Pt(IV)Ac-POA. DNA counterstaining with Hoechst 33258 (in blue). Bars: 20 μ m. The bar chart represents the quantification of Bax fluorescent intensity. *Statistical analysis: control vs each treatment and CDDP vs Pt(IV)Ac-POA; p values: (**) $p < 0.01$, (***) $p < 0.001$.

Figure 26 shows the double immunolabeling for Bcl-2 and mitochondria. After 48h-CT with CDDP at 40 μ M or Pt(IV)Ac-POA at 4 μ M, the Bcl-2 labelling increased compared to C6 control cells. After CDDP exposure, the Bcl-2 fluorescence increased compared to control and Pt(IV)Ac-POA-treated

cells, as the bar chart shows in **Figure 26**. On the contrary, no significant difference was found compared to the control and Pt(IV)Ac-POA-treated cells. The effect on mitochondria, before and after treatment, was like that seen in B50 cells. Indeed, while in the control samples the mitochondria appear fusiform and have a well-defined structure, following exposure to both compounds, these organelles condensing around the nucleus and an even more evident aspect after treatment with Pt(IV)Ac-POA.

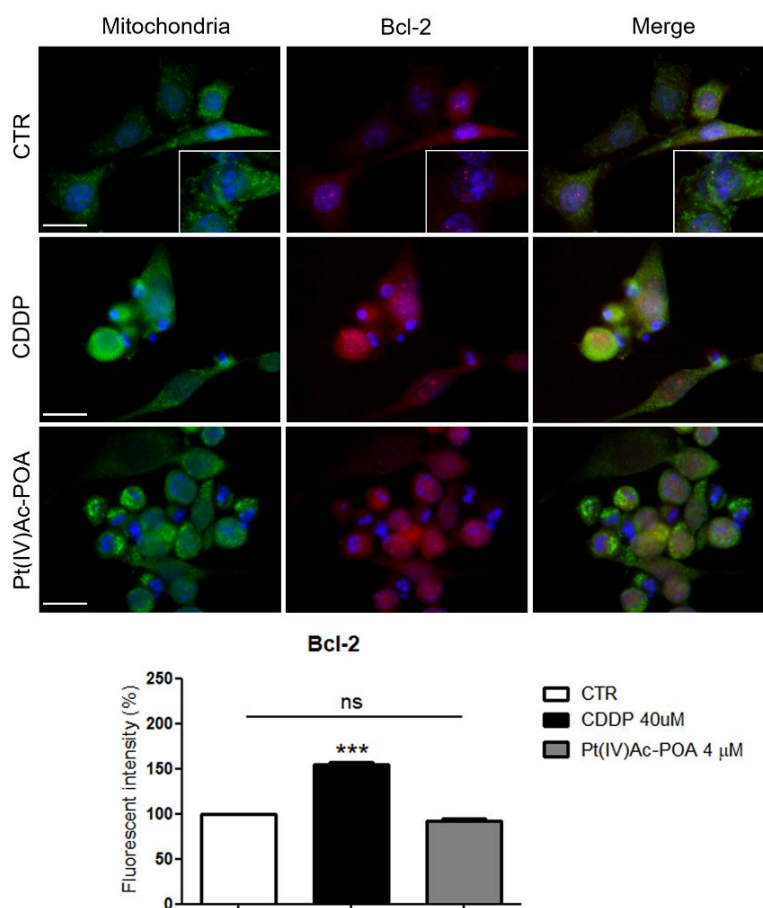


Figure 26. Double immunoreaction for mitochondria (green fluorescence) and Bcl-2 (red fluorescence) in control and treated cells with CDDP or Pt(IV)Ac-POA. DNA counterstaining with Hoechst 33258 (in blue). Bars: 20 μ m. The bar chart represents the quantification of Bcl-2 fluorescent intensity. *Statistical analysis: control *vs* each treatment and CDDP *vs* Pt(IV)Ac-POA; p values: (***) $p < 0.001$, ns: not significant.

Finally, the double immunoreaction for AIF and mitochondria (**Figure 27**), displayed how in C6 control cells, similarly to B50 cells, AIF colocalized with mitochondria, while after 48h-CT with CDDP at 40 μM or Pt(IV)Ac-POA at 4 μM , the AIF fluorescence was detected in cells nuclei. In Pt(IV)Ac-POA-treated sample, compared to CDDP-treated one, an increase in the number of cells with AIF colocalization within the nucleus was evaluated. An increase in nuclear labelling for AIF in early apoptosis was observed, although AIF was also present in late apoptosis. Besides, after both treatments, mitochondria produced clusters at the perinuclear level, losing the physiological morphology especially after exposure to the new compound.

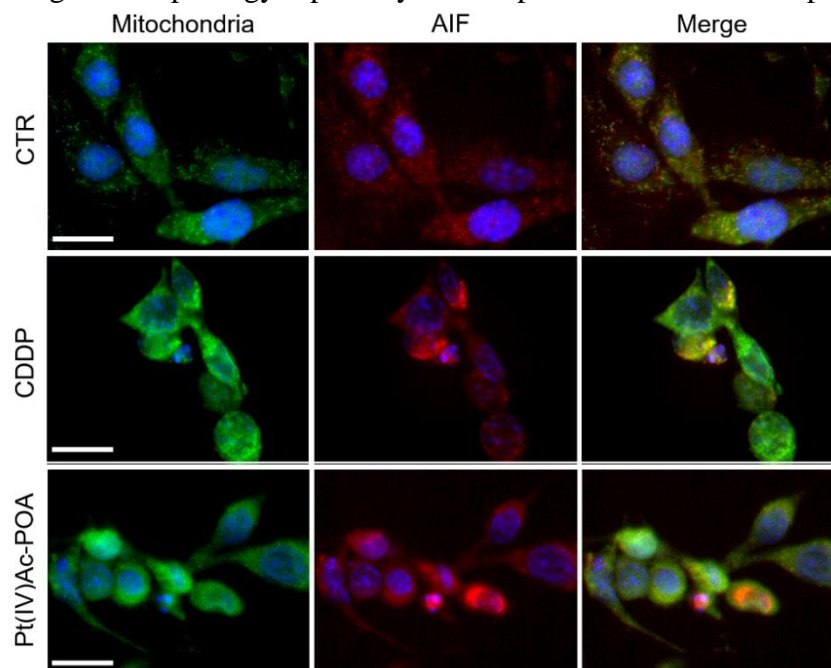


Figure 27. Double immunoreaction for mitochondria (green fluorescence) and AIF (red fluorescence) in control and treated cells with CDDP or Pt(IV)Ac-POA. DNA counterstaining with Hoechst 33258 (blue fluorescence). Bars: 20 μm .

After this analysis the focus was on the caspase-dependent pathways, to understand the effects induced on C6 cells by 48h-CT with Pt(IV)Ac-POA at 4 μM . Therefore, immunocytochemical detections for the principal markers involved in these pathways were performed. Immunocytochemistry confirmed the presence of positive cells to the active caspase-9 and active

caspase-3 after CDDP at 40 μM or Pt(IV)Ac-POA at 4 μM exposure, on the contrary in control condition no cells were marked (**Figure 28**). The presence of both markers near fragmented nuclei suggested the induction of mitochondrial-mediated pathway in apoptotic cells and corroborated the data described above. Furthermore, in cells caspase-immunopositive, cytoskeletal fragmentation and the onset of dense perinuclear masses took place after treatment. To compare the efficiency of the two treatments, a quantification of the active caspase-3-positive cells was carried out. The percentage of cleaved caspase-3 positive cells was $(1.13 \pm 0.66)\%$ in the control, $(18.50 \pm 1.21)\%$ in CDDP-treated samples and $(31.47 \pm 2.64)\%$ in Pt(IV)Ac-POA-treated cells, thus showing a significant increase in the activation of the intrinsic apoptotic pathway after exposure to new prodrug.

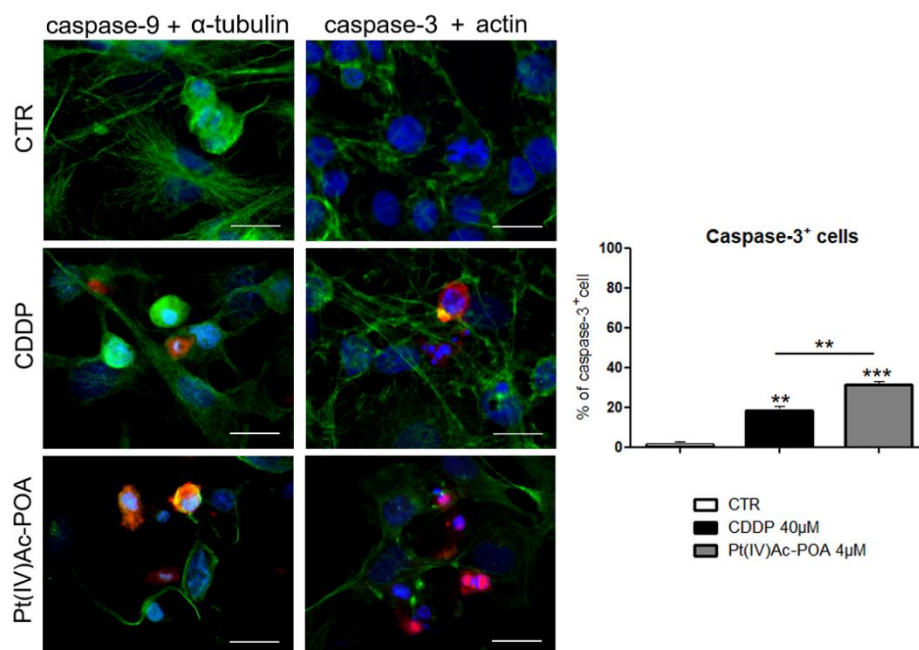


Figure 28. Controls and treated cells after 48h-CT with 40 μM CDDP or 4 μM Pt(IV)Ac-POA. The double immunocytochemical reaction for active caspase-9 and active caspase-3 (red fluorescence), α -tubulin and actin (green fluorescence); DNA counterstaining with Hoechst 33258 (in blue). Band chart represents the percentage values of caspase-3 immunopositive cells. *Statistical analysis: control vs treated samples vs each treatment and CDDP vs Pt(IV)Ac-POA; p values: (**) $p < 0.01$, (***) $p < 0.001$. Bars: 20 μm .

In control cells, PARP-1 fluorescence colocalized with the nucleus and the cytoskeletal tubulin was well-structured. After 48h-CT with 40 μ M CDDP or 4 μ M of the prodrug, PARP-1 was expressed at the nuclear level in cells during the early stages of apoptosis, whereas in late apoptosis with evidently fragmented nuclei, PARP-1, or more exactly p89, moved into the cytoplasm. After both treatments, cells lost their elongated shape due to cytoskeletal tubulin alterations (**Figure 29**). Although the effect of PARP-1 translocation was more evident in the sample treated with the new compound and there were more apoptotic cells, western blot showed greater expression of cleaved PARP-1 (p89 fragment) in cells exposed to CDDP compared to the other conditions. Therefore, the analysis of the possible activation of other cell death pathways was continued.

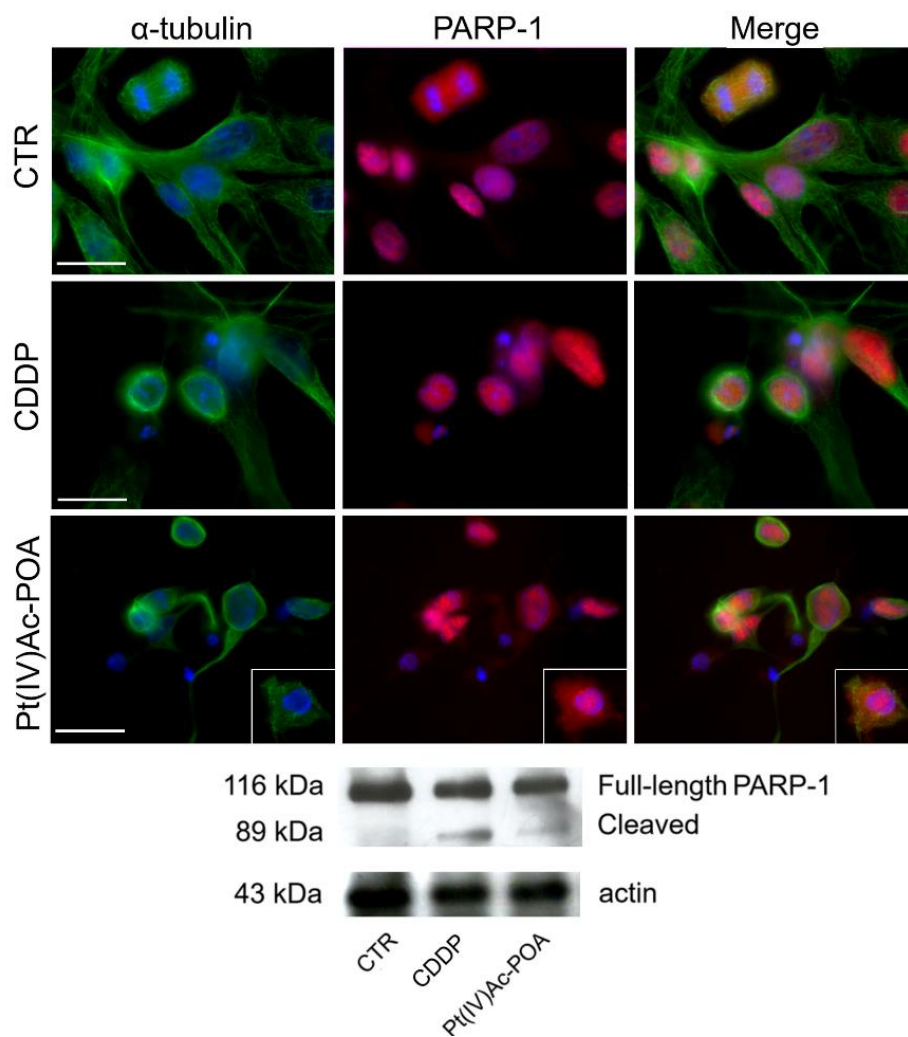


Figure 29. Double immunocytochemical detection of PARP-1 (in red) and α -tubulin (in green) in controls cells and after 40 μ M CDDP or 4 μ M Pt(IV)Ac-POA 48h-CT. DNA counterstaining with Hoechst 33258 (in blue). Inserts: PARP-1 translocation from nuclei to cytoplasm. Bars: 20 μ m. Western blot analysis shows the bands of full-length PARP-1 (116 kDa) and cleaved PARP-1 (89 kDa) compared to the loading control (CTR) and actin (43 kDa).

Immunopositivity to active caspase-8, a protein involved in the extrinsic apoptotic pathway, increased after both treatments compared to the control condition, in which no marked cells were observed (**Figure 30**). After

48h-CT with Pt(IV)Ac-POA a drastic decrease in cell number was evaluated. In addition, those cells with a non-fragmented nucleus displayed an intense immunopositivity to cleaved caspase-8, suggesting a preliminary step of the extrinsic apoptotic pathway. Additionally, after treatment, cells showed fragmented nuclei and an irregular morphology due to the cytoskeleton collapse.

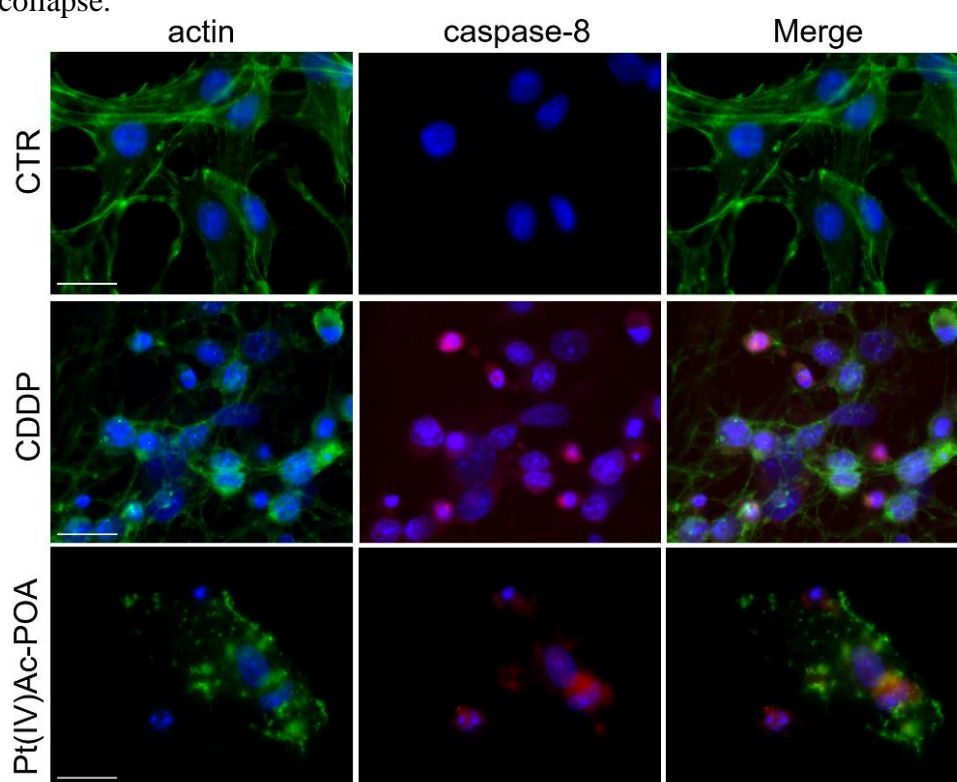


Figure 30. Double immunocytochemical detection of active caspase-8 (red fluorescence) and actin (green fluorescence) in C6 control cells and after 48h-CT with 40 μ M CDDP or 4 μ M Pt(IV)Ac-POA. DNA counterstaining with Hoechst 33258 (in blue). Bars: 20 μ m.

Caspase-8 is also involved in the initial phase of necroptosis. To confirm the activation of the extrinsic apoptotic pathway and possible preliminary activation of the necroptotic pathway, an immunocytochemical detection of RIP1 was performed. In control cells, RIP1 fluorescence was detectable in the cytoplasm with a uniform distribution. In contrast after treatments, some cells were marked only near the nuclei, suggesting a redistribution of RIP1.

Although only after 48h-CT with Pt(IV)Ac-POA there was an evident translocation of RIP1 from the cytoplasm within the nuclei, indeed in CDDP-treated cells RIP1 was in the perinuclear zone (Yoon S et al. 2016). This data may suggest that only after treatment with the new compound there was a possible activation of the necroptotic pathway (**Figure 31**).

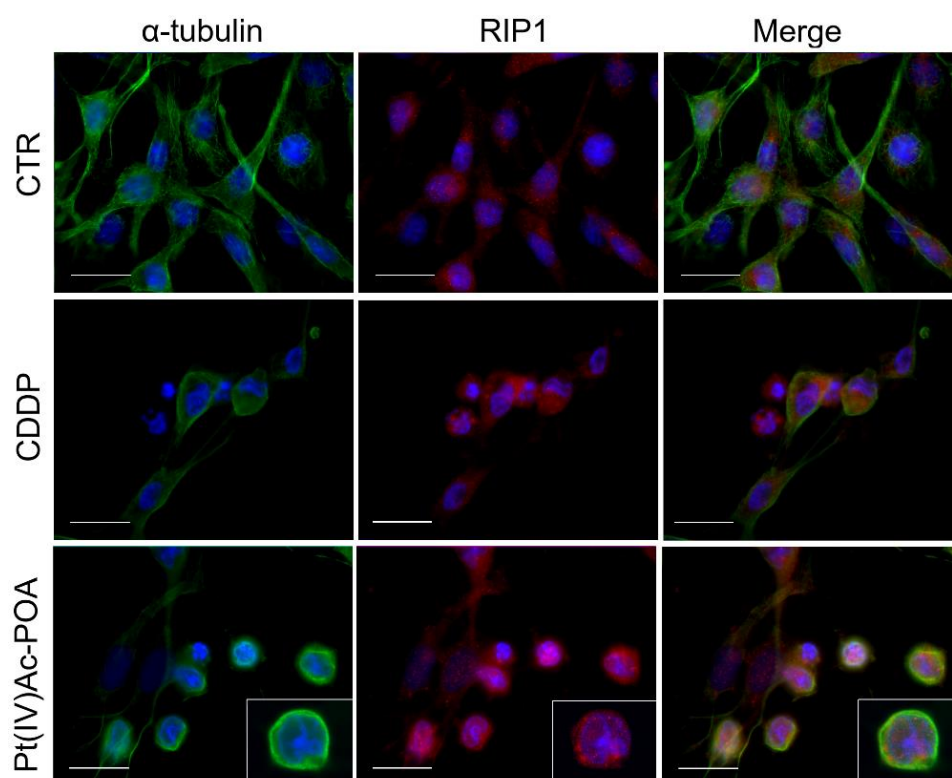


Figure 31. Double immunocytochemical detection of RIP1 (red fluorescence) and α -tubulin (green fluorescence). DNA counterstaining with Hoechst 33258 (blue fluorescence). Insert: RIP1 translocation within the condensed nucleus after treatment with Pt(IV)Ac-POA. Bars: 20 μ m.

4.2.5 Analysis of autophagic process activation

To analyse the activation of autophagy, LC3B and p62/SQSTM1 were evaluated by immunofluorescence reaction, since being two proteins principally involved in this process. The p62 protein, SQSTM1, is a ubiquitin-binding scaffold protein that colocalizes with ubiquitinated protein

aggregates. The protein can polymerize through an N-terminal PB1 domain, interacting with ubiquitinated proteins through the C-terminal UBA domain (Katsuragi Y et al. 2015). Images in **Figure 32A** show the double immunolabelling for p62/SQSTM1 and LC3B. In control cells, p62/SQSTM1 was localized in the cytoplasm and no colocalized with LC3B. After 48h-CT with CDDP at 40 μ M, immunofluorescence of both proteins increased and, LC3B was detectable also in cell nuclei. After exposure to Pt(IV)Ac-POA 4 μ M, nuclei remained negative for p62/SQSTM1 and LC3B, but compared to control cells, the two fluorescence colocalized. Western blot analysis for p62/SQSTM1 performed on C6 cells after 48h-CT to 40 μ M CDDP or 4 μ M Pt(IV)Ac-POA, compared to controls, gave another aspect of the activation of autophagy (**Figure 32B**). Indeed, western blotting density band analysis evidenced a declined expression of p62/SQSTM1 after both treatments, especially in CDDP-treated cells, suggesting a deep activation of the autophagic pathway.

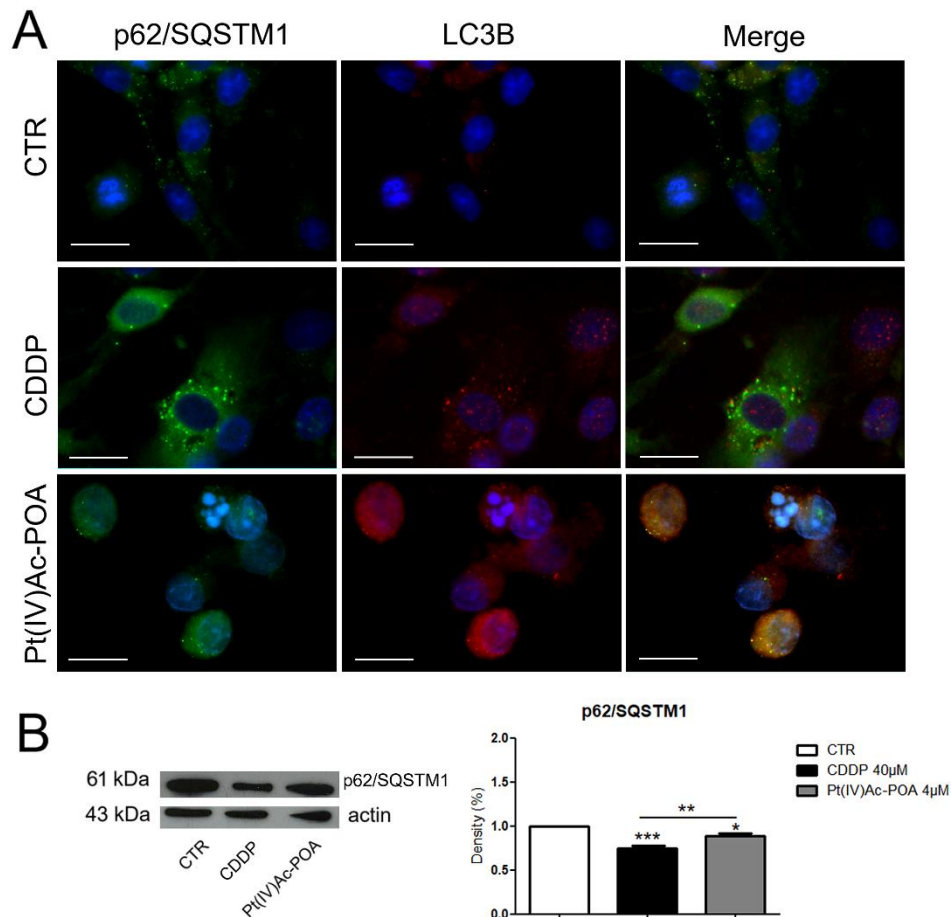


Figure 32. A) Double immunolabelling for p62/SQSTM1 (green) and LC3B (red). DNA counterstaining with Hoechst 33258 (in blue). Bars: 20 μm. **B)** Western blotting data of p62/SQSTM1. The bar chart representing density bands quantification of p62/SQSTM1 in the control sample and following CDDP 40 μM or 4 μM Pt(IV)Ac-POA 48h-CT. *Statistical analysis: control vs treated samples and CDDP vs Pt(IV)Ac-POA; p values: (***) $p < 0.05$, (**) $p < 0.01$, (***) $p < 0.001$.

4.2.6 Analysis of CBPs after Pt(IV)Ac-POA treatment

CBPs were also analysed in C6 glioma cells. Although the glial cells cannot produce an action potential like neuronal cells, these cells play a key role in the regulation of the extracellular microenvironment, especially the synaptic one. Glial cells are therefore fundamental for the correct

maintenance of the physiological processes of nervous tissue cells. An aberration of their role would, therefore, affect not only the onset of cellular transmission dysfunctions but also the genesis of neoplasms.

Double immunolabeling for PV and actin showed a predominantly immunopositivity in cell cytoplasm in each condition, with some differences in PV signal between C6 control cells and those exposed to both treatments. As can be seen in **Figure 33**, following 48h-CT with CDDP the PV labelling increase compared to control or to Pt(IV)Ac-POA-treated cells, as quantification of fluorescence intensity confirmed. In addition, following both treatments, cells that underwent cell death exhibited the fragmented nucleus and the actin cytoskeleton lost its morphology and collapsed around the nucleus.

After immunofluorescence for CR, the labelling was distributed in the cytoplasm of C6 control cells (**Figure 33**). Also, after 48h-CT with CDDP at 40 μM or with Pt(IV)Ac-POA at 4 μM , the relative fluorescence of CR was still present in the cytoplasm. Fluorescence intensity quantification revealed CDDP-treated cells an increase in CR fluorescence compared to the control conditions and after treatment with Pt(IV)Ac-POA. Compared to C6 control cells, immunolabeling for actin revealed structural alterations of the cytoskeleton in treated cells. Indeed, following exposure to CDDP or Pt(IV)Ac-POA, the nucleus appeared fragmented, associated with changes in cell morphology and cytoskeleton alteration that promote actin cytoskeleton reorganization around the fragmented nuclei.

Following 48h-CT with CDDP at 40 μM or with Pt(IV)Ac-POA at 4 μM , cells showed an intensify in CaM fluorescence compared to control, this data was also confirmed by quantification analysis, which displayed an evident increase in CaM labelling in cells treated with Pt(IV)Ac-POA. Immunolabeling for actin revealed strongly changes in cytoskeleton organisation, between control C6 cells and those exposed to both treatments.

Finally, images and the bar chart of CB reported in **Figure 33** showed a significant increase of protein signal only in CDDP-treated cells compared to control and Pt(IV)Ac-POA-treated cells. Moreover, immunolabeling for actin revealed an altered cytoskeletal organization observed in treated samples.

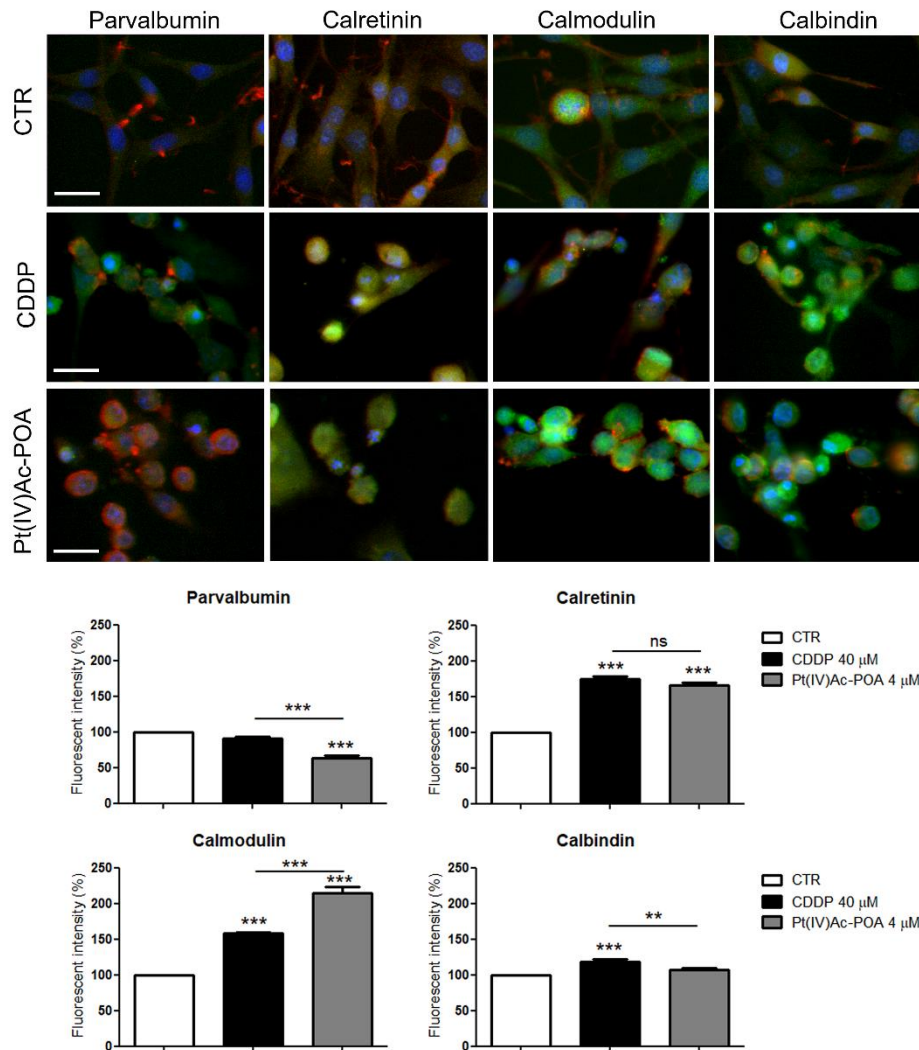


Figure 33. Immunocytochemical detection of CBPs: parvalbumin, calretinin calmodulin and calbindin (red fluorescence) and actin cytoskeleton (green fluorescence) in control C6 cells and after 48h-CT with CDDP 40 μ M or Pt(IV)Ac-POA 4 μ M. DNA was counterstained with Hoechst 33258 (in blue). Bar: 40 μ m. The bar charts with the percentage of fluorescence intensity for each CBPs in control and treated cells with CDDP or Pt(IV)Ac-POA. *Statistical analysis: control vs each treatment and CDDP vs Pt(IV)Ac-POA; ρ values: (**) $\rho < 0.01$, (***) $\rho < 0.001$, ns: not significant.

Western blot analysis was conducted on C6 control cells and after 48h-CT with CDDP 40 μ M or Pt(IV)Ac-POA 4 μ M, to corroborate the fluorescence data described above (**Figure 34**). From the data of the western blot a non-significance increment of CR was evaluated, the remaining results for CaM and CB, although different from those obtained from immunofluorescence quantifications, showed a significant increase in the expression of the two proteins after both treatments, suggesting a role of these two proteins in treatments response.

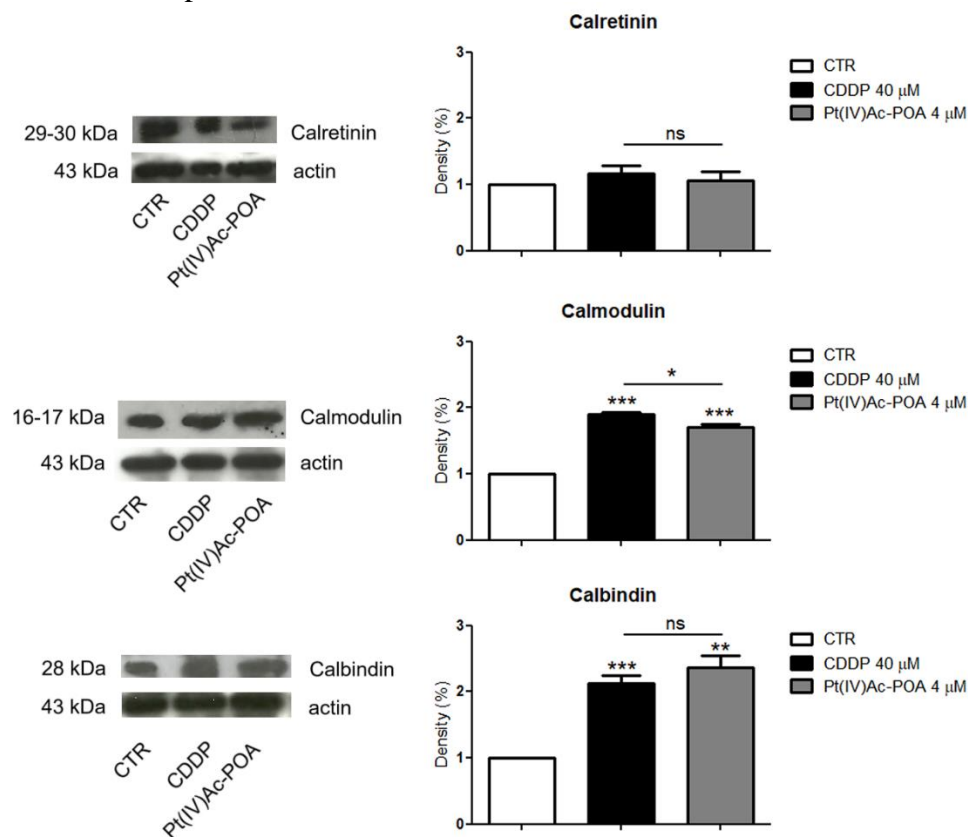


Figure 34. Western blot bands of CBPs: calretinin, calmodulin and calbindin after 48h-CT to CDDP 40 μ M or Pt(IV)Ac-POA 4 μ M, compared to the loading control (CTR) and actin (43 kDa). On the right of each western blot the respective bar chart of density bands quantification. *Statistical analysis: control vs each treatment and CDDP vs Pt(IV)Ac-POA; p values: (*) $p < 0.05$, (**) $p < 0.01$, (***) $p < 0.001$, ns: not significant.

4.2.7 Immunofluorescence analysis of PMCA1 after treatment

PMCA1 is another important protein in Ca^{2+} homeostasis and is often involved in the mechanism of action of anticancer drugs. As shown in the images in **Figure 35**, in control conditions the labelling associated with PMCA1 was higher than the cells treated with Pt(IV)Ac-POA 4 μM 48h-CT. Cells exposed to 40 μM CDDP exhibited greater PMCA1 fluorescence signal than control and Pt(IV)Ac-POA-treated cells. However, quantification of PMCA1 fluorescence intensity did not reveal significant differences though the three conditions. Also, immunolabeling for actin revealed that the cytoskeleton was well structured in control cells, while it lost its organization and collapsed near the nucleus following treatment with CDDP and Pt(IV)Ac-POA.

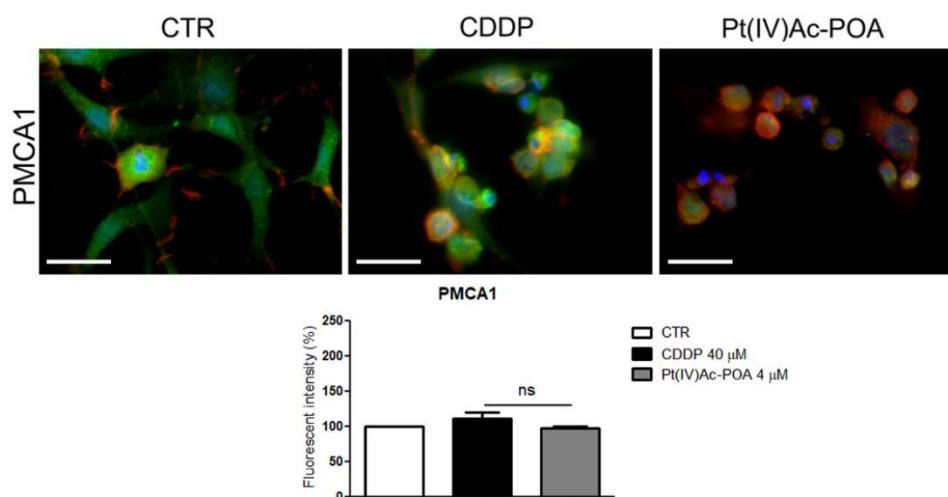


Figure 35. Double immunofluorescence for PMCA1 (green fluorescence) and actin (red fluorescence) in C6 cells in control condition and after 48h-CT with CDDP 40 μM or Pt(IV)Ac-POA 4 μM . DNA was counterstained with Hoechst 33258 (in blue). Bar: 40 μm . Bar chart with the percentage of fluorescence intensity for PMCA1 in the three conditions. *Statistical analysis: control vs each treatment and CDDP vs Pt(IV)Ac-POA; ns: not significant.

4.2.8 Analysis of the deacetylation effects induced by POA on C6 cells

The effect of 48h-CT with 4 μM POA on the C6 glioma cell line was investigated to understand how the free acid works in these cells compared to

B50 neuroblastoma cells. Compared to control condition, the results of cell cycle analysis showed that, after 48h-CT with POA at 4 μ M, a reduction in S phase was evident, associated with the presence of a sub-G₁ peak ascribable to an increased number of dead cells (**Figure 36A**). To confirm the presence of the apoptotic activation, the samples were subjected to reaction with Annexin V. In **Figure 36B** the cytograms obtained after flow cytometry analysis are reported. The results confirmed the presence of apoptotic cells (16%) after 48h-CT with POA alone, compared to the control condition (7%).

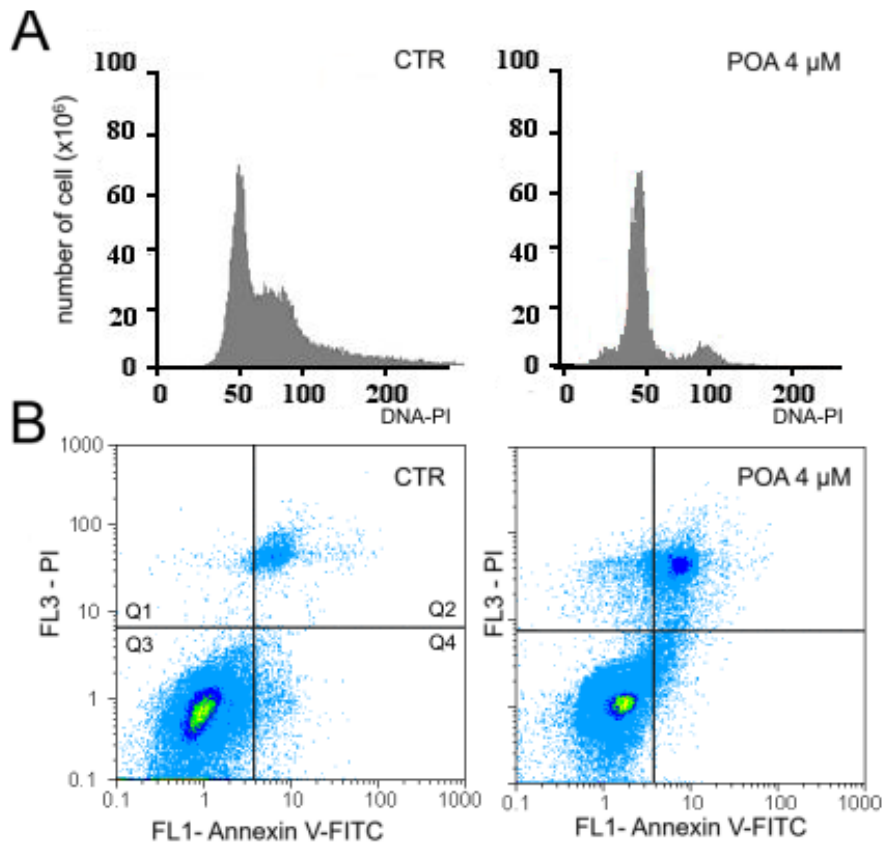


Figure 36. **A**) Cytograms of DNA content after PI staining in C6 control cells (CTR) and treated for 48h-CT with POA at 4 μ M. **B**) Dual parameter cytograms of FITC-labelled Annexin V (FL1) vs PI staining (FL3) representing control cells (CTR) and treated cells 48-CT with POA at 4 μ M.

Acetyl-H3 and PCNA were then studied by double immunoreaction to evaluate their expression after treatment for 48h-CT with POA 4 μ M. In **Figure 37A** the images of the immunofluorescence display how after treatment there was an increase in fluorescence intensity for acetyl-H3, on the contrary, a significant decrease in the PCNA fluorescent signal was observed. Despite, a non-significant reduction of PCNA expression in treated cells was observed by western blot analysis, a significant increase in histone H3 acetylation was obtained after POA treatment.

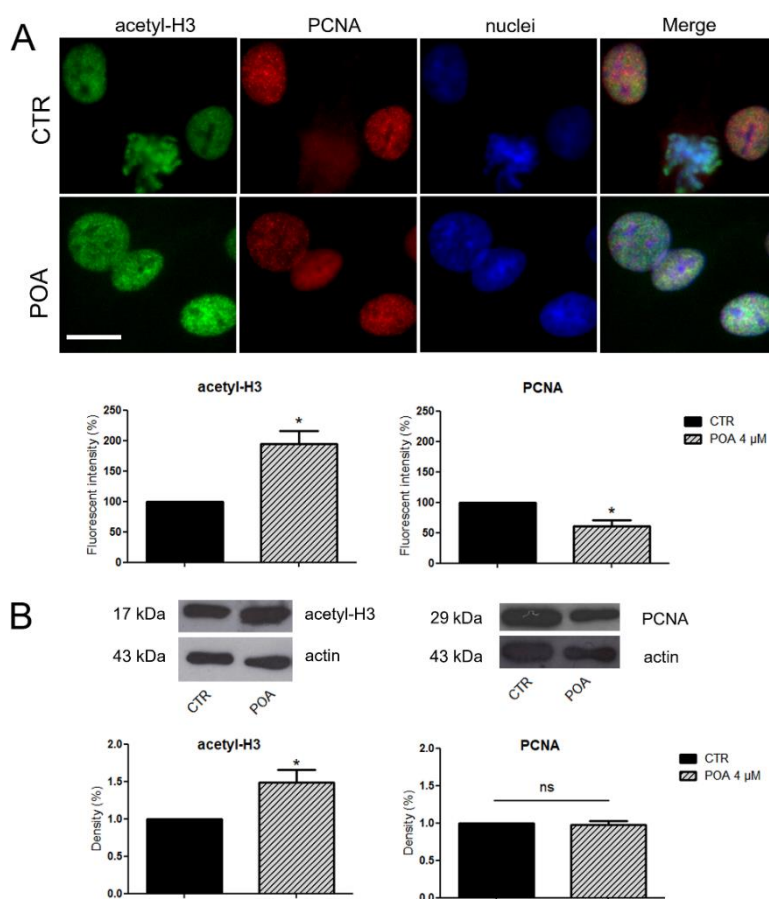


Figure 37. **A**) Double immunofluorescence reaction, with the relative quantification, for acetyl-H3 (in green) and PCNA (in red), nuclei were counterstained with Hoechst 33258 (in blue). Bar: 20 μ m. **B**) Western blot bands and density bar charts of acetyl-H3 and PCNA. Student's *t*-test: *statistical significance between control and POA-treated cells; p values: (*) $p < 0.05$, ns: not significant.

Similar to what observed in B50 cells, in C6 cells, the effect of the POA, as an HDACi, on chromatin decondensation, appeared ineffective at 48 h-CT (**Figure 38**), showing control-like characteristics in cells treated with the POA.

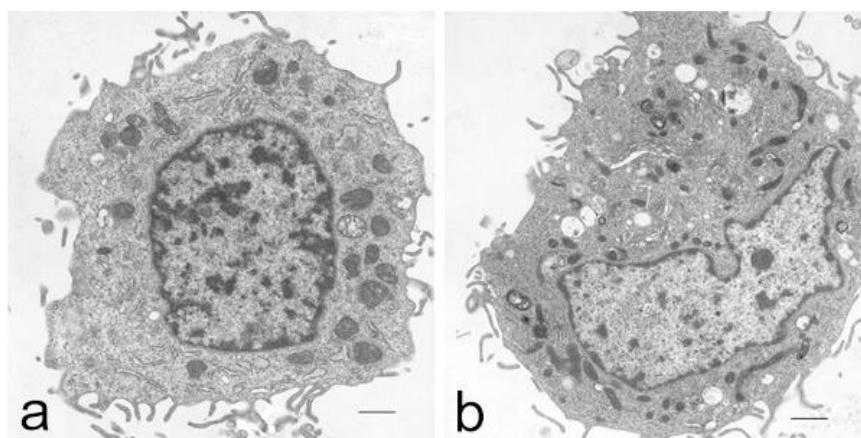


Figure 38. Ultrastructural analysis at the electron microscope reveals no difference in chromatin decondensation between control (**a**) and treated cells at 48h-CT with POA μM (**b**). Bars: 1.1 μm .

To verify whether what observed was the greatest effect of the POA, as for B50 cells, the short exposure times to POA 4 μM were analysed (**Figure 39**). The data obtained showed a maximum effect in the chromatin decondensation at 2h compared to the remaining treatments (4h, 8h, and 24h respectively).

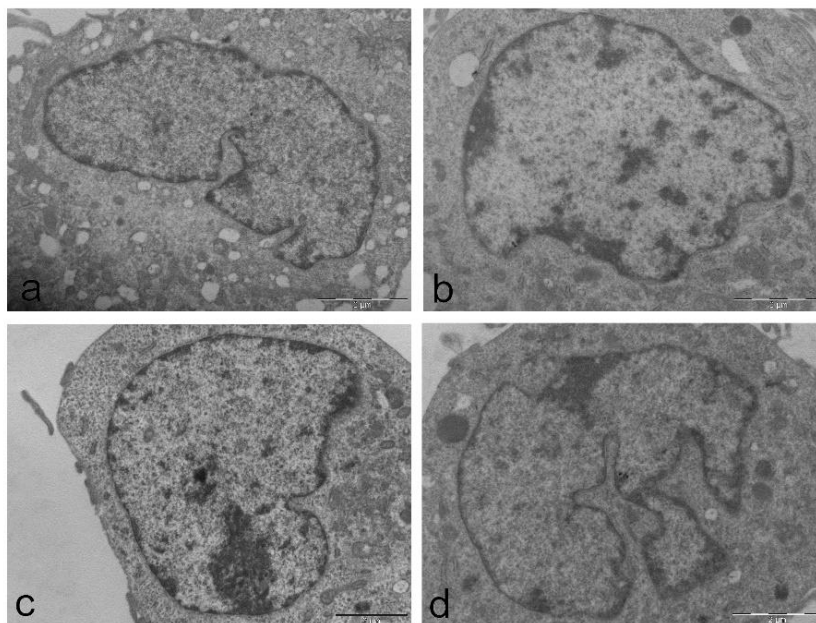


Figure 39. C6 cells after 4 μM POA treatment at 2h (a), 4h (b), 8h (c) and 24h (d), respectively. To note the strong chromatin decondensation after 2h of continuous exposure to POA: Bars: 2 μM .

Subsequently, this data was confirmed by the immunolabeling for the acetyl-H3 and by the western blot analysis of the sample treated for 2h with POA a 4 μM and the respective control. A significant difference was observed for PCNA only by western blot analysis (**Figure 40**).

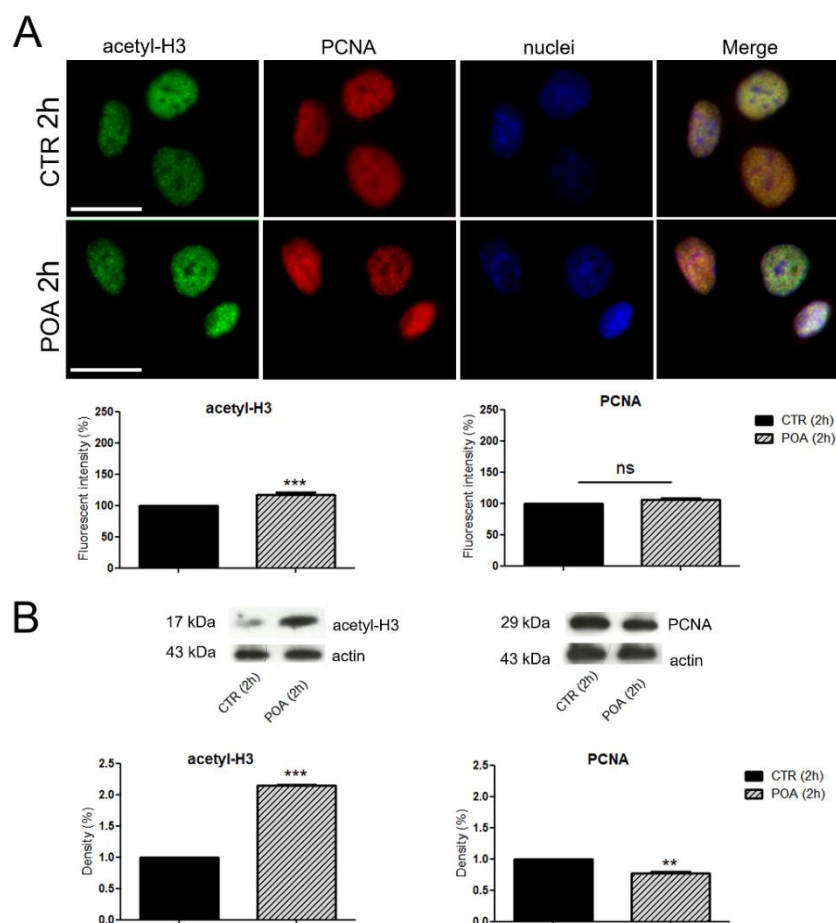


Figure 40. **A**) C6 control cells and treated with 4 μM POA at 2h-CT. Double immunofluorescence reaction, with the relative quantification, for acetyl-H3 (in green) and PCNA (in red), nuclei were counterstained with Hoechst 33258 (in blue). Bar: 20 μm . **B**) Western blot bands and density bar charts of acetyl-H3 and PCNA. Student's *t*-test: *statistical significance between control and POA-treated cells; ρ values: (**) $\rho < 0.01$, (***) $\rho < 0.001$, ns: not significant.

No changes induced by the treatment 48h-CT with POA at 4 μM were found on C6 cells compared to control, in the analyses on the pathways and CBPs previously described and carried out for 48h-CT Pt(IV)Ac-POA at 4 μM .

4.3 The effect of Pt(IV)Ac-POA on the human U251 cell line

The effects of CDDP and analogues have long been studied in the human U251 glioblastoma line. This cell line, following studies conducted in the laboratory of Cell Biology and Neurobiology, was particularly resistant to the standard dosages used for *in vitro* investigations. Several data have been previously obtained on the use of new compounds such as [Pt(O,O'-acac)(γ -acac)(DMS)] in the treatment of this cell line (Griamaldi M, 2015, Ph.D. thesis) and the observations obtained indicate the U251 cell line as a good model for the study of GBM, especially due to its strong intercellular heterogeneity.

4.3.1 Analysis of cell death and activation of the apoptotic pathway

The concentrations used for the U251 line treatment with Pt(IV)Ac-POA were selected by comparing the data previously obtained for standard *in vitro* treatment with CDDP (40 μ M) and new platinum(II) such as [Pt(O,O'-acac)(γ -acac)(DMS)]. Among the concentrations analysed by MTS assay, only Pt(IV)Ac-POA at 10 μ M was found to be effective on the U251 line. After 48h-CT treatment with Pt(IV)Ac-POA at 10 μ M and following counterstaining with PI the cells were divided into the different phases of the cell cycle, with a slight decrease of the S phase of (14.73 ± 0.51)% (**Figure 41A**). Evaluating the cytograms obtained from the cytofluorimetric analysis, the presence of a sub-G₁ peak (black arrow) was observed, corresponding to an accumulation of dead cells (**Figure 41A**, insert). By Annexin V assay was confirmed that compared to control condition, after 48h-CT with Pt(IV)Ac-POA at 10 μ M, an increase in the number of apoptotic cells was observed, especially of late apoptotic cells (**Figure 41B**).

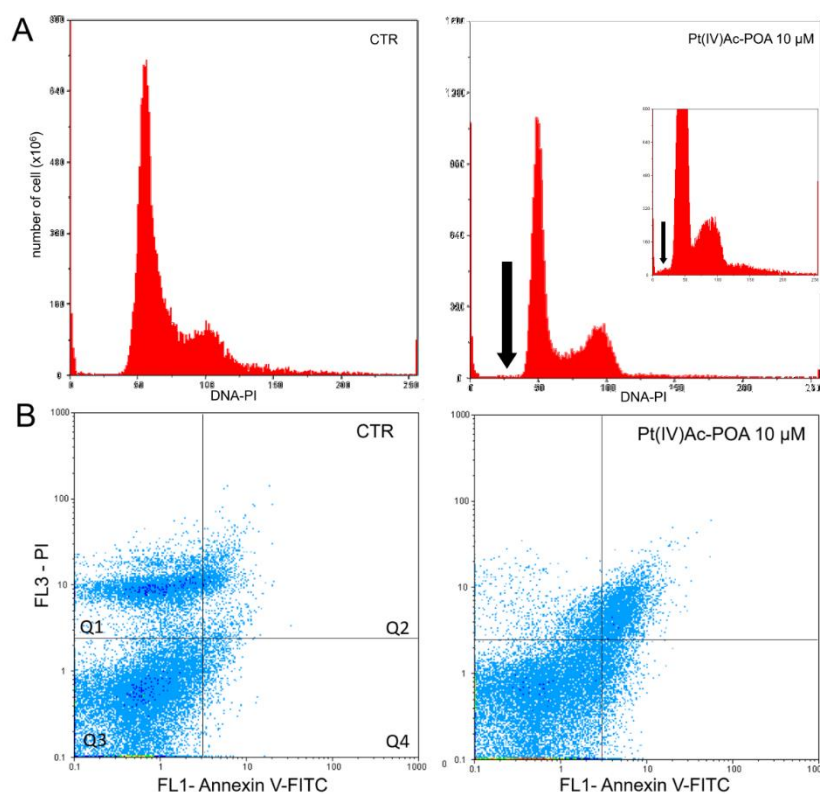


Figure 41. **A)** Cytograms of DNA content after staining with PI in U251 control cells and after treatment with Pt(IV)Ac-POA at 10 μ M for 48h-CT. Insert represents the graph of the sample treated with Pt(IV)Ac-POA 10 μ M compared to the same number of cells analysed in the control sample ($y: 800 \times 10^6$). The black arrow indicates the sub-G₁ peak corresponding to dead cells. **B)** Dual parameter cytograms of FITC-labelled Annexin V (FL1) versus PI staining (FL3) in the control (CTR) and in cells treated with Pt(IV)Ac-POA at 10 μ M. Quadrant Q1: necrotic cells, Q2: late apoptotic cell, Q3: viable cells, and Q4: early apoptotic.

4.3.2 Ultrastructural investigation at TEM

Thanks to the evaluation of the samples by electronic microscopy, it was possible to assess the different ultrastructural alterations induced after 48h-CT with Pt(IV)Ac-POA at 10 μ M. In the control cell, a nucleus with decondensed chromatin, a well-organized ER located in the perinuclear area and medium-sized mitochondria were observed (**Figure 42a**). On the contrary after continuous exposure to the new compound, several phenotypes of cell

death were detected such as apoptotic features *i.e.* chromatin condensation and disappearance of the nuclear envelope (**Figure 42b**), typical elements of autophagy such as the increase in the number of vacuoles containing degradation material (**Figure 42c**) and morphologies attributable to necroptosis (**Figure 42d**).

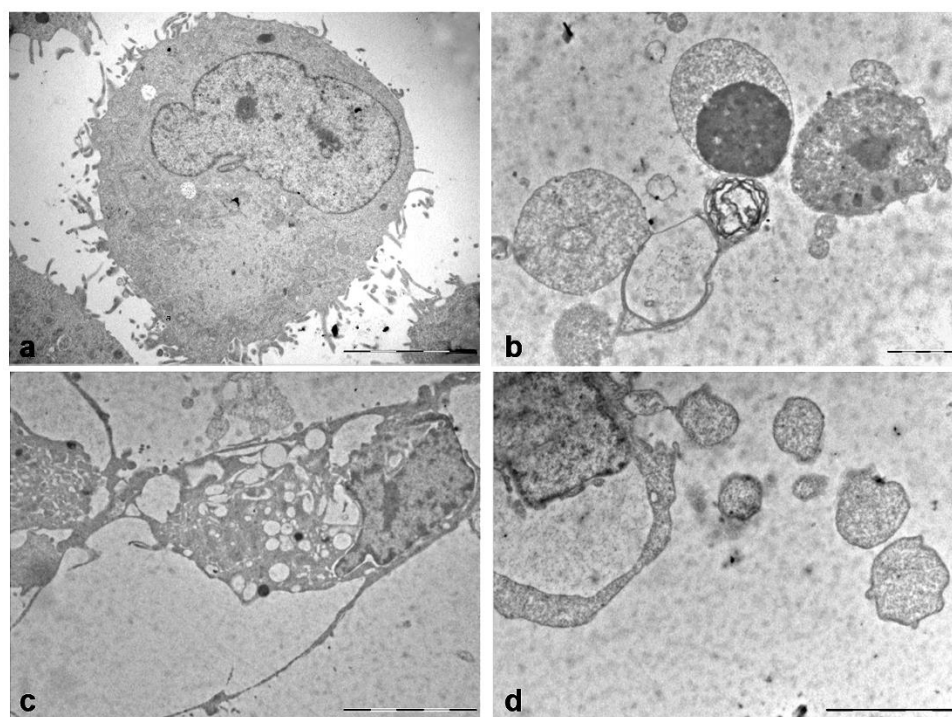


Figure 42. U251 cells ultrastructural analysis in the control condition (**a**) and after 10 μ M Pt(IV)Ac-POA 48h-CT (**b-d**). Apoptosis (**b**), autophagy (**c**) and necroptosis (**d**) are shown. Bars: 5 μ m.

4.3.3 Evaluation of different apoptotic cell death

Based on the different morphologies detected by electron microscopy, the presence of proteins mainly involved in the respective cell death pathways was evaluated by immunofluorescence. Moreover, data previously collected on U251 cells, showed a tendency of these cells to resist treatments, modifying cell death pathways and triggering resistance mechanisms, observed above all in the treatment with CDDP (Grimaldi M, 2015, Ph.D. thesis). Data relating to these survival processes, observed in the B50 line of

rat neuroblastoma, have already been published (Grimaldi M et al. 2019). Therefore, a second experimental condition *i.e.* “recovery condition” (REC) (see Materials and Methods) was added, aimed at bringing out the strategies of defense of tumour cells implemented after 48h-CT with chemotherapy.

The activation of the intrinsic and extrinsic apoptotic pathway was investigated by immunolabeling for active caspase-3 and active caspase-8, respectively (**Figure 43**). After 48h-CT with CDDP 40 μ M or Pt(IV)Ac-POA at 10 μ M, an increase in immunopositivity of both active caspases was observed, compared to the control condition, in which no labelling was found for the proteins of interest. A progressive increase in the relative investigated markers was found in the recovery samples compared to the control and the respective treatments at 48h-CT. Furthermore, the greatest apoptotic induction effect was observed in the recovery samples, especially in which exposed to 10 μ M Pt(IV)Ac-POA. This data suggests that although the cells have had a 7-day recovery time in fresh medium, U251 cells continue to die. The immunolabelling of the actin cytoskeleton reveals how respect to the well-defined structural organization in control cells, following treatment there was a complete degeneration of the cellular morphology with a cytoskeleton collapsed around the nuclei that were highly degraded. Also, from the quantification of the cell immunopositivity for the two cleaved caspases, the predominantly expressed pathway seemed to be the intrinsic one.

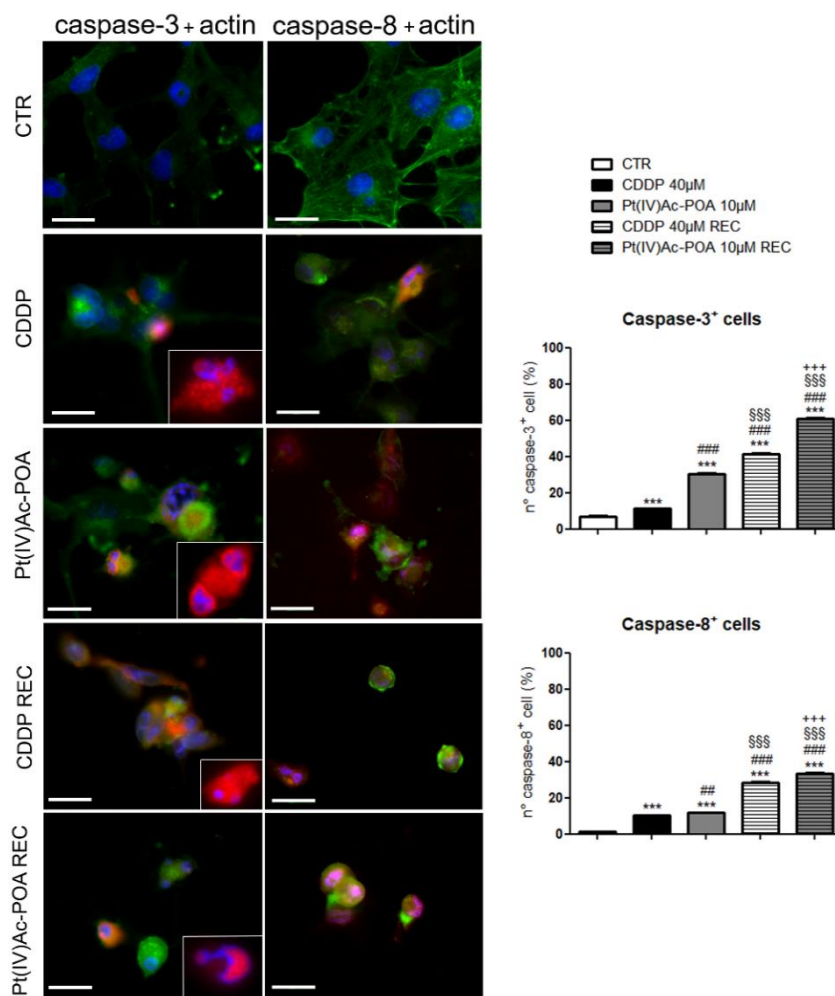


Figure 43. Immunolabelling for active caspase-3 and active caspase-8 (red fluorescence) and actin (green fluorescence) in U251 control cells, after 48h-CT with CDDP 40 μ M or Pt(IV)Ac-POA 10 μ M and in recovery conditions after exposure for 48h to CDDP or Pt(IV)Ac-POA. Hoechst 33258 counterstaining for the nuclei (in blue). Inserts: magnifications of apoptotic marked nuclei. Bars: 40 μ m. Bar charts represent the number of cells immunopositive to active caspase-3 or active caspase-8, respectively. *Statistical significance between control and each treatment condition; #statistical significance between CDDP and the other treatments conditions; \$statistical significance between Pt(IV)Ac-POA and the other recovery conditions; +statistical significance between recovery conditions CDDP and Pt(IV)AC-POA respectively; ρ values: (*) $\rho < 0.05$; (**) $\rho < 0.01$; (***) $\rho < 0.001$.

Following this analysis, the activation of the active caspase-3 substrate *i.e.* PARP-1 was investigated (**Figure 44**). In U251 control cells, PARP-1 was localized at the nucleus level, while the well-organized tubulin cytoskeleton supported cell morphology. After 48h-CT with CDDP 40 μ M and Pt(IV)Ac-POA 10 μ M, the cells underwent apoptosis, as suggested by the presence of cells with a degraded nucleus. Different cell death phases were observed: late apoptosis, in which there was no more colocalization between the fluorescence of PARP-1 and the nucleus, and early apoptosis in which PARP-1, or rather the p89 fragment, moved from the nucleus to the cytoplasm, a phenomenon that can be observed especially in the treated sample with Pt(IV)Ac-POA. The cells with a healthy phenotype detectable in the sample exposed to CDDP, on the other hand, showed a still nuclear PARP-1 signal. In recovery conditions of the sample exposed to the CDDP, a redistribution of the fluorescent signal of PARP-1 was observed in more spots-like labelling, observable in the lower-left cell. In these conditions, apoptosis was also observed, but also a morphology suggesting an ongoing autophagic process. The recovery condition of Pt(IV)Ac-POA-treated sample still revealed the presence of apoptosis (insert), while the cells with nuclear PARP-1 displayed a strongly altered tubulin cytoskeleton, indicating possible cellular damage. Finally, the western blot analysis for PARP-1 showed the activation of PARP-1 in all treatments compared to the control. It should be noted that in the Pt(IV)Ac-POA recovery condition there was a reduction in the expression of PARP-1, associated however with its activation and which could suggest a strong effect of Pt(IV)Ac-POA in reducing expression of this protein involved in DNA repair.

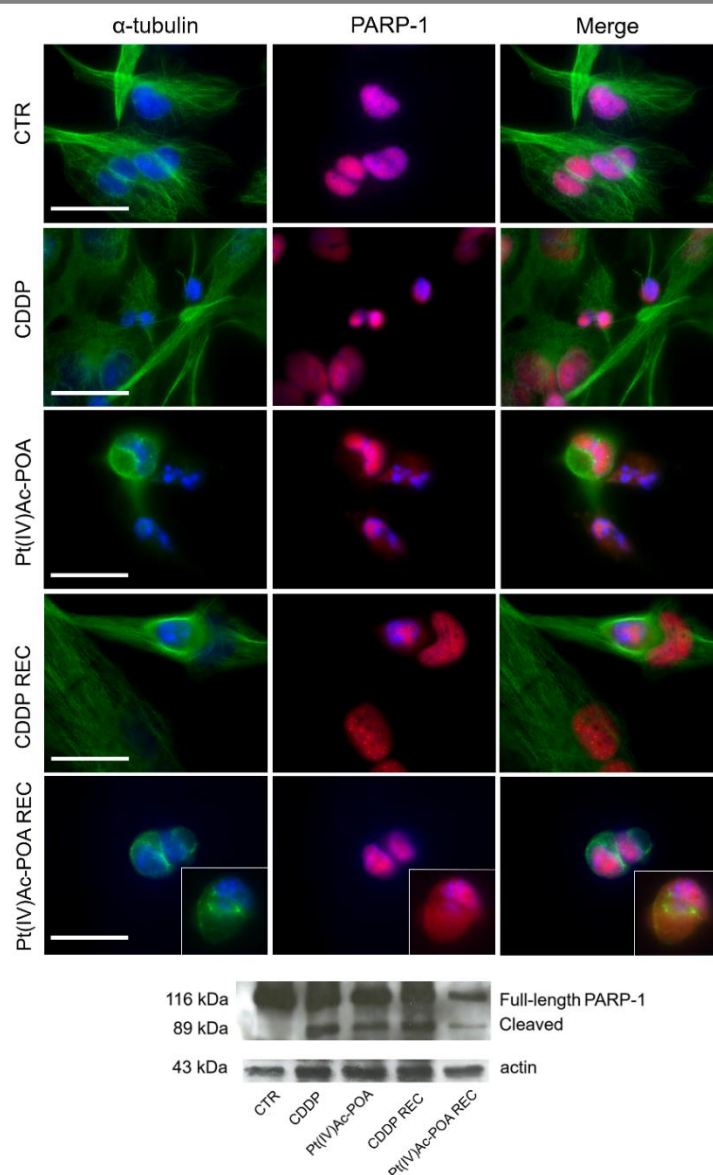


Figure 44. Double immunocytochemical detection of PARP-1 (in red) and α -tubulin (in green) in controls cells and after 40 μ M CDDP or 10 μ M Pt(IV)Ac-POA 48h-CT and respective recovery conditions. DNA counterstaining with Hoechst 33258 (in blue). Inserts: PARP-1 translocation from the nucleus to cytoplasm. Bars: 20 μ m. Western blot analysis shows the bands of full-length PARP-1 (116 kDa) and cleaved PARP-1 (89 kDa) compared to the loading control and actin (43 kDa).

As regards the pathway supported by the caspase-8, therefore of the extrinsic apoptotic pathway, the RIP1 protein was evaluated by immunofluorescence reaction (**Figure 45**). After immunolabelling for RIP1 it was observed in control cells that the fluorescent signal of the protein was diffused homogeneously for the entire cytoplasm and was not revealed at the nucleus level. After 48h-CT with CDDP 40 μ M, a redistribution of the fluorescent signal was evaluated around fragmented nuclei, while in cells that had almost similar characteristics to the control, the distribution of RIP1 remained predominantly cytoplasmic. In the samples exposed to Pt(IV)Ac-POA for 48h, there was an increase in the RIP1 signal around degraded nuclei, compared to the conditions described above. Furthermore, the tubulin cytoskeleton appeared strongly damaged, compared to the control conditions and the cells treated with CDDP. Under the recovery conditions of both treatments, the cells appeared non-viable, with an increase in the signal for RIP1 around the visibly damaged nuclei. In particular, the Pt(IV)Ac-POA sample showed cells with evident pyknosis.

In the necrosome formation, RIP1, or rather RIP3, interacts with MLKL that is essential to induce necroptosis. Conformational change in MLKL promotes its translocation to the plasma membrane, causing its permeabilization, but also to the nucleus in the early necroptosis stage (Weber K et al. 2018). In this regard, the possible translocation of MLKL was investigated following treatment with CDDP or Pt(IV)AC-POA both at 48h-CT and recovery conditions (**Figure 46**). In control cells, the MLKL labelling was purely cytoplasmic, while after treatment the fluorescent signal revealed a redistribution in cells with a fragmented nucleus. After treatment with CDDP 40 μ M the MLKL signal was like the control, with redistribution around a nucleus damaged, due to the collapse of the cytoskeleton around it. In the remaining treatments, an increase in MLKL fluorescence was detected, especially in cells with an apoptotic phenotype. To note, the localization of MLKL in the cell nucleus of the Pt(IV)Ac-POA recovery sample.

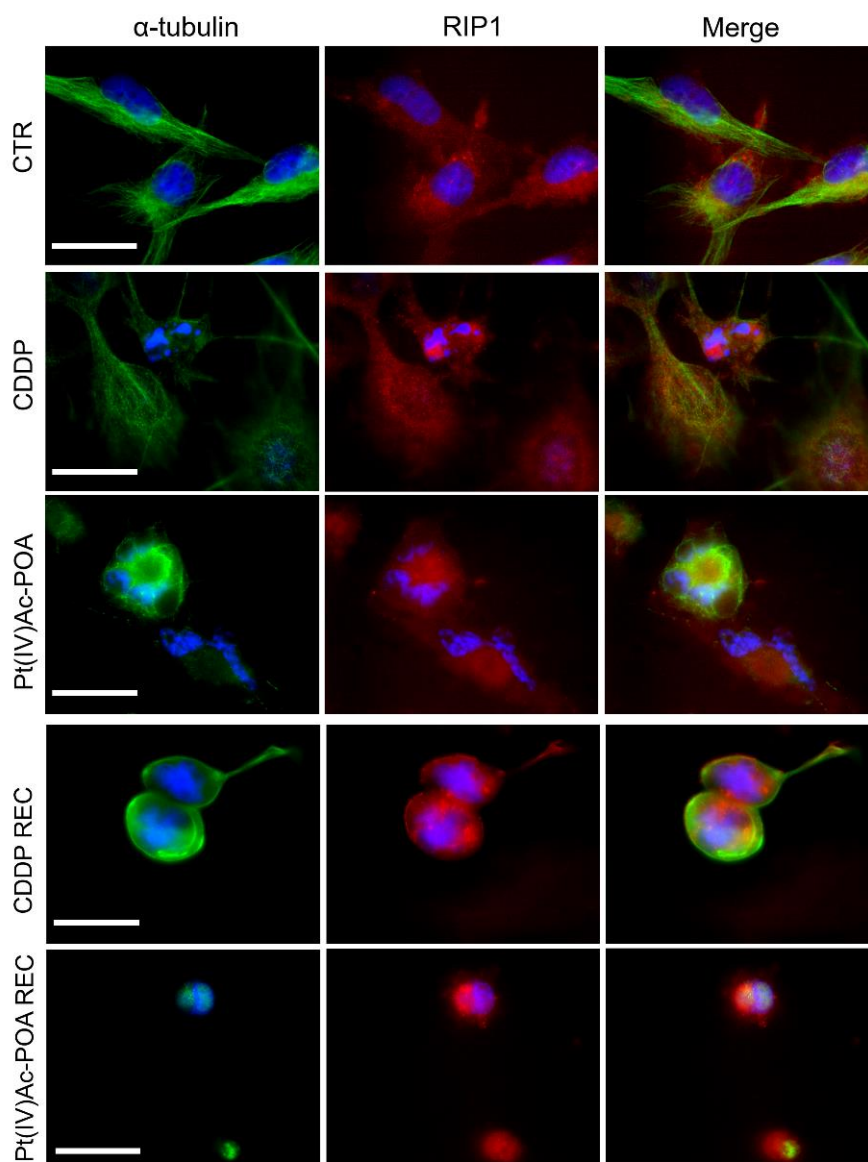


Figure 45. Double immunocytochemical detection of RIP1 (red fluorescence) and α -tubulin (green fluorescence). DNA counterstaining with Hoechst 33258 (blue fluorescence). U251 cells were analysed in each different conditions *i.e.* control, 48h-CT with CDDP 40 μ M or Pt(IV)AC-POA 10 μ M and recovery condition for CDDP or Pt(IV)Ac-POA. Bars: 20 μ m.

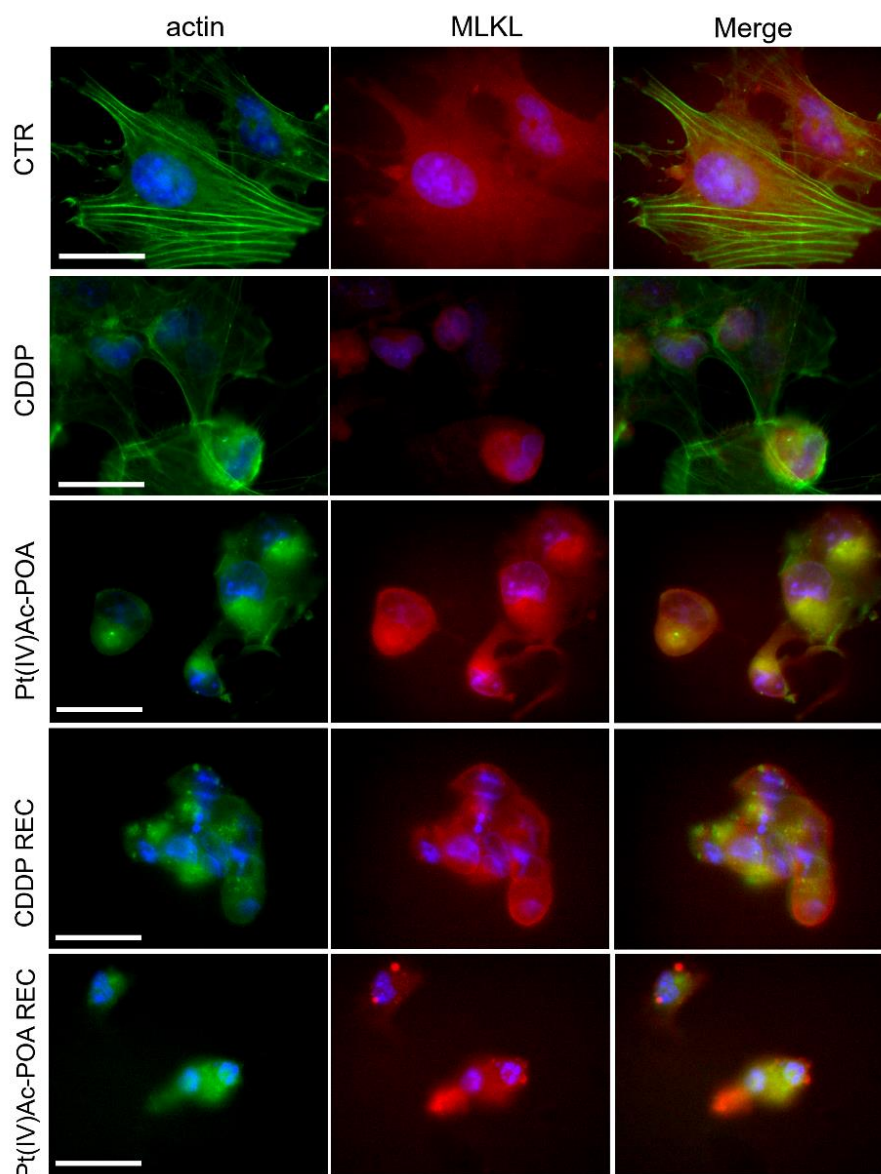


Figure 46. Double immunocytochemical detection of MLKL (red fluorescence) and actin (green fluorescence). DNA counterstaining with Hoechst 33258 (blue fluorescence). U251 cells were analysed in each different conditions *i.e.* control, 48h-CT with CDDP 40 μ M or Pt(IV)AC-POA 10 μ M and recovery condition for CDDP or Pt(IV)Ac-POA. Bars: 20 μ m.

Then also the activation of the independent caspase pathway was investigated by immunolabeling for the AIF protein and the mitochondria (**Figure 47**). In the control cells, the AIF protein was found to be at the level of the mitochondria, as suggested by the colocalization of the two associated fluorescence. Following treatment, AIF loses its physiological location and moves into the cytoplasm and then into the nucleus. At 48h-CT with CDDP at 40 μ M and Pt(IV)Ac-POA at 10 μ M the translocation of AIF to the nucleus was more evident, on the contrary in the two recovery conditions, despite the apoptosis present, it was more difficult to discriminate this process, as it seems there is a return of localization of AIF with the mitochondria, which could, therefore, be associated with a cellular recovery mechanism.

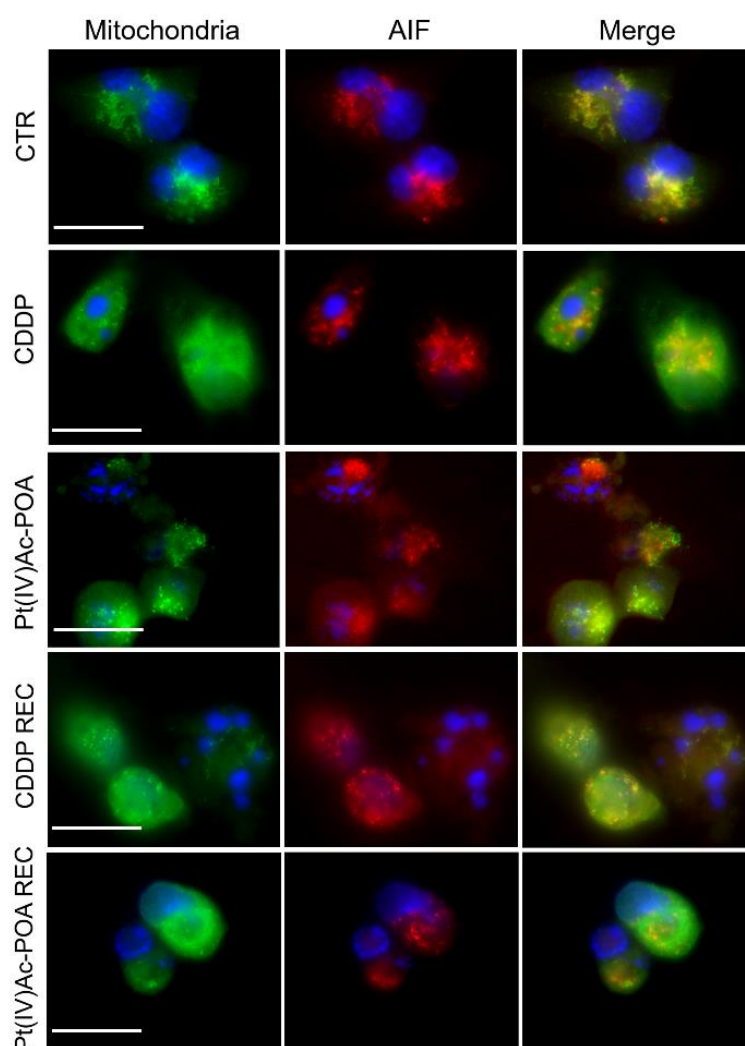


Figure 47. Double immunoreaction for mitochondria (green fluorescence) and AIF (red fluorescence) in control and treated cells. DNA counterstaining with Hoechst 33258 (blue fluorescence). U251 cells were analysed in each different conditions *i.e.* control, 48h-CT with CDDP 40 μM or Pt(IV)AC-POA 10 μM and recovery condition for CDDP or Pt(IV)Ac-POA. Bars: 20 μm.

4.3.4 Evaluation of autophagy pathway activation

As described in the previous analyses, after treatments, it was possible to detect the typical morphologies of autophagy. For this reason, the two proteins mainly involved in the autophagic pathway such as p62/SQSTM1 and LC3B were evaluated. In the control cells, the two associated fluorescence did not colocalize, p62/SQSTM1 was evaluated both in the cytoplasm and in the nucleus, while LC3B was predominantly cytoplasmatic. After treatments a colocalization of the two protein signals was detectable in all conditions, suggesting an activation of the autophagic process. The only distinct condition was the CDDP recovery sample in which the cells have strongly changed their morphology, increasing in size and considerably the basal expression of the two proteins of which fluorescence was not observed to be colocalized (**Figure 48A**).

Through western blot analysis, the levels of p62/SQSTM1 were examined in the respective treatments and control condition, however, despite a reduction in the expression levels of this protein, no statistically significant differences were obtained compared to the control samples (**Figure 48B**).

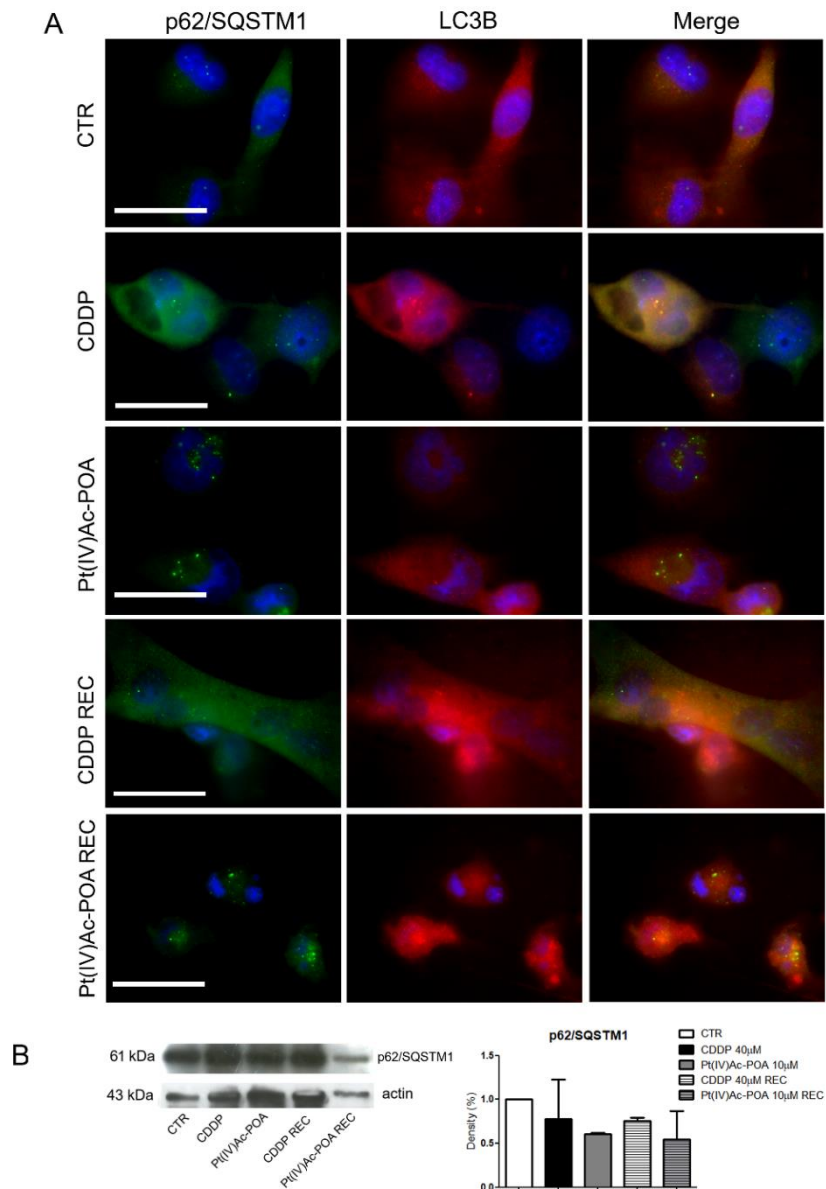


Figure 48. A) Double immunolabelling for p62/SQSTM1 (in green) and LC3B (in red). DNA counterstaining with Hoechst 33258 (in blue). Bars: 20 μ m. **B)** Western blotting data of p62/SQSTM1. The bar chart represents density bands quantification of p62/SQSTM1 in the control sample and following CDDP 40 μ M or 4 μ M Pt(IV)Ac-POA 48h-CT and their respective recovery conditions.

4.3.5 Analysis of Pt(IV)Ac-POA treatment on cytoplasmic organelles

Based on experiments already carried out on the U251 cell line treated with CDDP 40 μ M and platinum(II) 48h-CT (Grimaldi M, 2015, Ph.D. thesis) and the observations obtained on the involvement of cytoplasmic targets, cellular components such as the Golgi Apparatus and mitochondria were analysed to establish whether cytoplasmic organelles were also targets of treatment with Pt(IV)Ac-POA. From the obtained data it was shown how compared to the control conditions, after each treatment, there was a strong alteration of the organelle under study.

In control conditions, Golgi Apparatus fluorescence was clear and in the perinuclear area, suggesting a good structuring of the organelle, thanks also to the presence of a well-organized actin cytoskeleton. In contrast, after treatments, there was a degeneration of both Golgi cistern attachment and cytoskeletal structure. After 48h-CT with CDDP 40 μ M or Pt(IV)Ac-POA 10 μ M, a degradation of Golgi Apparatus was observed, resulting in a diffuse and homogeneous fluorescence purely localized around fragmented nuclei. This effect was considerably intensified in the Pt(IV)Ac-POA sample, where cytoskeleton and Golgi Apparatus were no longer distinguishable. On the contrary, in the CDDP recovery conditions, despite the presence of cells in a state of stress, there was a restoration of physiological conditions, associated with well-defined actin and Golgi Apparatus labelling as observed in control cells (**Figure 49**).

Very similar effects were also observed in the double immunolabelled analysis for the mitochondria and the tubulin cytoskeleton (**Figure 50**). In control conditions, the mitochondria were distributed evenly throughout the entire cytoplasm of the cell, delineating according to the pattern of microtubules of the well-organized cytoskeleton. After the respective treatments, a very intense effect was obtained in the 48h-CT samples exposed to Pt(IV)Ac-POA 10 μ M and the exposure action seems to persist even in recovery conditions. In the samples treated with CDDP at 40 μ M to 48h-CT, different cells showed similar characteristics to the control, which worsened in the recovery condition, but which in any case showed less intense effects than those obtained in cells treated with the new compound.

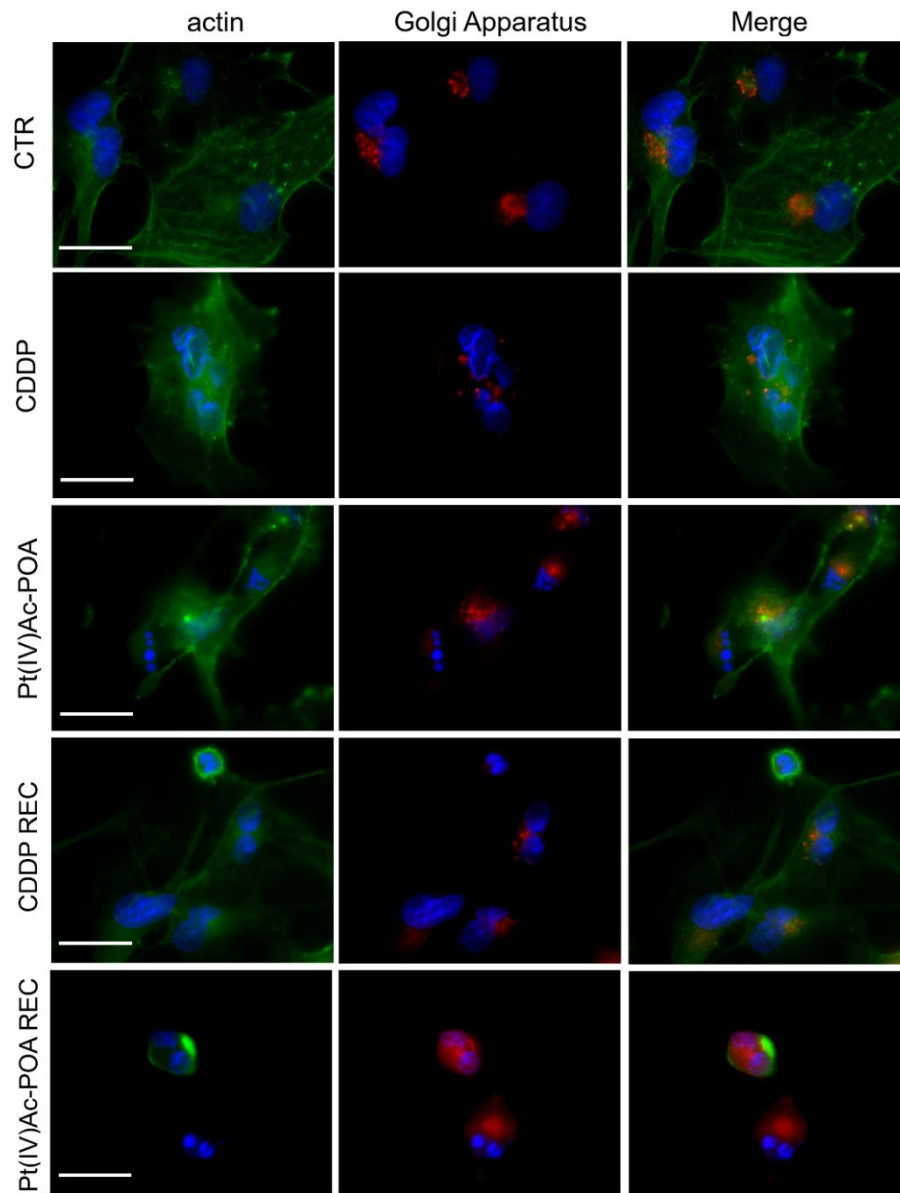


Figure 49. Double immunocytochemical detection of Golgi Apparatus (red fluorescence) and actin (green fluorescence). An investigation by fluorescence microscopy, U251 control cells and after 48h-CT with CDDP 40 μ M or Pt(IV)Ac-POA 10 μ M and the respective recovery conditions. DNA counterstaining with Hoechst 33258 (blue fluorescence). Bars: 20 μ m.

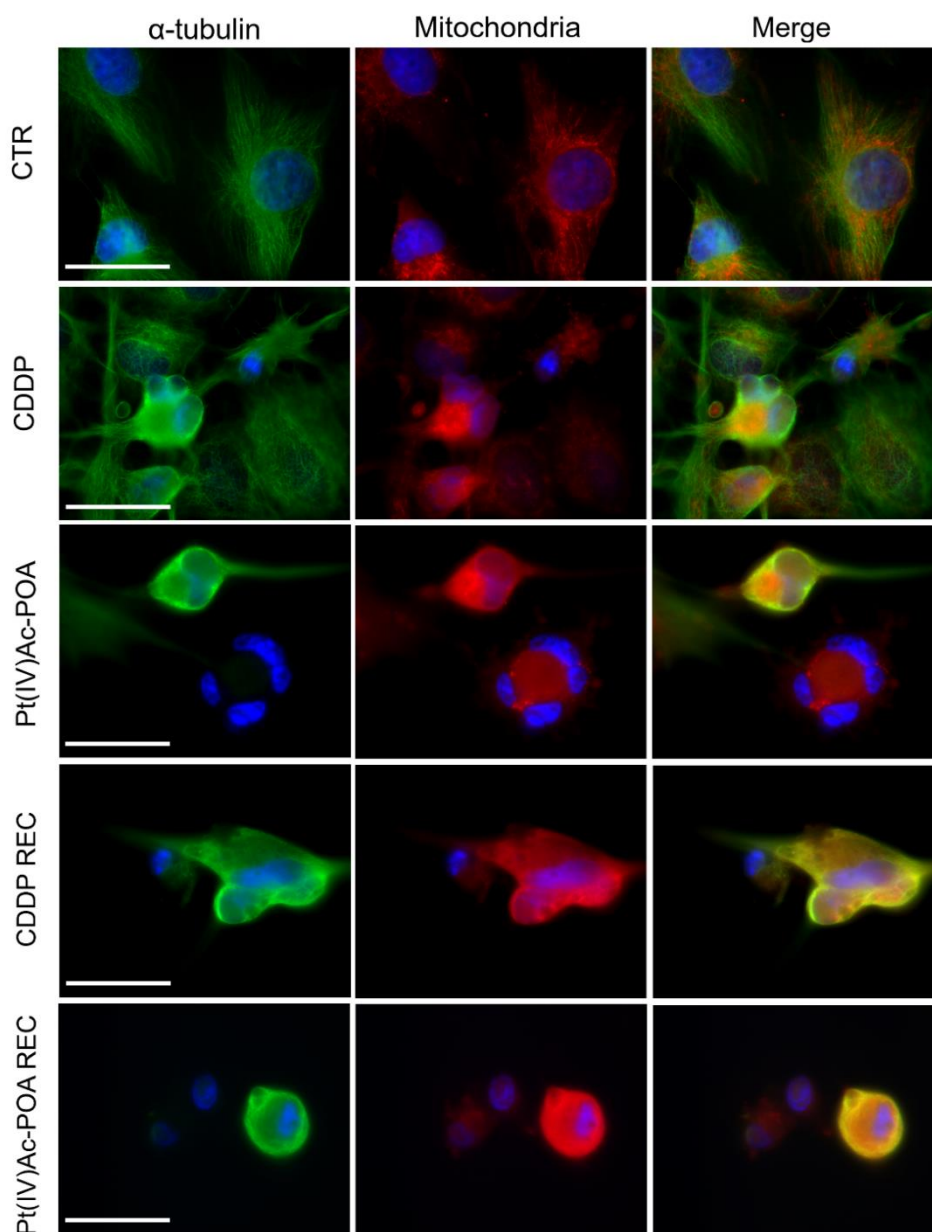


Figure 50. Double immunocytochemical detection of mitochondria (red fluorescence) and α -tubulin (green fluorescence) in control and after 48h-CT with CDDP 40 μ M or Pt(IV)Ac-POA 10 μ M and the respective recovery conditions. DNA counterstaining with Hoechst 33258 (blue fluorescence). Bars: 20 μ m.

4.3.6 Hadrontherapy with carbon ions on U251

Preliminary studies have been conducted on U251 cells using carbon ion hadrontherapy. The effects were evaluated by applying different experimental conditions, to observe the action of hadrontherapy alone and combined with the use of chemotherapeutic drugs such as CDDP or new compounds being studied such as Pt(IV)Ac-POA. The same concentrations of compounds were maintained, to compare the effects of combined therapy with those already observed with the treatments where the chemotherapeutic was already used. The data obtained (**Figure 51**), although very preliminary, showed that hadrontherapy and chemotherapeutic treatment can promote cell death of U251 tumour cells. Above all, we can see how the 4Gy radiation is more effective on U251 cells compared to 2Gy radiation. Indeed, the structural modifications of the cytoskeleton were observed in the samples pretreated with the compounds and then irradiated to 4Gy. However, the PARP-1 translocation was found only in some conditions *i.e.* CDDP+4Gy, Pt(IV)Ac-POA+2Gy, and Pt(IV)Ac-POA+4Gy, suggesting a great efficacy on U251 cells.

The observation of the 48h-CT conditions was then associated with the analysis of long-term effects, evaluating the various treatments in recovery conditions (**Figure 52**). To note that the effects of the pretreatment and/or irradiation were preserved only under specific conditions. Indeed, the samples only irradiated resumed being like the control, particularly in recovery conditions, as showed by cells in mitosis (white arrow). The treatments associated with CDDP both at 2Gy and 4Gy seemed to have a good yield, but the presence of cells with fusiform morphology would allow assuming the beginning of cellular recovery. The best result was obtained with Pt(IV)Ac-POA pretreatment, with both exposures to 2Gy and 4Gy. The possibility to obtain a good antitumor effect, even after exposure to 2Gy, would make this combined treatment a good strategy to reduce the high dose of therapy.

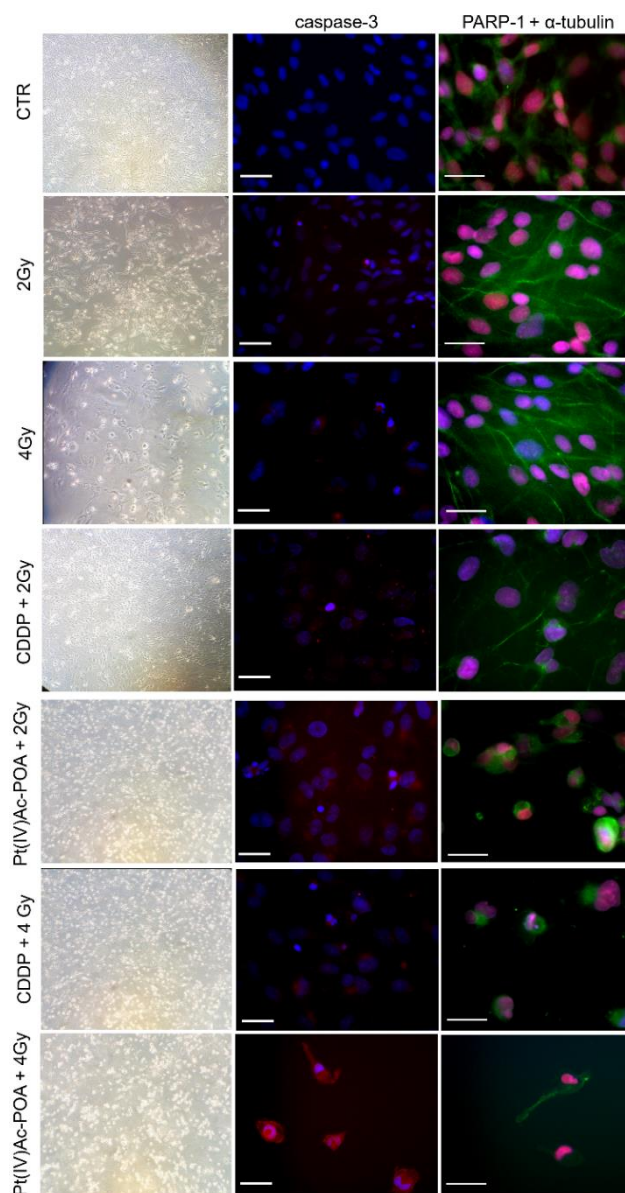


Figure 51. Representation of the experimental conditions for hadrontherapy. The left column indicates U251 cultured in flask before being processed for immunofluorescence reactions. Immunoreaction to active caspase-3 or PARP-1 (in red) with α -tubulin (in green). DNA counterstaining with Hoechst 33258 (in blue). Bars: 20 μ m.

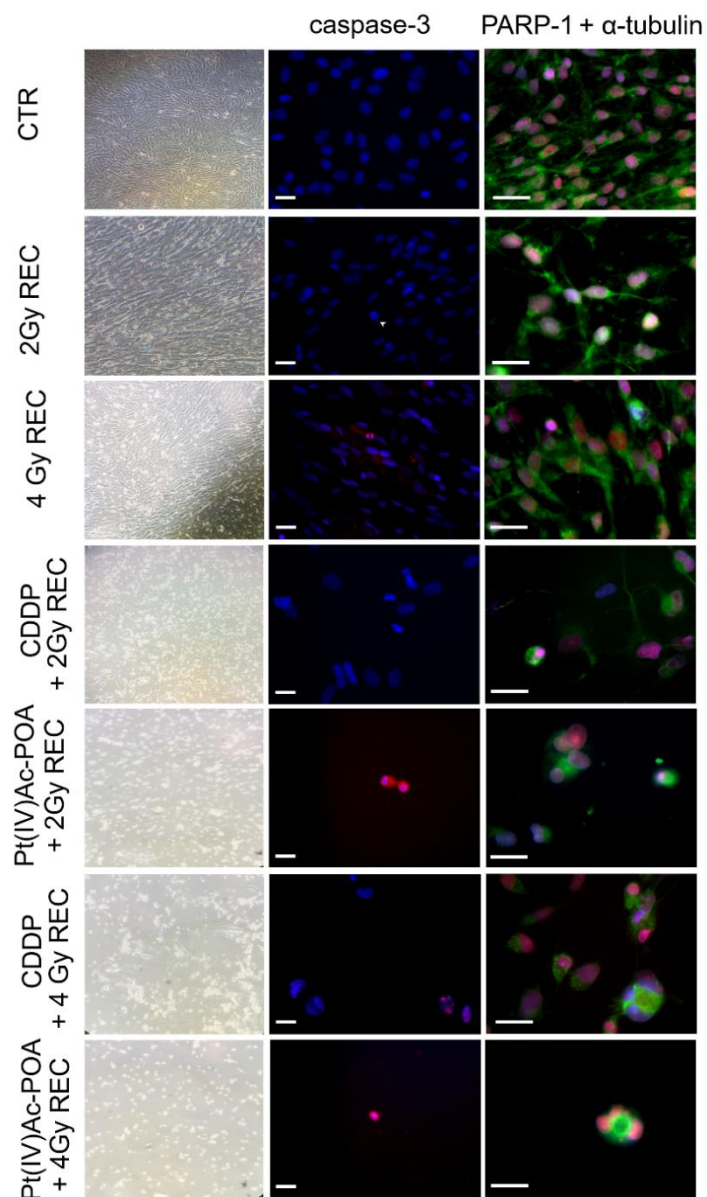


Figure 52. Representation of the experimental conditions for hadrontherapy after recovery condition. The left column indicates U251 cultured in flask before being processed for immunofluorescence reactions. Immunoreaction to active caspase-3 or PARP-1 (in red) with α -tubulin (in green). DNA counterstaining with Hoechst 33258 (in blue). White arrow indicates a mitosis Bars: 20 μ m.

4.3.7 *Taraxacum officinale* effects on free radical stress on U251

To assess whether the beneficial effects of the *Taraxacum officinale* could also be employed in the treatment of the U251 cell line, an MTS assay was performed to identify the concentrations of interest for this type of study *i.e.* 25 $\mu\text{g/ml}$, 250 $\mu\text{g/ml}$ and 2500 $\mu\text{g/ml}$. Following this investigation, the effects on the cell cycle were evaluated (**Figure 53**). However, all concentrations showed no effect on the cell cycle, which was therefore very similar to the control even after 48h-CT with *Taraxacum officinale* extract.

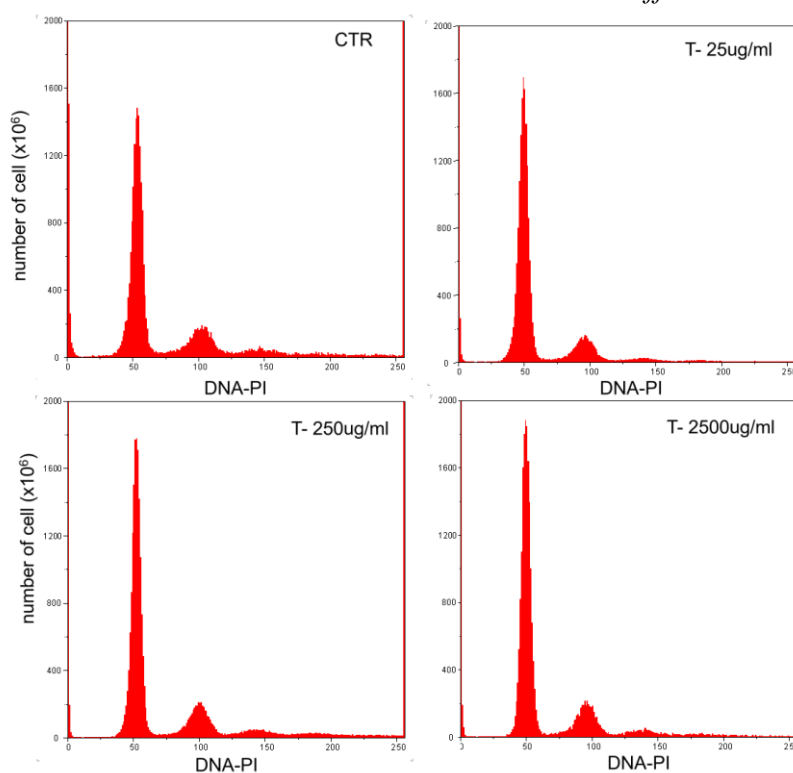


Figure 53. Flow cytometry after PI staining. Cytograms of DNA content of U251 control cells (CTR) and treated for 48h-CT with *Taraxacum officinale* root extract at different concentrations (25, 250 and 2500 $\mu\text{g/ml}$).

Since there was no alteration in the cell cycle, the possibility of the extract to reduce the effects of free radical stress was investigated. For this analysis, the three concentrations (25, 250, 2500 $\mu\text{g/ml}$) were evaluated both by treating the cells with the extract of *Taraxacum officinale* for 48h-CT and by using

this procedure as a pre-treatment for the subsequent exposure to Pt(IV)Ac-POA at 10 μ M.

The most significant effects were obtained at the concentration of 250 μ g/ml, concentration already used in other studies and therefore non-toxic for healthy cells (Zhu H et al. 2017). First, the presence of active caspase-3 positive cells was evaluated, to discriminate against a possible adjuvant effect between the treatments. The images reported in **Figure 54**, revealed a non-immunopositivity of the U251 control cells for cleaved caspase-3, while single apoptosis was found after 48-CT with the *Taraxacum officinale* extract at 250 μ g/ml. On the contrary, after combined treatment, an increase in immunopositive cells for active caspase-3 or in any case cells with a cell death phenotype, was observed, although not intensively. The 48-CT treated sample with Pt(IV)Ac-POA 10 μ M was used as a positive control.

Subsequently, proteins related to free radical stress and inflammation such as NOS2, or inducible NOS, and COX2 were analysed by immunofluorescence analysis. A decrease in the levels of both proteins following 48h-CT with the extract at a concentration of 250 μ g/ml was observed. To note that Pt(IV)Ac-POA at 10 μ M, in addition to inducing cell death and a perinuclear redistribution of mitochondria, also promoted an increase in the fluorescent signal for both NOS2 and COX2. The compound having a reducing action, could, therefore, influence the mechanisms of regulation of free radical stress and related mechanisms. However, this effect was decreased with the pre-treatment with the extract for 48h-CT, suggesting an action to restore normal physiological levels. Furthermore, the tumour cell, having a hypoxic microenvironment, could represent a target for the action of the *Taraxacum officinale*, which could, therefore, increase the sensitivity of the tumoral cell to the chemotherapeutic agent.

Besides, the reduction of inflammation-associated molecules could reduce the damage caused by it, especially in the nervous tissue where the cells are most sensitive.

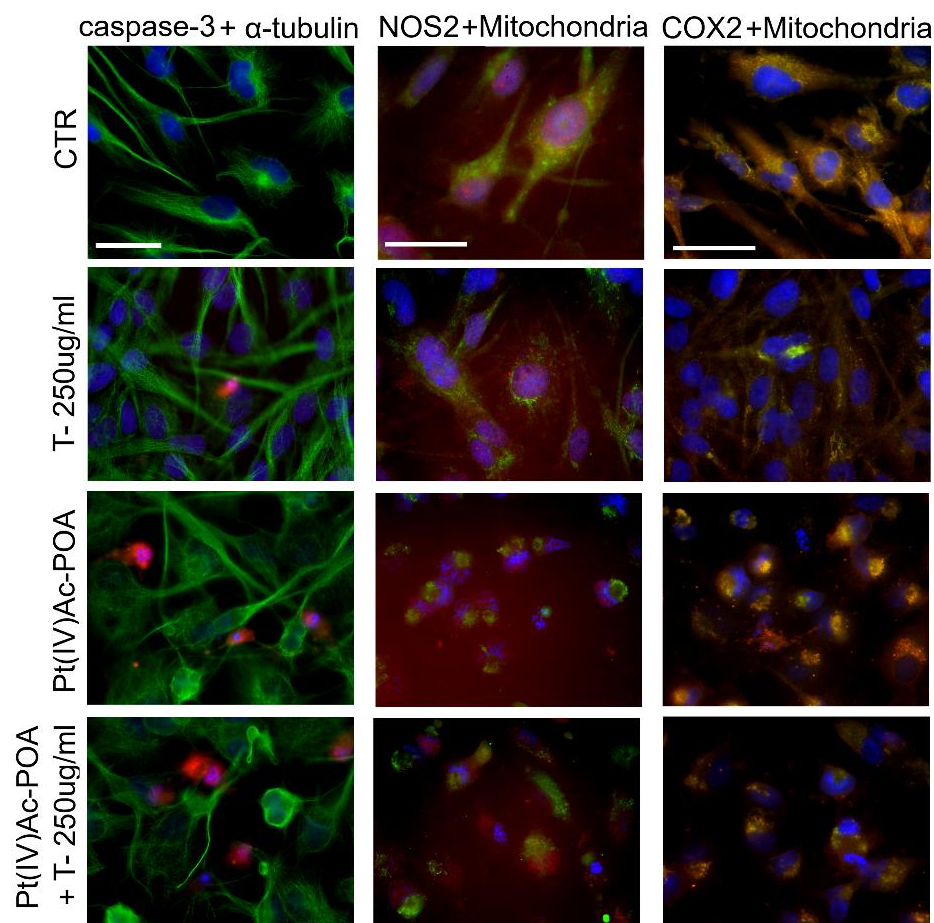


Figure 54. Double immunoreactions for active caspase-3 (red fluorescence) and α -tubulin (green fluorescence) are reported in the first column; in the middle double immunoreaction for NOS2 (red fluorescence) and mitochondria (green fluorescence); the last column indicates double immunoreaction for COX2 (red fluorescence) and mitochondria (green fluorescence). Each investigation was performed for cells in the control condition, after 48h-CT with 250 μ g/ml of *Taraxacum officinale* or Pt(IV)Ac-POA at 10 μ M. At last, pre-treatment with 250 μ g/ml of the extract 48h-CT, followed by treatment with Pt(IV)Ac-POA at 10 μ M 48h-CT. Bars: 20 μ m.

4.3.8 *Ganoderma lucidum* treatment and its effect on calmodulin protein

Ganoderma lucidum has long been used to treat various tumours, and its effect on the U251 line was then evaluated. After testing different concentrations of the *Ganoderma lucidum* supplement, through the MTS assay, in order not to induce any type of damage to control cells such as fibroblasts, three concentrations of interest were selected for flow cytometric analyses. After 48h-CT with the supplement, cytofluorimetric analysis of U251 cells DNA content was performed (**Figure 55**). Compared to the control, at the concentration of 10 mg/ml, the cells no longer showed a distribution in the various phases of the cycle, but there was a complete degeneration of the cell cycle. At the concentration of 5 mg/ml there was a more evident sub-G₁ peak than the control; to note a blockage of the cells in the G₂/M phase of the cell cycle. Finally, at the lowest concentration, 1 mg/ml, a pattern of cell distribution very similar to the control, but with less obvious peaks was observed. At this concentration, cells were not damaged considerably and therefore the U251 slowly start to proliferate again even after treatment. Based on these data, the concentration of 5mg/ml was chosen for subsequent treatments.

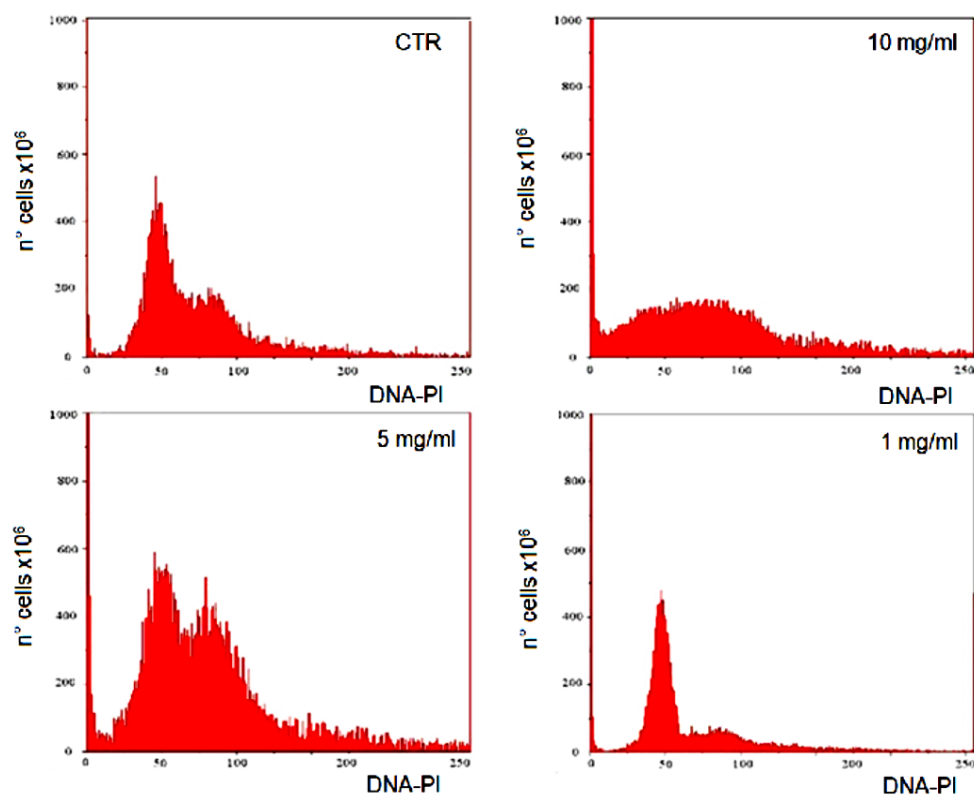


Figure 55. Cytograms of DNA content after staining with PI in U251 control cells and after treatment with *Ganoderma lucidum* based supplement (10, 5 and 1 mg/ml) 48h-CT.

Once the treatment concentration was chosen, double immunolabelling for NOS2 and actin was performed, in order to observe any changes in the free radicals stress and the possible effect on cell morphology *i.e.* reductions in cell volume and de-structuring of microfilaments. After 48h-CT with the supplement based on *Ganoderma lucidum*, a reduction in the NOS2 fluorescent signal was observed compared to the control conditions, suggesting a reduction in the level of nitrogen radical stress. The treatment with H₂O₂ at 300 μ M was tested as a positive control for the induction of NOS2 (**Figure 56**).

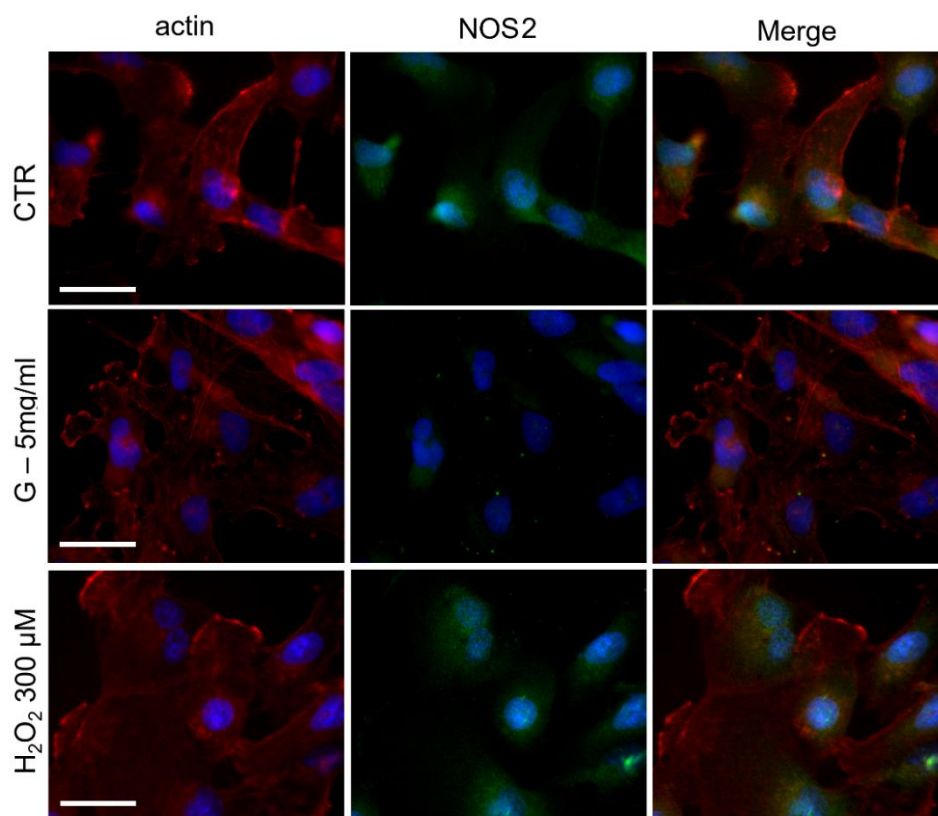


Figure 56. Double immunocytochemical detection in control (CTR) and 48h-CT to *Ganoderma lucidum* based supplement at 5mg/ml (G-5mg/ml) treated cells. Positive control obtained by U251 exposure to H₂O₂ at 300 μM. NOS2: green fluorescence, actin: red fluorescence, Hoechst 33258 counterstaining for the nuclei (in blue). Bars: 20 μm.

Another aspect that was evaluated following treatment with the *Ganoderma lucidum* supplement was to assess changes in CaM levels before and after treatment for 48h-CT. CaM plays an important role in numerous pathways, including the remodelling of the actin cytoskeleton, intercellular communication, and regulation of Ca²⁺ homeostasis, which is a key component in the physiological mechanisms of neuronal and glial cells. The images in **Figure 57** represent U251 control cells and cells after 48h-CT to the supplement based on *Ganoderma lucidum*. The actin cytoskeleton in the treated U251 cells showed no obvious morphological changes compared to

control cells, thus maintaining its structural integrity. CaM in U251 control cells appeared to be homogeneously distributed in the cytoplasm, this localization was maintained even after treatment, although there was an accumulation at the perinuclear level. This data could, therefore, suggest a direct action of the treatment even at the intracellular level, acting on mechanisms of essential signalling such as CaM.

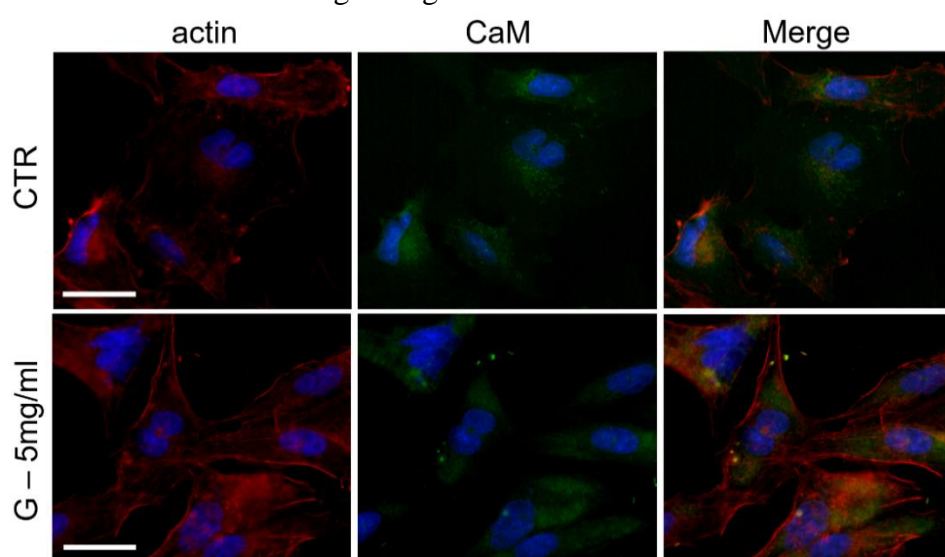


Figure 57. Double immunocytochemical detection in control (CTR) and 48h-CT to *Ganoderma lucidum* based supplement at 5mg/ml (G-5mg/ml) treated cells. CaM: green fluorescence, actin: red fluorescence, Hoechst 33258 counterstaining for the nuclei (in blue). Bars: 20 μ m.

4.3.9 Characterization of BK and KIR4.1 channel in U251 cell line

Wound healing assay after 24 h was used to verify cell migration, but above all to distinguish the cellular phenotype that could be considered “migrant”. The experimental plan consisted of a basal condition and 24 h after wound healing assay (t_1) (see Material and Methods). In these conditions, U251 cells, after immunolabelling to the actin cytoskeleton, showed two different morphologies: flattened cells and cells with polarised cytoplasmic protrusions, called “polarised cells” (**Figure 58**).

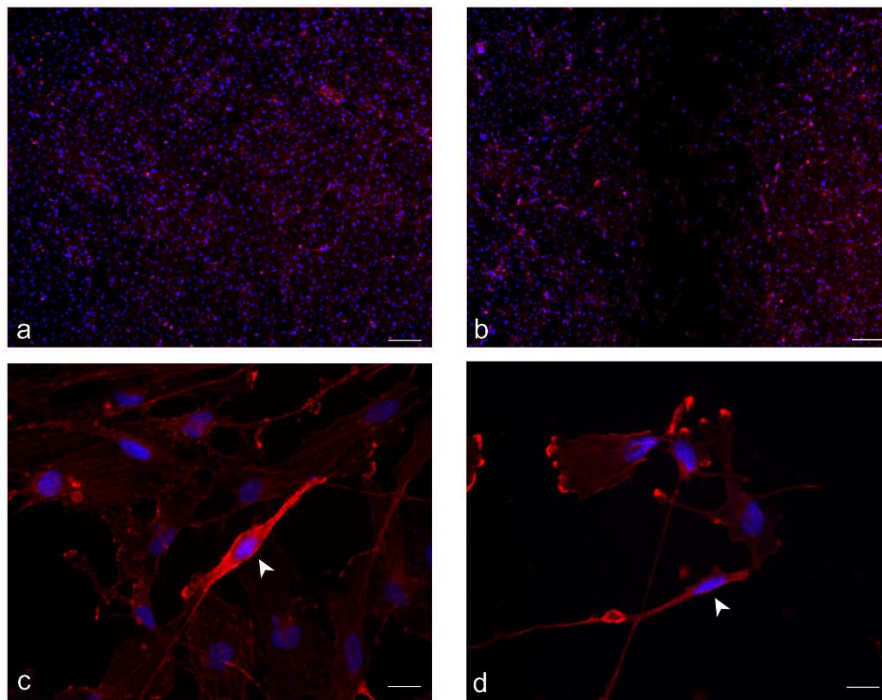


Figure 58. Actin immunostaining for U251 cells cytoskeleton (red fluorescence), revealing different cell morphologies at the basal condition and at t_1 (**a,c** and **b,d**, respectively); nuclear counterstaining with Hoechst 33258 (blue fluorescence). White arrowhead indicates polarized cells. Bars: 200 μm (**a** and **b**), 20 μm (**c** and **d**).

The migration marker, active-Cdc42, used to stained cell cytoplasm and identify cell morphology, revealed that in polarised cells immunoreactivity was enhanced compared with flattened cells (**Figure 59**). Especially, in polarised cells, the mean fluorescence density per cell progressively increased from basal to out, to intra scratch cells (**Figure 59 c**), whereas in the flattened cells, the fluorescence persisted constant (**Figure 59 a–c**).

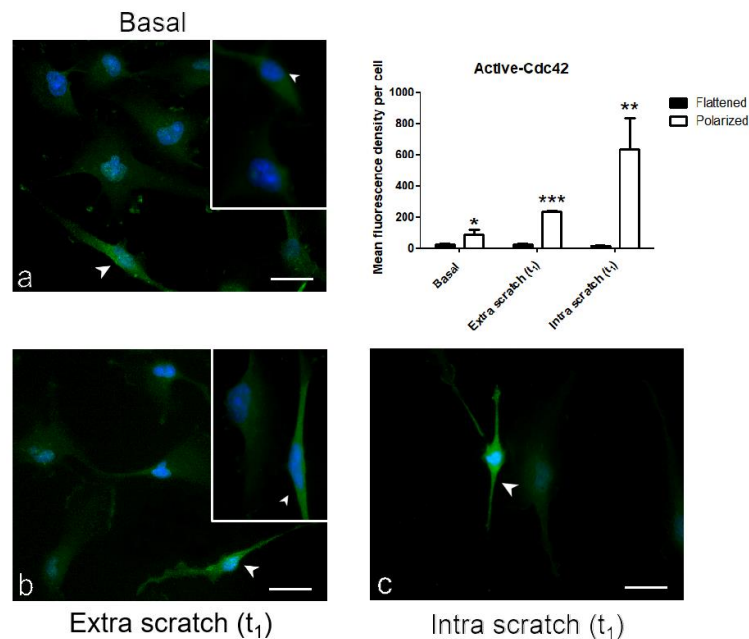


Figure 59. Active-Cdc42 immunolabelling (green fluorescence), in flattened and polarized cells, evaluated at basal condition (**a**) and at t_1 , both outside (extra scratch, **b**) and within (intra scratch, **c**) wounded area. Bar chart shows the mean fluorescence density per cell. Nuclei were counterstained with Hoechst 33258 (blue fluorescence). White arrowhead indicates polarised cells. Bars: 40 μm . Student's t -test: *statistical analysis between flattened and polarized cell in the three experimental conditions: p values: (*) $p < 0.05$; (**) $p < 0.01$; (***) $p < 0.001$.

The proliferation marker PCNA was used to identify proliferating U251 cells and discriminate against some differences in cell morphology as described above. No statistically significant differences were measured in flattened and polarised cells under different experimental conditions except for extra scratch cells between flattened and polarised cells (**Figure 60 a–c**). The difference in the type of immunolabelling was evaluated; in polarised cells was homogeneously distributed in the nucleus, while in flattened cells the fluorescence appeared spot-like, indicating that the latter were actively cycling cell.

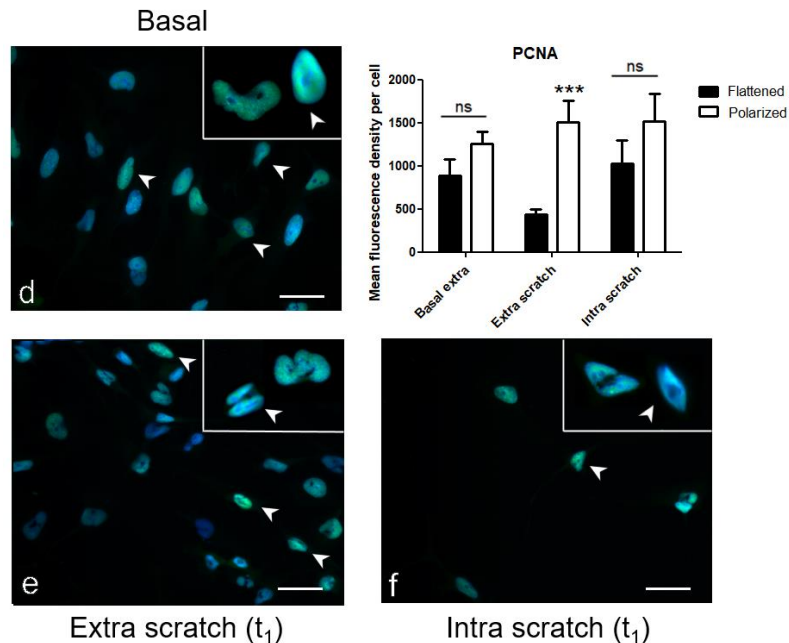


Figure 60. PCNA immunolabelling (green fluorescence), in flattened and polarised cells, evaluated at basal condition (a) and at t₁, both outside (extra scratch, b) and within (intra scratch, c) wounded area. Bar chart shows the mean fluorescence density per cell. Nuclei were counterstained with Hoechst 33258 (blue fluorescence). White arrowhead indicates polarised cells. Bars: 40 μ m. Student's t-test: *statistical analysis between flattened and polarized cell in the three experimental conditions: p values: (***) $p < 0.001$, ns: not significant.

Immunocytochemistry demonstrated the cytoplasmic expression of both Kir4.1 and BK channels, and a mislocation in the nucleus under basal conditions. In polarised cells, BK-immunopositivity was detectable in both the cytoplasm and nucleus (**Figure 61A**). The mean fluorescence density *per cell* was higher in the nucleus of cells extra scratch and intra the wounded area compared with the basal condition (**Figure 61B**). In the cytoplasm, a similar non-significant trend was observed. Kir4.1-immunopositivity was detected in both the cytoplasm and nucleus (**Figure 61C**). The mean fluorescence density was higher in both the cytoplasm and nucleus of cells extra the wounded area compared with the basal condition (**Figure 61D**). Therefore, scratch wounding may trigger the increased expression of BK and KIR4.1 in the nucleus and cytoplasm.

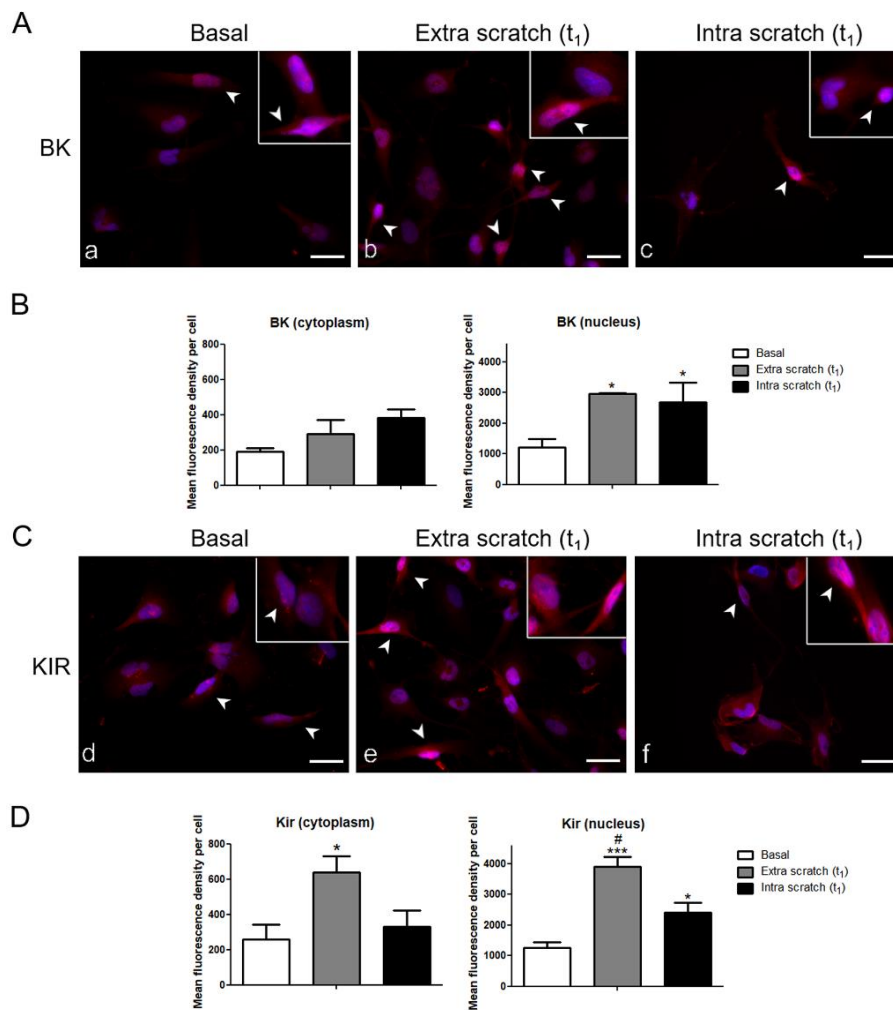


Figure 61. Immunocytochemical detection of BK (**Panel A**, red fluorescence) and Kir4.1 (**Panel B**, red fluorescence) in the nucleus and cytoplasm of polarized cells at basal condition (**a, d**) and at t_1 , both outside (**b, e**) and within (**c, f**) the wounded area. Nuclei were counterstained with Hoechst 33258 (blue fluorescence). Inserts: details of BK and Kir4.1 nuclear immunoreactivity. White arrowhead: polarised cells. Bars: 40 μm . Bar charts show the mean fluorescent density per cell of BK (**Panel C**) and Kir4.1 (**Panel D**) in the nucleus and cytoplasm. *Statistical analysis: cells at basal condition vs t_1 , outside and within the wounded area; #statistical significance between cells at t_1 within and outside wounded area. ρ values: (*) $\rho < 0.05$; (**) $\rho < 0.01$; (***) $\rho < 0.001$.

The EDTA-regressive technique displayed the ultrastructural localisation of BK and Kir4.1 channels in the U251 cell line. In the nucleus, the BK-labelling was mainly found near the heterochromatin rather than euchromatin. In particular, several marked spots were observed on RNA fibrils. The labelling of the BK channel was also present in the cytoplasm and near the cell membrane. BK-positive membrane protrusions were also observed (**Figure 62A b**). Ultrastructural analysis of Kir4.1 channels displayed a more heterogeneous localisation inside the nucleoplasm compared with BK labelling. The Kir4.1-labelling was also detected near the cytoplasmic membrane and membrane vesicle (**Figure 62B c,d**).

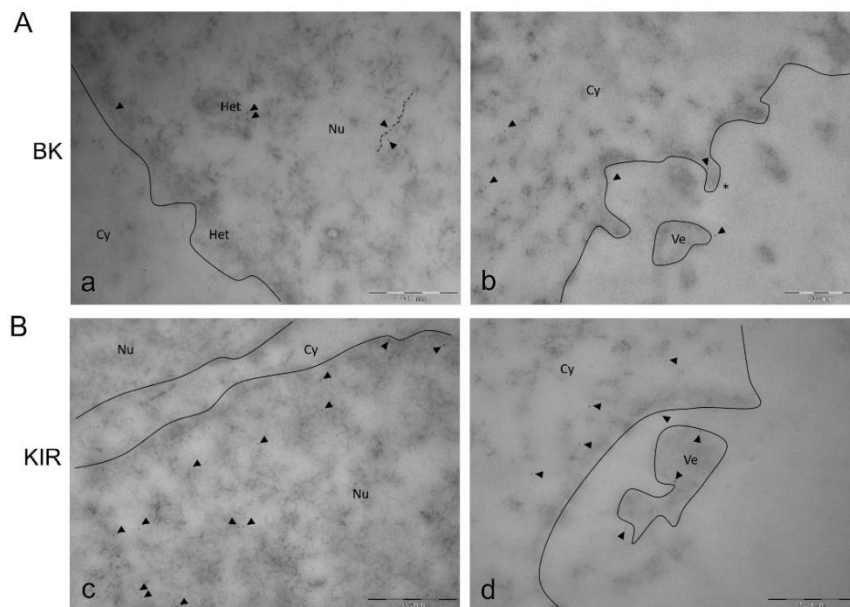


Figure 62. TEM ultrastructural analysis (EDTA-regressive staining technique): BK and Kir4.1 channels localization. **Panel A:** nuclear BK labelling mainly detected closed to the heterochromatinic space, compared to euchromatin (**a**), and cytoplasmic BK immunopositivity present nearby the cytoplasmic membrane, membrane protrusions (asterisk), also detectable in cell vesicles (**b**). **Panel B:** Kir4.1 immunolabelling heterogeneously localised inside the nucleoplasm (**c**), and cytoplasmic Kir4.1 staining mostly present nearby the membrane and membrane vesicle (**d**). Continuous line: nuclear membrane. Black spots: Immuno-gold labelling for BK- and Kir4.1; gold particles dimension: 6nm (black arrowhead). Dashed line: RNA fibrils. Cy: cytoplasm; Nu: nucleus; Het: heterochromatin; Ve: vesicle. Bars: 500nm.

5. Discussion

This thesis work is part of a broad scientific project that involves several research laboratories and that has the aim of identifying new treatments useful for overcoming the limits associated with conventional cancer therapies currently in use. Among these limits, chemoresistance is one of the major obstacles in the treatment of NS tumours, as the standard protocols, as well as the treatment with TMZ, can only in some cases improve the patient's prognosis, but not leading to a complete resolution. Also, the high heterogeneity that characterizes these cancers, in particular, GBM, represents a great challenge for the diagnosis and the development of tumour-specific therapies. Hence, based on these data, for more than ten years the laboratory, in which this work has been carried out, has been involved in identifying new platinum-based compounds that may have greater efficiency than the CDDP standard treatment, but with lower systemic toxicity. Several data obtained in our laboratory have confirmed the possibility of synthesizing new platinum-based compounds with good antitumor action and a lower cytotoxic effect on healthy cells (Piccolini VM et al. 2015), however, the problem of acquired chemoresistance remains a process to be clarified. In this regard, biomedical research has focused on new platinum(IV) compounds, which act as prodrugs, thus reducing the possible side effects of cytotoxicity outside tumour cells (Johnstone TC et al. 2016). Furthermore, the ability to associate biologically active axial ligands, *i.e.* HDACi, within the molecule, allows obtaining a synergistic effect that would implement the antitumor effect.

From 2017, the study of the new platinum-based compound Pt(IV)Ac-POA was undertaken and, to date, promising data have been published on the use of this prodrug in several lines of NS tumours (Ferrari B et al. 2019; Rangone B et al. 2018). Pt(IV)Ac-POA belongs to the platinum(IV) family and performs its cytotoxic action by acting as a prodrug. Indeed, it is inactive outside the tumour cells, while it is activated inside them through a reduction mechanism that leads to the splitting of the CDDP molecule and the two axial ligands including the POA (Gabano E et al. 2017). Thanks to the presence of POA, the Pt(IV)Ac-POA molecule is more lipophilic, thus increasing the intracellular accumulation of the prodrug compared to CDDP alone. Moreover, POA is considered a very active HDACi, thus indirectly producing an increase in acetylation at the chromatin level, increasing its

decondensation and consequently enhancing the exposure of DNA to the action of the CDDP (Gabano E et al. 2017; Novohradsky V et al. 2017).

The first step of this study was to characterize the effects of Pt(IV)Ac-POA treatment, on two different cell lines of NS tumours, such as B50 neuroblastoma and C6 glioma rat cell lines. These two lines, distinguished by different characteristics, have been chosen for their easy use as an *in vitro* model for the study of new antitumor compounds effects, as already described in various studies in the literature (Grimaldi M et al. 2019; Krajčí D et al. 2000). Furthermore, the choice fell on B50 and C6 cell line is the forecast to translate *in vitro* studies to *in vivo* model, in order to evaluate the aspects of neurotoxicity, also comparing them with the data previously obtained from other platinum-based compounds (Bernocchi G et al. 2011; Piccolini VM et al. 2015).

The U251 human GBM cell line represents the third line selected for the evaluation of the new compound action. This line has a very variable cellular phenotype, thus reflecting one of the negative aspects of GBM, *i.e.* heterogeneity. This feature drastically influences the efficacy of the treatments by not having specific targets available that can facilitate the action of cancer agents. Therefore, in addition to evaluating the effects of treatment with Pt(IV)Ac-POA, different approaches have been used to analyse: *i)* the using combined treatments to increase effectiveness and reduce the negative aspects of toxicity, *ii)* the role of ion channels, important for understanding the pathophysiology of this cell line especially in the migration mechanisms.

In the first part of the study, focused on two rat cell lines, *i.e.* B50 and C6 cells, by several analyses it has been observed that the new prodrug acts on both cell lines inducing cell death already at the concentration of 4 μ M. This concentration is 10 times lower than the standard CDDP concentrations (40 μ M) used for *in vitro* cytotoxicity experiments, suggesting more effectiveness of Pt(IV)Ac-POA compared to CDDP (Grimaldi M et al. 2019; Krajčí D et al. 2000).

From cytofluorimetric analyses carried out on B50 and C6 cells, following continuous exposure for 48 h to the prodrug, alterations of the cell cycle were detected with the formation of large sub-G₁ peaks indicating the presence of dead cells, subsequently found also as apoptosis by the analysis with Annexin V.

By ultrastructural analysis at electron microscopy, both B50 and C6 cell lines showed the activation of different cell death pathways following the 48h-CT

with Pt(IV)Ac-POA at 4 μ M. The morphologies evaluated in the samples are attributable to different cell death such as apoptosis with strong pyknosis, karyorrhexis, and disappearance of the nuclear envelope; autophagy characterized by the increase of cytoplasmic vacuoles and double-membrane autophagolysosomes; necroptosis with features like both apoptosis and necrosis, but which is counted among the cell deaths of the programmed type. The presence of necrosis was not found in treated samples, a positive aspect considering the cascade of inflammatory, and therefore harmful, events that this pathway induces. The activation of these cell death pathways was supported by fluorescence immunolabeling data of the main proteins involved in these mechanisms. Following 48 h exposure to the new compound, compared to control conditions, an increase of Bax immunofluorescence signal was detected correlated with a reduction of Bcl-2 fluorescence intensity, suggesting a major pro-apoptotic effect in the treated cell at the expense of anti-apoptotic signal. An increase in the immunopositivity of cleaved caspases-9 and -3 supports the activation of the intrinsic apoptotic pathway, finally corroborate by cleavage of PARP-1 evaluated by immunofluorescence reactions and western blot analysis. AIF involved in the caspase-independent apoptosis was also investigated. AIF translocation from mitochondria to the nucleus was observed after 48h-CT with Pt(IV)Ac-POA, indicating the activation of this cell death pathway. In each cell line, the induction of the extrinsic apoptotic pathway was detected by immunoreaction to cleaved caspase-8. In Pt(IV)Ac-POA-treated sample an increased in immunopositivity of active caspase-8 was also detected. Furthermore, the RIP1 translocation from the cytoplasm to the nucleus corroborated the activation of the extrinsic apoptosis process, also suggesting a possible involvement of the necroptotic mechanism. Therefore, as described above, the possibility of inducing a regulated death process represents a positive aspect in the treatment of tumours, in order to exclude all those secondary mechanisms that could reduce the effectiveness of treatment or otherwise compromise the pathological scenario.

Another pathway induced by 48-CT with Pt(IV)Ac-POA, previously evaluated at electron microscopy was autophagy. Autophagy may have a double role in cell death mechanisms. Indeed, it could be a way to induce cell death, type II cell death, or can be a strategy of cell survival and consequently a mechanism of drug resistance (Belounis A et al. 2016). The reduction in p62/SQSTM1 expression after Pt(IV)Ac-POA 48h-CT, may confirm the

activation of the autophagic pathway, in which p62 has a role. Several data in literature proposed that homeostatic maintenance of p62 levels may contribute to the outcome of the tumorigenic process (Liu WJ et al. 2016). The p62 levels evaluated after Pt(IV)Ac-POA 48h-CT exposure, was quantitatively closer to those measured in physiological condition, suggesting a possible role in preventing tumour progression. This result differs from previous experimental results obtained from CDDP treatment, showing that a strong decrease in p62 expression level is often associated to a chemoresistance phenomenon, correlated to a high activation of autophagic pathway, and so able to support cell survive (Lin JF et al. 2017; Chen J et al. 2018). In addition, previous data showed that also cytoplasmic organelles are CDDP targets (Bottone MG et al. 2008; Santin G et al. 2012) and this involvement was also investigated in B50 and C6 rat cell lines after 48h-CT with Pt(IV)Ac-POA. In this study, in treated cells, was produce drastic damage to mitochondria and Golgi Apparatus, indicating that also cytoplasmic organelles are a possible target of the new prodrug.

In neuronal and glial cells, Ca^{2+} ion is involved in the different functional pathway and dysregulation of its homeostasis could produce a severe impermeant not only in cell function but also induce apoptosis (Calvo M et al. 2015; Lory P et al. 2010). Furthermore $[\text{Ca}^{2+}]_i$ alterations are associated with several modifications in the regulation of cell proliferation and migration such as occur in several types of tumour (Marchi S and Pinton P 2018; Mignen O et al. 2017; Morciano G et al. 2018). Based on these data, a preliminary investigation of Ca^{2+} homeostasis regulation by CBPs and PMCA1 (Roberts-Thomson SJ et al. 2010; Schwaller B et al. 2002), was performed in B50 and C6 cells, after treatment with Pt(IV)AC-POA. Previous data demonstrated the involvement of Ca^{2+} regulation mechanism in the CDDP-induced effects (Bernocchi G et al. 2015; Brini M et al. 2017; Piccolini VM et al. 2015), therefore CDDP treatment was used as a standard treatment to compare Pt(IV)Ac-POA effects.

Experiments in immunofluorescence and western blotting were performed to demonstrate the influence of the two drugs on Ca^{2+} homeostasis, on both cell line, by evaluating the quantitative changes of PV proteins, a cytosolic CBP used as a marker for inhibitory interneurons, CR, a cytosolic buffer protein implicated in the modulation of Ca^{2+} homeostasis and neuronal excitability, CaM, a ubiquitous CBP involved in the regulation of various biological processes including energy metabolism, cell motility and exocytosis, CB, a

cytoplasmic CBP involved in the development of neurons, in neurite elongation and in the growth and formation of dendritic spines, and PMCA1, an ATPase pump involved in the control of Ca^{2+} homeostasis, in development and in organogenesis. This data will be useful to correlate it with oxidative stress and excessive production of ROS, processes induced by both compounds on the tumour lines in question. Comparing the data related to the expression of CR after the two treatments, a significant difference was not evident, suggesting that B50 and C6 cells maintain stem cell characteristics. CB, on the other hand, increased in both samples treated with CDDP and with Pt(IV)Ac-POA, but its expression was more significant in cells treated with CDDP. Considering the function of the protein, linked to the preservation of nerve cells during development (Bernocchi G et al. 2015), this could be related to a possible mechanism of resistance to CDDP induced by the cells. CaM, instead, increased significantly in Pt(IV)Ac-POA-treated cells compared to those with CDDP. This data agreed with the decrease of Bcl-2 and the presence of a greater percentage of apoptotic cells after this treatment. Moreover, the Ca^{2+} concentration increase in cytosol induced mitochondrial alterations that may lead to greater production of ROS and therefore to an increase in oxidative stress (Muscella A et al. 2011). The results related to the PMCA1 protein, confirmed the increase in Ca^{2+} level, indeed PMCA1 signal raised in both treatments compared to the control, however in cells exposed to Pt(IV)Ac-POA, PMCA1 was expressed in a reduced measure compared to the cells treated with CDDP (**Figure 1**).

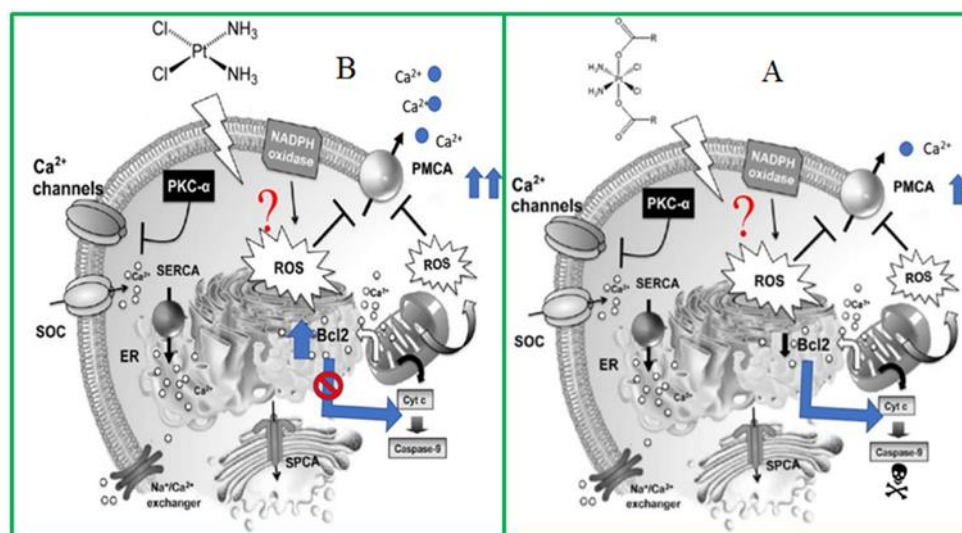


Figure 1. Comparison of the main mechanisms involved following treatment with a) CDDP; b) Pt(IV)Ac-POA (adapted from Muscella A et al. 2011).

This data contributes to confirming the indirect evaluation of the increase in intracellular Ca^{2+} induced by Pt(IV)Ac-POA. The data related to CDDP could support the hypothesis of the promotion of the drug resistance process in cells. Data on the expression of PV, showed a reduction following the two treatments compared to the control, in both cell lines. If compared, a greater reduction in the expression of PV was evident after treatment with Pt(IV)Ac-POA compared to CDDP. This could be attributed to a reduced long-term Ca^{2+} buffering action, thus indicating prolonged effects of the increased ion concentration.

Finally, the results presented show that Pt(IV)Ac-POA has an overall effect on the increase in Ca^{2+} , an effect that was probably related to its ability to trigger effective apoptosis.

In order to verify the action of the free acid POA at 48h-CT, its effect was initially evaluated by flow cytometry, demonstrating the induction of minimal apoptosis and a reduction in S phase. Then immunocytochemical and western blot investigations were conducted on acetyl-H3 levels, showing an increase in the levels of this acetylation, but not of the expression of the PCNA proliferation marker. To confirm the results obtained so far, some analyses have been carried out in electron microscopy to effectively evaluate the induction of chromatin decondensation following exposure to POA.

However, after 48h-CT at the POA in both the two cell lines no effect was obtained on chromatin decondensation. Based on these results, short-term effects were investigated, for which an increase in acetylation was obtained after 4 h or 2 h respectively in B50 and C6 cells. The different responses of the two cell lines could be associated with the neuronal and glial features that characterize the cells and consequently their functions. It is interesting to observe how C6 cells may have activated glia characteristics and therefore showing a strong euchromatic component (Mares V et al. 2003).

All the investigation describe so far was conducted on samples treated with POA at 4 μ M for 48h-CT, but any effects different to control conditions were evaluated. Other data obtained from samples treated with CDDP or Pt(IV)Ac-POA, showed drastic levels of H3 acetylation, due to the presence of the CDDP molecule that induces cell death and consequently reduced acetylation levels (data not shown). Therefore, data of POA confirmed that this compound has only a synergistic action when it is complexed with CDDP, implementing its function as an inhibitor of the enzyme histone deacetylase (Gabano E et al. 2017).

The second part of this study focused on the analysis of the effects induced by the new compound Pt(IV)Ac-POA on human glioblastoma cells U251. Thanks to data previously collected on this cell line, concerning the use of new platinum compounds, it was possible to compare the different concentrations and mechanisms activated following treatment with CDDP. The first step carried out was the choice of the dose to which the new compound was used, also referring to concentrations used in previous works on other cell lines (Ferrari B et al. 2019; Rangone B et al. 2018) and on the data obtained from the comparison between treatment with CDDP and a new platinum(II), *i.e.* [Pt(O,O'-acac)(γ -acac)(DMS)] (Grimaldi M, 2015, PhD thesis). The dose of 10 μ M Pt(IV)Ac-POA has proven to have the most significant effects after 48 h of continuous treatment, always remaining within a range of IC₅₀, therefore of relative toxicity. It should be noted that this concentration was found to be 4 times less than 40 μ M CDDP normally used *in vitro* treatment.

Although the effects on the cell cycle were not as intense as had been seen in the previous lines analysed, it was possible to find cell death, confirmed later by the presence of different apoptotic pathways. After treatment with the new compound, it was possible to detect through the analysis at electron microscopy the presence of different phenotypes of cell death such as

apoptosis, autophagy, and necroptosis; all forms of cell death among the types of programmed cell death. The positive aspect of treatment with Pt(IV)Ac-POA was to not have detected at 10 μ M necroptosis, compared to other concentrations used, indicating a possible lower pro-inflammatory effect and side effect for healthy cells.

Since GBM is a tumour with a tendency to form relapses, the “*recovery*” condition was used to mimic the recovery period following the chemotherapy treatment and consequently to observe a possible activation of resistance mechanisms in the U251 cell line.

Through immunofluorescence reactions, the presence of both active caspases -3 and -8 after 48h-CT with CDDP and Pt(IV)Ac-POA was detected, compared to the control conditions. A significant finding was the progressive increase of immunopositivity to the two cleaved caspases in the samples after recovery conditions, showing a steady increase in the fluorescent signal especially in cells treated with the new compound. This data would, therefore, suggest that the effect of treatment with Pt(IV)Ac-POA can be prolonged over time, inducing cell death even a long time after treatment. PARP-1 and RIP1, substrates of caspase-3 and -8 respectively, were both activated after treatments. In fact, about the intrinsic apoptotic pathway, the translocation of the p89 fragment from the nucleus to the cytoplasm was observed, although with a more visible effect in the 48h-CT samples exposed to the new compound. The cleavage of PARP-1 was also confirmed by western blot, by which the full length of PARP-1 and the fragment p89 were detected. Furthermore, in cells treated with CDDP and then subjected to recovery, a redistribution of the fluorescent protein was observed, indicating a possible damage compensation induced by the treatment. Moreover, in this condition, an autophagic-like morphology was detected, hypothesizing a mechanism of survival to the stress conditions operated by the U251 cells. As concerning RIP1, in treated cells this protein moved from cytoplasm to the nucleus, thus confirming the activation of the extrinsic apoptotic pathway and the preliminary step for necroptosis. Also in this case, for all three proteins analysed, after 48-CT with Pt(IV)Ac-POA the effect of cell death induction was maintained even in recovery conditions, on the contrary, after CDDP and its related recovery the cells showed always altered phenotype, but much more similar to control conditions.

Autophagy activation was corroborated in immunofluorescence reaction by the colocalization of the two proteins signal p62/SQSTM1 and LC3B. Indeed

in controls, any colocalization was observed, on the contrary after treatments the presence of the activation of autophagy mechanisms was detected. In this context, autophagy activation plays an important role in cell survival, in fact as described above, a strong reduction in p62 level could be associated with higher activation of autophagy process, correlated to a protective effect against stress conditions. On the contrary if p62 increases in its expression level could be a promotion of tumour progression (Liu WJ et al. 2016). However, despite no significant data was obtained by western blotting analysis, in the CDDP recovery condition, an autophagy morphology was detected, while the proapoptotic effect persisted in Pt(IV)Ac-POA recovery samples.

Finally, modifications at the level of the cytoplasmic organelles have suggested that they too can be targets of treatment with Pt(IV)Ac-POA. Specifically, it is important to note that in a recovery condition, the cells exposed to the new compound were characterized by a highly damaged Golgi Apparatus and mitochondria clustered, compared to cells treated with CDDP, in which a beginning of cellular improvement was observed, whereby the organelles resumed their physiological structure and localization.

The hadrontherapy with carbon ions represents, compared to the classical photon radiotherapy, an innovative method for the treatment of aggressive tumours that are refractory to treatment (Rieken S et al. 2012). The principle on which this technique is based allows obtaining the maximum irradiation dose in the area to be treated, reducing its diffusion of the surrounding healthy cells (Ohno T 2013). Furthermore, carbon ion hadrontherapy seems to show better effects than classical radiotherapy as it would reduce the migratory capacity of tumour cells (Rieken S et al. 2012).

What was observed in this study was the great capacity of the combined chemotherapy and hadrontherapy effect in inducing almost 90% U251 cell death, using the new platinum-based compound associated with 4Gy irradiation. This data was also confirmed by the recovery conditions, therefore by the long-term effect of the treatment, where it was possible to find the maintenance of the induced apoptotic effect. This effect could not be detected in samples pre-treated with CDDP or only exposed to irradiation, in which U251 cells showed a strong recovery from treatment. It should also be noted that even in the recovery conditions for the samples pre-treated with Pt(IV)Ac-POA and subsequently exposed to 2Gy, there was a still visible

effect of apoptotic induction, suggesting the possibility to select a lower dose of irradiation in order to reduce the possibility of side effect.

The U251 line was also subjected to treatment with phyto- and/or mycotherapeutic to evaluate its possible effects not so much in inducing apoptosis as in reducing the negative effects of chemotherapy and therefore improving the aspects linked to the patient's quality of life. As far as *Taraxacum officinale* is concerned, the effects already known in the literature for other types of tumours (Sheena N et al. 2018) have also been confirmed on the U251 line. The possibility of combining chemotherapeutic exposure with a pre-treatment with *Taraxacum officinale* root extract could create an adjuvant effect, able to increase the sensitivity of tumour cells, acting on the reduction of free radicals that characterize the tumour cell microenvironment. Similar effects were also found after treatment with the *Ganoderma lucidum* supplement, which in addition to inducing a reduction in free radicals, blocks the cell cycle, accumulating cells in the G₂/M phase and thus making them a possible target for an action combined with therapy.

The effects induced on CaM could also be the basis of a direct effect of the fungus, not only therefore in the modulation of the immune system through beta-glucans, but acting directly on intracellular mechanisms.

As these phyto- or -mycotherapeutic is a possible dietary supplement, the cancer patient could benefit directly from a targeted diet, which then may become active systematically.

Finally, the characterization of BK and Kir4.1 Ca²⁺-activated potassium channels in U251 cells allowed to lay the basis for a new type of therapeutic approach. Polarised cells resulted positive for the migration marker active-Cdc42, and the immunopositivity progressively increased from basal to extra to intra scratch, in contrast to flattened cells negative for active-Cdc42 immunostaining. Furthermore, in flattened cells was observed a spotted-like PCNA-immunolabelling, in contrast to the homogeneous staining in polarized cells. This data may corroborate the “go-or-grow” phenotypic switch of GBM cells, a phenomenon described for brain tumours, where migration and proliferation are mutually exclusive behaviours (Catacuzzeno L et al. 2015). The immunolabelling of BK and Kir4.1 channel was present both in the cytoplasm and nucleus of U251 cells. The immunofluorescence density in the cytoplasm and nucleus was lower in the basal condition, however, was raised in extra and intra wounded area. These data indicated

that the scratch wounding was necessary and enough for triggering the expression of BK and Kir4.1 in the nucleus and cytoplasm. In addition, the cell immunofluorescence density intra and extra the wounded area was comparable, indicating the expression of channels was present in both migrated and non-migrated cells. Therefore, electrophysiological data suggested that cells extra the wounded area expressed Kir4.1 and BK, however, both channels were not in a functional state (data not showed). Cytoplasm Kir4.1 immunolabelling was evaluated near the membrane and in membrane vesicles, whereas BK channels were also present in several protrusions.

TEM ultrastructural analysis displayed a heterogeneous labelling of Kir4.1 inside the nucleoplasm, while BK immunostaining in the nucleosome was mainly detected close to the heterochromatin compared with euchromatin, suggesting a possible involvement of BK channels in chromatin remodelling. These novel findings can encourage in designing new therapeutic strategies targeting ion channels to stop the invasiveness of glioma cells in surrounding healthy tissues.

6. Conclusions and perspectives

These data reinforce the idea that Pt(IV)Ac-POA would be a promising drug in cancer treatment, acting on different types of NS tumours.

The possibility of using the prodrug at lower concentrations than the CDDP *i.e.* 4 μ M for B50 and C6 cell lines and 10 μ M for the U251 line obtaining the same cytotoxic action, is extremely favourable in a context of use even *in vivo*, in which side effects such as toxicity to the body's healthy cells are often incurred.

Base on the encouraging data obtained on rat cell lines, future perspectives will, therefore, test the new compound *in vivo*, investigating the effects of Pt(IV)Ac-POA and eventually combined treatment strategies on: *i*) tumour formation, growth; *ii*) molecular and morphological changes in tissue and any damage/repair process of cytoarchitecture *iii*) signal transduction and neurotransmission. These analyses will be conducted especially during the development of the CNS when the absence of a fully developed BBB makes specific brain areas more sensitive to collateral effects of the chemotherapy. These analyses will be conducted especially in two different regions of the CNS such as the cerebellum and hippocampus. Indeed, during the rat postnatal life (11 to 30 days of life), these areas show an intense neurogenic activity; representing a good model to studying treatment-induced alteration in the tissue organization, histogenesis processes, and functions.

The results obtained in this work on the U251 cell line open up new perspectives also for the treatment of GBM. The use of combined actions such as hadrontherapy with carbon ions, as well as the administration of phyto-mycoterapeutic supplements could improve the standard therapy currently in use, in an overview bringing both improvements in the anticancer treatment itself and a targeted advancement to support the cancer patients.

An intense collaboration with other research centres has recently been initiated in our laboratory that aims to use the new compound in an extensive *in vitro* investigation, that will be carried out on different GBM lines (*i.e.* T98G, U87-MG, TMZ- and Paclitaxel-resistant cells), as well as on Glioblastoma-like Stem Cells (GSCs) isolated from patient with GBM. Indeed, based on recent studies, GSCs seem to be responsible for tumour heterogeneity and to trigger cellular mechanisms that induce GBM growth and its resistance to current therapies. About that, the novel findings on ion

channels can aid in designing new therapeutic strategies targeting to block the invasiveness or proliferation of GBM cells, trying to improve the treatments for this tumour so that to date the prognosis is still fatal.

References

- Abbott NJ, Patabendige AA, Dolman DE, Yusof SR, Begley DJ.** Structure and function of the blood-brain barrier. *Neurobiol Dis.* 2010;37:13-25
- Abdelsameea AA, Kabil SL.** Mitigation of cisplatin-induced peripheral neuropathy by canagliflozin in rats. *Naunyn Schmiedebergs Arch Pharmacol.* 2018;391:945-952
- Abdullaev IF, Rudkouskaya A, Mongin AA, Kuo YH.** Calcium-activated potassium channels BK and IK1 are functionally expressed in human gliomas but do not regulate cell proliferation. *PLoS One.* 2010;5:e12304
- Adams M, Gammill L, Bronner-Fraser M.** Discovery of transcription factors and other candidate regulators of neural crest development. *Dev Dynamics.* 2008;237:1021-1033
- Agarwala SS, Kirkwood JM.** Temozolomide, a novel alkylating agent with activity in the central nervous system, may improve the treatment of advanced metastatic melanoma. *Oncologist.* 2000;5:144-151
- Aggarwal BB, Gupta SC, Kim JH.** Historical perspectives on tumor necrosis factor and its superfamily: 25 years later, a golden journey. *Blood.* 2012;119:651-665
- Aghi MK, Liu TC, Rabkin S, Martuza RL.** Hypoxia enhances the replication of oncolytic herpes simplex virus. *Mol Ther.* 2009;17:51-56
- Agnihotri S, Gajadhar AS, Ternamian C, Gorlia T, Diefes KL, Mischel PS, Kelly J, McGown G, Thorncroft M, Carlson BL, Sarkaria JN, Margison GP, Aldape K, Hawkins C, Hegi M, et al.** Alkylpurine-DNA-N-glycosylase confers resistance to temozolomide in xenograft models of glioblastoma multiforme and is associated with poor survival in patients. *J Clin Invest.* 2012;122:253-266
- Agnihotri S, Burrell KE, Wolf A, Jalali S, Hawkins C, Rutka JT, Zadeh G.** Glioblastoma, a brief review of history, molecular genetics, animal models and novel therapeutic strategies. *Arch Immunol Ther Exp.* 2013;61:25-41
- Ahmed EM, Bandopadhyay G, Coyle B, Grabowska A.** HIF-independent, CD133-mediated mechanism of cisplatin resistance in glioblastoma cells. *Cell Oncol (Dordr).* 2018;41:319-328

- Al-Majed AA, Sayed-Ahmed MM, Al-Yahya AA, Aleisa AM, Al-Rejaie SS, Al-Shabanah OA.** Propionyl-L-carnitine prevents the progression of cisplatin-induced cardiomyopathy in a carnitine depleted rat model. *Pharmacol.Res.* 2006;53:278-286
- Albesiano E, Han JE, Lim M.** Mechanisms of Local Immunoresistance in Glioma. *Neurosurg Clin N Am.* 2010;21:17-29
- Alcindor T, Beauger N.** Oxaliplatin: a review in the era of molecularly targeted therapy. *Curr Oncol.* 2011;18:18-25
- Alifieris C, Trafalis DT.** Glioblastoma multiforme: pathogenesis and treatment. *Pharmacol Ther.* 2015;152:63-82
- Alpàr A, Attems J, Mulder J, Hökfelt T, Harkany T.** The renaissance of Ca²⁺-binding proteins in the nervous system: screening takes center stage. *Rev Cell Signal.* 2012;24:378-387
- Alshareef A, Gupta N, Zhang HF, Wu C, Haque M, Lai R.** High expression of β -catenin contributes to the crizotinib resistant phenotype in the stem-like cell population in neuroblastoma. *Sci Rep.* 2017;7:16863
- Altucci L, Stunnenberg HG.** Time for epigenetics. *Int J Biochem Cell Biol.* 2009;41:2-3
- Alvarez AA, Field M, Bushnev S, Longo MA, Sugaya K.** The effects of histone deacetylase inhibitors on glioblastoma derived cells. *J Mol Neurosci.* 2015;55:7-20
- Andera L.** Signaling activated by death receptors of the TNFR family. *Biomed Pap Med Fac Univ Palacky Olomouc Czech Repub.* 2009;153:173-180
- Ao X, Zou L, Wu Y.** Regulation of autophagy by the Rab GTPase network. *Cell Death Differ.* 2014;21:348-358
- Appella E, Anderson CW.** Post-translational modifications and activation of p53 by genotoxic stresses. *Rev Eur J Biochem.* 2001;268:2764-2772
- Appelqvist H, Waster P, Kagedal K, Ollinger K.** The lysosome: from waste bag to potential therapeutic target. *J Moll Cell Biol.* 2013;5:214-226
- Apraiz A, Boyano MD, Asumedi A.** Cell-centric view of apoptosis and apoptotic cell death inducing antitumoral strategies. *Cancer.* 2011;3:1042-1080
- Arcangeli A, Crociani O, Lastraioli E, Masi A, Pillozzi S, Becchetti A.** Targeting ion channels in cancer: a novel frontier in antineoplastic therapy. *Curr Med Chem.* 2009;16:66-93

- Aredia F, Scovassi AI.** Poly(ADP-ribose): a signaling molecule in different paradigms of cell death. *Biochem Pharmacol.* 2014;92:157-163
- Ardizzoni A, Boni L, Tiseo M, Fossella FV, Schiller JH, Paesmans M, Radosavljevic D, Paccagnella A, Zatloukal P, Mazzanti P, Bisset D, Rosell R; CISCA (CISplatin versus CARboplatin) Meta-analysis Group.** Cisplatin- versus carboplatin-based chemotherapy in first-line treatment of advanced non-small-cell lung cancer: an individual patient data meta-analysis. *J Natl Cancer Inst.* 2007;99:847-857
- Argyriou AA, Bruna J, Marmioli P, Cavaletti G.** Chemotherapy-induced peripheral neurotoxicity (CIPN): An update. *Crit Rev Oncol Hematol.* 2012;82:51-77
- Ariosa AR, Klionsky DJ.** Autophagy core machinery: overcoming spatial barriers in neurons. *J Mol Med.* 2016;94:1217-1227
- Arnesano F, Losacco M, Natile G.** An updated view of cisplatin transport. *European J Org Chem.* 2013;15:2701-2711
- Asselin E, Mills GB, Tsang BK.** XIAP regulates Akt activity and caspase-3-dependent cleavage during cisplatin-induced apoptosis in human ovarian epithelial cancer cells. *Cancer Res.* 2001;61:1862-1868
- Atadja PW.** HDAC inhibitors and cancer therapy. *Pro Drug Res.* 2011;67:175-195
- Audesirk T, Audesirk G, Ferguson C, Shugarts D.** Effects of inorganic lead on the differentiation and growth of cultured hippocampal and neuroblastoma cells. *Neurotoxicology.* 1991;12:529-538
- Avan A, Postma TJ, Ceresa C, Avan A, Cavaletti G, Giovannetti E, Peters GJ.** Platinum-induced neurotoxicity and preventive strategies: past, present and future. *Oncologist.* 2015;20:411-432
- Babu R, Adamson DC.** Rindopepimut: an evidence-based review of its therapeutic potential in the treatment of EGFRvIII-positive glioblastoma. *Core Evid.* 2012;7:93-103
- Bai LY, Omar HA, Chiu CF, Chi ZP, Hu JL, Weng JR.** Antitumor effects of (S)-HDAC42, a phenylbutyrate-derived histone deacetylase inhibitor, in multiple myeloma cells. *Cancer Chemother Pharmacol.* 2010;68:489-496
- Bano D, Dinsdale D, Cabrera-Socorro A, Maida S, Lambacher N, Mccoll B, Ferrando-May E, Hengartner MO, Nicotera P.** Alteration of the nuclear pore complex in Ca(2+)-mediated cell death. *Cell Death Differ.* 2010;17:119-133

- Bano D, Prehn JHM.** Apoptosis-Inducing Factor (AIF) in Physiology and Disease: The Tale of a Repented Natural Born Killer. *EBioMedicine*. 2018;30:29-37
- Barami K, Sloan AE, Rojiani A, Schell MJ, Staller A, Brem S.** Relationship of gliomas to the ventricular walls. *J Clin Neurosci*. 2009;16:195-201
- Barbieri A, Quagliariello V, Del Vecchio V, Falco M, Luciano A, Amruthraj NJ, Nasti G, Ottaiano A, Berretta M2, Iaffaioli RV, Arra C.** Anticancer and anti-inflammatory properties of *Ganoderma lucidum* extract effects on melanoma and triple-negative breast cancer treatment. *Nutrients*. 2017;9:210
- Barclay LA, Wales TE, Garner TP, Wachter F, Lee S, Guerra RM, Stewart ML, Braun CR, Bird GH, Gavathiotis E, Engen JR, Walensky LD.** Inhibition of Pro-apoptotic BAX by a noncanonical interaction mechanism. *Mol Cell*. 2015;57:873-886
- Barnhart BC, Alappat EC, Peter ME.** The CD95 type I/type II model. *Semin Immunol*. 2003;15:185-193
- Barth RF, Kaur B.** Rat brain tumor models in experimental neuro-oncology: the C6, 9L, T9, RG2, F98, BT4C, RT-2 and CNS-1 gliomas. *J Neurooncol*. 2009;94:299-312
- Basu A, Krishnamurthy S.** Cellular responses to Cisplatin-induced DNA damage. *J Nucleic Acids*. 2010;pii:201367
- Battle E, Clevers H.** Cancer stem cells revisited. *Nat Med*. 2017;23:1124-1134
- Baylin SB, Schuebel KE.** Genomic biology: the epigenomic era opens. *Nature*. 2007;448:548-549
- Beauchesne P.** Extra-neural metastases of malignant gliomas: Myth or reality? *Cancers*. 2011;3:461-477
- Belounis A, Nyalendo C, Le Gall R, Imbriglio TV, Mahma M, Teira P, Beaunoyer M, Cournoyer S, Haddad E, Vassal G, Sartelet H.** Autophagy is associated with chemoresistance in neuroblastoma. *BMC Cancer*. 2016;16:891
- Ben-Ari Y.** Cell death and synaptic reorganizations produced by seizures. *Rev Epilepsia*. 2001;3:5-7
- Benda P, Lightbody J, Sato G, Levine L, Sweet W.** Differentiated rat glial cell strain in tissue culture. *Science*. 1968;161:370-371
- Benedetti R, Conte M, Altucci L.** Targeting histone deacetylases in disease: where are we?. antioxidant redox signal. 2015;23:99-126

- Benfenati F, Valtorta F, Rossi MC, Onofri F, Sihra T, Greengard P.** Interactions of synapsin I with phospholipids: possible role in synaptic vesicle clustering and in the maintenance of bilayer structures. *J Cell Biol.* 1993;123:1845-1855
- Berchtold MW, Villalobo A.** The many faces of calmodulin in cell proliferation, programmed cell death, autophagy, and cancer. *Biochim Biophys Acta.* 2014;1843:398-435
- Bergmann A, Steller H.** Apoptosis, stem cells, and tissue regeneration. *Sci Signal.* 2010;3:8
- Berlanga P, Cañete A, Castel V.** Advances in emerging drugs for the treatment of neuroblastoma. *Rev Expert Opin Emerg Drugs.* 2017;22:63-75
- Bernocchi G, Bottone MG, Piccolini VM, Dal Bo V, Santin G, De Pascali SA, Migoni D, Fanizzi FP.** Developing central nervous system and vulnerability to platinum compounds. *Chemother Res Pract.* 2011;2011:315418
- Bernocchi G, Fanizzi FP, De Pascali SA, Piccolini VM, Gasperini C, Insolia V, Bottone MG.** Neurotoxic effects of platinum compounds: studies *in vivo* on intracellular calcium homeostasis in the immature Central Nervous System. *Toxics.* 2015;3:224-248.
- Bettters E, Liu Y, Kjaeldgaard A, Sundstrom E, Garcia-Castro MI.** Analysis of early human neural crest development. *Dev Biol.* 2010;344:578-592
- Bezecny P.** Histone deacetylase inhibitors in glioblastoma: pre-clinical and clinical experience. *Med Oncol.* 2014;31:985
- Blackiston DJ, McLaughlin KA, Levin M.** Bioelectric controls of cell proliferation: ion channels, membrane voltage and the cell cycle. *Cell Cycle.* 2009;8:3527-3536
- Bloechl-Daum B, Deuson RR, Mavros P, Hansen M, Herrstedt J.** Delayed nausea and vomiting continue to reduce patients' quality of life after highly and moderately emetogenic chemotherapy despite antiemetic treatment. *J Clin Oncol.* 2006;24:4472-4478
- Bodenner DL, Dedon PC, Keng PC, Borch RF.** Effect of diethyldithiocarbamate on cis-diamminedichloroplatinum (II)-induced cytotoxicity, DNA cross-linking, and gamma-glutamyl transpeptidase inhibition. *Cancer Res.* 1986;46:2745-2750
- Bolden JE, Peart MJ, Johnstone RW.** Anticancer activities of histone deacetylase inhibitors. *Nat Rev Drug Discov.* 2006;5:769-784

- Bordey A, Sontheimer H, Trouslard J.** Muscarinic activation of BK channels induces membrane oscillations in glioma cells and leads to inhibition of cell migration. *J Membr Biol.* 2000;176:31-40
- Borst P, Rottenberg S, Jonkers J.** How do real tumors become resistant to cisplatin?. *Cell Cycle.* 2008;7:1353-1359
- Bottone MG, Santin G, Aredia F, Bernocchi G, Pellicciari C, Scovassi AI.** Morphological Features of Organelles during Apoptosis: An Overview. *Cells.* 2013;2:294-305
- Bottone MG, Soldani C, Frascini A, Croce AC, Bottiroli G, Camboni T, Scovassi AI, Pellicciari C.** Enzyme-assisted photosensitization activates different apoptotic pathways in Rose Bengal acetate treated HeLa cells. *Histochem Cell Biol.* 2009;131:391-399
- Bottone MG, Soldani C, Veneroni P, Avella D, Pisu M, Bernocchi G.** Cell proliferation, apoptosis and mitochondrial damage in rat B50 neuronal cells after cisplatin treatment. *Cell Prolif.* 2008;41:506-520
- Boulikas T, Pantos A, Bellis E, Christofis P.** Designing platinum compounds in cancer: structures and mechanism. *Cancer Ther.* 2007;5:537-583
- Boya P, Kroemer G.** Lysosomal membrane permeabilization in cell death. *Oncogene.* 2008;27:6434-6451
- Brabec V, Griffith DM, Kisova A, Kostrhunova H, Zerzankova L, Marmion CJ, Kasparkova J.** Valuable insight into the anticancer activity of the platinum-histone deacetylase inhibitor conjugate, cis-[Pt(NH₃)₂malSAHA-2H]. *Mol Pharm.* 2012;9:1990-1999
- Bradshaw A, Wickremsekera A, Tan ST, Peng L, Davis PF, Itinteang T.** Cancer stem cell hierarchy in Glioblastoma Multiforme. *Front Surg.* 2016;3:21
- Braganza MZ, Kitahara CM, Berrington de González A, Inskip PD, Johnson KJ, Rajaraman P.** Ionizing radiation and the risk of brain and central nervous system tumors: a systematic review. *Rev Neuro Oncol.* 2012;14:1316-1324
- Brandes AA, Tosoni A, Franceschi E, Reni M, Gatta G, Vecht C.** Glioblastoma in adults. *Rev Crit Rev Oncol Hematol.* 2008;67:139-152
- Brandalise F, Cesaroni V, Gregori A, Repetti M, Romano C, Orrù G, Botta L, Girometta C, Guglielminetti ML, Savino E, Rossi P.** Dietary Supplementation of *Hericium erinaceus* Increases Mossy Fiber-CA3 Hippocampal Neurotransmission and

- Recognition Memory in Wild-Type Mice. *Evid Based Complement Alternat Med.* 2017;2017:3864340
- Breglio AM, Rusheen AE, Shide ED, Fernandez KA, Spielbauer KK, McLachlin KM, Hall MD, Amable L, Cunningham LL.** Cisplatin is retained in the cochlea indefinitely following chemotherapy. *Nat Commun.* 2017;8:1654
- Brenner C, Grimm S.** The permeability transition pore complex in cancer cell death. *Oncogene.* 2006;25:4744-4756
- Brenner D, Blaser H, Mak TW.** Regulation of tumour necrosis factor signalling: live or let die. *Nat Rev Immunol.* 2015;15:362-374
- Brescia P, Ortensi B, Fornasari L, Levi D, Broggi G, Pelicci G.** CD133 is essential for glioblastoma stem cell maintenance. *Stem Cells.* 2013;31:857-869
- Brini M, Cali T, Ottolini D, Carafoli E.** The plasma membrane calcium pump in health and disease. *Rev FEBS J.* 2013;280:5385-5397
- Brini M, Carafoli E, Cali T.** The plasma membrane calcium pumps: focus on the role in (neuro)pathology. *Rev Biochem Biophys Res Commun.* 2017;483:1116-1124
- Brisse HJ, McCarville MB, Granata C, Krug KB, Wootton-Gorges SL, Kanegawa K, Giammarile F, Schmidt M, Shulkin BL, Matthay KK, Lewington VJ, Sarnacki S, Hero B, Kaneko M, London WB et al.** Guidelines for imaging and staging of neuroblastic tumors: consensus report from the International Neuroblastoma Risk Group Project. *Radiology.* 2011;261:243-257
- Brodbelt A, Greenberg D, Winters T, Williams M, Vernon S, Collins VP.** Glioblastoma in England: 2007–2011. *Eur J Cancer.* 2015;51:533-542
- Brodeur GM, Hogarty MD, Mosse YP, Maris JM.** Neuroblastoma. In: Pizzo PA., Poplack DG editors. *Principle and practice of pediatric oncology.* 6th. Lippincott, Williams and Wilkins; Philadelphia. 2011;886-922
- Brozovic A, Ambriovic-Ristov A, Osmak M.** The relationship between cisplatin-induced reactive oxygen species, glutathione, and BCL-2 and resistance to cisplatin. *Crit Rev Toxicol* 2010;40:347-359
- Brumatti G, Salmanidis M, Ekert PG.** Crossing paths: interactions between the cell death machinery and growth factor survival signals. *Cell Mol Life Sci.* 2010;67:1619-1630

- Buchheit CL, Rayavarapu RR, Schafer ZT.** The regulation of cancer cell death and metabolism by extracellular matrix attachment. *Semin Cell Dev Biol.* 2012;23:402-411
- Buchheit CL, Weigel KJ, Schafer ZT.** Cancer cell survival during detachment from the ECM: multiple barriers to tumour progression. *Nat Rev Cancer.* 2014;14:632-641
- Burette A, Weinberg RJ.** Perisynaptic organization of plasma membrane calcium pumps in cerebellar cortex. *J Comp Neurol.* 2007;500:1127-1135
- Burgess A, Ruefli A, Beamish H, Warrener R, Saunders N, Johnstone R, Gabrielli B.** Histone deacetylase inhibitors specifically kill nonproliferating tumour cells. *Oncogene.* 2004;23:6693-6701
- Burnashev N, Rozov A.** Presynaptic Ca²⁺ dynamics, Ca²⁺ buffers and synaptic efficacy. *Rev Cell Calcium.* 2005;37:489-495
- Burnstock G, Di Virgilio F.** Purinergic signalling and cancer. *Purinergic Signal.* 2013;9:491-540
- Callejo A, Sedó-Cabezón L, Juan ID, Llorens J.** Cisplatin-induced ototoxicity: effects, mechanisms and protection strategies. *Toxics.* 2015;3:268-293
- Calvo M, Villalobos C, Núñez L.** Calcium imaging in neuron cell death. *Methods Mol Biol.* 2015;1254:73-85
- Camp AJ, Wijesinghe R.** Calretinin: modulator of neuronal excitability. *Rev Int J Biochem Cell Biol.* 2009;41:2118-2121
- Candè C, Cohen I, Daugas E, Ravagnan L, Larochette L, Zamzami N, Kroemer G.** Apoptosis-inducing factor (AIF): a novel caspase-independent death effector released from mitochondria. *Biochimie.* 2002;84:215-222
- Capano M, Virji S, Crompton M.** Cyclophilin-A is involved in excitotoxin-induced caspase activation in rat neuronal B50 cells. *Biochem J.* 2002;363:29-36
- Carlisi D, Lauricella M, D'Anneo A, Emanuele S, Angileri L, Di Fazio P, Santulli A, Vento R, Tesoriere G.** The histone deacetylase inhibitor suberoylanilide hydroxamic acid sensitises human hepatocellular carcinoma cells to TRAIL-induced apoptosis by TRAIL-DISC activation. *Eur J Cancer.* 2009;45:2425-2438.
- Carozzi VA, Chiorazzi A, Canta A, Lapidus RG, Slusher BS, Wozniak KM, Cavaletti G.** Glutamate carboxypeptidase inhibition reduces the severity of chemotherapy-induced peripheral neurotoxicity in rat. *Neurotox Res.* 2010;17:380-391

- Case RM, Eisner D, Gurney A, Jones O, Muallem S, Verkhatsky A.** Evolution of calcium homeostasis: from birth of the first cell to an omnipresent signalling system. *Rev Cell Calcium.* 2007;42:345-350
- Catacuzzeno L, Caramia M, Sforna L, Belia S, Guglielmi L, D'Adamo MC, Pessia M, Franciolini F.** Reconciling the discrepancies on the involvement of large-conductance Ca(2+)-activated K channels in glioblastoma cell migration. *Front Cell Neurosci.* 2015;9:152
- Ceccarelli M, Barthel FP, Malta TM, Sabedot TS, Salama SR, Murray BA, Morozova O, Newton Y, Radenbaugh A, Pagnotta SM, Anjum S, Wang J, Manyam G, Zoppoli P, Ling S, et al.** Molecular profiling reveals biologically discrete subsets and pathways of progression in diffuse glioma. *Cell.* 2016;164:550-563
- Celio MR.** Calbindin D-28k and parvalbumin in the rat nervous system. *Neuroscience.* 1990;35:375-475
- Cerri S, Piccolini VM, Santin G, Bottone MG, De Pascali SA, Migoni D, Iadarola P, Fanizzi FP, Bernocchi G.** The developmental neurotoxicity study of platinum compounds. Effects of cisplatin versus a novel Pt(II) complex on rat cerebellum. *Neurotoxicol Teratol.* 2011;33:273-281
- Chaichana KL, Jusue-Torres I, Navarro-Ramirez R, Raza SM, Pascual-Gallego M, Ibrahim A, Hernandez-Hermann M, Gomez L, Weingart JD, Olivi A, Blakeley J, Gallia GL, Lim M, Brem H, Quinones-Hinojosa A.** Establishing percent resection and residual volume thresholds affecting survival and recurrence for patients with newly diagnosed intracranial glioblastoma. *Neuro Oncol.* 2014;16:113-122
- Chaitanya GV, Alexander JS, Babu PP.** PARP-1 Cleavage Fragments: Signatures of Cell-Death Proteases in Neurodegeneration. *Cell Commun Signal.* 2010; 8:31
- Chakravarti A, Noll E, Black PM, Finkelstein DF, Finkelstein DM, Dyson NJ, Loeffler JS.** Quantitatively determined survivin expression levels are of prognostic value in human gliomas. *J Clin Oncol.* 2002;20:1063-1068
- Chang L, Wang A.** Calpain mediated cisplatin-induced ototoxicity in mice. *Neural Regen Res.* 2013;8:1995-2002
- Charles NA, Holland EC, Gilbertson R, Glass R, Kettenmann H.** The brain tumor microenvironment. *Glia.* 2012;60:502-514
- Chekhonin VP, Baklaushev VP, Yusubaliev GM, Pavlov KA, Ukhova OV, Gurina OI.** Modeling and immunohistochemical analysis of C6 glioma *in vivo*. *Bull Exp Biol Med.* 2007;143:501-509

- Chen CKJ, Zhang JZ, Aitken JB, Hambley TW.** Influence of equatorial and axial carboxylato ligands on the kinetic inertness of platinum(IV) complexes in the presence of ascorbate and cysteine and within DLD 1 cancer cells. *J Med Chem.* 2013;56:8757-8764
- Chen D, Milacic V, Frezza M, Dou QP.** Metal complexes, their cellular targets and potential for cancer therapy. *Curr Pharm Des.* 2009;15:777-779
- Chen J, McKay RM, Parada LF.** Malignant glioma: Lessons from genomics, mouse models and stem cells. *Cell.* 2012;149:36-47
- Chen J, Zhang L, Zhou H, Wang W, Luo Y, Yang H, Yi H.** Inhibition of autophagy promotes cisplatin-induced apoptotic cell death through Atg5 and Beclin 1 in A549 human lung cancer cells. *Mol Med Rep.* 2018;17:6859-6865
- Chen S, Zhou L, Zhang Y, Leng Y, Pei X, Lin H, Jones R, Orlowski RZ, Dai Y, Grant S.** Targeting SQSTM1/p62 induces cargo loading failure and converts autophagy to apoptosis via NBK/Bik. *Mol Cell Biol.* 2014;34:3435-3449
- Chen W, Li N, Chen T, Han Y, Li C, Wang Y, He W, Zhang L, Wan T, Cao X.** The lysosomal-associated apoptosis-inducing protein containing the pleckstrin homology (PH) and FYVE domains (LAPF), representative of a novel family of PH and FYVE domain-containing proteins, induces caspase-independent apoptosis via the lysosomal-mitochondrial pathway. *J Biol Chem.* 2005;280:40985-40995.
- Chen W, Wu J, Li L, Zhang Z, Ren J, Liang Y, Chen F, Yang C, Zhou Z, Su SS, Zheng X, Zhang Z, Zhong CQ, Wan H, Xiao M, et al.** Ppm1b negatively regulates necroptosis through dephosphorylating Rip3. *Nat Cell Biol.* 2015;17:434-444
- Cheng YJ, Wu R, Cheng ML, Du J, Hu XW, Yu L, Zhao XK, Yao YM, Long QZ, Zhu LL, Zhu JJ, Huang NW, Liu HJ, Hu YX, Wan F.** Carboplatin-induced hematotoxicity among patients with non-small cell lung cancer: Analysis on clinical adverse events and drug-gene interactions. *Oncotarget.* 2017;8:32228-32236
- Chikman B, Vasyanovich S, Lavy R, Habler L, Tolstov G, Kapiev A, Halevy A, Sandbank J.** COX2 expression in high-grade breast cancer: Evidence for prognostic significance in the subset of triple-negative breast cancer patients. *Med Oncol* 2014;31:989
- Chin CF, Wong DY, Jothibasu R, Ang WH.** Anticancer platinum (IV) prodrugs with novel modes of activity. *Curr Top Med Chem.* 2011;11:2602-2612
- Cho YS, Park HL.** Exploitation of necroptosis for treatment of caspase-compromised cancers. *Oncol Lett.* 2017;14:1207-1214

- Choi AM, Ryter SW, Levine B.** Autophagy in human health and disease. *N Engl J Med.* 2013;368:651-662
- Choudhari SK, Chaudhary M, Bagde S, Gadbail AR, Joshi V.** Nitric oxide and cancer: a review. *World J Surg Oncol.* 2013;11:118
- Ciarimboli G.** Membrane transporters as mediators of cisplatin side-effects. *Anticancer Res.* 2014;34:547-550
- Cilerdžić J, Vukojević J, Stajić M, Stanojković T, Glamočlija J.** Biological activity of *Ganoderma lucidum* basidiocarps cultivated on alternative and commercial substrate. *J E-thnopharmacol.* 2014;155:312-319
- Claudiu A. Vlada, MD, Jae-Sung Kim, PhD, and Kevin E. Behrns, MD.** Autophagy: Self-preservation through cannibalism of proteins and organelles. *Surgery.* 2015;157:1-5
- Cobbs CS, Whisenhunt TR, Wesemann DR, Harkins LE, Van Meir EG, Samanta M.** Inactivation of wild-type p53 protein function by reactive oxygen and nitrogen species in malignant glioma cells. *Cancer Res.* 2003;63:8670-8673
- Cohen GM.** Caspases: the executioners of apoptosis. *Biochem J.* 1997;326:1-16
- Collin T, Chat M, Lucas MG, Moreno H, Racay P, Schwaller B, Marty A, Llano I.** Developmental changes in parvalbumin regulate presynaptic Ca²⁺ signaling. *J Neurosci.* 2005;25:96-107
- Collins VP, Jones DT, Giannini C.** Pilocytic astrocytoma: pathology, molecular mechanisms and markers. *Acta Neuropathol.* 2015;129:775-788
- Colon NC, Chung DH.** Neuroblastoma. *Rev Adv Pediatr.* 2011;58:297-311
- Combs SE.** Proton and Carbon Ion Therapy of Intracranial Gliomas. *Prog Neurol Surg.* 2018;32:57-65
- Combs SE, Bruckner T, Mizoe JE, Kamada T, Tsujii H, Kieser M, Debus J.** Comparison of carbon ion radiotherapy to photon radiation alone or in combination with temozolomide in patients with high-grade gliomas: explorative hypothesis-generating retrospective analysis. *Radiother Oncol.* 2013;108:132-135
- Connors TA, Cleare MJ, Harrap KR.** Structure-activity relationships of the antitumor platinum coordination complexes. *Cancer Treat Rep.* 1979;63:1499-1502
- Conradt B.** Genetic control of programmed cell death during animal development. *Annu Rev Genet.* 2009;43:493-523

- Cornago M, Garcia-Alberich C, Blasco-Angulo N, Vall-Llaura N, Nager M, Herreros J, Comella JX, Sanchis D, Llovera M.** Histone deacetylase inhibitors promote glioma cell death by G2 checkpoint abrogation leading to mitotic catastrophe. *Cell Death Dis.* 2014;5:e1435
- Cory S, Adam JM.** The Bcl-2 family: regulator of the cellular life-death switch. *Nat Rev Cancer* 2002;2:647-656
- Crane CA, Ahn BJ, Han SJ, Parsa AT.** Soluble factors secreted by glioblastoma cell lines facilitate recruitment, survival, and expansion of regulatory T cells: Implications for immunotherapy. *Neuro Oncol.* 2012;14:584-595
- Crona DJ, Faso A, Nishijima TF, McGraw KA, Galsky MD, Milowsky MI.** A Systematic Review of Strategies to Prevent Cisplatin-Induced Nephrotoxicity. *Oncologist.* 2017;22:609-619
- Crosara Teixeira M, Braghiroli MI, Sabbaga J, Hoff PM.** Primary prevention of colorectal cancer: myth or reality? *Rev World J Gastroenterol.* 2014;20:15060-15069
- Cuddapah VA, Robel S, Watkins S, Sontheimer H.** A neurocentric perspective on glioma invasion. *Nat Rev Neurosci.* 2014;15:455-465
- Cuervo AM, Wong E.** Chaperone-mediated autophagy: roles in disease and aging. *Cell Res.* 2014;24:92-104
- Cummings BS, Lasker JM, Lash LH.** Expression of glutathione-dependent enzymes and cytochrome P450s in freshly isolated and primary cultures of proximal tubular cells from human kidney. *J.Pharmacol.Exp.Ther.* 2000;293:677-685
- Custódio JB, Cardoso CM, Santos MS, Almeida LM, Vicente JA, Fernandes MA.** Cisplatin impairs rat liver mitochondrial functions by inducing changes on membrane ion permeability: prevention by thiol group protecting agents. *Toxicology.* 2009;259:18-24
- Curry MC, Luk NA, Kenny PA, Roberts-Thomson SJ, Monteith GR.** Distinct regulation of cytoplasmic calcium signals and cell death pathways by different plasma membrane calcium ATPase isoforms in MDA-MB-231 breast cancer cells. *J Biol Chem.* 2012;287:28598-28608
- Czabotar PE, Lessene G, Strasser A, Adams JM.** Control of apoptosis by the BCL-2 protein family: implications for physiology and therapy. *Nat Rev Mol Cell Biol.* 2014;15:49-63

- D'Angelo E, De Filippi G, Rossi P, Taglietti V.** Ionic mechanism of electroresponsiveness in cerebellar granule cells implicates the action of a persistent sodium current. *J Neurophysiol.* 1998;80:493-503
- Damert A, Ikeda E, Risau W.** Activator-protein-1 binding potentiates the hypoxia-induciblefactor-1-mediated hypoxia-induced transcriptional activation of vascular-endothelial growth factor expression in C6 glioma cells. *Biochem J.* 1997;327:419-423
- Damsma GE, Alt A, Brueckner F, Carell T, Cramer P.** Mechanism of transcriptional stalling at cisplatin-damaged DNA. *Nat Struct Mol Biol.* 2007;14:1127-1133
- Danial NN, Korsmeyer SJ.** Cell death: critical control points. *Cell.* 2004;116:205-219
- Dasari S, Tchounwou PB.** Cisplatin in cancer therapy: molecular mechanisms of action. *Eur J Pharmacol.* 2014;740:364-378
- Davidovich P, Kearney CJ, Martin SJ.** Inflammatory outcomes of apoptosis, necrosis and necroptosis. *Biol Chem.* 2014;395:1163-1171
- De Brouwer S, De Preter K, Kumps C, Zabrocki P, Porcu M, Westerhout EM, Lakeman A, Vandesomepele J, Hoebeeck J, Van Maerken T, De Paepe A, Laureys G, Schulte JH, Schramm A, Van Den Broecke C, et al.** Meta-analysis of neuroblastomas reveals a skewed ALK mutation spectrum in tumors with MYCN amplification. *Clin Cancer Res.* 2010;16:4353-4362
- De Pascali SA, Papadia P, Ciccarese A, Pacifico C, Fanizzi FP.** First examples of β -diketonate platinum(II) complexes with sulfoxide ligands. *Eur J Inorg Chem.* 2005;5:788-796
- Debatin KM, Poncet D, Kroemer G.** Chemotherapy: targeting the mitochondrial cell death pathway. *Rev Oncogene.* 2002; 21:8786-8803
- Degterev A, Hitomi J, Gernscheid M, Ch'en IL, Korkina O, Teng X, Abbott D, Cuny GD, Yuan C, Wagner G, Hedrick SM, Gerber SA, Lugovskoy A, Yuan J.** Identification of RIP1 kinase as a specific cellular target of necrostatins. *Nat Chem Biol.* 2008;4:313-321
- Degterev A, Huang Z, Boyce M, Li Y, Jagtap P, Mizushima N, Cuny GD, Mitchison TJ, Moskowitz MA., Yuan J.** Chemical inhibitor of nonapoptotic cell death with therapeutic potential for ischemic brain injury. *Nat Chem Biol.* 2005;1:112-119
- Del Vecchio CA, Li G, Wong AJ.** Targeting EGF receptor variant III: tumor specific peptide vaccination for malignant gliomas. *Expert Rev Vaccines.* 2012;11:133-144

- Delbridge AR, Grabow S, Strasser A, Vaux DL.** Thirty years of BCL-2: translating cell death discoveries into novel cancer therapies. *Nat Rev Cancer.* 2016;16:99-109
- Demkow U, Stelmaszczyk-Emmel A.** Cardiotoxicity of cisplatin-based chemotherapy in advanced non-small cell lung cancer patients. *Respir Physiol Neurobiol.* 2013;187:64-67
- Deng X, Ewton DZ, Friedman E.** Mirk/Dyrk1B maintains the viability of quiescent pancreatic cancer cells by reducing levels of reactive oxygen species. *Cancer Res.* 2009;69:3317-3324
- Deretic V, Kimura T, Timmins G, Moseley P, Chauhan S, Mandell M.** Immunologic manifestations of autophagy. *J Clin Investig.* 2015;125:75-84
- Deretic V, Saitoh T, Akira S.** Autophagy in infection, inflammation and immunity. *Nat Rev Immunol.* 2013;13:722-737
- Desoize B.** Cancer and metals and metal compounds: part I--carcinogenesis. *Crit Rev.Oncol.Hematol.* 2002;42:1-3
- Desoize B, Madoulet C.** Particular aspect of platinum compounds used at present in cancer treatment. *Crit Rev Oncol Hematol.* 2002;42:317-325
- Dewson G, Kratina T, Czabotar P, Day CL, Adams JM, Kluck RM.** Bak activation for apoptosis involves oligomerization of dimers via their alpha6 helices. *Mol Cell* 2009;36:696-703
- Di Bartolomeo S, Corazzari M, Nazio F, Oliverio S, Lisi G, Antonioli M, Pagliarini V, Matteoni S, Fuoco C, Giunta L, D'Amelio M, Nardacci R, Romagnoli A, Piacentini M, Cecconi F, et al.** The dynamic interaction of AMBRA1 with the dynein motor complex regulates mammalian autophagy. *J Cell Biol.* 2010;191:155-168
- Di Leva F, Domi T, Fedrizzi L, Lim D, Carafoli E.** The plasma membrane Ca²⁺ ATPase of animal cells: structure, function and regulation. *Rev Arch Biochem Biophys.* 2008;476:65-74
- Dietrich J, Han R, Yang Y, Mayer-Pröschel M, Noble M.** CNS progenitor cells and oligodendrocytes are targets of chemotherapeutic agents in vitro and in vivo. *J Biol.* 2006;5: 22
- Dilruba S, Kalayda GV.** Platinum-based drugs: past, present and future. *Cancer Chemother Pharmacol.* 2016;77:1103-1124

- Domingues P, González-Tablas M, Otero Á, Pascual D, Miranda D, Ruiz L, Sousa P, Ciudad J, Gonçalves JM, Lopes MC, Orfao A, Tabernero MD.** Tumor infiltrating immune cells in gliomas and meningiomas. *Brain Behav Immun.* 2016;53:1-15
- Dong Z, Saikumar P, Weinberg JM, Venkatachalam MA.** Calcium in cell injury and death. *Annu Rev Pathol.* 2006;1:405-434
- Donson AM, Addo-Yobo SO, Handler MH, Gore L, Foreman NK.** MGMT promoter methylation correlates with survival benefit and sensitivity to temozolomide in pediatric glioblastoma. *Pediatr Blood Cancer.* 2007;48:403-407
- dos Santos NA, Martins NM, Curti C, Pires Bianchi ML, dos Santos AC.** Dimethylthiourea protects against mitochondrial oxidative damage induced by cisplatin in liver of rats. *Chem Biol Interact.* 2007;170:177-186
- Du C, Fang M, Li Y, Li L, Wang X.** Smac, a mitochondrial protein that promotes cytochrome c-dependent caspase activation by eliminating IAP inhibition. *Cell.* 2000;102:33-42
- Dubois LG, Campanati L, Righy C, D'Andrea-Meira I, Spohr TC, Porto-Carreiro I, Pereira CM, Balça-Silva J, Kahn SA, DosSantos MF, Oliveira Mde A, Ximenes-da-Silva A, Lopes MC, Faveret E, Gasparetto EL, et al.** Gliomas and the vascular fragility of the blood brain barrier. *Front Cell Neurosci.* 2014;8:418
- Dubouloz F, Deloche O, Wanke V, Cameroni E, De Virgilio C.** The TOR and EGO protein complexes orchestrate microautophagy in yeast. *Mol. Cell.* 2005;19:15-26
- Dugbartey GJ, Peppone LJ, de Graaf IA.** An integrative view of cisplatin-induced renal and cardiac toxicities: Molecular mechanisms, current treatment challenges and potential protective measures. *Toxicology.* 2016;371:58-66
- Duijkers FA, Gaal J, Meijerink JP, Admiraal P, Pieters R, de Krijger RR, van Noesel MM.** High anaplastic lymphoma kinase immunohistochemical staining in neuroblastoma and ganglioneuroblastoma is an independent predictor of poor outcome. *Am J Pathol.* 2012;180:1223-1231
- Dunn GP, Dunn IF, Curry WT.** Focus on TILs: Prognostic significance of tumor infiltrating lymphocytes in human glioma. *Cancer Immun.* 2007;7:12
- Egan DF, Shackelford DB, Mihaylova MM, Gelino S, Kohnz RA, Mair W, Vasquez DS, Joshi A, Gwinn DM, Taylor R, Asara JM, Fitzpatrick J, Dillin A, Viollet B, Kundu M, et al.** Phosphorylation of ULK1 (hATG 1) by AMP activated protein kinase connects energy sensing to mitophagy. *Science.* 2011;331:456-461

- Elmore S.** Apoptosis: a review of programmed cell death. *Toxicol Pathol.* 2007;35:495-516
- Elsamadicy AA, Chongsathidkiet P, Desai R, Woroniecka K, Farber SH, Fecci PE, Sampson JH.** Prospect of rindopepimut in the treatment of glioblastoma. *Expert Opin Biol Ther.* 2017;17:507-513
- Evans SM, Judy KD, Dunphy I, Jenkins WT, Hwang WT, Nelson PT, Lustig RA, Jenkins K, Magarelli DP, Hahn SM, Collins RA, Grady MS, Koch CJ.** Hypoxia is important in the biology and aggression of human glial brain tumors. *Clin Cancer Res.* 2004;10:8177-8184
- Facoetti A, Vischioni B, Ciocca M, Ferrarini M, Furusawa Y, Mairani A, Matsumoto Y, Mirandola A, Molinelli S, Uzawa A, Vilches FG, Orecchia R.** In vivo radiobiological assessment of the new clinical carbon ion beams at CNAO. *Radiat Prot Dosimetry.* 2015;166:379-382
- Falkenberg KJ, Johnstone RW.** Histone deacetylases and their inhibitors in cancer, neurological diseases and immune disorders. *Nat Rev Drug Discov.* 2014;13:673-691
- Farre JC, Subramani S.** Mechanistic insights into selective autophagy pathways: lessons from yeast. *Nat Rev Mol Cell Biol.* 2016;17:537-552
- Farrell CJ and Plotkin SR.** Genetic causes of brain tumors: neurofibromatosis, tuberous sclerosis, von Hippel-Lindau and other syndromes. *Neurol Clin.* 2007;25:925-946
- Fathpour P, Obad N, Espedal H, Stieber D, Keunen O, Sakariassen PØ, Niclou SP, Bjerkvig R.** Bevacizumab treatment for human glioblastoma. Can it induce cognitive impairment? *Neuro Oncol.* 2014;16:754-756
- Fatokun AA, Dawson VL, Dawson TM.** Parthanatos: mitochondrial-linked mechanisms and therapeutic opportunities. *Br J Pharmacol.* 2014;171:2000-2016
- Favaloro B, Allocati N, Graziano V, Di Ilio C, De Laurenzi V.** Role of apoptosis in disease. *Aging.* 2012;4:330-349
- Feng S, Yang Y, Mei Y, Ma L, Zhu DE, Hoti N, Castanares M, Wu M.** Cleavage of RIP3 inactivates its caspase-independent apoptosis pathway by removal of kinase domain. *Cell Signal.* 2007;19:2056-2067
- Feoktistova M, Geserick P, Kellert B, Dimitrova DP, Langlais C, Hupe M, Cain K, MacFarlane M, Hacker G, Leverkus M.** cIAPs block Ripoptosome formation, a RIP1/caspase-8 containing intracellular cell death complex differentially regulated by cFLIP isoforms. *Mol Cell.* 2011;43:449-463

- Ferrari B, Urselli F, Gilodi M, Camuso S, Priori EC, Rangone B, Ravera M, Veneroni P, Zanellato I, Roda E, Osella D, Bottone MG.** New Platinum-Based Prodrug Pt(IV)Ac-POA: Antitumour Effects in Rat C6 Glioblastoma Cells. *Neurotox Res.* 2019;[Epub ahead of print]
- Ferri KF, Kroemer G.** Organelle-specific initiation of cell death pathways. *Nat Cell Biol.* 2001;3:255-263
- Fioretti B, Castigli E, Maria R, Micheli, Bova R, Sciaccaluga M, Harper A, Franciolini F, Catacuzzeno L.** Expression and modulation of the intermediate conductance Ca^{2+} -activated K^{+} Channel in Glioblastoma GL-15 Cells. *Cell Physiol Biochem.* 2006;18:47-56
- Florea AM, Büsselberg D.** Cisplatin as an anti-tumor drug: cellular mechanisms of activity, drug resistance and induced side effects. *Cancers (Basel).* 2011;3:1351-2371
- Flynn JR, Wang L, Gillespie DL, Stoddard GJ, Reid JK, Owens J, Ellsworth GB, Salzman KL, Kinney AY, Jensen RL.** Hypoxia-regulated protein expression, patient characteristics, and preoperative imaging as predictors of survival in adults with glioblastoma multiforme. *Cancer.* 2008;113:1032-1042
- Fredlund E, Ringner M, Maris JM, Pahlman S.** High Myc pathway activity and low stage of neural differentiation associate with poor outcome in neuroblastoma. *Proc Natl Acad Sci USA.* 2008;105:14094-14099
- Frew AJ, Johnstone RW, Bolden JE.** Enhancing the apoptotic and therapeutic effects of HDAC inhibitors. *Cancer Lett.* 2009;280:125-133
- Frezza C, Cipolat S, Martins de Brito O, Micaroni M, Beznoussenko GV, Rudka T, Bartoli D, Polishuck RS, Danial NN, De Strooper B, Scorrano L.** OPA1 controls apoptotic cristae remodeling independently from mitochondrial fusion. *Cell.* 2006;126:177-189
- Frezza M, Hindo S, Chen D, Davenport A, Schmitt S, Tomco D, Dou QP.** Novel metals and metal complexes as platforms for cancer therapy. *Curr Pharm Des.* 2010;16:1813-1825
- Foghsgaard L, Wissing D, Mauch D, Lademann U, Bastholm L, Boes M, Elling F, Leist M, Jaattela M.** Cathepsin B acts as a dominant execution protease in tumor cell apoptosis induced by tumor necrosis factor. *J Cell Biol.* 2001;153:999-1010
- Folkerth RD.** Descriptive analysis and quantification of angiogenesis in human brain tumors. *J Neurooncol.* 2000;50:165-172

- Fu Q, Fu TM, Cruz AC, Sengupta P, Thomas SK, Wang S, Siegel RM, Wu H, Chou JJ.** Structural basis and functional role of intramembrane trimerization of the Fas/CD95 death receptor. *Mol Cell*. 2016;61:602-613
- Fuchs Y, Steller H.** Programmed cell death in animal development and disease. *Cell*. 2011;147:742-758
- Fuchs Y, Steller H.** Live to die another way: modes of programmed cell death and the signals emanating from dying cells. *Nat Rev Mol Cell Biol*. 2015;16:329-344
- Furnari FB, Fenton T, Bachoo RM, Mukasa A, Stommel JM, Stegh A, Hahn WC, Ligon KL, Louis DN, Brennan C, Chin L, DePinho RA, Cavenee WK.** Malignant astrocytic glioma: genetics, biology, and paths to treatment. *Rev Genes Dev*. 2007;21:2683-2710
- Furuta T, Ueda T, Aune G, Sarasin A, Kraemer KH, Pommier Y.** Transcription-coupled nucleotide excision repair as a determinant of cisplatin sensitivity of human cells. *Cancer Res*. 2002;62:4899-4902
- Gabano E, Ravera M, Zanellato I, Tinello S, Gallina A, Rangone B, Gandin V, Marzano C, Bottone MG, Osella D.** An unsymmetric cisplatin-based Pt(IV) derivative containing 2-(2-propynyl)octanoate: a very efficient multi-action antitumor prodrug candidate. *Dalton Trans*. 2017;46:14174-14185
- Galanski M, Arion VB, Jakupec MA, Keppler BK.** Recent developments in the field of tumor-inhibiting metal complexes. *Curr Pharm Des*. 2003;9:2078-2089
- Galluzzi L, Bravo-San Pedro JM, Kepp O, Kroemer G.** Regulated cell death and adaptive stress responses. *Cell Mol Life Sci*. 2016;73:2405-2410
- Galluzzi L, Kepp O, Krautwald S, Kroemer G, Linkermann A.** Molecular mechanisms of regulated necrosis. *Semin Cell Dev Biol*. 2014;35:24-32
- Galluzzi L, Maiuri MC, Vitale I, Zischka H, Castedo M, Zitvogel L, Kroemer G.** Cell death modalities: classification and pathophysiological implications. *Cell Death Differ*. 2007;14:1237-1243
- Galluzzi L, Senovilla L, Vitale I, Michels J, Martins I, Kepp O, Castedo M, Kroemer G.** Molecular mechanisms of cisplatin resistance. *Oncogene*. 2012;31:1869-1883
- Galluzzi L, Vitale I, Aaronson S, Abrams JM, Adam D, Agostinis P, Alnemri ES, Altucci L, Amelio I, Andrews DW, Annicchiarico-Petruzzelli M, Antonov AV, Arama E, Baehrecke EH, Barlev N, et al.** Molecular mechanisms of cell death:

- recommendations of the Nomenclature Committee on Cell Death 2018. *Cell Death Differ.* 2018;25:486-541
- Galluzzi L, Vitale I, Michels J, Brenner C, Szabadkai G, Harel-Bellan A, Castedo M, Kroemer G.** Systems biology of cisplatin resistance: past, present and future. *Cell Death Dis.* 2014;5:e1257
- Gerson SL.** Clinical relevance of MGMT in the treatment of cancer. *J Clin Oncol.* 2002;20:2388-2399
- Giannone G, Rondé P, Gaire M, Haiech J, Takeda K.** Calcium oscillations trigger focal adhesion disassembly in human U87 astrocytoma cells. *J Biol Chem.* 2002;277:26364-26371
- Gibson D.** Platinum(IV) anticancer prodrugs-hypotheses and facts. *Dalton Trans.* 2016;45:12983-12991
- Giorgi C, Agnoletto C, Bononi A, Bonora M, De Marchi E, Marchi S, Missiroli S, Patergnani S, Poletti F, Rimessi A, Suski JM, Wieckowski MR, Pinton P.** Mitochondrial calcium homeostasis as potential target for mitochondrial medicine. *Rev Mitochondrion.* 2012;12:77-85
- Gleichmann M, Mattson MP.** Neuronal calcium homeostasis and dysregulation. *Rev Antioxid Redox Signal.* 2011;14:1261-1273
- Godoy LC, Anderson CT, Chowdhury R, Trudel LJ, Wogan GN.** Endogenously produced nitric oxide mitigates sensitivity of melanoma cells to cisplatin. *Proc Natl Acad Sci USA.* 2012;109:20373-20378
- Goffart N, Kroonen J, Rogister B.** Glioblastoma-Initiating Cells: Relationship with Neural Stem Cells and the Micro-Environment. *Cancers.* 2013;5:1049-1071
- Goldberg AD, Allis CD, Bernstein E.** Epigenetics: a landscape takes shape. *Cell.* 2007;128:635-638
- Goldberg SB, Gettinger SN, Mahajan A, Chiang AC, Herbst RS, Sznol M, Tsiouris AJ, Cohen J, Vortmeyer A, Jilaveanu L, Yu J, Hegde U, Speaker S, Madura M, Ralabate A et al.** Pembrolizumab for patients with melanoma or non-small-cell lung cancer and untreated brain metastases: Early analysis of a non-randomised, open-label, phase 2 trial. *Lancet Oncol.* 2016;17:976-983
- Gonzales VM, Fuertes MA, Alonso C, Perez JM.** Is cisplatin-induced cell death always produced by apoptosis? *Mol Pharmacol.* 2001;59:657-663

- Goodsell DS.** The molecular perspective: cisplatin. *Stem Cells*. 2006;24:514-515
- Gough DR, Cotter TG.** Hydrogen peroxide: a Jekyll and Hyde signalling molecule. *Cell Death Dis*. 2011;2:213
- Grada Z, Hegde M, Byrd T, Shaffer DR, Ghazi A, Brawley VS, Corder A, Schönfeld K, Koch J, Dotti G, Heslop HE, Gottschalk S, Wels WS, Baker ML, Ahmed N.** TanCAR: A novel bispecific chimeric antigen receptor for cancer immunotherapy. *Mol Ther Nucleic Acids*. 2013;2:105
- Graf N, Lippard SJ.** Redox activation of metal-based prodrugs as a strategy for drug delivery. *Adv Drug Delivery Rev*. 2012;64:993-1004
- Griffith D, Morgan MP, Marmion C.** A novel anti-cancer bifunctional platinum drug candidate with dual DNA binding and histone deacetylase inhibitory activity. *Chem Commun (Camb)*. 2009;44:6735-6737
- Grimaldi M, Bo VD, Ferrari B, Roda E, De Luca F, Veneroni P, Barni S, Verri M, De Pascali SA, Fanizzi FP, Bernocchi G, Bottone MG.** Long-term effects after treatment with platinum compounds, cisplatin and [Pt(O,O'-acac)(γ -acac)(DMS)]: Autophagy activation in rat B50 neuroblastoma cells. *Toxicol Appl Pharmacol*. 2019;364:1-11
- Grimaldi M, Santin G, Insolia V, Dal Bo V, Piccolini VM, Veneroni P, Barni S, Verri M, De Pascali SA, Fanizzi FP, Bernocchi G, Bottone MG.** [Pt(O,O'-acac)(γ -acac)(DMS)] versus cisplatin: apoptotic effects in B50 neuroblastoma cells. *Histochem Cell Biol*. 2016;145:587-601
- Gritsenko PG, Iina O, Friedl P.** Interstitial guidance of cancer invasion. *Rev J Pathol*. 2012;226:185-199
- Grobben B, De Deyn PP, Slegers H.** Rat C6 glioma as experimental model system for the study of glioblastoma growth and invasion. *Rev Cell Tissue Res*. 2002;310:257-270
- Gupta RK, Patel AK, Shah N, Chaudhary AK, Jha UK, Yadav UC, Gupta PK, Pakuwal U.** Oxidative stress and antioxidants in disease and cancer: a review. *Asian Pac J Cancer Prev*. 2014;15:4405-4409
- Gusyatiner O, Hegi ME.** Glioma epigenetics: From subclassification to novel treatment options. *Semin Cancer Biol*. 2018;51:50-58
- Gyrd-Hansen M, Meier P.** IAPs: from caspase inhibitors to modulators of NF- κ B, inflammation and cancer. *Nat. Rev. Cancer* 2010;10:561-574.

- Hall BK.** The neural crest as a fourth germ layer and vertebrates as quadroblastic and triploblastic. *Evol Dev.* 2000;2:3-5
- Halliwell B.** Biochemistry of oxidative stress. *Biochem Soc Trans.* 2007;35:1147-1150
- Hamada N, Imaoka T, Masunaga S, Ogata T, Okayasu R, Takahashi A, Kato TA, Kobayashi Y, Ohnishi T, Ono K, Shimada Y, Teshima T.** Recent advances in the biology of heavy-ion cancer therapy. *J Radiat Res.* 2010;51:365-383
- Han S, Zhang C, Li Q, Dong J, Liu Y, Huang Y, Jiang T, Wu A.** Tumour-infiltrating CD4⁺ and CD8⁺ lymphocytes as predictors of clinical outcome in glioma. *Br J Cancer.* 2014;110:2560-2568
- Hanada T, Noda NN, Satomi Y, Ichimura Y, Fujioka Y, Takao T, Inagaki F, Ohsumi Y.** The Atg12-Atg5 conjugate has a novel E3-like activity for protein lipidation in autophagy. *J Biol Chem.* 2007;282:37298-37302
- Hanahan D, Weinberg RA.** Hallmarks of cancer: The next generation. *Cell.* 2011;144:646-674
- Hansford LM, Thomas WD, Keating JM, Burkhart CA, Peaston AE, Norris MD, Haber M, Armati PJ, Weiss WA, Marshall GM.** Mechanisms of embryonal tumor initiation: distinct roles for MycN expression and MYCN amplification. *Proc Natl Acad Sci U S A.* 2004;101:12664-12669
- Hara E, Rivas MV, Ward JM, Okanoya K, Jarvis ED.** Convergent differential regulation of parvalbumin in the brains of vocal learners. *PLoS One.* 2012;7:e29457
- Hardwick JM, Soane L.** Multiple functions of BCL-2 family proteins. *Cold Spring Harb Perspect Biol.* 2013;5
- Harris J, De Haro SA, Master SS, Keane J, Roberts EA, Delgado M, Deretic V.** T helper 2 cytokines inhibit autophagic control of intracellular Mycobacterium tuberculosis. *Immunity.* 2007;27:505-517
- Hausheer FH, Schilsky RL, Bain S, Berghorn EJ, Lieberman F.** Diagnosis, management, and evaluation of chemotherapy-induced peripheral neuropathy. *Semin Oncol.* 2006;33:15-49
- Hayashi-Nishino M, Fujita N, Noda T, Yamaguchi A, Yoshimori T, Yamamoto A.** A subdomain of the endoplasmic reticulum forms a cradle for autophagosome formation. *Nature Cell Biol.* 2009;11:1433-1437

- Hayton S, Maker GL, Mullaney I, Trengove RD.** Untargeted metabolomics of neuronal cell culture: A model system for the toxicity testing of insecticide chemical exposure. *J Appl Toxicol.* 2017;37:1481-1492
- He C, Klionsky DJ.** Regulation Mechanisms and Signaling Pathways of Autophagy. *Annu Rev Genet.* 2009;43:67-93
- Hegde M, Corder A, Chow KK, Mukherjee M, Ashoori A, Kew Y, Zhang YJ, Baskin DS, Merchant FA, Brawley VS, Byrd TT, Krebs S, Wu MF, Liu H, Heslop HE, et al.** Combinational targeting offsets antigen escape and enhances effector functions of adoptively transferred T cells in glioblastoma. *Mol Ther.* 2012;21:2087-2101
- Hegi ME, Diserens AC, Gorlia T, Hamou MF, de Tribolet N, Weller M, Kros JM, Hainfellner JA, Mason W, Mariani L, Bromberg JE, Hau P, Mirimanoff RO, Cairncross JG, Janzer RC, et al.** MGMT gene silencing and benefit from temozolomide in glioblastoma. *N Engl J Med.* 2005;352:997-1003
- Herceg Z, Lambert MP, van Veldhoven K, Demetriou C, Vineis P, Smith MT, Straif K, and Wild CP.** Towards incorporating epigenetic mechanisms into carcinogen identification and evaluation. *Carcinogenesis.* 2013;34:1955-1967
- Hide T, Makino K, Nakamura H, Yano S, Anai S, Takezaki T, Kuroda J, Shinojima N, Ueda Y, Kuratsu J.** New treatment strategies to eradicate cancer stem cells and niches in glioblastoma. *Neurol Med Chir.* 2013;53:764-772
- Higashida H, Yokoyama S, Hoshi N, Hashii M, Egorova A, Zhong ZG, Noda M, Shahidullah M, Taketo M, Knijnik R, Kimura Y, Takahashi H, Chen XL, Shin Y, Zhang JS.** Signal transduction from bradykinin, angiotensin, adrenergic and muscarinic receptors to effector enzymes, including ADP-ribosyl cyclase. *Rev Biol Chem.* 2001;382:23-30
- Higashimori H, Sontheimer H.** Role of Kir4.1 channels in growth control of glia. *Glia.* 2007;55:1668-1679
- Hilfiker S, Schweizer FE, Kao HT, Czernik AJ, Greengard P, Augustine GJ.** Two sites of action for synapsin domain E in regulating neurotransmitter release. *Nat Neurosci.* 1998;1:29-35
- Hirst M, Marra MA.** Epigenetics and human disease. *Int J Biochem Cell Biol.* 2009;41:136-146
- Hitomi J, Christofferson DE, Ng A, Yao J, Degterev A, Xavier RJ, Yuan J.** Identification of molecular signaling network that regulates a cellular necrotic cell death pathway. *Cell.* 2008;135:1311-1323

- Hodeify R, Megyesi J, Tarcsfalvi A, Safirstein RL, Price PM.** Protection of cisplatin cytotoxicity by an inactive cyclin-dependent kinase. *Am J Physiol Renal Physiol.* 2010;299:112-120
- Hodi FS, O'Day SJ, McDermott DF, Weber RW, Sosman JA, Haanen JB, Gonzalez R, Robert C, Schadendorf D, Hassel JC, Akerley W, van den Eertwegh AJ, Lutzky J, Lorigan P, Vaubel JM, et al.** Improved survival with ipilimumab in patients with metastatic melanoma. *N Engl J Med.* 2010;363:711-723
- Hogan PG, Rao A.** Store-operated calcium entry: Mechanisms and modulation. *Biochem Biophys Res Commun.* 2015;460:40-49
- Holland EC.** Glioblastoma multiforme: The Terminator. *Proc Natl Acad Sci USA.* 2000;97:6242-6244
- Holzer AK, Manorek GH, Howell SB.** Contribution of the major copper influx transporter CTR1 to the cellular accumulation of cisplatin, carboplatin, and oxaliplatin. *Mol.Pharmacol.* 2006;70:1390-1394
- Hsieh P, Yamane K.** DNA mismatch repair: molecular mechanism, cancer, and ageing. *Rev Mech Ageing Dev.* 2008;129:391-407
- Hu Q, Wu D, Chen W, Yan Z, Yan C, He T, Liang Q, Shi Y.** Molecular determinants of caspase-9 activation by the Apaf-1 apoptosome. *Proc Natl Acad Sci USA.* 2014;111:16254-1661.
- Hu X, Zhao Y, Wei L, Zhu B, Song D, Wang J, Yu L, Wu J.** CCDC178 promotes hepatocellular carcinoma metastasis through modulation of anoikis. *Oncogene.* 2017;36:4047-4059.
- Hu Z, Dong N, Lu D, Jiang X, Xu J, Wu Z, Zheng D, Wechsler DS.** A positive feedback loop between ROS and Mxi1-0 promotes hypoxia-induced VEGF expression in human hepatocellular carcinoma cells. *Cell Signal.* 2017;31:79-86
- Huang K, Zhang J, O'Neill KL, Gurumurthy CB, Quadros RM, Tu Y, Luo X.** Cleavage by Caspase 8 and Mitochondrial Membrane Association Activate the BH3-only Protein Bid during TRAIL-induced Apoptosis. *J Biol Chem.* 2016;291:11843-11851
- Huang WP, Klionsky DJ.** Autophagy in yeast: a review of molecular machinery. *Cell Struct Funct.* 2002;27:409-420
- Huber SM.** Oncochannles. *Cell Calc.* 2013;53:241-255

- Hughes MA, Powley IR, Jukes-Jones R, Horn S, Feoktistova M, Fairall L, Schwabe JW, Leverkus M, Cain K, MacFarlane M.** Co-operative and hierarchical binding of c-FLIP and Caspase-8: a unified model defines how c-FLIP isoforms differentially control cell fate. *Mol Cell*. 2016;61:834-849
- Huntoon CJ, Flatten KS, Wahner Hendrickson AE, Huehls AM, Sutor SL, Kaufmann SH, Karnitz LM.** ATR inhibition broadly sensitizes ovarian cancer cells to chemotherapy independent of BRCA status. *Cancer Res*. 2013;73:3683-3691
- Iacob G and Dinca EB.** Current data and strategy in glioblastoma multiforme. *J Med Life*. 2009;2:386-393
- Ichim G, Lopez J, Ahmed SU, Muthalagu N, Giampazolias E, Delgado ME, Haller M, Riley JS, Mason SM, Athineos D, Parsons MJ, van de Kooij B, Bouchier-Hayes L, Chalmers AJ, Rooswinkel RW, et al.** Limited mitochondrial permeabilization causes DNA damage and genomic instability in the absence of cell death. *Mol Cell*. 2015;57:860-872
- Ikeguchi M, Liu J, Kaibara N.** Expression of survivin mRNA and protein in gastric cancer cell line (MKN-45) during cisplatin treatment. *Apoptosis*. 2002;7:23-29
- Ikonomidou C.** Chemotherapy and the pediatric brain. *Mol Cell Pediatr*. 2018;5:8
- Ilangovan G, Li H, Zweier JL, Kuppusamy P.** *In vivo* measurement of tumor redox environment using EPR spectroscopy. *Mol Cell Biochem*. 2002;234:393-398
- Insinga A, Monestiroli S, Ronzoni S, Gelmetti V, Marchesi F, Viale A, Altucci L, Nervi C, Minucci S, Pelicci PG.** Inhibitors of histone deacetylases induce tumor-selective apoptosis through activation of the death receptor pathway. *Nat Med*. 2005;11:71-76
- International Agency for Research on Cancer (IARC).** Cisplatin. IARC Monographs on the Evaluation of Carcinogenic Risk of Chemicals to Humans. Lyon, France: International Agency for Research on Cancer, 1981. Some antineoplastic and immunosuppressive agents. 1981;26:151-164
- Iseri S, Ercan F, Gedik N, Yuksel M, Alican I.** Simvastatin attenuates cisplatin-induced kidney and liver damage in rats. *Toxicology*. 2007;230:256-264
- Ishida S, Lee J, Thiele DJ, Herskowitz I.** Uptake of the anticancer drug cisplatin mediated by the copper transporter Ctr1 in yeast and mammals. *Proc Natl Acad Sci USA*. 2002;99:14298-14302
- Ishiuchi S, Tsuzuki K, Yoshida Y, Yamada N, Hagimura N, Okado H, Miwa A, Kurihara H, Nakazato Y, Tamura M, Sasaki T, Ozawa S.** Blockage of Ca(2+)-

- permeable AMPA receptors suppresses migration and induces apoptosis in human glioblastoma cells. *Nat Med.* 2002;8:971-978
- Ishola TA, Chung DH.** Neuroblastoma. *Rev Surg Oncol.* 2007;16:149-156
- Itakura E, Mizushima N.** Atg14 and UVRAG: mutually exclusive subunits of mammalian Beclin 1 -PI3K complexes. *Autophagy.* 2009;5:534-536
- Iwanami A, Cloughesy TF, Cavenee WK, Mischel PS.** Arsenic reverses glioblastoma resistance to mTOR-targeted therapies. *Cell Cycle.* 2013;12:1473-1474
- Jaber N, Dou Z, Chen JS, Catanzaro J, Jiang YP, Ballou LM, Selinger E, Ouyang X, Lin RZ, Zhang J, Zong WX.** Class III PI3K Vps 34 plays an essential role in autophagy and in heart and liver function. *Proc Natl Acad Sci USA.* 2012;109:2003-2008
- Jacobs JFM, Idema AJ, Bol KF, Grotenhuis JA, de Vries IJM, Wesseling P, Adema GJ.** Prognostic significance and mechanism of Treg infiltration in human brain tumors. *J Neuroimmunol.* 2010;225:195-199
- Jeon HJ, Kang HJ, Jung HJ, Kang YS, Lim CJ, Kim YM, Park EH.** Anti-inflammatory activity of *Taraxacum officinale*. *J Ethnopharmacol.* 2008;115:82-88
- Jiang D, Wang L, Zhao T, Zhang Z, Zhang R, Jin J, Cai Y, Wang F.** Restoration of the tumor-suppressor function to mutant p53 by *Ganoderma lucidum* polysaccharides in colorectal cancer cells. *Oncol Rep.* 2017;37:594-600
- Jiang P, Mizushima N.** Autophagy and human disease. *Cell Res.* 2014;24:69-79
- Jiang X, Wang X.** Cytochrome C-mediated apoptosis. *Annu Rev Biochem.* 2004;73:87-106
- Jiang Y, Gue, C, Vasko MR, Kelley MR.** Implications of apurinic/apyrimidinic endonuclease in reactive oxygen signaling response after cisplatin treatment of dorsal root ganglion neurons. *Cancer Res.* 2008;68:6425-6434
- Jin Z, Li Y, Pitti R, Lawrence D, Pham VC, Lill JR, Ashkenazi A.** Cullin3-based polyubiquitination and p62-dependent aggregation of caspase-8 mediate extrinsic apoptosis signaling. *Cell.* 2009;137:721-735
- Jinno-Oue A, Shimizu N, Hamada N, Wada S, Tanaka A, Shinagawa M, Ohtsuki T, Mori T, Saha MN, Hoque AS, Islam S, Kogure K, Funayama T, Kobayashi Y, Hoshino H.** Irradiation with carbon ion beams induces apoptosis, autophagy, and cellular senescence in a human glioma-derived cell line. *Int J Radiat Oncol Biol Phys.* 2010;76:229-241

- John T, Lomeli N, Bota DA.** Systemic cisplatin exposure during infancy and adolescence causes impaired cognitive function in adulthood. *Behav Brain Res.* 2017;319:200-206
- Johnson DR, O'Neill BP.** Glioblastoma survival in the United States before and during the temozolomide era. *J Neurooncol.* 2012;107:359-364
- Johnstone C, Suntharalingam K, Lippard SJ.** The next generation of platinum drugs: targeted Pt(II) agents, nanoparticle delivery and Pt(IV) prodrugs. *Chem Rev.* 2016;116:3436-3486
- Johnstone TC.** The crystal structure of Oxaliplatin: a case of overlooked pseudo symmetry. *Polyhedron.* 2014;67
- Johnstone TC, Suntharalingam K, Lippard SJ.** The next generation of platinum drugs: targeted Pt(II) agents, nanoparticle delivery, and Pt(IV) prodrugs. *Chem Rev.* 2016;116:3436-3486
- Jong NN, Nakanishi T, Liu JJ, Tamai I, McKeage MJ.** Oxaliplatin transport mediated by organic cation/carnitine transporters OCTN1 and OCTN2 in overexpressing human embryonic kidney 293 cells and rat dorsal root ganglion neurons. *J Pharmacol Exp Ther.* 2011;338:537-547
- Judson I, Kelland L.** New developments and approaches in the platinum arena. *Drugs.* 2000;59:29-36
- Julien O, Wells JA.** Caspases and their substrates. *Cell Death Differ.* 2017;24:1380-1389
- Kabeya Y, Mizushima N, Uero T, Yamamoto A, Kirisako T, Noda T, Kominami E, Ohsumi Y, Yoshimori T.** LC3, a mammalian homologue of yeast Apg8p, is localized in autophagosome membranes after processing. *Embo Journal.* 2000;19:5720-5728
- Kamada T, Tsujii H, Blakely EA, Debus J, De Neve W, Durante M, Jäkel O, Mayer R, Orecchia R, Pötter R, Vatnitsky S, Chu WT.** Carbon ion radiotherapy in Japan: an assessment of 20 years of clinical experience. *Lancet Oncol.* 2015;16:93-100
- Karsy M, Gelbman M, Shah P, Balumbu O, Moy F, Arslan E.** Established and emerging variants of glioblastoma multiforme: review of morphological and molecular features. *Folia Neuropathol.* 2012;50:301-321
- Kart A, Cigremis Y, Karaman M, Ozen H.** Caffeic acid phenethyl ester (CAPE) ameliorates cisplatin-induced hepatotoxicity in rabbit. *Exp Toxicol Pathol.* 2010;62:45-52
- Katsuragi Y, Ichimura Y, Komatsu M.** p62/SQSTM1 functions as a signalling hub and a autophagy adaptor. *FEBS J.* 2015;282:4672-4678

- Kaufmann A, Beier V, Franquelim HG, Wollert T.** Molecular mechanism of autophagic membrane-scaffold assembly and disassembly. *Cell*. 2014;156: 469-481
- Kaushal GP, Kaushal V, Herzog C, Yang C.** Autophagy delays apoptosis in renal tubular epithelial cells in cisplatin cytotoxicity. *Autophagy*. 2008;4:710-712
- Kaushik S, Cuervo AM.** Chaperone-mediated autophagy: a unique way to enter the lysosome world. *Trends Cell Biol*. 2012;22:407-417
- Kavuri SM, Geserick P, Berg D, Dimitrova DP, Feoktistova M, Siegmund D, Gollnick H, Neumann M, Wajant H, Leverkus M.** Cellular FLICE-inhibitory protein (cFLIP) isoforms block CD95- and TRAIL death receptor-induced gene induction irrespective of processing of caspase-8 or cFLIP in the death-inducing signaling complex. *J Biol Chem*. 2011;286:16631-16646
- Kearney CJ, Cullen SP, Tynan GA, Henry CM, Clancy D, Lavelle EC, Martin SJ.** Necroptosis suppresses inflammation via termination of TNF- or LSP-induced cytokine and chemokine production. *Cell Death Differ* 2015;22:1313-1327
- Keith B, Simon MC.** Hypoxia-inducible factors, stem cells, and cancer. *Rev Cell* 2007;129:465-472
- Kelland L.** The resurgence of platinum-based cancer chemotherapy. *Nat Rev Cancer*. 2007;7:573-584
- Kenyon KA, Bushong EA, Mauer AS, Strehler EE, Weinberg RJ, Burette AC.** Cellular and subcellular localization of the neuron-specific plasma membrane calcium ATPase PMCA1a in the rat brain. *J Comp Neurol*. 2010;518:3169-3183
- Kheirleaid EA, Miller N, Chang KH, Curran C, Hennessey E, Sheehan M, Kerin MJ.** Mismatch repair protein expression in colorectal cancer. *J Gastrointest Oncol*. 2013;4:397-408
- Khoo HE, Prasad KN, Kong KW, Jiang Y, Ismail A.** Carotenoids and their isomers: color pigments in fruits and vegetables. *Molecules*. 2011;16:1710-1738
- Kiekow CJ, Figueiró F, Dietrich F, Vechia LD, Pires EN, Jandrey EH, Gnoatto SC, Salbego CG, Battastini AM, Gosmann G.** Quercetin derivative induces cell death in glioma cells by modulating NF- κ B nuclear translocation and caspase-3 activation. *Eur J Pharm Sci*. 2016;84:116-122
- Kilari D, Guancial E, Kim ES.** Role of copper transporters in platinum resistance. *World J Clin Oncol*. 2016;7:106-113

- Kim J, Kundu M, Viollet B, Guan KL.** AMPK and mTOR regulate autophagy through direct phosphorylation of Ulk1. *Nat Cell Biol.* 2011;13:132-141
- Kim MY, Zhang T, Kraus WL.** Poly(ADP-ribosylation) by PARP-1: PAR-laying NAD⁺ into a nuclear signal. *Genes Dev.* 2005;19:1951-1967
- Kim SS, Harford JB, Pirollo KF, Chang EH.** Effective treatment of glioblastoma requires crossing the blood–brain barrier and targeting tumors including cancer stem cells: The promise of nanomedicine. *Biochem Biophys Res Commun.* 2015;468:485-489
- Kioi M, Vogel H, Schultz G, Hoffman RM, Harsh GR, Brown JM.** Inhibition of vasculogenesis, but not angiogenesis, prevents the recurrence of glioblastoma after irradiation in mice. *J Clin Invest.* 2010;120:694-705
- Kipnis J.** Multifaceted interactions between adaptive immunity and the central nervous system. *Science.* 2016;353:766-771
- Klionsky DJ.** Autophagy: from phenomenology to molecular understanding in less than a decade. *Nat Rev Mol Cell Biol.* 2007;8:931-937
- Klionsky DJ, Emr SD.** Autophagy as a regulated pathway of cellular degradation. *Science.* 2000;290:1717-1721
- Knott JC, Mahesparan R, Garcia-Cabrera I, Bølge Tysnes B, Edvardsen K, Ness GO, Mørk S, Lund-Johansen M, Bjerkvig R.** Stimulation of extracellular matrix components in the normal brain by invading glioma cells. *Int J Cancer.* 1998;75:864-872
- Knowlton AA, Liu TT.** Mitochondrial Dynamics and Heart Failure. *Compr Physiol.* 2015;6:507-526
- Kolasinski SL.** Food, drink, and herbs: alternative therapies and gout. *Curr Rheumatol Rep.* 2014;16:409
- Kongara S, Karantza V.** The interplay between autophagy and ROS in tumorigenesis. *Front Oncol.* 2012;2:171
- Kostova I.** Platinum complexes as anticancer agents. *Recent Pat Anticancer Drug Discov.* 2006;1:1-22
- Kops GJ, Weaver BA, Cleveland DW.** On the road to cancer: aneuploidy and the mitotic checkpoint. *Nat Rev Cancer.* 2005;5:773-785

- Krajcí D, Mares V, Lisá V, Spanová A, Vorlíček J.** Ultrastructure of nuclei of cisplatin-treated C6 glioma cells undergoing apoptosis. *Eur J Cell Biol.* 2000;79:365-376
- Krajcí D, Mares V, Lisá V, Bottone MG, Pellicciari C.** Intranuclear microtubules are hallmarks of an unusual form of cell death in cisplatin-treated C6 glioma cells. *Histochem Cell Biol.* 2006;125:183-191
- Kroemer G, Galluzzi L, Brenner C.** Mitochondrial membrane permeabilization in cell death. *Physiol Rev.* 2007;87:99-163
- Kroemer G, Marino G, Levine B.** Autophagy and the integrated stress response. *Mol Cell.* 2010;40:280-293
- Krysko DV, Garg AD, Kaczmarek A, Krysko O, Agostinis P, Vandenabeele P.** Immunogenic cell death and DAMPs in cancer therapy. *Nat Rev Cancer.* 2012;12:860-875
- Kuffler SW, Nicholls JG.** The physiology of neuroglial cells. *Ergeb Physiol.* 1966;57:1-90
- Kuma A, Mizushima N, Ishihara N, Ohsumi Y.** Formation of the ~350-kDa Apg12-Apg5-Apg16 multimeric complex, mediated by Apg16 oligomerization, is essential for autophagy in yeast. *J Biol Chem.* 2002;277:18619-18625
- Kunkel TA, Erie DA.** DNA mismatch repair. *Annu Rev Biochem.* 2005;74:681-710
- Kunzelmann K.** Ion channels and cancer. *J Membr Biol.* 2005;205:159-173
- Kuo HC, Huang IC, Chen TY.** Cordyceps s.l. (Ascomycetes) species used as medicinal mushrooms are closely related with higher ability to produce cordycepin. *Int J Med Mushrooms.* 2015;17:1077-1085
- Kuo MT, Fu S, Savaraja N, Chen HH.** Role of the human high-affinity copper transporter in copper homeostasis regulation and cisplatin sensitivity in cancer chemotherapy. *Cancer Res.* 2012;72:4616-4621
- Kushner BH.** Neuroblastoma: a disease requiring a multitude of imaging studies. *Rev J Nucl Med.* 2004;45:1172-1188
- Lagneaux L, Gillet N, Stamatopoulos B, Delforge A, Dejeneffe M, Massy M, Meuleman N, Kentos A, Martiat P, Willems L, Bron D.** Valproic acid induces apoptosis in chronic lymphocytic leukemia cells through activation of the death receptor pathway and potentiates TRAIL response. *Exp Hematol.* 2007;35:1527-1537

- Laprie A, Hu Y, Alapetite C, Carrie C, Habrand JL, Bolle S, Bondiau PY, Ducassou A, Huchet A, Bertozzi AI, Perel Y, Moyal É, Balosso J, radiotherapy committee of SFCE and France Hadron.** Paediatric brain tumours: A review of radiotherapy, state of the art and challenges for the future regarding protontherapy and carbontherapy. *Cancer Radiother.* 2015;19:775-789
- Larysz D, Kula D, Kowal M, Rudnik A, Jarzab M, Blamek S, Bierzyńska-Macyszyn G, Kowalska M, Bazowski P, Jarzab B.** Epidermal growth factor receptor gene expression in high grade gliomas. *Folia Neuropathol.* 2011;49:28-38
- Lebelt A, Dzieciol J, Guzinska-Ustymowicz K, Lemancewicz D, Zimnoch L, Czykier E.** Angiogenesis in gliomas. *Folia Histochem Cytobiol.* 2008;46:69-72
- Lee MJ, Kim YS, Kummar S, Giaccone G, Trepel JB.** Histone deacetylase inhibitors in cancer therapy. *Curr Opin Oncol.* 2008;20:639-649
- Lee P, Murphy B, Miller R, Menon V, Banik NL, Giglio P, Lindhorst SM, Varma AK, Vndergrift WA 3rd, Patel SJ, Das A.** Mechanisms and clinical significance of histone deacetylase inhibitors: epigenetic glioblastoma therapy. *Anticancer Res.* 2015;35:615-625.
- Lee SY.** Temozolomide resistance in glioblastoma multiforme. *Genes Dis.* 2016;3:198-210
- Lee WJ, Roberts-Thomson SJ, Monteith GR.** Plasma membrane calcium-ATPase 2 and 4 in human breast cancer cell lines. *Biochem. Biophys Res Commun.* 2005;337:779-783
- Leng Y, Marinova Z, Reis-Fernandes MA, Nau H, Chuang DM.** Potent neuroprotective effects of novel structural derivatives of valproic acid: potential roles of HDAC inhibition and HSP70 induction. *Neurosci Lett.* 2010;476:127-132
- Lesueur P, Chevalier F, El-Habr EA, Junier MP, Chneiweiss H, Castera L, Müller E, Stefan D, Saintigny Y.** Radiosensitization effect of talazoparib, a parp inhibitor, on glioblastoma stem cells exposed to low and high linear energy transfer radiation. *Sci Rep.* 2018;8:3664
- Levine B, Kroemer G.** Autophagy in the pathogenesis of disease. *Cell.* 2008;132:27-42
- Lewit-Bentley A, Réty S.** EF-hand calcium-binding proteins. *Curr Opin Struct Biol.* 2000;10:637-643
- Li D, Xu T, Cao Y, Wang H, Li L, Chen S, Wang X, Shen Z.** A cytosolic heat shock protein 90 and cochaperone CDC37 complex is required for RIP activation during necroptosis. *Proc Natl Acad Sci USA.* 2015;12:5017-5022

- Li G, Qin Z, Chen Z, Xie L, Wang R, Zhao H.** Tumor microenvironment in treatment of glioma. *Open Med.* 2017;12:247-251
- Li H, Lei B, Xiang W, Wang H, Feng W, Liu Y, Qi S.** Differences in Protein Expression between the U251 and U87 Cell Lines. *Turk Neurosurg.* 2017;27:894-903
- Li H, Villalobo A.** Evidence for the direct interaction between calmodulin and the human epidermal growth factor receptor. *Biochem J.* 2002;362:499-505
- Li IC, Chen YL, Lee LY, Chen WP, Tsai YT, Chen CC, Chen CS.** Evaluation of the toxicological safety of erinacine A-enriched *Hericium erinaceus* in a 28-day oral feeding study in Sprague-Dawley rats. *Food Chem Toxicol.* 2014;70:61-67
- Li R, Chen X, You Y, Wang X, Liu Y, Hu Q, Yan W.** Comprehensive portrait of recurrent glioblastoma multiforme in molecular and clinical characteristics. *Oncotarget.* 2015;6:30968-30974
- Li T, Peng J, Zeng F, Zhang K, Liu J, Li X, Ouyang Q, Wang G, Wang L, Liu Z, Liu Y.** Association between polymorphisms in CTR1, CTR2, ATP7A, and ATP7B and platinum resistance in epithelial ovarian cancer. *Int J Clin Pharmacol Ther.* 2017;55:774-780
- Li WW, Li J, Bao JK.** Microautophagy: lesser-known self-eating. *Cell Mol Life Sci.* 2012;69:1125-1136
- Li Y, Seto E.** HDACs and HDAC inhibitors in cancer development and therapy. *Cold Spring Harb Perspect Med.* 2016;6
- Lin JF, Lin YC, Tsai TF, Chen HE, Chou KY, Hwang TI.** Cisplatin induces protective autophagy through activation of BECN1 in human bladder cancer cells. *Drug Des Devel Ther.* 2017,11:1517-1533
- Linde CI, Di Leva F, Domi T, Tosatto SC, Brini M, Carafoli E.** Inhibitory interaction of the 14-3-3 proteins with ubiquitous (PMCA1) and tissue-specific (PMCA3) isoforms of the plasma membrane Ca²⁺ pump. *Cell Calcium.* 2007;43:550-561
- Liu WJ, Ye L, Huang WF, Guo LJ, X ZG1, Wu HL, Yang C, Liu HF.** p62 links the autophagy pathway and the ubiquitin-proteasome system upon ubiquitinated protein degradation. *Cell Mol Biol Lett.* 2016;21:29
- Liu X, Chang Y, Reinhart P H, Sontheimer H.** Cloning and characterization of glioma BK, a novel BK channel isoform highly expressed in human glioma cells. *J Neurosci.* 2002;22:1840-1849

- Liu YL, Liu PF, Shao W, Du HP, Li ZZ, Guo C, Li ZF.** Effect of temozolomide on survival in elderly patients with glioblastoma and impaired performance status: a propensity score-matching analysis. *Onco Targets Ther.* 2017;10:4029-4035
- London WB, Castleberry RP, Matthay KK, Look AT, Seeger RC, Shimada H, Thorner P, Brodeur G, Maris JM, Reynolds CP, Cohn SL.** Evidence for an age cutoff greater than 365 days for neuroblastoma risk group stratification in the Children's Oncology Group. *J Clin Oncol.* 2005;23:6459-6465
- Lory P, Mezghrani A.** Calcium channelopathies in inherited neurological disorders: relevance to drug screening for acquired channel disorders. *Rev IDrugs.* 2010;13:467-471
- Los M, Mozoluk M, Ferrari D, Stepczynska A, Stroh C, Renz A, Herceg Z, Wang ZQ, Schulze-Osthoff K.** Activation and caspase-mediated inhibition of PARP: a molecular switch between fibroblast necrosis and apoptosis in death receptor signaling. *Mol Biol Cell.* 2002;13:978-988
- Lou E.** Can you hear them now? Tumor microtubules form cellular communication networks that protect gliomas from surgical lesions and chemotherapy treatments. *Neuro Oncol.* 2017;19:1289-1291
- Louis CU, Shohet JM.** Neuroblastoma: molecular pathogenesis and therapy. *Anna Rev Med.* 2015;66:9-63
- Louis DN, Ohgaki H, Wiestler OD, Cavenee WK, Burger PC, Jouvet A, Scheithauer BW, Kleihues P.** The 2007 WHO classification of tumours of the central nervous system. *Acta Neuropathol.* 2007;114:97-109
- Louis DN, Perry A, Burger P, Ellison DW, Reifenberger G, von Deimling A, Aldape K, Brat D, Collins VP, Eberhart C, Figarella-Branger D, Fuller GN, Giangaspero F, Giannini C, Hawkins C, et al.** International Society Of Neuropathology--Haarlem consensus guidelines for nervous system tumor classification and grading. *Brain Pathol.* 2014;24:429-435
- Louis DN, Perry A, Reifenberger G, von Deimling A, Figarella-Branger D, Cavenee WK, Ellison DW.** The 2016 World Health Organization classification of tumors of the Central Nervous System: a summary. *Acta Neuropathol.* 2016;131:803-820
- Luna-Vargas MP, Chipuk JE.** Physiological and pharmacological control of BAK, BAX, and beyond. *Trends Cell Biol.* 2016;26:906-917
- Lucio-Eterovic AK, Cortez MA, Valera ET, Motta FJ, Queiroz RG, Machado HR, Carlotti CG Jr, Neder L, Scrideli CA, Tone LG.** Differential expression of 12

- histone deacetylase (HDAC) genes in astrocytomas and normal brain tissue: class II and IV are hypoeexpressed in glioblastomas. *BMC Cancer* 2008;8:243
- Lyon JG, Mokarram N, Saxena T, Carroll SL, Bellamkonda RV.** Engineering challenges for brain tumor immunotherapy. *Adv Drug Deliv Rev.* 2017 May 15;114:19-32
- Ma L, Young J, Prabhala H, Pan E, Mestdagh P, Muth D, Teruya-Feldstein J, Reinhardt F, Onder TT, Valastyan S, Westermann F, Speleman F, Vandesompele J, Weinberg RA.** miR-9, a MYC/MYCN-activated microRNA, regulates E-cadherin and cancer metastasis. *Nat Cell Biol.* 2010;12:247-256
- Ma L, Zhang S, Du M.** Cordycepin from *Cordyceps militaris* prevents hyperglycemia in alloxan-induced diabetic mice. *Nutr Res.* 2015;35:431-439
- Machaca K.** Ca(2+) signaling, genes and the cell cycle. *Cell Calcium.* 2010;48:243-250
- Maes W, Verschuere T, Van Hoylandt A, Boon L, Van Gool S.** Depletion of regulatory T cells in a mouse experimental glioma model through Anti-CD25 treatment results in the infiltration of non-immunosuppressive myeloid cells in the brain. *Clin Dev Immunol.* 2013;2013:952469
- Mahoney DJ, Cheung HH, Mrad RL, Plenchette S, Simard C, Enwere E, Arora V, Mak TW, Lacasse EC, Waring J, Korneluk RG.** Both cIAP1 and cIAP2 regulate TNFalpha-mediated NF-kappaB activation. *Proc Natl Acad Sci USA.* 2008;105:11778-11783
- Majeski AE, Dice JF.** Mechanisms of chaperone-mediated autophagy. *Int J Biochem Cell Biol.* 2004;36:2435-2444
- Mallilankaraman K, Cárdenas C, Doonan PJ, Chandramoorthy HC, Irrinki KM, Golenár T, Csordás G, Madireddi P, Yang J, Müller M, Miller R, Kolesar JE, Molgó J, Kaufman B, Hajnóczky G, et al.** MCUR1 is an essential component of mitochondrial Ca²⁺ uptake that regulates cellular metabolism. *Nat Cell Biol.* 2012;14:1336-1343
- Manal M, Chandrasekar MJ, Gomathi Priya J, Nanjan MJ.** Inhibitors of histone deacetylase as antitumor agents: A critical review. *Bioorg Chem.* 2016;67:18-42
- Manini I, Caponnetto F, Bartolini A, Ius T, Mariuzzi L, Di Loreto C, Beltrami AP, Cesselli D.** Role of Microenvironment in Glioma Invasion: What We Learned from *In vitro* Models. *Rev Int J Mol Sci.* 2018;19:pii:E147

- Manjarrés IM, Rodríguez-García A, Alonso MT, García-Sancho J.** The sarco/endoplasmic reticulum Ca(2+) ATPase (SERCA) is the third element in capacitative calcium entry. *Cell Calcium*. 2010;47:412-418
- Mansour HH, Hafez HF, Fahmy NM.** Silymarin modulates cisplatin-induced oxidative stress and hepatotoxicity in rats. *J Biochem Mol Biol*. 2006;39:656-661
- Mansouri A, Ridgway LD, Korapati AL, Zhang Q, Tian L, Wang Y, Siddik ZH, Mills GB, Claret FX.** Sustained activation of JNK/p38 MAPK pathways in response to cisplatin leads to Fas ligand induction and cell death in ovarian carcinoma cells. *J Biol Chem*. 2003;278:19245-19256
- Marchesi F, Turriziani M, Tortorelli G, Avvisati G, Torino F, De Vecchis L.** Triazene compounds: mechanism of action and related DNA repair systems. *Rev Pharmacol Res Off J Ital Pharmacol Soc*. 2007;56:275-287
- Marchi S, Pinton P.** Alterations of calcium homeostasis in cancer cells. *Curr Opin Pharmacol*. 2016;29:1-6
- Mares V, Lisá V, Malík R, Kozáková H, Sedo A.** Cisplatin induced gamma-glutamyltransferase up-regulation, hypertrophy and differentiation in astrocytic glioma cells in culture. *Histol Histopathol*. 2003;18:687-693
- Margolin K, Ernstoff MS, Hamid O, Lawrence D, McDermott D, Puzanov I, Wolchok JD, Clark JI, Sznol M, Logan TF, Richards J, Michener T, Balogh A, Heller KN, Hodi FS.** Ipilimumab in patients with melanoma and brain metastases: An open-label, phase 2 trial. *Lancet Oncol*. 2012;13:459-465
- Marini AM, Strauss KI, Jacobowitz DM.** Calretinin-containing neurons in rat cerebellar granule cell cultures. *Brain Res Bull*. 1997;42:279-288
- Maris JM, Matthay KK.** Molecular biology of neuroblastoma. *J Clin Oncol*. 1999;17:2264-2279
- Maris JM, Hogarty MD, Bagatell R, Cohn SL.** Neuroblastoma. *Rev Lancet*. 2007;369:2106-2120
- Maris JM.** Recent Advances in Neuroblastoma. *Rev N Engl J Med*. 2010;362:2202-2211
- Markovic DS, Vinnakota K, Chirasani S, Synowitz M, Raguet H, Stock K, Sliwa M, Lehmann S, Kälin R, van Rooijen N, Holmbeck K, Heppner FL, Kiwit J, Matyash V, Lehnardt S, et al.** Gliomas induce and exploit microglial MT1-MMP expression for tumor expansion. *Proc Natl Acad Sci U S A*. 2009;106:012535

- Marks PA, Xu WS.** Histone deacetylase inhibitors: Potential in cancer therapy. *J Cell Biochem.* 2009;107:600-608
- Marmorstein R.** Structure of histone acetyltransferases. *J Mol Biol* 2001;311:433-444
- Martínez-Montemayor MM, Ling T, Suárez-Arroyo IJ, Ortiz-Soto G, Santiago-Negrón CL, Lacourt-Ventura MY, Valentín-Acevedo A, Lang WH, Rivas F.** Identification of Biologically Active *Ganoderma lucidum* Compounds and Synthesis of Improved Derivatives That Confer Anti-cancer Activities in vitro. *Front Pharmacol.* 2019;10:115
- Martins-Taylor K, Schroeder DI, LaSalle JM, Lalande M, Xu RH.** Role of DNMT3B in the regulation of early neural and neural crest specifiers. *Epigenetics.* 2012;7:71-82
- Marvaso G, Vischioni B, Jereczek-Fossa BA, Ciardo D, Fossati P, Giandini T, Morlino S, Carrara M, Romanelli P, Russi E, Valvo F, Valdagni R, Orecchia R.** Hadrontherapy from the Italian Radiation Oncologist point of view: face the reality. The Italian Society of Oncological Radiotherapy (AIRO) survey. *Radiol Med.* 2017;122:140-145
- Massaguer A, Gonzalez-Canto A, Escribano E, Barrabes S, Artigas G, Moreno V, Marchan V.** Integrin-targeted delivery into cancer cells of a Pt(IV) pro-drug through conjugation to RGD-containing peptides. *Dalton Trans.* 2015;44:202-212
- Masui K, Kato Y, Sawada T, Mischel PS, Shibata N.** Molecular and genetic determinants of glioma cell invasion. *Rev Int J Mol Sci.* 2017;18
- Maugeri R, Schiera G, Di Liegro CM, Fricano A, Iacopino DG, Di Liegro I.** Aquaporins and brain tumors. *Int J Mol Sci.* 2016;17:pii:E1029
- Mayanil CS.** Transcriptional and epigenetic regulation of neural crest induction during neurulation. *Dev Neurosci.* 2013;35:361-372
- Mazor T, Pankov A, Johnson BE, Hong C, Hamilton EG, Bell RJA, Smirnov IV, Reis GF, Phillips JJ, Barnes MJ, Idbaih A, Alentorn A, Kloezeman JJ, Lamfers MLM et al.** DNA methylation and somatic mutations converge on the cell cycle and define similar evolutionary histories in brain tumours. *Cancer Cell.* 2015;28:307-317
- McKay BC, Becerril C, Ljungman M.** P53 plays a protective role against UV- and cisplatin-induced apoptosis in transcription-coupled repair proficient fibroblasts. *Oncogene.* 2001;20:6805-6808

- McDonald AJ, Betette RL.** Parvalbumin-containing neurons in the rat basolateral amygdala: morphology and co-localization of Calbindin-D(28k). *Neuroscience*. 2001;102:413-425
- McNamara MG, Mason WP.** Antiangiogenic therapies in glioblastoma multiforme. *Expert Rev Anticancer Ther*. 2012;12:643-654
- Melguizo C, Prados J, González B, Ortiz R, Concha A, Alvarez PJ, Madeddu R, Perazzoli G, Oliver JA, López R, Rodríguez-Serrano F, Aránega A.** MGMT promoter methylation status and MGMT and CD133 immunohistochemical expression as prognostic markers in glioblastoma patients treated with temozolomide plus radiotherapy. *J Transl Med*. 2012;10:250
- Menke K, Schwermer M, Felenda J, Beckmann C, Stintzing F, Schramm A, Zuzak TJ.** Taraxacum officinale extract shows antitumor effects on pediatric cancer cells and enhance mistletoe therapy. *Complement Ther Med*. 2018;40:158-164
- Metcalf D., Isaacs AM.** The role of ESCRT proteins in fusion events involving lysosomes, endosomes and autophagosomes. *Biochem Soc Trans*. 2010;38:1469-1473
- Michalke B.** Platinum speciation used for elucidating activation or inhibition of Pt-containing anti-cancer drugs. *J Trace Elem Med Biol*. 2010;24:69-77
- Mignen O, Constantin B, Potier-Cartereau M, Penna A, Gautier M, Guéguinou M, Renaudineau Y, Shoji KF, Félix R, Bayet E, Buscaglia P, Debant M, Chantôme A, Vandier C.** Constitutive calcium entry and cancer: updated views and insights. *Eur Biophys J*. 2017;46:395-413
- Mihaly SR, Ninomiya-Tsuji J, Morioka S.** TAK1 control of cell death. *Cell Death Differ*. 2014;21:1667-1676
- Mikawa T, Leonart ME, Takaori-Kondo A, Inagaki N, Yokode M, Kondoh H.** Dysregulated glycolysis as an oncogenic event. *Cell Mol Life Sci*. 2015;72:1881-1892
- Miller RP, Tadagavadi RK, Ramesh G, Reeves WB.** Mechanism of cisplatin nephrotoxicity. *Toxins*. 2010;2:2490-2518
- Minucci S, Pelicci PG.** Histone deacetylase inhibitors and the promise of epigenetic (and more) treatments for cancer. *Nat Rev Cancer*. 2006;6:38-51
- Mirandola A, Molinelli S, Vilches Freixas G, Mairani A, Gallio E, Panizza D, Russo S, Ciocca M, Donetti M, Magro G, Giordanengo S, Orecchia R.** Dosimetric commissioning and quality assurance of scanned ion beams at the Italian National Center for Oncological Hadrontherapy. *Med Phys*. 2015;42:5287-5300

- Mizushima N, Levine B, Cuervo AM, Klionsky DJ.** Autophagy fights disease through cellular self digestion. *Nature*. 2008;451:1069-1075
- Modak S, Cheung NK.** Neuroblastoma: Therapeutic strategies for a clinical enigma. *Cancer Treat Rev*. 2010;36:307-317
- Modjtahedi N, Giordanetto F, Madeo F, Kroemer G.** Apoptosis-inducing factor: vital and lethal. *Trends Cell Biol*. 2006;16:264-272
- Mohamadi N, Kazemi SM, Mohammadian M, Toofani Milani A, Moradi Y, Yasemi M, Ebrahimi far M, Mazloumi Tabrizi M, Ebrahimi Shahmabadi H, Akbarzadeh Khiyavi A.** Toxicity of cisplatin-loaded poly butyl cyanoacrylate nanoparticles in a brain cancer cell line: anionic polymerization results. *Asian Pac J Cancer Prev*. 2017;18:629-632
- Molenaar RJ.** Ion Channels in Glioblastoma. *ISRN Neurology*. 2011;2011:590249
- Moncharmont C, Auberdiac P, Mélis A, Afqir S, Pacaut C, Chargari C, Merrouche Y, Magné N.** Cisplatin or carboplatin, that is the question. *Bull Cancer*. 2011;98:164-175
- Monclair T, Brodeur GM, Ambros PF, Brisse HJ, Cecchetto G, Holmes K, Kaneko M, London WB, Matthay KK, Nuchtern JG, von Schweinitz D, Simon T, Cohn SL, Pearson AD; INRG Task Force.** The International Neuroblastoma Risk Group (INRG) staging system: an INRG Task Force report. *J Clin Oncol*. 2009;27:298-303
- Montana V, Sontheimer H.** Bradykinin promotes the chemotactic invasion of primary brain tumors. *J Neurosci*. 2011;31:4858-4867
- Montell C.** The TRP superfamily of cation channels. *Sci STKE*. 2005;2005:re3
- Morciano G, Marchi S, Morganti C, Sbrano L, Bittremieux M, Kerkhofs M, Corricelli M, Danese A, Karkucinska-Wieckowska A, Wieckowski MR, Bultynck G, Giorgi C, Pinton P.** Role of mitochondria-associated ER membranes in calcium regulation in cancer-specific settings. *Neoplasia*. 2018;20:510-523
- Moreno L, Marshall V, Pearson ADJ.** At the frontier of progress of pediatric oncology: the neuroblastoma paradigm. *Br Med Bull*. 2013;108: 173-188
- Moreno-Smith M, Halder JB, Meltzer PS, Gonda TA, Mangala LS, Rupaimoole R, Lu C, Nagaraja AS, Gharpure KM, Kang Y, Rodriguez-Aguayo C, Vivas-Mejia PE, Zand B, Schmandt R, Wang H, et al.** ATP11B mediates platinum resistance in ovarian cancer. *J Clin Invest*. 2018;128:3199

- Mori M, Konno T, Morii T, Nagayama K, Imoto K.** Regulatory interaction of sodium channel IQ-motif with calmodulin C-terminal lobe. *Biochem Biophys Res Commun.* 2003;307:290-296
- Mori M, Tanifuji S, Mochida S.** Kinetic organization of Ca²⁺ signals that regulate synaptic release efficacy in sympathetic neurons. *Mol Pharmacol.* 2014;86:297-305
- Morris SW, Kirstein MN, Valentine MB, Dittmer KG, Shapiro DN, Saltman DL, Look AT.** Fusion of a kinase gene, ALK, to a nucleolar protein gene, NPM, in non-Hodgkin's lymphoma. *Science.* 1994;263:1281-1284
- Moscat J, Diaz-Meco MT, Albert A, Campuzano S.** Cell signaling and function organized by PB1 domain interactions. *Mol Cell.* 2006;23:631-640
- Mosse YP, Laudenslager M, Khazi D, Carlisle AJ, Winter CL, Rappaport E, Maris JM.** Germline PHOX2B mutation in hereditary neuroblastoma. *Am J Hum Genet.* 2004;75:727-730
- Mossé YP, Laudenslager M, Longo L, Cole KA, Wood A, Attiyeh EF, Laquaglia MJ, Sennett R, Lynch JE, Perri P, Laureys G, Speleman F, Kim C, Hou C, Hakonarson H, et al.** Identification of ALK as a major familial neuroblastoma predisposition gene. *Nature.* 2008;455:930-935
- Mostowy S, Sancho-Shimizu V, Hamon MA, Simeone R, Brosch R, Johansen T, Cossart P.** p62 and NDP52 proteins target intracytosolic Shigella and Listeria to different autophagy pathways. *J Biol Chem.* 2011;286:26987-26995
- Moulin M, Anderton H, Voss AK, Thomas T, Wong WWL, Bankovacki A, Feltham R, Chau D, Cook WD, Silke J, Vaux DL.** IAPs limit activation of RIP kinases by TNF receptor 1 during development. *The EMBO J.* 2012;31:1679-1691
- Munshi A, Kurland JF, Nishikawa T, Tanaka T, Hobbs ML, Tucker SL, Ismail S, Stevens C, Meyn RE.** Histone deacetylase inhibitors radiosensitize human melanoma cells by suppressing DNA repair activity. *Clin Cancer Res.* 2005;11:4912-4922
- Munoz JL, Rodriguez-Cruz V, Greco SJ, Nagula V, Scotto KW.** Temozolomide induces the production of epidermal growth factor to regulate MDR1 expression in glioblastoma cells. *Mol Cancer Ther* 2014;13:2399-2411
- Murphy M, Czabotar PE, Hildebrand JM, Lucet IS, Zhang JG, Alvarez-Diaz S, Lewis R, Lalaoui N, Metcalf D, Webb AI, Young SN, Varghese LN, Tannahill GM, Hatchell EC, Majewski IJ, et al.** The pseudokinase MLKL mediates necroptosis via molecular switch mechanism. *Immunity.* 2013;39:443-453

- Muscella A, Calabriso N, De Pascali SA, Urso L, Ciccicarese A, Fanizzi FP, Migoni D, Marsigliante S.** New platinum(II) complexes containing both an O,O'-chelated acetylacetonate ligand and a sulfur ligand in the platinum coordination sphere induce apoptosis in HeLa cervical carcinoma cells. *Biochem Pharmacol.* 2007;74:28-40
- Muscella A, Calabriso N, Fanizzi FP, De Pascali SA, Urso L, Ciccicarese A, Migoni D, Marsigliante S.** [Pt, (O,O'-acac)(γ -acac)(DMS)], a new Pt compound exerting fast cytotoxicity in MCF-7 breast cancer cells via the mitochondrial apoptotic pathway. *Br J Pharmacol.* 2008;153:34-49
- Muscella A, Calabriso N, Vetrugno C, Fanizzi FP, De Pascali SA, Storelli C, Marsigliante S.** The platinum (II) complex [Pt(O,O'-acac)(γ -acac)(DMS)] alters the intracellular calcium homeostasis in MCF-7 breast cancer cells. *Biochem Pharmacol.* 2011;81:91-103
- Muscella A, Calabriso N, Vetrugno C, Urso L, Fanizzi FP, De Pascali SA, Marsigliante S.** Sublethal concentrations of the platinum(II) complex [Pt(O,O'-acac)(γ -acac)(DMS)] alter the motility and induce anoikis in MCF-7 cells. *Br J Pharmacol.* 2010;60:1362-1377
- Muscella A, Vetrugno C, Migoni D, Biagioni F, Fanizzi FP, Fornai F, De Pascali SA, Marsigliante S.** Antitumor activity of [Pt(O,O'-acac)(γ -acac)(DMS)] in mouse xenograft model of breast cancer. *Cell Death Dis.* 2014;5:e1014
- Mutlu H, Akca Z, Erden A, Aslan T, Ucar K, Kaplan B, Buyukcelik A.** Lack of sunlight exposure influence on primary glioblastoma survival. *Asian Pac J Cancer Prev.* 2014;15:4165-4168
- Nagata S.** Apoptotic DNA fragmentation. *Exp Cell Res.* 2000;256:12-18
- Nagatogawa H, Ichimura Y, Ohsumi Y.** Atg8, a ubiquitin-like protein required for autophagosome formation, mediates membrane tethering and hemifusion. *Cell.* 2007;130:165-178
- Natsume A, Yoshida J.** Gene therapy for high-grade glioma: current approaches and future directions. *Cell Adh Migr.* 2008;2:186-191
- Najafov A, Chen H, Yuan J.** Necroptosis and Cancer. *Trends Cancer.* 2017;3:294-301
- Nedergaard M, Rodríguez JJ, Verkhratsky A.** Glial calcium and diseases of the nervous system. *Rev Cell Calcium.* 2010;47:140-149
- Negrini S, Gorgoulis VG, Halazonetis TD.** Genomic instability-an evolving hallmark of cancer. *Nat Rev Mol Cell Biol.* 2010;11:220-228

- Neuwelt EA, Bauer B, Fahlke C, Fricker G, Iadecola C, Janigro D, Leybaert L, Molnar Z, O'Donnell ME, Povlishock JT.** Engaging neuroscience to advance translational research in brain barrier biology. *Nat Rev Neurosci.* 2011;12:169-182
- Nikolova T, Kiweler N2, Krämer OH.** Interstrand Crosslink Repair as a Target for HDAC Inhibition. *Trends Pharmacol Sci.* 2017;38:822-836
- Nixon RA.** The role of autophagy in neurodegenerative disease. *Nat Med.* 2013;19:983-997
- Noda S, Yoshimura S, Sawada M, Naganawa T, Iwama T, Nakashima S, Sakai N.** Role of ceramide during cisplatin-induced apoptosis in C6 glioma cells. *J Neurooncol.* 200;52:11-21
- Norberg E, Gogvadze V, Vakifahmetoglu H, Orrenius S, Zhivotovsky B.** Oxidative modification sensitizes mitochondrial apoptosis-inducing factor to calpain-mediated processing. *Free Radic Biol Med.* 2010;48:791-797
- Norden AD, Drappatz J, Wen PY.** Antiangiogenic therapies for high-grade glioma. *Nat Rev Neurol.* 2009;5:610-620
- Novohradsky V, Zanellato I, Marzano C, Pracharova J, Kasparkova J, Gibson D, Gandin V, Osella D, Brabec V.** Epigenetic and antitumor effects of platinum(IV)-octanoato conjugates. *Sci Rep.* 2017;7:3751
- Núñez R, Sancho-Martínez SM, Novoa JM, López-Hernández FJ.** Apoptotic volume decrease as a geometric determinant for cell dismantling into apoptotic bodies. *Cell Death Differ.* 2010;17:1665-1671
- O'Neill KL, Huang K, Zhang J, Chen Y, Luo X.** Inactivation of prosurvival Bcl-2 proteins activates Bax/Bak through the outer mitochondrial membrane. *Genes Dev.* 2016;30:973-988
- Oakes SA, Scorrano L, Opferman JT, Bassik MC, Nishino M, Pozzan T, Korsmeyer SJ.** Proapoptotic BAX and BAK regulate the type 1 inositol trisphosphate receptor and calcium leak from the endoplasmic reticulum. *Proc Natl Acad Sci U S A.* 2005;102:105-110
- Oehme I, Deubzer HE, Lodrini M, Milde T, Witt O.** Targeting of HDAC8 and investigational inhibitors in neuroblastoma. *Expert Opin Investig Drugs.* 2009;18:1605-1617
- Oh GS, Kim HJ, Shen A, Lee SB, Khadka D, Pandit A, So HS.** Cisplatin-induced kidney dysfunction and perspective of improving treatment strategies. *Electrolyte Blood Press.* 2014;12:55-65

- Ohnishi T, Matsumura H, Izumoto S, Hiraga S, Hayakawa T.** A novel model of glioma cell invasion using organotypic brain slice culture. *Cancer Res.* 1998;58:2935-2940
- Ohno T.** Particle radiotherapy with carbon ion beams. *EPMA J.* 2013;4:9
- Okada M, Miyake K, Tamiya T.** Glioblastoma treatment in the elderly. *Neurol Med Chir.* 2017;57:667-676
- Okunade GW, Miller ML, Pyne GJ, Sutliff RL, O'Connor KT, Neumann JC, Andringa A, Miller DA, Prasad V, Doetschman T, Paul RJ, Shull GE.** Targeted ablation of plasma membrane Ca²⁺-ATPase (PMCA) 1 and 4 indicates a major housekeeping function for PMCA1 and a critical role in hyperactivated sperm motility and male fertility for PMCA4. *J Biol Chem.* 2004;279:33742-33750
- Olsen ML, Sontheimer H.** Mislocalization of Kir channels in malignant glia. *Glia.* 2004;46:63-73
- Onishi M, Ichikawa T, Kurozumi K, Date I.** Angiogenesis and invasion in glioma. *Rev Brain Tumor Pathol.* 2011;28:13-24
- Ono Y, Nonomura N, Harada Y, Fukui T, Tokizane T, Sato E, Nakayama M, Nishimura K, Takahara S, Okuyama A.** Loss of p73 induction in a cisplatin-resistant bladder cancer cell line. *Mol Urol.* 2001;5:25-30
- Øra I, Eggert A.** Progress in treatment and risk stratification of neuroblastoma: impact on future clinical and basic research. *Rev Semin Cancer Biol.* 2011;21:217-228
- Osswald M, Solecki G, Wick W, Winkler F.** A malignant cellular network in gliomas: potential clinical implications. *Neuro Oncol.* 2016;18:479-485
- Otey CA, Boukhelifa M, Maness P.** B35 neuroblastoma cells: an easily transfected, cultured cell model of Central Nervous System Neurons. *Methods Cell Biol.* 2003;71:287-304
- Ovadje P, Ammar S, Guerrero JA, Arnason JT, Pandey S.** Dandelion root extract affects colorectal cancer proliferation and survival through the activation of multiple death signalling pathways. *Oncotarget.* 2016;7:73080-73100
- Owens C, Irwin M.** Neuroblastoma: the impact of biology and cooperation leading to personalized treatments. *Crit Rev Clin Lab Sci.* 2012;49:85-115
- Pabla N, Dong B.** Cisplatin nephrotoxicity: mechanism and renoprotective strategies. *Kidney Int.* 2008;73:994-1007

- Pajtler KW, Mack SC, Ramaswamy V, Smith CA, Witt H, Smith A, Hansford JR, von Hoff K, Wright KD, Hwang E, Frappaz D, Kanemura Y, Massimino M, Faure-Contier C, Modena P, Tabori U, Warren KE, et al.** The current consensus on the clinical management of intracranial ependymoma and its distinct molecular variants. *Acta Neuropathol.* 2017;133:5-12
- Pacher P, Beckman JS, Liaudet L.** Nitric oxide and peroxynitrite in health and disease. *Physiol Rev.* 2007;87:315-424
- Paoli P, Giannoni E, Chiarugi P.** Anoikis molecular pathways and its role in cancer progression. *Biochim Biophys Acta.* 2013;1833:3481-3498
- Park HH.** Caspase recruitment domains for protein interactions in cellular signaling (Review). *Int J Mol Med.* 2019;43:1119-1127
- Park JR, Eggert A, Caron H.** Neuroblastoma: biology, prognosis, and treatment. *Rev Hematol Oncol Clin North Am.* 2010;24:65-86
- Park JR, Bagatell R, London WB, Maris JM, Cohn SL, Mattay KK, Hogarty M; COG Neuroblastoma Committee.** Children's Oncology Group's 2013 blueprint for research: Neuroblastoma. *Pediatr Blood Cancer.* 2013;60:985-993
- Park SB, Goldstein D, Krishnan AV, Lin CS, Friedlander ML, Cassidy J, Koltzenburg M, Kiernan MC.** Chemotherapy induced peripheral neurotoxicity: a critical analysis. *CA Cancer J Clin.* 2013;63:419-437
- Parkash J, Asotra K.** Calcium wave signaling in cancer cells. *Life Sci.* 2010;87:587-595
- Parrish AB, Freel CD, Kornbluth S.** Cellular mechanisms controlling caspase activation and function. *Cold Spring Harb Perspect Biol* 2013;5
- Parsons DW, Jones S, Zhang X, Lin JC, Leary RJ, Angenendt P, Mankoo P, Carter H, Siu IM, Gallia GL, Olivi A, McLendon R, Rasheed BA, Keir S, Nikolskaya T, et al.** An integrated genomic analysis of human glioblastoma multiforme. *Science.* 2008;321:1807-1812
- Pasparakis M, Vandenabeele P.** Necroptosis and its role in inflammation. *Nature.* 2015;517:331-320
- Patanè S.** Cardiotoxicity: Cisplatin and long-term cancer survivors. *Int J Cardiol.* 2014;175:201-202
- Patel M, Kim J, Ruzevick J, Li G, Lim M.** The future of glioblastoma therapy: synergism of standard of care and immunotherapy. *Cancers.* 2014;6:1953-1985

- Paterson RR.** Ganoderma - a therapeutic fungal biofactory. *Phytochemistry*. 2006;67
- Pei D, Luther W, Wang W, Paw BH, Stewart RA, George RE.** Distinct neuroblastoma associated alterations of PHOX2B impair sympathetic neural differentiation in zebrafish models. *Plos Genet*. 2013;9:e1003533
- Perazzoli G, Prados J, Ortiz R, Caba O, Cabeza L, Berdasco M, González B, Melguizo C.** Temozolomide resistance in Glioblastoma cell lines: implication of MGMT, MMR, P-Glycoprotein and CD133 expression. *PLoS One*. 2015;10:e0140131
- Perez RP.** Cellular and molecular determinants of cisplatin resistance. *Eur J Cancer*. 1999;34:1535-1544.
- Persechini A, Stemmer PM.** Calmodulin is a limiting factor in the cell. *Rev Trends Cardiovasc Med*. 2002;12:32-37
- Persons DL, Yazlovitskaya EM, Pelling JC.** Effect of extracellular signal-regulated kinase on p53 accumulation in response to cisplatin. *J Biol Chem*. 2000;275:35778-35785
- Piccolini VM, Bottone MG, Bottiroli G, De Pascali SA, Fanizzi FP, Bernocchi G.** Platinum drugs and neurotoxicity: effects on intracellular calcium homeostasis. *Cell Biol Toxicol*. 2013;29:339-353
- Piccolini VM, Esposito A, Dal Bo V, Insolia V, Bottone MG, De Pascali SA, Fanizzi FP, Bernocchi G.** Cerebellum neurotransmission during postnatal development: [Pt(O,O'-acac)(γ -acac)(DMS)] vs cisplatin and neurotoxicity. *Int J Dev Neurosci*. 2015;40:24-34
- Pichler V, Mayr J, Heffeter P, Domotor O, Enyedy EA, Hermann G, Groza D, Kollensperger G, Galanksi M, Berger W, Keppler BK, Kowol CR.** Maleimide-functionalised platinum(IV) complexes as a synthetic platform for targeted drug delivery. *Chem Commun*. 2013;49:2249-2251
- Pignatelli B, Duran M.** Overcoming resistance of cancer stem cells. *Lancet Oncol*. 2012;13:187-188
- Plogmann D, Celio MR.** Intracellular concentration of parvalbumin in nerve cells. *Brain Res*. 1993;600:273-279
- Poff A, Koutnik AP, Egan KM, Sahebjam S, D'Agostino D, Kumar NB.** Targeting the Warburg effect for cancer treatment: Ketogenic diets for management of glioma. *Semin Cancer Biol*. 2019;56:135-148

- Pohl A, Erichsen M, Stehr M, Hubertus J, Bergmann F, Kammer B, von Schweinitz D.** Image-defined Risk Factors Correlate with Surgical Radicality and Local Recurrence in Patients with Neuroblastoma. *Klin Padiatr.* 2016;228:118-123
- Ponten J.** Properties of human malignant glioma cells *in vitro*. *Med Biology.* 1978;56:184-193
- Prasad M, Naik ST.** Management of root rot and heart rot of *Acacia mangium* Willd. *Karnataka Journal of Agricultural Sciences.* 2002;15:321-326
- Prasad MS, Sauka-Spengler T, Labonne C.** Induction of the neural crest state: control of stem cell attributes by gene regulatory, post transcriptional and epigenetic interactions. *Dev Biol.* 2012;366:10-21
- Puri P, Chandra A.** Autophagy modulation as a potential therapeutic target for liver diseases. *J Clin Exp Hepatol.* 2014;4:51-59
- Purkayastha A, Sharma N, Sridhar MS, Abhishek D.** Intramedullary Glioblastoma multiforme of Spine with intracranial supratentorial metastasis: progressive disease with a multifocal picture. *Asian J Neurosurg.* 2018;13:1209-1212
- Purow B, Schiff D.** Advances in the genetics of glioblastoma: are we reaching critical mass *Nat Rev Neurol.* 2009;5:419-426
- Quan W, Lee MS.** Role of autophagy in the control of body metabolism. *Endocrinol Metab.* 2013;28:6-11
- Qiang L, Yang Y, Ma YJ, Chen FH, Zhang LB, Liu W, Qi Q, Lu N, Tao L, Wang XT, You QD, Guo QL.** Isolation and characterization of cancer stem like cells in human glioblastoma cell lines. *Cancer Lett.* 2009;279:13-21
- Qiu YY, Mirkin BL, Dwivedi RS.** Inhibition of DNA methyltransferase reverses cisplatin induced drug resistance in murine neuroblastoma cells. *Elsevier.* 2005;29:456-463
- Qu L, Li S, Zhuo Y, Chen J, Qin X, Guo G.** Anticancer effect of triterpenes from *Ganoderma lucidum* in human prostate cancer cells. *Oncology letters.* 2017;14:7467-7472
- Rangone B, Ferrari B, Astesana V, Masiello I, Veneroni P, Zanellato I, Osella D, Bottone MG.** A new platinum-based prodrug candidate: Its anticancer effects in B50 neuroblastoma rat cells. *Life Sci.* 2018;210:166-176.
- Ransom CB, Sontheimer H.** BK channels in human glioma cells. *J Neurophysiol* 2001;85:790-803

- Rasmussen BK, Hansen S, Laursen RJ, Kosteljanetz M, Schultz H, Nørgård BM, Guldborg R, Gradel KO.** Epidemiology of glioma: clinical characteristics, symptoms, and predictors of glioma patients grade I-IV in the Danish Neuro-Oncology Registry. *J Neurooncol.* 2017;135:571-579
- Ratajczak MZ, Zuba-Surma E, Kucia M, Reza R, Wojakowski W, Ratajczak J.** The pleiotropic effects of the SDF-1-CXCR4 axis in organogenesis, regeneration and tumorigenesis. *Leukemia.* 2006;20:1915-1924
- Ratto D, Corana F, Mannucci B, Priori EC, Cobelli F, Roda E, Ferrari B, Occhinegro A, Di Iorio C, De Luca F, Cesaroni V, Girometta C, Bottone MG, Savino E, Kawagishi H et al.** Hericium erinaceus Improves Recognition Memory and Induces Hippocampal and Cerebellar Neurogenesis in Frail Mice during Aging. *Nutrients.* 2019;11:pii:E715.
- Raveendran R, Braude JP, Wexselblatt E, Novohradsky V, Stuchlikova O, Brabec V, Gandin V, Gibson D.** Pt(IV) derivatives of cisplatin and oxaliplatin with phenylbutyrate axial ligands are potent cytotoxic agents that act by several mechanisms of action. *Chem Sci.* 2016;7:2381-2391
- Ravera M, Gabano E, Zanellato I, Bonarrigo I, Alessio M, Arnesano F, Galliani A, Natile G, Osella D.** Cellular trafficking, accumulation and DNA platination of a series of cisplatin-based dicarboxylato Pt(IV) prodrugs. *J Inorg Biochem.* 2015;150:1-8
- Ravera M, Gabano E, Zanellato I, Bonarrigo I, Escribano E, Moreno V, Font-Bardia M, Calvet T, Osella D.** Synthesis, characterization and antiproliferative activity on mesothelioma cell lines of bis(carboxylato)platinum(IV) complexes based on picoplatin. *Dalton Trans.* 2012;41:3313-3320
- Ravikumar B, Sarkar S, Davies JE, Futter M, Garcia-Arencibia M, Green-Thompson ZW, Jimenez-Sanchez M, Korolchuk VI, Lichtenberg M, Luo S, Massey DC, Menzies FM, Moreau K, Narayanan U, Renna M, Siddiqi FH, et al.** Regulation of mammalian autophagy in physiology and pathophysiology. *Physiol Rev.* 2010;90:1383-1435
- Rayavarapu RR, Heiden B, Pagani N, Shaw MM, Shuff S, Zhang S, Schafer ZT.** The role of multicellular aggregation in the survival of ErbB2-positive breast cancer cells during extracellular matrix detachment. *J Biol Chem.* 2015;290:8722-8733
- Razavi SM, Lee KE, Jin BE, Aujla PS, Gholamin S, Li G.** Immune Evasion Strategies of Glioblastoma. *Front Surg.* 2016;3:11
- Reardon DA, Wen PY.** Therapeutic advances in the treatment of glioblastoma: rationale and potential role of targeted agents. *Rev Oncologist.* 2006;11:152-164

- Reboulleau CP.** Inositol metabolism during neuroblastoma B50 cell differentiation: Effects of differentiating agents on inositol uptake. *J Neurochem.* 1990;55:641-650
- Reifenberger G, Wirsching HG, Knobbe-Thomsen CB, Weller M.** Advances in the molecular genetics of gliomas - implications for classification and therapy. *Nat Rev Clin Oncol.* 2017;14:434-452
- Ren D, Tu HC, Kim H, Wang GX, Bean GR, Takeuchi O, Jeffers JR, Zambetti GP, Hsieh JJ, Cheng EH.** BID, BIM, and PUMA are essential for activation of the BAX- and BAK-dependent cell death program. *Science.* 2010;330:1390-1393
- Résibois A, Rogers JH.** Calretinin in rat brain: an immunohistochemical study. *Neuroscience.* 1992;46:101-134
- Riedl SJ, Salvesen GS.** The apoptosome: signalling platform of cell death. *Nat Rev Mol Cell Biol.* 2007;8:405-413
- Rieken S, Habermehl D, Wuerth L, Brons S, Mohr A, Lindel K, Weber K, Haberer T, Debus J, Combs SE.** Carbon ion irradiation inhibits glioma cell migration through downregulation of integrin expression. *Int J Radiat Oncol Biol Phys.* 2012;83:394-399
- Riemenschneider MJ, Hegi ME, Reifenberger G.** MGMT promoter methylation in malignant gliomas. *Target Oncol.* 2010;5:161-165
- Rimessi A, Coletto L, Pinton P, Rizzuto R, Brini M, Carafoli E.** Inhibitory interaction of the 14-3-3{epsilon} protein with isoform 4 of the plasma membrane Ca(2+)-ATPase pump. *J Biol Chem.* 2005;280:37195-37203
- Rizzuto R, De Stefani D, Raffaello A, Mammucari C.** Mitochondria as sensors and regulators of calcium signalling. *Nat Rev Mol Cell Biol.* 2012;13:566-578
- Robert C, Long GV, Brady B, Dutriaux C, Maio M, Mortier L, Hassel JC, Rutkowski P, McNeil C, Kalinka-Warzocha E, Savage KJ, Hernberg MM, Lebbé C, Charles J, Mihalciou C, et al.** Nivolumab in previously untreated melanoma without BRAF mutation. *N Engl J Med.* 2015;372:320-330
- Robert C, Ribas A, Wolchok JD, Hodi FS, Hamid O, Kefford R, Weber JS, Joshua AM, Hwu WJ, Gangadhar TC, Patnaik A, Dronca R, Zarour H, Joseph RW, Boasberg P, et al.** Anti-programmed-death-receptor-1 treatment with pembrolizumab in ipilimumab-refractory advanced melanoma: a randomised dose-comparison cohort of a phase 1 trial. *Lancet.* 2014;384:1109-1117

- Roberts-Thomson SJ, Curry MC, Monteith GR.** Plasma membrane calcium pumps and their emerging roles in cancer. *World J Biol Chem.* 2010;1:248-253
- Rocha CRR, Silva MM, Quinet A, Cabral-Neto JB, Menck CFM.** DNA repair pathways and cisplatin resistance: an intimate relationship. *Clinics.* 2018;73:e478s
- Rolle K.** miRNA Multiplayers in glioma. From bench to bedside. *Acta Biochim Pol.* 2015;62:353-365
- Romanov J, Walczak M, Ibiricu I, Schüchner S, Ogris E, Kraft C, Martens S.** Mechanism and functions of membrane binding by the Atg5-Atg12/ Atg16 complex during autophagosome formation. *EMBO J.* 2012;31:4304-4317
- Roos A, Ding Z, Loftus JC, Tran NL.** Molecular and microenvironmental determinants of glioma stem-like cell survival and invasion. *Front Oncol.* 2017;7:120
- Rosato RR and Grant S.** Histone deacetylase inhibitors: insights into mechanisms of lethality. *Expert Opin Ther Targets.* 2005;9:809-824
- Rosenberg B, Vancamp L, Krigas T.** Inhibition of cell division in *Escherichia coli* by electrolysis products of platinum electrode. *Nature.* 1965;205:698-699
- Rossi S.** The National Centre for Oncological Hadrontherapy (CNAO): Status and perspectives. *Phys Med.* 2015;31:333-351
- Rossi P, Buonocore D, Altobelli E, Brandalise F, Cesaroni V, Iozzi D, Savino E, Marzatico F.** Improving training condition assessment in endurance cyclists: effects of *Ganoderma lucidum* and *Ophiocordyceps sinensis* dietary supplementation. *Evid Based Complement Alternat Med.* 2014;2014:979613.
- Rossi P, Cesaroni V, Brandalise F, Occhinegro A, Ratto D, Perrucci F, Lanaia V, Girometta C, Orrù G, Savino E.** Dietary Supplementation of Lion's Mane Medicinal Mushroom, *Heridium erinaceus* (Agaricomycetes), and Spatial Memory in Wild-Type Mice. *Int J Med Mushrooms.* 2018;20:485-494
- Roth P, Preusser M, Weller M.** Immunotherapy of Brain Cancer. *Oncol Res Treat.* 2016;39:326-334
- Roy S, Kar M, Roy S, Saha A, Padhi S, Banerjee B.** Role of β -catenin in cisplatin resistance, relapse and prognosis of head and neck squamous cell carcinoma. *Cell Oncol.* 2017;41:185-200
- Rubinsztein DC, Shpilka T, Elazar Z.** Mechanisms of autophagosome biogenesis. *Curr Biol.* 2012;22:29-34

- Russell RC, Tian Y, Yuan H, Park HW, Chang YY, Kim J, Kim H, Neufeld TP, Dillin A, Guan KL.** ULK1 induces autophagy by phosphorylating Beclin-1 and activating VPS34 lipid kinase. *Nat Cell Biol.* 2013;15:741-750
- Sabharwal SS, Schumacker PT.** Mitochondrial ROS in cancer: initiators, amplifiers or an Achilles' heel? *Nat Rev Cancer.* 2014;14:709-721
- Sagnè C, Agulhon C, Ravassard P, Darmon M, Hamon M, El Mestikawy S, Gasnier B, Giros B.** Identification and characterization of a lysosomal transporter for small neutral amino acids. *Pro Natl Acad Sci USA.* 2001;98:7206-7211
- Sahu R, Kaushik S, Clement CC, Cannizzo ES, Scharf B, Follenzi A, Potolicchio I, Nieves E, Cuervo AM, Santambrogio L.** Microautophagy of cytosolic proteins by late endosomes. *Dev Cell.* 2011;20:131-139
- Sakahira H, Enari M, Nagata S.** Cleavage of CAD inhibitor in CAD activation and DNA degradation during apoptosis. *Nature.* 2015;526:728
- Salkoff L, Butler A, Ferreira G, Santi C, Wei A.** High-conductance potassium channels of the SLO family. *Nat Rev Neurosci.* 2006;7:921-931
- Salazar BM, Balczewski EA, Ung CY, Zhu S.** Neuroblastoma, a paradigm for big data science in pediatric oncology. *Int J Mol Sci.* 2016;18
- Samberkar S, Gandhi S, Naidu M, Wong KH, Raman J, Sabaratnam V.** Lion's Mane, *Herichium erinaceus* and Tiger Milk, *Lignosus rhinocerotis* (Higher Basidiomycetes) Medicinal Mush-rooms Stimulate Neurite Outgrowth in Dissociated Cells of Brain, Spinal Cord, and Retina: An In Vitro Study. *Int J Med Mushrooms.* 2015;17:1047-1054
- Sancho-Martínez SM, Prieto-García L, Prieto M, López-Novoa JM, López-Hernández FJ.** Subcellular targets of cisplatin cytotoxicity: an integrated view. *Pharmacol Ther.* 2012;136:35-55
- Sanodiya BS, Thakur GS, Baghel RK, Prasad GB, Bisen PS.** *Ganoderma lucidum*: a potent pharmacological macrofungus. *Curr Pharm Biotechnol.* 2009;10:717-742
- Santin G, Piccolini VM, Barni S, Veneroni P, Giansanti V, Dal Bo V, Bernocchi G, Bottone MG.** Mitochondrial fusion: a mechanism of cisplatin-induced resistance in neuroblastoma cells? *Neurotoxicology.* 2013;34:51-60
- Santin G, Piccolini VM, Veneroni P, Barni S, Bernocchi G, Bottone MG.** Different patterns of apoptosis in response to cisplatin in B50 neuroblastoma rat cells. *Histol Histopathol.* 2011;26:831-842

- Santin G, Scietti L, Veneroni P, Barni S, Bernocchi G, Bottone MG.** Effects of Cisplatin in neuroblastoma rat cells: damage to cellular organelles. *Int J Cell Biol.* 2012;2012:424072
- Santos JG, Da Cruz WMS, Schönthal AH, Salazar MD, Fontes CAP, Quirico-Santos T, Da Fonseca CO.** Efficacy of a ketogenic diet with concomitant intranasal perillyl alcohol as a novel strategy for the therapy of recurrent glioblastoma. *Oncol Lett.* 2018;15:1263-1270
- Sanz-Blasco S, Valero RA, Rodríguez-Crespo I, Villalobos C, Núñez L.** Mitochondrial Ca²⁺ overload underlies Abeta oligomers neurotoxicity providing an unexpected mechanism of neuroprotection by NSAIDs. *PLoS One.* 2008;3:2718
- Sasmitha AO, Wong YP, Ling APK.** Biomarkers and therapeutic advances in glioblastoma. *Asia Pac J Clin Oncol.* 2018;14:40-51
- Sattler T, Mayer A.** Cell-Free Reconstitution of Microautophagic Vacuole Invagination and Vesicle Formation. *J Cell Biol.* 2000;151:529-538
- Schatzmann HJ.** ATP-dependent Ca⁺⁺-extrusion from human red cells. *Experientia.* 1966;22:364-365
- Schiffmann SN, Cheron G, Lohof A, d'Alcantara P, Meyer M, Parmentier M, Schurmans S.** Impaired motor coordination and Purkinje cell excitability in mice lacking calretinin. *Proc Natl Acad Sci USA.* 1999;96:5257-5262
- Schläger C, Körner H, Krueger M, Vidoli S, Haberl M, Mielke D, Brylla E, Issekutz T, Cabañas C, Nelson PJ, Ziemssen T, Rohde V, Bechmann I, Lodygin D, Odoardi F, et al.** Effector T-cell trafficking between the leptomeninges and the cerebrospinal fluid. *Nature.* 2016;530:349-353
- Schuh K, Cartwright EJ, Jankevics E, Bundschu K, Liebermann J, Williams JC, Armesilla AL, Emerson M, Oceandy D, Knobloch KP, Neyses L.** Plasma membrane Ca²⁺ ATPase 4 is required for sperm motility and male fertility. *J Biol Chem.* 2004;279:28220-28226
- Shamas-Din A, Kale J, Leber B, Andrews DW.** Mechanisms of action of Bcl-2 family proteins. *Cold Spring Harb Perspect Biol.* 2013;5:a008714
- Schexnayder C, Broussard K, Onuaguluchi D, Poché A, Ismail M, McAtee L, Llopis S, Keizerweerd A, McFerrin H, Williams C.** Metformin Inhibits Migration and Invasion by Suppressing ROS Production and COX2 Expression in MDA-MB-231 Breast Cancer Cells. *Int J Mol Sci.* 2018;19

- Schmid D, Pypaert M, Munz C.** Antigen-loading compartments for major histocompatibility complex class II molecules continuously receive input from autophagosomes. *Immunity*. 2007;26:79-92
- Schmidt O, Pfanner N, Meisinger C.** Mitochondrial protein import: from proteomics to functional mechanisms. *Nat Rev Mol Cell Biol*. 2010;11:655-667
- Schmit K, Michiels C.** TMEM Proteins in Cancer: A Review. *Front Pharmacol*. 2018;9:1345
- Schramm A, Köster J, Marschall T, Martin M, Schwermer M, Fielitz K, Büchel G, Barann M, Esser D, Rosenstiel P, Rahmann S, Eggert A, Schulte JH.** Next-generation RNA sequencing reveals differential expression of MYCN target genes and suggests the mTOR pathway as a promising therapy target in MYCN-amplified neuroblastoma. *Int J Cancer*. 2013;132:106-115
- Schubert D, Heinemann S, Carlisle W, Tarikas H, Kimes B, Patrick J, Steinbach JH, Culp W, Brandt BL.** Clonal cell lines from the rat central nervous system. *Nature*. 1974;249:224-227
- Schug ZT, Gonzalez F, Houtkooper RH, Vaz FM, Gottlieb E.** BID is cleaved by caspase-8 within a native complex on the mitochondrial membrane. *Cell Death Differ*. 2011;18:538-548
- Schurmans S, Schiffmann SN, Gurden H, Lemaire M, Lipp HP, Schwam V, Pochet R, Imperato A, Böhme GA, Parmentier M.** Impaired long-term potentiation induction in dentate gyrus of calretinin-deficient mice. *Proc Natl Acad Sci USA*. 1997;94:10415-10420
- Schütz K, Carle R, Schieber A.** Taraxacum--a review on its phytochemical and pharmacological profile. *J Ethnopharmacol*. 2006;107:313-323
- Schwaller B.** The continuing disappearance of "pure" Ca²⁺ buffers. *Rev Cell Mol Life Sci*. 2009;66:275-300
- Schwaller B.** Cytosolic Ca²⁺ buffers. *Cold Spring Harb Perspect Biol*. 2010;2:a004051
- Schwaller B.** Calretinin: from a "simple" Ca(2+) buffer to a multifunctional protein implicated in many biological processes. *Rev Front Neuroanat*. 2014;8:3
- Schwaller B, Meyer M, Schiffmann S.** 'New' functions for 'old' proteins: the role of the calcium-binding proteins calbindin D-28k, calretinin and parvalbumin, in cerebellar physiology. Studies with knockout mice. *Rev Cerebellum*. 2002;1:241-258

- Sciumè G, Santoni A, Bernardini G.** Chemokines and glioma: invasion and more. *Rev J Neuroimmunol.* 2010;224:8-12
- Scovassi AI, Soldani C, Veneroni P, Bottone MG, Pellicciari C.** Changes of mitochondria and relocation of the apoptosis inducing factor during apoptosis. *Ann NY Acad Sci.* 2009;1171:12-17
- Sedletska Y, Fourrier L, Malinge JM.** Modulation of MutS ATP-dependent functional activities by DNA containing a cisplatin compound lesion (base damage and mismatch). *J Mol Biol.* 2007;369:27-40
- Segal M, Korkotian E.** Roles of calcium stores and store-operated channels in plasticity of dendritic spines. *Neuroscientist.* 2016;22:477-485
- Seo JH, Ahn Y, Lee SR, Yeol Yeo C, Chung Hur K.** The major target of the endogenously generated reactive oxygen species in response to insulin stimulation is phosphatase and tensin homolog and not phosphoinositide-3 kinase (PI-3 kinase) in the PI-3 kinase/Akt pathway. *Mol Biol Cell.* 2005;16:348-357
- Sengupta N and Seto E.** Regulation of histone deacetylase activities. *J Cell Biochem.* 2004; 93:57-67
- Sermeus A, Cosse JP, Crespín M, Mainfroid V, de Longueville F, Ninane N, Raes M, Remacle J, Michiels C.** Hypoxia induces protection against etoposide-induced apoptosis: molecular profiling of changes in gene expression and transcription factor activity. *Mol Cancer.* 2008;7:27
- Serrano-Puebla A, Boya P.** Lysosomal membrane permeabilization in cell death: new evidence and implications for health and disease. *Ann N Y Acad Sci.* 2016;1371:30-44
- Shah MA, Schwartz GK.** Cell cycle-mediated drug resistance: an emerging concept in cancer therapy. *Clin Cancer Res.* 2001;7:2168-2181
- Shahar T, Nossek E, Steinberg DM, Rozovski U, Blumenthal DT, Bokstein F, Sitt R, Freedman S, Corn BW, Kanner AA, Ram Z.** The impact of enrollment in clinical trials on survival of patients with glioblastoma. *J Clin Neurosci.* 2012;19:1530-1534
- Shao F, Liu C.** Revisit the candidacy of brain cell types as the cell(s) of origin for human high-grade glioma. *Front Mol Neurosci.* 2018;11:48
- Shao Y, Gao Z, Marks PA, Jiang X.** Apoptotic and autophagic cell death induced by histone deacetylase inhibitors. *Proc Natl Acad Sci USA.* 2004;101:18030-18035

- Sheena N, Ajith T, Janardhanan K.** Prevention of nephrotoxicity induced by the anti-cancer drug cisplatin, using *Ganoderma lucidum*, a medicinal mushroom occurring in South India. *Current Science*. 2003;85:478-482
- Shen DW, Ma J, Okabe M, Zhang G, Xia D, Gottesman MM.** Elevated expression of TMEM205, a hypothetical membrane protein, is associated with cisplatin resistance. *J Cell Physiol*. 2010;225:822-828
- Shen DW, Pouliot LM, Hall MD, Gottesman MM.** Cisplatin resistance: A cellular self-defense mechanism resulting from multiple epigenetic and genetic changes. *Pharmacol Rev*. 2012;64:706-721
- Shen T, Morlock G, Zorn H.** Production of cyathane type secondary metabolites by submerged cultures of *Herichium erinaceus* and evaluation of their antibacterial activity by di-rect bioautography. *Fungal Biol Biotechnol*. 2015;2:8
- Sherman SE, Lippard SJ.** Structural aspects of platinum anticancer drug interactions with DNA. *Chem Rev*. 1987;86:1153-1181
- Sheth S, Mukherjea D, Rybak LP, Ramkumar V.** Mechanisms of Cisplatin-Induced Ototoxicity and Otoprotection. *Front Cell Neurosci*. 2017;11:338
- Shohet J, Foster J.** Neuroblastoma. *BMJ*. 2017;357:j1863
- Shohet JM, Ghosh R, Coarfa C, Ludwig A, Benham AL, Chen Z, Patterson DM, Barbieri E, Mestdagh P, Sikorski DN, Milosavljevic A, Kim ES, Gunaratne PH.** A genomic wide search for promoters that respond to increased MYCN reveals both new oncogenic and tumor suppressor microRNAs associated with aggressive neuroblastoma. *Cancer Res*. 2011;71:3841-3851
- Shohet JM.** Redefining functional MYCN gene signatures in neuroblastoma. *Proc Natl Acad Sci USA*. 2012;109:19041-19042
- Shyamala K, Yanduri S, Girish HC, Murgod S.** Neural crest: The fourth germ layer. *J Oral Maxillofac Pathol*. 2015;19:221-229
- Sigstedt SC, Hooten CJ, Callewaert MC, Jenkins AR, Romero AE, Pullin MJ, Kornienko A, Lowrey TK, Slambrouck SV, Steelant WF.** Evaluation of aqueous extracts of *Taraxacum officinale* on growth and invasion of breast and prostate cancer cells. *Int J Oncol*. 2008;32:1085-1090
- Singh SB, Ornatowski W, Vergne I, Naylor J, Delgado M, Roberts E, Ponpuak M, Master S, Pilli M, White E, Komatsu M, Deretic V.** Human IRGM regulates

- autophagy and cell-autonomous immunity functions through mitochondria. *Nat Cell Biology*. 2010;12:1154-1165
- Smith BC, Denu JM.** Chemical mechanisms of histone lysine and arginine modifications. *Biochim Biophys Acta*. 2009;1789:45-57
- Smith MA, Schnellmann RG.** Calpains, mitochondria, and apoptosis. *Cardiovasc Res*. 2012;96: 32-37
- So H, Kim H, Kim Y, Kim E, Pae HO, Chung HT, Kim HJ, Kwon KB, Lee KM, Lee HY, Moon SK, Park R.** Evidence that cisplatin-induced auditory damage is attenuated by downregulation of pro-inflammatory cytokines via Nrf2/HO-1. *J Assoc Res Otolaryngol*. 2008;9:290-306
- Soldani C, Bottone MG, Pellicciari C, Scovassi AI.** Two-color fluorescence detection of Poly (ADPRibose) Polymerase-1 (PARP-1) cleavage and DNA strand breaks in etoposide-induced apoptotic cells. *Eur J Histochem*. 2001;45:389-392
- Soomro SH, Ting LR, Qing YY, Ren M.** Molecular biology of glioblastoma: Classification and mutational locations. *J Pak Med Assoc*. 2017;67:1410-1414
- Sosa V, Moliné T, Somoza R, Paciucci R, Kondoh H, LLeonart ME.** Oxidative stress and cancer: an overview. *Ageing Res Rev*. 2013;12:376-390
- Spix C, Pastore G, Sankila R, Stiller CA, Steliarova-Foucher E.** Neuroblastoma: incidence and survival in European children (1978-1997): Report from the automated childhood cancer information system project. *Eur J Cancer*. 2006;42:2081-2091
- Speleman F, Park JR, Henderson TO.** Neuroblastoma: A Tough Nut to Crack. *Rev Am Soc Clin Oncol Educ Book*. 2016;35:548-557
- Sprowl JA, Ciarimboli G, Lancaster CS, Giovinazzo H, Gibson AA, Du G, Janke LJ, Cavaletti G, Shields AF, Sparreboom A.** Oxaliplatin-induced neurotoxicity is dependent on the organic cation transporter OCT2. *Proc Natl Acad Sci USA*. 2013;110:11199-11204
- Srinivasula SM, Hegde R, Saleh A, Datta P, Shiozaki E, Chai J, Lee RA, Robbins PD, Fernandes-Alnemri T, Shi Y, Alnemri ES.** A conserved XIAP-interaction motif in caspase-9 and Smac/DIABLO regulates caspase activity and apoptosis. *Nature*. 2001;410:112-116
- Stallings RL.** MicroRNA involvement in the pathogenesis of neuroblastoma: potential for MicroRNA mediated therapeutics. *Curr Pharm Des*. 2009;15:456-462

- Stathopoulos PB, Schindl R, Fahrner M, Zheng L, Gasmi-Seabrook GM, Muik M, Romanin C, Ikura M.** STIM1/Orai1 coiled-coil interplay in the regulation of store-operated calcium entry. *Nat Commun.* 2013;4:2963
- Steinle M., Palme D., Misovic M., Rudner J., Dittmann K., Lukowski R., Ruth P., Huber SM.** Ionizing radiation induces migration of glioblastoma cells by activating BK channels. *Radiother Oncol.* 2011;101:122-126
- Stiles CD, Rowitch DH.** Glioma stem cells: a midterm exam. *Neuron.* 2008;58:832-846
- Stordal B, Pavlakis N, Davey R.** Oxaliplatin for the treatment of cisplatin-resistant cancer: a systematic review. *Cancer Treat Rev.* 2007;33:347-357
- Starkov AA.** The role of mitochondria in reactive oxygen species metabolism and signaling. *Ann N Y Acad Sci.* 2008;1147:37-52
- Strasser A, Jost PJ, Nagata S.** The many roles of FAS receptor signaling in the immune system. *Immunity.* 2009;30:180-192
- Strehler EE.** Plasma membrane calcium ATPases as novel candidates for therapeutic agent development. *J Pharm Pharm Sci.* 2013;16:190-206
- Sturm D, Bender S, Jones DT, Lichter P, Grill J, Becher O, Hawkins C, Majewski J, Jones C, Costello JF, Iavarone A, Aldape K, Brennan CW, Jabado N, Pfister SM.** Paediatric and adult glioblastoma: multiform (epi)genomic culprits emerge. *Nat Rev Cancer.* 2014;14:92-107
- Sun L, Wang H, Wang Z, He S, Chen S, Liao D, Wang L, Yan J, Liu W, Lei X, Wang X.** Mixed lineage kinase domain-like protein mediates necrosis signaling downstream of RIP3 kinase. *Cell.* 2012;148:213-227
- Sun Q, Fan W, Chen K, Ding X, Chen S, Zhong Q.** Identification of Barkor as a mammalian autophagy-specific factor for Beclin 1 and class III phosphatidylinositol 3-kinase. *Proc Natl Acad Sci USA.* 2008;105:19211-19216
- Suzuki H, Aoki K, Chiba K, Sato Y, Shiozawa Y, Shiraishi Y, Shimamura T, Niida A, Motomura K, Ohka F, Yamamoto T, Tanahashi K, Ranjit M, Wakabayashi T, Yoshizato T, et al.** Mutational landscape and clonal architecture in grade II and III gliomas. *Nat Genet.* 2015;47:458-468
- Suzuki K, Kubota Y, Sekito T, Ohsumi Y.** Hierarchy of Atg proteins in pre-autophagosomal structure organization. *Genes Cells.* 2007;12:209-218

- Swift CC, Eklund MJ, Kravcka JM, Alazraki AL.** Updates in diagnosis, management, and treatment of neuroblastoma. *Radiographics*. 2018;38:566-580
- Szyf M.** Epigenetics, DNA methylation, and chromatin modifying drugs. *Annu Rev Pharmacol Toxicol*. 2009;49:243-263
- Sweeney B, Vora M, Ulbricht C, Basch E.** Evidence-based systematic review of dandelion (*Taraxacum officinale*) by natural standard research collaboration. *J Herb Pharmacother*. 2005;5:79-93
- Taghipour Zahir S, Mortaz M, Baghi Yazdi M, Sefidrokh Sharahjin N, Shabani M.** Calvarium mass as the first presentation of glioblastoma multiforme: A very rare manifestation of high-grade glioma. *Neurochirurgie*. 2018;64:76-78
- Tait SW, Green DR.** Mitochondria and cell death: outer membrane permeabilization and beyond. *Nat Rev Mol Cell Biol*. 2010;11:621-632
- Takahashi M, Fukami S, Iwata N, Inoue K, Itohara S, Itoh H, Haraoka J, Saido T.** *In vivo* glioma growth requires host-derived matrix metalloproteinase 2 for maintenance of angioarchitecture. *Pharmacol Res*. 2002;46:155-163
- Tang D, Wu D, Hirao A, Lahti JM, Liu L, Mazza B, Kidd VJ, Mak TW, Ingram AJ.** ERK activation mediates cell cycle arrest and apoptosis after DNA damage independently of p53. *J Biol Chem*. 2002;277:12710-12717
- Tekirdag K, Cuervo AM.** Chaperone-mediated autophagy and endosomal microautophagy: Joint by a chaperone. *J Biol Chem*. 2018;293:5414-5424
- Tenev T, Bianchi K, Darding M, Broemer M, Langlais C, Wallberg F, Zachariou A, Lopez J, MacFarlane M, Cain K, Meier P.** The Ripoptosome, a signalling platform that assembles in response to genotoxic stress and loss of IAPs. *Mol Cell*. 2011;43:432-448
- Thakkar JP, Dolecek TA, Horbinski C, Ostrom QT, Lightner DD, Barnholtz-Sloan JS, Villano JL.** Epidemiologic and molecular prognostic review of glioblastoma. *Cancer Epidemiol Biomarkers Prev* 2014;23:1985-1996
- Thomas SG, Huang S, Li S, Staiger CJ, Franklin-Tong VE.** Actin depolymerization is sufficient to induce programmed cell death in self-incompatible pollen. *JCB*. 2007;174:221-229
- Thuringer D, Chanteloup G, Boucher J, Pernet N, Boudesco C, Jego G, Chatelier A, Bois P, Gobbo J, Cronier L, Solary E, Garrido C.** Modulation of the IRly rectifying

- potassium channel Kir4.1 by the pro-invasive miR-5096 in GBM cells. *Oncotarget*. 2017;8:37681-37693
- Timerbaev AR, Hartinger CG, Aleksenko SS, Keppler BK.** Interactions of antitumor metallodrugs with serum proteins: advances in characterization using modern analytical methodology. *Chem Rev*. 2006;106:2224-2248
- Tobiume K, Matsuzawa A, Takahashi T, Nishitoh H, Morita K, Takeda K, Minowa O, Miyazono K, Noda T, Ichijo H.** ASK1 is required for sustained activations of JNK/p38 MAP kinases and apoptosis. *EMBO Rep*. 2001;2:222-228
- Toescu EC.** Hypoxia sensing and pathways of cytosolic Ca²⁺ increases. *Rev Cell Calcium*. 2004;36:187-199
- Tomiya A, Tachibana K, Suzuki K, Seino S, Sunayama J, Matsuda KI, Sato A, Matsumoto Y, Nomiya T, Nemoto K, Yamashita H, Kayama T, Ando K, Kitanaka C.** MEK-ERK-dependent multiple caspase activation by mitochondrial proapoptotic Bcl-2 family proteins is essential for heavy ion irradiation-induced glioma cell death. *Cell Death*. 2010;1:60
- Tooze SA, Yoshimori T.** The origin of the autophagosomal membrane. *Nat Cell Biol*. 2010;12:831-835
- Torsvik A, Stieber D, Enger P, Golebiewska A, Molven A, Svendsen A, Westermarck B, Nicloulhale K, Enger M, Bjerkvig R.** U-251 revisited: genetic drift and phenotypic consequences of long-term cultures of glioblastoma cells. *Cancer Med*. 2014;812-824
- Torti D, Trusolino L.** Oncogene addiction as a foundational rationale for targeted anti-cancer therapy: promises and perils. *EMBO Mol Med*. 2011;3:623-636
- Trochet D, Bourdeaut F, Janoueix-Lerosey I, Deville A, de Pontual L, Schleiermacher G, Coze C, Philip N, Frébourg T, Munnich A, Lyonnet S, Delattre O, Amiel J.** Germline mutations of the paired-like homeobox 2B (PHOX2B) gene in neuroblastoma. *Am J Hum Genet*. 2004;74:761-764
- Turner K, Sontheimer H.** Cl and K channels and their role in primary brain tumour biology. *Philos Trans R Soc Lond B Biol Sci*. 2014;369:20130095
- Ungerstedt JS, Sowa Y, Xu WS, Shao Y, Dokmanovic M, Perez G, Ngo L, Holmgren A, Jiang X, Marks PA.** Role of thioredoxin in the response of normal and transformed cells to histone deacetylase inhibitors. *Proc Natl Acad Sci USA*. 2005;102:673-678
- Upton JW, Kaiser WJ, Mocarski ES.** Virus inhibition of RIP3-dependent necrosis. *Cell Host Microbe*. 2010;7:302-313

- Upton JW, Kaiser WJ, Mocarski ES.** DAI/ZBP1/DLM-1 complexes with RIP3 to mediate virus-induced programmed necrosis that is targeted by murine cytomegalovirus vIRA. *Cell Host Microbe.* 2012;11:290-297
- Uttenweiler A, Schwarz H, Neumann H, Mayer A.** The vacuolar transporter chaperone (VTC) complex is required for microautophagy. *Mol Biol Cell.* 2007;18:166-175
- van Tellingen O, Yetkin-Arik B, de Gooijer MC, Wesseling P, Wurdinger T, de Vries HE.** Overcoming the blood–brain tumor barrier for effective glioblastoma treatment. *Drug Resist Updat.* 2015;19:1-12
- Van Wijk SJ, Hageman GJ.** Poly(ADP-ribose) polymerase-1 mediated caspase-independent cell death after ischemia/reperfusion. *Free Radic Biol Med.* 2005;39:81-90
- Vanden Berghe T, Linkermann A, Jouan-Lanhouet S, Walczak H, Vandenabeele P.** Regulated necrosis: the expanding network of non-apoptotic cell death pathways. *Nat Rev Mol Cell Biol.* 2014;15:135-147
- Vandenabeele P, Galluzzi L, Vanden Berghe T, Kroemer G.** Molecular mechanisms of necroptosis an ordered cellular esplosion. *Nat Rev Mol Cell Biol.* 2010;11:700-714
- Valentijn AJ, Zouq N, Gilmore AP.** Anoikis. *Biochem Soc Trans.* 2004;32:421-425
- Valtorta F, Greengard P, Fesce R, Chiergatti E, Benfenati F.** Effects of the neuronal phosphoprotein synapsin I on actin polymerization. I. Evidence for a phosphorylation-dependent nucleating effect. *J Biol Chem.* 1992;267:11281-11288
- VanOosten RL, Moore JM, Karacay B, Griffith TS.** Histone deacetylase inhibitors modulate renal cell carcinoma sensitivity to TRAIL/Apo-2L-induced apoptosis by enhancing TRAIL-R2 expression. *Cancer Biol Ther.* 2005;4:1104-1112
- Vaseva AV, Marchenko ND, Ji K, Tsirka SE, Holzmann S, Moll UM.** p53 opens the mitochondrial permeability transition pore to trigger necrosis. *Cell.* 2012;149:1536-1548
- Veenhuis M, Salomons FA, Van Der Klei IJ.** Peroxisome biogenesis and degradation in yeast: a structure/function analysis. *Microsc Res Tech.* 2000;51:584-600
- Vergara C, Latorre R, Marrion N, Adelmant JP.** Calcium-activated potassium channels. *Curr Opin Neurobiol.* 1998;8:321-329

- Verhagen AM, Ekert PG, Pakusch M, Silke J, Connolly LM, Reid GE, Moritz RL, Simpson RJ, Vaux DL.** Identification of DIABLO, a mammalian protein that promotes apoptosis by binding to and antagonizing IAP proteins. *Cell*. 2000;102:43-53
- Veskoukis AS, Tsatsakis AM, Kouretas D.** Dietary oxidative stress and antioxidant defense with an emphasis on plant extract administration. *Cell Stress Chaperones*. 2012;17:11-21
- Virag L, Szabo C.** The therapeutic potential of poly(ADP-ribose) polymerase inhibitors. *Pharmacol. Rev* 2002;54:375-429
- Vitale I, Galluzzi L, Castedo M, Kroemer G.** Mitotic catastrophe: a mechanism for avoiding genomic instability. *Nat Rev Mol Cell Biol*. 2011;12:385-392
- Vitale I, Manic G, De Maria R, Kroemer G, Galluzzi L.** DNA damage in stem cells. *Mol Cell*. 2017;66:306-319
- von Karstedt S, Montinaro A, Walczak H.** Exploring the TRAILs less travelled: TRAIL in cancer biology and therapy. *Nat Rev Cancer*. 2017;17:352-366
- Vousden KH and Lane DP.** p53 in health and disease. *Nat Rev Mol Cell Biol*. 2007;8:275-283
- Wachtel-Galor S, Yuen J, Buswell JA, Benzie IFF.** A Medicinal Mushroom. *Ganoderma lucidum* (Lingzhi or Reishi). *Herbal Medicine: Biomolecular and Clinical Aspects*. 2011; 2nd edition. Chapter 9
- Waissbluth S, Daniel SJ.** Cisplatin-induced ototoxicity: transporters playing a role in cisplatin toxicity. *Hear Res*. 2013;299:37-45
- Wait SD, Prabhu RS, Burri SH, Atkins TG, Asher AL.** Polymeric drug delivery for the treatment of glioblastoma. *Neuro Oncol*. 2015;17:9-23
- Wakamatsu Y, Watanabe Y, Nakamura H, Kondoh H.** Regulation of the neural crest cell fate by N-myc: promotion of ventral migration and neural differentiation. *Development*. 1997;124:1953-1962
- Wang F, Gómez-Sintes R, Boya P.** Lysosomal membrane permeabilization and cell death. *Traffic*. 2018;19:918-931
- Wang D, Lippard SJ.** Cellular processing of platinum anticancer drugs. *Nat Rev Drug Discovery*. 2005;4:307-320

- Wang D, Sadée W, Quillan JM.** Calmodulin binding to G protein-coupling domain of opioid receptors. *J Biol Chem.* 1999;274:22081-22088
- Wang H, Sun L, Su L, Rizo J, Liu J, Wang LF, Wang FS, Wang X.** Mixed lineage kinase domain-like protein MLKL causes necrotic membrane disruption upon phosphorylation by RIP3. *Mol Cell.* 2014;54:133-146
- Wang H, Yu SW, Koh DW, Lew J, Coombs C, Bowers W, Federoff HJ, Poirier GG, Dawson TM, Dawson VL.** Apoptosis-inducing factor substitutes for caspase executioners in NMDA-triggered excitotoxic neuronal death. *J Neurosci.* 2004;24:10963-10973
- Wang PW, Abedini MR, Yang LX, Ding AA, Figeys D, Chang JY, Tsang BK, Shieh DB.** Gelsolin regulates cisplatin sensitivity in human head-and-neck cancer. *Int J Cancer.* 2014;135:2760-2769
- Wang Y, Dawson VL, Dawson TM.** Poly(ADP-ribose) signals to mitochondrial AIF: a key event in parthanatos. *Exp Neurol.* 2009;218:193-202
- Wang YB, Peng C, Liu YH.** Low dose of bradykinin selectively increases intracellular calcium in glioma cells. *J Neurol Sci.* 2007;258:44-51
- Warrier S, Pavanram P, Raina D, Arvind M.** Study of chemoresistant CD133⁺ cancer stem cells from human glioblastoma cell line U138MG using multiple assays. *Cell Biol Int.* 2012;36:1137-1143
- Warth A, Mittelbronn M, Wolburg H.** Redistribution of the water channel protein aquaporin-4 and the K⁺ channel protein Kir4.1 differs in low- and high-grade human brain tumors. *Acta Neuropathol.* 2005;109:418-426
- Waseem M, Bhardwaj M, Tabassum H, Raisuddin S, Parvez S.** Cisplatin hepatotoxicity mediated by mitochondrial stress. *Drug Chem Toxicol.* 2015;38:452-459
- Watkins S, Robel S, Kimbrough IF, Robert SM, Ellis-Davies G, Sontheimer H.** Disruption of astrocyte-vascular coupling and the blood-brain barrier by invading glioma cells. *Nat Commun.* 2014;5:4196
- Weaver AK, Bomben VC, Sontheimer A.** Expression and function of calcium-activated potassium channels in human glioma cells. *Glia.* 2006;54:223-233
- Webb TR, Slavish J, George RE, Look AT, Xue L, Jiang Q, Cui X, Rentrop WB, Morris SW.** Anaplastic lymphoma kinase: role in cancer pathogenesis and small-molecule inhibitor development for therapy. *Expert Rev Anticancer Ther.* 2009;9:331-356

- Weber K, Roelandt R, Bruggeman I, Estornes Y, Vandenabeele P.** Nuclear RIPK3 and MLKL contribute to cytosolic necrosome formation and necroptosis. *Commun Biol.* 2018;1:6
- Weichert W.** HDAC expression and clinical prognosis in human malignancies. *Cancer Lett* 2009;280:168-176.
- Weidberg H, Shvets E, Elazar Z.** Biogenesis and cargo selectivity of autophagosomes. *Annu Rev Biochem.* 2011;80:125-156
- Weller M, Butowski N, Tran DD, Recht LD, Lim M, Hirte H, Ashby L, Mechtler L, Goldlust SA, Iwamoto F, Drappatz J, O'Rourke DM, Wong M, Hamilton MG, Finocchiaro G, et al.** Rindopepimut with temozolomide for patients with newly diagnosed, EGFRvIII-expressing glioblastoma (ACT IV): a randomised, double-blind, international phase 3 trial. *Lancet Oncol.* 2017;18:1373-1385
- Weller M, Wick W, Hegi ME, Stupp R, Tabatabai G.** Should biomarkers be used to design personalized medicine for the treatment of glioblastoma? *Future Oncol.* 2010;6:1407-1414
- Wen PY and Kesari S.** Malignant gliomas in adults. *N Engl J Med.* 2008;359:492-507
- Wen PY, Macdonald DR, Reardon DA, Cloughesy TF, Sorensen AG, Galanis E, Degroot J, Wick W, Gilbert MR, Lassman AB, Tsien C, Mikkelsen T, Wong ET, Chamberlain MC, Stupp R, et al.** Updated response assessment criteria for high-grade gliomas: response assessment in neuro-oncology working group. *J Clin Oncol.* 2010;28:1963-1972
- Wertz IE, Dixit VM.** Ubiquitin-mediated regulation of TNFR1 signaling. *Cytokine Growth Factor Rev.* 2008;19:313-324
- Wesseling P, Capper D.** WHO 2016 Classification of gliomas. *Neuropathol Appl Neurobiol.* 2018;44:139-150
- Westermarck UK, Wilhelm M, Frenzel A, Henriksson MA.** The MYCN oncogene and differentiation in neuroblastoma. *Semin Cancer Biol.* 2011;21:256-266
- Wexselblatt E, Gibson D.** What do we know about the reduction of Pt(IV) pro-drugs? *J Inorg Biochem.* 2012;117:220-229
- Wheate NJ, Walker S, Craig GE, Oun R.** The status of platinum anticancer drug in the clinic and in clinical trials. *Dalton Trans.* 2010;39:8113-8127

- Whittle SB, Smith V, Doherty E, Zhao S, McCarty S, Zage PE.** Overview and recent advances in the treatment of neuroblastoma. *Expert Rev Anticancer Ther.* 2017;17:369-386
- Wick W, Weller M, van den Bent M, Sanson M, Weiler M, von Deimling A, Plass C, Hegi M, Platten M, Reifenberger G.** MGMT testing-the challenges for biomarker-based glioma treatment. *Nat Rev Neurol.* 2014;10:372-385
- Wilson JJ, Lippard SJ.** Synthetic methods for the preparation of platinum anticancer complexes. *Chem Rev.* 2014;114:4470-4495
- Wilwert JL, Madhoun NM, Coughlin DJ.** Parvalbumin correlates with relaxation rate in the swimming muscle of sheepshead and kingfish. *J Exp Biol.* 2006;209:227-237
- Wirngo FE, Lambert MN, Jeppesen PB.** The Physiological Effects of Dandelion (*Taraxacum Officinale*) in Type 2 Diabetes. *Rev Diabet Stud.* 2016;13:113-131
- Witt O, Deubzer HE, Lodrini M, Milde T, Oehme I.** Targeting Histone Deacetylases in Neuroblastoma. *Curr Pharm Des.* 2009;15:436-47
- Wong E, Cuervo AM.** Integration of clearance mechanisms: the proteasome and autophagy. *Cold Spring Harb Perspect Biol.* 2010;2:a006734
- Wong PM, Puente C, Ganley IG, Jiang X.** The ULK1 complex: sensing nutrient signals for autophagy activation. *Autophagy.* 2013;9:124-137
- Wu G, Chai J, Suber TL, Wu JW, Du C, Wang X, Shi Y.** Structural basis of IAP recognition by Smac/DIABLO. *Nature.* 2000;408:1008-1012
- Wu GS, Guo JJ, Bao JL, Li XW, Chen XP, Lu JJ, Wang YT.** Anti-cancer properties of triterpenoids isolated from *Ganoderma lucidum* - a review. *Expert Opin Investig Drugs.* 2013;22:981-992
- Wu M, Swartz MA.** Modeling tumor microenvironments *in vitro*. *J Biomech Eng.* 2014;136:021011
- Würth R, Pattarozzi A, Gatti M, Bajetto A, Corsaro A, Parodi A, Sirito R, Massollo M, Marini C, Zona G, Fenoglio D, Sambuceti G, Filaci G, Daga A, Barbieri F, et al.** Metformin selectively affects human glioblastoma tumor-initiating cell viability: A role for metformin-induced inhibition of Akt. *Cell Cycle.* 2013;12:145-156
- Xie R, Nguyen S, McKeehan WL, Liu L.** Acetylated microtubules are required for fusion of autophagosomes with lysosomes. *BMC Cell Biol.* 2010;11:89

- Xiong H, Cheng Y, Zhang X, Zhang X.** Effects of taraxasterol on iNOS and COX-2 expression in LPS-induced RAW 264.7 macrophages. *J Ethnopharmacol.* 2014;155:753-757
- Xu WS, Perez G, Ngo L, Gui CY, Marks PA.** Induction of polyploidy by histone deacetylase inhibitor: a pathway for antitumor effects. *Cancer Res.* 2005;65:7832-7839
- Xu Z, Chen X, Zhong Z, Chen L, Wang Y.** Ganoderma lucidum polysaccharides: immunomodulation and potential anti-tumor activities. *Am J Chin Med.* 2011;39:15-27
- Yalçın B, Kremer LC, van Dalen EC.** High-dose chemotherapy and autologous haematopoietic stem cell rescue for children with high-risk neuroblastoma. *Cochrane Database Syst Rev.* 2015;10:CD006301
- Yamasaki M, Makino T, Masuzawa T, Kurokawa Y, Miyata H, Takiguchi S, Nakajima K, Fujiwara Y, Matsuura N, Mori M, Doki Y.** Role of multidrug resistance protein 2 (MRP2) in chemoresistance and clinical outcome in oesophageal squamous cell carcinoma. *Br J Cancer.* 2011;104:707-713
- Yáñez M, Gil-Longo J, Campos-Toimil M.** Calcium binding proteins. *Adv Exp Med Biol.* 2012;740:461-482
- Yang I, Han SJ, Sughrue ME, Tihan T, Parsa AT.** Immune cell infiltrate differences in pilocytic astrocytoma and glioblastoma: evidence of distinct immunological microenvironments that reflect tumor biology. *J Neurosurg.* 2011;115:505-511
- Yang L, Lin C, Wang L, Guo H, Wang X.** Hypoxia and hypoxia-inducible factors in glioblastoma multiforme progression and therapeutic implications. *Rev Exp Cell Res.* 2012;318:2417-2426
- Yang J, Sun X, Mao W, Sui M, Tang J, Shen Y.** Conjugate of Pt(IV)-histone deacetylase inhibitor as a prodrug for cancer chemotherapy. *Mol Pharm.* 2012;9:2793-2800
- Yang Z, Klionsky DJ.** Mammalian autophagy: core molecular machinery and signaling regulation. *Curr Opin Cell Biol.* 2010;22:124-131
- Yao S, Cheng M, Zhang Q, Wasik M, Kelsh R, Winkler C.** Anaplastic lymphoma kinase is required for neurogenesis in the developing central nervous system of zebrafish. *PLoS One.* 2013;8:e63757
- Yavin E, Gabai A, Gil S.** Nerve growth factor mediates monosialoganglioside-induced release of fibronectin and J1/tenascin from C6 glioma cells. *J Neurochem.* 1991;56:105-112

- Yew DT, Luo CB, Heizmann CW, Chan WY.** Differential expression of calretinin, calbindin D28K and parvalbumin in the developing human cerebellum. *Brain Res Dev Brain Res.* 1997;103:37-45
- Yilmaz HR, Sogut S, Ozyurt B, Ozugurlu F, Sahin S, Isik B, Uz E, Ozyurt H.** The activities of liver adenosine deaminase, xanthine oxidase, catalase, superoxide dismutase enzymes and the levels of malondialdehyde and nitric oxide after cisplatin toxicity in rats: protective effect of caffeic acid phenethyl ester. *Toxicol Ind Health.* 2005;21:67-73
- Yin J, Valin KL, Dixon ML, Leavenworth JW.** The Role of Microglia and Macrophages in CNS Homeostasis, Autoimmunity, and Cancer. *Rev J Immunol Res.* 2017;2017:5150678
- Yla-Antilla P, Vihinen H, Jokitalo E, Eskelinen EL.** 3D tomography reveals connections between the phagophore and endoplasmic reticulum. *Autophagy.* 2009;5:1180-1185
- Yoon S, Bogdanov K, Kovalenko A, Wallach D.** Necroptosis is preceded by nuclear translocation of the signaling proteins that induce it. *Cell Death Differ.* 2016;23:253-260
- Yoshii SR, Mizushima N.** Monitoring and measuring autophagy. *Int J Mol Sci.* 2017;18:1865
- Yousefi S, Perozzo R, Schmid I, Ziemiecki A, Schaffner T, Scapozza L, Brunner T, Simon HU.** Calpain-mediated cleavage of Atg5 switches autophagy to apoptosis. *Nat Cell Biol.* 2006;8:1124-1132
- Yu AL, Gilman AL, Ozkaynak MF, London WB, Kreissman SG, Chen HX, Smith M, Anderson B, Villablanca JG, Matthay KK, Shimada H, Grupp SA, Seeger R, Reynolds CP, Buxton A et al.** Anti-GD2 antibody with GM-CSF, interleukin-2, and isotretinoin for neuroblastoma. *N Engl J Med.* 2010;363:1324-1334
- Yuan S, Yu X, Topf M, Ludtke SJ, Wang X, Akey CW.** Structure of an apoptosome-procaspase-9 CARD complex. *Structure.* 2010;18:571-583
- Zamble DB, Mikata Y, Eng CH, Sandman KE, Lippard SJ.** Testis specific HMG domain protein alters the respons of cells to cisplatin. *J Inorg Biochem.* 2002;91:451-462
- Zaman S, Wang R, Gandhi V.** Targeting the apoptosis pathway in hematologic malignancies. *Leuk Lymphoma.* 2014;55:1980-1992
- Zhang J, Stevens MF, Bradshaw TD.** Temozolomide: mechanisms of action, repair and resistance. *Curr Mol Pharmacol.* 2012;5:102-114

- Zhang M, Chakravarti A.** Novel radiation-enhancing agents in malignant gliomas. *Semin. Radiat. Oncol.* 2006;16:29-37
- Zhang P, Yi LH, Meng GY, Zhang HY, Sun HH, Cui LQ.** Apelin-13 attenuates cisplatin-induced cardiotoxicity through inhibition of ROS-mediated DNA damage and regulation of MAPKs and AKT pathways. *Free Radic Res.* 2017;51:449-459
- Zhang X, Peng L, Liang Z, Kou Z, Chen Y, Shi G, Li X, Liang Y, Wang F, Shi Y.** Effects of Aptamer to U87-EGFRvIII cells on the proliferation, radiosensitivity, and radiotherapy of Glioblastoma cells. *Mol Ther Nucleic Acids.* 2018;10:438-449
- Zhang X, Xiong H, Liu L.** Effects of taraxasterol on inflammatory responses in lipopolysaccharide-induced RAW 264.7 macrophages. *J Ethnopharmacol.* 2012;141:206-211
- Zhang Y, Ma WY, Kaji A, Bode AM, Dong Z.** Requirement of ATM in UVA-induced signaling and apoptosis. *J Biol Chem.* 2002;277:3124-3131
- Zheng YR, Suntharalingam K, Johnstone TC, Yoo H, Lin W, Brooks JG, Lippard SJ.** Pt(IV) prodrugs designed to bind non-covalently to human serum albumin for drug delivery. *J Am Chem Soc.* 2014;136:8790-8798
- Zhu H, Zhao H, Zhang L, Xu J, Zhu C, Zhao H, Lv G.** Dandelion root extract suppressed gastric cancer cells proliferation and migration through targeting lncRNA-CCAT1. *Biomed Pharmacother.* 2017;93:1010-1017
- Zong H, Parada LF, Baker SJ.** Cell of origin for malignant gliomas and its implication in therapeutic development. *Cold Spring Harb. Perspect. Biol.* 2015;7:pii: a020610
- Zou Y, Biao L, Xu F, Liu R, Liu Z, Fu Y.** Structural study on the interactions of oxaliplatin and linear DNA. *Scanning.* 2016;38:880-888

List of original manuscripts

A Brief Communication on a Cell Line of Neural Stem Cells B50 Cells Treated With a New Cisplatin-Based Drug

Ferrari B¹, Astesana V¹, De Pascali SA², Fanizzi FP² and Bottone MG^{1*}

¹Dipartimento di Biologia e Biotecnologie "L. Spallanzani" Università di Pavia, via Ferrata 9, 27100, Pavia, Italy

²University of Salento, Di.S.Te.B.A., Campus Ecotekne, via Provie Lecce-Monteroni, 73100, Lecce, Italy

*Corresponding Author: Maria Grazia Bottone, Dipartimento di Biologia e Biotecnologie "L. Spallanzani" Università di Pavia, via Ferrata 9, 27100, Pavia, Italy, Tel: 0382986319; Email: mariagrazia.bottone@unipv.it

Mini Review

Volume 2 Issue 1

Received Date: June 04, 2018

Published Date: June 12, 2018

Mini Review

The B50 neuronal cell line was derived, in the 1974, from neuroblastoma in the neonatal rat central nervous system (CNS), and to date it's a cell line widely used in different studies. B50 cells offer several advantages to researchers for the study of CNS neurons in culture: they are simple to grow, to differentiate and to transfect. B50 cells have been extensively used in the study of death, toxicology and neuronal cell differentiation. Since 2008, Bottone and collaborators use this model to investigate the effects of cisplatin (cisPt) and new platinum compounds on the stem component of a brain tumour: neuroblastoma. Neuroblastoma is the most common extra-cranial solid tumour in infants and children and accounts for 8-10% of all childhood cancers. It causes the 15% of cancer deaths in the paediatric population. The incidence of neuroblastoma is 10.2 cases per million in children under 15 years of age and almost 500 new cases are reported each year [1].

Neuroblastoma can be seen as the result of a neural nature cell differentiation failure. The neural crest is a population of cells from neural folds and at the time of closure of the neural tube, these cells will be found in the dorsal part, but soon they will move away migrating in the surrounding tissues. The development of these crests is regulated by transcription factors Adam, et al. (2008) [2], post-transcriptional, post-translational modifications and epigenetic events [3].

The traditional treatment of neuroblastoma includes: chemotherapy, surgical resection and / or radiotherapy. However, many aggressive neuroblastomas have developed resistance to chemotherapeutic agents, increasing the probability of relapses. Induction chemotherapy is carried out by a combination of cyclophosphamide, doxorubicin, cisplatin, carboplatin, etoposide, topotecan, ifosfamide, and vincristine. The treatment does not exclude complications, because it can lead to growth disorders, endocrinopathies and the appearance of secondary malignancies [4].

[Pt(O,O'-acac)(γ-acac)(DMS)], called also PtAcacDMS, is a new platinum-based compound, that has shown less toxicity compared to cisPt. Indeed, during normal development of CNS, in rat cerebellum sections treated with the new compound, early minor apoptotic events was observed with a reduction in alteration of granule cell migration and in the growth of Purkinje cell dendrites [5]. Furthermore, PtAcacDMS enters in cells faster, about a quarter of more time than cisPt [6, 7].

Despite cisPt, PtAcacDMS target is not primarily DNA, in fact, it shows low reactivity with nucleobases and a specific reactivity with intracellular sulphur ligands. In rat neuroblastoma cells (B50), it has been observed that cisPt induces activation of the intrinsic apoptotic pathway, through the alteration of mitochondrial membrane

permeability [8]. Using immunocytochemical, cytometric and morphological techniques, it has also been shown that these compounds exert a cytostatic action and activate apoptosis by different pathways [9]. Morphological alterations of Golgi Apparatus, in B50 cells treated with cisPt, may be related to structural changes of the cytoskeletal system that is reflect in a strong production of vesicles and a spatial redistribution in dense masses [10]. After treatment with PtAcacDMS, an evident rearrangement has been detectable at the RE level: membranes completely disrupted and cisterns compressed into the cytoplasm without a uniform distribution was observed [9]. Recently, Grimaldi and collaborators (2016) have shown that the long-term effects of PtAcacDMS, exert cytotoxicity (induce cell death by apoptosis) in the neuronal B50 cell line but do not induce drug resistance. Furthermore, the alteration of the permeability of the external mitochondrial membrane induced by PtAcacDMS treatment causes the loss of the maintenance of Ca^{2+} and ATP homeostasis. The lack of this energetic molecule determines the blocking of the pumps responsible to the expulsion of Ca^{2+} from the cell, leading an increase in intracellular Ca^{2+} concentration. PtAcacDMS also causes the inhibition of Ca^{2+} transport pumps activity such as PMCA (Plasma Membrane Calcium ATPase), but not SERCA (Sarco/End plasmatic Reticulum Calcium ATPase) or SPCA (Secretary Pathway Calcium ATPase) and Na^{2+}/Ca^{2+} pump. ROS production is also evident by inducing the activity of NAD (P) H oxidase, which directly induce DNA damage [11].

Based on these assumptions, we compared the effect of cisPt and PtAcacDMS treatment on intracellular calcium homeostasis in B50 cells. The presented data were obtained by fluorescent immunohistochemically and microscopic techniques. Images reported in (Figure 1) show immunolabelling for calcium-binding proteins Calmodulin (CaM) and Calretinin (CR). In eukaryotic cell, CaM has an important role in the regulation of several cellular functions. Interacting with many target protein, CaM controls cell proliferation and death processes *i.e.* apoptosis, autophagy and necroptosis [12, 13], regulating the physiology of cancer cells (including cancer stem cells) and the progression, growth, angiogenesis and metastases associated with the tumour. CR is a protein associated with development and regulates processes such as proliferation, differentiation and cell death. Moreover, even if still much discussed, it seems to be involved in neuro-protection.

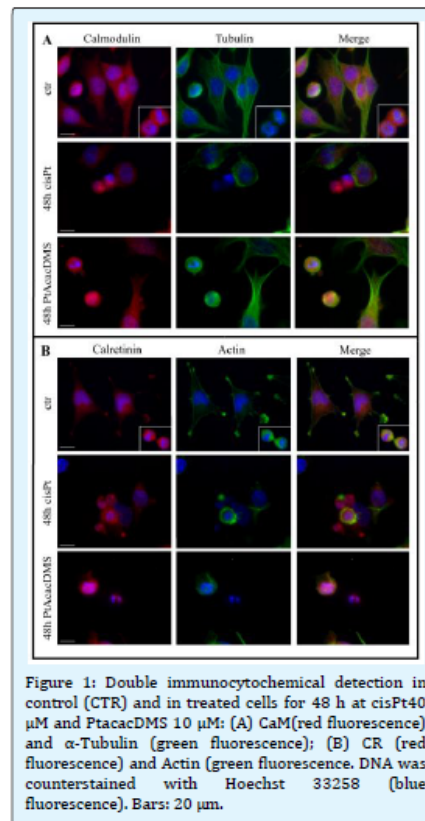


Figure 1: Double immunocytochemical detection in control (CTR) and in treated cells for 48 h at cisPt40 μ M and PtacacDMS 10 μ M: (A) CaM (red fluorescence) and α -Tubulin (green fluorescence); (B) CR (red fluorescence) and Actin (green fluorescence). DNA was counterstained with Hoechst 33258 (blue fluorescence). Bars: 20 μ m.

This analysis was conducted on B50 neuroblastoma rat cells cultured in Dulbecco's Modified Eagle Medium (DMEM) supplemented with L-glutamine (2 mM), penicillin 100 IU ml^{-1} , streptomycin (100 mg l^{-1}) and 10% fetal bovine serum (FBS). Cell culture was carried out at 37°C in a 5% CO_2 humidified chamber.

Journal of Embryology & Stem Cell Research

After treatment with cisPt (40µM) and PtAcacDMS (10µM) for 48h at continuous exposure an immunohistochemistry detection for CaM and CR was performed, associated with a labelling for the tubulinic and actininc cytoskeleton respectively and a counterstained with Hoechst 33258for the nuclei (Table 1). For images acquisition an Olympus BX51 microscope equipped with a 100-W mercury lamp was used under the following conditions: 330-385 nm excitation filter (excf),

400 nm dichroic mirror (dm) and 420 nm barrier filter (bf) for Hoechst 33258; 450-480 nm excf, 500 nm dm and 515 nm bf for the fluorescence of Alexa 488; 540 nm excf, 580 nm dm and 620 nm bf for Alexa 594. Images were recorded with an Olympus MagniFire camera system and processed with the Olympus Cell F software. The analysis of the differences between the treated samples was conducted, evaluating three independent experiments for each condition and protein analysed.

Antigen	Primary antibody	Dilution in PBS	Secondary antibody	Dilution in PBS
Calmodulin	Abcam, mouse monoclonal IgG ₁	1:200	Anti-mouse IgG1 Alexa Fluor 594	1:200
Calretinin	Swant, rabbit polyclonal	1:2000	Anti-mouse IgG1 Alexa Fluor 594	1:200
-Tubulin	Invitrogen, mouse monoclonal	1:100	Anti-mouse IgG1 Alexa Fluor 488	1:200
Actin	Invitrogen, Alexa 488-Phalloidin	1:40		

Table 1: Primary and secondary antibodies used for immunocytochemical reactions at fluorescence microscope.

Images reported in (Figure 1) demonstrate that after treatment with PtAcacDMS and cisPt, there was an increase of red fluorescence relating to both CaM and CR respectively. A rearrangement of the actinic and tubulin cytoskeleton (green fluorescence) was observed compared to control sample. A clear intensification of CaM fluorescence was detectable in cells treated with PtAcacDMS compared to those treated with cisPt. This data is well correlated with the presence of a higher percentage of apoptotic cells obtained after PtAcacDMS treatment. Moreover, the increase of Ca²⁺ in cytosol correlates with mitochondrial alterations Grimaldi, et al. (2016) [7] which also induce higher ROS production and therefore an increase in oxidative stress [14].

These preliminary data, which will have to be confirmed by quantitative evaluations, appear promising and in line with others presented in the literature and give us the possibility to consider PtAcacDMS as a new strategy for tumours treatment, in particular by its action on pathways involved in CaM-dependent systems [15-19].

References

- Park JR, Eggert A, Caron H (2008) Neuroblastoma: biology, prognosis, and treatment. *Rev HematolOncolClin North Am* 55(1): 97-120.
- Adams M, Gammill L, Bronner-Fraser M (2008) Discovery of transcription factors and other candidate regulators of neural crest development. *Dev Dynamics* 237(4): 1021-1033.
- Mayanil CS (2013) Transcriptional and epigenetic regulation of neural crest induction during neurulation. *Dev Neurosci* 35(5): 361-372.
- Yalçın B, Kremer LC, Caron HN, van Dalen EC (2013) High-dose chemotherapy and autologous haematopoietic stem cell rescue for children with high-risk neuroblastoma. *Cochrane Database Syst Rev* (8): CD006301.
- Bernocchi G, Bottone MG, Piccolini VM, Dal Bo V, Santin G, et al. (2011) Developing central nervous system and vulnerability to platinum compounds. *Chemother Res Pract*.
- Muscella A, Calabriso N, De Pascali SA, Urso L, Ciccarese A, et al. (2007) platinum(II) complexes containing both an O,O'-chelated acetylacetonate ligand and a sulfur ligand in the platinum coordination sphere induce apoptosis in HeLa cervical carcinoma cells. *Biochem Pharmacol* 74(1): 28-40.
- Grimaldi M, Santin G, Insolia V, Dal Bo V, Piccolini VM, et al. (2016) [Pt(O,O'-acac)(γ-acac)(DMS)] versus cisplatin: apoptotic effects in B50 neuroblastoma cells. *Histochem Cell Biol* 145(5): 587-601.

Journal of Embryology & Stem Cell Research

8. Bottone MG, Soldani C, Veneroni P, Avella D, Pisu M, et al. (2008) Cell proliferation, apoptosis and mitochondrial damage in rat B50 neuronal cells after cisplatin treatment. *Cell Prolife* 41(3): 506-520.
9. Santin G, Piccolini VM, Veneroni P, Barni S, Bernocchi G, et al. (2011) Different patterns of apoptosis in response to cisplatin in B50 neuroblastoma rat cells. *Histol Histopathol* 26(7): 831-42.
10. Santin G, Scietti L, Veneroni P, Barni S, Bernocchi G, et al. (2012) Effects of Cisplatin in neuroblastoma rat cells: damage to cellular organelles. *Int J Cell Biol* 2012: 424072.
11. Muscella A, Calabriso N, Vetrugno C, Fanizzi FP, De Pascali SA, et al. (2011) The platinum (II) complex [Pt(O,O'-acac)(γ-acac)(DMS)] alters the intracellular calcium homeostasis in MCF-7 breast cancer cells. *BiochemPharmacol* 81(1): 91-103.
12. Smaili SS, Quest AF, Hetz C, Lavandro S (2013) Editorial: signaling in cell death, survival, proliferation and degeneration. *Curr Mol Med* 13(2): 239-240.
13. Nomura M, Ueno A, Saga K, Fukuzawa M, Kaneda Y (2014) Accumulation of cytosolic calcium induces necroptotic cell death in human neuroblastoma. *Cancer Res* 74(4): 1056-1066.
14. Muscella A, Calabriso N, Vetrugno C, Fanizzi FP, De Pascali SA, et al. (2011) The signalling axis mediating neuronal apoptosis in response to [Pt(O,O'-acac)(γ-acac)(DMS)]. *BiochemPharmacol* 81(11): 1271-1285.
15. Berchtold MW, Villalobo A (2014) the many faces of calmodulin in cell proliferation, programmed cell death, autophagy, and cancer. *Biochim Biophys Acta* 1843(2): 398-435.
16. Cerri S, Piccolini VM, Santin G, Bottone MG, De Pascali SA, et al. (2011) The developmental neurotoxicity study of platinum compounds. Effects of cisplatin versus a novel Pt (II) complex on rat cerebellum. *Neurotoxicol Teratol* 33(2): 273-281.
17. De Pascali SA, Papadia P, Ciccarese A, Pacifico C, Fanizzi FP (2005) First examples of β-diketonate platinum (II) complexes with sulfoxide ligands. *Eur J Inorg Chem* 2005(4): 788-796.
18. De Pascali SA, Papadia P, Capoccia S, Marchiò L, Lanfranchi M, et al. (2009) Hard/soft selectivity in ligand substitution reactions of beta-diketonate platinum(II) complexes. *Dalton Trans* (37): 7786-7795.
19. Kawai Y, Nakao T, Kunimura N, Kohda Y, Gemba M (2006) Relationship of intracellular calcium and oxygen radicals to cisplatin-related renal cell injury. *J Pharmacol Sci* 100(1): 65-72.



Author's Personal Copy

Life Sciences 210 (2018) 166–176



Contents lists available at ScienceDirect

Life Sciences

journal homepage: www.elsevier.com/locate/lifescie

A new platinum-based prodrug candidate: Its anticancer effects in B50 neuroblastoma rat cells

Beatrice Rangone^{a,1}, Beatrice Ferrari^{b,1}, Valentina Astesana^b, Irene Masiello^b, Paola Veneroni^b, Ilaria Zanellato^a, Domenico Osella^a, Maria Grazia Bottone^{b,*}

^a Dipartimento di Scienze e Innovazione Tecnologica, Università del Piemonte Orientale "A. Avogadro", viale Terasi Michel 11, 15121 Alessandria, Italy
^b Dipartimento di Biologia e Biotecnologie "L. Spallanzani", Università di Pavia, via Ferrata 9, 27100 Pavia, Italy

ARTICLE INFO

Keywords:
 B50
 Neuroblastoma cells
 Cisplatin
 Cell death
 Immunocytochemistry

ABSTRACT

AIMS: Neuroblastoma is a rare cancer that affects children, mostly under the age of 5. This type of cancer starts in very early forms of immature nerve cells or developing cells found in embryo or fetus. To date cisplatin represents one of the most potent antitumor agent in own, however, the onset of systemic side effects and the induction of drug resistance limit its use in the clinic for long-term treatment. In the present study we have analysed the effects of a new compound of platinum(IV) conjugates, named Pt(IV)Ac-POA, which is able to generate a synergistic antineoplastic action when released along with cisplatin upon intracellular Pt(IV) → Pt(II) reduction.

Main methods: To assess the growth inhibition of the compounds under investigation, a cell viability test, i.e. the resazurin reduction assay was used on the B50 neuroblastoma rat cells. Further analysis on the cell cycle and metabolic alterations were carried out through flow cytometry. Morphological changes and activation of different cell death pathways after treatment, were observed at transmission electron microscope and by immunocytochemistry at fluorescence microscopy. Protein expression was examined by western blot analysis.

Key findings: This compound bearing bioactive axial ligand, such as the active histone deacetylase inhibitor (HDACI) (2-propionyl)octanoic acid (POA), induced cell death through different pathways at a concentration ten times lower than cisplatin.

Significance: The results showed that Pt(IV)Ac-POA could represent a promising improvement of Pt-based chemotherapy against neuroblastoma.

1. Introduction

One of the most active agents used in the systemic treatment of cancer is cisplatin. This metal-drug and its analogues (carboplatin and oxaliplatin) represent the standard therapy for a wide range of childhood and adult tumours, including some nervous system cancers, such as neuroblastoma [10]. This type of cancer is the most common extracranial tumour in children. It represents 8–10% of all childhood cancers and could start in embryonic or fetal life [12]. The benefit of cisplatin is hampered by severe side effects, including neurotoxicity, such as some studies conducted on rats treated with this drug have demonstrated [19,37]. Damages against the Peripheral Nervous System (PNS) are well-known [13] and some morpho-functional alterations were detected both during development [3] and in adult Central Nervous System (CNS) ([48]; Kelly et al. [30]).

A goal of biomedical research is the synthesis of new antitumor agents, having the same therapeutic effect of the reference drug, but with less systemic toxicity. In this context, the class of platinum(IV) derivatives, Pt(IV), is gaining increasing attention. It is generally accepted that Pt(IV) complexes act as prodrugs, i.e. they are reduced to cytotoxic Pt(II) analogues within the hypoxic tumour cells [24,27,50] (Scheme 1).

The two axial ligands, released along with the Pt(II) metabolite, can be synergistic or adjuvant agents, giving rise to multi-action Pt(IV) drugs [20,23,31]. In particular, Pt(IV) complexes bearing histone deacetylase inhibitors (HDACI) would benefit of the widely-described synergistic effect that these molecules exert on DNA-damaging agents as cisplatin. Indeed, HDAC inhibition increases histone acetylation, decreasing histone-DNA interactions and allowing for chemo-sensitization versus DNA-damaging agents [6,35]. Members of medium chain fatty

* Corresponding author at: Dipartimento di Biologia e Biotecnologie "L. Spallanzani", Università di Pavia, via Ferrata 9, 27100 Pavia, Italy.

E-mail address: bottone@unipv.it (M.G. Bottone).

¹ Both authors contributed equally to this work.

<https://doi.org/10.1016/j.lfs.2018.08.048>

Received 12 June 2018; Received in revised form 27 July 2018; Accepted 20 August 2018

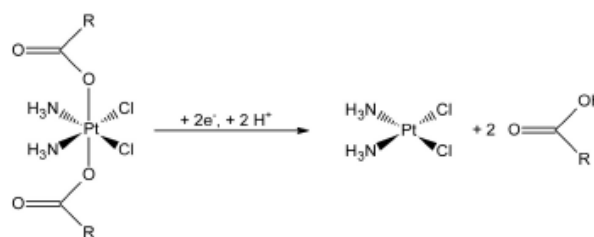
Available online 23 August 2018

0024-3205/© 2018 Elsevier Inc. All rights reserved.

Author's Personal Copy

B. Ruggione et al.

Life Sciences 210 (2018) 166–176



Scheme 1. Activation by reduction mechanism of a generic cisplatin-based Pt(IV) compound. R = alkyl or aryl substituent.

acid (MCFA) family as valproate (VPA) and phenyl-butyrate (PhB), have proved themselves as HDACi, and have been abundantly discussed in literature ([39,40,43]; Witt et al. 2017).

Here we report on a new Pt(IV) complex, based on cisplatin containing a different MCFA-HDACi, namely 2-(2-propynyl)octanoate (POA), along with an inert acetate (Ac) as axial ligands. POA has been reported to be more active than VPA inducing histone hyperacetylation in cerebellar granule cells [34], and showing antiproliferative activity on neuroblastoma cancer cells (neurogenesis and differentiation) [5]. The resulting complex (OC-6-44)-acetatodiamminedichlorido(2-(2-propynyl)octanoato)platinum(IV), named Pt(IV)Ac-POA (Scheme 2), has showed a promising antitumor activity both in vitro and in vivo on several human cancer cell lines [21] with less side effects than cisplatin, as generally Pt(IV) derivatives do.

On these bases, the aim of our study is to evaluate the effects on the B50 neuroblastoma rat cells induced by exposure to Pt(IV)Ac-POA, to understand the activation of cell death pathways and the morphological and functional changes.

2. Materials and methods

2.1. Cell culture and treatments

B50 neuroblastoma rat cells (Istituto Zooprofilattico Sperimentale della Lombardia e dell'Emilia Romagna, catalogue no. BS T.C.I. 115), were cultured in Dulbecco's Modified Eagle Medium (DMEM) supplemented with L-glutamine (2 mM), penicillin 100 IU mL⁻¹, streptomycin (100 mg L⁻¹) and 10% fetal bovine serum (FBS). Cell culture was carried out at 37 °C in a 5% CO₂ humidified chamber. Cells were challenged with Pt(IV)Ac-POA or free POA or free cisplatin for 48 h continuous treatment, CT, then viability assay, flow cytometry,

immuno-cytochemistry and molecular analysis were performed.

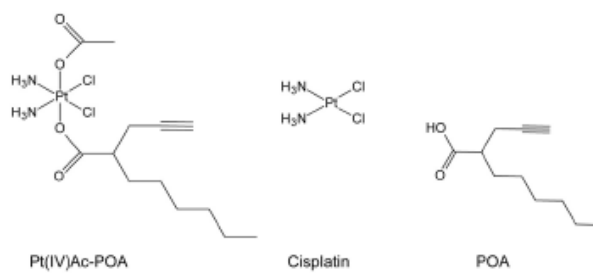
The cells were incubated with 40 μM cisplatin (Teva Pharma, Milan, Italy) for 48 h at 37 °C. This concentration was chosen considering in vivo experiments experimental design (i.e., a single injection of 5 μg/g b.w.) in the normal development nervous system [7] and corresponds to the dose most commonly used in the chemotherapy [4,17]. B50 cells were chosen since they offer several advantages for studying CNS neurons in culture [42]. Moreover these cells were previously used to investigate the mechanisms of cisplatin-induced cytotoxicity.

2.2. Antiproliferative activity and combination index

To assess the growth inhibition of the compounds under investigation, a cell viability test, i.e. the resazurin reduction assay was used. Briefly, cells were seeded in black sterile tissue-culture treated 96-well plates. At the end of treatment (48 h), viability was assayed by 100 μg mL⁻¹ resazurin (Acros Chemicals, France) in fresh medium for 1 h at 37 °C, and the amount of the reduced product, i.e. resorufin, was measured by means of fluorescence (excitation 535 nm, emission 595 nm) with a Tecan Infinite F200Pro plate reader (Tecan Austria). In each experiment, cells were exposed to the drugs at different concentrations and the final data were calculated from at least three replicates of the same experiment performed in triplicate. The fluorescence of 8 wells containing medium without cells were used as blank. Fluorescence data were normalized to 100% cell viability for non-treated cells.

Half inhibitory concentration (IC₅₀), defined as the concentration of the drug reducing cell viability by 50%, was obtained from the dose-response curve fitting using Origin Pro (version 8, Microcal Software, Inc., Northampton, MA, USA).

In the combination index (CI) analysis [15], Pt(IV)Ac-POA



Scheme 2. Sketch of cisplatin, 2-(2-propynyl)octanoic acid, POA, and its Pt(IV) mixed derivative (OC-6-44)-acetatodiamminedichlorido(2-(2-propynyl)octanoato)platinum(IV), Pt(IV)Ac-POA.

conjugate was viewed as a combination of cisplatin and POA at fixed 1:1 dose ratio [53], according to its stoichiometry. The residual viability was compared to those obtained with free cisplatin or free POA as single treatments, by means of the simple formula:

$$CI = \frac{C1_m}{C1_a} + \frac{C2_m}{C2_a}$$

where C1 and C2 are the drug concentrations of metabolites cisplatin and POA in Pt(IV)Ac-POA (C1m and C2m) or when administrated as single treatment (C1a and C2a) to obtain the same level of residual viability. The value of CI allows evaluating drug interaction: $CI \approx 1$ indicates an additive effect, $CI < 1$ and a $CI > 1$ indicate synergism and antagonism, respectively.

2.3. Cell uptake

Cell uptake was measured according to a already published procedure (Ravera et al.) [44]. Briefly, cells were seeded in T25 flasks and continuously treated for 4 h with 1 and 10 μM concentrations of Pt(IV)Ac-POA or free cisplatin, respectively. At the end of the exposure, cells were washed, detached from the flasks and harvested in fresh complete medium. An automatic cell counting device (Countess[®], Life Technologies), was used to measure the cell number and the mean diameter from every cell count. About 5×10^6 cells were transferred into a glass tube, centrifuged, and the supernatant was carefully removed by aspiration. Cellular pellets were stored at -20°C until mineralization. After defrosting, cells were mineralized with HNO_3 in an ultrasonic bath. Platinum determination was performed by inductively coupled plasma-mass spectrometry (ICP-MS, Thermo Optek X Series 2). The level of Pt found in cells after the treatment was normalized upon the cell number and the cellular volume, in order to obtain the intracellular Pt concentration. The ratio between the intracellular and the extracellular (in the culture medium) Pt concentration is defined accumulation ratio, AR [20].

2.4. Flow cytometry

B50 cells were treated in 75 cm^2 plastic flasks with different concentrations of Pt(IV)Ac-POA for 48 h at 37°C (continued exposure to 1, 4 and 10 μM). After treatments, cells were detached by mild trypsinization (0.25% in phosphate-buffered saline, PBS, with 0.05% EDTA) to obtain single-cell suspensions to be processed for flow cytometry with a Partec PAS III flow cytometer (Münster, Germany), equipped with argon laser excitation (power 200 mW) at 488 nm. Data were analysed with the built-in software (Flowmax, Partec).

2.5. Cell cycle analysis and identification of apoptotic cells

Cells were washed in PBS, permeabilized in 70% ethanol for 10 min, treated with RNase A 100 U mL^{-1} and then stained for 10 min at room temperature with Propidium Iodide (PI) 50 $\mu\text{g mL}^{-1}$ (Sigma-Aldrich, Milan, Italy) 1 h before flow cytometric analysis. PI red fluorescence was detected with a 610-nm long-pass emission filter. At least 20,000 cells per sample were measured to obtain the distribution among the different phases of the cell cycle and the percentage of apoptotic cells.

2.6. Analysis of cell death with Annexin V assay

Single-cell suspensions, obtained as described above, were incubated with Annexin V-FITC (Annexin V-FITC Apoptosis Detection Kit, Abcam, Italy) for 10 min in the dark. Propidium Iodide was used as a counterstain to discriminate necrotic/dead cells from apoptotic cells. Fluorescence was revealed by means flow cytometry at 488 nm excitation and with 530/30 (FITC) and 585/42 nm (PI) band-pass emission filters.

2.7. Transmission electron microscopy (TEM)

B50 cells treated with different concentrations of Pt(IV)Ac-POA (1, 4 and 10 μM) were harvested by mild trypsinization (0.25% trypsin in PBS containing 0.05% EDTA) and collected by centrifugation at 800 rpm for 5 min in fresh tubes. The samples were immediately fixed with 2.5% glutaraldehyde in culture medium (2 h at room temperature), centrifuged at 2000 rpm for 10 min and washed several times with PBS. Then, samples were post-fixed in 1% OsO_4 for 2 h at room temperature and washed in water. The cell pellets were pre-embedded in 2% agar, dehydrated with increasing concentrations of acetone (30, 50, 70, 90 and 100%, respectively). Finally, the pellets were embedded in EPON resin and polymerized at 60°C for 48 h. Ultrathin sections were obtained with ultramicrotome Rechter, then placed on nickel grids and stained with uranyl acetate and lead citrate. Sections were observed under a Zeiss EM 900 transmission electron microscope operating at 80 kV. The plates, after being developed, have been computerized through Epson Perfection 4990 Photo scanner at a resolution of 600 dpi and then processed using the Epson Scan software.

2.8. Measurement of mitochondrial membrane potential with JC-1

Changes in mitochondrial membrane potential were monitored using the JC-1 dye (namely, 5,5',6,6'-tetrachloro-1,1',3,3'-tetraethylbenzimidazolylcarbocyanine iodide, Molecular Probes, Invitrogen, Italy). B50 cells, harvested as described above, were incubated in culture medium with 2 μM JC-1 for 20 min at 37°C in the dark. After two washes with PBS at 37°C , the suspension was analysed at 488 nm excitation and with 530/30 and 585/42 nm band-pass emission filters.

2.9. Immunocytochemical reactions at fluorescence microscope

B50 cells were grown on coverslips and treated with the compound under investigation Pt(IV)Ac-POA at the concentration of 4 μM . After 48 h, the cells were fixed with 4% formalin for 20 min and post-fixed with 70% ethanol at -20°C for at least 24 h. Samples were rehydrated for 10 min in PBS and then immunolabeled with primary antibodies for 60 min at room temperature in a dark moist chamber. After some washes in PBS, coverslips were incubated with secondary antibodies for 45 min. After that, sections were counterstained for DNA with 0.1 $\mu\text{g mL}^{-1}$ Hoechst 33258 (Sigma-Aldrich, Milano, Italy), washed with PBS, and mounted in a drop of Mowiol (Calbiochem, Inalco, Italy), for fluorescence microscopy analysis. An Olympus BX51 microscope equipped with a 100-W mercury lamp was used under the following conditions: 330–385 nm excitation filter (excf), 400 nm dichroic mirror (dm) and 420 nm barrier filter (bf) for Hoechst 33258; 450–480 nm excf, 500 nm dm and 515 nm bf for the fluorescence of Alexa 488; 540 nm excf, 580 nm dm and 620 nm bf for Alexa 594. Images were recorded with an Olympus MagniFire camera system and processed with the Olympus Cell F software. The percentage of caspase-positive cells was obtained by counting the cells on coverslips.

Primary and secondary antibodies used for immunocytochemical reactions at fluorescence microscope are reported in Table 1.

2.10. Western blotting

After treatments with cisplatin and Pt(IV)Ac-POA cells were washed twice with PBS and lysed in RIPA buffer (Tris HCl 1 M pH 7.6, EDTA 0.5 M pH 8, NaCl 5 M, NP40 Nonidet 100%, with the addition of proteases and phosphatases inhibitors) at 4°C for 30 min. Proteins were quantified using the Bradford reagent (Sigma Aldrich, Italy). Samples were electrophoresed in a 15% SDS-PAGE minigel and transferred onto a nitrocellulose membrane (Bio-Rad, Hercules, CA) by a semidry blotting for 1.30 h under a constant current of 60 mA. The membranes were saturated for 30 min with PBS containing 0.2% Tween-20 and 5% skim milk, and incubated overnight with monoclonal mouse anti-PCNA

Table 1
Primary and secondary antibodies used for immunocytochemical reactions at fluorescence microscope.

Primary antibody	Secondary antibody	Dilution	Dilution
Caspase-9	Alcon 594-conjugated anti-rabbit antibody (Molecular Probes, Invitrogen)	1:200 in PBS	1:200 in PBS
Caspase-3	Alcon 594-conjugated anti-rabbit antibody (Molecular Probes, Invitrogen)	1:200 in PBS	1:200 in PBS
PARP-1	Alcon 594-conjugated anti-rabbit antibody (Molecular Probes, Invitrogen)	1:200 in PBS	1:200 in PBS
Caspase-8	Alcon 594-conjugated anti-rabbit antibody (Molecular Probes, Invitrogen)	1:200 in PBS	1:200 in PBS
RP71	Alcon 594-conjugated anti-rabbit antibody (Molecular Probes, Invitrogen)	1:200 in PBS	1:200 in PBS
Golgi	Alcon 594-conjugated anti-rabbit antibody (Molecular Probes, Invitrogen)	1:200 in PBS	1:200 in PBS
Mitochondria	Alcon 594-conjugated anti-human antibody (Molecular Probes, Invitrogen)	1:200 in PBS	1:200 in PBS
Lysosomes	Alcon 488-conjugated anti-human antibody (Molecular Probes, Invitrogen)	1:400 in PBS	1:400 in PBS
α -Tubulin	Alcon 488-conjugated anti-mouse antibody (Molecular Probes, Invitrogen)	1:200 in PBS	1:200 in PBS
PCNA	Alcon 594-conjugated anti-mouse antibody (Molecular Probes, Invitrogen)	1:200 in PBS	1:40 in PBS
Actin	Alcon 594-conjugated anti-mouse antibody (Molecular Probes, Invitrogen)	1:40 in PBS	1:40 in PBS

* Becton et al. [9]

antibody (1:5000, Abcam, Cambridge, USA). After several washes with PBS-Tween, the membranes were incubated for 30 min with the proper secondary antibody conjugated with horseradish peroxidase (1:2000, Dako, Italy). Immunoreactive bands were detected with the reagent Luminata[™] Crescendo (Merck Millipore, Billerica, MA), according to the appropriate instructions, and revealed on Amersham Hyperfilm[™] ECL (GE Healthcare, Little Chalfont, UK) slabs. The density of the protein bands were normalized with the respective actin and subsequently with the loading control using ImageJ software.

2. II. Statistical analysis

Every experiment was performed with three independent replicates and the obtained scores were expressed as the mean \pm SD (standard deviation) or SEM (standard error of mean). Data differences were analysed for statistical significance by means of a Student's *t*-test.

3. Results

3.1. Antiproliferative activity, combination index and cellular accumulation

Pt(IV)Ac-POA was tested on the B50 neuroblastoma rat cell line along with free cisplatin and free POA as reference compounds. Noteworthy, Pt(IV)Ac-POA exhibited an IC₅₀ value one orders of magnitude lower (higher potency) than the prototypal metal-drug cisplatin (Table 2 and Fig. 1A). Fig. 1A shows that the preformed Pt(IV)Ac-POA was by far more active than both drugs when administered alone.

In order to further verify if POA enhances the antitumor effect of cisplatin, a combination index was computed. Pt(IV)Ac-POA conjugate was viewed as a combination of cisplatin and POA at fixed 1:1 dose ratio, according to its stoichiometry (see Materials and Methods). At every level of residual viability, CI analysis showed a strong synergistic effect (CI around 0.01) (Fig. 1B).

A key parameter of the mechanisms of action of a drug is its cellular accumulation [36]. Accordingly, when B50 cells were challenged with Pt(IV)Ac-POA, CT 4 h (Table 2), the Pt accumulation ratio (AR) resulted around 12 times higher than that of free cisplatin, in tune with its higher potency (Table 2).

A further investigation on the antiproliferative propensity of Pt(IV)Ac-POA was carried out. The level of the proliferation marker PCNA (Proliferating Cell Nuclear Antigen), correlated in the literature with the degree of glioma malignancy [26] or the efficiency of antitumor treatment [32], was evaluated by western blotting. Fig. 2 shows the PCNA expression in cells after CT with 40 μ M cisplatin or 4 μ M Pt(IV)Ac-POA.

Data indicated a reduction (compared to control) in PCNA expression in cells after all treatments, in particular after exposition to Pt(IV)Ac-POA, thus indicating a synergistic inhibition of PCNA by the combo compound (Fig. 2).

3.2. Cell cycle distribution

The first graph of Fig. 3A represents the distribution of DNA in B50 cells. Decreasing Pt(IV)Ac-POA concentrations (namely 10, 4 and 1 μ M)

Table 2
Antiproliferative activity (IC₅₀) obtained after 48 h CT and accumulation ratio (AR) obtained after 4 h CT. All data are means \pm SEM of at least three independent replicates.

Compound	B50	
	IC ₅₀ (μ M)	AR
POA	750 \pm 120	–
Cisplatin	3.8 \pm 0.6	2.3 \pm 0.5
Pt(IV)Ac-POA	0.37 \pm 0.05	26.9 \pm 0.1

B. Rangone et al.

Life Sciences 210 (2018) 166–176

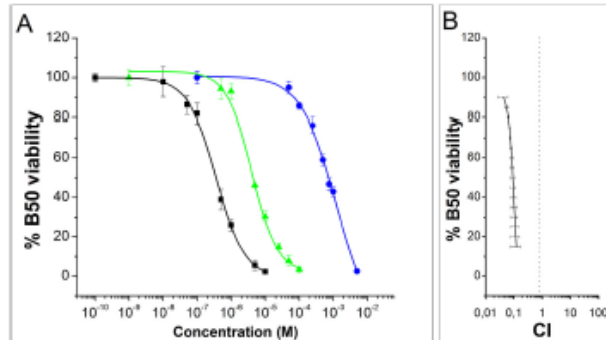


Fig. 1. (A) B50 cells were treated for 48 h with cisplatin (green triangles), POA (blue dots), or the 1:1 the combo molecule Pt(IV)Ac-POA (black squares). Data are means \pm standard deviation of a representative experiment. Residual viability was assessed by means of the resazurin reduction assay and data were fitted with a four-parameter function (green, blue, and black lines, respectively). Residual viability data were compared to obtain the Combination Index (CI) value. (CI < 1: synergism; CI around 1 additive effect; CI > 1 antagonism). (B) CI plot (black line) for the 1:1 the combo molecule Pt(IV)Ac-POA. (For interpretation of the references to colour in this figure legend, the reader is referred to the web version of this article.)

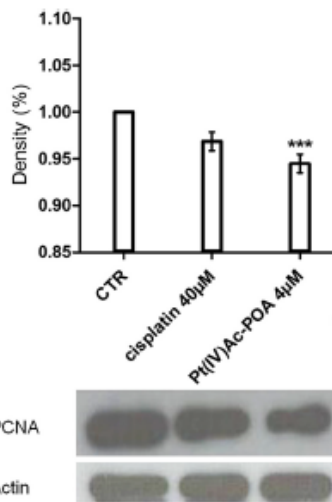


Fig. 2. Western blotting of PCNA following 48 h CT with 40 μ M cisplatin or 4 μ M Pt(IV)Ac-POA. The density of the bands was normalized over actin and over the untreated control (CTR). Data are means \pm SEM. Statistical analysis: number of observations per control and treated samples: 3; * p < 0.05; ** p < 0.01; *** p < 0.001.

were used for 48 h CT. Untreated cells (CTR) were distributed among the cell phases (G_1 , S, G_2), the intensity of S phase indicated that the cells were proliferating. Conversely, the treatment with 10 μ M CT deeply modified the histogram distribution. We observed a massive number of cells in sub- G_1 phase (dead cells), while peaks G_1 , S and G_2 were almost absent. After 4 μ M CT the sub- G_1 peak was still evident, while the presence of G_1 and S peaks and the absence of G_2 peak indicated arrested proliferation. After 1 μ M CT, the cells were still distributed in the different phases of cell cycle, along with a small sub- G_1 peak.

3.3. Ultrastructural analysis

In control, (Fig. 3Ba) the sample cell was characterized by the presence of a nucleus in peripheral position, a decondensed chromatin and a large nucleolus. Reticulum endoplasmic and Golgi Apparatus were present in perinuclear zone and there were small-to-medium size mitochondria in cytoplasm and sporadic lysosomes. In Fig. 3Bb cell after 10 μ M CT exhibited typical necrosis morphology. Indeed, an evident subcellular disorganization and disaggregation of organelles and cytoskeletal components were observed. Moreover, the fragmentation of the nucleus and highly condensed chromatin (karyorrhexis) were also detectable.

Treatments with 1 μ M (Fig. 3Bc) and, even more, with 4 μ M (Fig. 3Bd) seem to induce autophagy. A reduction of nucleus volume (pyknosis) and an increase of lysosomes and autophagic vacuole number were observed. Some vacuoles contained membranous cytoplasmic residues in the degradation phase, which can be attributable to autophagosomes. In addition, elongated mitochondria were observed, a characteristic of a cell that tries to survive [46].

One cell in apoptosis and another in necroptosis were evidenced in Fig. 3Be and Bf, several types of cell death were detectable in the sample treated at 4 μ M.

3.4. Flow cytometric analysis after staining with Annexin V and PI

To assess the induction of apoptosis after 4 and 10 μ M CT with Pt(IV)Ac-POA, a test with Annexin V/PI staining was performed. Fig. 3C shows that in the control almost all cells are living, while after treatments the number of viable cells tended to decrease drastically. In particular, at 4 μ M an increase of late apoptotic cells (Q3, yellow bars) compared to control (62.6 ± 0.8 vs 21 ± 0.2) was observed. At 10 μ M CT necrotic cells (Q2, red bars) increased compared to 4 μ M CT (45.79 ± 0.32 vs 10.88 ± 0.44).

For this reason, the concentration of 4 μ M of Pt(IV)Ac-POA was chosen hereafter for the standard 48 h CT.

3.5. Activation of apoptotic pathways

The intrinsic pathway is activated by several stimuli making permeable the mitochondrial membrane. The results obtained with JC-1 assay in cytofluorometric analysis demonstrated a perturbation of the mitochondrial membrane potential (MMP). In treated cells, the fluorescence changed from orange (JC-1 aggregates, Q3), observed in the control, to green fluorescent (monomeric JC-1, Q4), indicating a significant depolarization of MMP [1] (Fig. 4A and B).

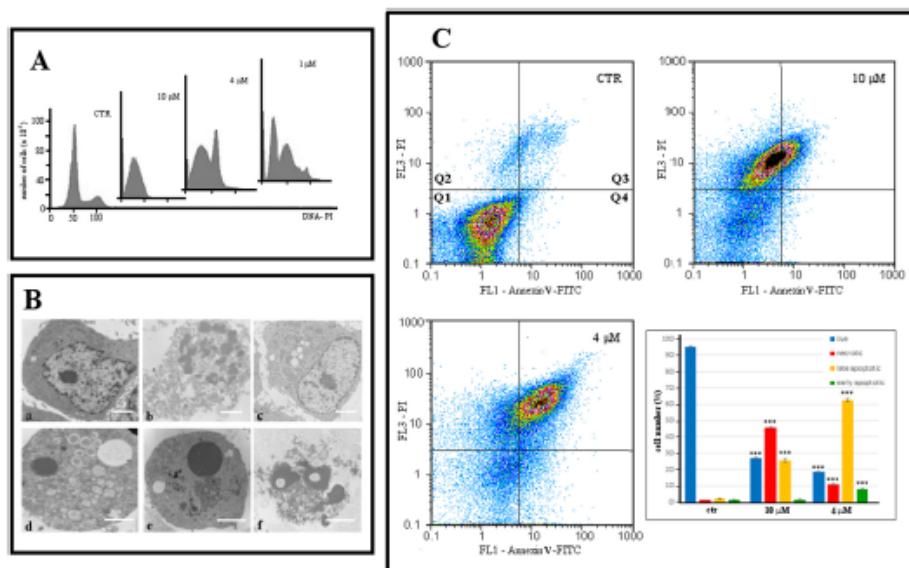


Fig. 3. (A) Histograms of DNA content in Flow cytometry after PI staining in B50 control cells (CTR) and treated for 48 h with Pt(IV)Ac-POA at different concentrations (10, 4 and 1 μ M). (B) Electron microscopy. a) B50 cell in control condition. b) B50 cell after treatment with Pt(IV)Ac-POA at 10 μ M for 48 h. c) B50 cell after treatment with Pt(IV)Ac-POA at 1 μ M for 48 h. d, e, f) B50 cells after treatment with Pt(IV)Ac-POA at 4 μ M for 48 h. Pictures d–f show examples of cell death for d) autophagy, e) apoptosis, and f) necroptosis. Bars: 1.5 μ m. (C) Dual parameter cytograms of FITC-labelled Annexin V (FL1) versus PI staining (FL3) of the control (CTR, upper left plot) and of cells treated with Pt(IV)Ac-POA at 10 (upper right plot) and 4 μ M (lower left plot) concentrations, respectively. The histogram represents the average of three independent experiments, showing the values percentage of Annexin V/PI positive cells; in quadrant Q1 (viable cells), Q2 (necrotic), Q3 (late apoptotic) and Q4 (early apoptotic). Statistical analysis: number of observations per control and treated samples: 5; * $p < 0.05$; ** $p < 0.01$; *** $p < 0.001$.

Furthermore, to evaluate the activation of apoptotic pathway, immunocytochemical detection for active caspase-9, -3 and for PARP-1 was performed.

In the intrinsic apoptotic pathway, the executive caspase-3 was activated by caspase-9; in control condition, cells were not immunopositive to caspase-3, as testified by the presence of only proliferative viable cells (mitosis is visible in the lower-left box of Fig. 5B). In this condition, actin cytoskeletal was well organized in filaments within all cytoplasm. After treatment, the cells underwent apoptosis: the immunopositivity of both caspase-9 and caspase-3 (red fluorescence) was increased. In this condition, cell morphology was altered: the cells had a round shape and their nucleus appeared fragmented (visible in the lower left panel of Fig. 5B). The actin cytoskeleton collapsed, with inhomogeneous distribution localized around the nucleus.

The percentage of caspase-3 positive cells was $3 \pm 0.5\%$ in the control and $52 \pm 2\%$ in the samples after CT.

Poly [ADP-ribose] polymerase 1, PARP-1, is an enzyme involved in repair processes of DNA. Its proteolytic cleavage fragments, i.e. "cleaved PARP-1" are one of the hallmark of apoptosis, since PARP-1 is a preferential substrate for caspase-3. The longer fragment is released from the nucleus to the cytosol, due to its lower DNA-binding affinity [14]. Accordingly, PARP-1 (red fluorescence) was found colocalized in nuclei in control and in early apoptotic cells (Fig. 5C), while it moved to the cytoplasm in late apoptotic cells, where nuclei resulted clearly fragmented. The cytoskeletal tubulin showed alterations and formed aggregates, so the cells lost their tapered shape.

Caspase-8 is involved in the extrinsic apoptotic pathway; and its

activation is induced by the death receptors Fas, tumour necrosis factor receptor-1 and death receptor-3. In Fig. 5D, a high increase in caspase-8 cytoplasmic immunopositivity (red fluorescence) was observed in cells treated only.

To confirm the activation of the extrinsic apoptotic pathway, an immunocytochemical detection of RIP1 (receptor-interacting protein kinase 1), which is a caspase-8 substrate, was performed. In control cells (Fig. 5E), RIP1 was expressed in the cytoplasm with a homogeneous distribution, but the treatment caused a redistribution of RIP1 from the cytoplasm to a perinuclear zone, indicating that active RIP1 translocated from the cytoplasm, which was totally destroyed in tardive apoptosis.

3.6. Evaluation of autophagy

LC3 is an ubiquitin-like protein that is cleaved at its C-terminal to form LC3B-I (14 kDa). LC3B-I is then conjugated to phosphatidylethanolamine in the autophagosome membrane to form LC3B-II (16 kDa) [28]. In control cells, LC3B was detected both in the nucleus and in the cytoplasm and did not colocalize with lysosomes in the cytoplasm. On the contrary after CT, LC3B moved mostly into the cytoplasm of apoptotic cells (Fig. 5F). In particular, in early apoptosis LC3B colocalized with lysosomes in the cytoplasm (represented in the box), whereas in late apoptosis there was no colocalization and lysosomes decreased.

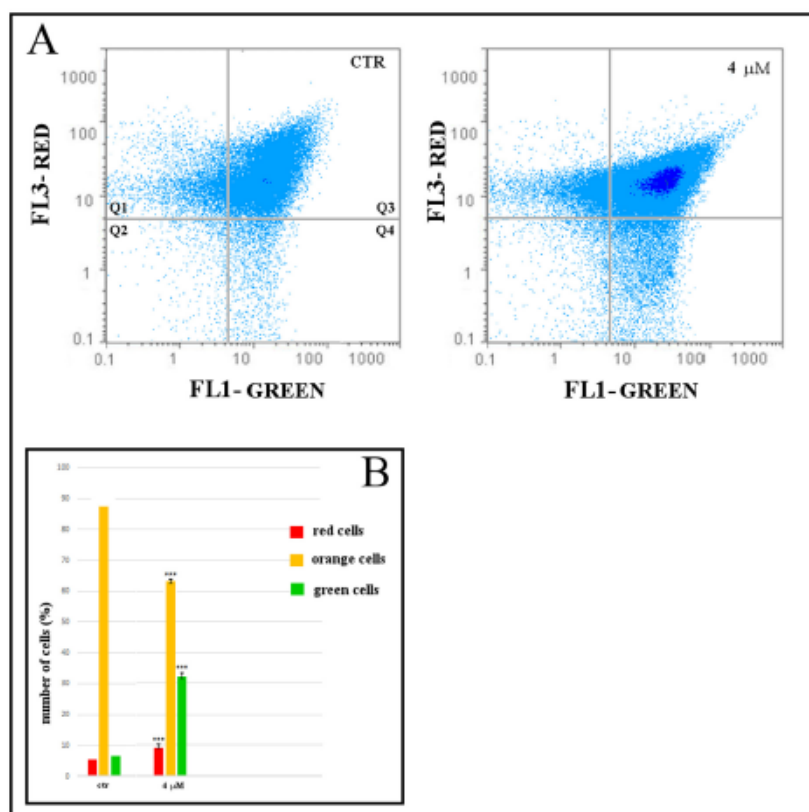


Fig. 4. Effect of Pt(IV)Ac-POA treatment on mitochondrial potential of B50 cells. (A) Cytometric analysis of green-versus-red fluorescence of JC-1 showing cell filling into the red fraction (Q1), the orange fraction (Q3) and green fraction (Q4). Representative plots of the control (CTR, upper left plot) and 4 μ M Pt(IV)Ac-POA (upper right plot) treated samples. (B) Histograms with percentage of JC-1 positive cells: green, red and orange cells bar chart. Statistical analysis: number of observations per control and treated samples: 3; * $p < 0.05$; ** $p < 0.01$; *** $p < 0.001$. (For interpretation of the references to colour in this figure legend, the reader is referred to the web version of this article.)

3.7. Effects of Pt(IV)Ac-POA on intracellular organelles

We evaluated also the effects of Pt(IV)Ac-POA on cytoplasmic organelles, such as Golgi Apparatus and mitochondria. In control cells (Fig. 6A), immunofluorescence for Golgi apparatus (red fluorescence) appeared homogeneous with a perinuclear localization while the actin cytoskeleton maintained its organization. After CT, cells underwent to death showing evident alterations. In this condition, the nucleus was fragmented and the actin cytoskeleton collapsed around it; Golgi Apparatus lost its tubular connections and resulted distributed in the cytoplasm.

In control, mitochondria (red fluorescence) with a spotted-like shape, localized in cytoplasm and near the nucleus, were observed (Fig. 6B). Compared to control, treated cells showed mitochondria with morphological alterations, in particular the immunofluorescence for mitochondria appeared homogeneous and these organelles clustered

and formed dense masses around the nucleus.

4. Discussion and conclusions

Cisplatin has been used for almost half a century in the chemotherapeutic treatment of different types of cancer [29]. Many side effects, including nephrotoxicity, neurotoxicity, ototoxicity, etc., limit its clinical application [49].

In recent years, many attempts have been made to obtain molecules that can overcome these problems [51]. Particularly, new platinum(II)-based compounds, which have as the cellular targets the amino acid residues of protein, have been synthesized [16,38] and were used compared to cisplatin treatment, showing a lower cytotoxicity in vivo studies on development of rat cerebellum and hippocampus [8]. In addition, in vitro studies, these new platinum(II)-based compounds have been shown to induced, similarly to cisplatin, apoptotic cell death

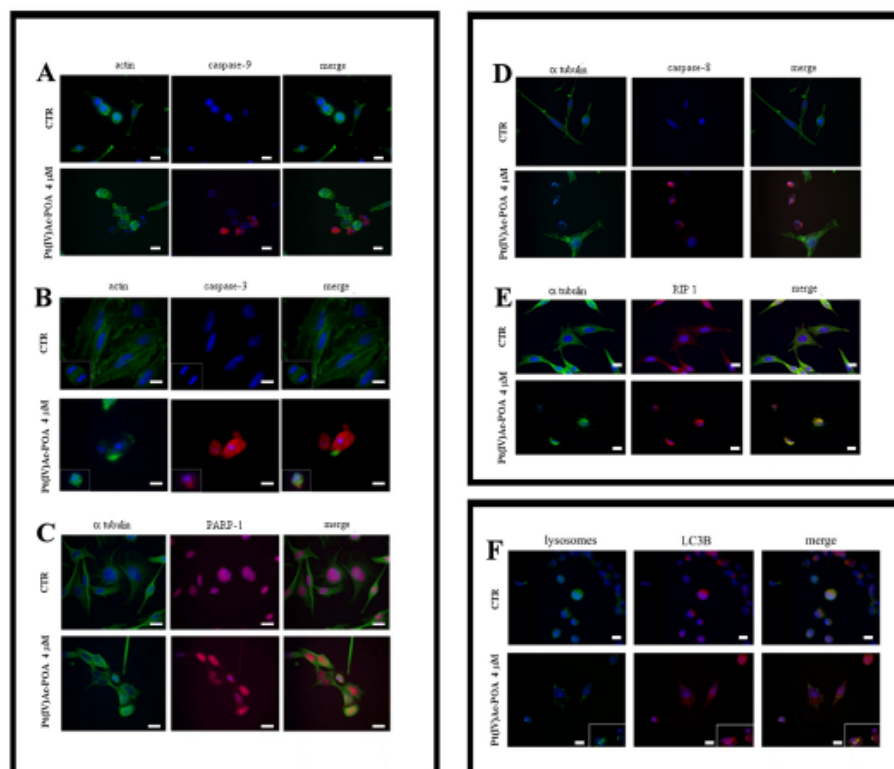


Fig. 5. Double immunocytochemical detection in control (CTR) and 48 h Pt(IV)Ac-POA at 4 μ M treated cells: (A) caspase-9 (red fluorescence) and actin (green fluorescence); (B) caspase-3 (red fluorescence) and actin (green fluorescence); (C) PARP-1 (red fluorescence) and α tubulin (green fluorescence); (D) caspase-3 (red fluorescence) and α tubulin (green fluorescence); (E) RIP1 (red fluorescence) and α tubulin (green fluorescence); (F) LC3B (red fluorescence) and lysosomes (green fluorescence). DNA was counterstained with Hoechst 33258 (blue fluorescence). Bar: 20 μ m. (For interpretation of the references to colour in this figure legend, the reader is referred to the web version of this article.)

in B50 neuroblastoma rat cells at concentration 4 times lower than cisplatin [25].

Nowadays, platinum(IV) prodrugs are actively investigated [23]. In particular, a new prodrug, namely Pt(IV)Ac-POA, has been recently synthesized [21]. This complex is a new multi-action prodrug candidate, designed as a cisplatin/POA “combo” molecule. This considerable advantage is due to its ability to deliver at the same time huge amounts of cisplatin and POA in cells. This enhancement of cellular uptake is mainly due to the lipophilicity of the Pt(IV)Ac-POA assembly with respect to the hydrophilic cisplatin and the amphiphilic POA (in anionic form at physiologic pH) precursors, enhancement referred as “*synergistic cellular accumulation*” [21].

The action of POA as an HDAC inhibitor represents a promising strategy specifically for neuroblastoma chemotherapy [41,52]. In particular, HDAC8 inhibition enhances the effects of DNA-damaging drugs, as cisplatin, inducing overall chemosensitization and decreasing chemoresistance [52]. Furthermore, POA has showed a strong

antiproliferative activity associated with morphological changes in neuroblastoma cells (neuritogenesis and differentiation) [5]. The limit of HDACi is the need of high dosages, giving rise to considerable side effects [41]. Pt(IV)Ac-POA could bypass the problem because Pt(IV)-based complexes are stable in the bloodstream [18] and enter tumour cells to higher extent than free POA [27]. In aggregate, Pt(IV)Ac-POA could offer the advantages of cisplatin (DNA-damaging activity) and of POA (HDAC inhibition) without the limiting toxicities of both agents when administered individually on neuroblastoma.

Viability assays showed that this prodrug has a higher antiproliferative activity than cisplatin on B50 cell line, since its half-maximal inhibitory concentration (IC_{50}) after 48 h CT was 0.37 compared to 3.8 μ M for cisplatin. The higher activity of Pt(IV)Ac-POA has been further confirmed by the decreased PCNA expression and by the different cell cycle distribution.

Pt(IV)Ac-POA exhibited a strong synergistic effect in respect to the free drug, taking advantage of an exceptional increase of cellular

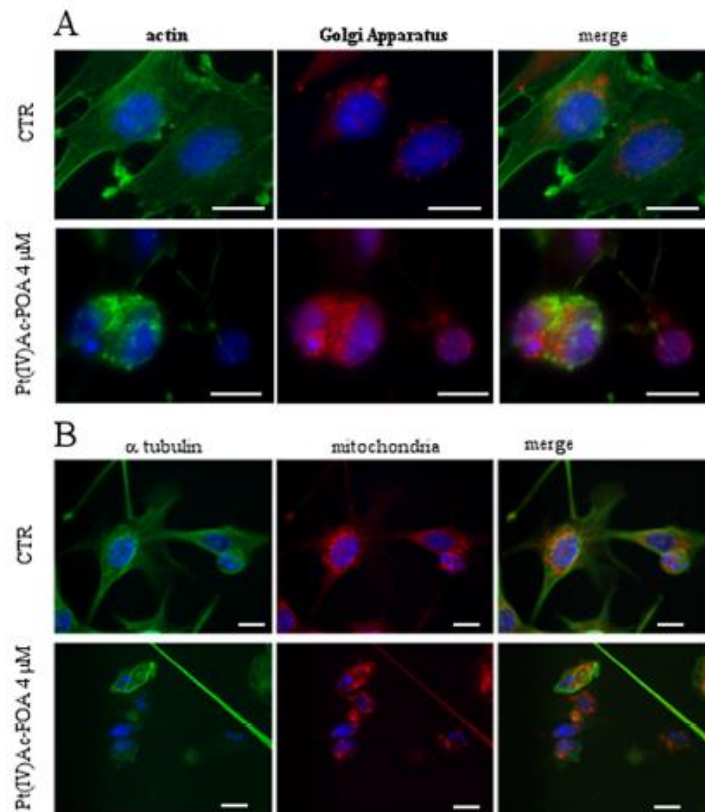


Fig. 6. (A) Golgi apparatus (red fluorescence) and actin (green fluorescence) in control and 48 h Pt(IV)Ac-FOA at 4 μM treated cells. (B) Double immunocytochemical detection of mitochondria (red fluorescence) and α tubulin (green fluorescence) in control and 48 h Pt(IV)Ac-FOA at 4 μM treated cells. DNA was counterstained with Hoechst 33258 (blue fluorescence). Bars: 20 μm. (For interpretation of the references to colour in this figure legend, the reader is referred to the web version of this article.)

uptake, often referred as "synergistic cellular accumulation" (e.g. [21]).

Results obtained by Santin et al. proved that cisplatin induced 22% of caspase-3 positive apoptotic cells in B50 cell line [45], while Pt(IV)Ac-FOA, used at a concentration ten times less than cisplatin, causes a higher apoptotic effect (52%).

Electron microscopy analysis demonstrated that after 10 μM CT, cells exhibited necrotic morphology, while after 4 μM CT, cells showed apoptotic morphology. In addition, cells with autophagic characteristics were also detectable, as the activation of autophagy which may occur in type II cell death. An immunocytochemical staining of different markers confirmed the activation of different pathways. The treated samples were immunopositive to cleaved PARP-1 and caspases-9, -3, -8 and RIP1 demonstrating the activation of both the intrinsic and extrinsic apoptotic pathways. Since RIP1 is also involved in a preliminary step of the necroptotic pathway, we could not exclude its activation as some cells showed the typical necroptotic morphology [2,22]. The

colocalization of the staining for LC3B and lysosomes suggested the activation of the autophagic pathway [47].

JC-1 staining showed a drop of the mitochondrial membrane potential, a further indication that Pt(IV)Ac-FOA is able to induce apoptosis. Indeed, this dye is a valuable indicator of the health and functional state of the cells [33]. Like cisplatin [3], the new prodrug also targets cytoplasmic organelles: after fluorescent immunolabelling mitochondria appeared small and rounded and often organized in clusters in dying cells. In control cells, Golgi apparatus had flattened perinuclear tanks, while after treatment it was observed as round bodies in cytoplasm. The actinic and tubulin cytoskeleton disassembled and reorganized, assuming a more homogeneous appearance.

Considering that Pt(IV)Ac-FOA prodrug acts on B50 neuroblastoma rat cells at concentration ten times lower respect to cisplatin and induced different patterns of cell death, it could represent a potential alternative to cisplatin.

B. Rangone et al.

Life Sciences 210 (2018) 166–176

Conflict of interest

The authors declare no conflict of interest.

Author contributions

All authors had full access to all experimental data and assume responsibility for the integrity and accuracy of data and analysis.

MG Bottone: study concept and design, analysis and interpretation of data, writing and finalizing the manuscript and supervision; B Rangone: analysis and interpretation of data, writing the manuscript; B Ferrari: analysis and interpretation of data, writing the manuscript; V Artesiani: analysis and interpretation of data, writing the manuscript; I Maselli: Acquisition, analysis and interpretation of data; P Veneroni technical assistance for cell culture; I Zanellato: analysis and interpretation of data, writing the manuscript; D Osella: analysis and interpretation of data, writing and finalizing the manuscript.

Beatrice Rangone and Beatrice Ferrari: both authors contributed equally to this work.

Acknowledgements

This research is supported by the University of Pavia: Fondi Ricerca Giovani (FRG 2016) and by the Compagnia di San Paolo: research project "BIPLANES". We are indebted to the Inter-University Consortium for Research on the Chemistry of Metals in Biological Systems (CIRCMSB, Bari) and UE COST CM1105 Action "Functional metal complexes that bind to biomolecules" for stimulating discussions during the group meetings and short-term missions. We thank Dr. Giuliano Mazzini (IGM-CNR, Pavia) for assistance in the analysis in Flow cytometry.

References

- [1] E. Bolner, X. Li, W. Gerczyca, M.R. Melamed, Z. Daryniakiewicz, Analysis of apoptosis by laser scanning cytometry, *Cytometry* 35 (1999) 181–195.
- [2] J. Inzinzio, L. Vieira-Cordeiro, S. Enns, Necroptotic cell death signaling and execution pathway: lessons from knockout mice, *Mediat. Inflamm.* 2015 (2015) 128076, <https://doi.org/10.1155/2015/128076>.
- [3] G. Bernocchi, M.G. Bottone, V.M. Piccolini, V. Dal Bo, G. Santin, S.A. De Pascali, D. Mignoli, P.F. Zanetti, Developing central nervous system and vulnerability to platinum compounds, *Chemother. Res. Pract.* 2011 (2011) 315418, <https://doi.org/10.1155/2011/315418>.
- [4] D.L. Bodamer, P.C. Daddon, P.C. Kang, J.C. Katz, R.F. Booth, Selective protection against cis-diamminedichloroplatinum (II)-induced toxicity in kidney, gut, and bone marrow by *dehydroepiandrosterone*, *Cancer Res.* 46 (1986) 2751–2755.
- [5] U. Rafiq, K. Ekin, U. Eberbeck, C.L. Bacon, E. O'Driscoll, C. O'Connell, V. Bessini, A. Kawa, E. Lapchik, E. Beck, C.M. Regan, H. Nau, Studies on the tetrazolium pharmacophore of valproic acid analogues: evidence of interactions at a hydrophobic centre, *Eur. J. Pharmacol.* 354 (2–3) (1998) 289–299, [https://doi.org/10.1016/S0014-2999\(98\)00462-2](https://doi.org/10.1016/S0014-2999(98)00462-2).
- [6] J.E. Bolden, M.J. Post, R.W. Johnston, Anticancer activities of histone deacetylase inhibitors, *Nat. Rev. Drug Discov.* 5 (2006) 769–784, <https://doi.org/10.1038/nrd2133>.
- [7] M.G. Bottone, C. Soldani, P. Veneroni, D. Avella, M.R. Piva, G. Bernocchi, Cell proliferation, apoptosis and mitochondrial damage in rat R50 neuronal cells after cisplatin treatment, *Cell Prolif.* 41 (2008) 506–520, <https://doi.org/10.1111/j.1365-2184.2008.00550.x>.
- [8] M.G. Bottone, G. Santin, V.M. Piccolini, V. Dal Bo, G. Bernocchi, Cisplatin neurotoxicity induces cell death in vivo and in vitro: Cisplatin: Pharmacology, Clinical Use and Adverse Effects, Nova Science Publishers, 2011, https://www.novapublishers.com/catalog/producer_info.php?product_id=37177.
- [9] M.G. Bottone, G. Santin, C. Soldani, P. Veneroni, A.L. Soszka, C. Alpini, Intracellular distribution of Taukynase as detected by multicolor immunofluorescence techniques, *Eur. J. Histochem.* 56 (2012) e4, <https://doi.org/10.4081/ejh.2012.e4>.
- [10] T. Boulikas, A. Pantos, E. Belle, P. Christofit, Designing platinum compounds in cancer: structures and mechanisms, *J. Cancer Ther.* 5 (2007) 557–583.
- [11] G.M. Brodsky, M.D. Hogarty, Y.P. Minou, J.M. Marié, *Neuroblastoma*, in: P.A. Pizzo, D.G. Poplack (Eds.), *Principles and Practice of Pediatric Oncology*, 6th ed., Lippincott, Williams and Wilkins, Philadelphia (PA), USA, 2011, pp. 886–922.
- [12] G. Cavalletti, B. Fregeni, F. Lanzani, L. Mattavelli, E. Susani, P. Alberti, D. Corlinovic, P. Bidoli, Chemotherapy-induced peripheral neurotoxicity assessment: a critical revision of the currently available tests, *Eur. J. Cancer* 46 (2010) 479–494, <https://doi.org/10.1016/j.ejca.2009.12.008>.
- [13] G.V. Chaitanya, J.S. Alexander, P.P. Babu, PARP-1 cleavage fragments: signatures of cell-death proteases in neurodegeneration, *Cell Commun. Signal* 8 (2010) 31, <https://doi.org/10.1186/1478-811X-8-31>.
- [14] T.C. Chou, P. Talley, Quantitative analysis of dose-effect relationships: the combined effects of multiple drugs or enzyme inhibitors, *Adv. Enzym. Regul.* 22 (1984) 27–55, [https://doi.org/10.1016/0065-2571\(84\)90007-4](https://doi.org/10.1016/0065-2571(84)90007-4).
- [15] S.A. De Pascali, P. Papadia, A. Ciccarese, C. Pacifico, F.P. Zanetti, First examples of platinum-platinum II complexes with nucleic acids, *Eur. J. Inorg. Chem.* 5 (2005) 784–796, <https://doi.org/10.1002/ejic.200400665>.
- [16] J. Dietrich, R. Han, Y. Yang, M. Mayer-Trischel, M. Noble, CNS progenitor cells and oligodendrocytes are target of chemotherapeutic agents in vivo and in vitro, *J. Biol. Chem.* 281 (2006) 22–34, <https://doi.org/10.1074/jbc.M510280>.
- [17] R.C. Dolman, G.B. Deacon, T.W. Hambley, Studies of the binding of a series of platinum(IV) complexes to plasma proteins, *J. Inorg. Biochem.* 88 (3–4) (2002) 260–269, [https://doi.org/10.1016/S0162-0134\(01\)00260-9](https://doi.org/10.1016/S0162-0134(01)00260-9).
- [18] C. Frangola, C.A. Boicelli, M. Orsini, C. Addario, P. Chiari, M. Viale, Protective effect of proline hydrochloride on cisplatin-induced alterations in rat kidney, *Anti-Cancer Drugs* 13 (10) (2002) 1043–1054, <https://doi.org/10.1097/00001813-200210000-00008>.
- [19] E. Gabano, M. Ravera, D. Osella, Piva and cure of bifunctional platinum(IV) anticancer prodrugs two are (not always) better than one, *Dalton Trans.* 43 (2014) 98213–99820, <https://doi.org/10.1039/c4dt00091h>.
- [20] E. Gabano, M. Ravera, I. Zanellato, S. Tinello, A. Gallia, B. Rangone, V. Gandia, C. Marzano, M.G. Bottone, D. Osella, An unsymmetrical cisplatin-based Pt(IV) derivative containing 2-(3-propenyl)octanoate: a very efficient multi-action anticancer prodrug candidate, *Dalton Trans.* 46 (2017) 14174–14185, <https://doi.org/10.1039/c6dt02020a>.
- [21] L. Galluzzi, O. Kopp, G. Kroemer, Mitochondrial regulation of cell death: a phylogenetically conserved control, *Microb. Cell Fact.* 3 (2016) 101–108, <https://doi.org/10.15698/mic2016.03.483>.
- [22] D. Gibson, Platinum(IV) anticancer prodrugs - hypothesis and facts, *Dalton Trans.* 45 (3) (2016) 12985–12991, <https://doi.org/10.1039/c6dt01414c>.
- [23] N. Graf, S.J. Lippard, Redox activation of metal-based prodrugs as a strategy for drug delivery, *Adv. Drug Deliv. Rev.* 64 (2012) 993–1004, <https://doi.org/10.1016/j.addr.2012.01.007>.
- [24] M. Giammalvi, G. Santin, V. Invidia, V. Dal Bo, V.M. Piccolini, P. Veneroni, S. Banti, M. De Pascali, S.A. Verd, F.P. Zanetti, G. Bernocchi, M.G. Bottone, [Pt(OAc)(acac)(y-acac)(DMS)] versus cisplatin apoptotic effects in R50 neuroblastoma cells, *Histochem. Cell Biol.* 145 (5) (2016) 587–601, <https://doi.org/10.1007/s00418-015-1396-1>.
- [25] K. Guzikowska-Ustymowicz, A. Pryczynicz, A. Kemona, J. Czynbawska, Correlation between proliferation markers PCNA, Ki-67, MCM-2 and antiapoptotic protein Bcl-2 in colorectal cancer, *Anticancer Res.* 29 (8) (2009) 3049–3052.
- [26] T.C. Johnston, K. Sauerbrey, S.J. Lippard, The next generation of platinum drugs: targeted Pt(II) agents, nanoparticle delivery, and Pt(IV) prodrugs, *Chem. Rev.* 116 (2016) 3436–3486, <https://doi.org/10.1021/acs.chemrev.5b00597>.
- [27] Y. Kabeya, N. Mizushima, T. Ueno, A. Yamamoto, T. Kirisako, T. Noda, E. Kimizuka, Y. Ohsumi, T. Yoshimori, LC3, a mammalian homologue of yeast Apg8p, is localized in autophagosome membranes after processing, *EMBO J.* 19 (2000) 5720–5728, <https://doi.org/10.1093/emboj/19.21.5720>.
- [28] L. Kalland, The resurgence of platinum-based cancer chemotherapy, *Nat. Rev. Cancer* 7 (2007) 573–584, <https://doi.org/10.1038/nrc2167>.
- [29] M.R. Kelley, Y. Jiang, C. Guo, A. Reed, H. Meng, M.R. Vashe, Role of the DNA base excision repair protein, APE1 in cisplatin, oxaliplatin, or carboplatin induced sensory neuropathy, *PLoS One* 9 (2014) e106485, <https://doi.org/10.1371/journal.pone.0106485>.
- [30] R.G. Kenny, S.W. Chuah, A. Crawford, C.J. Marmion, Platinum(IV) Prodrugs - a step closer to Ehrlich's vision? *Eur. J. Inorg. Chem.* 2017 (2017) 1596–1612, <https://doi.org/10.1002/ejic.201601278>.
- [31] M. Kutwin, E. Sawose, S. Jaworski, M. Wierzbicki, B. Strojny, M. Gendek, A. Chwalibog, Assessment of the proliferation status of glioblastoma cell and tumor status after nanoplatinum treatment, *PLoS One* (2017) 12(5), <https://doi.org/10.1371/journal.pone.0178277>.
- [32] A.V. Kuznetsov, R. Margreiter, A. Amberger, V. Saks, M. Grimm, Changes in mitochondrial redox state, membrane potential and calcium permeate mitochondrial dysfunction in doxorubicin-induced cell death, *Biochim. Biophys. Acta* 1813 (6) (2011) 1144–1152, <https://doi.org/10.1016/j.bbamcr.2011.05.002>.
- [33] Y. Leng, Z. Maizova, M.A. Reis-Ferreira, H. Nau, D.M. Chang, Potent neuroprotective effects of novel structural derivatives of valproic acid: potential roles of HDAC inhibition and HSP70 induction, *Neurosci. Lett.* 476 (2010) 127–130, <https://doi.org/10.1016/j.neulet.2009.04.013>.
- [34] Y. Li, E. Seo, HDACs and HDAC inhibitors in cancer developmental therapy, *Cold Spring Harb. Perspect. Med.* 6 (10) (2016), <https://doi.org/10.1101/cshperspect.a026831>.
- [35] E. Lindqvist, E. Holzer, Cellular distribution and cellular reactivity of platinum(II) complexes, *Biochem. Pharmacol.* 52 (1996) 7–14, [https://doi.org/10.1016/0006-2952\(96\)0106-2](https://doi.org/10.1016/0006-2952(96)0106-2).
- [36] M. Liu, C.C. Chiara, M. Bumo-Tany, R.R. Mella, L.C. Racanan, R.R. Golvin, H. Raib, A pathophysiologic role for T lymphocytes in murine acute cisplatin nephrotoxicity, *J. Am. Soc. Nephrol.* 17 (2006) 765–774, <https://doi.org/10.1681/ASN.2005010102>.
- [37] A. Mucchelli, N. Calabro, C. Vetrugno, F.P. Zanetti, S.A. De Pascali, C. Strelli, S. Marzagliano, The platinum (II) complex [Pt(OAc)(y-acac)(DMS)] alters the intracellular calcium homeostasis in MCF-7 breast cancer cells, *Biochim. Pharmacol.* 81 (2011) 91–103, <https://doi.org/10.1016/j.bcp.2010.09.012>.
- [38] V. Novichkova, L. Zorzanova, J. Stupankova, O. Vana, R. Ravendran, D. Gibson,

Author's Personal Copy

B. Rangone et al.

Life Sciences 210 (2018) 166–176

- J. Kasparkova, V. Brabec, New insights into the molecular and epigenetic effects of anti-tumor Pt(IV)-oxalate acid conjugates in human ovarian cancer cells, *Biochem. Pharmacol.* 95 (2015) 133–144, <https://doi.org/10.1016/j.bcp.2015.04.003>.
- [40] V. Novobradsky, I. Zanollato, C. Mazzoni, J. Pacharova, J. Kasparkova, D. Gibson, V. Gardin, D. Onella, V. Brabec, Epigenetic and anti-tumor effects of platinum(IV)-octanoate conjugates, *Sci. Rep.* 7 (1) (2017) 3751, <https://doi.org/10.1038/s41598-017-02864-w>.
- [41] I. Oehme, H.E. Deshner, M. Ledriani, T. Milde, O. Witt, Targeting of HDAC5 and investigational inhibitors in neuroblastoma, *Expert Opin. Invest. Drugs* 18 (11) (2009) 1605–1617, <https://doi.org/10.1517/14726230903241658>.
- [42] C.A. Ouy, M. Boudjadja, P. Masson, K55 neuroblastoma cells: an early manufactured cultured cell model of central nervous system neurons, *Methods Cell Biol.* 71 (2003) 287–304.
- [43] R. Ravendran, J.P. Brault, E. Wenzelhan, V. Novobradsky, O. Stuchlikova, V. Brabec, V. Gardin, D. Gibson, Pt(IV) derivatives of cisplatin and oxaliplatin with phenylthio urea axial ligands are potent cytotoxic agents that act by several mechanisms of action, *Chem. Sci.* 7 (2016) 2581–2591, <https://doi.org/10.1039/C5SC04235D>.
- [44] M. Ravera, E. Gabano, I. Zanollato, A. Gallina, E. Perin, A. Arzani, S. Castiglioni, D. Onella, Cisplatin and valproate released from the bifunctional [Pt(IV)Cl₂(NH₂)₂(valproate)₂] anti-tumor prodrug or from liposome formulations: who does what? *Dalton Trans.* 46 (2017) 1559–1566, <https://doi.org/10.1039/C6DT03749F>.
- [45] G. Santin, V.M. Piccolini, P. Veronesi, S. Bardi, G. Bernocchi, M.G. Bottoni, Different patterns of apoptosis in response to cisplatin in R50 neuroblastoma rat cells, *Histo. Histochem.* 26 (7) (2011) 831–842, <https://doi.org/10.14670/HH-26-530>.
- [46] G. Santin, V.M. Piccolini, S. Bardi, P. Veronesi, V. Gianesini, V. Dal Bo, G. Bernocchi, M.G. Bottoni, Mitochondrial fusion: a mechanism of cisplatin-induced resistance in neuroblastoma cells? *Neurooncology* 34 (2013) 51–60, <https://doi.org/10.1093/neuonc/nnt110>.
- [47] I. Tanida, T. Ueno, E. Kominami, LC3 and autophagy, *Methods Mol. Biol.* 445 (2008) 77–88, https://doi.org/10.1007/978-1-59745-157-4_4.
- [48] I. Troy, K. McFarland, S. Littman-Power, R.J. Kelly, E.T. Walpole, D. Wyld, D. Thomson, Cisplatin-based therapy: a neurological and neuropsychological review, *Psychoncology* 9 (2008) 25–36, [https://doi.org/10.1002/psyc.1099-1811\(200808\)0229:1<25::AID-PON229>3.0.CO;2](https://doi.org/10.1002/psyc.1099-1811(200808)0229:1<25::AID-PON229>3.0.CO;2).
- [49] D. Wang, S.J. Lippard, Cellular processing of platinum anticancer drugs, *Nat. Rev. Drug Discov.* 4 (2005) 307–320, <https://doi.org/10.1038/nrd1698>.
- [50] E. Wenzelhan, D. Gibson, What do we know about the reduction of Pt(IV) prodrugs? *J. Inorg. Biochem.* 117 (2012) 220–229, <https://doi.org/10.1016/j.jinorgbio.2012.06.013>.
- [51] N.J. Whittle, S. Walker, G.E. Craig, R. Oan, The status of platinum anticancer drug in the clinic and in clinical trials, *Dalton Trans.* 39 (2010) 8113–8127, <https://doi.org/10.1039/c0dt00202a>.
- [52] O. Witt, H.E. Deshner, M. Ledriani, T. Milde, I. Oehme, Targeting histone deacetylase in neuroblastoma, *Curr. Pharm. Des.* 15 (4) (2009) 436–447, <https://doi.org/10.2174/138161209780315774>.
- [53] I. Zanollato, C.D. Boidi, G. Lingua, P.G. Betta, S. Crocchia, E. Monti, D. Onella, In vitro anti-metastatic activity of cisplatin-gemcitabine combination: evidence for sequence-dependent effects, *Cancer Chemother. Pharmacol.* 67 (2) (2010) 265–273, <https://doi.org/10.1007/s00280-010-1314-0>.



Contents lists available at ScienceDirect

Toxicology and Applied Pharmacology

journal homepage: www.elsevier.com/locate/taap

Long-term effects after treatment with platinum compounds, cisplatin and [Pt(O,O'-acac)(γ-acac)(DMS)]: Autophagy activation in rat B50 neuroblastoma cells



Maddalena Grimaldi^{a,1}, Veronica Dal Bo^{a,1}, Beatrice Ferrari^a, Elisa Roda^{a,b}, Fabrizio De Luca^a, Paola Veneroni^a, Sergio Barni^a, Manuela Verrì^a, Sandra A. De Pascali^c, Franco P. Fanizzi^c, Graziella Bemocchi^a, Maria G. Bottone^{a,*}

^a Laboratory of Cell Biology and Neurobiology, Department of Biology and Biotechnology "L. Spallanzani", University of Pavia, Italy

^b Laboratory of Clinical & Experimental Toxicology, Pavia Poison Centre, National Toxicology Information Centre, Toxicology Unit, ICS Maugeri SpA, IRCCS Pavia, Via Maugeri 10, Pavia, Italy

^c General and Inorganic Chemistry Laboratory, Department of Biological and Environmental Sciences and Technologies (DiSTeRA), University of Lecce, Italy

ARTICLE INFO

Keywords:
CisPt
PtAcacDMS
Apoptosis
Autophagy
Drug resistance
Neuroblastoma rat cells

ABSTRACT

Cisplatin (cisPt), among the best known components of multi drug front line therapies used for the treatments of solid tumors, such as the childhood neuroblastoma, acts through DNA linking. Nevertheless, the cisPt effectiveness is compromised by the onset of severe side effects, including neurotoxicity that results in neurodegeneration, cell death, and drug resistance. In the field of experimental oncology, aimed at overcoming cytotoxicity and chemoresistance, great efforts are devoted to the synthesis of new platinum-based drugs, such as [Pt(O,O'-acac)(γ-acac)(DMS)] (PtAcacDMS), which shows a specific reactivity with sulfur residues of enzymes involved in apoptosis. Autophagy, an evolutionary conserved degradation pathway for recycling of cytoplasmic components, represents one of the mechanisms adopted by cancer cells which contribute to drug resistance. In the present study, standard acute (48 h exposure) and long term effects (7 day-recovery after treatment or 7 day-recovery followed by reseeding and 96 h growth), of cisPt and PtAcacDMS (40 and 10 μM, respectively) were investigated in vitro employing rat B50 neuroblastoma as a cancer model. Using fluorescence and electron microscopy, as well as biochemical techniques, our data highlight a key role of the autophagic process in B50 cells. Specifically, long term effects caused by cisPt lead to inhibition of the apoptotic process and paralleled by the activation of autophagy, thus evidencing that autophagy has a protective role after cisPt exposure, allowing cells to survive. Whereas, long term effects produced by PtAcacDMS lead toward both apoptosis and autophagy activation. In conclusion, autophagy may represent an alternative cell death pathway, circumventing drug-resistance strategies employed by cancer cells to survive chemotherapy.

1. Introduction

Cisplatin (cis-dichlorodiammineplatinum, cisPt) is one of the most used and effective cytotoxic agents in the treatments of a wide range of malignancies (Bresden et al., 2000). CisPt interacts with purine bases of DNA forming adducts or cross-links, either between adjacent bases on the same strand or on opposing strands (Dasari and Tchounwou, 2014). DNA lesions block transcription and translation, thus leading to inhibition of cell cycle and apoptosis induction. CisPt also acts as a

cytoplasmic level in B50 cells (Bottone et al., 2008; Santin et al., 2011, 2012).

Although effective, the clinical use of cisPt is limited by severe side effects, including nephrotoxicity, ototoxicity, neurotoxicity, and drug-resistance (McWhinney et al., 2009; Bemocchi et al., 2011; Galluzzi et al., 2012; Astolfi et al., 2013). Resistance mechanisms include the inability of cisPt to cross the plasma membrane, the intracellular detoxification through glutathione and/or metallothioneins, an efficient DNA repair activity (Rabik and Dolan, 2007), the activation of an anti-

Abbreviations: B50, neuroblastoma rat cell lines; cisPt, cisplatin; PtAcacDMS, [Pt(O,O'-acac)(γ-acac)(DMS)]; CNS, central nervous system; TEM, Transmission Electron Microscopy; CO₂, carbon dioxide; μM, micromolar; hrs, hours

* Corresponding author at: Department of Biology and Biotechnology "L. Spallanzani", University of Pavia, via Ferrata 9, 27100 Pavia, Italy.

E-mail address: bottone@unipv.it (M.G. Bottone).

¹ Both Maddalena Grimaldi and Veronica Dal Bo contributed equally to this work.

<https://doi.org/10.1016/j.taap.2018.12.005>

Received 1 August 2018; Received in revised form 26 November 2018; Accepted 5 December 2018

Available online 06 December 2018

0041-008X/ © 2018 Elsevier Inc. All rights reserved.

apoptotic pathway (Pasetto et al., 2006) and autophagy (Platini et al., 2010; Bao et al., 2015; Lin et al., 2017). Recently, it has been demonstrated that autophagy acts as a beneficial stress response, triggered by cisPt-induced death mechanisms (Del Bello et al., 2013). In the rapidly evolving fields of experimental oncology and personalized medicine, essential challenges include overcoming cytotoxicity and chemoresistance. With this aim, one of the adopted strategies is the synthesis of new platinum compounds, such as [Pt(O, O'acac)(γ -acac)(DMS)] (PtAcacDMS) (De Pascali et al., 2006; Wang et al., 2018). This novel drug preferentially interacts with non-genomic targets, as demonstrated in previous studies, revealing a mechanism of action which differs from cisPt, although this is yet to be fully clarified (Muscella et al., 2007, 2008). Specifically, it is well known that cisPt tends to react with DNA, considered its main pharmacological target, giving rise to DNA-protein intrastrands and interstrands, and DNA-DNA cross-links. These DNA rearrangement phenomena can lead to cell death due to resulting physiological process inhibition, i.e. DNA transcription or replication induced by the distortion of the double helix (Jordan and Carmo-Fonseca, 2000; De Castro et al., 2018).

Differently, the alternative action mechanism of PtAcacDMS, essentially cytosolic, might be responsible for the ability of this potential anticancer agent to overcome the drug resistance induction, one of the principal causes of cisPt-based tumour treatment failure. Indeed, PtAcacDMS has shown a higher *in vitro* and *in vivo* pharmacological uptake, activity and tolerability than cisPt (De Castro et al., 2018). In particular, PtAcacDMS reacts with amino acidic residues belonging to enzymes or other proteins implicated in the apoptotic pathway (Muscella et al., 2007, 2008). Notably, PtAcacDMS has a greater cytotoxic effect on cancer than cisPt, though accompanied by a lower CNS neurotoxicity (Bernocchi et al., 2015), inducing milder changes on fundamental events of rat cerebellar neuroarchitecture development, e.g. lower apoptotic phenomena, less altered granule cell migration and Purkinje cell dendrite growth as well as preserved inhibitory synapses formation (Bernocchi et al., 2011; Piccolini et al., 2015). Furthermore, literature data reported that PtAcacDMS induces cell death in several cancer cell lines such as MCF-7 breast cancer and SH-SY5Y human neuroblastoma cells (Muscella et al., 2011, 2014). Another recent *in vitro* investigation of neuroblastoma cells has revealed a greater cytotoxic effect with PtAcacDMS treatment compared to cisPt, moreover cisPt has shown an evident inhibition of apoptosis in long-term exposure conditions (Grimaldi et al., 2016). In the present study, cytotoxic effects after standard acute testing (48 h-exposure) and long-term exposure (7 day-recovery phase after treatment or 7 day-post-exposure recovery period followed by reseeded and 96 h-growth) of the two different platinum compounds were investigated *in vitro* in rat B50 neuroblastoma. Cancer cells were exposed at a dose of 40 μ M and 10 μ M of cisPt and PtAcacDMS respectively, focusing on different cell death pathways, i.e. apoptosis and autophagy. Autophagy is an evolutionary conserved intracellular process for the turnover and degradation of long-lived proteins and organelles, fundamentally active at low levels in the cells; this survival mechanism is enhanced by acute stress conditions such as starvation, hypoxia and pathogen infection (Klionsky, 2007; Fimia et al., 2013). It plays a neuroprotective role in the developing CNS (Bottone et al., 2015), nonetheless still participating in cell death caused by intense stress or long-term stimuli the so-called type II programmed cell death (Levine and Kroemer, 2008). Autophagy is also implicated in maintenance of tumorigenesis (Demarchi et al., 2006) and it may represent a mechanism allowing tumour cells to survive anticancer therapies (Longo et al., 2008; Wang et al., 2013).

Thus, with the aim to make an *in depth* investigation into the onset and progression of apoptotic and autophagic pathways caused by cisPt- and PtAcacDMS-treatment the processes of immunocytochemical, biophysical, western blotting and ultrastructural analysis were performed. The investigation focused on changes in morphology and localization of cytoplasmic organelles, i.e. mitochondria and lysosomes which are essential elements involved in both cell death pathways. The following

proteins known as autophagic markers were studied (i) Beclin-1 and ATG5 (Liang et al., 2001; Codogno and Meijer, 2006; Zhao et al., 2018) involved in autophagosomal membrane formation (ii) p62/SQSTM1, a scaffold protein which transports ubiquitinated proteins to the autophagolysosomes (Komatsu and Ichimura, 2010) and (iii) LC3 (microtubule-associated protein-MAP-Light Chain 3) required for the binding of substrates to the autophagosome (Kabeja et al., 2000; Zhao et al., 2018). Our ultimate goal was to elucidate whether autophagy may represent a drug-resistance survival mechanism or merely a cell death strategy thereby further improving the knowledge of the novel platinum compound PtAcacDMS.

2. Material and methods

2.1. Cell culture

Rat B50 neuroblastoma cells (ATCC, Rockville, MD, USA) were cultured in 75 cm² flasks in Dulbecco's minimal essential medium (DMEM) supplemented with 10% fetal bovine serum, 1% glutamine, 100 IU/ml penicillin and streptomycin (Celbio, Milan, Italy) and maintained at 37 °C in a humidified atmosphere (95% air/5% CO₂). Twenty-four hour before experiments, cells were seeded on glass coverslips for fluorescence microscopy, or grown in 75 cm² plastic flasks for flow cytometric, western blotting and ultrastructural (by transmission electron microscopy, TEM) analysis.

2.2. Pharmacological treatments

2.2.1. Exposure conditions

Cell exposure to the different platinum compounds was performed according to the following protocols:

- i) standard acute test (48 h-exposure) to cisPt (Teva Pharma, Milan, Italy) or PtAcacDMS (De Pascali et al., 2006) at a dose of 40 μ M and 10 μ M, respectively, at 37 °C. CisPt administrated concentration was selected considering previous *in vitro* investigations (Bottone et al., 2008) as well as *in vivo* experimental designs, employing a single subcutaneous injection (5 μ g/g b.w.) in 10-days old rats, corresponding to the therapeutic dose suggested by Bodenner et al. (1986) and Dietrich et al. (2006), already used in clinical practice. PtAcacDMS concentration was chosen based on previous *in vitro* findings on B50 cells (Grimaldi et al., 2016);
- ii) standard acute test (48 h-exposure) to cisPt (40 μ M) or PtAcacDMS (10 μ M), followed by a 7 day-recovery phase in drug-free normal DMEM, namely recovered condition;
- iii) standard acute test (48 h-exposure) to cisPt (40 μ M) or PtAcacDMS (10 μ M), followed by a 7 day-recovery phase in drug-free medium, further followed by re-seeding and growth in drug-free complete DMEM for 96 h, namely reseeded condition.

2.2.2. Selected drugs concentration

The cisPt and PtAcacDMS concentrations (40 μ M and 10 μ M, respectively), were selected based on previous experimental findings:

- (i) *in vivo* studies, administering CisPt (MW 300.05) via the subcutaneous injection at a dose of 5 microg/g b.w. (= 3.4 mM) in rats (Scherini et al., 1992 and Bottone et al., 2008), corresponding to the therapeutic dose suggested by Bodenner et al., 1986 and Dietrich et al., 2006. Based on this dose, assuming that about 60 mL corresponds to the whole blood volume in rat and considering our cell population density, we calculated a CisPt dose of about 40 μ M to be used to treat a cell culture flask.
- (ii) *in vitro* dose- and time-response experiments demonstrating that both compounds, tested at concentration ranging from 1 to 200 μ M, were able to induce apoptosis and cytoplasmic organelles damage in a number of cell lineages, showing different sensitivity

Table 1
Primary and secondary antibodies used for immunofluorescence.

Antigen	Primary antibody	Dilution in PBS	Secondary antibody	Dilution in PBS
HSP70	Monoclonal mouse (Thermo Scientific, Waltham, USA)	1:50	Alexa Fluor 488 goat anti-mouse (Molecular Probes, Invitrogen, USA)	1:200
Auricularin ^a serum for lysosome detection recognizing lysosomal proteins	Human anti-mouse serum (donor given by IRCCS San Matteo Pavia, Italy)	1:500	Alexa Fluor 594 goat anti-human (Molecular Probes, Invitrogen, USA)	1:200
Bcl-2 ¹	Polyclonal rabbit (Cell Signaling, Danvers, USA)	1:100	Alexa Fluor 488 goat anti-rabbit (Molecular Probes, Invitrogen, USA)	1:200
LC3B	Monoclonal rabbit anti-LC3B (Cell Signaling, Danvers, USA)	1:200	Alexa Fluor 488 goat anti-rabbit (Molecular Probes, Invitrogen, USA)	1:200
p62/SQSTM1	Monoclonal mouse (Abcam, Cambridge, USA)	1:100	Alexa Fluor 488 goat anti-mouse (Molecular Probes, Invitrogen, USA)	1:200

^a Borrono et al. (2012).

to the drug, with maximal effects at concentrations comparable to the present chosen dose (Shi et al., 1995; Muscella et al., 2007; Santin et al., 2012; Santin et al., 2013; De Castro et al., 2018);

(ii) *in vitro* investigations describing the use of 40 μ M cisPt on a variety of tumour cell lines, based on its ability to cause apoptosis (Sakalli Çetin et al., 2017; Qian et al., 2018), cell cycle and mitochondrial respiratory complex alterations (Kachadourian et al., 2007; Chiang et al., 2014).

(iv) our *in vitro* dose-response investigations, demonstrating that 10 μ M PIAcacDMS was the most apoptogenic dose, with effect comparable to that observed after 40 μ M cisPt-exposure, while higher PIAcacDMS concentrations (i.e. 40 and 20 μ M) triggered necrotic cells death (Grimaldi et al., 2016).

2.3. Immunofluorescence reactions

After treatments, the samples grown on coverslips were fixed with 4% formalin and post-fixed with 70% ethanol for 30 min at -20°C , and stored at -20°C . Samples were rehydrated for 15 min in PBS and then immunolabeled with selected monoclonal and polyclonal primary antibodies (Table 1) diluted in PBS. This 1 h-incubation were performed at room temperature in a dark moist chamber. Cells were then washed three times with PBS, and incubated for 1 h with the proper secondary antibodies (Table 1) diluted in PBS. Cells were therefore counterstained for DNA with 0.1 $\mu\text{g}/\text{mL}$ of Hoechst 33258 (Sigma-Aldrich, Milano, Italy) for 6 min, washed with PBS, and finally mounted in a drop of Mowiol (Calbiochem-Inalco, Italy) for confocal and fluorescent microscopy. For each experimental condition, three independent experiments were carried out.

2.4. TEM ultrastructural investigation

The cells were harvested by mild trypsinization (0.25% trypsin in PBS containing 0.05% EDTA), immediately fixed with 2% glutaraldehyde (Polysciences, Inc., Warrington, PA, USA) in the culture medium (1 h at 4°C) and post-fixed in 1% OsO_4 (Sigma Chemical Co., St. Louis, MO, USA) in PBS for 1 h at room temperature. Cells were then centrifuged (10 min, 800g), washed and cell pellets were embedded in 2% agar, thoroughly rinsed with Sørensen buffer (pH 7.2) and dehydrated in ethanol. Then, the pellets were embedded in Epon resin and polymerized at 60°C for 24 h. Ultrathin sections (600 Å) were cut with RECHERT ultramicrotome, mounted on nickel grids and stained with uranyl acetate and lead citrate. Sections were observed and pictured under a Zeiss EM 900 transmission electron microscope.

2.5. Confocal fluorescence microscopy

For confocal laser scanning microscopy, Leica TCS-SP system mounted on a Leica DMIRBE-inverted microscope was used. For fluorescence excitation, an Ar/UV laser at 364 nm was used for Hoechst 33258, an Ar/Vis laser at 488 nm was used for FITC and a He/Ne laser at 543 nm was used for Alexa 594. Spaced (0.5 μm) optical sections were recorded using a $63\times$ oil immersion objective. The "colocalization" analysis was done considering 30 cells for sample, and three points of colocalization in at least 15 cells. Images were collected in the 1024×1024 pixel format, stored on a magnetic mass memory and processed by Leica confocal software.

2.6. Fluorescence microscopy

A BX51 Olympus microscope equipped with a 100 W mercury lamp was used with: 330–385 nm excitation filter (exc.f), 400 nm dichroic mirror (dm), and 420 nm barrier filter (bf) for Hoechst 33258; 450–480 nm exc.f, 500 nm dm and 515 nm bf for the fluorescence of Alexa 488; 540 nm exc.f, 580 nm dm, and 620 nm bf for Alexa 594. Images were recorded with an Olympus MagnaFire cam and processed

Table 2
Primary and secondary antibodies used for Western Blotting experiments.

Antigen	Primary antibody	Dilution in PBS	Secondary antibody	Dilution in PBS
Actin	Mouse anti-actin (Sigma Aldrich, Italy)	1:2000	Goat anti-mouse horseradish peroxidase (Dako, Italy)	1:2000
Beclin-1	Polyclonal rabbit (Cell Signaling, Danvers, USA)	1:1000	Goat anti-rabbit horseradish peroxidase (Dako, Italy)	1:2000
LC3B	Monoclonal rabbit anti-LC3B (Cell Signaling, Danvers, USA)	1:1000	Goat anti-rabbit horseradish peroxidase (Dako, Italy)	1:2000
p62/SQSTM1	Monoclonal mouse (Abcam, Cambridge, USA)	1:1000	Goat anti-mouse horseradish peroxidase (Dako, Italy)	1:2000
ATG5	Monoclonal rabbit anti-ATG5 (Abcam, Cambridge, USA)	1:1000	Goat anti-rabbit horseradish peroxidase (Dako, Italy)	1:2000

with the Olympus Cell F software.

2.7. Western blotting analysis

After treatments, the cells were washed twice with PBS and lysed in RIPA buffer (Tris HCl 1 M pH7.6, EDTA 0.5 M pH8, NaCl 5M, NP40 Nonidet 100%, H₂O₄ with the addition of proteases and phosphatases inhibitors) at 4 °C for 20 min. Bradford reagent (Sigma Aldrich, Milan, Italy) was used for the count of protein amount. Samples were electrophoresed in a 7.5% or 12% SDS-PAGE minigel and transferred onto a nitrocellulose membrane (BioRad, CA) by a semidry blotting for 1.45 h under a constant current of 36 mA. The membranes were saturated overnight with PBS containing 0.2% Tween-20 and 5% skim milk, and incubated for 1 h with selected antibodies listed in Table 2. After washes, membranes were incubated for 30 min with the proper secondary antibodies conjugated with horseradish peroxidase (1:2000, Dako, Italy). Visualization of immunoreactive bands was performed by ECL System and Hyperfilm Photographic Film (Amersham Life Sciences, UK) using the manufacturer's instructions. Image J software was used to obtain the density bar chart of the protein bands which are normalized with the loading control. At least three independent experiments were carried out.

2.8. Statistical analysis

In the present study, data are presented as mean \pm SD over the mean experimental values of each of three independent experiments. Statistical analysis was carried out using one-way ANOVA and Post hoc Dunnett's test (software package GraphPad Prism Inc.). p values ranging from < 0.001 to < 0.05 were considered to indicate statistical significance.

3. Results

3.1. Alteration of cytoplasmic organelles: mitochondrial and lysosomal changes

The activation of apoptosis and autophagy after treatments with the two diverse platinum compounds was evaluated by performing a double immunofluorescence (Fig. 1), revealing both lysosomes (red fluorescence) and mitochondria (green fluorescence) homogeneously distributed in the cytoplasm (Fig. 1a). Immunofluorescence labelling, distinctive for these organelles, neither demonstrated co-localization in the control cells (Fig. 1a) nor in cisPt-treated cells after a standard acute test (Fig. 1b). Notably, after a 48 h-exposure to both cisPt or PtAcacDMS the cellular morphology changed with cells assuming elongating features and undergoing apoptosis (Fig. 1b, b'). In PtAcacDMS-treated cells (standard acute test) small and round mitochondria as well as lysosomes organized into homogeneous clusters were observable (Fig. 1b'). After a 7 day-recovery period in a drug-free medium areas of immunofluorescence co-localization typically characterized by several orange spots were detected indicating possible mitochondrial degradation in lysosome vesicles (Fig. 1c, c'). After a reseeded period, cisPt treated-cells returned to normal morphology, appearing similar to controls and without signs of immunofluorescence co-localization, i.e. absence of orange spots (Fig. 1d') thus suggesting the successful attempt

of the cell to survive. On the contrary after reseeded apoptotic events and orange spots were still observed in the cytoplasm of cells previously exposed to PtAcacDMS (Fig. 1d'), possibly indicating a substantial mitochondrial clearance inside lysosomal vesicles. Additionally, the lysosomes were more abundant in PtAcacDMS-treated cells after the standard acute test (48 h-exposure).

3.2. Apoptosis and autophagy interplay: typical ultrastructural features

TEM analysis was performed to elucidate any possible apoptotic and autophagic characteristic after drug-treatments (Fig. 2). B50 control cells possess a typical morphology, showing a kidney-shaped nucleus, characterized by de-condensed chromatin and nucleolus (Fig. 2a) and the Golgi apparatus located in the perinuclear area. Small mitochondria and granular endoplasmic reticulum were observed, whereas primary and secondary lysosomes appeared sporadic, indicating physiological basal autophagic activity. After cisPt or PtAcacDMS standard acute test - 48 h-exposure (Fig. 2b, b'), the cells underwent apoptosis, displaying classical features, e.g. cytoplasmic segmentation, condensed chromatin, double membrane apoptotic bodies (Fig. 2b' arrowhead) and cytoplasmic vacuoles (Fig. 2b' arrowhead). Nonetheless, autophagic cells were also present after a 48h-exposure to both compounds, demonstrating intense autophagic activity, as indicated by the occurrence of several degraded autophagic bodies containing cytoplasmic material (Fig. 2c, c'). After a 7 day-recovery in a cisPt-free medium, cells presented a decentralized nucleus and the cytoplasm appeared crowded with double membrane vacuoles containing membranous residues called "myelin bodies" (Fig. 2d arrowhead). Similarly the 7 day-recovered cells previously treated with PtAcacDMS were characterized by an autophagic morphology, showing small mitochondria and several secondary lysosomes, these latter representing autophagosomes at different stages of maturation (Fig. 2d' arrowhead). Furthermore, at the cell periphery, the plasma membrane formed some blebs also evident in reseeded cells previously treated with cisPt (Fig. 2e), enclosing cytoplasmic components as a consequence of cytoskeletal damage. Notably in reseeded cells, formerly exposed to cisPt, the cytoplasm exhibited normal-shaped mitochondria (arrowhead) and only some heterophagosomes, indicating that no massive cytoplasmic degradation is occurring. Conversely after PtAcacDMS-treatment, recovered cells still displayed apoptotic characteristics such as heterochromatinic areas that could be representative of karyorrhexis (Fig. 2e'). The displayed apoptotic features together with the presence of autophagic bodies within the cytoplasm (Fig. 2d', e', insert) seemed to indicate that the two processes could mutually cooperate in directing cells to die.

3.3. Autophagy activation after exposure to platinum compounds: confocal microscopy investigation

Autophagic activity was evaluated by western blotting analysis and double immunofluorescence staining, exhibiting several markers representative of autophagy occurrence and lysosome increase. In order to explore possible immunofluorescence co-localization and/or autophagolysosomes formation the confocal microscopy was used.

3.3.1. Beclin-1 immunofluorescence and lysosomes modifications

In B50 control cells, Beclin-1 was detected both in the nucleus and

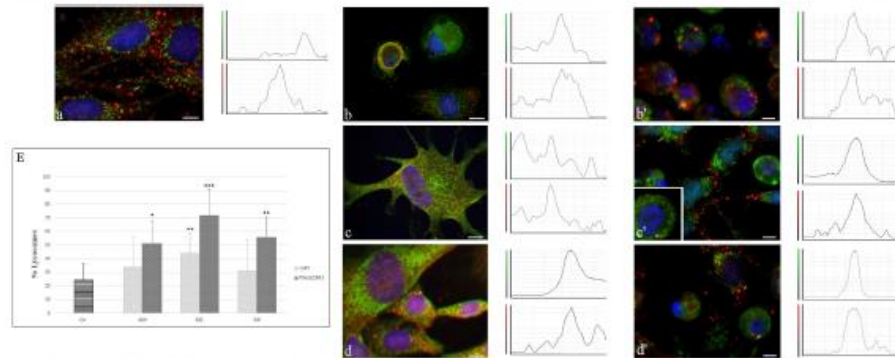


Fig. 1. Fluorescence microscopy (lysosomes - mitochondria immunocytochemical detection), emission spectra and lysosome quantification. Double immunocytochemical detection of lysosomes (red fluorescence) and mitochondria (green fluorescence) in control cells (a), cisPt standard acute test - 48 h exposed cells (b), recovered and reseeded cells after cisPt (c and d, respectively), PtAcacDMS - standard acute test - 48 h exposed cells (b'), recovered and reseeded cells after PtAcacDMS (c' and d', respectively). On the right, near the micrographs, are the emission spectra referring to the green and red fluorescence respectively, showing the presence or absence of colocalization of the two fluorescence. Nuclei were counterstained with Hoechst 33258 (blue fluorescence). Scale bar: 20 μ m. The histogram (E) shows the percentage of lysosomes (%) in the cells; data are presented as mean \pm SD over the mean experimental values of each of three independent experiments. p values: (*) < 0.05; (**) < 0.01; (***) < 0.001. (For interpretation of the references to colour in this figure legend, the reader is referred to the web version of this article.)

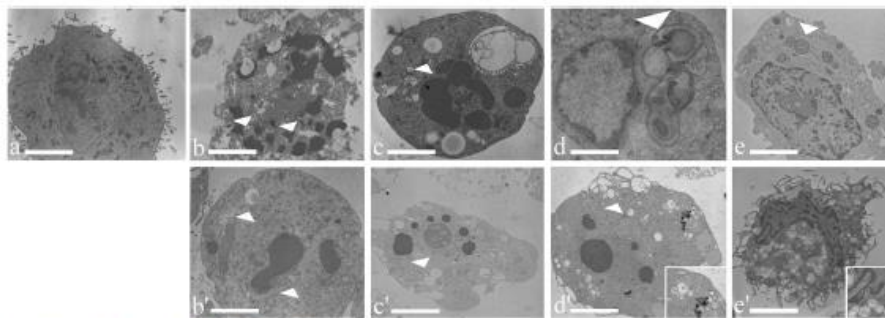


Fig. 2. TEM analysis: Apoptosis and autophagy activation. Transmission electron microscopy evaluation of apoptotic and autophagic features after cisPt - (b-c) and PtAcacDMS - (b'-e') treatment. Ultrastructural morphology of control cells (a), cisPt - standard acute test - 48 h exposed cells (b, in which arrowhead indicates apoptotic bodies, in c arrowhead indicates autophagic bodies), recovered cells (d in which arrowhead shows autophagic bodies), and reseeded cells (e, in which arrowhead indicates mitochondria). Ultrastructural morphology of PtAcacDMS - standard acute test - 48 h exposed cells (b'-e', in which arrowhead cytoplasmic vacuoles), recovered cells (d', in which arrowhead indicates an autophagic bodies), reseeded cells (e'). Insert (d', e'): autophagic bodies. Bars: 1.5 μ m.

the cytoplasm without any co-localization at a lysosomes level (Fig. 3a). After a standard acute test (48 h-exposure) to cisPt, apoptotic cells were observed (Fig. 3b). Early apoptosis was characterized by the immunoreactivity for both Beclin-1 and lysosomes, co-localizing inside the cytoplasm thus participating to the autophagosomal membrane formation. Whereas in late apoptosis, the lysosomes were markedly decreased until their complete disappearance. After a standard acute test (48 h-exposure) to PtAcacDMS, Beclin-1 was uniformly distributed in clusters inside the cytoplasm, where sporadic immunofluorescence spots of co-localization with lysosomal vesicles were observed (Fig. 3b'). Several cells in early and late apoptotic stages were also detected. After a 7 day-recovery in a drug-free medium, cells showed a

mutated morphology (Fig. 3c, c'), appearing with a round-flowered shape, probably due to the increase of cytoplasmic volume. Beclin-1 immunopositivity evident in the cytoplasm co-localized with lysosomes staining. Notably, a substantial increase of lysosomes occurred. Reseeded cells, previously exposed to cisPt (Fig. 3d) showed lysosomes immunopositivity still co-localizing with that of autophagic protein Beclin-1. Certain reseeded cells, formerly treated with PtAcacDMS showed apoptotic features while in some others few fluorescent spots representative of co-localization were detected, with an evident decrease of Beclin-1 staining (Fig. 3d').

Western blotting analysis further showed a significant increase of Beclin-1 level after 48 h-exposure to cisPt and after treatment with both

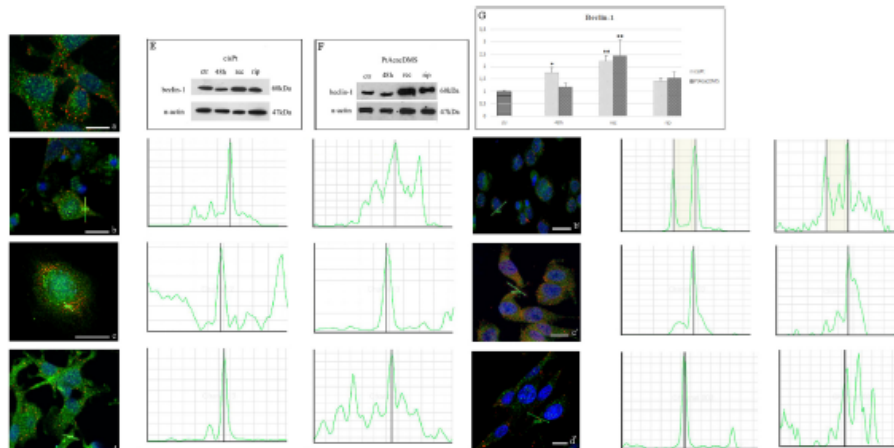


Fig. 3. Confocal microscopy (Beclin-1 - lysosomes immunocytochemistry), fluorescence emission spectra and Western Blotting data. Double immunocytochemical detection of Beclin-1 (green fluorescence) and lysosomes (red fluorescence) in control cells (a), cisPt- and PtAcacDMS-standard acute test - 48 h-exposed cells (b and b', respectively), recovered and reseeded cells (c-c' and d-d', respectively). Nuclei were counterstained with Hoechst 33258 (blue fluorescence). Bar: 20 μ m. On the right, near the micrographs, are the emission spectra referring to the green and red fluorescence respectively, showing the presence or absence of colocalization of the two fluorescence. Density bands of Beclin-1 (60 kDa) and α -actin (47 kDa) obtained by western blotting analysis are shown in E and F, for cisPt- and PtAcacDMS- treatments, respectively. In G, histogram shows quantitative analysis of Beclin-1 in control cells, standard acute test - 48 h exposed cells, recovered and reseeded cells after cisPt or PtAcacDMS. Data are presented as mean \pm SD over the mean experimental values of each of three independent experiments, p values: (*) < 0.05; (**) < 0.01. (For interpretation of the references to colour in this figure legend, the reader is referred to the web version of this article.)

cisPt- and PtAcacDMS in recovered cells, otherwise, no significant difference was observed after the reseeded period following cisPt exposure nor after treatment with PtAcacDMS (Fig. 3E, F).

3.3.2. LC3 and lysosomal proteins: expression and localization changes

LC3 is an ubiquitin-like protein cleaved at its C-terminal by a protease to form LC3B-I. When autophagy is activated, LC3B-I is conjugated to the phosphatidylethanolamine by the ubiquitin-like system formed by ATG7 and ATG3 and converted into LC3B-II isoform, allowing the association with autophagosomal membrane (Kabeya et al., 2000).

In control cells, LC3B localized both in nucleus as well as in cytoplasm, and a complete lack of co-localization with lysosomes was detected (Fig. 4a). The cells underwent apoptosis after standard acute test (48 h-exposure) to both cisPt and PtAcacDMS: in early apoptosis some fluorescent spots representative of co-localization were evident, while in late apoptosis LC3B did not co-localize with lysosomes. LC3 was entirely placed in the cytoplasm, mainly in PtAcacDMS-treated cells, and the number of lysosomes was dramatically decreased (Fig. 4b, b'). After a 7-day-recovery period cells formerly treated with both cisPt or PtAcacDMS showed an altered shape, displaying a soma mutation from slim to round and also increasing in volume. Furthermore a massive autophagic process occurred as indicated by the presence of several fluorescent spots representative of co-localization (Fig. 4c, c'). Reseeded cells, previously exposed to cisPt still showed spots of co-localization but exhibited a lower fluorescence intensity. In some cells LC3B returned into the nucleus (Fig. 4d). The same immunostaining pattern with a decreased immunofluorescence degree was observed in reseeded condition after PtAcacDMS treatment (Fig. 4d').

Accordingly western blotting analysis confirmed the activation of autophagy both in recovered and reseeded cells previously exposed to

PtAcacDMS as shown by the presence of the two LC3B isoforms (Fig. 4E and G). Similarly both in cisPt-treated cells or in reseeded ones a basal level of autophagy was evident while after the 7 day-recovery period a more significant increase of LC3B-II isoform was detected, suggesting the full activation of the process (Fig. 4E and G).

3.3.3. p62/SQSTM1 expression levels and lysosomes monitoring

In control cells, the scaffold protein p62 was located both in the nucleus and in the cytoplasm (Fig. 5a), since it contains nuclear import and export signals and shuttles between nucleus and cytoplasm (Johansen and Lamark, 2011). In early and late apoptotic cells, p62 was entirely localized in the cytoplasm and not detectable at nuclear level, as occurred after standard acute test (48 h-exposure) to cisPt or PtAcacDMS (Fig. 5b, b'). No sign of co-localization with lysosomes was observed. In recovered cells previously treated with cisPt, p62 appeared in the cytoplasm next to the lysosomes without any co-localization, according to the proper scaffold function of this protein. It participates to the formation of dense aggregates of non-degraded proteins accumulated in the cytoplasm (Fig. 5c). In reseeded cells after cisPt-exposure p62 localized back in the nucleus, thus indicating the end of the autophagic process (Fig. 5d). In recovered cells, formerly treated with PtAcacDMS, p62 returned at least in part at nuclear level, suggesting a decrease of autophagy (Fig. 5c'), while after the reseeded period the protein was localized mostly in the cytoplasm where an intense immunolabelling was observed (Fig. 5d'). High levels of p62 were detected by western blotting analysis (Fig. 5E) both in controls as well as after standard acute test (48 h-exposure) to cisPt or PtAcacDMS. The amount of protein slightly increased in recovered cells formerly treated with cisPt. In recovered and reseeded cells, after previous PtAcacDMS-exposure, a strong increase of p62 levels was evident, suggesting that the autophagic process was activated and apparent for longer durations

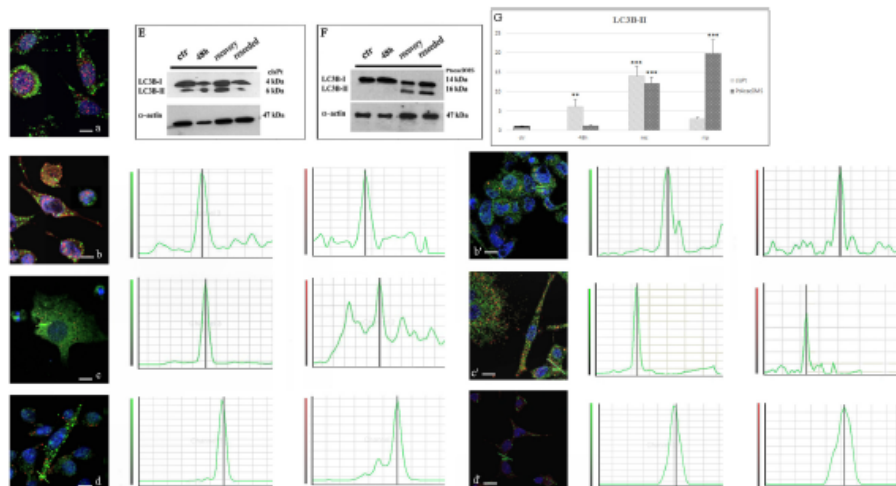


Fig. 4. Confocal microscopy (LC3B - lysosomes immunocytochemistry), fluorescence emission spectra and Western Blotting data. Double immunocytochemical detection of LC3B (green fluorescence) and lysosomes (red fluorescence) in control cells (a), cisPt- and PtAcacDMS-standard acute test - 48 h-exposed cells (b and b', respectively), recovered and reseeded cells (c-c' and d-d', respectively). Nuclei were counterstained with Hoechst 33258 (blue fluorescence). Bar: 20 μ m. On the right, near the micrographs, are the emission spectra referring to the green and red fluorescence respectively, showing the presence or absence of colocalization of the two fluorescence. Density bands of LC3B-I (cleaved form 14 kDa), LC3B-II (lipidated form 16 kDa) and α -actin (47 kDa) obtained by western blotting analysis are shown in E and F, for cisPt- and PtAcacDMS- treatments, respectively. In G, histogram shows quantitative analysis of LC3B-II (lipidated form) in control cells, standard acute test - 48 h-exposed cells, recovered and reseeded cells after cisPt or PtAcacDMS. Data are presented as mean \pm SD over the mean experimental values of each of three independent experiments. p values: (***) < 0.001; (**) < 0.01. (For interpretation of the references to colour in this figure legend, the reader is referred to the web version of this article.)

after drug removal (Fig. 5F).

3.3.4. ATG5 protein increase: key role in autophagy activation

Further western blotting analysis were conducted on ATG5, another protein which acts during the first steps of the autophagic process and involved in the autophagosomal membrane formation. Compared to controls and 48 h-exposed cells (standard acute test), high levels of ATG5 were detected both in recovered and reseeded cells previously treated with cisPt (Fig. 6), suggesting the activation of autophagy and congruent with our formerly reported data concerning Beclin-1. In addition, an increase of ATG5 protein levels was observed in reseeded cells previously exposed to PtAcacDMS in accordance with the cleavage of LC3, mainly described during the reseeded period (see above). Indeed, based on our results, ATG5 appeared to be a key part of the activation complex involved in LC3B lipidation.

4. Discussion

In recent years, great effort was devoted to understand the functional relationship between apoptosis and autophagy. In response to several stimuli, autophagy may constitute a stress adaptation aimed at avoiding cell death, thus suppressing apoptosis. Otherwise, in other scenarios autophagy can be considered an alternative pathway to cellular demise, known as type II cell death (Baehrecke, 2005; Gump and Thorburn, 2011). At molecular level, apoptosis and autophagy may share common pathways which can lead to several cellular responses (Maiuri et al., 2007). Recently, autophagy was observed to be a response mechanism, triggered by cells in treatment for malignant

cancers and neuronal disorders (Kondo et al., 2005; Maycotte and Thorburn, 2011; Harris and Rubinsztein, 2011; Choi et al., 2013). In the present study, the activation of autophagy was demonstrated in B50 neuroblastoma cells after treatments with two different chemotherapeutic agents, i.e. CisPt and PtAcacDMS. The former is a conventional anticancer drug, already used in clinical practice for treatment of both adult and childhood malignancies (Dasari and Tchounwou, 2014). The latter is an innovative platinum-based compound, recently synthesized by De Pascali and colleagues (De Pascali et al., 2006), with the aim to overcome the severe adverse side effects of chemotherapy and improving its efficacy. Our preliminary in vitro and in vivo studies comparing PtAcacDMS and cisPt demonstrated the enhanced efficacy of this novel compound, showing cytotoxic effects four times higher than those observed after cisPt treatment, nonetheless paralleled by an increased cerebral uptake of the new compound accompanied by a slighter CNS neurotoxicity. In accordance to a body of literature (Muscella et al., 2007 and 2008; Jordan and Carmo-Fonseca, 2000; De Castro et al., 2018), these data also corroborated the notion that the two compounds act through different cellular targets (Grimaldi et al., 2016).

The present investigation demonstrated that a standard acute test (48 h-exposure) using both cisPt or PtAcacDMS at a selected dose of 40 and 10 μ M respectively, induced apoptosis in B50 cells, as evidenced by TEM analyses. Apoptotic events were still observed in reseeded cells previously treated with PtAcacDMS whereas reseeded cells return to physiological morphology after cisPt exposure, indicating the recovery to physiological condition. The long-term cytotoxic effects of these platinum drugs involved the activation of autophagy, denoted by the double membrane vesicles known as autophagosomes. Observed at

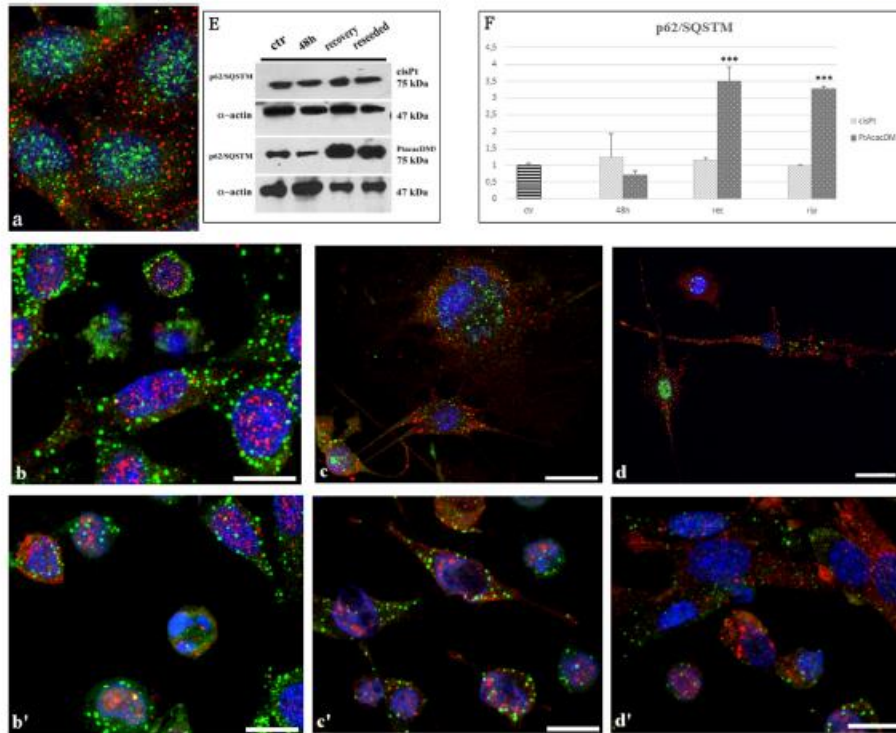


Fig. 5. Confocal microscopy (p62/SQSTM1 - lysosomes immunocytochemistry), and Western Blotting results. Double immunocytochemical detection of p62/SQSTM1 (green fluorescence) and lysosomes (red fluorescence) in control cells (a), cisPt- and PtAcacDMS-standard acute test - 48 h exposed cells (b and b', respectively), recovered and reseeded cells (c-c' and d-d', respectively). Nuclei were counterstained with Hoechst 33258 (blue fluorescence). Bar: 18 μ m. Density bands of p62/SQSTM1 (75 kDa) and α -actin (47 kDa) obtained by western blotting analysis are shown in E, for cisPt and PtAcacDMS. In F, histogram shows quantitative analysis of p62/SQSTM1 in control cells, standard acute test - 48 h exposed cells, recovered and reseeded cells after cisPt or PtAcacDMS. Data are presented as mean \pm SD over the mean experimental values of each of three independent experiments. p values: (***) < 0.001. (For interpretation of the references to colour in this figure legend, the reader is referred to the web version of this article.)

several stages of maturation in the cytoplasm of recovered cells after cisPt-exposure as well as in both recovered and reseeded cells previously treated with PtAcacDMS. These reported data are in line with previous investigations, showing that cisPt at concentrations ranging from 25 to 50 μ M is able to induce autophagy in a number of cell lineages, showing different sensitivity to this antineoplastic agent (Wang and Wu, 2014; Lin et al., 2017; Chen et al., 2017; Chen et al., 2018).

Since autophagy represents the major regulated mechanism for the degradation of long-lived proteins and the only known pathway for organelle degradation (Lee et al., 2012; Okamoto, 2014), the co-localization outcome revealed by our immunofluorescence analysis which involved mitochondria and lysosomes may indicate the occurrence of catalytic events in which mitochondria are engulfed inside lysosomes during the autophagic process. In fact, after cisPt treatment, fluorescent spots (representatives of co-localization) were only detected in recovered cells but not in reseeded ones, while conversely after exposure

to PtAcacDMS, co-localization areas were observed both in recovered and reseeded cells suggesting that autophagy lasted for a longer period. Furthermore, deeper findings on activation and the role of autophagy came from autophagic protein analysis (Beclin-1, LC3B and p62/SQSTM1 and ATG5), demonstrating changes in their expression and localization. Beclin-1 is involved in the nucleation step of the autophagosome formation (Kang et al., 2011) and forms the catalytic core complex with Vps34, class III mammalian phosphatidylinositol-3 kinase (PIK3C3), allowing the phosphorylation of phosphatidylinositol which produces PI3P which is critically involved in the autophagosomes membrane bio-genesis and material trafficking (Thoresen et al., 2010). As shown by our immunocytochemical results, during cellular homeostasis, Beclin-1 was localized in the cytoplasm, mainly in the perinuclear zone and inside the nucleus. This finding is in line with the critical role of Beclin-1 in regulating autophagy, given that, under homeostatic conditions this process is inhibited by the interaction between Beclin-1 and the anti-apoptotic factor Bcl-2 (Zhang et al., 2009;

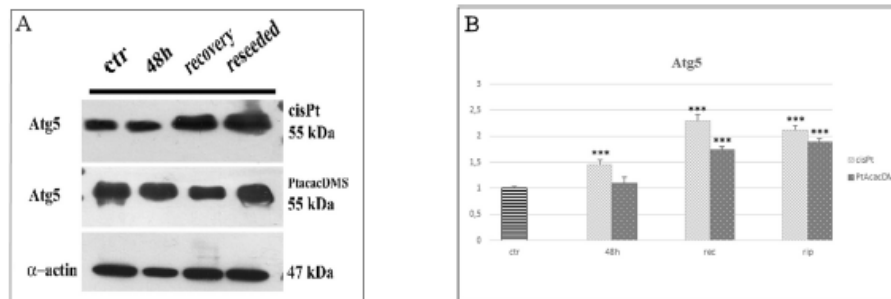


Fig. 6. ATG5 protein data by Western Blotting.

Data obtained by WB analysis for cisPt- or PtAcacDMS-treatments. In A, density bands of ATG5 (55 kDa) and α -actin (47 kDa). In B, histograms showing quantitative analysis of ATG5 in control cells, cisPt- and PtAcacDMS-standard acute test-48 h exposed cells, recovered and reseeded cells. Data are presented as mean \pm SD over the mean experimental values of each of three independent experiments. p values: (***) < 0.001.

Zhao et al., 2018). Once autophagy is induced, Bcl-2 is phosphorylated disrupting the interaction with Beclin-1 which can perform its function (Gordy and He, 2012; Fan and Zong, 2013). Notably, after both cisPt- and PtAcacDMS exposure Beclin-1 increased in the cytoplasm of recovered cells, as also confirmed by western blotting analysis, showing co-localization with lysosomes. Diversely, in reseeded cells, previously treated with PtAcacDMS, the immunopositivity for Beclin-1 decreased. Therefore, we may hypothesized that the autophagic process detectable in recovered cells after PtAcacDMS exposure could leave place, at least in part, to apoptotic events, therefore the nucleation of new autophagic vesicles might be not necessary at this stage. These data are also confirmed by previous results, in which cleavage and consequent inactivation of PARP-1 (Rodríguez-Vargas et al., 2016) were observed in reseeded cells after treatment with PtAcacDMS (Grimaldi et al., 2016). Moreover, concerning cisPt, our results are in accordance to previous experimental findings demonstrating that cisPt (25 μ M, 24 h-exposure) induced protective autophagy in human BC cells, through the up-regulation of beclin-1 (Lin et al., 2017). Furthermore, in line with our data, Chen and colleagues recently demonstrated that cisPt triggered autophagic responses by up-regulating beclin-1 and Atg5 expression levels (Chen et al., 2018).

Concerning ATG5, it is required for the growth of the phagophore during the elongation step (Graf et al., 2009) which depends on the binding of ATG5 to ATG12 and thus forming a key-complex (~55 kDa) in the lipidation of LC3B-I into LC3B-II. LC3B-II associated with both internal and external membrane of the elongating vesicle (Kuma et al., 2002) and it is responsible for the specific recognition of substrates. Our findings evidenced an increase of ATG5 protein levels in recovered cells after both cisPt and PtAcacDMS, shown by western blotting investigations, indicated a massive autophagy activation. Nonetheless, after PtAcacDMS exposure, higher ATG5 levels were determined in reseeded cells compared to those measured in recovered ones. Furthermore, confocal microscopy data demonstrated that LC3B was inside the cytoplasm after both cisPt- and PtAcacDMS-exposure and the co-localization with lysosomes confirmed the induction of autophagy. The lipidated form of LC3B (LC3B-II) was detectable in recovered cells after both treatments. LC3B-II was also observed in reseeded cells, formerly exposed to PtAcacDMS indicating a persisting autophagic process (elongation step). On the other hand, reseeded cells, previously treated with cisPt did not express the activated form of LC3B, suggesting that autophagy might have disappeared, this mechanism being a possible survival strategy for the cell (Guo et al., 2015; Wang et al., 2017). Our present findings are in accordance to previous studies demonstrating a significant increased LC3B-II accumulation after 24 h-exposure to 25 μ M

cisPt in human bladder cancer cells (Lin et al., 2017), as determined by Western blot, immunofluorescence and TEM. Similarly, a significantly enhanced (LC3B)-I/II conversion, resulting in LC3B-II increase and phagosome formation was reported in several human ovarian cancer cell lines (i.e. RMG-1, OV90, and OV433) as well as in human lung cancer cells (i.e. A549) after cisPt exposure (20–50 μ M cisPt for 24 h) (Wang and Wu, 2014; Chen et al., 2018).

Finally, regarding the analyzed scaffold protein p62/SQSTM1, it binds directly to LC3B-II thus conveying ubiquitinated proteins and conferring cargo selectivity to autophagosomal vesicles (Johansen and Lamark, 2011). During the 7-day recovery period after both platinum compound treatments p62/SQSTM1 localized closely to lysosomes showing high fluorescence intensity. In reseeded cells, previously exposed to cisPt, it localized in the nucleus indicating an interruption or, at least, a decrease of the autophagy. Instead, after PtAcacDMS treatment, p62/SQSTM1 was still in the cytoplasm of reseeded cells. The significant decrease of p62/SQSTM1 levels both in recovered and reseeded cells entirely confirmed the autophagy progression even long-lasting after drug-exposure, given that p62/SQSTM1 is itself degraded into autophagosomes together with substrates (Komatsu and Ichimura, 2010). These data were also in accordance to previous in vitro experiments in human bladder cancer cells, reporting p62 clearance and autophagolysosome formation after cisPt exposure at a dose of 25 μ M (Lin et al., 2017).

Taken together, our findings, in agreement with a body of literature (Bao et al., 2015; Zhan et al., 2016; Lin et al., 2017; Zhao et al., 2018), highlight the role of autophagy in B50 neuroblastoma cell line after exposure to both cisPt and PtAcacDMS at the chosen doses of 40 and 10 μ M respectively. After exposure to the platinum-based drugs, the early onset of apoptosis was followed by autophagy activation, subsequent to a recovery phase and growth in drug-free medium. Interestingly, after the 7-day recovery period we observed that cells underwent different fates depending on the above reported drugs treatment. After cisPt exposure and recovery during the reseeded stage, cells displayed a conventional morphology similar to that observed in controls, suggesting the protective role played by autophagy which may represent a survival mechanism occurring in cancer cells. On the contrary, reseeded cells, previously exposed to PtAcacDMS and then recovered, showed apoptotic features together with activation of autophagy machinery, suggesting that cells did not restore their homeostatic function and underwent cell death.

In summary, we suggest that PtAcacDMS, still effective at a dose 4 times lower than that employed for cisPt (10 vs 40 μ M, respectively), may represent an alternative molecule in the treatment of cancer due to

its higher efficacy and its ability to potentially overcome cisPt-resistance related to autophagy induction.

Conflict of interest

All of the authors have read and approved the paper and it has not been published previously nor is it being considered by any other peer-reviewed journal. All authors agree to the submission of this manuscript to the journal. The authors declare that they have no conflict of interest.

Funding

This research was supported by (i) Italian Ministry of Education, University and Research (MIUR): Dipartimenti di Eccellenza Program (2018–2022) - Dept. of Biology and Biotechnology "L. Spallanzani", University of Pavia, (ii) Fondazione Banca del Monte di Lombardia (Grant 2011) and (iii) MIUR (Cofin 2009).

Acknowledgments

We thank Dr. Patrizia Vaghi for confocal images that were taken at the Centro Grandi Strumenti, University of Pavia.

References

Asnolfi, I., Ghiselli, S., Guarnoni, V., Chiccani, M., Simoni, F., Oliviero, F., Ielli, G., Mariani, A., 2013. Correlation of adverse effects of cisplatin administration in patients affected by solid tumours: a retrospective evaluation. *Oncol. Rep.* 29, 1285–1292. <https://doi.org/10.3892/or.2013.2270>.

Badrack, E.H., 2005. Autophagy: dual roles in life and death? *Nat. Rev. Mol. Cell Biol.* 6, 505–510. <https://doi.org/10.1038/nrm1666>.

Rao, L., Jaramillo, M.C., Zhang, Z., Zhang, Y., Yao, M., Zhang, D.D., Yi, X., 2015. Induction of autophagy contributes to cisplatin resistance in human ovarian cancer cells. *Mol. Med. Rep.* 11, 91–98. <https://doi.org/10.3892/mmr.2014.2671>.

Bernocchi, G., Bortone, M.G., Piccinini, V.M., Dal Bo, V., Santini, G., De Pascali, S.A., Magoni, D., Fanzini, F.P., 2011. Developing central nervous system and vulnerability to platinum compounds. *Chemother. Res. Pract.* 2011, 315418. <https://doi.org/10.1155/2011/315418>.

Bernocchi, G., Fanzini, F.P., De Pascali, S.A., Piccinini, V.M., Gasperini, C., Insolia, V., Bortone, M.G., 2015. Neurotoxic effects of platinum compounds: studies in vivo on intracellular calcium homeostasis in the immature central nervous system. *Toxicol.* 3, 224–248. <https://doi.org/10.3390/tox3020224>.

Bodmer, D.L., Dodson, P.C., Keng, P.C., Borch, R.F., 1986. Effect of diethylthiocarbamate on cis-diamminedichloroplatinum (II)-induced cytotoxicity, DNA cross-linking, and gamma-glutamyl transpeptidase inhibition. *Cancer Res.* 46, 2745–2750.

Bortone, M.G., Soldani, C., Veneroni, P., Avila, D., Pisu, M., Bernocchi, G., 2008. Cell proliferation, apoptosis and mitochondrial damage in rat R50 neuronal cells after cisplatin treatment. *Cell Prolif.* 41, 506–520. <https://doi.org/10.1111/j.1365-2184.2008.00530.x>.

Bortone, M.G., Santini, G., Soldani, C., Veneroni, P., Scovazzi, A.I., Alpaoli, C., 2012. Intracellular distribution of Taukayases as detected by multicolor immunofluorescence techniques. *Eur. J. Histochem.* 56, 64. <https://doi.org/10.4081/eh.2012.64>.

Bortone, M.G., Fanzini, F.P., Bernocchi, G., 2015. In vivo and in vitro immunohistochemical visualization of neural cell apoptosis and autophagy. In: McEigh, A., Lissi, I. (Eds.), *Immunocytochemistry and Related Techniques*. NeuroMethods 101. Humana Press, New York, pp. 153–178. https://doi.org/10.1007/978-1-4939-2313-7_9.

Revdon, C.R., Phillips, K.A., Abdolell, M., Bunton, T., Tancock, I.F., 2000. Cognitive function in breast cancer patients receiving adjuvant chemotherapy. *J. Clin. Oncol.* 18, 2695–2701. <https://doi.org/10.1200/JCO.2000.18.14.2695>.

Chen, X., Zhang, L., Ding, S., Lei, Q., Fang, W., 2017. Cisplatin combination drugs induce autophagy in HeLa cells and interact with HSA via electrostatic binding affinity. *RSC Adv.* 7, 22270–22279.

Chen, J., Zhang, L., Zhou, H., Wang, W., Liu, Y., Yang, H., Yi, H., 2018. Inhibition of autophagy promotes cisplatin-induced apoptotic cell death through Atg5 and Beclin1 in A549 human lung cancer cells. *Mol. Med. Rep.* 17, 6859–6865.

Chiang, K.C., Tsui, K.H., Chang, L.C., Yeh, C.N., Feng, T.H., Chen, W.T., Chang, P.L., Chiang, H.Y., Juang, H.H., 2014. Cisplatin modulates B cell translocation gene 2 to attenuate cell proliferation of prostate carcinoma cells in both p53-dependent and p53-independent pathways. *Sci. Rep.* 4 (25111). <https://doi.org/10.1038/srep05111>.

Choi, A.M., Ryser, S.W., Levine, B., 2013. Autophagy in human health and disease. *N. Engl. J. Med.* 368, 1845–1846. <https://doi.org/10.1056/NEJMe1205406>.

Codogno, P., Meijer, A.J., 2006. ATG5: more than an autophagy factor. *Nat. Cell Biol.* 8, 1045–1047. <https://doi.org/10.1038/ncb1306-1045>.

Diazzi, S., Tchoumou, P.R., 2014. Cisplatin in cancer therapy: molecular mechanisms of action. *Eur. J. Pharmacol.* 740, 364–378. <https://doi.org/10.1016/j.ejphar.2014.07.025>.

De Castro, F., Resnardi, M., Antonaci, G., Del Coco, L., De Pascali, S.A., Mascola, A., Manigliano, S., Fanzini, F.P., 2018. Response of cisplatin resistant Skov-3 cells to [Pt(O,O'-Acac)(Y-Acac)(DMS)] treatment revealed by a metabolomic 1H-NMR study. *Molecules* 23, 2301. <https://doi.org/10.3390/molecules23092301>.

De Pascali, S.A., Magoni, D., Papaia, P., Mascola, A., Marigliano, S., Ciccarese, A., Fanzini, F.P., 2006. New water-soluble platinum(II) phenanthroline complexes tested as cisplatin analogues: first-time comparison of cytotoxic activity between analogous four- and five-coordinate species. *Dalton Trans.* (42), 5077–5087. <https://doi.org/10.1039/B610945D>.

De Rello, R., Toscano, M., Moretti, D., Macellari, E., 2013. Cisplatin-induced apoptosis inhibits autophagy, which acts as a pro-survival mechanism in human melanoma cells. *PLoS One* 8, e57236. <https://doi.org/10.1371/journal.pone.0057236>.

Demachi, F., Bertoli, C., Copetti, T., Tanida, I., Brancolini, C., Fekedulegn, E.L., Schneider, C., 2005. Galpoin is required for macroautophagy in mammalian cells. *J. Cell Biol.* 175, 595–605. <https://doi.org/10.1083/jcb.200501024>.

Dierckx, J., Han, R., Yang, Y., Mayer-Prischel, M., Noble, M., 2006. CNS progenitor cells and oligodendrocytes are targets of chemotherapeutic agents in vitro and in vivo. *J. Biol. Chem.* 281, 121–129. <https://doi.org/10.1074/jbc.M511010>.

Fan, Y.J., Zeng, W.X., 2013. The cellular decision between apoptosis and autophagy. *Chin. J. Cancer* 32, 121–129. <https://doi.org/10.5732/cj.012.10106>.

Fania, G.M., Kroemer, G., Piacentini, M., 2013. Molecular mechanisms of selective autophagy. *Cell Death Differ.* 20, 1–2. <https://doi.org/10.1038/cd.2012.97>.

Galluzzi, L., Senovilla, L., Vitale, I., Michels, J., Martins, I., Keop, O., Curcio, M., Kroemer, G., 2012. Molecular mechanisms of cisplatin resistance. *Oncogene* 31, 1869–1883. <https://doi.org/10.1038/onc.2011.384>.

Goody, C., He, Y.W., 2012. The cross-talk between autophagy and apoptosis: where does this lead? *Protein Cell* 3, 17–27. <https://doi.org/10.1007/s13238-011-1127-x>.

Graf, M.R., Jia, W., Johnson, R.S., Dent, P., Mitchell, C., Loda, R.M., 2009. Autophagy and the functional roles of Atg5 and Beclin-1 in the anti-tumor effects of the anti-androgen 17alpha-diol neurosteroid on malignant glioma cells. *J. Steroid Biochem. Mol. Biol.* 115, 137–145. <https://doi.org/10.1016/j.jsb.2009.03.013>.

Germadi, M., Santini, G., Insolia, V., Dal Bo, V., Piccinini, V.M., Veneroni, P., Rinali, S., Verri, M., De Pascali, S.A., Fanzini, F.P., Bernocchi, G., Bortone, M.G., 2016. [Pt(O,O'-Acac)(Y-acac)(DMS)] versus cisplatin: apoptotic effects in R50 neuroblastoma cells. *Histochem. Cell Biol.* 145, 587–601. <https://doi.org/10.1007/s00418-015-1396-1>.

Gump, I.M., Thorburn, A., 2011. Autophagy and apoptosis: what is the connection? *Trends Cell Biol.* 21, 387–392. <https://doi.org/10.1016/j.tcb.2011.03.007>.

Guo, M.L., Liao, K., Peryassamy, P., Yang, L., Cai, Y., Cullen, S.E., Buch, S., 2015. Cocaine-mediated microglial activation involves the ER stress-autophagy and Autophagy 11, 995–1009. <https://doi.org/10.1080/15548627.2015.1052205>.

Harris, H., Rubenstein, D.C., 2011. Control of autophagy as a therapy for neurodegenerative disease. *Nat. Rev. Neurol.* 8, 108–117. <https://doi.org/10.1038/nrn.2011.200>.

Jahromi, T., Lamark, T., 2011. Selective autophagy mediated by autophagic adaptor proteins. *Autophagy* 7, 279–296. <https://doi.org/10.4161/auto.7.3.14487>.

Jordan, P., Carmo-ROSA, M., 2000. Molecular mechanisms involved in cisplatin cytotoxicity. *Cell. Mol. Life Sci.* 57, 1229–1235.

Kabeya, Y., Mizushima, N., Ueno, T., Yamamoto, A., Kirisako, T., Noda, T., Kominami, E., Ohsumi, Y., Yoshimori, T., 2000. LC3, a mammalian homologue of yeast Apg8p, is localized in autophagosome membranes after processing. *EMBO J.* 19, 5720–5728. <https://doi.org/10.1093/emboj/19.21.5720>.

Kachadourian, R., Leitner, H.M., Day, R.J., 2007. Selected fibrosis promoters: the toxicity of cisplatin in human lung adenocarcinoma cells: a role for glutathione depletion. *Int. J. Oncol.* 31, 161–168.

Kang, R., Zeh, H.J., Lotze, M.T., Tang, D., 2011. The Beclin 1 network regulates autophagy and apoptosis. *Cell Death Differ.* 18, 571–580. <https://doi.org/10.1038/cdd.2010.191>.

Klionsky, D.J., 2007. Autophagy: from phenomenology to molecular understanding in less than a decade. *Nat. Rev. Mol. Cell Biol.* 8, 931–937. <https://doi.org/10.1038/nrm2245>.

Komatsu, M., Ichimura, Y., 2010. Physiological significance of selective degradation of p62 by autophagy. *FEBS Lett.* 584, 1374–1378. <https://doi.org/10.1016/j.febslet.2010.02.017>.

Kondo, Y., Kawano, T., Sawaya, R., Kondo, S., 2005. The role of autophagy in cancer development and response to therapy. *Nat. Rev. Cancer* 5, 726–734. <https://doi.org/10.1038/nrc1692>.

Kuma, A., Mizushima, N., Ishiura, N., Ohsumi, Y., 2002. Formation of the approximately 350-kDa Apg12-Apg5-Apg16 multimeric complex, mediated by Apg16 oligomerization, is essential for autophagy in yeast. *J. Biol. Chem.* 277, 18619–18625. <https://doi.org/10.1074/jbc.M111889200>.

Lee, H., Noh, J.Y., Oh, Y., Kim, Y., Chang, J.W., Chung, C.W., Lee, S.T., Kim, M., Ryu, H., Jung, Y.K., 2012. BE1 plays an essential role in ER stress-mediated aggregation of mutant huntingtin via the inhibition of autophagy flux. *Hum. Mol. Genet.* 21, 101–114. <https://doi.org/10.1093/hmg/ddt445>.

Levine, B., Kroemer, G., 2008. Autophagy in the pathogenesis of disease. *Cell* 132, 27–42. <https://doi.org/10.1016/j.cell.2007.12.018>.

Liang, X.H., Yu, J., Brown, K., Levine, B., 2001. Beclin 1 contains a leucine-rich nuclear export signal that is required for its autophagy and tumor suppressor function. *Cancer Res.* 61, 3443–3449.

Liu, J.F., Liu, Y.C., Yao, T.F., Chen, H.F., Chen, K.Y., Hwang, T.I., 2017. Cisplatin induces protective autophagy through activation of Beclin1 in human bladder cancer cells. *Drug Des. Devel. Ther.* 11, 1517–1533. <https://doi.org/10.2147/DDDT.S126464>.

Longo, L., Piazzi, F., Scardino, A., Alabio, O., Vassallo, G., Testitore, L., 2008. Autophagy inhibition enhances doxorubicin-induced apoptosis in hepatocellular carcinoma. *Mol. Cancer Ther.* 7, 2476–2485. <https://doi.org/10.1158/1535-7163.MCT-08-0361>.

- Maiuri, M.C., Zalcman, E., Kimchi, A., Kromer, G., 2007. Self-eating and self-killing: cross-talk between autophagy and apoptosis. *Nat. Rev. Mol. Cell Biol.* 8, 741–752. <https://doi.org/10.1038/nrm2239>.
- Mayotte, P., Thorburn, A., 2011. Autophagy and cancer therapy. *Cancer Biol. Ther.* 11, 127–137. <https://doi.org/10.4161/cbt.11.2.14627>.
- McWhinney, S.R., Goldberg, R.M., McLeod, H.L., 2009. Platinum neurotoxicity pharmacogenetics. *Mol. Cancer Ther.* 8, 10–16. <https://doi.org/10.1158/1535-7163.MCT-08-0840>.
- Muscella, A., Calabrino, N., De Pascoli, S.A., Urso, I., Ciccarese, A., Fanizzi, F.P., Magoni, D., Marsigliante, S., 2007. New [Pt(O, O'-acac)] complexes containing both an O,O'-chelated acetylacetonate ligand and a sulfur ligand in the platinum coordination sphere induce apoptosis in H1a cervical carcinoma cells. *Biochem. Pharmacol.* 74, 28–40. <https://doi.org/10.1016/j.bcp.2007.03.027>.
- Muscella, A., Calabrino, N., Fanizzi, F.P., De Pascoli, S.A., Urso, I., Ciccarese, A., Magoni, D., Marsigliante, S., 2008. [Pt(O, O'-acac)(gamma-acac)(DMS)], a new Pt compound exerting fast cytotoxicity in MCF-7 breast cancer cells via the mitochondrial apoptotic pathway. *Br. J. Pharmacol.* 153, 34–49. <https://doi.org/10.1038/sj.bjp.0707576>.
- Muscella, A., Calabrino, N., Verugno, C., Fanizzi, F.P., De Pascoli, S.A., Sironi, C., Marsigliante, S., 2011. The platinum (II) complex [Pt(O, O'-acac)(gamma-acac)(DMS)] alters the intracellular calcium homeostasis in MCF-7 breast cancer cells. *Biochem. Pharmacol.* 81, 91–103. <https://doi.org/10.1016/j.bcp.2010.09.012>.
- Muscella, A., Verugno, C., Calabrino, N., Cossa, L.G., De Pascoli, S.A., Fanizzi, F.P., Marsigliante, S., 2014. [Pt(O, O'-acac)(gamma-acac)(DMS)] alters SH-SY5Y cell migration and invasion by the inhibition of Na⁺/H⁺ exchanger isoform 1 occurring through a PKC α /ERK/mTOR Pathway. *PLoS One* 9, e112186. <https://doi.org/10.1371/journal.pone.0112186>.
- Okamoto, K., 2014. Organophagy: eliminating cellular building blocks via selective autophagy. *J. Cell Biol.* 205, 435–445. <https://doi.org/10.1083/jcb.201402054>.
- Pacetto, L.M., D'Andrea, M.R., Rossi, F., Montefrini, S., 2006. Oxaliplatin-related neurotoxicity: how and why? *Q. Rev. Oncol. Hematol.* 59, 159–168. <https://doi.org/10.1016/j.critrev.2006.01.001>.
- Piccolini, V.M., Esposito, A., Dal Bo, V., Incolta, V., Romone, M.G., De Pascoli, S.A., Fanizzi, F.P., Bernocchi, G., 2015. Cerebellum neurotransmission during postnatal development: [Pt(O, O'-acac)(X)(gamma-acac)(DMS)] vs cisplatin and neurotoxicity. *Int. J. Dev. Neurosci.* 40, 24–34. <https://doi.org/10.1016/j.ijdevneu.2014.10.006>.
- Platani, F., Pérez-Tomé, R., Ambrosio, S., Testore, L., 2010. Understanding autophagy in cell death control. *Curr. Pharm. Des.* 16, 101–113. <https://doi.org/10.2174/158161210789941810>.
- Qian, P., Yan, L.J., Li, Y.Q., Yang, H.T., Duan, H.Y., Wu, J.T., Fan, X.W., Wang, S.L., 2018. Cyanidin ameliorates cisplatin-induced cardiotoxicity via inhibition of ROS-mediated apoptosis. *Exp. Ther. Med.* 15, 1959–1965. <https://doi.org/10.3892/etm.2017.5617>.
- Rahbi, C.A., Dolan, M.E., 2007. Molecular mechanisms of resistance and toxicity associated with platinumating agents. *Cancer Treat. Rev.* 33, 9–23. <https://doi.org/10.1016/j.ctrv.2006.09.005>.
- Rodríguez-Vargas, J.M., Rodríguez, M.I., Májula-Medagón, J., García-Díaz, Á., González-Flores, A., López-Rivas, A., Virgí, I., Iluzi, G., Schreiber, V., Dauter, F., Olivieri, F.J., 2016. Autophagy requires poly(ADP-ribose) polymerase-dependent AMPK nuclear export. *Cell Death Differ.* 23, 2007–2018. <https://doi.org/10.1038/cdd.2016.80>.
- Sakalli Çetin, E., Nazroglu, M., Gök, R., Övey, I.S., Arslan Köpür, P., 2017. Selenium potentiates the anticancer effect of cisplatin against oxidative stress and calcium ion signaling-induced intracellular toxicity in MCF-7 breast cancer cells: involvement of the TRPV1 channel. *J. Recept. Signal Transduct. Res.* 37, 84–93. <https://doi.org/10.3109/10799893.2016.1160931>.
- Santini, G., Piccolini, V.M., Venesoni, P., Baril, S., Bernocchi, G., Bottono, M.G., 2011. Different patterns of apoptosis in response to cisplatin in R50 neuroblastoma rat cells. *Histol. Histopathol.* 26, 831–842. <https://doi.org/10.14670/HH-26.831>.
- Santini, G., Scietti, L., Venesoni, P., Baril, S., Bernocchi, G., Bottono, M.G., 2012. Effects of Cisplatin in neuroblastoma rat cells: damage to cellular organelles. *Int. J. Cell Biol.* 2012, 424072. <https://doi.org/10.1155/2012/424072>.
- Santini, G., Piccolini, V.M., Baril, S., Venesoni, P., Giassanti, V., Dal Bo, V., Bernocchi, G., Bottono, M.G., 2013. Mitochondrial fusion: a mechanism of cisplatin-induced resistance in neuroblastoma cells? *Neurotoxicology* 34, 51–60. <https://doi.org/10.1016/j.neuro.2012.10.011>.
- Scherini, F., Neechi, D., Vignola, C., Bernocchi, G., 1992. Co-Dichlorodiamine septium album GABAergic structures in the immature rat cerebellum. *Neuroscience* 50, 987–997. [https://doi.org/10.1016/0306-4522\(92\)90221-6](https://doi.org/10.1016/0306-4522(92)90221-6).
- Shi, Y., Fankoh, A., Radwanji, L.G., Penn, L.Z., Miller, R.G., Mills, G.R., 1995. Rapamycin enhances apoptosis and increases sensitivity to cisplatin in vitro. *Cancer Res.* 55, 1982–1988.
- Thoresen, S.B., Pedersen, N.M., Ljønsdal, K., Srensen, H., 2010. A phosphatidylinositol 3-kinase class III sub-complex containing VPS15, VPS34, Beclin 1, UVRAG and RIF-1 regulates cytokinesis and degradative endocytic traffic. *Exp. Cell Res.* 316, 3368–3378. <https://doi.org/10.1016/j.yexcr.2010.07.008>.
- Wang, J., Wu, G.S., 2014. Role of autophagy in cisplatin resistance in ovarian cancer cells. *J. Biol. Chem.* 289, 17163–17173.
- Wang, H., Zhang, S., Zhong, J., Zhang, J., Luo, Y., Pengfei, G., 2013. The proteasome inhibitor lactacystin exerts its therapeutic effects on glioma via apoptosis: an in vitro and in vivo study. *J. Int. Med. Res.* 41, 72–81. <https://doi.org/10.1177/0300060513476992>.
- Wang, G.Y., Bi, Y.G., Liu, X.D., Zhao, Y., Han, J.F., Wei, M., Zhang, Q.Y., 2017. Autophagy was involved in the protective effect of metformin on hyperglycemia-induced cardiomyocyte apoptosis and Connexin43 downregulation in H9c2 cells. *Int. J. Med. Sci.* 14, 698–704. <https://doi.org/10.7150/ijms13990>.
- Wang, F.Y., Tang, X.M., Wang, Y., Huang, K.R., Feng, H.W., Chen, Z.F., Liu, Y.N., Liang, H., 2018. Mitochondria-targeted platinum(II) complexes induce apoptosis-dependent autophagic cell death mediated by ER-stress in A549 cancer cells. *Eur. J. Med. Chem.* 155, 639–650. <https://doi.org/10.1016/j.ejmech.2018.06.018>.
- Zhan, L., Zhang, Y., Wang, W., Song, E., Fan, Y., Li, L., Wei, B., 2016. Autophagy as an emerging therapy target for ovarian carcinoma. *Oncotarget* 7, 83476–83487. <https://doi.org/10.18632/oncotarget.13060>.
- Zhang, H., Kong, X., Kang, J., Su, J., Li, Y., Zhong, J., Sun, L., 2009. Oxidative stress induced pan-ERK autophagy and mitochondrial dysfunction in human glioma U251 cells. *Toxicol. Sci.* 110, 376–388. <https://doi.org/10.1093/toxsci/kfp101>.
- Zhao, C., Mei, Y., Chen, X., Jiang, L., Jiang, J., Song, X., Xiao, H., Zhang, J., Wang, J., 2018. Autophagy plays a pro-survival role against methamphetamine-induced apoptosis in H9c2 cells. *Toxicol. Lett.* 294, 156–165. <https://doi.org/10.1016/j.toxlet.2018.05.017>.



Article

Hericium erinaceus Improves Recognition Memory and Induces Hippocampal and Cerebellar Neurogenesis in Frail Mice during Aging

Daniela Ratto ¹, Federica Corana ², Barbara Mannucci ², Erica Cecilia Priori ¹, Filippo Cobelli ¹, Elisa Roda ^{1,3}, Beatrice Ferrari ¹, Alessandra Occhinegro ¹, Carmine Di Iorio ¹, Fabrizio De Luca ¹, Valentina Cesaroni ⁴, Carolina Girometta ⁴, Maria Grazia Bottone ¹, Elena Savino ⁴, Hirokazu Kawagishi ⁵ and Paola Rossi ^{1,*}

¹ Department of Biology and Biotechnology “L. Spallanzani”, University of Pavia, 27100 Pavia, Italy; daniela.ratto01@universitadipavia.it (D.R.); ericacecilia.priori01@universitadipavia.it (E.C.P.); filippo.cobelli01@universitadipavia.it (F.Cob.); elisa.roda@unipv.it (E.R.); beatrice.ferrari01@universitadipavia.it (B.F.); alessandra.occhinegro01@universitadipavia.it (A.O.); carmine.diiorio01@universitadipavia.it (C.D.I.); fabrizio.deluca01@universitadipavia.it (F.D.L.); mariagrazia.bottone@unipv.it (M.G.B.)

² Centro Grandi Strumenti, University of Pavia, 27100 Pavia, Italy; federica.corana@unipv.it (F.Cor.); barbara.mannucci@unipv.it (B.M.)

³ Laboratory of Clinical & Experimental Toxicology, Pavia Poison Centre, National Toxicology Information Centre, Toxicology Unit, ICS Maugeri SpA, IRCCS Pavia, 27100 Pavia, Italy

⁴ Department of Earth and Environmental Sciences, University of Pavia, 27100 Pavia, Italy; valentina.cesaroni01@universitadipavia.it (V.C.); carolina.girometta01@universitadipavia.it (C.G.); elena.savino@unipv.it (E.S.)

⁵ Research Institute of Green Science and Technology, Shizuoka University; 422-8529 Shizuoka, Japan; kawagishi.hirokazu@shizuoka.ac.jp

* Correspondence: paola.rossi@unipv.it; Tel: +0039-0382-896076

Received: 7 March 2019; Accepted: 25 March 2019; Published: 27 March 2019

Abstract: Frailty is a geriatric syndrome associated with both locomotor and cognitive decline, implicated in both poor quality of life and negative health outcomes. One central question surrounding frailty is whether phenotypic frailty is associated with the cognitive impairment during aging. Using spontaneous behavioral tests and by studying the dynamic change during aging, we demonstrated that the two form of vulnerability, locomotor and recognition memory decline, develop in parallel and therefore, integration of the motoric and cognitive evaluations are imperative. We developed an integrated frailty index based on both phenotypic and recognition memory performances. *Herichium erinaceus* (*H. erinaceus*) is a medicinal mushroom that improves recognition memory in mice. By using HPLC-UV-ESI/MS analyses we obtained standardized amounts of erinacine A and hericenones C and D in *H. erinaceus* extracts, that were tested in our animal model of physiological aging. Two-month oral supplementation with *H. erinaceus* reversed the age-decline of recognition memory. Proliferating cell nuclear antigen (PCNA) and doublecortin (DCX) immunohistochemistry in the hippocampus and cerebellum in treated mice supported a positive effect of an *H. erinaceus* on neurogenesis in frail mice.

Keywords: aging; phenotypic frailty; cognitive decline; *Herichium erinaceus*; erinacines; hericenones; medicinal mushrooms supplementation; neurogenesis

1. Introduction

Recent reports on the European population suggest that by 2060, 30% of Europeans will be over the age of 65. Frailty is a geriatric syndrome associated with poor quality of life and negative health outcomes, such as acute illness, falls, hospitalization, disability, dependency, and mortality, adjusted for comorbidities [1,2,3], in the absence of recognized disabilities or organ-specific diseases. Health declines in frailty are accelerated and accompanied by the failure of homeostatic mechanisms [4,5].

Fried defined phenotypic frailty as an aging-associated phenotype expressing at least three of the following symptoms: weakness, weight loss, slow walking speed, fatigue, and a low level of physical activity [1]. Most older people gradually become frail and oscillations between non-frail, pre-frail, and frail are not uncommon [6]. Cognitive impairment is a decline of cognitive functions such as remembering, reasoning, and planning, ranging from mild forms of forgetfulness to severe dementia. Cognition-impaired frailty in human studies was associated with global cognition and perceptual speed, but not with episodic memory [7]. Quality of life in the elderly is particularly affected by impairments in the functioning of the memory system [8]. In order to evaluate the inclusion of cognitive performances in frailty clinical diagnosis [9], it is necessary to first determine whether phenotypic frailty is associated with cognitive impairment [10].

Several epidemiological studies have reported that higher levels of phenotypic frailty increases the risk of cognitive impairment and dementia [11,12,13], and that higher levels of cognitive impairment or dementia increase the risk of phenotypic frailty [14,15,16]. This suggests that frailty may be an early indicator for subsequent cognitive decline. Understanding the mechanisms by which phenotypic frailty is linked to cognitive impairment has implications for the management of those susceptible for both phenotypic frailty and cognitive impairment.

Hericium erinaceus (*H. erinaceus*) is found in Europe, Asia, North America, Oceania, and generally throughout the north temperate latitudes. In Italy, it is considered quite rare; it occurs along the Apennines mountain chain, near Sicily and Sardinia, while in the North only few sporadic sightings have been reported.

H. erinaceus is an edible mushroom widely used as herbal medicine, in all areas mentioned above and in a few East Asian countries. Since 1990, studies on *H. erinaceus* secondary metabolites reported several (about 70) structurally related terpenoids, such as erinacines, hericenones, hericerins, hericenols, and erinacerins [17,18,19].

All of the above-mentioned molecules, except erinacines, share a geranyl side chain bonded to a resorcinol framework; that is, they are aromatic compounds containing the 6-alkyl-2,4-dihydroxybenzoic acid unit also known as β -resorcylylate [20]. Erinacines are classified as cyathane-type diterpenoids, including 20 members of 24 different diterpenoids in *H. erinaceus* [18]. The standardization of dietary supplements from medicinal mushrooms is still in its early stages, because proper standards and protocols are lost and cannot guarantee product quality [21,22].

Existing data have suggested that there is a neuroprotective effect of dietary supplementation with *H. erinaceus* in mice subjected to middle cerebral artery occlusion [23]. Furthermore, *H. erinaceus* provided a partial recovery of intellectual function of patients with a mild cognitive impairment or against other forms of neurodegenerative diseases, including dementia and Alzheimer's [24,25,26]. It has been shown that erinacines A–I and hericenones C–H are responsible for the neuroprotective effects of stimulating Nerve Growth Factor (NGF) [27,28] and of brain derived neurotrophic factor (BDNF) synthesis in vitro [29,30]. A possible role of polysaccharides in neuroprotection has been suggested as well [25,27,31]. Additionally, the effects of *H. erinaceus* on recognition memory and on hippocampal mossy fiber-CA3 neurotransmission in wild-type middle-aged mice was recently published [32,33]. Among the neurogenic zones, hippocampus is the most interesting area in the adult brain, because it is involved in higher cognitive function, such as memory processes and certain affective behaviors. In particular adult and persistent hippocampal neurogenesis generates new excitatory neurons in the dentate gyrus and contributes in a significant way to plasticity across the life span [34].

In the current report, we have created a frailty index for locomotor and recognition memory performance and we examined the relationship between them in aging, wild-type mice. Furthermore,

we observed the effect of an *H. erinaceus* supplement (He1) containing a known amount of Erinacine A, Hericenone C, and Hericenone D on frailty. Moreover, we assessed the He1 effect on hippocampal and cerebellum neurogenesis in frailty animals, by investigating specific protein markers representative of cell proliferation activity and newborn neurons occurrence.

2. Materials and Methods

2.1. Animals

Fifteen wild-type male mice (strain C57BL-6J), starting at 11 months old, were maintained in single cages in the Animal Care Facility at University of Pavia on a 12-h light/dark cycle. Water and food were provided ad libitum. All experiments were carried out in accordance with the guidelines laid out by the institution's animal welfare committee, the Ethics Committee of Pavia University (Ministry of Health, License number 774/2016-PR).

In vivo experiments were performed at six different experimental times (Figure 1), between 11 and 23.5 months old.

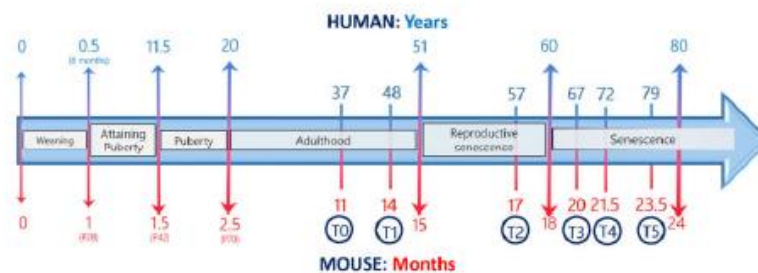


Figure 1. Comparative age between men and mice during their life span and the chosen experimental times (modified by Dutta and Sengupta, 2016).

Seven out of fifteen mice, starting from 21.5 months old, received for two months a drink made by a mixture of He1 mycelium and sporophore as ethanol extracts solubilized in water, in such a way that every mouse received 1 mg of supplement per day. This amount was chosen to mimic the oral supplementation in humans (about 1g/day). Daily consumption of water and supplements was monitored for each mouse.

At each experimental time, mice were weighed; no statistically significant change was recorded either during aging or between the He1 and control groups.

2.2. Apparatus and Procedures

We performed a spontaneous behavioral test to study locomotor activity and recognition memory in mice. For all experiments, researchers were blinded to the group assignment (control and He1). Mice activity was quantified by SMART video tracking system with a selected sampling time of 40 ms/point (2 Biological Instruments, Besozzo, Varese, Italy) and Sony CCD color video camera (PAL). All mice, at different times from T0 until T5, performed two spontaneous tests, Emergence and Novel Object Recognition (NOR) tasks. Emergence and NOR tasks are used to assess recognition memory for the environment and the object, respectively.

2.2.1. Emergence Test

We carried out emergence tests in accordance with procedures described by Brandalise et al., 2017 [32]. In the emergence test, we measured total distance and resting time covered in the familiar

compartment as locomotor parameters, while we measured the number of exits, latency of first exit, and the time of exploration outside as cognitive indicators (Table 1).

Table 1. selected parameters to measure locomotor and cognitive performances in each task. DI = discrimination index between novel/repositioned and familiar object. NOR = novel object recognition.

Test	Locomotor Parameters	Cognitive Parameters
Emergence	Resting Time In (s)	Exit Number (n)
	Total Distance In (cm)	Latency of First Exit (s)
		Time of Exploration (s)
(Open Arena)		
NOR	Resting Time (s)	Number of Approaches: DI Time of Approaches: DI
	Total Distance (cm)	
	Max Speed (cm/s)	
	Mean Speed (cm/s)	

2.2.2. Novel Object Recognition Task

We carried out novel object recognition tasks in accordance with procedures described by Brandalise et al., 2017 [32], consisting of three primary phases: open arena, familiarization, and test. To assess locomotor activity, mice were observed for 15 min while freely exploring the open-field arena in the absence of objects. Locomotor parameters of mean speed, maximum speed, resting time, and the total distance covered in the arena (Table 1) were all considered. During test phase, we measured the number of approaches and the time of approaches to the familiar and the novel objects as cognitive parameters (Table 1). To evaluate the discrimination between novel and familiar objects, we calculated the Mean Novelty Discrimination Index (DI) by using the following formula (1) [35].

$$DI = (n-f)/(n+f) \quad (1)$$

where n is the average time or number of approaches to the novel object and f is the average time or number of approaches to the familiar one (Table 1). This index ranges from -1 to 1 , where -1 means complete preference for the familiar object, 0 means no preference, and 1 means complete preference for the novel object.

2.3. The Frailty Index

A variant of Parks's methodology [36,37] was used to calculate the Frailty Index (FI). In Parks's procedure for creating the FI, a graded scale was calculated as follows: values that were 1 standard deviation (SD) above or below the mean reference value were given a frailty value of 0.25; values that differed by 2 SD were scored as 0.5; values that differed by 3 SD were given a value of 0.75, and values that were more than 4 SD above or below the mean received a frailty value of 1. Parameters that differed from T0 reference values by less than 1 SD received a score of 0.

Park's procedure, as described above, was changed in order to obtain more accurate values during aging. The mean value and the standard deviation (SD) for each of the parameters were calculated at T0. The values obtained in each mouse at different times, from T0 to T5, were compared to the mean value at T0, by using the following formula (2):

$$FI = ((\text{Value} - \text{Mean Value at T0}) / (\text{SD at T0})) * 0.25 \quad (2)$$

This procedure was applied for both Locomotor FI and Cognitive FI. Finally, to obtain LAC (Locomotor And Cognitive) FI we averaged the Locomotor and Cognitive FIs.

2.4. *H. erinaceus*

The He1 (strain 1 of *H. erinaceus*) was isolated from a basidioma collected in 2013 in Siena province (Region Tuscany, Italy) from a live specimen of *Quercus ilex* [38]. The basidioma was aseptically cut in small portions (about 1 mm³) that were placed into Petri dishes with 2% malt extract agar as a culture medium (MEA, Biokar Diagnostics). Chloranphenicol at 50 ppm was added in this first step. Incubation was performed at 24 °C in complete darkness. The strain was maintained in the Italian Culture Collection of Pavia University (MicUNIPV).

2.4.1. Extraction Procedures

Lyophilized mycelium and sporophores of He1 were extracted in 70% ethanol, per the procedure described by Gerbec et al. [39]. In details, one gram of dry substrate was blended with 10 mL of 70% ethanol and left in the thermostat overnight at 50°C. Before withdrawing, the material was stirred for one hour and was centrifuged at 4000 rpm for three minutes. The supernatant was stored at -20°C.

2.4.2. HPLC-UV-ESI/MS Method

HPLC-UV-ESI/MS analyses were carried out on a Thermo Scientific LCQ FLEET system, equipped with a PAD-UV detector working at 254 nm (Thermo Scientific®, San Jose, CA, USA). The chromatographic separation was performed using an Ascentis Express F5 HPLC column (150 × 3.0 mm, 2.7 µm particle size Sigma Aldrich, Milan, Italy) maintained at 40 °C, with a flow rate of 0.3 mL/min and an injection volume of 20 µL. The following gradient method was utilized with water containing 0.1% formic acid (solvent A) and acetonitrile (solvent B): 0–9 min (30–50% B), 9–27 min (50–60% B), 27–54 min (60–100% B), 54–69 min (100–30% B), and 69–75 min (30% B); all solvents are from Sigma Aldrich, Milan, Italy. The HPLC system was interfaced to the ion trap mass spectrometer with an Electro Spray Ionization (ESI) ion source. The compounds were analyzed under positive (ESI+) ion conditions. The ion spray and capillary voltage were set at 5kV and 10V, respectively, in positive ion mode. The capillary temperature was 400 °C. The acquisition was performed both in Full Scan mode (mass range 200–2000 Da) and MS/MS Dependent Scan mode. The data station utilized the Xcalibur MS Software Version 2.1 (Thermo Scientific®, San Jose, CA, USA).

Erinacine A and hericenones C and D were used as standards [40,41]. Stock solutions (1 mg/mL) of erinacine A and hericenones C and D were prepared in 70% ethanol. Standard solutions with the final concentration range of 1–25 µg/mL for erinacine A and 20–100 µg/mL for hericenones C and D were prepared. Linear least-square regression analysis for the calibration curves showed correlation coefficients of 0.9968, 0.9945, and 0.9951, respectively, for erinacine A, hericenones C, and hericenones D with respect to the peak area, demonstrating a good linear relationship in the different ranges tested. Each concentration was analyzed in triplicate.

2.5. Tissue Sampling: Hippocampal and Cerebellar Specimens Preparation

Mice were anesthetized by isoflurane inhalation (Aldrich, Milwaukee, WI, USA) before decapitation.

The brain and cerebellum were immediately excised as previously described [42], washed in 0.9% NaCl, and fixed by immersion for 48 h at room temperature in Carnoy's solution (6 absolute ethanol/3 chloroform/1 acetic acid). The tissues were then kept in absolute ethanol for one hour, followed by acetone for 50 min, and finally embedded in Paraplast X-TRA (Sigma Aldrich, Milan, Italy). Eight micron-thick sections, collected on silane-coated slides, of brain and cerebellar vermis were cut in the sagittal plane.

2.6. Immunohistochemistry: Fluorescence Microscopy Assessment and Quantification of Cell Proliferation and Neurogenesis

To avoid possible staining differences due to small changes in the procedure, the immunoreactions were carried out simultaneously on slides from controls and treated animals. Paraffin-embedded sections were deparaffinized in xylene, rehydrated through a series of graded alcohol treatments and rinsed in phosphate-buffered saline (PBS, Sigma).

PCNA (PC10), a 37 kDa molecular weight protein also known as cyclin, was employed as marker of cell proliferation. In particular, in cells fixed with organic solvents, the PCNA was demonstrated to be strongly associated in the nuclear regions where DNA synthesis is occurring [43]. DCX is considered a marker for neuronal precursors and migrating neuroblasts during neurogenesis recovery [44]. The presence and distribution of PCNA and DCX was assessed using commercial antibodies on murine specimens, focusing on the hippocampus and cerebellum. Brain and cerebellar sections of control and He1 mice were incubated overnight at room temperature with the primary

antibody: (i) mouse monoclonal antibody against PCNA (1:600, Abcam, Cambridge, MA, USA), and (ii) goat polyclonal antibody against DCX (1:100, Santa Cruz Biotechnology, Santa Cruz, CA, USA). After washing in phosphate buffer saline (PBS), sections were incubated for one hour with the secondary antibody: (i) Alexa Fluor 488-conjugated anti-mouse (1:100, Molecular Probes, Space, Milano, Italy) and (ii) Alexa Fluor 594-conjugated anti-goat (1:100, Molecular Probes, Space, Milano, Italy), in a dark, moist chamber. Then the nuclei were counterstained for 10 min with 0.1 µg/mL Hoechst 33258 (Sigma Aldrich, Milan, Italy). After PBS washing, coverslips were mounted in a drop of Mowiol (Calbiochem, San Diego, CA, USA).

Sections were observed by fluorescence microscopy with an Olympus BX51 equipped with a 100-W mercury lamp used under the following conditions: 330–385 nm excitation filter (excf), 400 nm dichroic mirror (dm), and 420 nm barrier filter (bf) for Hoechst 33258; 450–480 nm excf, 500 nm dm, and 515 nm bf for the fluorescence of Alexa 488; 540 nm excf, 580 nm dm, and 620 nm bf for Alexa 594. Images were recorded with an Olympus MagnaFire cam and processed with the Olympus Cell F software.

Immunofluorescence quantification was performed by calculating the percentage of PCNA or DCX immunocytochemically positive nuclei or cytoplasm of nervous cells (from the hippocampus and cerebellum) of a total number (about 300) for each animal and experimental condition, in a minimum of 10 randomly selected high-power microscopic fields.

2.7. Statistics

Data are reported as mean ± standard error of the mean (SEM). We performed Bartlett and Shapiro Wilk Tests to establish and confirm the normality of parameters. To verify statistically significant differences, we used a one-way Anova for repeated measures of the aging of mice and a two-way Anova for the effect of *H. erinaceus* supplementation. The statistical analysis for immunofluorescence was carried out using an Unpaired Student's t-test. The differences are considered statistically significant for $p < 0.05$ (*), $p < 0.01$ (**), $p < 0.001$ (***), and $p < 0.0001$ (****). Statistical analyses were performed with GraphPad Prism 7.0 software (GraphPad Software Inc., La Jolla, CA, USA).

3. Results

3.1. Locomotor and Recognition Memory during Physiological Aging

We first investigated locomotor performance and recognition memory during physiological aging in healthy mice ($n = 15$) using different spontaneous behavioral tests. Novelty recognition memory for a new environment and for novel objects was tested by way of emergence and NOR tasks, respectively.

We carried out behavioral spontaneous tests in mice at 11 (T0), 14 (T1), 17 (T2), 20 (T3), 21.5 (T4), and 23.5 (T5) months old. For the reader to understand the practical application of these tests, a comparison of the different developmental stages between humans and mice during their life span, according to Dutta and Sengupta is outlined in Figure 1 [45]. To monitor the physiological aging in mice, we choose six experimental times: T0 and T1 corresponding to adulthood phase, T2 to reproductive senescence, and T3, T4, and T5 to senescence phase.

Figure 2A shows the locomotor parameters measured in the open arena during aging. Total distance and resting time decreased from T0 to T1, stabilizing at T3. Mean speed in the open arena changed at T2 and then worsened with the aging. Maximum speed worsened later, in senescence phases T4 and T5.

Figures 2B and 2C show the cognitive parameters measured in emergence and in NOR, respectively. In the emergence test latency to the first exit, the exit number and the exploring time worsened from T0 to T1 and then remained relatively stable, whereas the latency to the first exit worsening again in the senescence phase. In the NOR test, the time of approach and the number of approaches decreased in T2 and even more in senescence phase.

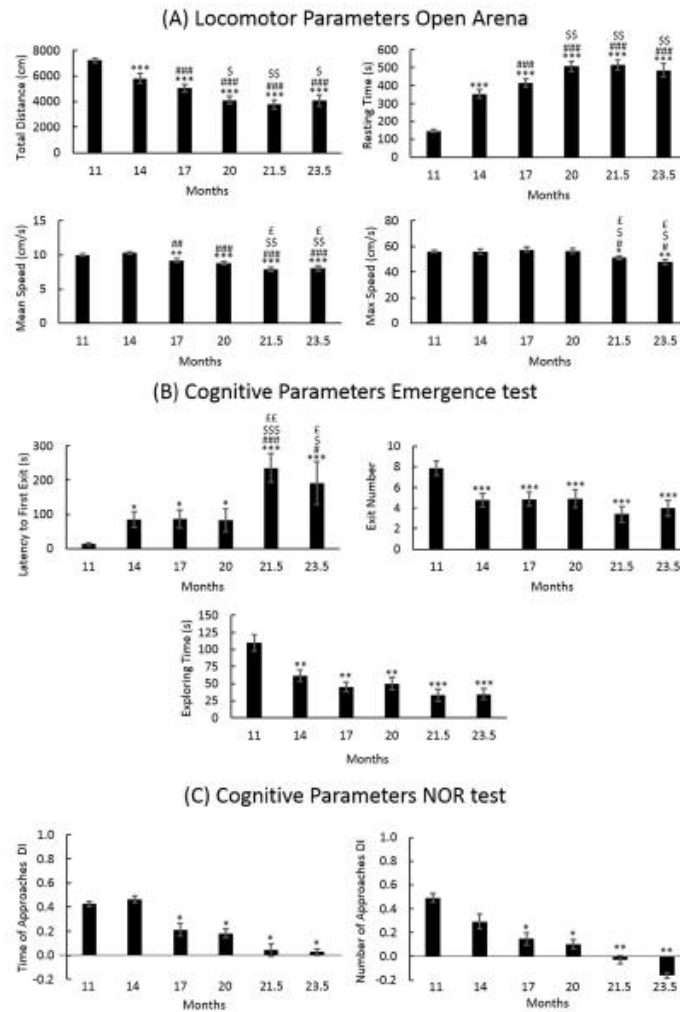


Figure 2. Locomotor and cognitive parameters during aging. (A) Locomotor parameters: total distance, resting time, mean speed, and max speed measured in open arena during aging. (B) cognitive parameters: latency to first exit, exit number, and exploring time measured in emergence, and (C) cognitive parameters: discrimination index (DI) of the time of approaches and of the number of approaches measured in NOR test. Statistical results were performed by Anova for repeated measures: * vs T0, # vs T1, \$ vs T2, and £ vs T3. For all symbols reported $p < 0.05$ (*, #, \$, £), $p < 0.01$ (**, ##, \$\$, ££), $p < 0.001$ (***, ###, \$\$\$, £££).

3.1.1. Locomotor Frailty Index

We calculated the Locomotor Frailty Index (FI) for each of the parameters reported in Table 1, then averaged the values for each experimental time. Figure 3, Panel A shows the Locomotor FIs from T0 to T5 and the linear least-square regression analysis, with $R^2 = 0.8912$. Results from a one-way ANOVA are reported in Figure 3. These results suggest that during physiological aging, locomotor performances decline linearly from the adulthood to the senescence stage.

The slope obtained by the linear least-square regression analysis (slope value = 0.1044) indicated that for every three months passed, locomotor activity decreased by about 35.43%, yielding a significantly different Locomotor FI value from the previous one each time.

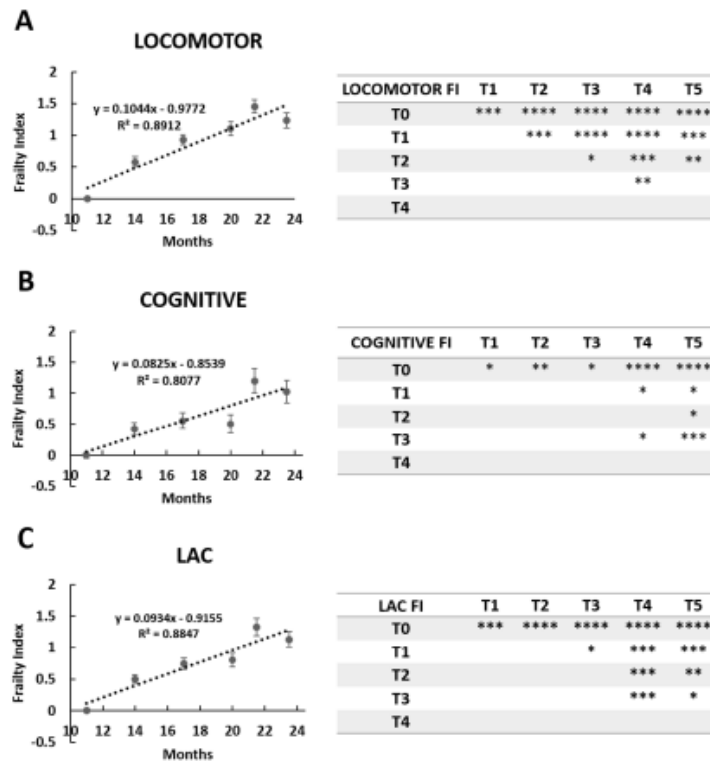


Figure 3. Locomotor, cognitive, and LAC (locomotor and cognitive) decline during physiological aging in mice. Locomotor (panel (A)), cognitive (panel (B)), and LAC (panel (C)) Frailty Index during physiological aging in mice. Linear regressions of experimental points and statistical results were reported. $p < 0.05$ (*), $p < 0.01$ (**), $p < 0.001$ (***).

3.1.2. Cognitive Frailty Index

Novelty recognition memory was evaluated, resulting in a calculation of the Cognitive Frailty Index (FI) during aging (Figure 3B). Cognitive FI was calculated using a linear least-square regression analysis, with $R^2 = 0.8077$. Results from a one-way ANOVA are reported in Figure 3.

The slope obtained by the linear least-square regression analysis (slope value = 0.0825) indicated that for every 3 months passed, recognition memory declined by about 26.04%, yielding a significantly different Cognitive FI value the previous one each time.

3.1.3. Cognitive Frailty Index

In order to evaluate a global trend of both phenotypic and cognitive decline in physiological aging, we calculated the Locomotor and Cognitive FI (LAC frailty index) by averaging all frailty indices obtained prior to evaluating the locomotor and cognitive performances during aging (Figure 3C). The LAC FI significantly increased from T0 to T5. Similarly, as previously described for Locomotor FI and Cognitive FI, the LAC FI values follow a linear trend ($R^2 = 0.8847$) (Figure 3C). The slope obtained by the linear least-square regression analysis (slope value = 0.0934) indicated that for every 3 months passed, the frailty of the mouse increased by about 30.7%.

3.2. Identification and Quantification of Erinacine A, Hericenone C, and Hericenone D

In order to identify and quantify the bioactive metabolites of interest, we analyzed the mycelium and sporophore extracts of He1 using HPLC-UV-ESI/MS. Erinacine A and hericenones C and D were identified by comparing both retention times and ESI/MS spectra with the authentic standards.

Characteristic ions of Erinacine A in the ESI/MS spectrum (Figure 4) are sodium and potassium adducts of a single molecule as well as a dimer (Table 2). Hericenone C and D spectra (Figure 5) present just $[M+H]^+$ and $[M+Na]^+$ ions (Table 2).

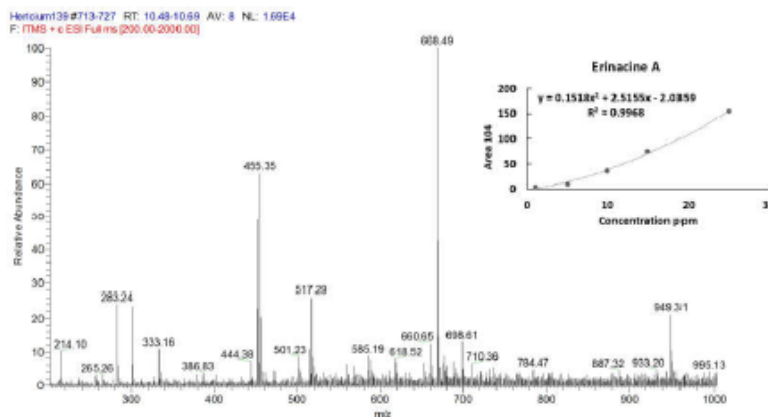


Figure 4. ESI/MS spectrum of Erinacine A. Panel (top, right) reports calibration curves and linear regression curve for Erinacine A.

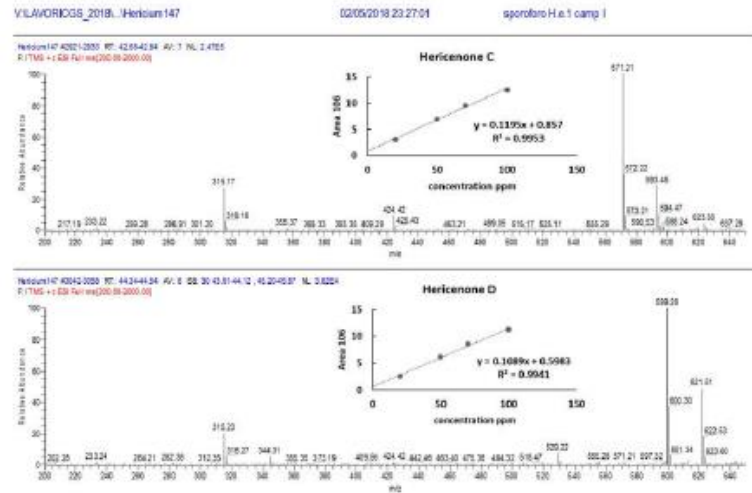


Figure 5. ESI/MS spectra of Hericenone C and D. Panels (top, right) report calibration curves for Hericenone C and D.

Table 2. shows the Erinacine A, Hericenones C and D molecular formula, molecular weight, chemical structure, characteristic structure, and content in 1 g of dried He1 mycelium and sporophore.

	Molecular Formula	Molecular Weight (g/mol.)	Chemical Structure	Characteristic Ions (m/z)	Content (µg/g)
Erinacine A	$C_{21}H_{34}O_6$	432.56		455 [M+Na] ⁻ 452 [2M+K+H] ²⁺ 668 [3M+K+H] ²⁺ 949 [2M+HCOOH+K] ⁺	150 in mycelium
Hericenone C	$C_{27}H_{46}O_6$	570.81		571 [M+H] ⁻ 593 [M+Na] ⁺	500 in basidioma
Hericenone D	$C_{27}H_{46}O_6$	598.87		599 [M+H] ⁻ 621 [M+Na] ⁺	<20 in basidioma

Erinacine A was detected using HPLC/ESI-MS. By comparing the retention time and molecular ion or mass spectra, we confirmed the peak identification. We quantified it by comparing the peak areas with those of the standard (Figure 6). The calibration curve was constructed by injecting

standard mixture solutions at five concentrations (1, 5, 10, 15, and 25 µg/mL). The linear least-square regression analysis for the calibration curve showed a correlation coefficient of $r = 0.9968$. The level of Erinacine A present in mycelium of He1 calculated by the calibration curve was 150 µg/g (Table 2).

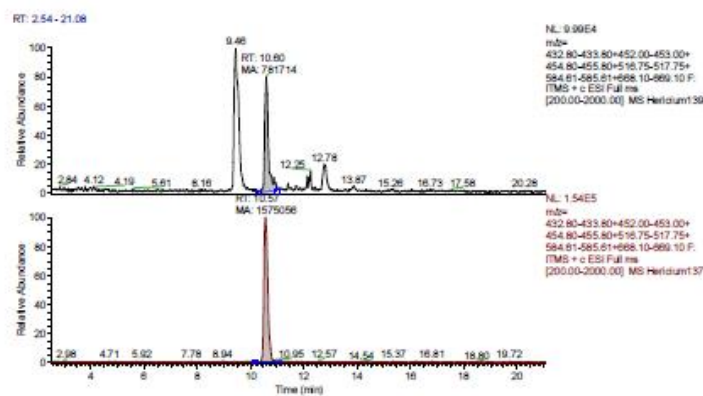


Figure 6. MS (Mass Spectrum) traces of He1 mycelium and Erinacine A (Rt 10.57) standard. Peak area of Erinacine A is pointed out.

The hericenones C and D chromatographic conditions produced a good resolution of adjacent peaks. UV detection provided sufficient sensitivity for each analyte, allowing proper quantification of both compounds by comparing the peak areas in the UV trace with those of the standards (Figure 7). Calibration curves were constructed by injecting the standard mixture solutions at four concentrations (20, 50, 75, 100 µg/mL). Linear least-square regression analysis for the calibration curves showed correlation coefficients of $r = 0.9945$ and $r = 0.9951$, respectively, for hericenones C and D. The levels of hericenones C and D present in He1 basidioma, calculated by calibration curves, were 500 µg/g and less than 20 µg/g, respectively (Table 2).

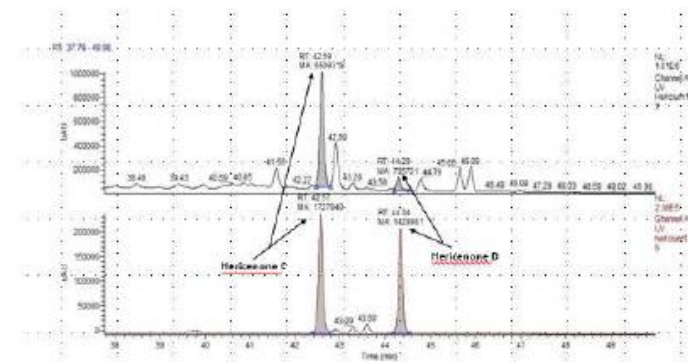


Figure 7. UV (Ultra Violet) traces of He1 sporophore (top) and Hericenone C (Rt 42.57) and D (Rt 44.34) standards (bottom). Peak areas corresponding to Hericenone C and D are pointed out.

3.3. He1 Supplementation Improved Recognition Memory Performances during Aging

We investigated cognitive and locomotor performances after oral *H. erinaceus* supplementation on frail mice. Seven mice with a T4 LAC FI score measured of more than 1.30 received a mixture of components made by He1 mycelium and basidioma for two months until T5.

Figure 8 shows the frailty index before (T4) and after He1 supplementation (T5). He1 supplementation improved recognition memory in mice during aging, characterized by a Cognitive FI decrease from 1.71 ± 0.21 to 0.72 ± 0.22 . Locomotor performances before and after He supplementation were not significant different. Considering together locomotor and memory performances by means of the LAC index, He1 regressed aged-related frailty, but this change in LAC index was completely driven by the improve in memory function.

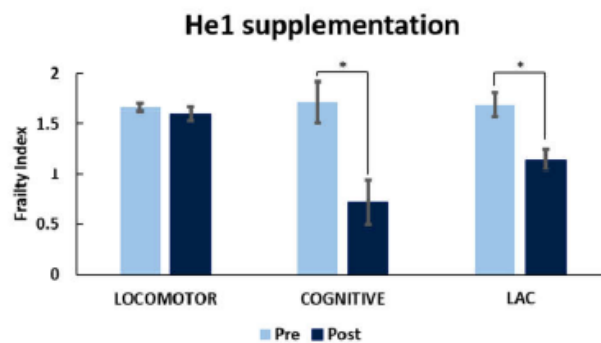


Figure 8. *H. erinaceus* improved recognition memory during mice aging. Value measured pre-supplementation (pre) and post-supplementation (post) on locomotor, recognition memory, and LAC (Locomotor And Cognitive) FI. $p < 0.05$ (*).

3.4. He1 Supplementation Improved Hippocampal and Cerebellum Proliferation and Neurogenesis

To examine the molecular mechanism involved in the He1 effect on aging mice, we performed immunocytochemical studies on different cerebral tissues, i.e. the hippocampus and cerebellum, testing both the proliferating cell nuclear antigen (PCNA) and doublecortin (DCX) as specific markers of active proliferation and neurogenesis, respectively. We performed immunocytochemistry on He1 frail mice and on untreated (control) animals at T5.

Preliminary data seem to demonstrate that cell proliferating activity achieved the highest expression in both brain areas in He1 mice compared to control animals. Specifically, the PCNA nuclear immunolabelling appeared more marked in the hippocampal dentate gyrus (DG) granule cells and in the CA3 pyramidal neurons, while the immunopositive cells (possibly granular or glial cells) predominantly localized in the width of the outer molecular layer in the cerebellar cortex (Figure 9A). Notably, clusters of PCNA-positive cells, possibly newborn granule cells, were observed suggesting the occurrence of a recovered proliferation wave (Figure 9A). Accordingly, quantitative analysis demonstrated that the PCNA labelling frequency detected in He1 treated mice ($22.89\% \pm 6.09$) reached significantly higher values compared to those measured in controls ($10.80\% \pm 3.09$, $p < 0.05$) in the hippocampus. Similarly, the PCNA labelling frequency detected in He1 mice ($25.60\% \pm 6.66$) reached significantly higher values compared to those measured in controls ($8.19\% \pm 4.43$, $p < 0.05$), in the cerebellum (Figure 9B).

In He1 mice, hippocampus showed a more marked DCX labelling compared to control animals. In particular, DCX immunolabelling appeared more intense in the dentate gyrus (DG) granule cells

in the hippocampus (Figure 10A, panel a and b). In the cerebellar cortex the immunopositivity was less expressed, nonetheless mainly localized in cells present in the molecular layer (Figure 10A, panel c and d). Quantitative analysis showed that the DCX labelling frequency in He1 mice achieved significantly higher values compared to those measured in control animals in hippocampus ($8.45\% \pm 3.02$ vs $0.22\% \pm 0.45$, respectively, with $p < 0.05$). In the cerebellum the DCX labelling frequency displayed a trend of increase in He1 mice but did not reach the threshold for the statistically significant difference compared to controls (4.68 ± 3.06 vs $0.26\% \pm 0.79$, respectively, with $p = 0.073$) (Figure 10B). It should be noted that the DCX labelling frequency in control animals is only about 0.2% in both hippocampus and cerebellum. As the PCNA labelling identifies DNA repair as well as duplication, and DCX positivity links to the presence of newborn neurons, the increased expression of this cytochemical marker may be the manifestation of different biological responses involving the recovery of cell proliferation and neurogenesis, potentially highlighting the occurrence of an upswing phase owed to the neurobiological effects exerted by the oral supplementation with He1.

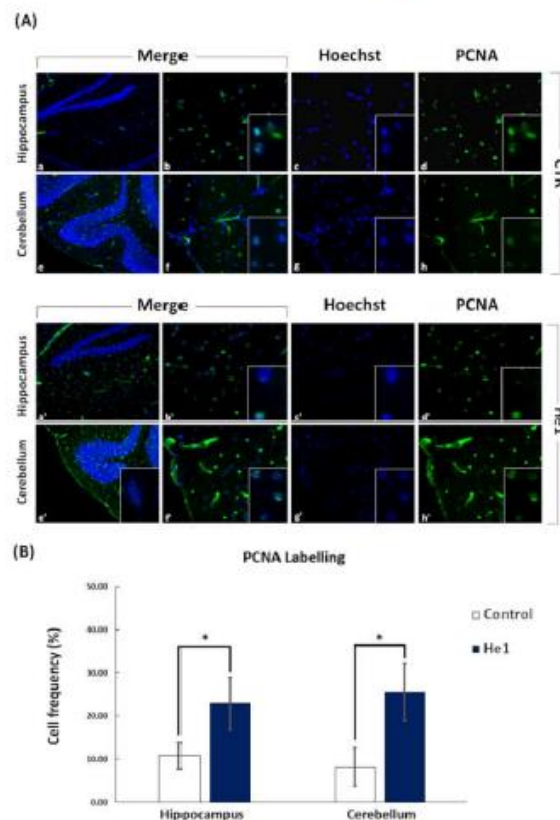


Figure 9. Panel (A) shows cell proliferating activity immunocytochemically detected by PCNA (Proliferating Cell Nuclear Antigen) labelling, observed at T5 after 2 months oral supplementation with He1 in both hippocampus and cerebellum, (a'–d' and e'–h', respectively), compared to control

untreated mice (CTR) (a–h). Cell proliferation was significantly enhanced in He1 mice, with the labelling appearing more intense in the hippocampal DG granule cells and in CA3 pyramidal neurons (a'–d') and in cerebellar molecular layer (e'–h'), compared to controls (a–d and e–h, respectively), predominantly localized in the DG granule cells and in CA3 pyramidal neurons, as also in the width of the cerebellar. Objective magnification: 20 x (a, e and a', e'); 40 x (b–d, f–h and b'–d', f'–h'); 100 x (insert in b–d, f–h, b'–d', f'–h'). Panel (B) shows changes in the percentage of PCNA labelling index of hippocampal and cerebellar cells in He1 mice. $p < 0.05$ (*).

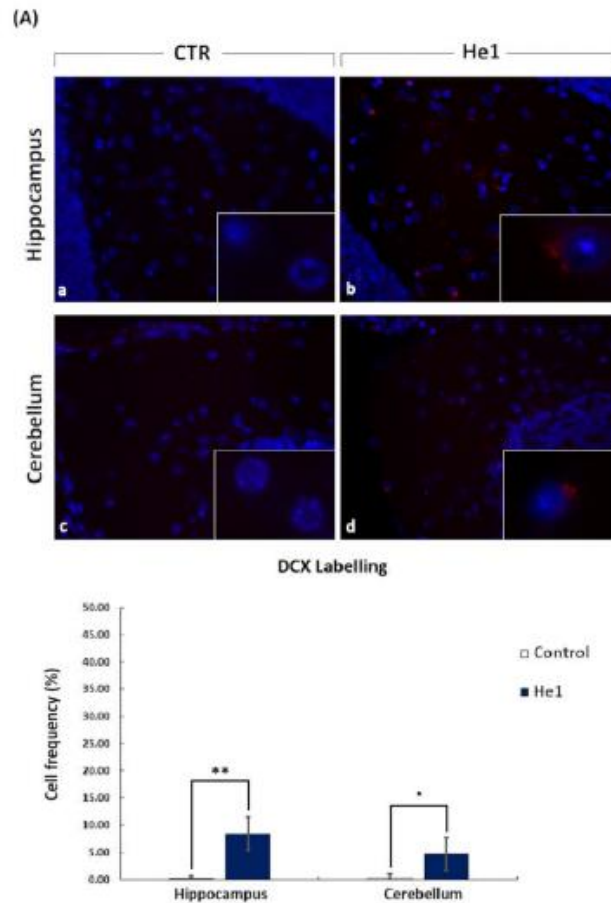


Figure 10. Panel (A) shows doublecortin (DCX) immunocytochemistry, observed at T5 after 2 months oral supplementation with He1 in hippocampus and cerebellum (b and d), compared to control mice (a and c). Objective magnification: 40 x (a–d); 100 x (inserts). Panel (B) shows the cell frequency percentage of DCX labelling in the hippocampal dentate gyrus and cerebellar molecular layer in control and He1 mice. $p < 0.01$ (**), $p = 0.07$ (*).

4. Discussion

The aim of this study was to develop an index to monitor locomotor and cognitive frailty in aging mice *in vivo* and to study the effect of *H. erinaceus* extracts containing a known amount of erinacines A and hericenones C and D. The mechanism of action of He1 was evaluated by immunocytochemistry.

We developed a frailty index score (LAC FI) based both on locomotor and cognitive decline during aging. To achieve a translational approach, we chose to monitor locomotor indicators that compare well to phenotypic frailty indicators in humans, such as gait speed and the level of physical activity [1]. We therefore measured the mean and maximum speed, resting time, and the total distance covered in an open arena test.

In concordance with Fried's phenotype model [1] and with Parks observations on activity level [36], the current paper demonstrates that the locomotor performances of mice progressively worsened during aging. The locomotor FI increased significantly during aging, with a linear progression from 11 to 23.5 months. We have developed a simplified, non-invasive method to monitor the development of frailty during mice aging, using a FI measured according to Whitehead [37].

Researchers use often the Stenberg Item Recognition Paradigm (SIRP) to measure cognitive impairment during aging in humans [46,47], during which a small group of items, called the positive set, is presented for the subject to memorize. After a delay, a single item is presented that may (familiar) or may not have (novel) been shown before and the subject is asked to answer "yes" or "no" to indicate their recognition of the item. The NOR and the emergence test in mice assess the same ability to recognize a familiar and a novel object [48] or a new environment. We measured exit numbers, the latency of the first exit and the time of exploration in the emergence test and the number and time of approaches in the NOR test [32] as cognitive parameters. We preferred to use different parameters, as suggested by Ennaceur et al., because it has been recognized that this methodology supports the validity and interpretation of the data of a behavioral experiment [49].

Locomotor and Cognitive Frailty Index scores were interpolated by a straight line. The slope of the linear regression indicates that locomotor performances decrease at a steeper rate than cognitive performances during the mouse's life span. Therefore, the data, therefore, indicate that locomotor frailty is associated with lower performance in recognition memory. These data suggest that when mice meet frailty criteria, they should be seen as mice at risk of cognitive decline.

Standardization, efficacy, and the mechanism of action of medicinal mushroom products is a pressing problem [21]. Thanks to the comparison with standard measures, we have identified and quantified erinacines A in the mycelium, and hericenones C and D in the sporophore of He1 using the HPLC-UV-ESI/MS technique. It is worth noting that the content of 0.15 mg/g of erinacine A present in mycelium in this *Herichium* strain is comparable to that reported by Krzyczkowski et al. under the use of the most favorable combination of nutrients [50]. By monitoring the temperature and ventilation during the processing, Chen et al. subsequently obtained the highest content of erinacine A, suggesting a carbon-to-nitrogen ratio of 6 and a pH value of 4 may be important parameters in promoting the biosynthesis of erinacine A [51].

Basidioma of *H. erinaceus* contains a considerable quantity of bioactive molecules such as hericenones. The quantity of hericenones C and D in our sample of *H. erinaceus* was 0.5 mg/g and 0.02 mg/g, respectively, similar to that reported by Lee et al. in some wild-type and local varieties of *H. erinaceus* strains [52].

To be able to best generalize our results to humans, we decided to use an amount of the mycelium and basidioma extracts to mimic the supplementation used in humans. It should be noted that *in vitro* and *in vivo* effects of erinacine A and hericenones on NGF synthesis [53], on reducing amyloid burden [51], on reducing amyloid plaques, and on recovering from impairments in Morris water maze tasks [54] were obtained by using a daily millimolar concentration starting from 1- until 30 mg/Kg body weight [55]. In our experimental condition, we used 100-fold lower concentration.

Using the same experimental condition, we previously described the effect of *H. erinaceus* on improving recognition memory and the increase in spontaneous and evoked excitatory synaptic

current in mossy fiber-CA3 synapses [32,33]. Similarly, Rossi et al. showed that two months of *H. erinaceus* treatment increased locomotor performances in mice [33]. The current paper confirms that He1 supplementation may increase recognition memory performance in mice during aging and may also revert the cognitive decline in frail mice.

Hippocampal neurogenesis is pivotally involved in higher cognitive function and, new excitatory dentate gyrus (DG) granule cells, generated by adult hippocampal neurogenesis, contributes significantly to neural plasticity throughout the entire life duration. Our data showed in hippocampus the recovery of cell proliferation in DG granule cells and CA3 pyramidal neurons and the presence of progenitor cells in DG granule cells. These data are in accordance with a recent *in vivo* study by Ryu et al. [56], supporting the notion that *H. erinaceus* extract administration promotes hippocampal neurogenesis in the adult mouse brain.

There is, currently, a dearth of literature available on the cerebellum area. An *in vitro* investigation showed the ability of *H. erinaceus* to promote the normal development of cerebellar cells, demonstrating a regulatory effect on the myelin genesis process [57]. Recently, Trovato and colleagues [58] demonstrated *in vivo* the neuroprotective action of *H. erinaceus* through the up-regulation of lipoxin A4 and modulation of stress responsive vitagene proteins. Our data supports the occurrence of a cell proliferation upswing in the cerebellum, as evidenced by the presence of several PCNA-immunopositive cells, possibly granular cells. Traditionally, the adult cerebellum is commonly considered as a “non-neurogenic” area. Nonetheless, our present results concerning cerebellar cortex demonstrated the presence of DCX-immunopositive cells localized in the molecular layer of He1-treated mice, suggesting the occurrence of newborn immature nervous cells.

In accordance with our preliminary results, recent investigations hypothesized the existence of stem cell populations within the cortex of the adult cerebellum that express stem cell markers and that can give rise to neuronal progeny when expanded *in vitro* and subsequently transplanted back into the murine cerebellum [59]. Therefore, further in-depth experiments, testing additional molecular markers, need to be carried out to confirm these data, initially identifying the PCNA-immunopositive proliferating cell type and then corroborating the occurrence of a “non-canonical” cerebellar neurogenic process in adult mice.

5. Conclusions

In conclusion, we suggest that during aging, the two forms of vulnerability in locomotor and cognitive performances develop in parallel and therefore, we need to integrate motoric and cognitive evaluations. As suggested by Lauretani et al., an investigation of the “brain-muscle loop” in a simultaneous assessment of all aspects that may progressively lead to loss of independence is imperative [60]. Furthermore, *H. erinaceus* is a seemingly good candidate to regress recognition memory decline during aging, possibly through an increase in neurogenesis in the hippocampus and cerebellum. These findings raise the possibility that *H. erinaceus* extracts could be a new therapeutic strategy for preventing or treating neurodegenerative diseases such as dementia and Alzheimer’s, as suggested by other authors [24,25,26]. Future studies should investigate the mechanisms involved in this at a cellular level.

Author Contributions: D.R., A.O., C.D.I. carried out the behavior experimental tasks and the experimental analysis. F.C., B.M., V.C., C.G. carried out HPLC-UV-ESI/MS. E.C.P., F.C., B.F., F.D.L. carried out the immunohistological experiments and analysis. D.R., E.R., P.R. wrote the manuscript. M.G.B., H.K., E.S. critically analyzed and reviewed the manuscript.

Funding: This research was supported by the Italian Ministry of Education, University and Research (MIUR): Dipartimenti di Eccellenza Program (2018–2022)—Dept. of Biology and Biotechnology “L. Spallanzani”, University of Pavia.

Acknowledgments: We thank Ilaria Cabrini and the Università staff of the University of Pavia for support in our crowdfunding “Noi coltiviamo la memoria.” We thank Istituto Per Lo Studio e La Cura Del Diabete S.r.l.(Caserta), Guna S.p.A, Named S.p.A, Miconet S.r.l., A.V.D Reform, Bromatech S.r.l, METEDA S.r.l., for supporting us as donors. We thank experts from BioMed Proofreading® LLC for a first English editing. All authors read and approved the final manuscript.

Conflicts of Interest: The authors declare no conflict of interest.

References

1. Fried, L.P.; Tangen, C.M.; Walston, J.; Newman, A.B.; Hirsch, C.; Gottdiener, J.; Seeman, T.; Tracy, R.; Kop, W.J.; Burke, G.; et al. Frailty in older adults: Evidence for a phenotype. *J. Gerontol. A Biol. Sci. Med. Sci.* **2001**, *56*, 46–56.
2. Bandeen-Roche, K.; Xue, Q.L.; Ferrucci, L.; Walston, J.; Guralnik, J.M.; Chaves, P.; Zeger, S.L.; Fried, L.P. Phenotype of Frailty: Characterization in the women's health and aging studies. *J. Gerontol. A Biol. Sci. Med. Sci.* **2001**, *61*, 262–266, doi:10.1093/gerona/61.3.262.
3. Hogan, D.B.; Mackinght, C.; Bergman, H. Models, definitions, and criteria of Frailty. *Aging Clin. Exp. Res.* **2003**, *15*, 1–29.
4. Ferrucci, L.; Cavazzini, C.; Corsi, A.; Bartali, B.; Russo, C.R.; Lauretani, F.; Ferrucci, L.; Cavazzini, C.; Corsi, A.M.; Bartali, B.; et al. Biomarkers of frailty in older persons. *J. Endocrinol. Invest.* **2002**, *25*, 10–15.
5. Taffet, G.E. Physiology of aging. In *Geriatric Medicine*; Springer: New York, NY, USA, 2003; pp. 27–35.
6. Espinoza, S.E.; Jung, I.; Hazuda, H. Frailty transitions in the San Antonio Longitudinal Study of Aging. *J. Am. Geriatr. Soc.* **2012**, *60*, 652–660, doi:10.1111/j.1532-5415.2011.03882.x.
7. Boyle, P.A.; Buchman, A.S.; Wilson, R.S.; Leurgans, S.E.; Bennett, D.A. Physical frailty is associated with incident mild cognitive impairment in community-based older persons. *J. Am. Geriatr. Soc.* **2010**, *58*, 248–255, doi:10.1111/j.1532-5415.2009.02671.x.
8. Brodzia, A.; Brewczyński, A.; Bajor, G. Clinical significance of knowledge about the structure, function, and impairments of working memory. *Med. Sci. Monit.* **2013**, *19*, 327–338, doi:10.12659/MSM.883900.
9. Sternberg, S.A.; Wershof-Schwartz, A.; Karunanathan, S.; Bergman, H.; Mark-Clarfield, A. The identification of frailty: A systematic literature review. *J. Am. Geriatr. Soc.* **2011**, *59*, 2129–2138, doi:10.1111/j.1532-5415.2011.03597.x.
10. Robertson, D.A.; Savva, G.M.; Kenny, R.A. Frailty and cognitive impairment—a review of the evidence and causal mechanisms. *Ageing Res. Rev.* **2013**, *12*, 840–851, doi:10.1016/j.arr.2013.06.004.
11. Auyeung, T.W.; Lee, J.S.W.; Kwok, T.; Woo, J. Physical frailty Predicts future cognitive decline—a four-year prospective study in 2737 cognitively normal older adults. *J. Nutr. Health Aging* **2011**, *15*, 690–694.
12. Mitnitski, A.; Fallah, N.; Rockwood, K. A multistate model of cognitive dynamics in relation to frailty in older adults. *Ann. Epidemiol.* **2011**, *21*, 507–516, doi:10.1016/j.annepidem.2011.01.006.
13. Samper-Terrent, R.; Al-Snih, S.; Raji, M.A.; Markides, K.S.; Ottenbacher, K.J. Relationship between frailty and cognitive decline in older Mexican Americans. *J. Am. Geriatr. Soc.* **2008**, *56*, 1845–1852, doi:10.1111/j.1532-5415.2008.01947.x.
14. Aranda, M.P.; Ray, L.A.; Snih, S.A.; Ottenbacher, K.J.; Markides, K.S. The protective effect of neighborhood composition on increasing frailty among older Mexican Americans: A barrio advantage? *J. Aging Health* **2011**, *23*, 1189–1217, doi:10.1177/0898264311421961.
15. Doba, N.; Tokuda, Y.; Goldstein, N.E.; Kushiro, T.; Hinohara, S. A pilot trial to predict frailty syndrome: The Japanese Health Research Volunteer Study. *Exp. Gerontol.* **2012**, *47*, 638–643, doi:10.1016/j.exger.2012.05.016.
16. Raji, M.A.; Al Snih, S.; Ostir, G.V.; Markides, K.S.; Ottenbacher, K.J. Cognitive status and future risk of frailty in older Mexican Americans. *J. Gerontol. Biol. Sci. Med. Sci.* **2010**, *65*, 1228–1234, doi:10.1093/gerona/gdq121.
17. Kawagishi, H.; Ando, M.; Mizuno, T. Hericenone A and B as cytotoxic principles from the mushroom *Hericium erinaceum*. *Tetrahedron Lett.* **1990**, *31*, 373–376, doi:10.1016/S0040-4039(00)94558-1.
18. Friedman, M. Chemistry, Nutrition, and Health-Promoting Properties of *Hericium erinaceum* (Lion's Mane) Mushroom Fruiting Bodies and Mycelia and Their Bioactive Compounds. *J. Agric. Food Chem.* **2015**, *63*, 7108–7123, doi:10.1021/acs.jafc.5b02914.
19. He, X.; Wang, X.; Fang, J.; Chang, Y.; Ning, N.; Guo, H.; Huang, L.; Huang, X.; Zhao, Z. Structures, biological activities, and industrial applications of the polysaccharides from *Hericium erinaceum* (Lion's Mane) mushroom: A review. *Int. J. Biol. Macromol.* **2017**, *97*, 228–237, doi:10.1016/j.ijbiomac.2017.01.040.
20. Cookson, R.; Barrett, T.N.; Barrett, A.G. β -Keto-dioxinones and β,δ -diketo-dioxinones in biomimetic resorcyolate total synthesis. *Acc. Chem. Res.* **2015**, *48*, 628–642, doi:10.1021/ar5004169.
21. Wasser, S.P. Medicinal mushroom science: Current perspectives, advances, evidences, and challenges. *Biomed. J.* **2014**, *37*, 345–356, doi:10.4103/2319-4170.138318.

22. Wasser, S.P. Medicinal Mushrooms in Human Clinical Studies. Part I. Anticancer, Oncoimmunological, and Immunomodulatory Activities: A Review. *Int. J. Med. Mushrooms* **2017**, *19*, 279–317, doi:10.1615/IntJMedMushrooms.v19.i4.10.
23. Hazekawa, M.; Kataoka, A.; Hayakawa, K.; Uchimasu, T.; Furuta, R.; Irie, K.; Yoshida, M.; Fujioka, T.; Egashira, N.; Oishi, R.; et al. Neuroprotective effect of repeated treatment with *Herichium erinaceum* in mice subjected to middle cerebral artery occlusion. *J. Health Sci.* **2010**, *56*, 296–303, doi:10.1248/jhs.56.296.
24. Mori, K.; Inatomi, S.; Ouchi, K.; Azumi, Y.; Tuchida, T. Improving effects of the mushroom Yamabushitake (*Herichium erinaceum*) on mild cognitive impairment: A double-blind placebo-controlled clinical trial. *Phytother. Res.* **2009**, *23*, 367–372, doi:10.1002/ptr.2634.
25. Kawagishi, H.; Zhuang, C. Compounds for dementia from *Herichium erinaceum*. *Drug Future* **2008**, *33*, 149–155, doi:10.1358/dof.2008.033.02.1173290.
26. Tsai-Teng, T.; Chin-Chu, C.; Li-Ya, L.; Wan-Ping, C.; Chung-Kuang, L.; Chien-Chang, S.; Chi-Ying, H.F.; Chien-Chih, C.; Shiao, Y.J. Erinacine A-enriched *Herichium erinaceum* mycelium ameliorates Alzheimer's disease-related pathologies in APPsw/PS1dE9 transgenic mice. *J. Biomed. Sci.* **2016**, *23*, 49, doi:10.1186/s12929-016-0266-z.
27. Mori, K.; Obara, Y.; Hirota, M.; Azumi, Y.; Kinugasa, S.; Inatomi, S.; Nakahata, N. Nerve growth factor-inducing activity of *Herichium erinaceum* in 1321N1 human astrocytoma cells. *Biol. Pharm. Bull.* **2008**, *31*, 1727–1732, doi:10.1248/bpb.31.1727.
28. Kawagishi, H.; Shimada, A.; Hosokawa, S.; Mori, H.; Sakamoto, H.; Ishiguro, Y.; Sakemi, S.; Bordner, J.; Kojima, N.; Furukawa, S. Erinacines E, F, and G, stimulators of nerve growth factor (NGF)-synthesis, from the mycelia of *Herichium erinaceum*. *Tetrahedron Lett.* **1996**, *37*, 7399–7402, doi:10.1016/0040-4039(96)01687-5.
29. Chiu, C.H.; Chyau, C.C.; Chen, C.C.; Lee, L.Y.; Chen, W.P.; Liu, J.L.; Lin, W.H.; Mong, M.C. Erinacine A-Enriched *Herichium erinaceum* Mycelium Produces Antidepressant-Like Effects through Modulating BDNF/PI3K/Akt/GSK-3 β Signaling in Mice. *Int. J. Mol. Sci.* **2018**, *19*, pii: e341, doi:10.3390/ijms19020341.
30. Rupic, Z.; Rascher, M.; Kanaki, S.; Köster, R.W.; Stadler, M.; Wittstein, K. Two New Cyathane Diterpenoids from Mycelial Cultures of the Medicinal Mushroom *Herichium erinaceum* and the Rare Species, *Herichium flagellum*. *Int. J. Mol. Sci.* **2018**, *19*, pii: E740, doi:10.3390/ijms19030740.
31. Wong, K.H.; Naidu, M.; David, P.; Abdulla, M.A.; Abdullah, N.; Kuppasamy, U.R.; Sabaratnam, V. Peripheral Nerve Regeneration Following Crush Injury to Rat Peroneal Nerve by Aqueous Extract of Medicinal Mushroom *Herichium erinaceum* (Bull.: Fr) Pers. (Aphyllphoromycetidaeae). *Evid. Based Complement. Alternat. Med.* **2011**, 580752, doi:10.1093/ecam/nea062.
32. Brandalise, F.; Cesaroni, V.; Gregori, A.; Repetti, M.; Romano, C.; Orrù, G.; Botta, L.; Girometta, C.; Guglielminetti, M.L.; Savino, E.; et al. Dietary Supplementation of *Herichium erinaceum* Increases Mossy Fiber-CA3 Hippocampal Neurotransmission and Recognition Memory in Wild-Type Mice. *Evid. Based Complement. Alternat. Med.* **2017**, 3864340, doi:10.1155/2017/3864340.
33. Rossi, P.; Cesaroni, V.; Brandalise, F.; Occhinegro, A.; Ratto, D.; Perrucci, F.; Lanaia, V.; Girometta, C.; Orrù, G.; Savino, E. Dietary Supplementation of Lion's Mane Medicinal Mushroom, *Herichium erinaceum* (Agaricomycetes), and Spatial Memory in Wild-Type Mice. *Int. J. Med. Mushrooms* **2018**, *20*, 485–494, doi:10.1615/IntJMedMushrooms.2018026241.
34. Kempermann, G.; Song, H.; Gage, F.H. Neurogenesis in the adult hippocampus. *Cold Spring Harb. Perspect. Biol.* **2015**, *7*, doi:10.1101/cshperspect.a018812.
35. Silvers, J.M.; Harrod, S.B.; Mactutus, C.F.; Booze, R.M. Automation of the novel object recognition task for use in adolescent rats. *J. Neurosci. Methods* **2007**, *166*, 99–103, doi:10.1016/j.jneumeth.2007.06.032.
36. Parks, R.J.; Fares, E.; Macdonald, J.K.; Ernst, M.C.; Sinal, C.J.; Rockwood, K.; Howlett, S.E. A Procedure for Creating a Frailty Index Based on Deficit Accumulation in Aging Mice. *J. Gerontol. Biol. Sci. Med. Sci.* **2012**, *67*, 217–227, doi:10.1093/gerona/glr193.
37. Whitehead, J.C.; Hildebrand, B.A.; Sun, M.; Rockwood, M.R.; Rose, R.A.; Rockwood, K.; Howlett, S.E. A clinical frailty index in aging mice: Comparisons with frailty index data in humans. *J. Gerontol. Biol. Sci. Med. Sci.* **2014**, *69*, 621–632, doi:10.1093/gerona/glt136.
38. Cesaroni, V.; Brusoni, M.; Cusaro, C.M.; Girometta, C.; Perini, C.; Picco, A.M.; Rossi, P.; Salerni, E.; Savino, E. Phylogenetic comparison between Italian and worldwide *Herichium* species. *IJMM* **2019**, submitted.
39. Gerbec, B.; Tavčar, E.; Gregori, A.; Kreft, S.; Berovic, M. Solid State Cultivation of *Herichium erinaceum* Biomass and Erinacine: A Production. *J. Bioprocess. Biotech.* **2015**, *5*, 1–5, doi:10.4172/2155-9821.1000210.

40. Kawagishi, H.; Ando, M.; Sakamoto, H.; Yoshida, S.; Ojima, F.; Ishiguro, Y.; Ukai, N.; Furukawa, S. Hericenones C, D and E, stimulators of nerve growth factor (NGF)-synthesis, from the mushroom *Hericium erinaceum*. *Tetrahedron Lett.* **1991**, *32*, 4561–4564, doi:10.1016/0040-4039(91)80039-9.
41. Kawagishi, H.; Ando, M.; Sakamoto, H.; Yoshida, S.; Ojima, F.; Ishiguro, Y.; Ukai, N.; Furukawa, S. Erinacines A, B and C, strong stimulators of nerve growth factor (NGF)-synthesis, from the mycelia of *Hericium erinaceum*. *Tetrahedron Lett.* **1994**, *35*, 1569–1572, doi:10.1016/S0040-4039(00)76760-8.
42. D'Angelo, E.; Rossi, P.; DeFilippi, G.; Magistretti, J.; Taglietti, V. The relationship between synaptogenesis and expression of voltage-dependent currents in cerebellar granule cells in situ. *J. Physiol. Paris* **1994**, *88*, 197–207.
43. Shi, J.; Zhong, X.; Song, Y.; Wu, Z.; Gao, P.; Zhao, J.; Sun, J.; Wang, J.; Liu, J.; Wang, Z. Long non-coding RNA RUNX1-IT1 plays a tumour-suppressive role in colorectal cancer by inhibiting cell proliferation and migration. *Cell Biochem. Funct.* **2019**, *37*, 11–20, doi:10.1002/cbf.3368.
44. Ayanlaja, A.A.; Xiong, Y.; Gao, Y.; Ji, G.; Tang, C.; Abdikani Abdullah, Z.; Gao, D. Distinct Features of Doublecortin as a Marker of Neuronal Migration and Its Implications in Cancer Cell Mobility. *Front. Mol. Neurosci.* **2017**, *10*, 199, doi:10.3389/fnmol.2017.00199.
45. Dutta, S.; Sengupta, P. Men and mice: Relating their ages. *Life Sci.* **2016**, *152*, 244–248, doi:10.1016/j.lfs.2015.10.025.
46. Sternberg Task. Dual Mechanisms of Cognitive Control, Washington University in St. Louis. Available online: <http://pages.wustl.edu/dualmechanisms/sternberg-task#sternbergdesc> (accessed on 26 March 2019).
47. Nosofsky, R.M.; Little, D.R.; Donkin, C.; Fific, M. Short-term memory scanning viewed as exemplar-based categorization. *Psychol. Rev.* **2011**, *118*, 280–315, doi:10.1037/a0022494.
48. Brodziak, A.; Kołat, E.; Rózyk-Myrta, A. In Search of Memory Tests Equivalent for Experiments on Animals and Humans. *Med. Sci. Monit.* **2014**, *20*, 2733–2739, doi:10.12659/MSM.891056.
49. Ennaceur, A.L.; Michalikova, S.; Bradford, A.; Ahmed, S. Detailed analysis of the behavior of Lister and Wistar rats in anxiety, object recognition and object location tasks. *Behav. Brain. Res.* **2005**, *159*, 247–266.
50. Krzyczkowski, W.; Malinowska, E.; Herold, F. Erinacine A biosynthesis in submerged cultivation of *Hericium erinaceum*: Quantification and improved cultivation. *Eng. Life Sci.* **2010**, *10*, 446–457.
51. Chen, C.C.; Tzeng, T.T.; Chen, C.C.; Ni, C.L.; Lee, L.Y.; Chen, W.P.; Shiao, Y.J.; Shen, C.C. Erinacine S, a rare sesterterpene from the mycelia of *Hericium erinaceum*. *J. Nat. Prod.* **2016**, *79*, 438–441, doi:10.1016/j.jnpp.2004.11.006.
52. Lee, D.G.; Kang, H.W.; Park, C.G.; Ahn, Y.S.; Shin, Y. Isolation and identification of phytochemicals and biological activities of *Hericium erinaceum* and their contents in *Hericium* strains using HPLC/UV analysis. *J. Ethnopharmacol.* **2016**, *184*, 219–225, doi:10.1016/j.jep.2016.02.038.
53. Kawagishi, H.; Mori, H.; Uno, A.; Kimura, A.; Chiba, S. A sialic acid-binding lectin from the mushroom *Hericium erinaceum*. *FEBS Lett.* **1994**, *340*, 56–58.
54. Tzeng, T.T.; Chen, C.C.; Chen, C.C.; Tsay, H.J.; Lee, L.Y.; Chen, W.P.; Shen, C.C.; Shiao, Y.J. The cyanthine diterpenoid and sesterterpene constituents of *Hericium erinaceum* mycelium ameliorate Alzheimer's disease-related pathologies in APP/PS1 transgenic mice. *Int. J. Mol. Sci.* **2018**, *19*, 598, doi:10.3390/ijms19020598.
55. Li, I.C.; Lee, L.Y.; Tzeng, T.T.; Chen, W.P.; Chen, Y.P.; Shiao, Y.J.; Chen, C.C. Neurohealth Properties of *Hericium erinaceum* Mycelia Enriched with Erinacines. *Behav. Neurosci.* **2018**, *1–10*, doi:10.1155/2018/5802634.
56. Ryu, S.; Kim, H.G.; Kim, J.Y.; Kim, S.Y.; Cho, K.O. *Hericium erinaceum* Extract Reduces Anxiety and Depressive Behaviors by Promoting Hippocampal Neurogenesis in the Adult Mouse Brain. *J. Med. Food.* **2018**, *21*, 174–180, doi:10.1089/jmf.2017.4006.
57. Kolotushkina, E.V.; Moldavan, M.G.; Voronin, K.Y.; Skibo, G.G. The influence of *Hericium erinaceum* extract on myelination process in vitro. *Fiziol. Zhurnal* **2003**, *49*, 38–45.
58. Trovato, R.; Siracusa, R.; Di Paola, M.; Scuto, M.L.; Ontario, O.; Bua, P.; Di Mauro, M.A.; Toscano, C.C.T.; Petralia, L.; Maiolino, A.; et al. Redox modulation of cellular stress response and lipoxin A4 expression by *Hericium erinaceum* in rat brain: Relevance to Alzheimer's disease pathogenesis. *Immun. Ageing* **2016**, *13*, 23, doi:10.1186/s12979-016-0078.
59. Ahlfeld, J.; Filser, S.; Schmidt, F.; Wefers, A.K.; Merk, D.J.; Glaß, R.; Herms, J.; Schüller, U. Neurogenesis from Sox2 expressing cells in the adult cerebellar cortex. *Sci. Rep.* **2017**, *7*, 6137, doi:10.1038/s41598-017-06150-x.

60. Lauretani, F.; Meschi, T.; Ticinesi, A.; Maggio, M. "Brain-muscle loop" in the fragility of older persons: From pathophysiology to new organizing models. *Aging Clin. Exp. Res.* **2017**, *6*, 1305–1311, doi:10.1007/s40520-017-0729-4.



© 2019 by the authors. Licensee MDPI, Basel, Switzerland. This article is an open access article distributed under the terms and conditions of the Creative Commons by Attribution (CC-BY) license (<http://creativecommons.org/licenses/by/4.0/>).



New Platinum-Based Prodrug Pt(IV)Ac-POA: Antitumour Effects in Rat C6 Glioblastoma Cells

Beatrice Ferrari¹ · Francesca Urselli¹ · Martina Gilodi¹ · Serena Camuso¹ · Erika Cecilia Priori¹ · Beatrice Rangone² · Mauro Ravera² · Paola Veneroni¹ · Iliaria Zanellato² · Elisa Roda^{1,3} · Domenico Osella² · Maria Grazia Bottone¹

Received: 30 March 2019 / Revised: 30 March 2019 / Accepted: 13 June 2019
© Springer Science+Business Media, LLC, part of Springer Nature 2019

Abstract

Gliomas are the most frequent primary tumours of the nervous system, characterised by high degree of malignancy, widespread invasion and high-rate proliferation. Cisplatin and analogue are currently employed in clinical trials as active chemotherapeutic agents for the systemic treatment of this type of malignancy. Despite therapy benefits, clinical use of these agents is hampered by severe side effects including neurotoxicity. Therefore, the aim of the present study was to analyse the effect of a new compound of platinum(IV) conjugate, named Pt(IV)Ac-POA, which can generate a synergistic antineoplastic action when released along with cisplatin, after a specific reduction reaction within tumour cells. To assess the effects of the novel compound on rat C6 glioma cells, cell cycle and cell death activation analyses were carried out using flow cytometry. Morphological changes and activation of different cell death pathways were evaluated by both transmission electron microscopy and immunofluorescence microscopy. Protein expression was investigated by western blotting analysis. The novel compound Pt(IV)Ac-POA, bearing as axial ligand (2-propynyl)octanoic acid (POA), which is a histone deacetylase inhibitor (HDACi), acts as a prodrug in tumour cells, inducing cell death through different pathways at a concentration lower than those tested for other platinum analogues. The current results showed that Pt(IV)Ac-POA could represent a promising improvement of Pt-based chemotherapy against gliomas, either inducing a chemosensitisation and reducing chemoresistance.

Keywords C6 · Glioma cells · Cisplatin · HDACi · Cell death · Immunocytochemistry

Introduction

Gliomas are the most frequent primary tumours of the nervous system (NS) characterised by high degree of malignancy, widespread invasion and high-rate proliferation (Sciumè et al. 2010). Gliomas develop mainly in correspondence of brain areas with a higher functional activity

(Kiekow et al. 2016) and might evolve into highly aggressive glioblastoma multiforme (GBM) (Maher et al. 2001). Due to these peculiar characteristics, gliomas are among the most aggressive malignancies and refractory to therapies (Wen et al. 2010).

Cisplatin (*cis*-dichlorodiammine platinum (II)) is one of the most active agents used in cancer treatment. This metal-based compound represents the standard therapy for different types of childhood and adult cancers, including gliomas. Despite cisplatin efficacy to induce cancer cell death, its benefit is hindered by harsh side effects such as damages at the peripheral nervous system (PNS) (Cavaletti et al. 2010) and some morpho-functional alterations of the central nervous system in adult and during development (Troy et al. 2000; Bemocchi et al. 2011). Moreover, the onset of acquired drug resistance after long periods of treatment reduces the cisplatin antitumour action (Zisowsky et al. 2007; Florea and Büsselberg 2011; Galluzzi et al. 2012).

✉ Maria Grazia Bottone
bottone@unipv.it

¹ Laboratory of Cell Biology and Neurobiology, Department of Biology and Biotechnology "L. Spallanzani", University of Pavia, Via Ferrata 9, 27100 Pavia, Italy

² Department of Sciences and Technological Innovation (DiSTI), University of Piemonte Orientale "A. Avogadro", Viale Teresa Michel 11, 15121 Alessandria, Italy

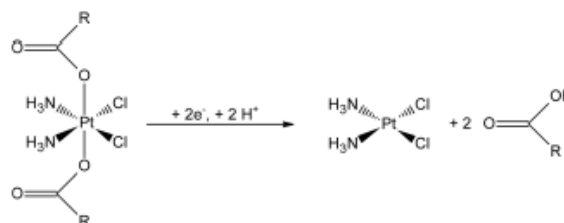
³ Laboratory of Clinical and Experimental Toxicology, Pavia Poison Centre, National Toxicology Information Centre, Toxicology Unit, ICS Maugeri Spa, IRCCS Pavia, Via Maugeri 10, Pavia, Italy

Therefore, the purpose of biomedical research has been to synthesise new antitumour agents, possessing the same chemotherapeutic effect of the reference cisplatin, but causing less systemic toxicity. In this context, the class of platinum(IV) derivatives, Pt(IV), is gaining attention. Pt(IV) complexes act as prodrugs: the two axial ligands, which have released along with the Pt(II) metabolite upon reduction in the hypoxic tumour cell microenvironment, can be synergistic or adjuvant agents, giving rise to Pt(IV) drug multi-action (Gabano et al. 2014; Gibson 2016; Johnstone et al. 2016; Kenny et al. 2017) (Fig. 1).

Among these novel compounds, a new platinum-based prodrug (*OC-6-44*)-acetatodiamminedichlorido(2-(2-propynyl)octanoato)platinum(IV), named Pt(IV)Ac-POA, has been synthesised. This prodrug has an octahedral structure based on cisplatin and contains as axial ligands the free acid POA, a MCFA-HDACi (Medium-Chain Fatty Acids–Histone DeAcetylase Inhibitor), along with an inert acetate (Ac) (Fig. 2). The possibility to co-administer cisplatin with Histone DeAcetylase inhibitors (HDACi), which indirectly decrease the histone–DNA interactions, seems to play a good effect on DNA-adduct formation (Hřebáčková et al. 2010) and chemo-sensitisation versus DNA-damaging agents (Bolden et al. 2006; Li and Seto 2016). In addition, the combination between the cisplatin and MCFA produces a Pt(IV) complex more lipophilic than cisplatin alone, showing an antitumour activity both in vitro and in vivo on several human cancer cell lines (Gabano et al. 2017), possessing less side effects than cisplatin. Previous data obtained on neuroblastoma cells exposed to Pt(IV)Ac-POA showed encouraging results (Rangone et al. 2018).

Therefore, in the present study, we explored the effects induced by the novel prodrug Pt(IV)Ac-POA on rat C6 glioma cells, focusing on the activation of diverse cell death pathways and also evaluating morphological and functional alterations. In particular, a panel of specific markers representative of different cellular pathways was investigated, employing a battery of complementary techniques, i.e. flow cytometry, western blotting analysis, transmission electron microscopy and immunofluorescence staining.

Fig. 1 Reduction mechanism-induced activation of a generic cisplatin-based Pt(IV) compound. R = alkyl or aryl substituent



Materials and Methods

Cell Culture and Treatments

Glial C6 cells (ATTC CCL 107, Rockville, MD, USA, passage 50) were cultured on glass cover slips in Dulbecco's modified Eagle's medium containing 10% fetal bovine serum, 1% di glutamine and 100 U/ml di penicillin–streptomycin (Celbio), at 37 °C in a 5% CO₂ humidified chamber. Cells were exposed to Pt(IV)Ac-POA (1, 4 and 10 μM) for 48 h of continuous treatment (CT) at 37 °C; then flow cytometry, immunocytochemistry, ultrastructural analysis and molecular determinations were performed.

The chosen Pt(IV)Ac-POA concentrations were selected based on previous in vitro results obtained on rat B50 neuroblastoma cell line (Rangone et al. 2018).

As widely accepted, rat C6 glioma used as an experimental model system for GBM represents an efficient means in the evaluation of anticancer therapies (Grobben et al. 2002).

Flow Cytometry

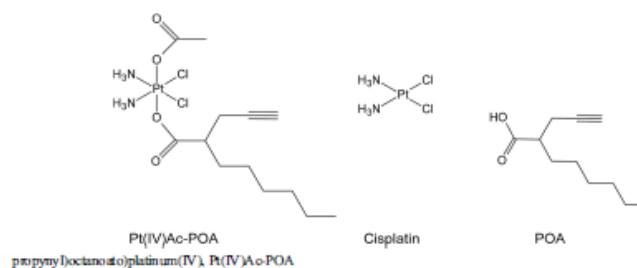
C6 cells were treated in 75-cm² plastic flasks with cisplatin or Pt(IV)Ac-POA for 48 h of continued exposure at 37 °C. After treatments, cells were detached by mild trypsinisation (0.25% in phosphate-buffered saline, PBS, with 0.05% EDTA) to obtain single-cell suspensions to be processed with a Partec PAS III flow cytometer (Münster, Germany), equipped with argon laser excitation (power 200 mW) at 488 nm. Data were analysed with the built-in software (Flowmax, Partec).

Cell-Cycle Analysis and Identification of Dead Cells

Cells were quickly washed in PBS, permeabilised in 70% ethanol for 10 min, treated with RNase A 100 U ml⁻¹ and then stained at room temperature with propidium iodide (PI) 50 μg ml⁻¹ (Sigma-Aldrich, Milan, Italy) 1 h before flow cytometric analysis. PI red fluorescence was detected with 610-nm long-pass emission filter. At least 20,000 cells per sample were measured to obtain the distribution among the different phases of the cell cycle and the percentage of dead cells.

Neurotox Res

Fig. 2 Drawing of cisplatin, 2-(2-propynyl)octanoic acid, POA, and its Pt(IV) mixed derivative (OC-6-44)-acetato diamminedichlorido(2-(2-



Analysis of Cell Death with Annexin V Assay

Single-cell suspensions, obtained as described above, were incubated with Annexin V-FITC (Annexin V-FITC Apoptosis Detection Kit; Abcam, Italy) for 10 min in the dark. PI was used as a counterstain to discriminate necrotic/dead cells from apoptotic cells. Fluorescence was revealed by means of flow cytometry at 488 nm excitation and with 530/30 (FITC) and 585/42 nm (PI) band-pass emission filters.

Transmission Electron Microscopy (TEM)

Control and Pt(IV)Ac-POA-treated C6 were harvested by mild trypsinisation (0.25% trypsin in PBS containing 0.05% EDTA) and collected by centrifugation at 800 rpm for 5 min in fresh tubes. The samples were immediately fixed with 2.5% glutaraldehyde in culture medium (2 h at room temperature), centrifuged at 2000 rpm for 10 min and washed several times with PBS. Then, samples were post-fixed in 1% OsO₄ for 2 h at room temperature and washed in water. The cell pellets were pre-embedded in 2% agar, dehydrated with increasing concentrations of acetone (30%, 50%, 70%, 90% and 100%, respectively). Finally, the pellets were embedded in Epon resin and polymerised at 60 °C for 48 h. Ultrathin sections were obtained with ultramicrotome Rechter, then placed on nickel grids and stained with uranyl acetate and lead citrate. Lastly, sections were observed under a Zeiss EM 900 transmission electron microscope operating at 80 kV. The plates, after being developed, have been computerised through Epson Perfection 4990 Photo scanner at a resolution of 800 dpi and then processed using the Epson Scan software.

Immunocytochemical Reactions: Fluorescence Microscopy Evaluation

Cells were grown on coverslips and treated with the compound under investigation Pt(IV)Ac-POA at the concentration of 4 μM. After 48 h, the cells were fixed with 1%

formalin for 20 min and post-fixed with 70% ethanol at -20 °C for at least 24 h. Samples were rehydrated for 10 min in PBS and then immunolabelled with primary antibodies for 1 h at room temperature in a dark moist chamber. After some washes in PBS, coverslips were incubated with secondary antibodies for 45 min. After that, sections were counterstained for DNA with 0.1 μg ml⁻¹ Hoechst 33258 (Sigma-Aldrich, Milan, Italy), washed with PBS and mounted in a drop of Mowiol (Calbiochem, Inalco, Italy) for fluorescence microscopy analysis. An Olympus BX51 microscope equipped with a 100-W mercury lamp was used under the following conditions: 330–385 nm excitation filter (excf), 400 nm dichroic mirror (dm) and 420 nm barrier filter (bf) for Hoechst 33258; 450–480 nm excf, 500 nm dm and 515 nm bf for the fluorescence of Alexa 488; 540 nm excf, 580 nm dm and 620 nm bf for Alexa 594. Images were recorded with an Olympus MagniFire camera system and processed with the Olympus Cell F software.

Primary and secondary antibodies used for immunocytochemical reactions using fluorescence microscopy are summarised in Table 1.

Western Blotting

After treatment with Pt(IV)Ac-POA, cells were washed twice with PBS and lysed in RIPA buffer (Tris-HCl 1 M pH 7.6, EDTA 0.5 M pH 8, NaCl 5 M, NP40 Nonidet 100%, with the addition of protease and phosphatase inhibitors) at 4 °C for 30 min. Proteins were quantified using the Bradford reagent (Sigma Aldrich, Italy). Samples were electrophoresed in a 10% SDS-PAGE minigel and transferred onto a nitrocellulose membrane (BioRad, Hercules, CA) by a semidry blotting for 1.30 h under a constant current of 60 mA. The membranes were saturated for 30 min with PBS containing 0.2% Tween-20 and 5% skim milk, and incubated overnight with monoclonal mouse anti-SQSTM1/p62 antibody (1:1000, ~61 kDa; Abcam, Cambridge, USA). After several washes with PBS-Tween, the membranes were incubated for

Table 1. Primary and secondary antibodies employed for immunofluorescence microscopy

Primary antibody	Dilution	Secondary antibody	Dilution	
Caspase-9	Polyclonal rabbit anti-caspase-9 (Cell Signaling Technology, Danvers, USA)	1:200 in PBS	Alexa 594-conjugated anti-rabbit antibody (Molecular Probes, Invitrogen)	1:200 in PBS
Caspase-3	Monoclonal rabbit anti-caspase-3 (Cell Signaling Technology, Danvers, USA)	1:200 in PBS	Alexa 594-conjugated anti-rabbit antibody (Molecular Probes, Invitrogen)	1:200 in PBS
PARP-1	Monoclonal rabbit anti-PARP1 (Cell Signaling Technology, Danvers, USA)	1:200 in PBS	Alexa 594-conjugated anti-rabbit antibody (Molecular Probes, Invitrogen)	1:200 in PBS
Caspase-8	Monoclonal rabbit anti-caspase-8 (Cell Signaling Technology, Danvers, USA)	1:100 in PBS	Alexa 594-conjugated anti-rabbit antibody (Molecular Probes, Invitrogen)	1:200 in PBS
RIP1	Polyclonal rabbit anti-RIP1 (Santa Cruz Biotechnology)	1:200 in PBS	Alexa 594-conjugated anti-rabbit antibody (Molecular Probes, Invitrogen)	1:200 in PBS
Golgi	Human autoimmune serum recognising proteins of Golgi apparatus ^a	1:200 in PBS	Alexa 594-conjugated anti-human antibody (Molecular Probes, Invitrogen)	1:200 in PBS
Mitochondria	Human autoimmune serum recognising the 70-kDa E2 subunit of the pyruvate dehydrogenase complex ^b	1:200 in PBS	Alexa 594-conjugated anti-human antibody (Molecular Probes, Invitrogen)	1:200 in PBS
LC3B	Polyclonal rabbit anti-LC3B (Cell Signaling Technology, Danvers, USA)	1:400 in PBS	Alexa 488-conjugated anti-rabbit antibody (Molecular Probes, Invitrogen)	1:200 in PBS
Lysosomes	Human autoimmune serum recognising lysosomal proteins ^a	1:400 in PBS	Alexa 594-conjugated anti-human antibody (Molecular Probes, Invitrogen)	1:200 in PBS
SQSTM1/p62	Monoclonal mouse anti-SQSTM1/p62 (Abcam, Cambridge, USA)	1:100 in PBS	Alexa 594-conjugated anti-human antibody (Molecular Probes, Invitrogen)	1:200 in PBS
α -Tubulin	Monoclonal mouse anti- α -tubulin (Invitrogen)	1:100 in PBS	Alexa 488-conjugated anti-mouse antibody (Molecular Probes, Invitrogen)	1:200 in PBS
Actin	Alexa 488-phalloidin (Molecular Probes, Invitrogen)	1:40 in PBS		

^{a,b}Rangone et al. 2018

30 min with the proper secondary antibody conjugated with horseradish peroxidase (1:2000; Dako, Italy). Immunoreactive bands were detected with the reagent Luminata™ Crescendo or Luminata™ Forte (Merck Millipore, Billerica, MA), according to the appropriate instructions, and revealed on Amersham Hyperfilm™ ECL (GE Healthcare, Little Chalfont, UK) slabs. The density of the protein bands was normalised with the respective actin and subsequently with the loading control using Image J software.

Statistical Analysis

Each experiment was performed as three independent replicates and the obtained scores were expressed as the mean \pm SD (standard deviation) or SEM (standard error of mean). Data differences were analysed for statistical significance by means of Student's *t* test or with one-way ANOVA and post hoc Dunnett's test (software package GraphPad Prism Inc.). *P* values ranging from < 0.001 to < 0.05 were considered statistically significant.

Results

Cell-Cycle Distribution and Cell Death

Graphs in Fig. 3 represent the DNA distribution in C6 control and 48 h-CT cells exposed to Pt(IV)Ac-POA at different concentrations (10, 4 and 1 μM). In control condition, cells were distributed among the different cell phases (G_1 , S, G_2) clearly showing its proliferating activity as indicated by the intensity of S phase. The graph of Pt(IV)Ac-POA treated sample (10 μM CT) showed a deeply modified DNA content distribution, and a massive number of debris were indeed detected, while peaks G_1 , S and G_2 were almost absent. After 4 μM CT to the same compound, graph showed an enlarged sub- G_1 peak, indicating a high mortality of cell population, and a distribution of DNA content comparable to those detected in cisplatin-treated cells, nonetheless already obtained at a concentration ten times lower than that of reference drug. Conversely, after Pt(IV)Ac-POA 1 μM CT, cells displayed their distribution in the different cycle phases, but a small sub- G_1 peak was still identifiable.

These reported data are in accordance with previous experimental findings (Rangone et al. 2018), showing that the new prodrug is able to induce cell death already at the concentration of 4 μM , with a significant decrease in the number of living cells. Based on these results, the concentration of 4 μM Pt(IV)Ac-POA was selected, under the

standard condition (48 h-CT), and then employed for all the following determinations.

A test with Annexin V/PI staining was performed to assess the induction of apoptosis after 4 μM Pt(IV)Ac-POA 48 h-CT. In Fig. 4, graphs show that in the control condition, almost all cells were living, while after treatment, the number of viable cells tended to decrease drastically. Specifically, the quadrants Q1, Q2, Q3 and Q4 identify necrotic cells, cells in late apoptosis, live cells and early apoptotic cells, respectively. Histogram displays that compared to control condition, 4 μM Pt(IV)Ac-POA exposure caused an increase in the concentration of late apoptotic cell number (62.81 ± 1.32 vs. 7.06 ± 0.35) with a strong reduction of live cells (12.26 ± 0.58 vs. 86.59 ± 4.36).

Ultrastructural Analysis

Our previous in vitro data showed that, after exposure to 4 μM Pt(IV)Ac-POA, cells underwent different types of programmed cell death. Therefore, in order to understand the activation of several mechanisms, morphological changes were analysed by electronic microscopy. In control condition (Fig. 5a), cells were characterised by the presence of the nucleus in central position showing decondensed chromatin. Golgi apparatus was organised in perinuclear zone; moreover, in cytoplasm, medium-sized mitochondria were seen. Additionally, (1) short cytoplasmic extensions at the cellular periphery level and (2) sporadic lysosomes with possible basal

Fig. 3 Cytofluorimetric analysis. Graphs showing DNA content after PI staining in rat C6 glioma lineage. Control samples vs. treated cells after 48 h-CT to Pt(IV)Ac-POA (10, 4 and 1 μM)

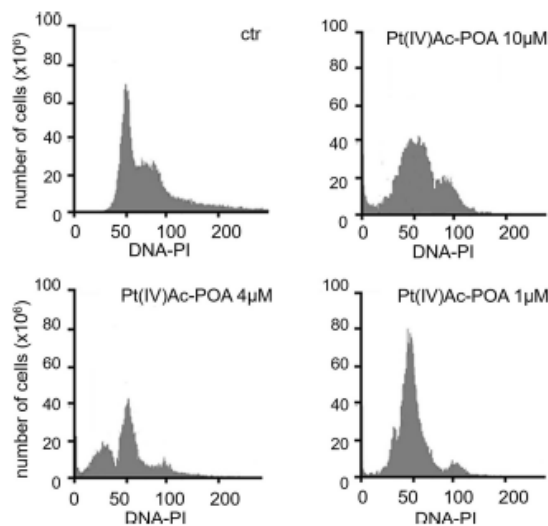
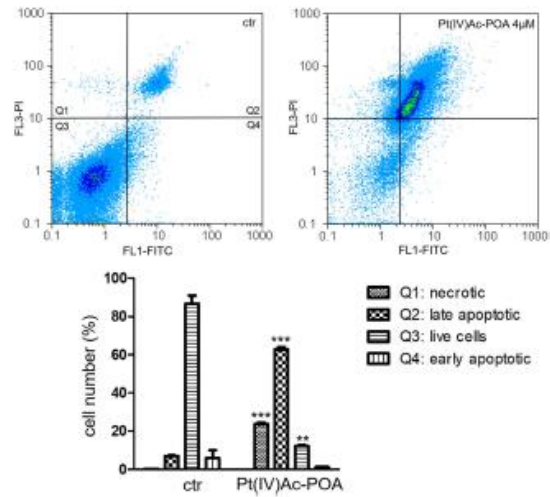


Fig. 4 Flow cytometric data after Annexin V and PI staining. Dual parameter cytograms of FITC-labelled Annexin V (FL1) versus PI staining (FL3) in control (ctr, left plot) and 4 μ M Pt(IV)Ac-POA treated cells (right plot). Histogram represents the average of three independent experiments, showing the percentage values of Annexin V/PI positive cells: Q1, Q2, Q3 and Q4 quadrants show necrotic, late apoptotic, viable and early apoptotic cells, respectively. Statistical analysis: number of observations per control and treated samples: ** $p < 0.01$; *** $p < 0.001$



autophagic activity were also observed. After Pt(IV)Ac-POA exposure (Fig. 5b), cells exhibited an apoptotic morphology,

typically characterised by chromatin condensation, absence of nuclear envelope and partial cytosol degradation. As shown in

Fig. 5 Ultrastructural analysis by TEM. (a) C6 cell in control condition. (b-d) C6 cells after 4 μ M Pt(IV)Ac-POA 48 h-CE apoptotic cell (b), autophagic cell (c) with some autophagolysosomes (insert, black arrowhead) and necrotic (d) are shown. Bars = 1.1 μ m

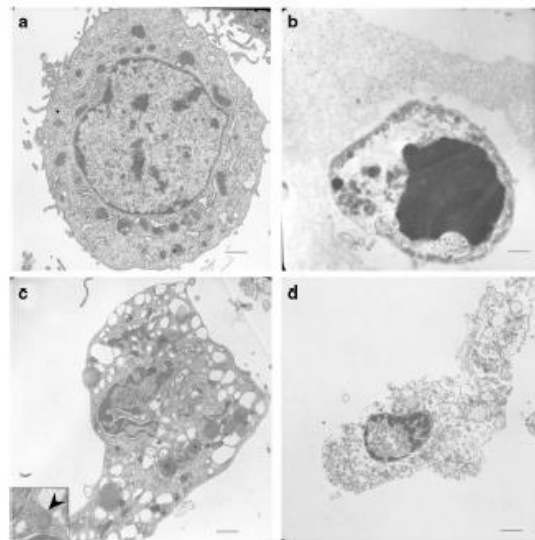


Fig. 5c, some autophagic features were detectable after prodrug exposure, i.e. cytoplasmic autophagic vacuoles, probably autophagolysosomes, characterised by a double membrane and containing cell debris (black arrowhead and insert).

Furthermore, some necroptosis hallmarks were detected (Fig. 5d): several cells showed some characteristics similar to both apoptotic ones, such as karyorrhexis, as well as to necrotic ones, i.e. cytoplasmic vacuolations and plasma membrane rupture.

Effects of Pt(IV)Ac-POA on Intracellular Organelles

Former investigations showed that cytoplasmic organelles, such as Golgi apparatus and mitochondria, are target of platinum compounds. In particular, studies in rat B50 neuroblastoma cells demonstrated that after 48-h exposure to cisplatin and platinum(II)-based compound, mitochondria formed a cluster and went towards fragmentation (Santin et al. 2012, 2013; Grimaldi et al. 2016). Thus, we evaluated the effects of 4 μ M Pt(IV)Ac-POA on Golgi apparatus and mitochondria. In control cells (Fig. 6a), Golgi apparatus immunofluorescence (red fluorescence) showed a normal appearance, consisting in a network with homogeneous distribution in the perinuclear zone and, partially, throughout the cell body.

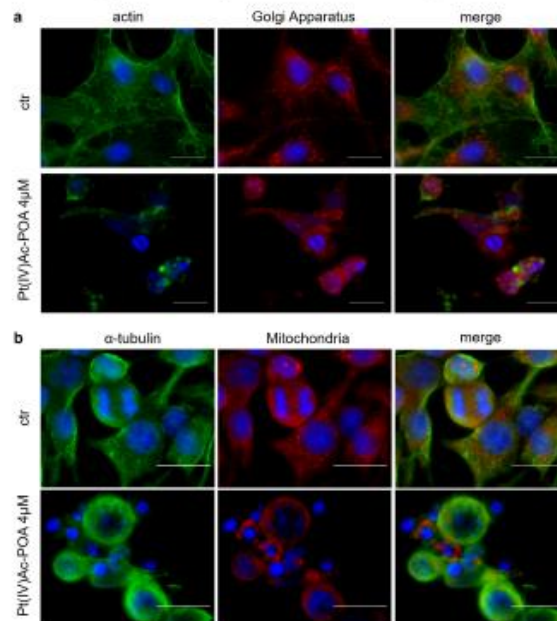
Moreover, actin-positive cytoskeleton (green fluorescence) maintained usual shape and internal organisation. After Pt(IV)Ac-POA 48 h-CT, cells showed alterations evidently related to cell death: actin-positive cytoskeleton collapsed around the nuclei, which appeared fragmented, and Golgi apparatus lost its physiological tubular connections, exhibiting a variable number of distinct elements with globular aspect distributed in the cytoplasm.

Regarding mitochondria (red fluorescence), in control cells immunolabelling displayed a spotted-like appearance, with cytoplasm and perinuclear localisation (Fig. 6b). Differently, after Pt(IV)Ac-POA CT, cells showed manifest morphological alterations. In particular, immunofluorescence lost its spotted-like feature, appearing more homogeneous and mitochondria clustered around apoptotic nuclei, forming dense masses. Tubulin cytoskeleton collapsed, and cells lost their fusiform shape.

Activation of Apoptotic Pathways

To explore the main mechanisms involved in cell death, occurring in C6 cells after 4 μ M Pt(IV)Ac-POA exposure, and to corroborate data obtained by electron microscopy, immunocytochemical detection of peculiar markers

Fig. 6 Intracellular organelles investigation by fluorescence microscopy, after 4 μ M Pt(IV)Ac-POA 48 h-CT. (a) Double immunocytochemical detection of Golgi apparatus (red fluorescence) and actin (green fluorescence) in control and treated cells. (b) Double immunocytochemical detection of mitochondria (red fluorescence) and α -tubulin (green fluorescence) in control and treated cells. DNA counterstaining with Hoechst 33258 (blue fluorescence). Bars = 20 μ m



representative of these pathways was performed using fluorescence microscopy.

After Pt(IV)Ac-POA CT, immunofluorescence data confirmed the presence of caspase-9 and caspase-3 (active form) positive cells (red fluorescence), while, contrarily, a lack of marked cells was observed in control condition, characterised by proliferating cells (presence of mitosis) (Fig. 7). Caspase-9 is the initial caspase involved in the intrinsic apoptotic pathway, being responsible to activate the executive caspase-3. The expression of both markers, near fragmented nuclei, suggested the induction of mitochondrial-mediated pathway in apoptotic cells. Furthermore, these caspase-immunopositive cells were also characterised by cytoskeletal fragmentation and the presence of dense perinuclear masses.

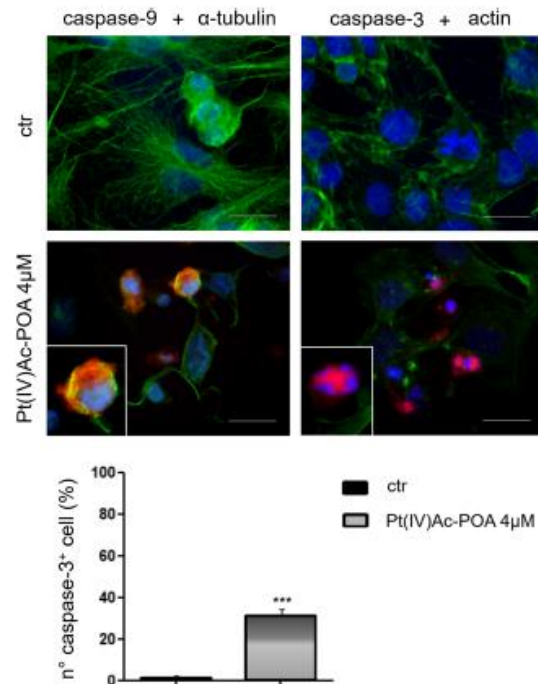
To compare the effectiveness of the prodrg treatment, a quantification of the caspase-3 immunopositive cells was carried out. The measured percentages were 1.13 ± 0.66 and 31.47 ± 2.64 in control and Pt(IV)Ac-POA-treated cells, respectively, thus revealing a significant increased

activation of the intrinsic apoptotic pathway after exposure to the new Pt(IV) compound.

Poly [ADP-ribose] polymerase 1 (PARP1), involved in DNA damage repair processes, acts as survival factor in case of limited damages to DNA, while, when extensive DNA damage arises, it promotes cell death (Virag and Szabo 2002). In fact, when a severe DNA damage occurs, caspase-3 cleaves PARP1 in two fragments, i.e. p89 and p24 (Soklani et al. 2001; Arodia and Scovassi 2014). In the present investigation, the former peptide fragment p89, being considered a specific apoptotic marker, was evaluated by immunocytochemistry.

In control cells, PARP1 (red fluorescence) localised within the nucleus and the cytoskeletal tubulin appeared well structured, providing the integrity of fusiform cell morphology. After 4 μ M Pt(IV)Ac-POA 48 h-CT, PARP1 was expressed at nuclear level in cells during the early stages of apoptosis, whereas in late apoptosis, in which nuclei were evidently fragmented, PARP1, or rather p89, moved to the cytoplasm. Moreover, after treatment, cells lost their tapered shape due to

Fig. 7 Intrinsic apoptotic pathway investigated by fluorescence microscopy in controls and treated (48 h CT to 4 μ M Pt(IV)Ac-POA) cells. Double immunocytochemical reaction for caspase-9 and caspase-3 (red fluorescence), α -tubulin and actin (green fluorescence); DNA counterstaining with Hoechst 33258 (blue fluorescence). *Inserts:* high-magnification micrographs showing in detail caspases-immunopositive apoptotic cells; fragmented nuclei and collapsed cytoskeleton are also visible. Histogram represents the percentage values of caspase-3-immunopositive cells. Statistical analysis: number of observations per control and treated samples: *** $p < 0.001$. Micrograph bars = 20 μ m



cytoskeletal tubulin alterations and aggregate formation, causing more roundish and irregular morphology (Fig. 8).

Caspase-8, involved in the extrinsic apoptotic pathway, is synthesised as an inactive single polypeptide chain zymogen pro-caspase. This caspase is activated by proteolytic cleavage by death receptors Fas, tumour necrosis factor receptor receptor-1 and death receptor receptor-3.

An increase in caspase-8 cytoplasmic immunopositivity (red fluorescence) was observed in Pt(IV)Ac-POA treated cells (Fig. 9a), while, contrarily, no immunopositive cells were detectable in control samples. Notably, after Pt(IV)Ac-POA CT, cells displayed fragmented nuclei and an irregular morphology due to cytoskeleton collapse.

Caspase-8 is also involved in initial stage of alternative cell death mechanism such as necroptosis, which induced inter alia by oxidative stress (Hitomi et al. 2008). Necroptosis is a type of cell death induced by the autophosphorylation of RIP-1, a caspase-8 substrate, and RIP-3, thus forming a necrosis complex (Feng et al. 2007).

To confirm the activation of the extrinsic apoptotic pathway and a possible preliminary activation of necroapoptotic pathway, in the present investigation the immunocytochemical detection of RIP1 (receptor-interacting protein kinase 1) was performed. In control cells, RIP1 was uniformly expressed in the cytoplasm. In contrast, after Pt(IV)Ac-POA CT, some cells were marked close to the nuclei only, suggesting that, after activation, a redistribution of RIP1 occurred, with the peptide moving from the cytoplasm to a perinuclear zone, with the nuclei appearing destroyed in tardive apoptosis (Fig. 9b).

Analysis of the Activation of Autophagic Process

Caspase-8 activation, particularly associated with the oligomerisation of p62, is also involved in autophagy-

induced apoptosis (Islam et al. 2018). Thus, to analyse autophagy activation, an immunocytochemical study was conducted to investigate the expression/changes of two proteins pivotally involved in this process: LC3B and SQSTM1/p62.

The ubiquitin-like protein LC3 is cleaved at its C terminus and forms LC3B-I, which is then conjugated with phosphatidylethanolamine in the autophagosome membrane to form LC3B-II (Kabeya et al. 2000), suggesting the activation of autophagy, which can contribute to type II cell death.

After immunolabelling, LC3B was expressed both in the nucleus and the cytoplasm and no colocalisation with the lysosomes was observed in control cells (Fig. 10).

In 4 μ M Pt(IV)Ac-POA treated cells, LC3B was mainly distributed in the cytoplasm of cells presenting fragmented nucleus, a typical sign of cell death. In some cells, LC3B colocalised with lysosomes, and an increase in the number of lysosomes was detected.

To deeply investigate this data, the number of lysosomes per cell was measured. The quantification, repeated three times on independent experiments, was performed on control and treated cell ($n = 10$ quadrants per condition), evaluating the number of lysosomes using the Autocounter procedure on ImageJ software. The data obtained were reported in the histograms in Fig. 10, and a significant increase in lysosome amount ($56.86 \pm 0.97\%$) was observed after Pt(IV)Ac-POA 48 h-CT compared to control condition.

The p62 protein, also called sequestosome-1 (SQSTM1), is a ubiquitin-binding scaffold protein which colocalises with ubiquitinated protein aggregates. The protein can polymerise through an N-terminal PB1 domain, interacting with ubiquitinated proteins through the C-terminal UBA domain (Komatsu and Ichimura 2010). Micrographs in Fig. 11 show the double immunolabelling for SQSTM1/p62 and LC3B. In

Fig. 8 Double immunocytochemical detection of PARP1 (red fluorescence) and tubulin (green fluorescence) in controls and cells exposed to 4 μ M Pt(IV)Ac-POA 48 h-CT. DNA counterstaining with Hoechst 33258 (blue fluorescence). *insets*: high magnification micrographs showing PARP1 translocation from nuclei to cytoplasm in early and late apoptotic cells. Bars = 20 μ m

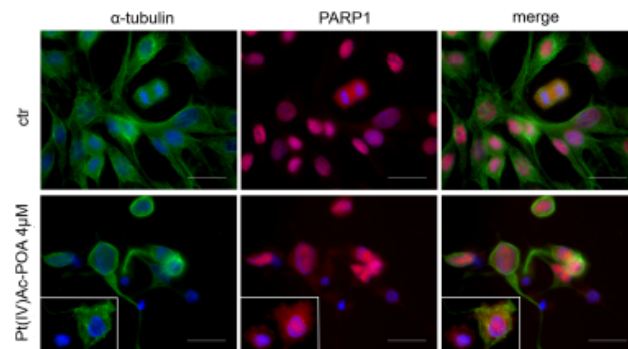
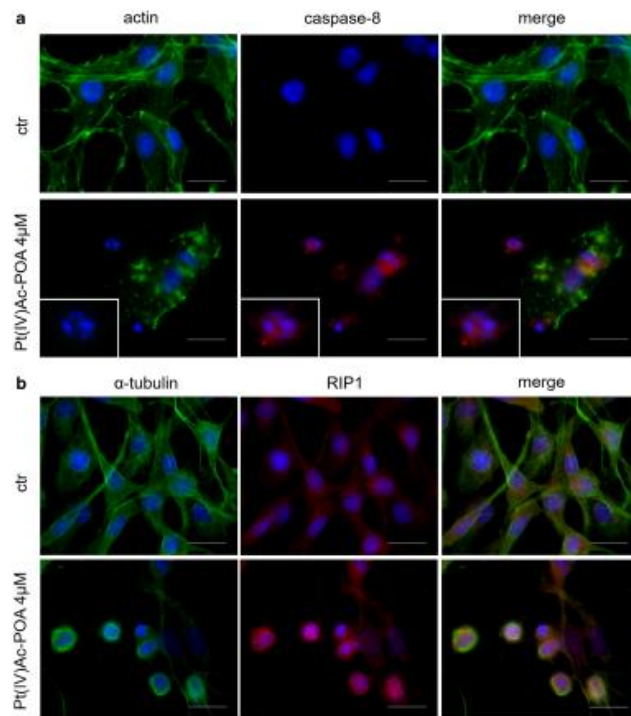


Fig. 9 Extrinsic apoptotic pathway investigated by fluorescence microscopy in control and 4 μM Pt(IV)Ac-POA 48 h treated cells. (a) Double immunocytochemical detection of caspase-8 (red fluorescence) and actin (green fluorescence). *Insert:* Caspase-8-immunopositive apoptotic cell displaying fragmented nucleus. (b) Double immunocytochemical detection of RIP1 (red fluorescence) and tubulin (green fluorescence). DNA counterstaining with Hoechst 33258 (blue fluorescence). Bars = 20 μm



control cells, SQSTM1/p62 was localised in the cytoplasm while no localisation with LC3B was detected. Similarly, after Pt(IV)Ac-POA 48 h-CT, SQSTM1/p62 was expressed in the cytoplasm, notably exhibiting colocalisation with LC3B.

Western blot analysis for SQSTM1/p62, performed analysing C6 cells exposed to 4 μM Pt(IV)Ac-POA 48 h-CT compared to controls, further confirmed immunocytochemical findings. Western blotting density band analysis evidenced a declined expression of SQSTM1/p62 after 4 μM Pt(IV)Ac-POA 48 h-CT, compared to control sample (Fig. 11). Each experiment was repeated three times and the ImageJ software was used to obtain the protein band density, which were normalised with the respective loaded control. The quantification subsequently confirmed the significant decrease of SQSTM1/p62 protein after 4 μM Pt(IV)Ac-POA 48 h-CT compared to control cells.

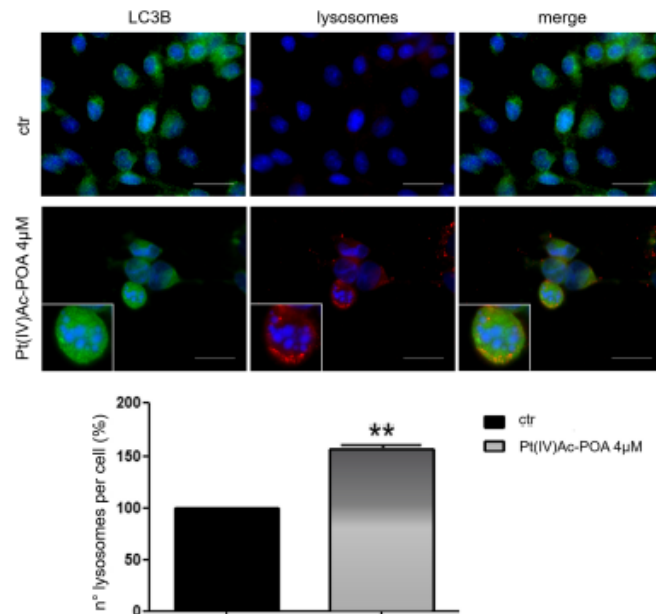
Discussion

Cisplatin has been one of the most active agents used in the chemotherapeutic protocols for several cancers; however, a lot of severe side effects, such as nephrotoxicity, neurotoxicity and ototoxicity, limit its clinical application (Hammers et al. 1991; Florea and Büsnelberg 2011).

Therefore, in recent years, a main goal of medical researchers was to obtain novel molecules able to overcome adverse effects, nonetheless displaying high anticancer efficacy.

New platinum(II)-based compounds, which interact with intracellular targets as the amino acid residues of protein, have been recently synthesised (De Pascali et al. 2005; Muscella et al. 2011; Johnstone et al. 2016). Compared to cisplatin, these drugs showed lower cytotoxicity in *in vivo* studies

Fig. 10 Immuno fluorescence study: autophagy activation investigated in C6 controls and 4 μ M Pt(IV)Ac-POA 48 h treated cells. Double immunolabelling for LC3B (green fluorescence) and lysosomes (red fluorescence). *Insert:* Detail of LC3B- and lysosome-immunofluorescence colocalisation in cell with compromised nucleus. Histogram showing the percentage number of lysosomes per cell (data normalised to control). Statistical analysis: number of observations per control and treated samples: ** $p < 0.01$. Micrograph bars = 20 μ m



(Fenoglio et al. 2015; Piccolini et al. 2015) and a better efficacy in vitro, already at lower concentrations (Grimaldi et al. 2018). Another class of platinum-based compounds are the platinum(IV) prodrugs which gained attention and are still under investigation (Arsenijevic et al. 2017; Göschl et al. 2017). A new multi-action prodrug, namely Pt(IV)Ac-POA, has been lately synthesised (Gabano et al. 2017) and designed as a cisplatin/POA combination molecule increasing the ability to deliver at the same time huge amounts of cisplatin and POA in cells. The 'synergistic cellular accumulation' of Pt(IV)Ac-POA is mainly due to the lipophilicity of the molecule assembly with respect to the hydrophilic cisplatin and the amphiphilic POA (in anionic form at physiologic pH) precursors that increase cellular uptake. Moreover, POA, acting as HDAC8 inhibitor, enhances the effects of DNA-damaging drugs, inducing chemosensitisation and decreasing chemoresistance to cisplatin (Witt et al. 2009; Gabano et al. 2017; Rangone et al. 2018).

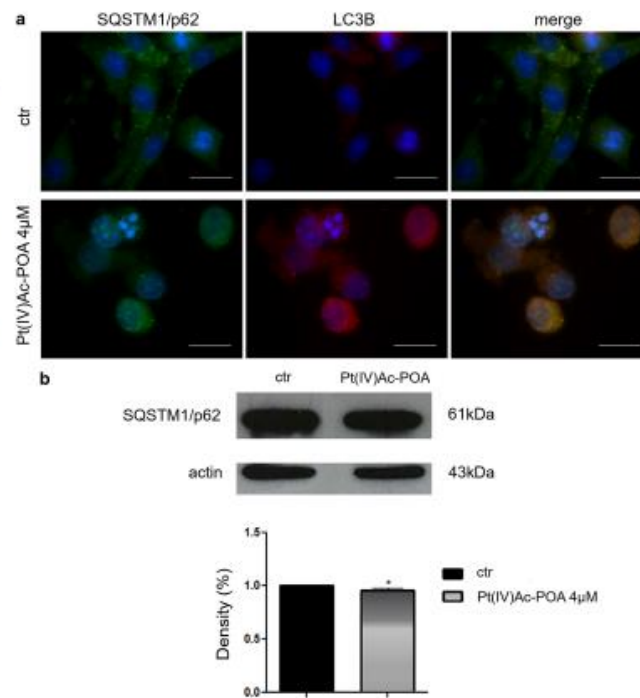
In the present study, we demonstrated the efficacy of Pt(IV)Ac-POA 48 h-CT to induce cell death in rat C6 glioma lineage. We further obtained some information about the mechanism by which cells died after prodrug exposure. Actually, as determined by flow cytometric analysis after PI staining, Pt(IV)Ac-POA was able to induce programmed cell

death through different mechanisms, already at 4 μ M, a concentration ten times lower than that usually employed for cisplatin (Santín et al. 2013; Sakalı Çetin et al. 2017; Grimakdi et al. 2018; Qian et al. 2018). The presence of numerous apoptotic cells after treatment was confirmed by Annexin-V assay, while, at ultrastructural level, alternative cell death mechanisms, i.e. necroptosis and autophagy, were identified by electron microscopy. These data are in line with previous in vitro experimental findings (Rangone et al. 2018), showing the new prodrug antineoplastic action in a different cell lineage, i.e. rat B50 neuroblastoma cell.

Immunocytochemical staining corroborated these data, investigating specific markers and confirming the activation of different pathways. This technique allowed to specifically evaluate Pt(IV)Ac-POA 48 h-CT effects on intracellular organelles, revealing that the new prodrug is able to act on cytoplasmic targets, as previously demonstrated for another platinum(II) compound, i.e. Pt(O,O'-acac)(γ -acac)(DMS) in different cell lineage (Grimaldi et al. 2016). Specifically, already at 4 μ M Pt(IV)Ac-POA 48 h-CT, Golgi apparatus lost its flattened tubular organisation in perinuclear zone, producing round bodies distributed in cytoplasm.

The prodrug treatment also produced changes of the physiological morphology of mitochondria, which

Fig. 11 Analysis of the autophagy activation in C6 controls and 4 μ M Pt(IV)Ac-POA 48 h treated cells. (a) Double immunolabelling for p62/SQSTM1 (green fluorescence) and LC3B (red fluorescence). DNA counterstaining with Hoechst 33258 (blue fluorescence). Bars = 20 μ m. (b) Western blotting data of p62/SQSTM1. Histogram representing density bands quantification of p62/SQSTM1 in control sample and following 4 μ M Pt(IV)Ac-POA 48 h-CT. The means, obtained from three independent experiments, have been normalised to control (ctr) and expressed as the mean \pm standard error of mean (SEM). Statistical analysis: number of observations per control and treated samples: * $p < 0.05$



showed a small and rounded organisation and often clustered within dying cells.

It is well known that mitochondria have a central role in numerous signalling pathways including programmed cell death (Osman et al. 2011; Estaquier et al. 2012). Therefore, we hypothesised that the observed dense mass formation around the nucleus was possibly due to mitochondria fragmentation, also suggesting the induction of deep changes in cell physiology caused by Pt(IV)Ac-POA exposure. Moreover, in treated cells, the occurrence of actin and tubulin cytoskeletal reorganisation was detected as a homogeneous and less-defined immunofluorescence.

After 4 μ M Pt(IV)Ac-POA 48 h-CT, treated cells displayed immunopositivity for both cleaved caspases-9 and -3, showing an increase in the percentage of caspase-3-positive cells compared to control conditions. The translocation of the cleaved fragment p89 of PARP1 from the nucleus to the cell cytoplasm further confirms the activation of the intrinsic apoptotic pathway.

Furthermore, the caspase-8 and RIP1 immunoreactivity of Pt(IV)Ac-POA treated cells demonstrated the activation of extrinsic apoptotic pathway, without excluding that RIP1 translocation to cell nucleus might represent a preliminary step of the necroptotic pathway, as observed in treated samples by electron microscopy.

Taken together, the present finding, obtained using a wide panel of different techniques, suggest that the novel prodrug Pt(IV)Ac-POA may induce autophagy, which represents an alternative pathway of programmed cell death, compared to apoptosis observed in previous investigations. The autophagy activation could be a strategy to induce cancer cell death without compromising the integrity of healthy tissue. Nonetheless, it has to be taken into consideration that in tumours, autophagy is often correlated with being acquired after a long period of treatment (Wang and Wu 2014; Belounis et al. 2016). Notably, a significant increase in lysosome number was detected after treatment with Pt(IV)Ac-POA 48 h-CT, suggesting an increase in the basal level of autophagy. These data were also

confirmed by immunofluorescence results showing both LC3B lysosomes as well as SQSTM1/p62-LC3B colocalisations, which are ascribable to the formation of autophagolysosome and autophagosome. The decrease in SQSTM1/p62 expression after Pt(IV)Ac-POA 48 h-CT may corroborate the activation of autophagic pathway, in which p62 may have a role. A body of literature demonstrated that autophagy and p62 are two interdependent elements of the protein control system, acting in a networked manner to maintain proteostasis, also revealing a frequent p62 upregulation in cancer cells and during tumour progression events (Moscat et al. 2016; Islam et al. 2018). It has been recently proposed that homeostatic maintenance of p62 levels in tumour by autophagy-dependent or -independent mechanisms may contribute to the final outcome of the tumorigenic process, also having important implications for the design of prospective therapeutic strategies for cancer targeting autophagy or p62-regulated signalling pathways (Liu et al. 2016). The p62 levels measured after Pt(IV)Ac-POA 48 h-CT exposure, quantitatively closer to those measured in physiological condition, could have a role in preventing tumour progression. This result differs from previous experimental findings on cisplatin showing a chemoresistance phenomenon promoted by a strong decrease in p62 expression level, associated to a high activation of autophagic pathway, able to promote cell survive (Lin et al. 2017; Chen et al. 2018).

Hence, a further long-term study using the novel prodrug Pt(IV)Ac-POA will be necessary to deeply understand if the observed autophagic process would evolve towards cell death, namely secondary apoptosis, rather than providing cells with a 'protection' mechanism, thus giving resistance to the new compound.

Conclusions

Taken together, the present findings support the use of this new prodrug as a potential alternative to the employment of cisplatin and its analogues, considering that Pt(IV)Ac-POA is already effective on rat C6 glioma cells at a concentration ten times lower than that used for the in vitro standard treatment with cisplatin (4 μ M vs. 40 μ M, respectively). This prodrug dose was nonetheless able to induce different cell death pathways. Pt(IV)Ac-POA contains peculiar chemical groups, which, once they enter the cell, allow the chromatin access to chemotherapy agents, thus offering a good approach to increase the effectiveness of cisplatin to damage the DNA. Hence, the molecular structural stability outside cancer cells and new subcellular targets, which characterise novel Pt(IV) compounds, could be the two key elements which enable to prevent drug resistance and to improve the chemotherapeutic efficacy.

Acknowledgments We thank Dr. Giuliano Mazzini (IGM-CNR, Pavia) for his excellent assistance in the analysis in flow cytometry.

Funding information This research was supported by the University of Pavia: Fondi Ricerca Giovani (FRG 2018) and by the University of Piemonte Orientale (FAR 2017). We are indebted to the Inter-University Consortium for Research on the Chemistry of Metals in Biological Systems (CIRCMSB, Bari) for stimulating discussions during the group meetings and short-term missions. This research was supported by Italian Ministry of Education, University and Research (MIUR): Dipartimenti di Eccellenza Program (2018–2022) - Dept. of Biology and Biotechnology "L. Spallanzani", University of Pavia."

Compliance with Ethical Standards

Conflict of interest The authors declare that they have no conflict of interest.

References

- Aredia F, Scovassi AI (2014) Poly(ADP-ribose): a signaling molecule in different paradigms of cell death. *Biochem Pharmacol* 92:157–163. <https://doi.org/10.1016/j.bcp.2014.06.021>
- Arsenijevic M, Milovanovic M, Jovanovic S, Arsenijevic N, Markovic BS, Gazdic M, Volarevic V (2017) In vitro and in vivo anti-tumor effects of selected platinum(IV) and dinuclear platinum(II) complexes against lung cancer cells. *J Biol Inorg Chem* 22:807–817. <https://doi.org/10.1007/s00775-017-1459-y>
- Belouinis A, Nyalendo C, Le Gall R, Imbriglio TV, Mahma M, Tein P, Baumoyer M, Courmoyer S, Hakkid E, Vassal G, Santet H (2016) Autophagy is associated with chemoresistance in neuroblastoma. *BMC Cancer* 16:891. <https://doi.org/10.1186/s12885-016-2906-9>
- Bernocchi G, Bottoni MG, Piccolini VM, Dal Bo V, Santin G, De Pascali SA, Migoni D, Faniuzzi FP (2011) Developing central nervous system and vulnerability to platinum compounds. *Chemother Res Pract* 2011:315418–315414. <https://doi.org/10.1155/2011/315418>
- Bolden JE, Peart MJ, Johnstone RW (2006) Anticancer activities of histone deacetylase inhibitors. *Nat Rev Drug Discov* 5:769–784. <https://doi.org/10.1038/nrd2133>
- Cavaletti G, Frigeni B, Lanzani F, Mattavelli L, Susani E, Alberti P, Cortinovis D, Bidoli P (2010) Chemotherapy-induced peripheral neurotoxicity assessment: a critical revision of the currently available tools. *Eur J Cancer* 46:479–494. <https://doi.org/10.1016/j.ejca.2009.12.008>
- Chen J, Zhang L, Zhou H, Wang W, Luo Y, Yang H, Yi H (2018) Inhibition of autophagy promotes cisplatin-induced apoptotic cell death through Atg5 and Beclin 1 in A549 human lung cancer cells. *Mol Med Rep* 17:6859–6865. <https://doi.org/10.3892/mmr.2018.8686>
- De Pascali SA, Papadia P, Giacarone A, Pacifico C, Faniuzzi FP (2005) First examples of β -diketonate platinum(II) complexes with sulfoxide ligands. *Eur J Inorg Chem* 5:788–796. <https://doi.org/10.1002/ejic.200400665>
- Estaqueir J, Vallette F, Vayssières JL, Mignotte B (2012) The mitochondrial pathways of apoptosis. *Adv Exp Med Biol* 942:157–183. https://doi.org/10.1007/978-94-007-2869-1_7
- Feng S, Yang Y, Mei Y, Ma L, Zhu DE, Hoti N, Castaneras M, Wu M (2007) Clavage of RIP3 inactivates its caspase-independent apoptosis pathway by removal of kinase domain. *Cell Signal* 19:2056–2067. <https://doi.org/10.1016/j.cellsig.2007.05.016>
- Fenoglio C, Albicini F, De Pascali SA, Milanese G, Fumagalli M, Migoni D, Faniuzzi FP, Bernocchi G (2015) Renal fibrogenesis and platinum

- compounds in a rat model: a novel Pt(II) complex vs. cisplatin. *Anticancer Res* 35:739–751
- Florea AM, Büsnelberg D (2011) Cisplatin as an anti-tumor drug: cellular mechanisms of activity, drug-resistance and induced side effects. *Cancers* 3:1351–1371. <https://doi.org/10.3390/cancers3011351>
- Gabuno E, Ravera M, Osella D (2014) Pros and cons of bifunctional platinum(IV) antitumor prodrugs: two are (not always) better than one. *Dalton Trans* 43:9813–9820. <https://doi.org/10.1039/c4dt00911h>
- Gabuno E, Ravera M, Zandlato I, Tinello S, Gallina A, Rangone B, Gandin V, Marzano C, Bottone MG, Osella D (2017) An unsymmetric cisplatin-based Pt(IV) derivative containing 2-(2-propynyl)octanoate: a very efficient multi-action antitumor prodrug candidate. *Dalton Trans* 46:14174–14185. <https://doi.org/10.1039/c7dt02928d>
- Galluzzi L, Vitale I, Senovilla L, Eisenberg T, Carmona-Gutierrez D, Vacchelli E, Robert T, Ripoche H, Jägermann N, Pucciard C, Servant N, Hupé P, Lazar V, Dessan P, Barillot E et al (2012) Independent transcriptional reprogramming and apoptosis induction by cisplatin. *Cell Cycle* 11:3472–3480. <https://doi.org/10.4161/cc.21789>
- Gibson D (2016) Platinum(IV) anticancer prodrugs—hypotheses and facts. *Dalton Trans* 45:12983–12991. <https://doi.org/10.1039/c6dt01414c>
- Göschl S, Schräber-Bryczak E, Pichler V, Coeh K, Heffeler P, Jungwirth U, Jakupac MA, Berger W, Keppler BK (2017) Comparative studies of oxalplatin-based platinum(IV) complexes in different *in vitro* and *in vivo* tumor models. *Metallomics* 9:309–322. <https://doi.org/10.1039/c6mt00226a>
- Grimaldi M, Santin G, Insolia V, Dal Bo V, Piccolini VM, Veneroni P, Bottone MG (2016) [Pt(O,O'-acac)(γ-acac)(DMS)] versus cisplatin: apoptotic effects in B50 neuroblastoma cells. *Histochem Cell Biol* 145:587–601. <https://doi.org/10.1007/s00418-015-1396-1>
- Grimaldi M, Dal Bo VD, Ferrari B, Rosta E, De Luca F, Veneroni P, Barni S, Verri M, De Pascoli SA, Fanizzi FP, Bemocchi G, Bottone MG (2018) Long-term effects after treatment with platinum compounds, cisplatin and [Pt(O,O'-acac)(γ-acac)(DMS)]: autophagy activation in rat B50 neuroblastoma cells. *Toxicol Appl Pharmacol* 364:1–11. <https://doi.org/10.1016/j.taap.2018.12.005>
- Grobben B, De Deyn PP, Slegers H (2002) Rat C6 glioma as experimental model system for the study of glioblastoma growth and invasion. *Cell Tissue Res* 310:257–270. <https://doi.org/10.1007/s00441-002-0651-7>
- Harmers FP, Gispán WH, Neijt JP (1991) Neurotoxic side-effects of cisplatin. *Eur J Cancer* 27:372–376. [https://doi.org/10.1016/0277-5379\(91\)90549-S](https://doi.org/10.1016/0277-5379(91)90549-S)
- Hitomi J, Christoferson DE, Ng A, Yao J, Degterev A, Xavier RJ, Yuan J (2008) Identification of a molecular signaling network that regulates a cellular necrotic cell death pathway. *Cell* 135:1311–1323. <https://doi.org/10.1016/j.cell.2008.10.044>
- Hrebudkova J, Hrnčeta J, Eckschlagner T (2010) Valproic acid in the complex therapy of malignant tumors. *Curr Drug Targets* 11:361–379. <https://doi.org/10.2174/138945010790711923>
- Islam MA, Sooro MA, Zhang P (2018) Autophagic regulation of p62 is critical for cancer therapy. *Int J Mol Sci* 19:E1405. <https://doi.org/10.3390/ijms19051405>
- Johnstone TC, Sundharalingam K, Lippard SJ (2016) The next generation of platinum drugs: targeted Pt(II) agents, nanoparticle delivery, and Pt(IV) prodrugs. *Chem Rev* 116:3436–8346. <https://doi.org/10.1021/acs.chemrev.5b00597>
- Kabeysa Y, Mizushima N, Ueno T, Yamamoto A, Kirisako T, Noda T, Komatsu E, Ohsumi Y, Yoshimori T (2000) LC3, a mammalian homologue of yeast Apg8p, is localized in autophagosome membranes after processing. *EMBO J* 19:5720–5728. <https://doi.org/10.1093/emboj/19.21.5720>
- Kenny RG, Chuah SW, Crawford A, Marmion CJ (2017) Platinum(IV) prodrugs—a step closer to Ehrlich's vision? *Eur J Inorg Chem* 2017:1596–1612. <https://doi.org/10.1002/ejic.201601278>
- Kielow CJ, Figuziño F, Dietrich F, Dalla Vecchia L, Pires EN, Jandrey EH, Gnosto SC, Salbego CG, Battastini AM, Gosmann G (2016) Quercetin derivative induces cell death in glioma cells by modulating NF-κB nuclear translocation and caspase-3 activation. *Eur J Pharm Sci* 84:116–122. <https://doi.org/10.1016/j.ejps.2016.01.019>
- Komatsu M, Ichimura Y (2010) Physiological significance of selective degradation of p62 by autophagy. *FEBS Lett* 584:1374–1378. <https://doi.org/10.1016/j.febslet.2010.02.017>
- Li Y, Soto E (2016) HDACs and HDAC inhibitors in cancer development and therapy. *Cold Spring Harb Perspect Med* 6:10. <https://doi.org/10.1101/cshperspect.a026831>
- Lin JF, Lin YC, Tzsi TF, Chen HE, Chou KY, Hwang TI (2017) Cisplatin induces protective autophagy through activation of BECN1 in human bladder cancer cells. *Drug Des Devel Ther* 11:1517–1533. <https://doi.org/10.2147/DDDT.S126464>
- Liu WJ, Ye L, Huang WF, Guo LJ, Xu ZG, Wu HL, Yang C (2016) p62 links the autophagy pathway and the ubiquitin-proteasome system upon ubiquitinated protein degradation. *Cell Mol Biol Lett* 21:29. <https://doi.org/10.1186/s11658-016-0031-z>
- Maher EA, Furnari FB, Bachoo RM, Rowitch DH, Louis DN, Cavenee WK, DePinho RA (2001) Malignant glioma: genetics and biology of a grave matter. *Genes Dev* 15:1311–1333. <https://doi.org/10.1101/gad.891601>
- Moscat J, Karin M, Diaz-Meco MT (2016) p62 in cancer: signaling adaptor beyond autophagy. *Cell* 167:606–609. <https://doi.org/10.1016/j.cell.2016.09.030>
- Muscella A, Calabrisio N, Vetrugno C, Fanizzi FP, De Pascoli SA, Stortelli C, Marsigliante S (2011) The platinum (II) complex [Pt(O,O'-acac)(γ-acac)(DMS)] alters the intracellular calcium homeostasis in MCF-7 breast cancer cells. *Biochem Pharmacol* 81:91–103. <https://doi.org/10.1016/j.bcp.2010.09.012>
- Osman C, Voelker DR, Langer T (2011) Making heads or tails of phospholipids in mitochondria. *J Cell Biol* 192:7–16. <https://doi.org/10.1083/jcb.201006159>
- Piccolini VM, Esposito A, Dal Bo V, Insolia V, Bottone MG, De Pascoli SA, Fanizzi FP, Bemocchi G (2015) Cerebellum neurotransmission during postnatal development: [Pt(O,O'-acac)(γ-acac)(DMS)] vs cisplatin and neurotoxicity. *Int J Dev Neurosci* 40:24–34. <https://doi.org/10.1016/j.ijdevneu.2014.10.006>
- Qian P, Yan LJ, Li YQ, Yang HT, Duan HY, Wu JT, Fan XW, Wang SL (2018) Cyanidin ameliorates cisplatin-induced cardiotoxicity via inhibition of ROS-mediated apoptosis. *Exp Ther Med* 15:1959–1965. <https://doi.org/10.3892/etm.2017.75617>
- Rangone B, Ferrari B, Astesana V, Masiello I, Veneroni P, Zandlato I, Osella D, Bottone MG (2018) A new platinum-based prodrug candidate: its anticancer effects in B50 neuroblastoma rat cells. *Life Sci* 210:166–176. <https://doi.org/10.1016/j.lfs.2018.08.048>
- Sakalli Çetin E, Nazroglu M, Çiğ B, Övey İS, Aslan Koşar P (2017) Selenium potentiates the anticancer effect of cisplatin against oxidative stress and calcium ion signaling-induced intracellular toxicity in MCF-7 breast cancer cells: involvement of the TRPV1 channel. *J Recept Signal Transduct Res* 37:84–93. <https://doi.org/10.3109/10799893.2016.1160931>
- Santin G, Scietti L, Veneroni P, Barni S, Bemocchi G, Bottone MG (2012) Effects of cisplatin in neuroblastoma rat cells: damage to cellular organelles. *Int J Cell Biol* 2012:424072–424076. <https://doi.org/10.1155/2012/424072>
- Santin G, Piccolini VM, Barni S, Veneroni P, Giansanti V, Dal Bo V, Bemocchi G, Bottone MG (2013) Mitochondrial fusion: a mechanism of cisplatin-induced resistance in neuroblastoma cells? *Neuro Toxicology* 34:51–60. <https://doi.org/10.1016/j.neuro.2012.10.011>
- Sciumè G, Santoni A, Bernalini G (2010) Chemokines and glioma: invasion and more. *Rev J Neuroimmunol* 224:8–12. <https://doi.org/10.1016/j.jneuroim.2010.05.019>

Neurotox Res

- Soldani C, Bottone MG, Pellicciari C, Scovassi AI (2001) Two-color fluorescence detection of poly (ADP-ribose) polymerase-1 (PARP-1) cleavage and DNA strand breaks in etoposide-induced apoptotic cells. *Eur J Histochem* 45:389–392
- Troy L, McFarland K, Littman-Power S, Kelly BJ, Walpole ET, Wyld D, Thomson D (2000) Cisplatin-based therapy: a neurological and neuropsychological review. *Psychooncology* 9:29–39. [https://doi.org/10.1002/\(SICI\)1099-1611\(200010/2\)9:1<29::AID-PON428>3.0.CO;2-Z](https://doi.org/10.1002/(SICI)1099-1611(200010/2)9:1<29::AID-PON428>3.0.CO;2-Z)
- Virag L, Szabo C (2002) The therapeutic potential of poly(ADP-ribose) polymerase inhibitors. *Pharmacol Rev* 54:375–429
- Wang J, Wu GS (2014) Role of autophagy in cisplatin resistance in ovarian cancer cells. *J Biol Chem* 289:17163–17173. <https://doi.org/10.1074/jbc.M114.558288>
- Wen PY, Macdonald DR, Reardon DA, Cloughesy TF, Sorensen AG, Galanis E, Degroot J, Wick W, Gilbert MR, Lassman AB, Tsien C, Mikkelsen T, Wong ET, Chamberlain MC, Stupp R, Lamborn KR, Vogelbaum MA, van den Bent MJ, Chang SM (2010) Updated response assessment criteria for high-grade gliomas: response assessment in neuro-oncology working group. *J Clin Oncol* 28:1963–1972. <https://doi.org/10.1200/JCO.2009.26.3541>
- Witt O, Deubzer HE, Lodrini M, Milde T, Oehme I (2009) Targeting histone deacetylases in neuroblastoma. *Curr Pharm Des* 15:436–447. <https://doi.org/10.2174/138161209787315774>
- Zisowsky J, Koegel S, Leyers S, Devarakonda K, Kassack MU, Osmak M, Jaehde U (2007) Relevance of drug uptake and efflux for cisplatin sensitivity of tumor cells. *Biochem Pharmacol* 73:298–307. <https://doi.org/10.1016/j.bcp.2006.10.003>

Publisher's Note Springer Nature remains neutral with regard to jurisdictional claims in published maps and institutional affiliations.

Received: 23 January 2019 | Revised: 11 June 2019 | Accepted: 20 June 2019
 DOI: 10.1002/cne.24735

RESEARCH ARTICLE



Prolidase enzyme is required for extracellular matrix integrity and impacts on postnatal cerebellar cortex development

Violetta Insolia¹ | Erica C. Priori¹ | Caterina Gasperini¹ | Federica Coppa¹ |
 Marco Cocchia¹ | Erika Iervasi¹ | Beatrice Ferrari¹ | Roberta Besio² |
 Silvia Maruelli² | Graziella Bernocchi¹ | Antonella Forlino² | Maria G. Bottone¹

¹Department of Biology and Biotechnology,
 University of Pavia, Pavia, Italy

²Department of Molecular Medicine,
 Biochemistry Unit, University of Pavia, Pavia,
 Italy

Correspondence

Maria G. Bottone, Department of Biology and
 Biotechnology, University of Pavia, Via Ferrata
 9, Pavia 27100, Italy.
 Email: bottone@unipv.it

Funding information

Italian Ministry of Education, University and
 Research (MIUR); Sybil (Systems biology for
 the functional validation of genetic
 determinants of skeletal diseases), Grant/
 Award Number: 602300; FP7-HEALTH -
 Specific Programme "Cooperation"; Health;
 European Community

Abstract

The extracellular matrix is essential for brain development, lamination, and synaptogenesis. In particular, the basement membrane below the pial meninx (pBM) is required for correct cortical development. The last step in the catabolism of the most abundant protein in pBM, collagen Type IV, requires prolidase, an exopeptidase cleaving the imidodipeptides containing pro or hyp at the C-terminal end. Mutations impairing prolidase activity lead in humans to the rare disease prolidase deficiency characterized by severe skin ulcers and mental impairment. Thus, the dark-like (*dal*) mouse, in which the prolidase is knocked-out, was used to investigate whether the deficiency of prolidase affects the neuronal maturation during development of a brain cortex area. Focusing on the cerebellar cortex, thinner collagen fibers and disorganized pBM were found. Aberrant cortical granule cell proliferation and migration occurred, associated to defects in brain lamination, and in particular in maturation of Purkinje neurons and formation of synaptic contacts. This study deeply elucidates a link between prolidase activity and neuronal maturation shedding new light on the molecular basis of functional aspects in the prolidase deficiency.

KEYWORDS

basement membrane, cerebellar development, cortical dysplasia, prolidase deficiency

1 | INTRODUCTION

The organization and adjustments of extracellular matrix (ECM) components are essential in the brain, especially during pre- and postnatal development (Kwok, Yang, & Fawcett, 2014; Malemud, 2006; Soleman, Filippov, Dityatev, & Fawcett, 2013). It is becoming more evident that the roles of the ECM are multiple and variable. In fact, the central nervous system (CNS) ECM actively influences cell migration, axonal guidance, myelination and synaptogenesis during

development, and in adulthood plays an important role in maintaining synaptic stability and in restricting aberrant remodeling (Barros, Franco, & Müller, 2011; Burnside & Bradbury, 2014; Dityatev & Rusakov, 2011; Dityatev, Schachner, & Sonderegger, 2010; Frischknecht, Chang, Rasband, & Seidenbecher, 2014; Li, Liu, Yan, & Yang, 2014; Mettouchi, 2012; Rhodes & Simons, 2007; Suttkus, Morawski, & Arendt, 2014). In particular, basement membrane (BM) below the pial meninx (pBM) is a specialized structure of the ECM made up of a variety of ECM proteins including laminin, fibronectin, collagen IV, nidogen and proteoglycans (Timpi, 1989), whose integrity and proper assembly are essential for a correct histogenesis and cortical lamination (Hecht, Siegenthaler, Patterson, & Pleasure, 2010; Li et al., 2008; Oohashi, Edamatsu, Bekku, & Carulli,

Violetta Insolia and Erica C. Priori are co-first authors.

RRID: AB_10000343, AB_309747, AB_2336820, AB_2386821, AB_471163, AB_628210,
 AB_303394, AB_10000347, AB_2269341, AB_477257, AB_2465454, AB_2576217,
 AB_2556545, AB_2536090, AB_2534117, AB_476894, AB_476897, AB_2617137.

2015). Abnormal brain development has been observed after the targeted deletions of basement membrane constituents, such as deletion of the nidogen-binding site of laminin- γ 1 (Halfter, Dong, Yip, Willem, & Mayer, 2002; Smyth et al., 1999), laminin- α 1 chain (Ichikawa-Tomikawa et al., 2012), and dystroglycan (Moore et al., 2002). Moreover, many human pathologies can be grouped as "disorders of cortical development" in which BM defects were described at the pial surface such as microcephaly, microlissencephaly, pachygyria, and Zellweger syndrome (Francis et al., 2006).

The prolylase enzyme (peptidase D, EC: 3.4.13.9) is a cytosolic metallo enzyme relevant for the metabolism of many biologically important molecules which contain a large amount of Pro/Hyp in their primary structure, as collagens (Besio, Baratto, et al., 2013; Surazynski, Mityk, Palka, & Phang, 2008), and has a key role in the recycling of Pro/Hyp residues. Indeed, it is the only enzyme able to cleave dipptides with proline or hydroxyproline residues at their C-terminal end (Lupi, Tenni, Rossi, Cetta, & Forlino, 2008). Thus, prolylase activity may be the rate limiting factor for the degradation and synthesis of proline-rich proteins (Vanhoof, Goossens, De Meester, Hendriks, & Scharpe, 1995; Wess, Nanavati, Vogel, & Maggio, 1993). Furthermore, it was demonstrated that Type I and IV collagens are responsible for the activation of prolylase activity (Palka & Phang, 1997).

The alteration in prolylase enzyme, detected as either decreased or increased activity, characterizes many diseases, including those of CNS in humans (Kama, Surazynski, & Palka, 2000). The lack of prolylase activity is responsible for prolylase deficiency (PD; OMIM 170100), an extremely rare human autosomal recessive disorder (incidence of 1–2/1,000,000) caused by mutations in the prolylase gene, *PEPD* (chromosome location 19p12–p13.2). PD patients present a variable onset (from early childhood until adulthood), and a broad spectrum of phenotypes including severe skin lesions, vascular anomalies and variable degrees of mental impairment and developmental delay (Besio, Giola, et al., 2013; Butbul Aviel et al., 2012; De Rijcke et al., 1989; Falik-Zaccai et al., 2010; Ferreira & Wang, 2015; Hechtman, 2014; Lupi et al., 2008; Royce & Steinmann, 2002; Wang et al., 2006). Moreover, through brain magnetic resonance imaging (MRI), multiple bilateral micro thromboses (Arata et al., 1991) and subcortical white matter lesions, accompanied by leptomeningeal enhancement (Butbul Aviel et al., 2012) were described. These findings were compatible with vasculitis (Falik-Zaccai et al., 2010). PD diagnosis is based on the identification of *PEPD* pathogenic variants or on the detection of the strongly reduced prolylase activity (Besio et al., 2011).

In 2011 a mutant mouse was identified as a valuable model of prolylase deficiency. These mice present a spontaneous 4 bp deletion in exon 14 of the *PEPD* gene, exhibit a darkened coat color in homozygosity, from which their name "*dal*" for dark-like, and are characterized by iminodipeptiduria. *Dal* mice develop congenital cardiomyocyte hypertrophy due to the disruption of collagen-mediated integrin signaling and a bone phenotype (Besio et al., 2015; Cota et al., 2008; Jung et al., 2011). A preliminary characterization of the CNS of heterozygous *dal*^{+/+} and homozygous *dal*^{/dal} mice, showed brain morphological defects in cerebral cortex and cerebellum accompanied by pBM disorganization (Insolia & Piccolini, 2014).

Our study aimed to deeply characterize the brain anomalies in the *dal* mouse model of PD to understand the role of prolylase in brain cortex development and neuronal maturation and to understand the cellular/molecular basis of the human mental retardation associated to this pathology. The attention has been focused on the investigation of developing cerebellum during the first weeks of life since it has a well-characterized and relatively simple morphology and recapitulates the fundamental events of ontogenesis (Altman, 1982; Cerri, Piccolini, & Bernocchi, 2010; Ito, 2006; Ramos, Van Dine, Gilbert, Leheste, & Torres, 2015). Focusing on post mitotic maturing Purkinje neurons (key cells in the cerebellar circuit representing the sole output of the cerebellar cortex [Ito, 2006]), we studied various neurogenic events that contribute to the maturation of Purkinje cells, specifically the proliferation of granule cells and their migration along the Bergman glial fibers, and the formation of synaptic contacts of cerebellar circuits.

2 | MATERIALS AND METHODS

2.1 | Animals

The prolylase deficiency dark-like mice (*dal*^{+/+}; *Mus musculus*), on a mixed CBA \times C3H background, were kindly provided by Dr. Gunn TM (Great Falls, MI) and C3H wild-type (wt) mice were purchased from Charles River. The animals were maintained under standard experimental animal care protocol following the Italian Laws (Protocol N 1/2010) in the animal facility at the Dept. of Molecular Medicine of the University of Pavia (Italy).

2.2 | Genotyping

To detect the presence of the mutant allele lacking 4 bp in exon 14, genomic DNA was extracted from tail clip biopsies and exon 14 of the *Pepl* gene (BNSMUST0000075068.13) was PCR amplified using the following primers: 5'-AGCGATCGATGAACCTG-3' (1,160–1,177), sense and 5'-TCCAAGAGTGGTCAATGAA-3' (1,249–1,268), reverse. The presence of the 104 bp mutant and the 108 bp wt amplicons was identified by electrophoresis using 3% low melting agarose gel.

2.3 | Prolylase activity assay

Heterozygous and homozygous *dal* mice ($n = 5$, *dal*^{+/+} and $n = 3$ *dal*^{/dal}) and wt littermates ($n = 8$) were sacrificed by cervical dislocation at 21 days postnatal (P21) and cerebrum and cerebellum were isolated after calvarial removal. The samples were collected in 50 mM Tris-HCl, pH 7.8, minced and sonicated on ice for 10 s. The lysate was clarified by centrifugation for 15 min at 4°C and protein content was evaluated using the RC-DC Protein quantitation assay (BioRad, Hercules, CA, USA) using albumin as standard. The samples were stored at –80°C. Prolylase activity was determined in cerebrum and cerebellum as in Besio et al. (2011). Briefly 40 μ g of total protein lysate were incubated in presence of 1 mM MgCl₂ and 0.75 mM reduced glutathione for 20 min at 50°C to activate the prolylase enzyme, 100 mM Gly-Pro substrate was then added and the reaction was stopped after 20 min by addition of 0.45 M trichloroacetic acid. Following centrifugation

for 15 min at 16500g at 4°C, the prolidase activity was evaluated on 50 μ L of the supernatant by means of Chinard's Reagent (Chinard, 1952) and expressed as percentage of control samples (100%).

2.4 | Histological analysis

Heterozygous and homozygous *ddl* mice and *wt* littermate were sacrificed at P10, P21, P30, and P60 ($n = 5$ per genotype and age). The brains were quickly collected and the two hemispheres separated. One half of the brain was fixed in Carnoy's solution (six absolute ethanol/three chloroform/one acetic acid) for 48 hr at room temperature (RT), then placed in absolute ethanol for 1 hr and in acetone for 50 min and embedded in Paraplast X-tra (Sigma Aldrich, Milan, Italy). Six sections (8 μ m thick) were cut sagittally in sagittal plane and were collected on silan-coated slides. For each sample 12/15 slides were prepared. To proceed with the histological analysis the slides were deparaffinized in xylene (Carlo Erba, Comaredo, Italy), rehydrated in a decreasing ethanol series and rinsed in phosphate-buffered saline (PBS, Sigma Aldrich, Milan, Italy) following standard procedures. The other halves of cerebella were kept at -20°C for western blotting analysis.

All the experiments were run simultaneously for heterozygous, homozygous and *wt* mice. Only sagittal sections of lobules were taken into consideration for histological and morphological analysis.

All the images refer to the apex of the lobules VIa, VIb, VII, and VIII in the *vermis* since these lobules share the same developmental timing and pattern; when other lobules were considered it is always specified in the figure captions.

2.5 | Hematoxylin and eosin staining

The sections were immersed for 10 min in Carazzi's hematoxylin (Sigma Aldrich, Milan, Italy) at RT, washed in running tap water and

immersed in eosin (Sigma Aldrich, Milan, Italy) for 5 s. Sections were washed in distilled water, dehydrated in absolute ethanol, cleared in xylene (Carlo Erba, Comaredo, Italy), and mounted in Eukitt (Kindler, Freiburg, Germany).

2.6 | Picro sirius red staining

Brain sections were dipped for 1 hr in a picro sirius red solution, made by 0.5 g of sirius red powder (Direct Red 80, Sigma Aldrich, Milan, Italy) dissolved in 500 mL of saturated aqueous solution of picric acid (Picric acid solution, 1.3% in H_2O , Sigma Aldrich, Milan, Italy). Then, the samples were washed in 5% acidified water, dehydrated in absolute ethanol, cleared in xylene, and finally mounted in Eukitt (Kindler, Freiburg, Germany).

2.7 | Immunohistochemistry

The slides were incubated, at RT, for 7 min in a blocking buffer for the suppression of the endogenous peroxidases (3% H_2O_2 in 10% methanol in PBS), then for 20 min in fetal calf serum in order to block nonspecific antigen binding sites. The incubation with the primary antibody (Table 1) was carried out at RT for 1 hr in PBS overnight in a dark moist chamber for the following antibodies: mouse monoclonal anti-PV 11 kDa (1:5,000; Swant, Marly, Switzerland, RRID: AB_10000343); rabbit polydonal antiphospho-Tau (pSer519/202) 46–68 kDa (1:100, Sigma Aldrich, Milan, Italy); rabbit polyclonal anti-GABA α 6 51 kDa (1:250; Millipore, Billerica, MA, USA, RRID: AB_309747).

Thereafter, the sections were sequentially incubated with biotinylated secondary anti-rabbit or anti-mouse antibodies (1:200; Vector Laboratories, Burlingame, CA, USA, RRID: AB_2336820) for 30 min and horseradish peroxidase conjugated avidin-biotin complex (Vector Laboratories, Burlingame, CA, USA, RRID: AB_2336821) for 30 min at

TABLE 1 Primary and secondary antibodies used in immunohistochemistry

Primary antibodies for immunohistochemistry				
Antibody	Immunogen	Manufacturing details	Research Resource Identifiers (RRIDs)	Dilution
Antiparvalbumin	Purified cells from carp muscles	Mouse, monodonal, Swant/Marly, Switzerland, #235	AB_10000343	1:5,000
Antiphospho-Tau (pSer519/202)	Synthetic peptide derived from human Tau around the phosphorylation site of Ser519/202	Rabbit, polyclonal, Sigma Aldrich, Milan, Italy, #SAB4504598	Na	1:100
Anti-GABA α	Affinity-purified GABA α receptor isolated from bovine brain. Clone 62-3G1	Mouse, monodonal, Millipore, Billerica, MA, USA, #05-474	AB_309747	1:250
Secondary antibodies for immunohistochemistry				
Antibody	Immunogen	Manufacturing details	Research Resource Identifiers (RRIDs)	Dilution
Biotinylated goat anti-rabbit IgG	Gamma immunoglobulin	Goat, Vector Laboratories, Burlingame, CA, USA, #PK-6101	AB_2336820	1:200
Biotinylated horse anti-mouse IgG	Gamma immunoglobulin	Horse, Vector Laboratories, Burlingame, CA, USA, #PK-6102	AB_2336821	1:200

Abbreviation: Na, not available.

TABLE 2 Primary and secondary antibodies used in immunofluorescence

Primary antibodies for immunofluorescence				
Antibody	Immunogen	Manufacturing details	Research Resource Identifiers (RRIDs)	Dilution
Anti-laminin	Isolated from the basement membrane of Englebreth Holm-Swarm (EHS) mouse sarcoma	Rabbit, polyclonal Sigma Aldrich, Milan, Italy, #L9393	AB_477163	1:100
Anti-reelin	Generated against amino acids 3,239–3,460 of reelin of human origin	Mouse, monoclonal Santa Cruz Biotechnology, Santa Cruz, CA, USA, #sc-25,346	AB_628210	1:1,000
Anti-PCNA	Protein A-rat PCNA (proliferating nuclear antigen) fusion obtained from pC2T	Mouse, polyclonal, Millipore, Billerica, MA, USA, #ab29	AB_303394	1:600
Anti-cbinderin	Purified from chicken gut	Mouse, monoclonal, Swant, Marly, Switzerland, #300	AB_10000347	1:5,000
Anti-MAP2	Generated against amino acids 1–300 mapping at the N-terminus of MAP2 of human origin	Rabbit, polyclonal, Santa Cruz Biotechnology, Santa Cruz, CA, USA #28197	AB_2269341	1:250
Anti-NF-H	Carboxy terminal tail segment of enzymatically dephosphorylated pig Neurofilament H-subunit	Mouse, monoclonal, Abcam, Cambridge, MA, USA, #N0142	AB_477257	1:100
Anti-VGLUT2	Recombinant protein from rat VGLUT2.	Guinea pig, polyclonal, Millipore, Billerica, MA, USA, #AB2251-I	AB_2665454	1:1,500
Secondary antibodies for immunofluorescence				
Antibody	Immunogen	Manufacturing details	Research Resource Identifiers (RRIDs)	Dilution
Anti-rabbit IgG (H + L), Alexa Fluor 488	Gamma immunoglobins heavy and light chains	Goat, Thermo Fisher Scientific, Milan, Italy #A11034	AB_2576217	1:200
Anti-rabbit IgG (H + L), Alexa Fluor 594	Gamma immunoglobins heavy and light chains	Goat, Thermo Fisher Scientific, Milan, Italy #R37117	AB_2556545	1:200
Anti-mouse IgG (H + L), Alexa Fluor 594	Gamma immunoglobins heavy and light chains	Rabbit, Thermo Fisher Scientific, Milan, Italy #27027	AB_2536090	1:200
Anti-guinea pig IgG (H + L), Alexa Fluor 488	Gamma immunoglobins heavy and light chains	Goat, Thermo Fisher Scientific, Milan, Italy #A-11073	AB_2534117	1:200

RT. Then, 0.05% 3,3'-diaminobenzidine tetrahydrochloride (DAB; Sigma Aldrich, Milan, Italy) with 0.01% H₂O₂ in Tris-HCl buffer (0.05 M, pH 7.6) was used as a chromogen. After each reaction step, sections were washed thoroughly in PBS (two changes of 5 min each). Sections were dehydrated in ethanol, cleared in xylene, and mounted in Eukitt (Kndler, Freiburg, Germany). For control staining, sections were incubated with PBS instead of the primary antibody. No immunoreactivity was present in this condition.

The slides were observed with an Olympus BX51 microscope, and the images were acquired with an Optronics MagnaFire Camera through the CellF program (Olympus Segrate, Italy). Brightness and contrast parameters were optimized with the same software keeping the settings constant and selecting a fixed threshold.

2.8 | Immunofluorescence

After the deparaffinization procedure, some antigens were detected through immunofluorescence reactions. To avoid the nonspecific antigen binding sites the brain sections were treated for 30 min at RT with a PBS-blocking solution (100 mg BSA, 10 µL Tween 20, 3.3 mL glycine

0.3 M in PBS 1x). Then, the slices were incubated 1 hr in a dark moist chamber with the primary antibodies (Table 2) in PBS 1x: rabbit polyclonal anti-laminin (1:100; Sigma Aldrich, Milan, Italy, RRID: AB_477163); mouse monoclonal anti-reelin 388 kDa (1:1,000; Santa Cruz Biotechnology, Santa Cruz, CA, USA, RRID: AB_628210); mouse polyclonal antiproliferation cell nuclear antigen (PCNA) 29 kDa (1:600; Oncogene Science, Cambridge, MA, USA, Inc., RRID: AB_303394); mouse polyclonal anti-cbinderin (CB) 28 kDa (1:5,000; Swant, Marly, Switzerland, RRID: AB_10000347); rabbit polyclonal anti-MAP2 (1:250; Santa Cruz Biotechnology, Santa Cruz, CA, USA, RRID: AB_2269341); rabbit polyclonal anti-phospho-Tau (pSer519/202) 46–68 kDa (1:100; Sigma Aldrich, Milan, Italy); mouse monoclonal anti-NF-H 200 kDa (1:100; Abcam, Cambridge, MA, USA, RRID: AB_477257); guinea pig polyclonal anti-VGLUT2 56 kDa (1:1,500; Millipore, Billerica, MA, USA, RRID: AB_2665454).

Sections were washed in PBS and incubated with the appropriate secondary antibodies in PBS for 1 hr: Alexa-Fluor 594 anti-rabbit (1:200, Thermo Fisher Scientific, Milan, Italy, RRID: AB_2556545); Alexa-Fluor 594 anti-mouse (1:200, Thermo Fisher Scientific, Milan, Italy, RRID: AB_2536090); Alexa-Fluor 488 anti-rabbit (1:200, Thermo

Fisher Scientific, Milan, Italy, RRID: AB_2576217); Alexa-Fluor 488 anti-guinea pig (1:200, Thermo Fisher Scientific, Milan, Italy, RRID: AB_2534117). For the detection of a second antigen on the same section, the slides were twice washed in PBS for 5 min and then, re-incubated with the primary antibody following the same protocol as described above. After washing in PBS, the nuclei were counter-stained with 0.1 µg/mL Hoechst 33258 for 6 min, and coverslips were lastly mounted in a drop of Mowiol (Calbiochem, San Diego, CA, USA).

The slides were analyzed by fluorescence microscopy with an Olympus BX51 equipped with a 100 W mercury lamp used under the following conditions: 330–385 nm excitation filter (excf), 400 nm dichroic mirror (dm), and 420 nm barrier filter (bf) for Hoechst 33258, 450–480 nm excf, 500 nm dm, and 515 nm bf for Alexa 488, and 540 nm excf, 480 nm dm, and 620 nm bf for Alexa 594. Images were recorded with an Optronics MagnaFire camera through Cell F software. Images were optimized for color, brightness and contrast by using the same software keeping the settings constant and selecting a fixed threshold. For control staining, sections were incubated with PBS instead of the primary antibodies. No immunoreactivity was present in these sections (data not shown).

2.9 | Western blotting

Cerebellum lysates were obtained from wt, *dal*^{+/+} and *dal/dal* mice at P10 and P60, by homogenization in lysis buffer (5 mM HEPES pH 7.4, 320 mM sucrose, 2 mM EDTA pH 8.0, phosphatase and protease inhibitors [Sigma Aldrich, Milan, Italy]), the protein concentration was determined by Bradford Assay (Sigma Aldrich, Milan, Italy). Proteins (40 µg) were separated by sodium dodecyl sulfate polyacrylamide gel electrophoresis (SDS-PAGE) under reducing conditions using 12% polyacrylamide (Sigma Aldrich, Milan, Italy) gel. The proteins were electro-transferred to a nitrocellulose membrane (Hybond-P, GE Healthcare, Little Chalfont, UK), at 100 V and 38 mA for 2 hr. The membrane was then washed with PBS-0.02% Tween (PBS-T; Tween 20, Sigma Aldrich, Milan, Italy) and then blocked in 5% milk for 1 hr at RT. The membrane was then incubated with the primary antibody anti-CB 28 kDa (1:1,000;

Sigma Aldrich, Milan, Italy, RRID: AB_476894) in PBS-T 0.02% (Table 3) o/n at 4°C.

For normalization, the mouse monoclonal anti actin 42 kDa (1:2,000; Sigma Aldrich, Milan, Italy, RRID: AB_476697), in PBS-T was used. Goat polyclonal antibody antimouse (1:2,000; Agilent, Santa Clara, CA, USA, RRID: AB_2617137) was used as secondary antibody. LuminataTM Crescendo western HRP substrate and LuminataTM normal western HRP substrate (Millipore, Billerica, MA, USA) were used as substrates. Amersham Hyperfilm ECL (GE Healthcare, Little Chalfont, UK) was used.

Each experiment was carried out in triplicate and the band quantification was performed with the software Image J.

2.10 | Laminin-reelin overlapping

The laminin and reelin are two proteins expressed in the pBM. To evaluate their overlapping expression, the "polyline" function was used (Cell F software, Olympus). This function allowed to follow the positive pBM with high precision. In three sections of each slide for each animal, the length of the positive pBM was measured on the apical surface of the central lobules already mentioned. In particular, the measurements concerned the tracts in which the two markers were overlapping and the one in which it was detectable only the reelin and not the laminin. The total length of the pBM was the sum of both measurements. The average value ± SD of the length of "overlapping" and "no laminin" tracts were calculated for each genotype (wt, *dal*^{+/+}, and *dal/dal*). The length of "overlapping" and "no laminin" was expressed as percentage of the total pBM-length measured.

2.11 | Thickness of pBM collagen

The color of collagen fibers stained with picro sirius red and viewed under polarized light depends upon fiber thickness; as fiber thickness increases, the color changes from green to red (Vogel, Siebert, Hofmann, & Frantz, 2015). To determine the proportion of different stained collagen fibers, we used an automated function provided by the Cell F software, in which "green average" and "red average"

TABLE 3 Primary and secondary antibodies used in western blotting

Primary antibodies for Western blotting				
Antibody	Immunogen	Manufacturing details	Research Resource Identifiers (RRIDs)	Dilution
Anticalbindin	Bovine kidney calbindin-D	Mouse, monoclonal, Sigma Aldrich, Milan, Italy, #C9848	AB_476894	1:1,000
Antiactin	Slightly modified β-cytoplasmic actin N-terminal peptide, Ac-Asp-Asp-Ile-Na-Na-Leu-Val-Ile-Asp-Asn-Gly-Ser-Gly-Lys, conjugated to KLH	Mouse, monoclonal, Sigma Aldrich, Milan, Italy, #A2228	AB_476697	1:2,000
Secondary antibodies for Western blotting				
Antibody	Immunogen	Manufacturing details	Research Resource Identifiers (RRIDs)	Dilution
Antimouse	IgG immunoglobulins isolated from mouse serum	Goat, polyclonal, Agilent, Santa Clara, CA, USA, #P0447	AB_2617137	1:2,000

measured the average value of all intensity (density of pixels) of green and red, respectively, within the selection. Then, the green and red averages were expressed as a percentage of the total number of collagen pixels detected in the image.

2.12 | Thickness of external granular cell layer

The thickness of the total external granular cell layer (EGL) and of the two subgroups of cells within this layer, the proliferative (marked in red fluorescence by PCNA antibody) and pre-migrating granule cells (marked in blue fluorescence after Hoechst counterstaining) were evaluated. To this purpose the function "arbitrary line" provided by the Cell F software allowed to measure the layers thickness using a line spanning all the EGL, whose length was recorded, and it was perpendicular to the pial surface. The thickness measurements were carried out using 25 lines per image and data were expressed in Arbitrary Unit due to the absence of microscope calibration. The average values \pm SD of the thickness of "total EGL" and "proliferative EGL" layers were calculated for each genotype (wt, *dal/+*, and *dal/dal*). The thickness of the pre-migrating EGL layer was calculated by difference between the total and the proliferative EGL thickness.

2.13 | Cell count

For several markers it was useful to count the number of "normal" positive cells/structures and the altered positive ones. The software used was Cell F with the function of "multi-point counting". The results were then analyzed according to the purpose of the counting:

- Parvalbumin: the number of sharp and flat pinceaux at the Purkinje axon hillock was counted. From this counting those Purkinje neurons in which it was not possible to define the shape of the pinceaux were excluded. Then, the count of each brain section was used to make an average per slide and at the end per genotype. These mean values were shown in a graph.
- phospho-tau^(pSer202-509), at P60 Purkinje soma, and some other neurons within the molecular layer (ML), internal granular cell layer (IGL) and white matter were labeled and counted. The number of these cells was reported to compare the results among the genotypes.
- VGLUT2 and tau: VGLUT2+ and VGLUT2-Purkinje cell somata were counted. Then, among the VGLUT2+, Purkinje tau+ cells were counted (Purkinje soma VGLUT+ and tau+).

2.14 | Phospho-tau^(pSer202-509) positive Purkinje neurons

At P60, immunoreactions with phospho-tau^(pSer202-509) antibody labeled some Purkinje dendrites in the molecular layer (ML). To obtain a quantitative data, the function "closed polygon" of Cell F software was used to trace the perimeter of the ML; then the area and the optical density (OD) within the perimeter traced were measured. The perimeter of each positive dendrite was traced using the function

"magic wand" and the area and OD were calculated within the perimeter of each positive dendrite.

The area occupied by Purkinje positive dendrites within the ML was expressed as percentage of total ML.

2.15 | Statistical analysis

Three brain sections per slide, per animal ($n = 5$) were used for quantitative analysis and statistical observations. All the measurements concerned the vermis cerebellar lobules VIa, VIb, VII, and VIII. The results of wt, *dal/+*, and *dal/dal* were compared as follows: wt versus *dal/+*, wt versus *dal/dal*, and *dal/+* versus *dal/dal*. The results were analyzed through one-way analysis of variance, followed by post hoc analysis using SigmaPlot and the results were expressed as mean \pm SD; a p value < 0.05 was considered significant. All the immunohistochemistry and immunofluorescence quantification were performed with a blinding approach and fields were randomly chosen; the camera and magnification settings were maintained constant selecting a fixed threshold.

3 | RESULTS

3.1 | Prolidase activity is reduced in *dal* mice

Prolidase activity was measured in cerebellum and cerebral cortex. As expected, in both tissues the enzyme activity was strongly reduced in *dal/dal* mice ($3.7 \pm 1.4\%$ in cerebellum and $4.3 \pm 3.7\%$ in cerebrum) compared to controls (expressed as 100%). A prolidase activity of $39 \pm 8.8\%$ and $36.7 \pm 21\%$ in cerebellum and cerebrum, respectively, was detected in heterozygous animals.

3.2 | Morphological abnormalities in cerebellar cortex in *dal* mice

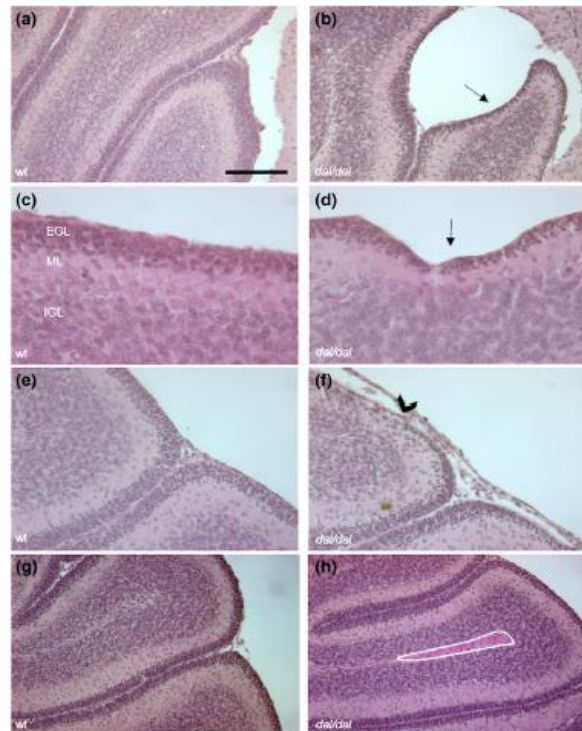
Morphological analyses of cerebellar cortex were carried out at P10 and P60, comparing wt and *dal* animals. At P10, the majority of the histogenesis and morphogenesis processes, such as the proliferation, migration and differentiation of neurons as well as the formation of fundamental synaptic contacts, are active. Instead, P60 represents the stage of mature cerebellum in which the above-mentioned processes ended.

All the images focused on the apex of the lobules VIa, VIb, VII, and VIII in the vermis since these lobules share the same developmental timing and pattern (Altman, 1982; Cerri et al., 2010). In few cases, the lobules IV and V were also examined. The type of alterations we found did not differ usually comparing *dal/dal* and *dal/+* animals; therefore, with the term "*dal*" both phenotypes are included.

Hematoxylin and eosin staining highlighted defects in the cerebellar cortex in the layering as well as in the morphology of the lobules in *dal* animals at different postnatal days.

In particular, at P10 (Figure 1) the morphology of the apical portion of the lobules IV-V was altered in *dal* animals, creating undulations on the surface (Figure 1b,d). In mutant mice, in some lobules, usually VIa-

FIGURE 1 Morphological alteration in the cerebellum in *dal* mice at P10. The apical portion of the lobules IV–VI were compared in wt (a, c, e, g) and *dal/dal* animals (b, d, f, h) by hematoxylin and eosin staining. The lobules of *dal/dal* mice were characterized by: undulations of the pial surface (black arrows; b, d); a reduction in the EGL thickness (black arrowhead; f) and overgrew blood vessels within the lobules (delineated with a white line; h). EGL, external granular layer; IGL, internal granular layer; ML, molecular layer. Magnification: scale bar of 200 μm (a, b, g, h); 50 μm (c, d); 100 μm (e, f) [Color figure can be viewed at wileyonlinelibrary.com]



With a reduction in the External Granular cell Layer (EGL) thickness was evident (Figure 1f). Moreover, as evidenced by eosin staining, overgrown blood vessels (BV) of different sizes penetrating the tissue and within the lobules were detected in all *dal* mice (Figure 1h).

At P60 pial surface anomalies as undulations were detected (Figure 2b) similar to those found at P10 (Figure 1b,d), and Molecular Layer (ML) portions partially detached from the tissue below (Figure 2c,d). In these cases, between the two ML portions, blood cells were detectable. Moreover, overgrown blood vessels penetrated cerebellar cortex detaching ML portions forming a sort of “ML island” (Figure 2f,g). In some cases, the BV penetrated the cortex and interrupted the EGL (Figure 2h). Furthermore, several granule cells had nuclei intensely stained by hematoxylin (Figure 2i) in some lobules (IV–V; VIII–IX) spread throughout their length, from the apex (Figure 2j) to the bottom (Figure 2j) of the fissure. In addition, at P60 ectopic granule and Purkinje cells were also visually detached from the lobule and immersed within the ML (Figure 2k) or in the “ML island” (Figure 2g; black box).

3.3 | Pial basal membrane irregularity of the cerebellar cortex of *dal* mice

At P10 in wt animals, the EGL below the pBM had a homogeneous thickness along the cerebellar cortex (Figure 3a) and the pBM was a continuous layer (Figure 3b,c). On the contrary, *dal* mice showed a reduction in EGL thickness (Figure 3e–h) and an altered pBM organization as revealed by the lack of laminin staining (Figure 3f). In both wt and mutant mice reelin was detected in the pBM (Figure 3g), but only in *dal* mice, in correspondence of the alterations, it was found in the EGL and in part in the ML as well as in the soma of Purkinje neurons (Figure 3g).

The absence of laminin and the overlap of the two markers in correspondence of apical cerebellar lobules were measured. In particular, laminin and reelin overlapped for $99 \pm 0.003\%$ in wt, $87 \pm 4.5\%$ in *dal/+* and $77 \pm 10\%$ in *dal/dal*, the remaining percentage represents portion of pBM positive only for reelin. The differences were not significant comparing *dal/+* versus *dal/dal* mice, but statistically significant comparing wt versus *dal/+* and *dal/dal* ($p < .01$) (Figure 3i).

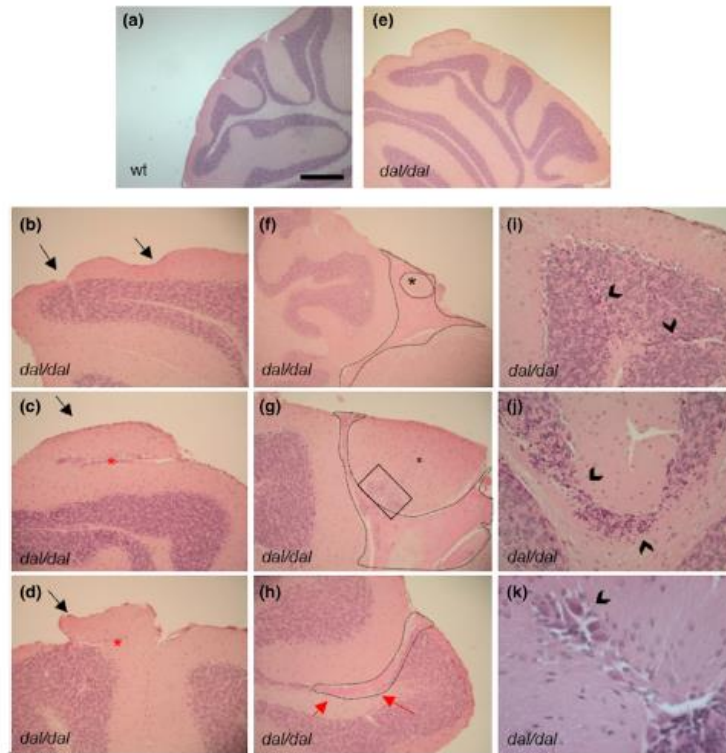


FIGURE 2 Morphological abnormalities in cerebellum of *dal* mice at P60. The morphology of the lobules IV–VI and VIII–IX were compared in wt (a) and *dal/dal* animals (b–k) by hematoxylin and eosin staining. The same anomaly was not always present in all the specimens in the same cerebellar sections, thus such variability forced us sometimes to choose the most representative anomalies of *dal/dal* or *dal/+* in comparisons with wt animals in not comparable regions of the cerebellum. The lobules of *dal/dal* mice were characterized by: pial surface anomalies (black arrows; b, c, d); partial ML detachment in which blood cells were visible (red asterisks; c, d); isolated “ML island” (black asterisks; f, g) surrounded by huge blood vessels (delineated with black dotted line; g, h); interrupted EGL (red arrows; h); ectopic granule cells (black box; g) and Purkinje neurons (black arrowhead; i); granule cells with intensely stained nuclei (black arrowheads; j, k). Magnification: scale bar of 400 μ m (a, e); 150 μ m (b–d, g, h); 80 μ m (f, j), 75 μ m (f) and 40 μ m (k) [Color figure can be viewed at wileyonlinelibrary.com]

The ECM profile included the analysis of collagens. The collagens component of the pBM was evaluated using picro sirius red staining, which highlighted the differences between wt and *dal* mice regarding the thickness of collagen structure within the pBM (Figure 3j,k). In particular, the color of collagen fibers stained with picro sirius red depends upon fiber thickness; as fiber thickness increases, the color changes from green/yellow to orange/red. A significant increase ($p < .001$) in the thinner fibers in *dal/+* and *dal/dal* mice compared with wt was found [optical density mature fibers,

wt 5.5 ± 0.6 ; *dal/+* 7.9 ± 0.9 ; *dal/dal* 8.04 ± 1.2 ; optical density immature fibers, wt 9.26 ± 2.7 ; *dal/+* 11.6 ± 2.7 ; *dal/dal* 10.36 ± 3.4] (Figure 3).

3.4 | Altered granule cell proliferation and maturation in *dal* mice

During the cerebellar postnatal development, immature granule cells, located in the EGL, proliferate adjacent to the pBM and then migrate

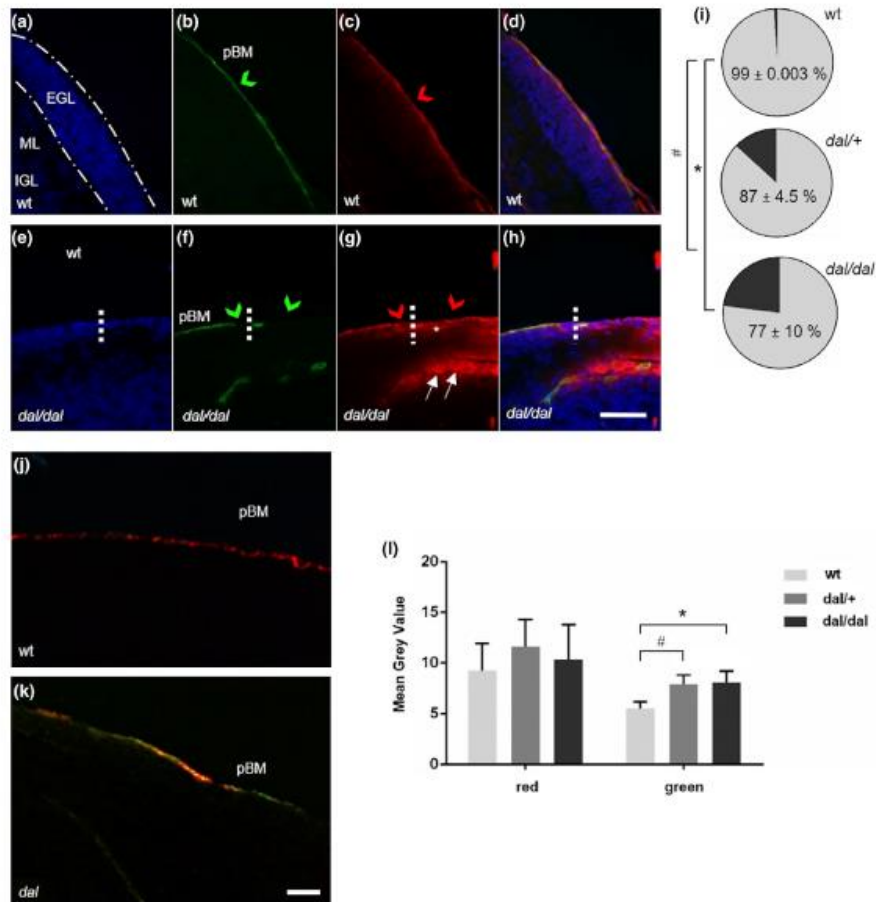


FIGURE 3 Impaired extracellular matrix organization in *dal* mice. (a–h) Immunofluorescence reactions at P10 for laminin (green) and reelin (red), markers for the pial basement membrane (pBM) were performed in wt (a–d) and *dal/dal* (e–h) animals. The nuclei (blue) are stained using Hoechst. The EGL thickness is delimited with white interrupted line (a) and the pBM is indicated with arrowheads (green and red for laminin and reelin immunopositivity, respectively; b, c, f, g); the abrupt reduction in the EGL thickness of *dal* mice is indicated with a white dotted line (e–h); the immunopositivity of reelin in the EGL and in part in the ML is highlighted by a white asterisk, while in Purkinje neurons by white arrows (g). (i) Pie charts represent the measurements of pBM positive to laminin and reelin when overlapped (light gray) and the length of pBM positive only for reelin with the absence of laminin (dark gray). These measures were expressed as percentage of cerebellar pial surface covering lobules from VIa, VIb, VII to VIII. (j, k) Picro sirius red staining of pBM collagen component. Images of wt and *dal* mouse under polarized light revealed thinner collagen fibers in green and thicker collagen fibers in red. (l) A significant difference in collagen fibers size was detected in *dal/+* and *dal/dal* mice ($*p < .05$ wt vs. *dal/dal*; $#p < .05$ wt vs. *dal/+*). Values are expressed as mean ± SD. EGL, external granular layer; IGL, internal granular layer; ML, molecular layer; pBM, pial basement membrane. Magnification: scale bar of 100 μm (a–h); 40 μm (j, k) [Color figure can be viewed at wileyonlinelibrary.com]

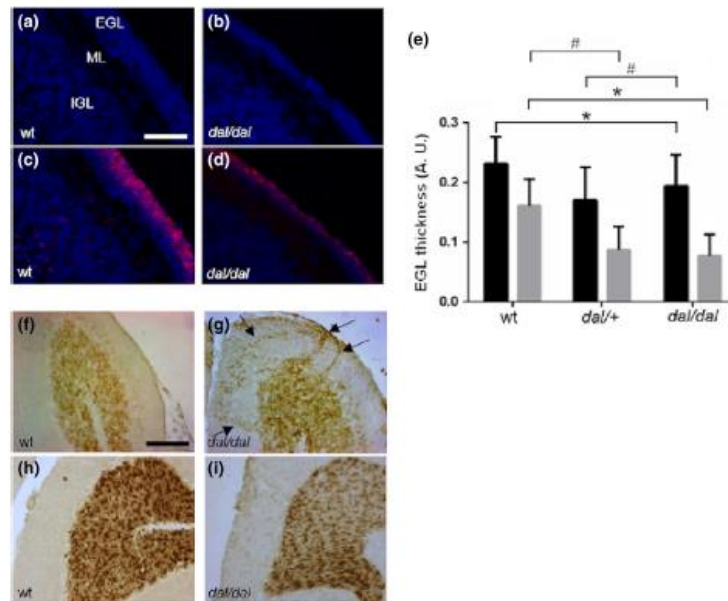


FIGURE 4 Proliferation and migration of granule neurons are impaired in *dal* mice. (a–d) Immunofluorescence reactions at P10 for PCNA (red), marker for cellular proliferation, were performed in wt (a, b) and *dal/dal* (c, d) animals. The nuclei (blue) were stained using Hoechst. (e) The histogram represents the thickness of whole EGL (black bars) and proliferating EGL (light gray bars). Values are expressed as mean \pm SD, A.U. (Arbitrary Unit) (black bars: * $p < .05$ wt vs. *dal/dal*; # $p < .05$ wt vs. *dal/+*; light gray bars: * $p < .05$ wt vs. *dal/dal*; # $p < .05$ wt vs. *dal/+*). (f–i) Immunohistochemical reaction for GABA α 6 were performed in wt (f, h) and *dal/dal* (g, i) at P10 and P60 to highlight mature granule cells in the ML and IGL. (g) Black arrowheads highlight clusters of migrating immature granule cells. Magnification: scale bar of 100 μ m (a–d), scale bar of 200 μ m (f–i) [Color figure can be viewed at wileyonlinelibrary.com]

through the ML toward the internal granular layer (IGL). In particular, in the EGL it is possible to distinguish a proliferative layer and a pre-migratory layer (Figure 4a,c). In mutant mice a reduction in the thickness of the PCNA-positive proliferative layer compared to wt was evident ($p < .05$ wt vs. *dal/dal*; # $p < .05$ wt vs. *dal/+*; light gray bars: * $p < .05$ wt vs. *dal/dal*; # $p < .05$ wt vs. *dal/+*) (Figure 4a–e).

GABA α 6 was used to mark mature granule cells of the IGL (Figure 4f–i). The scattering of immunopositive granule cells is different within the IGL comparing the different lobules and according to the histological maturation. The lobules that develop last (Vla, Vlb, and VII) showed a weaker staining for GABA α 6; this was visible in the wt, *dal/+*, and *dal/dal* mice. However, at P10 in *dal/dal* mice clusters of migrating GABA α 6 positive granule cells were evident in the ML (Figure 4f,g) (wt 108.48 \pm 12.23 and *dal* 107.26 \pm 54.14). At P60 (Figure 4h,i) in *dal/dal* mice, the presence of mature and strongly immunopositive granule cells within the IGL was not homogeneous as in the wt; there were weakly

immunopositive cells also in the ML (wt 130.47 \pm 51.70 and *dal* 134.44 \pm 12.28).

3.5 | Purkinje neuron morphology and synaptic contacts are impaired in *dal* mice

The morphology of Purkinje neurons was investigated by Calbindin (CB) staining. In wt mice, at both ages P10 (Figure 5a,c) and P60 (Figure 5e,f) the Purkinje neurons were intensely marked with a perfect dendritic arborisation. At P10, Purkinje alterations in *dal/dal* mice with cerebellar apical anomalies and layering defects as loss of Purkinje cells or differently oriented Purkinje dendrites were evident (Figure 5b,d).

At P60, the dendrites of Purkinje neurons of *dal/dal* mice appeared less branched and ectopic Purkinje neurons within the IGL, lacking dendrite branches, were also detected (Figure 5g,h,j).

The Purkinje morphology and the intensity of the labeling were similar at P10 and P60 mice. By western blot analysis (Figure 5k) no relevant difference in CB amount among wt and *dal* mice was detected at P10. However,

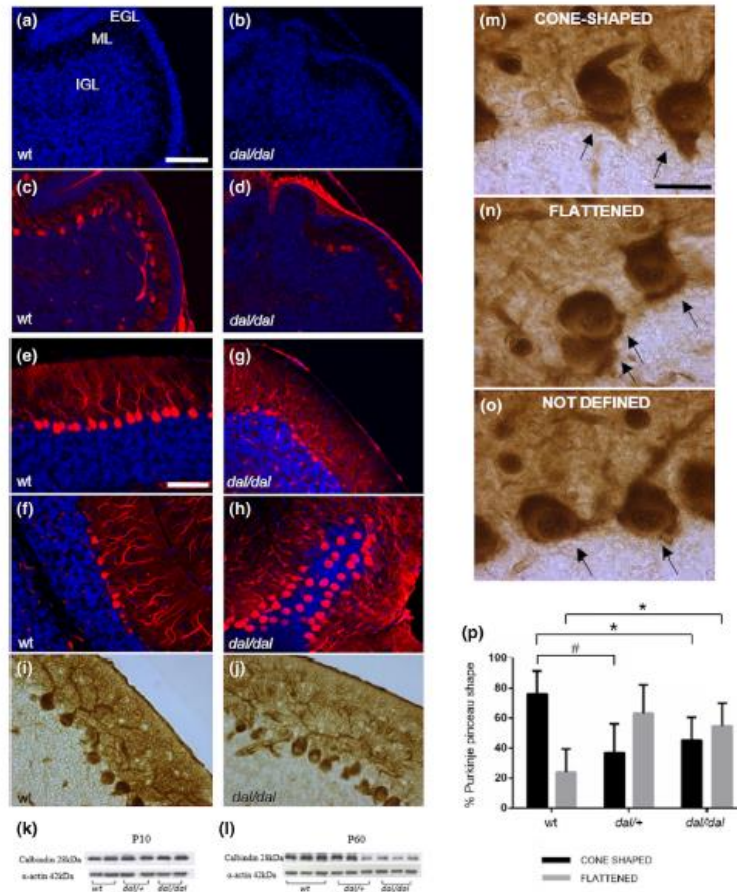


FIGURE 5 Abnormal morphology of *dal* mice Purkinje neuron. (a–h) Immunofluorescence reactions for calbindin (red), a calcium binding protein expressed by Purkinje cells, were performed in wt (a, f) and *dal/dal* (b, h) at P10 (a–d) and P60 (e–h). The nuclei (blue) were stained using Hoechst. (i–j) Immunohistochemical reaction at P60 for calbindin highlights less dendrite branches in *dal/dal* (j) compared to wt (i). (k–l) Western blot analysis for calbindin at P10 and P60. (m–o) Immunohistochemical reaction at P60 for parvalbumin highlights the shape of pinceaux (black arrows) as cone-shaped (m), flattened (n), or not defined (o). (p) The histogram represents the percentage of cone-shaped (black bars) and flattened pinceaux (light gray bars) in wt, heterozygous and homozygous [black bars: * $p < .001$ wt vs. *dal/dal*; # $p < .001$ wt vs. *dal/+*; light gray bars: * $p < .05$ wt vs. *dal/dal*]. Magnification: scale bars of 100 μ m (a–h); 20 μ m (i–m) [Color figure can be viewed at wileyonlinelibrary.com]

at P60 a statistical significant decrease in CB amount was evident in *dal* mice compared to wt (*dal/+* $83 \pm 0.01\%$; *dal/dal* $58 \pm 0.07\%$; $p < .001$). A significant difference between *dal/+* and *dal/dal* was also present ($p < .005$).

The parvalbumin (PV) immunolabeling was used to evaluate the morphology of the Purkinje pinceaux at the axon hillock (Figure 5m–o).

Generally, the pinceaux should be cone-shaped. To verify the aspect of the pinceaux, the number of visible well-defined cone-shaped pinceaux and of the altered ones with a flattened shape were counted. A significant difference was detected between the number of cone-shaped pinceaux among the three genotypes (wt $76 \pm 15\%$; *dal/+* $37 \pm 19\%$;

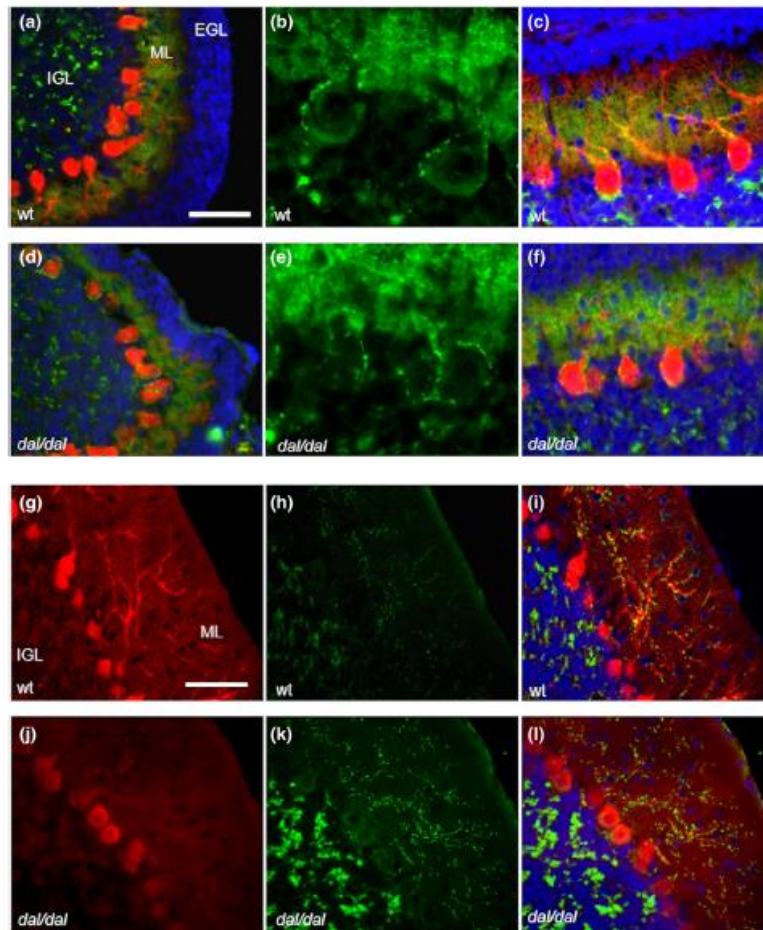


FIGURE 6 Synaptic contact between VGLUT2 climbing fibers and Purkinje neurons is altered in *dal* mice. (a–l) Double immunofluorescence reactions for VGLUT2 (green), marker for climbing fibers, and Calbindin (red), marker for Purkinje neurons, were performed in wt (a–c, g–i) and *dal/dal* (d–f, j–l) animals at P10 (a–f) and P60 (g–l). The nuclei (blue) are stained using Hoechst. Magnification: scale bar of 100 μ m (a, d), 50 μ m (b, e, g–n), 75 μ m (c–f) [Color figure can be viewed at wileyonlinelibrary.com]

dal/dal $45 \pm 15\%$; $p < .001$). A significant increase in the number of flattened pinceaux in *dal/dal* animals compared to wt was instead detected (wt $24 \pm 15\%$; *dal/+* $63 \pm 19\%$; *dal/dal* $55 \pm 15\%$; $p < .05$ wt vs. *dal/dal*).

The alterations of Purkinje pinceaux morphology at the axon hillock and changes in immunolabeling patterns was also detected by glutamic acid decarboxylase 67 (GAD67) (data not shown).

VGLUT2 marks climbing fibers in the ML and mossy fibers in the IGL in adult mice. At P10 VGLUT2 staining labels both parallel fiber terminals and climbing fiber terminals (Watanabe & Kano, 2011). Purkinje neurons make contacts with climbing fiber terminals in ML (Figure 6). Double immunofluorescence reaction, using CB and VGLUT2 allowed to study if morphologically compromised

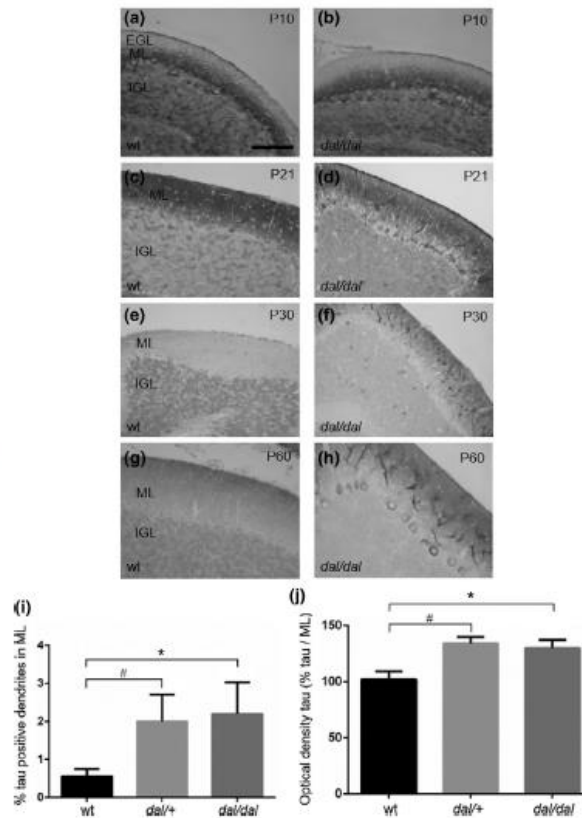
Purkinje neurons were still able to make synaptic contacts and if the correct synaptogenesis was still occurring. At P10 the labeling in wt was homogeneous (Figure 6a–c) and there were no particular changes in the *dal/dal* mice, even in correspondence of apical anomalies (Figure 6d–f). The positivity for VGLUT2 was mainly concentrated on the proximal portion of Purkinje dendrite branches and in correspondence of Purkinje cell soma, especially in fissures in wt, while in *dal/dal* mice most lobules showed the positivity over the entire dendritic tree of Purkinje neurons. As the postnatal development is proceeding, the positivity of VGLUT2 should change. At P60 these synapse arrangements showed a different pattern compared to P10. In fact, in P60 mice, VGLUT2 immunoreactive terminals were mainly identifiable on the main branches of Purkinje cell dendrite, in both wt and *dal/dal* mice (Figure 6g–i). Rarely, in mature brain the positivity was found around the soma. No differences were found considering the labeling of VGLUT1

parallel fibers in the three genotypes at both ages (data not shown).

3.6 | Abnormal persistence of phosphorylated tau protein in P60 mutant mice

The Tau protein is relevant to stabilize microtubules, its phosphorylation is necessary for their reorganization during development. Thus, phosphorylated Tau protein is physiologically present at P10 and decreases following brain maturation. In adults its permanence may be associated to neurodegeneration or developmental delay. The positivity for phospho-Tau^(pSer202/309) was similarly detected at P10 in the ML and IGL in both wt and *dal/dal* mice (Figure 7a,b), but it was different following the cerebellar maturation. In wt the labeling at P21 (Figure 7c) was very similar to the P10; while a reduced signal was detected at P30 and at P60 as expected (Figure 7e and g, respectively). On the contrary,

FIGURE 7 Abnormal persistence of phosphorylated tau protein in mutant mice. Immunohistochemical staining for phospho-tau^(pSer202/309) marker for neurodegeneration at later developmental stages, were performed in wt (a, c, e, g) and in *dal/dal* (b, d, f, h) at P10 (a, b), P21 (c, d), P30 (e, f), P60 (g, h). Magnification: scale bar of 200 μ m (a, b); 100 μ m (c–h). (i) The histogram represents the quantitative evaluation of the area occupied by positive Purkinje dendrites along lobules from VIa to VIII normalized for the area of total ML and expressed as percentage in P60 mice. Statistically significant difference comparing *dal* mice vs. wt ($*p < .05$ wt vs. *dal/dal*; $\#p < .05$ wt vs. *dal/+*) was detected. (j) The histogram represents the quantitative evaluation of the optical density (OD) of ML in P60 mice. Statistically significant difference comparing the ML OD of both *dal* mice vs. wt ($*p < .05$ wt vs. *dal/dal*; $\#p < .05$ wt vs. *dal/+*) was detected



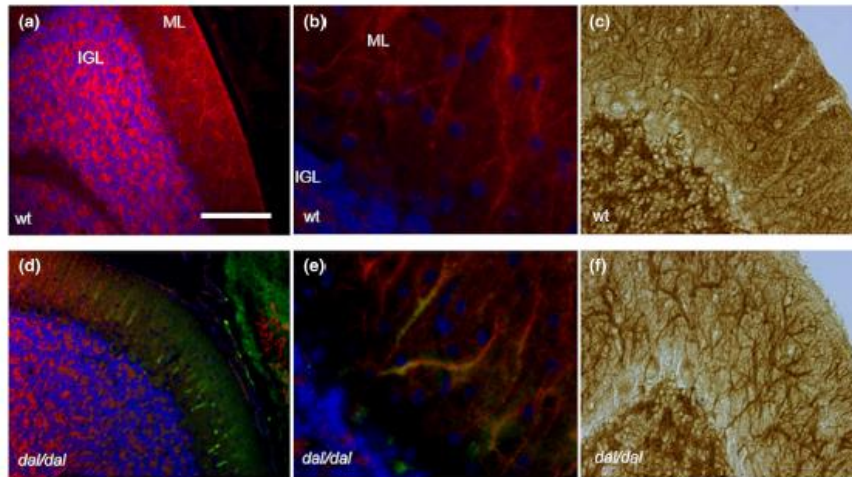


FIGURE 8 Purkinje neurons abnormalities in *dal* mice. Double immunofluorescence reactions for MAP2 (red), cytoskeletal marker, and phospho-tau^(S5e202/509) (green), neurodegenerative marker, were performed in wt (a, b) and in *dal/dal* (d, e) at P60. The nuclei were stained using Hoechst (blue). Magnification: scale bar of 100 μ m (a, d) and 20 μ m (b, e). [c, f] Immunohistochemical reactions for MAP2 highlights thick dendrite branches in *dal/dal* (f) compared to wt (c) at P60 [Color figure can be viewed at wileyonlinelibrary.com]

in *dal/dal* mice a high positivity for pTau was evident at all analyzed ages (P21, P30, and P60) (Figure 7d,f,h).

The pTau-positive Purkinje dendrites area along lobules from VIa to VIII, at P60 was evaluated. In wt only the $0.4 \pm 0.1\%$ of ML area was occupied by positive Purkinje dendrites, $2 \pm 0.6\%$ in *dal/+* and $2.1 \pm 0.9\%$ in *dal/dal* (*dal* vs. wt, $p < .05$) (Figure 7i). ML optical density (OD) was also evaluated and its increase in both *dal/+* ($p < .05$) and in *dal/dal* ($p < .05$) compared to the wt animals was detected (wt $102 \pm 7.3\%$; *dal/+* $134 \pm 6\%$; *dal/dal* $130 \pm 7.2\%$) (Figure 7j).

3.7 | Altered Purkinje microtubules organization and synaptic contacts in *dal* mice

The presence of phospho-tau^(S5e202/509) (Figure 8) at P60 in *dal* mice indicated an increase in the instability of microtubules, therefore the concomitant presence of MAP2 (a microtubule stabilizer protein) was evaluated (Figure 8a,b,d,e). Double immunofluorescence reactions showed that in the wt only MAP2 staining was detectable, the positivity for MAP2 was always homogeneous (Figure 8a-c) and mainly localized in the thinner Purkinje dendrite branches. In *dal/dal* mice different labeling could be detected: (a) some Purkinje neurons were immunopositive to phospho-tau^(S5e202/509) with a decrease in the labeling for MAP2 (Figure 8d); (b) the Purkinje dendrites were labeled by phospho-tau^(S5e202/509) and the positivity for MAP2 did not change (Figure 8e). There was no lobule specificity for these observations and it was not

correlated to the number of neurons immunopositive for phospho-tau^(S5e202/509). Anyway, in *dal/dal* mice the MAP2 immunostaining revealed thicker Purkinje dendrite branches (Figure 8f). It is not possible to exclude that these branches acquired an enlarged caliber or they represented the main dendrite branches of Purkinje cells.

To better investigate at P60 in *dal/dal* mice the localization of phospho-tau^(S5e519/202) within Purkinje neuron, a double immunofluorescence reaction was carried out using calbindin and phospho-tau^(S5e202/509) (Figure 9a-d). The positivity of phospho-tau^(S5e519/202) in *dal/dal* mice was found in Purkinje neurons and in particular in thicker dendrite branches (Figure 9b,c) and in some cell body (Figure 9d), in lobules apex as well as in fissures, without lobules specificity. Moreover, it was highlighted that Purkinje neurons in wt were perfectly shaped and labeled by CB (Figure 9a), while in *dal/dal*, Purkinje neurons positive for the phospho-tau^(S5e519/202) were less labeled by CB (Figure 9d).

In the mature brain heavy-neurofilament (NF-H) labels axons of basket cells, which form synaptic contacts with Purkinje dendrite branches in the ML, and the basket pinceaux around the Purkinje axon hillock. At P60, in wt mice, the basket-like structure around the Purkinje soma was strongly labeled as well as the axons, which run perpendicular to the Purkinje dendrite tree (Figure 9e). In *dal/dal* mice was evident a strong decrease in the positivity for this marker highlighting thinner basket-like structures and less or weaker stained axons in the ML (Figure 9g). In particular, double immunofluorescence reactions for NF-H and phospho-tau^(S5e202/509)

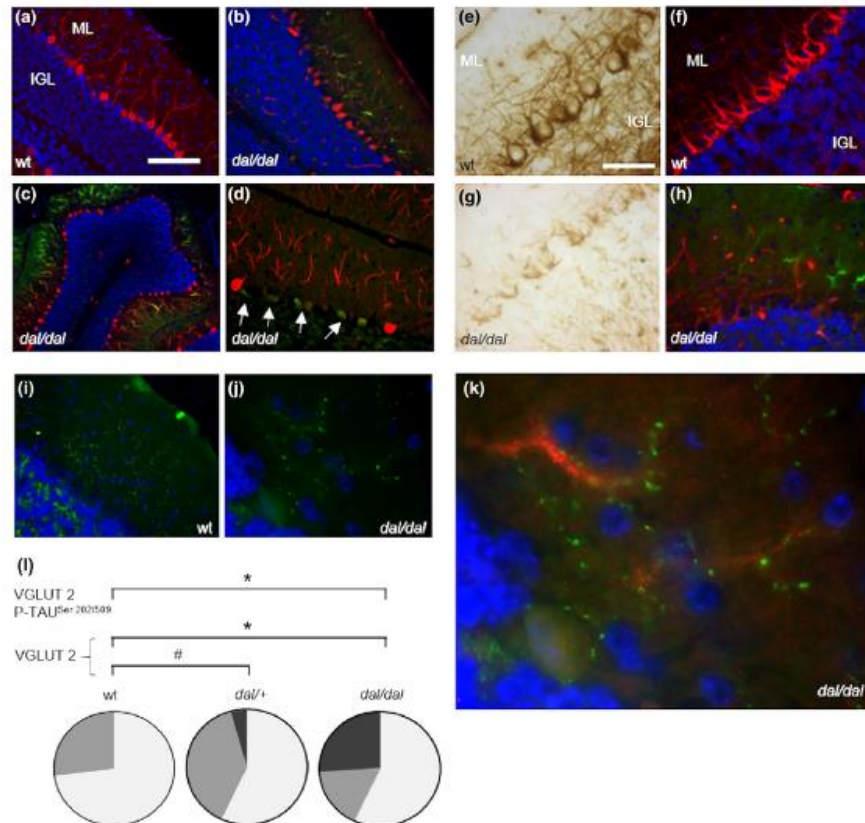


FIGURE 9 Purkinje neurons abnormalities in *dal* mice. Double immunofluorescence reactions for calbindin (red) and phospho-tau^{pSer202/509} (green) were performed in wt (a, b) and in *dal/dal* (d, e) at P60. The nuclei were stained using Hoechst (blue). (d) White arrows mark dendrite branches and cell body of Purkinje neurons immunopositive for phospho-tau (pSer202/509). Magnification: scale bar of 100 μ m (a, b, d) and 150 μ m (c). Immunohistochemical reaction for NF-H (e, g), marker for mossy fiber and double immunofluorescence reactions for NF-H (red) and phospho-tau^{pSer202/509} (green) were performed in wt (f) and in *dal/dal* (h) at P60. The nuclei were stained using Hoechst (blue). Magnification: scale bar of 100 μ m. (i–k) Immunofluorescence reactions for VGLUT2 (green) with phospho-tau^{pSer202/509} (red) at P60. The nuclei were stained using Hoechst (blue). White arrows (i, j) point the Purkinje nucleus. Magnification: scale bar of 20 μ m (M), scale bar of 30 μ m (j, k). (l) Pie charts represent: in gray color Purkinje soma VGLUT2⁺; in light gray, Purkinje soma VGLUT2⁺; in black, Purkinje neuron VGLUT2⁺ and phospho-tau^{pSer202/509} (* $p < .05$ wt vs. *dal/dal*; # $p < .05$ wt vs. *dal/+*) [Color figure can be viewed at wileyonlinelibrary.com]

(Figure 9h) revealed a decrease in the NF-H positivity close to Purkinje neurons expressing the phospho-tau^{pSer202/509} (Figure 9h). Moreover, abnormal or less developed pincaux were observed.

Double immunofluorescence reaction was carried out for VGLUT2 and phospho-tau^{pSer202/509} (Figure 9i–k).

At P60 VGLUT2 should be present mainly on Purkinje dendrite branches.

In *dal/dal* mice the immunopositivity was instead detected also around Purkinje cell soma (43% in *dal/+* and 42.5% in *dal/dal*), although 27% soma distribution was present in wt as well (wt vs. *dal/+* $p < .001$; wt vs. *dal/dal* $p < .001$). None of the 27% of VGLUT⁺ Purkinje soma in wt was also labeled by tau. In *dal/+* mice among the 43% of VGLUT⁺ Purkinje soma, 4.3% was also tau⁺ ($p < .05$). Instead in *dal/dal* mice among the 42.5% of VGLUT⁺

Purkinje soma, 26% were also tau* ($p < .05$) (Figure 9). No differences were found considering the double immunofluorescence reaction for VGLUT1 and phospho-tau^(pSer202/307) in the three genotypes at both ages (data not shown).

4 | DISCUSSION

In the present research, we studied the postnatal cerebellar cortex development and neuronal maturation in dark-like mice, heterozygous and homozygous for a loss-of-function mutation in the gene encoding prolidase.

In our studies we detected similar anomalies in both heterozygous and homozygous animals. Likely the 50% of the enzyme is not sufficient to guarantee the proper brain development.

Since prolidase exerts an indirect impact on the ECM remodeling, being involved in the collagen and procollagen metabolism (Kama et al., 2000), some ECM components were analyzed. In particular, the attention has been focused on those of pBM, as it is a specialized structure of ECM and a fundamental regulator of cortical development (Halfter et al., 2002). Pial BM was present in both wt and *dal* mice cerebellar cortex. However, in wt was uniform and continuous, whereas in *dal* was discontinuous and irregular. The pBM collagens in *dal* mice were represented by a majority of thicker structure than in the pBM of wt animals. The Type IV collagen is the most abundant in the CNS and acts as a scaffold to integrate laminin and other ECM components into sheet-like BM, which in turn, are thought to be essential for pBM assembly (Burnside & Bradbury, 2014; Pöschl et al., 2004). Since the collagen turnover is partially regulated by the prolidase enzyme (Surazynski et al., 2008), the collagen structural alterations and then the wrong positioning of the other pBM components in *dal* mice might be related to the absence or reduced activity of this enzyme. Laminin and reelin did not overlap each other all over the pBM. Moreover, the reelin was also found extracellularly in correspondence of apical anomalies suggesting defects in neurotransmission patterns (Senkov, Andjus, Radenovic, Soriano, & Dityatev, 2014). It was previously demonstrated that changes in the quantity, structure and distribution of collagens in tissues might affect cell signaling, metabolism, and function (Guszczyn & Sobolewski, 2004; Kama et al., 2000). Moreover, it is well documented that the impairment of pial ECM components leads to syndromes associated to cortical dysplasia (Barkovich, Guerrini, Kuzniecky, Jackson, & Dobyns, 2012; Francis et al., 2006; Halfter et al., 2002), molecular layer heterotopia (Ramos et al., 2013; Ramos et al., 2014), and morphological anomalies of the cerebellum (Cerri et al., 2010; Ichikawa-Tomikawa et al., 2012; Qiu, Cang, & Goff, 2010; Siegenthaler & Pleasure, 2011). In this light, it is possible to speculate that the apical anomalies (as the surface abnormalities, layering defects and heterotopias) could be linked to the pBM impairment. These could also explain why the anomalies were not diffused along the cerebellar cortex, but were scattered only in regions without lobule specificity, as the pBM defects herein recorded. The pBM organization and integrity is essential for the proliferation and then migration of neuronal precursors during prenatal and postnatal cerebellar development (Barros et al., 2011; Folsom & Fatemi, 2013; Lakatosova & Ostankova, 2012; Porcionatto, 2006).

The proliferating granule cells are located in the more apical surface of cerebellar lobules (close to the basal lamina) during the first postnatal stages (Altman, 1972); a layer thinning in *dal* mice was accompanied by a decrease in the PCNA protein amount in the developing brain of *dal* mice compared to wt. Once the granule cells proliferate in the EGL, they should migrate, toward the IGL, following the scaffold provided by the radial glial cells that are able to anchor their end-feet to the laminin protein sheet of pBM (Ichikawa-Tomikawa et al., 2012). In *dal* mice there were gaps in the laminin sheet that caused the retraction of radial glia fibers: they appeared interrupted without reaching the pial surface, or devoid of radial orientation or absent in correspondence of the apical surface anomalies (Insolia & Piccolini, 2014). These physical changes in the radial glia may interfere with the ability of granule neurons to find a suitable fiber near the EGL/ML interface to migrate properly. Furthermore, it was demonstrated that even after a granule neuron has found a suitable glial fiber, the traveling along these fibers may be less efficient (Komuro & Yacubova, 2003; Qu & Smith, 2005; Xu et al., 2013). It is also possible that some granule neurons migrate normally along adequate fibers and that only a subpopulation of neurons are dramatically detained in their migration as it was pointed out by GABA_A6 immunopositivity through which the migration/maturation of granule cells was followed. GABA_A6 is a marker of mature granule neurons and should be present only after the migration, when granules are in the IGL (Cerri et al., 2010; Laurie, Seeburg, & Wisden, 1992; Thompson & Stephenson, 1994). In *dal* mice, a wrong pattern of migration/maturation was highlighted at P10. In fact, clusters of migrating granule cells were found scattered in the ML and labeled by GABA_A6. Then at P60, the granule cells were still labeled in the IGL, but this positivity was not homogeneous in intensity, suggesting defects in the inhibitory synaptic system in the cerebellar glomeruli (Takayama & Inoue, 2004).

The limit in evaluating cell proliferation and migration using thickness of PCNA positive layer and GABA_A6 immunostaining should be taken into account in data interpretation.

It has been well-established that an altered migration and maturation of granule cells affect the cerebellum lamination, the distribution of Purkinje neurons in a monolayer and the growth of Purkinje cell dendrites, since the granule cells secrete trophic factors for Purkinje cell differentiation (Altman, 1982; Altman & Bayer, 1997; Cerri et al., 2010; Goldowitz & Hamre, 1998; Hatten, 1999; Xu et al., 2013). Indeed, in *dal* mice Purkinje cell morphology was altered, with dendrite trees poor of branches. Moreover, there were Purkinje neurons in ectopic positions within the internal granule cell layer, or distributed in a multilayer, confirming inappropriate cortical lamination: this finding was highlighted with calbindin immunohistochemistry, but was clearly detected with hematoxylin and eosin as well.

Purkinje neurons are key cells in the cerebellar cortex circuit since represent the sole output of the cerebellar cortex (Ito, 2006). Therefore, to get information concerning not only the morphology, but also the functionality of these neurons, the calcium homeostasis markers of Purkinje cells were considered together with other excitatory and inhibitory neurotransmission markers. The expression of CB and PV by Purkinje neurons, a fast and slow Ca²⁺ binding protein, respectively, was investigated. Both revealed anomalies in the Purkinje

neurons. The CB, as marker of Purkinje neurons highlighted alterations of dendrite tree branches and their organization within the ML. Moreover, there was a decrease in the amount of CB detected through western blotting in *dal* mice compared to wt at P60, although has been reported that morphological impairment of Purkinje neurons cannot be necessarily attributed to a reduction in CB content (Schwaller, Meyer, & Scniffmann, 2002). The PV marker led to the detection of alterations of the basket pinceaux at the Purkinje axon hillock. In fact, it was observed an increase of aberrant flat pinceaux instead of physiological cone-shaped one in *dal* mice.

Then, it must be taken into great consideration that the morphology, polarization, migration, and cell-connectivity of cells are dictated by cytoskeleton filamentous network of proteins whose regulation is essential during the different developmental stages of the brain (Matus, 1988; Menon & Gupton, 2016). In *dal* mice the cytoskeleton components MAP2, a microtubule stabilizer protein, tau protein, that in the phosphorylated form at Ser519/202 residues destabilizes the microtubules, and the NF-H were studied. First stages of cerebellar cortex development are characterized by high levels of MAP2 and phospho-tau^(pSer202/509) due to microtubule rearrangements (Avila, Lucas, Perez, & Hernandez, 2004; Riederer & Matus, 1985). At P60 in wt mice, the positivity was maintained in the cerebellar cortex for MAP2 while there was a strong decrease for phospho-tau^(pSer202/509). The presence in mature neurons of this latter marker is no more considered physiological. In this context, in *dal* mice, different cell populations were found immunopositive to phospho-tau^(pSer202/509) in the ML, IGL and in the white matter. It is important to highlight that Purkinje neurons labeled by phospho-tau^(pSer202/509) were also spread in the cerebellar lobules; the positivity was in the soma and/or in the dendrites and was associated to altered microtubules organization as evidenced by MAP2 staining. The positive dendrites were always of big caliber. These findings suggest that either the phospho-tau^(pSer202/509) positivity was localized in the main Purkinje dendrite or the dendrites positive for this marker were enlarged.

To understand whether the presence of tau is indicative of further functional damages of Purkinje cells, the attention has been focused on the evaluations of synaptic contacts of phospho-tau^(pSer202/509) positive-Purkinje neurons. Therefore, the NF-H, as a marker of inhibitory basket cell axons (White & Sillitoe, 2013); VGLUT1 and VGLUT2 as markers of parallel and climbing fibers, respectively, were evaluated (Boulland et al., 2004).

In wt mice, NF-H was not present at P10 yet, while at P60 highlighted the axons of basket cells, which form synaptic contacts with Purkinje dendrite branches in the ML, and the basket pinceaux at the Purkinje axon hillock. In *dal* mice, a strong decrease in NF-H labeling was evident since there were a loss of positive axons in the ML and flattened basket at Purkinje axon hillock, in particular in those Purkinje neurons positive for the phospho-tau^(pSer202/509) either in cell soma or in dendrites, confirming anomalies in the inhibitory pattern system.

In *dal* mice there were no significant changes in VGLUT1 (parallel fibers) positivity. Instead, there were some anomalies concerning the climbing fibers (VGLUT2 immunopositive), especially in the mature cerebellum. The mature stage (as P60) is characterized by a mono-

innervation of climbing fiber for each Purkinje neuron on the proximal portion of dendrite arborization (Strata, Tempia, Zagrebelsky, & Rossi, 1997; Watanabe & Kano, 2011). In *dal* mice, there were still Purkinje soma positive to VGLUT2 and the positivity in the ML was significantly higher in *dal* mice compared to wt. These results suggested that the critical pruning process of climbing fibers was not concluded, or it was delayed. Interestingly, a percentage of Purkinje neurons labeled by phospho-tau^(pSer202/509) presented the retention of climbing fibers in the somas. Different hypothesis could be formulated (not necessarily mutually exclusive): Purkinje dendrites maturation, altered in *dal* mice, strongly influences the development of synaptic contacts (Qiao et al., 2013); the presence of phospho-tau^(pSer202/509) could be either a first sign of neurodegeneration that is described as associated to synaptic alterations or a sign of developmental delay in the maturation of microtubules cytoskeleton and Purkinje cell synapses contacts (Goedert et al., 1993; Wang & Liu, 2008); imbalance in Ca²⁺ homeostasis (Hof et al., 1999; Schwaller et al., 2002; Vecellio, Schwaller, Meyer, Hunziker, & Celio, 2000); presence of extracellular reelin within the cerebellar layers in adult mice leading to the potentiation of glutamatergic neurotransmission together with the increase in spine density (Senkov et al., 2014). As previously described, the changes in *dal* mice could be linked to the impaired maturation of Purkinje neurons (Takayama, Nakagawa, Watanabe, Mishina, & Inoue, 1996; Yuzaki, 2004).

The morphological alterations of *dal* mice were not only related to these molecular and cellular pathways, but also to the physical damages of cortical portions caused by injuring blood vessels. In *dal* mice, there was an overgrowth of blood vessels both in term of number and size. The causes could be several: *dal* mice embryonically develop the cardiomyocyte hypertrophy (Jung et al., 2011), that physiologically results in a net induction of angiogenesis (Laughlin, Bowles, & Duncker, 2012); prolidase indirectly is involved in the angiogenesis signaling pathways (Rhodes & Simons, 2007). These big blood vessels were observed not only in correspondence of cerebellum, but also close to the hippocampal formation (Insolia & Piccolini, 2014).

Additionally, the pBM defect, as well as the layering alterations and apical anomalies (as cortical undulations) were also present in the neocortex in both P10 and P60 mice (Insolia & Piccolini, 2014).

In conclusion, to explain the ontogeny of the multiple anomalies in *dal* mice cerebellum, we propose a cascade of molecular/morphological events that begins with the absence of a full functional prolidase enzyme. The deficiency in prolidase results in the alteration in collagen metabolism, and in the increase in the thinner collagen structures as well as disorganized pBM. Such damage leads to the localized aberrant cortical granule cell proliferation and migration with consequent defects in brain lamination, cortical dysplasia and maturation of Purkinje neuron; calcium homeostasis imbalance; phosphorylation of tau proteins which is considered a pathological marker associated to alterations in the inhibitory and excitatory synaptic neurotransmission systems.

Of note, prolidase deficiency in humans is an autosomal recessive disorder and the characteristic untreatable skin lesions are evident only in presence of homozygous mutations. Similarly, the bone phenotype as well as the cardiomyocyte hypertrophy, previously described

in the *dal* model, were only detectable in homozygous state. Even if behavioral tests will be necessary (in term of motor coordination or in cage daily life), we believe that the molecular and histochemical alterations described in *dal* mice could affect the behavior and could cause the mental retardation in both heterozygous and homozygous *dal* mice. On the other end, no neurological defects were reported in human prolidase mutant carriers, thus a compensatory mechanism in humans could account for such difference. We hypothesize that in mouse brain even a decreased amount of prolidase leads to brain alterations, while in humans the phenotype manifests only with the complete lack of the enzyme.

Further studies directed toward the ultrastructure analysis of basement membrane integrity, and toward the electrophysiological characterization will be indispensable. Additionally, the cerebrum cortical anomalies and heterotopias should be evaluated in more details. To better understand the timing of ECM and brain anomalies appearance and to clarify if anomalies found are either a neurodegenerative event or a neurodevelopmental delay, it will be important to further investigate both earlier steps of development and older mice.

ACKNOWLEDGMENTS

This work was supported by the European Community, FP7, "Sybil" project (grant No. 602300) to A.F. This research was supported by the Italian Ministry of Education, University and Research (MIUR): Dipartimenti di Eccellenza Program (2018–2022)—Dept. of Biology and Biotechnology "L. Spallanzani", University of Pavia.

CONFLICT OF INTEREST

All the authors have read and approved the article that it has not been previously published. No conflict of interest to declare.

DATA ACCESSIBILITY

Research data are not shared.

ORCID

Graziella Bernocchi  <https://orcid.org/0000-0001-5816-7418>

Maria G. Bottono  <https://orcid.org/0000-0003-4570-8785>

REFERENCES

Altman, J. (1972). Postnatal development of the cerebellar cortex in the rat. I. The external granular layer and the transitional molecular layer. *Journal of Comparative Neurology*, 145(3), 353–398. <https://doi.org/10.1002/cne.901450305>

Altman, J. (1982). Morphological development of the rat cerebellum and some of its mechanism. *Experimental Brain Research Supplement*, 6, 8–46.

Altman, J., & Bayer, S. A. (1997). *Development of the cerebellar system: In relation to its evolution, structure, and functions*. Boca Raton: CPC Press.

Arata, J., Tada, J., Yamada, T., Oono, T., Yasutomi, H., & Oka, E. (1991). Angiopathic pathogenesis of clinical manifestations in prolidase

deficiency. *Arch*, 127(1), 124–125. <https://doi.org/10.1001/archderm.1991.01680010136028>

Avila, J., Lucas, J. J., Perez, M., & Hernandez, F. (2004). Role of tau protein in both physiological and pathological conditions. *Physiological Reviews*, 84(2), 361–384. <https://doi.org/10.1152/physrev.00024.2003>

Barkovich, A. J., Guerrini, R., Kuzniecky, R. L., Jackson, G. D., & Dobyns, W. B. (2012). A developmental and genetic classification for malformations of cortical development: Update 2012. *Brain*, 135(5), 1348–1369. <https://doi.org/10.1093/brain/awo019>

Barros, C. S., Franco, S. J., & Müller, U. (2011). Extracellular matrix Functions in the nervous system. *Cold Spring Harbor Perspectives in Biology*, 3(1), a005108. <https://doi.org/10.1101/cshperspect.a005108>

Besio, R., Baratto, M. C., Gioia, R., Morzani, E., Nicolis, S., Cucca, L., ... Forlino, A. (2013). A Mn(II)-Mn(II) center in human prolidase. *Biochimica et Biophysica Acta*, 1834(1), 197–204. <https://doi.org/10.1016/j.bbapap.2012.09.008>

Besio, R., Gioia, R., Cosu, F., Morzani, E., Nicolis, S., Cucca, L., ... Forlino, A. (2013). Kinetic and structural evidences on human prolidase pathological mutants suggest strategies for enzyme functional rescue. *PLoS One*, 8(3), e58792. <https://doi.org/10.1371/journal.pone.0058792>

Besio, R., Maruelli, S., Gioia, R., Villa, I., Grabowski, P., Gallagher, O., ... Forlino, A. (2015). Lack of prolidase causes a bone phenotype both in human and in mouse. *Bone*, 72, 53–64. <https://doi.org/10.1016/j.bone.2014.11.009>

Besio, R., Morzani, E., Gioia, R., Nicolis, S., Rossi, A., Casella, L., & Forlino, A. (2011). Improved prolidase activity assay allowed enzyme kinetic characterization and faster prolidase deficiency diagnosis. *Clinica Chimica Acta*, 412(19–20), 1814–1820. <https://doi.org/10.1016/j.cca.2011.06.011>

Boulland, J., Qureshi, T., Seal, R., Rafiki, A., Gundersen, V., Bergersen, L., ... Chaudhry, F. (2004). Expression of the vesicular glutamate transporters during development indicates the widespread corelease of multiple neurotransmitters. *The Journal of Comparative Neurology*, 480(3), 264–280. <https://doi.org/10.1002/cne.20354>

Burnside, E. R., & Bradbury, E. J. (2014). Manipulating the extracellular matrix and its role in brain and spinal cord plasticity and repair. *Neuro-pathology and Applied Neurobiology*, 40(1), 26–59. <https://doi.org/10.1111/nan.12114>

Butbul Aviel, Y., Mandel, H., Avilan Hersh, E., Bergman, R., Adiv, O. E., Luder, A., & Brik, R. (2012). Prolidase deficiency associated with systemic lupus erythematosus (SLE): Single site experience and literature review. *Pediatric Rheumatology Online Journal*, 10(1), 18. <https://doi.org/10.1186/1546-0096-10-18>

Cerri, S., Piccolini, V. M., & Bernocchi, G. (2010). Postnatal development of the central nervous system: Anomalies in the formation of cerebellum fissures. *Anatomical Record (Hoboken)*, 293(3), 492–501. <https://doi.org/10.1002/ar.21082>

Chinard, F. P. (1952). Photometric estimation of proline and ornithine. *The Journal of Biological Chemistry*, 199(1), 91–95.

Cota, C. D., Liu, R. R., Sumberac, T. M., Jung, S., Venkata, D., Millet, Y. H., & Gunn, T. M. (2008). Genetic and phenotypic studies of the dark-like mutant mouse. *Genesis*, 46(10), 562–573. <https://doi.org/10.1002/dvg.20432>

De Rijcke, S., De Maubeuge, J., Laporte, M., Bron, D., Hariga, C., & Ledoux, M. (1989). Prolidase deficiency. Apropos of a peculiar case. *Annales de Dermatologie et de Vénérologie*, 116(4), 309–312.

Dityatev, A., & Rusakov, D. A. (2011). Molecular signals of plasticity at the tetrapartite synapse. *Current Opinion in Neurobiology*, 21(11), 353–359. <https://doi.org/10.1016/j.conb.2010.12.006>

Dityatev, A., Schachner, M., & Sonderegger, P. (2010). The dual role of the extracellular matrix in synaptic plasticity and homeostasis. *Nature Reviews Neuroscience*, 11(2), 735–746. <https://doi.org/10.1038/nrn2898>

Falík-Zaccari, T. C., Khayat, M., Luder, A., Frenkel, P., Magen, D., Brik, R., ... Mandel, H. (2010). A broad spectrum of developmental delay in a large cohort of prolidase deficiency patients demonstrates marked

- interfamilial and intrafamilial phenotypic variability. *American Journal of Medical Genetics. Part B, Neuropsychiatric Genetics*, 153B(1), 46–56. <https://doi.org/10.1002/ajmg.b.30945>
- Ferreira, C., & Wang, H. (2015). In M. P. Adam, H. H. Arlunger, R. A. Pagon, S. E. Wallace, L. J. H. Bean, K. Stephens, & A. Amemiya (Eds.), *Prolidase deficiency* (1993rd–2015th ed.). Seattle, WA: University of Washington, Seattle.
- Folsom, T. D., & Fatemi, S. H. (2013). The involvement of reelin in neurodevelopmental disorders. *Neuropharmacology*, 68, 122–135. <https://doi.org/10.1016/j.neuropharm.2012.08.015>
- Francis, F., Meyer, G., Fallet-Bianco, C., Moreno, S., Kappeler, C., Socorro, A. C., ... Chelly, J. (2006). Human disorders of cortical development: From past to present. *The European Journal of Neuroscience*, 23(4), 877–893. <https://doi.org/10.1111/j.1460-9568.2006.04649.x>
- Frischknecht, R., Chang, K.-J., Rasband, M. N., & Seidenbecher, C. I. (2014). Neural ECM molecules in axonal and synaptic homeostatic plasticity. *Progress in Brain Research*, 214, 81–100. <https://doi.org/10.1016/B978-0-444-63486-3.00004-9>
- Goedert, M.,akes, R., Crowther, R. A., Six, J., Lübke, U., Vandermeeren, M., ... Lee, V. M. (1993). The abnormal phosphorylation of tau protein at Ser-202 in Alzheimer disease recapitulates phosphorylation during development. *Proceedings of the National Academy of Sciences of the United States of America*, 90(11), 5066–5070. <https://doi.org/10.1073/pnas.90.11.5066>
- Goldowitz, D., & Hamre, K. (1998). The cells and molecules that make a cerebellum. *Trends in Neurosciences*, 21(9), 375–382. [https://doi.org/10.1016/S0166-2234\(98\)01313-7](https://doi.org/10.1016/S0166-2234(98)01313-7)
- Guszczyński, T., & Sobolewski, K. (2004). Deregulation of collagen metabolism in human stomach cancer. *Pathobiology*, 71(6), 308–313. <https://doi.org/10.1159/000081726>
- Halter, W., Dong, S., Yip, Y.-P., Willem, M., & Mayer, U. (2002). A critical function of the pial basement membrane in cortical histogenesis. *The Journal of Neuroscience*, 22(14), 6029–6040. <https://doi.org/10.1523/JNEUROSCI.123-14-06029.2002>
- Hatten, M. E. (1999). Central nervous system neuronal migration. *Annual Review of Neuroscience*, 22, 511–539. <https://doi.org/10.1146/annurev.neuro.22.1.511>
- Hecht, J. H., Siegenthaler, J. A., Patterson, K. P., & Pleasure, S. J. (2010). Primary cellular meningeal defects cause neocortical dysplasia and dyslamination. *Annals of Neurology*, 68(4), 454–464. <https://doi.org/10.1002/ana.22103>
- Hechtman, P. (2014). Prolidase deficiency. In D. Valle, A. L. Beaudet, B. Vogelstein, K. W. Kinzler, S. E. Antonarakis, A. Ballabio, et al. (Eds.), chap 82 *The online metabolic and molecular bases of inherited disease* (OMMBID). New York, NY: McGraw-Hill.
- Hof, P. R., Glezer, I. I., Condé, F., Flagg, R. A., Rubin, M. B., Nimchinsky, E. A., & Weisenborn, D. M. V. (1999). Cellular distribution of the calcium-binding proteins parvalbumin, calbindin, and calretinin in the neocortex of mammals: Phylogenetic and developmental patterns. *Journal of Chemical Neuroanatomy*, 16(2), 77–116. [https://doi.org/10.1016/S0891-0618\(98\)00065-9](https://doi.org/10.1016/S0891-0618(98)00065-9)
- Ichikawa-Tomikawa, N., Ogawa, J., Douet, V., Xu, Z., Kamikubo, Y., Sakurai, T., ... Arikawa-Hirasawa, E. (2012). Laminin $\alpha 1$ is essential for mouse cerebellar development. *Matrix Biology*, 31(1), 17–28. <https://doi.org/10.1016/j.matbio.2011.09.002>
- Insolia, V., & Piccolini, V. M. (2014). Brain morphological defects in prolidase deficient mice: First report. *European Journal of Histochemistry*, 58(3), 2417. <https://doi.org/10.4081/ehj.2014.2417>
- Ito, M. (2006). Cerebellar circuitry as a neuronal machine. *Progress in Neurobiology*, 78(3–5), 272–303. <https://doi.org/10.1016/j.pneumbio.2006.02.006>
- Jung, S., Silvius, D., Nolan, K. A., Borchert, G. L., Millet, Y. H., Phang, J. M., & Gunn, T. M. (2011). Developmental cardiac hypertrophy in a mouse model of prolidase deficiency. *Birth Defects Research Part A: Clinical and Molecular Teratology*, 91(4), 204–217. <https://doi.org/10.1002/bda.20789>
- Kama, E., Surazynski, A., & Palka, J. (2000). Collagen metabolism disturbances are accompanied by an increase in prolidase activity in lung carcinoma planeoepitheliale. *International Journal of Experimental Pathology*, 81(5), 341–347. <https://doi.org/10.1111/j.1365-2613.2000.00168.x>
- Komuro, H., & Yacubova, E. (2003). Recent advances in cerebellar granule cell migration. *Cellular and Molecular Life Sciences*, 60(6), 1084–1098. <https://doi.org/10.1007/s00018-003-2248-z>
- Kwok, J. C. F., Yang, S., & Fawcett, J. W. (2014). Brain extracellular matrix in health and disease. *Progress in Brain Research*, 214, 179–192.
- Lakatosova, S., & Ostátníková, D. (2012). Reelin and its complex involvement in brain development and function. *The International Journal of Biochemistry & Cell Biology*, 44(9), 1501–1504. <https://doi.org/10.1016/j.biocel.2012.06.002>
- Laughlin, M. H., Bowles, D. K., & Duncker, D. J. (2012). The coronary circulation in exercise training. *American Journal of Physiology. Heart and Circulatory Physiology*, 302(1), 10–23. <https://doi.org/10.1152/ajpheart.00574.2011>
- Laurie, D. J., Seeburg, P. H., & Wisden, W. (1992). The distribution of 13 GABA_A receptor subunit mRNAs in the rat brain. II. Olfactory bulb and cerebellum. *The Journal of Neuroscience*, 12(3), 1063–1076. <https://doi.org/10.1523/JNEUROSCI.12-03-01063.1992>
- Li, S., Jin, Z., Koirala, S., Bu, L., Xu, L., Hynes, R. O., ... Piao, X. (2008). GPR56 regulates pial basement membrane integrity and cortical lamination. *The Journal of Neuroscience*, 28(22), 5817–5826. <https://doi.org/10.1523/JNEUROSCI.0853-08.2008>
- Li, Y., Liu, M., Yan, Y., & Yang, S. T. (2014). Neural differentiation from pluripotent stem cells: The role of natural and synthetic extracellular matrix. *World Journal of Stem Cells*, 6(1), 11–23. <https://doi.org/10.4252/wjscv6.i1.11>
- Lupi, A., Tenni, R., Rossi, A., Cetta, G., & Forlino, A. (2008). Human prolidase and prolidase deficiency: An overview on the characterization of the enzyme involved in proline recycling and on the effects of its mutations. *Amino Acids*, 35(4), 739–752. <https://doi.org/10.1007/s00726-008-0055-4>
- Malemud, C. J. (2006). Matrix metalloproteinases (MMP) in health and disease: An overview. *Frontiers in Bioscience*, 11, 1696–1701. <https://doi.org/10.2741/1915>
- Matus, A. (1988). Microtubule-associated proteins: Their potential role in determining neuronal morphology. *Annual Review of Neuroscience*, 11(3), 29–44. <https://doi.org/10.1146/annurev.ne.11.030188.000333>
- Menon, S., & Gupton, S. L. (2016). Building blocks of functioning brain: Cytoskeletal dynamics in neuronal development. *International Review of Cell and Molecular Biology*, 322, 183–245. <https://doi.org/10.1016/bs.icmb.2015.10.002>
- Mettouchi, A. (2012). The role of extracellular matrix in vascular branching morphogenesis. *Cell Adhesion & Migration*, 6(6), 528–534. <https://doi.org/10.4161/cam.22862>
- Moore, S. A., Saito, F., Chen, J., Michele, D. E., Henry, M. D., Messing, A., ... Campbell, K. P. (2002). Deletion of brain dystroglycan recapitulates aspects of congenital muscular dystrophy. *Nature*, 418(6896), 422–425. <https://doi.org/10.1038/nature00838>
- Oohashi, T., Edamitsu, M., Bekku, Y., & Carulli, D. (2015). The hyaluronan and proteoglycan link proteins: Organizers of the brain extracellular matrix and key molecules for neuronal function and plasticity. *Experimental Neurology*, 274(Pt. B), 134–144. <https://doi.org/10.1016/j.expneurol.2015.09.010>
- Palka, J., & Phang, J. M. (1997). Prolidase activity in fibroblasts is regulated by interaction of extracellular matrix with cell surface integrin receptors. *Journal of Cellular Biochemistry*, 67(2), 166–175.
- Porcionatto, M. A. (2006). The extracellular matrix provides directional cues for neuronal migration during cerebellar development. *Brazilian Journal of Medical and Biological Research*, 39(3), 313–320. <https://doi.org/10.1590/s0100-879x2006000300001>
- Pöschl, E., Schlötzer-Schrehardt, U., Bradvogel, B., Saita, K., Ninomiya, Y., & Mayer, U. (2004). Collagen IV is essential for basement

- membrane stability but dispensable for initiation of its assembly during early development. *Development*, 131(7), 1619–1628. <https://doi.org/10.1242/dev.01037>
- Qiao, S., Kim, S. H., Heck, D., Goldowitz, D., LeDoux, M. S., & Homayouni, R. (2013). Dab2IP GTPase activating protein regulates dendrite development and synapse number in cerebellum. *PLoS One*, 8(1), e53635. <https://doi.org/10.1371/journal.pone.0053635>
- Qiu, Z., Cang, Y., & Goff, S. P. (2010). Abl family tyrosine kinases are essential for basement membrane integrity and cortical lamination in the cerebellum. *The Journal of Neuroscience*, 30(43), 14430–14439. <https://doi.org/10.1523/JNEUROSCI.12861-10.2010>
- Qu, Q., & Smith, F. (2005). Neuronal migration defects in cerebellum of the large *myd* mouse are associated with disruptions in Bergmann glia organization and delayed migration of granule neurons. *Cerebellum*, 4(4), 261–270. <https://doi.org/10.1080/14734220500358351>
- Ramos, R. L., Siu, N. Y., Brunken, W. J., Yee, K. T., Gabel, L. A., Van Dine, S. E., & Hoplight, B. J. (2014). Cellular and axonal constituents of neocortical molecular layer heterotopia. *Developmental Neuroscience*, 36(6), 477–489. <https://doi.org/10.1159/000365100>
- Ramos, R. L., Van Dine, S. E., George, E., Patel, D., Hoplight, B. J., Leheste, J. R., ... Torres, G. (2013). Molecular layer heterotopia of the cerebellar vermis in mutant and transgenic mouse models on a C57BL/6 background. *Brain Research Bulletin*, 97, 63–68. <https://doi.org/10.1016/j.brainresbull.2013.05.001>
- Ramos, R. L., Van Dine, S. E., Gilbert, M. E., Leheste, J. R., & Torres, G. (2015). Neurodevelopmental malformations of the cerebellar vermis in genetically engineered rats. *Cerebellum*, 14, 624–631. <https://doi.org/10.1007/s12311-015-0657-9>
- Rhodes, J. M., & Simons, M. (2007). The extracellular matrix and blood vessel formation: Not just a scaffold. *Journal of Cellular and Molecular Medicine*, 11(2), 176–205. <https://doi.org/10.1111/j.1582-4934.2007.00031.x>
- Riederer, B., & Matus, A. (1985). Differential expression of distinct microtubule-associated proteins during brain development. *Proceedings of the National Academy of Sciences of the United States of America*, 82, 6006–6009.
- Royce, P. M., & Steinmann, B. (2002). Prolidase deficiency. In P. M. Royce & B. Steinmann (Eds.), *Connective tissue and its heritable disorders*. New York, NY: Wiley-Liss.
- Schwaller, B., Meyer, M., & Schiffrin, S. (2002). 'New' functions for 'old' proteins: The role of the calcium-binding proteins calbindin D-28k, calretinin and parvalbumin, in cerebellar physiology. Studies with knock-out mice. *Cerebellum*, 1(4), 241–258. <https://doi.org/10.1080/147342202320883551>
- Senkov, O., Andjus, P., Radenovic, L., Soriano, E., & Dityatev, A. (2014). Neural ECM molecules in synaptic plasticity, learning, and memory. *Progress in Brain Research*, 214, 53–80. <https://doi.org/10.1016/B978-0-444-63486-3.00003-7>
- Siegenthaler, J. A., & Pleasure, S. J. (2011). We have got you 'covered': How the meninges control brain development. *Current Opinion in Genetics & Development*, 21(3), 249–255. <https://doi.org/10.1016/j.gde.2010.12.005>
- Smyth, N., Vatansever, H. S., Murray, P., Meyer, M., Fife, C., Paulsson, M., & Edgar, D. (1999). Absence of basement membranes after targeting the LAMC1 gene results in embryonic lethality due to failure of endoderm differentiation. *The Journal of Cell Biology*, 144(1), 151–160.
- Soleman, S., Filippov, M. A., Dityatev, A., & Fawcett, J. W. (2013). Targeting the neural extracellular matrix in neurological disorders. *Neuroscience*, 253, 194–213. <https://doi.org/10.1016/j.neuroscience.2013.08.050>
- Strata, P., Tempia, F., Zagrebelsky, M., & Rossi, F. (1997). Reciprocal trophic interactions between climbing fibres and Purkinje cells in the rat cerebellum. *Progress in Brain Research*, 114, 263–282. [https://doi.org/10.1016/S0079-6123\(08\)63369-5](https://doi.org/10.1016/S0079-6123(08)63369-5)
- Surazynski, A., Miltyk, W., Palka, J., & Phang, J. M. (2008). Prolidase-dependent regulation of collagen biosynthesis. *Amino Acids*, 35(4), 731–738. <https://doi.org/10.1007/s00726-008-0051-8>
- Suttks, A., Morawski, M., & Arendt, T. (2014). Protective properties of neural extracellular matrix. *Molecular Neurobiology*, 53(1), 73–82. <https://doi.org/10.1007/s12035-014-8990-4>
- Takayama, C., & Inoue, Y. (2004). Morphological development and maturation of the GABAergic synapses in the mouse cerebellar granular layer. *Developmental Brain Research*, 150(2), 177–190. <https://doi.org/10.1016/j.devbrainres.2004.03.011>
- Takayama, C., Nakagawa, S., Watanabe, M., Mshina, M., & Inoue, Y. (1996). Developmental changes in expression and distribution of the glutamate receptor channel delta 2 subunit according to the Purkinje cell maturation. *Brain Research. Developmental Brain Research*, 92(2), 147–155. [https://doi.org/10.1016/0165-3806\(95\)00212-X](https://doi.org/10.1016/0165-3806(95)00212-X)
- Thompson, C. L., & Stephenson, F. A. (1994). GABAA receptor subtypes expressed in cerebellar granule cells: A developmental study. *Journal of Neurochemistry*, 62(5), 2037–2044. <https://doi.org/10.1046/j.1471-4159.1994.62052037.x>
- Timpi, R. (1989). Structure and biological activity of basement membrane proteins. *European Journal of Biochemistry*, 180(3), 487–502. <https://doi.org/10.1111/j.1432-1033.1989.tb14673.x>
- Vanhoof, G., Goossens, F., De Meester, I., Hendriks, D., & Schape, S. (1995). Proline motifs in peptides and their biological processing. *The FASEB Journal*, 9(9), 736–744.
- Vecellio, M., Schwaller, B., Meyer, M., Hunziker, W., & Celio, M. R. (2000). Alterations in Purkinje cell spines of calbindin D-28 k and parvalbumin knock-out mice. *The European Journal of Neuroscience*, 12(3), 945–954. <https://doi.org/10.1046/j.1460-9568.2000.00986.x>
- Vogel, B., Siebert, H., Hofmann, U., & Frantz, S. (2015). Determination of collagen content within picrosirius red stained paraffin-embedded tissue sections using fluorescence microscopy. *MethodsX*, 2, 124–134. <https://doi.org/10.1016/j.mex.2015.02.007>
- Wang, H., Kurien, B. T., Lundgren, D., Patel, N. C., Kaufman, K. M., Miller, D. L., ... Scofield, R. H. (2006). A nonsense mutation of PEPD in four Amish children with prolidase deficiency. *American Journal of Medical Genetics. Part A*, 140(6), 580–585. <https://doi.org/10.1002/ajmg.a.31134>
- Wang, J. Z., & Liu, F. (2008). Microtubule-associated protein tau in development, degeneration and protection of neurons. *Progress in Neurobiology*, 85(2), 148–175. <https://doi.org/10.1016/j.pneurobio.2008.03.002>
- Watanabe, M., & Kano, M. (2011). Climbing fiber synapse elimination in cerebellar Purkinje cells. *The European Journal of Neuroscience*, 34(10), 1697–1710. <https://doi.org/10.1111/j.1460-9568.2011.07894.x>
- Weiss, J., Nanavati, S., Vogel, Z., & Maggio, R. (1993). Functional role of proline and tryptophan residues highly conserved among G protein-coupled receptors studied by mutational analysis of the m3 muscarinic receptor. *The EMBO Journal*, 12(1), 331–338.
- White, J. J., & Sillito, R. V. (2013). Postnatal development of cerebellar zones revealed by neurofilament heavy chain protein expression. *Frontiers in Neuroanatomy*, 7, 9. <https://doi.org/10.3389/fnana.2013.00009>
- Xu, H., Yang, Y., Tang, X., Zhao, M., Liang, F., Xu, P., ... Fan, X. (2013). Bergmann glia function in granule cell migration during cerebellum development. *Molecular Neurobiology*, 47(2), 833–844. <https://doi.org/10.1007/s12035-013-8405-y>
- Yuzaki, M. (2004). The delta2 glutamate receptor: A key molecule controlling synaptic plasticity and structure in Purkinje cells. *Cerebellum*, 3(1), 89–93. <https://doi.org/10.1080/14734220410028921>

How to cite this article Insolia V, Priori EC, Gasperini C, et al. Prolidase enzyme is required for extracellular matrix integrity and impacts on postnatal cerebellar cortex development. *J Comp Neurol*. 2019;1–20. <https://doi.org/10.1002/cne.24735>

Pt(IV)Ac-POA: New Platinum Compound Induced Caspase Independent Apoptosis In B50 Neuroblastoma Stem Cells

Ferrari B¹, Camuso S¹, Priori EC¹, De Luca F¹, Roda E^{1,3}, Osella D² and Bottone MG^{1*}

¹Department of Biology and Biotechnology, University of Pavia, Italy

²Department of Sciences and Technological Innovation (DiSIT)*University of Eastern Piedmont, Italy

³Laboratory of Clinical & Experimental Toxicology, Pavia Poison Centre, National Toxicology Information Centre, Toxicology Unit, ICS Maugeri Spa, IRCCS Pavia, Italy

*Corresponding author: Maria Grazia Bottone, Department of Biology and Biotechnology, University of Pavia, Via Ferrata 9, 27100, Pavia, Italy, Tel: 3388527987; Email: bottone@unipv.it

Research Article

Volume 3 Issue 2

Received Date: August 17, 2019

Published Date: September 06, 2019

Abstract

Neuroblastoma is a tumour that affects adults and children, characterized by a stem cells component. To date, cisplatin is the main antitumor agent used in the clinical treatment of this tumour; however, it induces side effects such as neurotoxicity in healthy cells and induces chemo resistance to therapy in cancer cells. New platinum-based compounds, platinum (II) have recently been synthesized, and due to their chemical characteristics, they are able to identify new cellular targets. These complexes act as prodrugs and performing their cytotoxic effect as platinum (II) after a reduction reaction within the hypoxic tumour cells. Among these prodrugs, Pt(IV)Ac-POA appears to be very promising, thanks to the presence of ligand (2-propynyl)octanoic acid (POA), which acts as an inhibitor of histone deacetylase (HDACi) and leads to the increase of histone acetylation, decreasing the interactions between histone and DNA, so as to produce chemo-sensitization to DNA-damaging agents. The greater cytotoxic effect of Pt(IV)Ac-POA on tumour cells, would therefore be mainly due to the mechanism of inhibition of histone deacetylase, which would increase the accessibility of DNA to platination mechanisms that induce cell death. In this study the results show that Pt(IV)Ac-POA, used at a concentration ten times lower than cisplatin, can induce apoptosis in B50 cells in culture both through the intrinsic pathway and through the independent caspase pathway. The data, obtained by immunohistochemical techniques in fluorescence microscopy, show that treatment with Pt(IV)Ac-POA has a greater proapoptotic effect on stem cells compared to the cisplatin standard treatment.

Keywords: B50 Cells; Apoptosis; Cisplatin; Pt(IV)Ac-POA

Introduction

Cisplatin is one of the most active chemotherapeutic drug used in the treatment of different type of solid cancer, including some nervous system tumours, such as Neuroblastoma [1]. Neuroblastoma is a frequently extracranial tumour in infancy, representing 8-10% of all cancer in childhood. To date, cisplatin is largely employed in Neuroblastoma treatment, but despite its benefit, its use is hampered by severe systemic side effects and the onset of drug resistance [2-4]. For this reason, in the last years the goal of biomedical research has been the synthesis of new antitumor agents, with the same antitumor effect of the reference drug, but associated to less systemic toxicity.

To overcome limits of classical oncotherapy, new platinum (IV) pro drugs have been synthesised. The Pt(IV) complexes act as pro drugs and reducing themselves to cytotoxic analogues of Pt(II) inside hypoxic tumour cells [5-7]. Among these, the new Pt(IV)Ac-POA pro drug represents a promising tool, bearing as axial ligand (2-propynyl) octanoic acid (POA), an histone deacetylase inhibitor (HDACi). Pt(IV)Ac-POA is able to produce a synergistic action in the hypoxic tumour cell microenvironment. Indeed, HDAC inhibition increases histone acetylation, decreasing histone-DNA interactions and allowing for chemo-sensitization versus DNA-damaging agents [8-10]. The new prodrug has showed also a higher activity due to the high cellular accumulation by virtue of high lipophilicity and to the inhibition of histone deacetylase which leads to increased exposure of nuclear DNA, thereby permitting higher platination levels and promoting cancer cells death.

In this study we evaluated the effect of the new Pt(IV)Ac-POA on the B50 Neuroblastoma rat cells, focusing on the activation of different cell death pathways and the morphological and functional changes induced by treatment.

The B50 neuronal cell line offer several advantages to the study of neurons in culture, in fact they are simple to grow, to differentiate and to transfect. Concerning to our research, B50 cells have been extensively used in the study of death and toxicology.

Materials and Methods

B50 Neuroblastoma rat cells were cultured in 75 cm² flask, in Dulbecco's Modified Eagle Medium (DMEM) supplemented with L-glutamine (2 mM), penicillin 100 IU ml⁻¹, streptomycin (100 mg l⁻¹) and 10% fetal bovine serum (FBS), and at 37°C in a 5% CO₂ humidified chamber.

Cells were seed on glass coverslips placed in a 6 multi-well and then treated with cisplatin at 40 µM or Pt(IV)Ac-POA at 4 µM for 48h at continuous exposure. These concentrations for cisplatin and Pt(IV)Ac-POA were based on previous works and obtained by IC₅₀ analysis, respectively [11,12].

After treatment with cisplatin (40 µM) and Pt(IV)Ac-POA (4 µM) for 48h at continuous exposure an immunohistochemistry detection for Bax, Bcl-2 and AIF was performed, associated with a labelling for the mitochondria and a counterstained with Hoechst 33258 for the nuclei (Table 1). Images were obtained by an Olympus BX51 microscope equipped with a 100-W mercury lamp and used under the following conditions: 330-385 nm excitation filter (excf), 400 nm dichroic mirror (dm) and 420 nm barrier filter (bf) for Hoechst 33258; 450-480 nm excf, 500 nm dm and 515 nm bf for the fluorescence of Alexa 488; 540 nm excf, 580 nm dm and 620 nm bf for Alexa 594. Images were then recorded with an Olympus MagniFire camera system and processed with the Olympus Cell F software.

Antigen	Primary antibody	Dilution in PBS	Secondary antibody	Dilution in PBS
Bax	Polyclonal rabbit (Santa Cruz Biotechnology)	1:200	Anti-rabbit IgG1 Alexa Fluor 594 (Molecular Probes, Invitrogen)	1:200
Bcl-2	Polyclonal rabbit (Santa Cruz Biotechnology)	1:200	Anti-rabbit IgG1 Alexa Fluor 594 (Molecular Probes, Invitrogen)	1:200
AIF	Polyclonal rabbit (Cell Signaling Technology)	1:200	Anti-rabbit IgG1 Alexa Fluor 594 (Molecular Probes, Invitrogen)	1:200
Mitochondria	Human autoimmune serum *	1:200	Anti-human IgG1 Alexa Fluor 488 (Molecular Probes, Invitrogen)	1:200

Table 1: Primary and secondary antibodies used for immunocytochemical reactions at fluorescence microscope Rangone, et al. [12].

Differences between control and treated samples were analysed, evaluating three independent experiments for each condition and protein analysed. The percentage of mean fluorescence intensity was calculated with ImageJ software and the obtained scores were expressed as the mean \pm SEM (standard error of mean). Data differences were analysed for statistical significance by one-way ANOVA and post hoc Bonferroni's test (software package GraphPad Prism Inc.). p values ranging from < 0.001 to < 0.05 were considered statistically significant.

Results

To analyse the activation of cell death pathways, following treatment with cisplatin at 40 μ M or Pt(IV)Ac-

POA 4 μ M, immunocytochemical reactions were conducted to put in evidence the proteins involved in these processes: Bax, Bcl-2 and AIF.

After immunolabelling, in the B50 control cells, Bax (red fluorescence) was located in the cytoplasm and not localized with the mitochondria represented by green fluorescence (Figure 1). On the contrary, after both treatments, the Bax-immunolabelling was distributed nearby the mitochondria, where a clear colocalization of the Bax fluorescence with the organelles was observed. Semi quantitative analysis of the immunofluorescence intensity of Bax, showed an increased intensity in cells treated with Pt(IV)Ac-POA, compared to the control and treated-cells, in particular in cells with apoptotic nucleus.

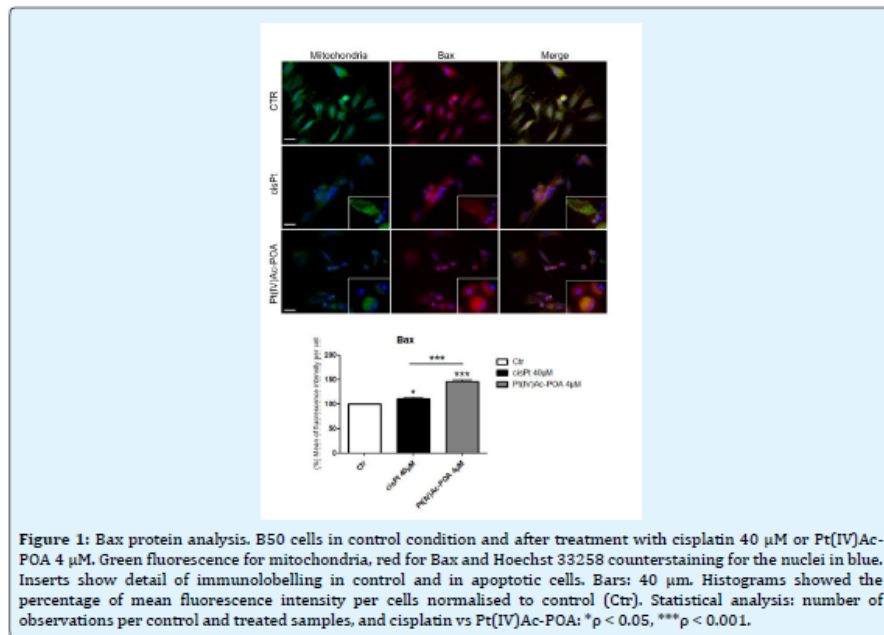


Figure 1: Bax protein analysis. B50 cells in control condition and after treatment with cisplatin 40 μ M or Pt(IV)Ac-POA 4 μ M. Green fluorescence for mitochondria, red for Bax and Hoechst 33258 counterstaining for the nuclei in blue. Inserts show detail of immunolabelling in control and in apoptotic cells. Bars: 40 μ m. Histograms showed the percentage of mean fluorescence intensity per cells normalised to control (Ctr). Statistical analysis: number of observations per control and treated samples, and cisplatin vs Pt(IV)Ac-POA: * $p < 0.05$, *** $p < 0.001$.

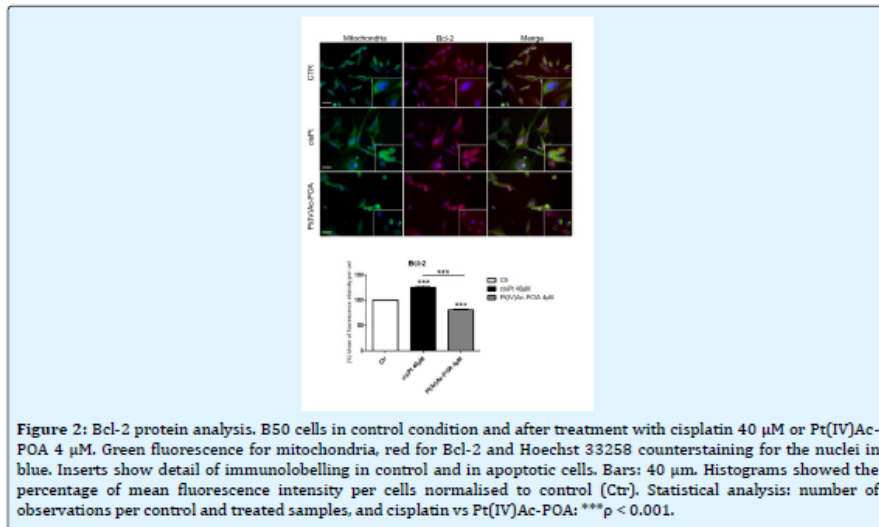
Images reported in Figure 2 show a double immunolabeling for Bcl-2, marked in red, and the mitochondria, green fluorescence. In B50 control cells, immunolabelling for Bcl-2 protein was distributed in the cytoplasm and any colocalization with the mitochondria

fluorescence was detectable. After treatment with cisplatin at 40 μ M and Pt(IV)Ac-POA at 4 μ M, respectively, Bcl-2 translocated to the mitochondria in early apoptosis, while its expression decreases, resulting almost absent in late apoptosis, as can be seen in the inserts. To note, in

Journal of Embryology & Stem Cell Research

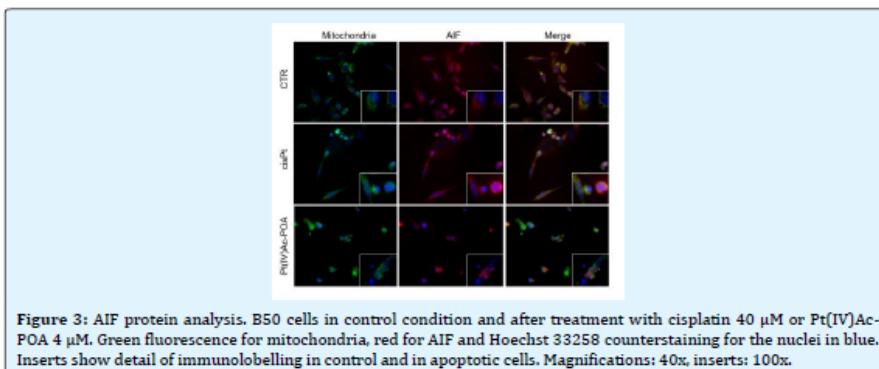
cells exposed to treatment with cisplatin, an increasing in Bcl-2 fluorescence was observed and corroborated by semi quantitative analysis. In fact, B50 cells that show a

control-like phenotype after treatment show an increase in fluorescence for the protein under examination.



Immunolabel for AIF, red fluorescence, revealed that in B50 control cells, AIF fluorescence localizes with the mitochondria (green fluorescence) (Figure 3). After treatment with cisplatin at 40 μM or Pt(IV)Ac-POA at 4

μM , the fluorescence related to AIF was no longer associated with labelling for mitochondria, but was found at the nuclear level which, following treatment, appears fragmented and with apoptotic features.



At last, in each condition analysed, a severe alteration in mitochondria structure were observed after both treatments compared to control. Indeed, in control cells mitochondria were characterized by a fusiform aspect and a homogeneous localization in the cytoplasm. Following treatment with cisplatin or Pt(IV)Ac-POA, the mitochondria lose their structure, appeared smaller and more rounded, clustering in dense masses around cells nuclei. A strong reduction in the number and in the cell size were evident after exposure Pt(IV)Ac-POA compared to control and cisplatin-treated cells. In particular, after cisplatin exposure some cells showed a treatment-resistant phenotype, the mitochondria maintain morphology comparable to that found in control cells and proteins of interest remained in the physiological compartment. This data was not observed after treatment with Pt(IV)Ac-POA or at least was detected in a minor way compared to cisplatin, suggesting a greater proapoptotic effect of the new compound.

Conclusion

Results presented in this work show that the prodrug can activate both the apoptotic pattern in B50 cell lines: the intrinsic apoptotic pathway and the independent caspase pattern. After treatment with Pt(IV)Ac-POA a morphological change in mitochondria, which undergo fission, were observed associated to i) an increase in the Bax protein level, ii) the translocation of AIF from the mitochondria to the nucleus and iii) a decrease in Bcl-2. Quantified values, which are statistically significantly, corroborates the greater effect of the new compound, active already at 4 μ M, than cisplatin (40 μ M). After Pt(IV)Ac-POA 4 μ M treatment, as had already been demonstrated by Rangone, et al. [12], the number of cells dying due to apoptosis or autophagy is also greater, compared to the standard treatment with cisplatin, where, the cells that do not show an apoptotic morphology and cells are characterized by an increasing in Bcl-2 protein expression, suggesting a cisplatin-chemo resistance.

Conflict of Interest

The authors declare that they have no conflict of interest

Acknowledgment

This research was supported by Italian Ministry of Education, University and Research (MIUR): Dipartimenti di Eccellenza Program (2018–2022) - Dept. of Biology and Biotechnology "L. Spallanzani", University of Pavia

Funding Information

This research is supported by the University of Pavia: Fondi Ricerca Giovani (FRG 2018) and by the Compagnia di San Paolo: research project "BIPLANES". We are indebted to the Inter-University Consortium for Research on the Chemistry of Metals in Biological Systems (CIRCMSB, Bari) and UE COST CM1105 Action "Functional metal complexes that bind to biomolecules" for stimulating discussions during the group meetings and short-term missions.

This research was supported by Italian Ministry of Education, University and Research (MIUR): Dipartimenti di Eccellenza Program (2018–2022) - Dept. of Biology and Biotechnology "L. Spallanzani", University of Pavia.

References

1. Boulikas T, Pantos A, Bellis E, Christofis P (2007) Designing platinum compounds in cancer: structures and mechanism. *Cancer Ther* 5: 537-583.
2. Yanagisawa R, Kubota N, Hidaka E, Sakashita K, Tanaka M, et al. (2018) Cisplatin-induced nephrotoxicity in patients with advanced Neuroblastoma. *Pediatr Blood Cancer* 65(9): e27253.
3. Wei M, Yuan X (2019) Cisplatin-induced ototoxicity in children with solid tumor. *J Pediatr Hematol Oncol* 41(2): e97-e100.
4. Aveic S, Corallo D, Porcù E, Pantile M, Boso D, et al. (2018) TP-0903 inhibits neuroblastoma cell growth and enhances the sensitivity to conventional chemotherapy. *Eur J Pharmacol* 818: 435-448.
5. Graf N, Lippard SJ (2012) Redox activation of metal-based prodrugs as a strategy for drug delivery. *Adv Drug Deliv Rev* 64(11): 993-1004.
6. Wexselblatt E, Gibson D (2012) What do we know about the reduction of Pt(IV) pro-drugs?. *J Inorg Biochem* 117: 220-229.
7. Johnstone TC, Suntharalingam K, Lippard SJ (2016) The next generation of platinum drugs: targeted Pt(II) agents, nanoparticle delivery, and Pt(IV) prodrugs. *Chem Rev* 116: 3436-3486.
8. Li Y, Seto E (2016) HDACs and HDAC Inhibitors in cancer development and therapy. *Cold Spring Harb Perspect Med* 6(10): 026831.

Journal of Embryology & Stem Cell Research

9. Novohradsky V, Zerankova L, Stepankova J, Vrana O, Raveendran R, et al. (2015) New insights into the molecular and epigenetic effects of antitumor Pt(IV)-valproic acid conjugates in human ovarian cancer cells. *Biochem Pharmacol* 95(3): 133-144.
10. Witt O, Deubzer HE, Lodrini M, Milde T, Oehme I (2009) Targeting histone deacetylases in neuroblastoma. *Curr Pharm Des* 15(4): 436-447.
11. Santin G, Scietti L, Veneroni P, Barni S, Bernocchi G, et al. (2012) Effects of Cisplatin in neuroblastoma rat cells: damage to cellular organelles. *Int J Cell Biol* 2012: 424072.
12. Rangone B, Ferrari B, Astesana V, Masiello I, Veneroni P, et al. (2018) A new platinum-based prodrug candidate: Its anticancer effects in B50 neuroblastoma rat cells. *Life Sci* 210: 166-176.

